MICROBIAL HYDROGEN METABOLISM

EDITED BY: Chris Greening and Eric Boyd
PUBLISHED IN: Frontiers in Microbiology

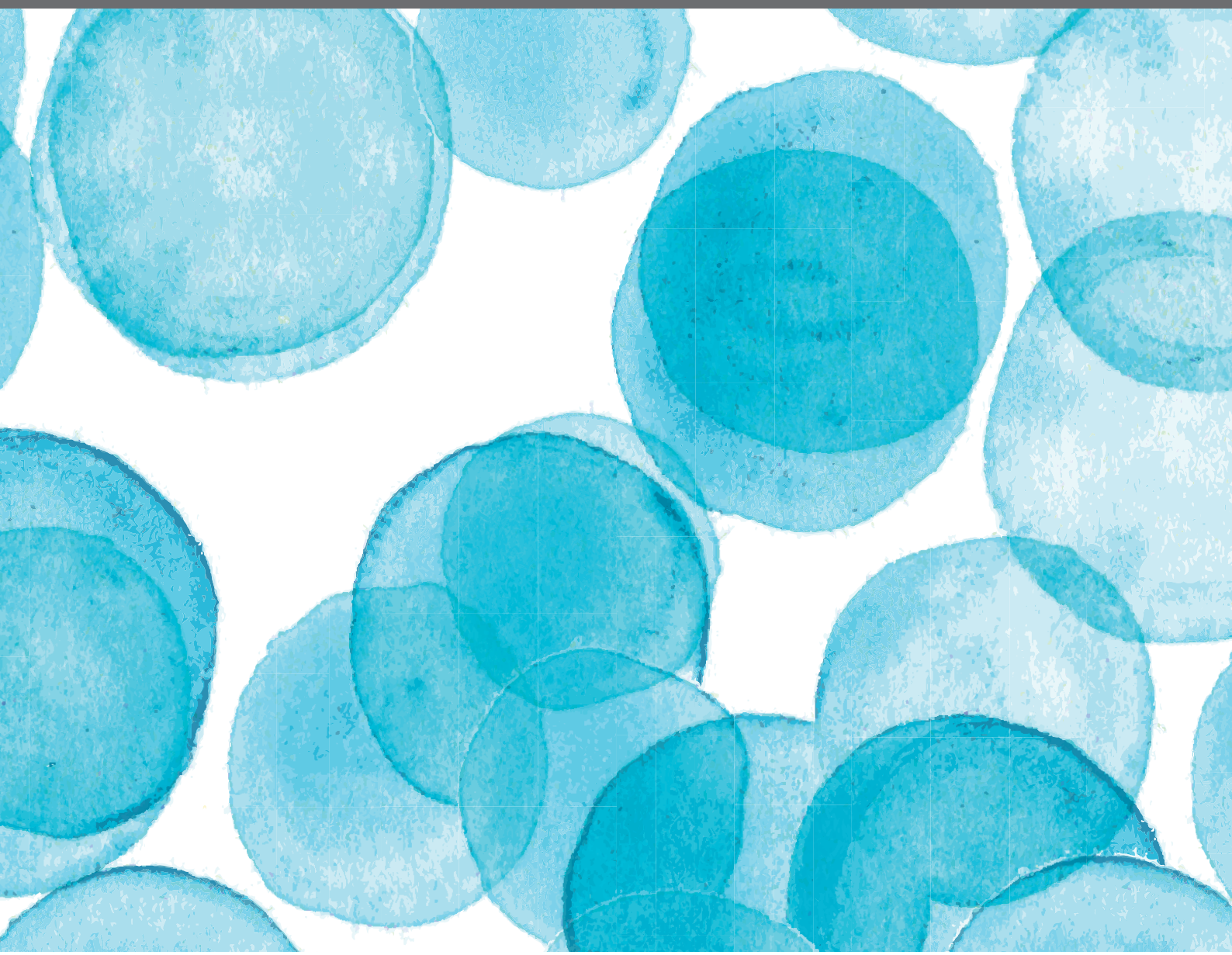

frontiers Research Topics

ISSN 1664-8714
ISBN 978-2-88963-540-5
DOI 10.3389/978-2-88963-540-5

About Frontiers

Frontiers is more than just an open-access publisher of scholarly articles: it is a pioneering approach to the world of academia, radically improving the way scholarly research is managed. The grand vision of Frontiers is a world where all people have an equal opportunity to seek, share and generate knowledge. Frontiers provides immediate and permanent online open access to all its publications, but this alone is not enough to realize our grand goals.

Frontiers Journal Series

The Frontiers Journal Series is a multi-tier and interdisciplinary set of open-access, online journals, promising a paradigm shift from the current review, selection and dissemination processes in academic publishing. All Frontiers journals are driven by researchers for researchers; therefore, they constitute a service to the scholarly community. At the same time, the Frontiers Journal Series operates on a revolutionary invention, the tiered publishing system, initially addressing specific communities of scholars, and gradually climbing up to broader public understanding, thus serving the interests of the lay society, too.

Dedication to Quality

Each Frontiers article is a landmark of the highest quality, thanks to genuinely collaborative interactions between authors and review editors, who include some of the world's best academicians. Research must be certified by peers before entering a stream of knowledge that may eventually reach the public - and shape society; therefore, Frontiers only applies the most rigorous and unbiased reviews.
Frontiers revolutionizes research publishing by freely delivering the most outstanding research, evaluated with no bias from both the academic and social point of view. By applying the most advanced information technologies, Frontiers is catapulting scholarly publishing into a new generation.

What are Frontiers Research Topics?

Frontiers Research Topics are very popular trademarks of the Frontiers Journals Series: they are collections of at least ten articles, all centered on a particular subject. With their unique mix of varied contributions from Original Research to Review Articles, Frontiers Research Topics unify the most influential researchers, the latest key findings and historical advances in a hot research area! Find out more on how to host your own Frontiers Research Topic or contribute to one as an author by contacting the Frontiers Editorial Office: researchtopics@frontiersin.org

MICROBIAL HYDROGEN METABOLISM

Topic Editors:
Chris Greening, Monash University, Australia
Eric Boyd, Montana State University, United States

Citation: Greening, C., Boyd, E., eds. (2020). Microbial Hydrogen Metabolism. Lausanne: Frontiers Media SA. doi: 10.3389/978-2-88963-540-5

Table of Contents

frontiers in Microbiology

EDITORIAL
published: 30 January 2020
doi: 10.3389/fmicb.2020.00056

Editorial: Microbial Hydrogen Metabolism

Chris Greening[1]* *and Eric Boyd*[2]*

[1] School of Biological Sciences, Monash University, Clayton, VIC, Australia, [2] Department of Microbiology and Immunology, Montana State University, Bozeman, MT, United States

Keywords: hydrogen, hydrogen metabolism, hydrogenase, fermentation, respiration

Editorial on the Research Topic

Microbial Hydrogen Metabolism

Among the most ancient and widespread metabolic traits of microbial life is the ability to interconvert molecular hydrogen (H_2; Lane et al., 2010; Schwartz et al., 2013; Peters et al., 2015). Two classes of metalloenzymes, [FeFe]-hydrogenase and [NiFe]-hydrogenase, catalyze the reversible oxidation of H_2 to electrons and protons (Volbeda et al., 1995; Peters et al., 1998); a third class of hydrogenase, termed [Fe]-hydrogenase or Hmd, catalyzes the reduction of the substrate methenyltetrahydromethanopterin with H_2 (Shima et al., 2008). The three classes of enzyme differ structurally and are phylogenetically unrelated. As such, they represent profound examples of convergent evolution (Wu and Mandrand, 1993; Vignais and Billoud, 2007; Greening et al., 2016).

Approximately a third of sequenced microorganisms, spanning at least 70 microbial phyla, encode hydrogenases and are thus predicted to be capable of interconverting H_2 (Peters et al., 2015; Greening et al., 2016). The earliest evolving hydrogenase enzymes harbor a [NiFe] co-factor and these are thought to have functioned oxidatively (Boyd et al., 2014; Weiss et al., 2016), with [FeFe]-hydrogenases thought to have emerged more recently (Mulder et al., 2010). Both [NiFe] and [FeFe]-hydrogenases have since diversified to function in aerobic and anaerobic, heterotrophic, and autotrophic, and chemotrophic and phototrophic metabolic backgrounds (Kovács et al., 2005; Tamagnini et al., 2007; Thauer et al., 2010; Schwartz et al., 2013; Koch et al., 2014; Schuchmann and Muller, 2014; Pinske and Sawers, 2016). Many bacteria and archaea oxidize H_2 as a low potential electron donor, an activity typically (albeit not exclusively) attributed to various lineages of [NiFe]-hydrogenase enzymes. Various bacteria, archaea, and microbial eukaryotes also evolve H_2 as a diffusible end product during fermentative metabolism through the activity of [FeFe]- or [NiFe]-hydrogenases (Horner et al., 2000; Kim and Kim, 2011; Marreiros et al., 2013; Schwartz et al., 2013; Pinske and Sawers, 2016). In many organisms, the ability to metabolize H_2 is a facultative trait that is regulated through the expression and maturation of hydrogenases (Schwartz et al., 2013; Greening and Cook, 2014). In such taxa, H_2 represents a substrate that organisms utilize to supplement their energy metabolism, thereby allowing for an expansion of their niche space in ecosystems where other sources of reductant are low or variable in supply (e.g., Amenabar et al., 2018).

The implications of H_2 in ecosystem level processes is increasingly being realized in both environmental and biomedical settings. A wide range of ecosystems have now been described where H_2 cycling supports the bulk of primary production and where it forms the basis by which species interact, leading to ecologically structured communities. Much of the research on H_2 metabolism to date has focused on ecosystems where H_2 is present at elevated concentrations due to biological

Edited by:
Patricia Coutinho Dos Santos, Wake Forest University, United States

Reviewed by:
Shawn E. McGlynn, Tokyo Institute of Technology, Japan

***Correspondence:**
Chris Greening
chris.greening@monash.edu
Eric Boyd
eboyd@montana.edu

Specialty section:
This article was submitted to Microbial Physiology and Metabolism, a section of the journal Frontiers in Microbiology

Received: *20 November 2019*
Accepted: *13 January 2020*
Published: *30 January 2020*

Citation:
Greening C and Boyd E (2020) Editorial: Microbial Hydrogen Metabolism. Front. Microbiol. 11:56. doi: 10.3389/fmicb.2020.00056

activity (e.g., anoxic sediments, gastrointestinal tracts; Sørensen et al., 1981; Wolf et al., 2016; Greening et al., 2019; Kessler et al., 2019) or geological activity (e.g., hydrothermal vents, subsurface systems; Petersen et al., 2011; Brazelton et al., 2012; Telling et al., 2015; Dong et al., 2019; Lindsay et al., 2019). More recently, it has been recognized that atmospheric H_2 can serve as source of reductant for aerobic soil microorganisms and that this can influence the composition of the atmosphere (Conrad, 1996; Constant et al., 2010; Ji et al., 2017; Cordero et al., 2019). In parallel, medical microbiologists have shown that H_2 metabolism is critical for the virulence of numerous pathogens, including *Helicobacter*, Clostridia, and Enterobacteriaceae (Kaji et al., 1999; Olson and Maier, 2002; Maier et al., 2004, 2013).

This special issue, featuring 10 articles from 46 different authors, explores microbial H_2 metabolism from the molecular to the ecosystem scale. In the area of anaerobic metabolism, there are articles exploring the metabolism of H_2-metabolizing bacteria capable of sulfate reduction, acetogenesis, halorespiration, and fermentation. Two articles investigate H_2 oxidation in sulfate-reducing bacteria using the model system *Desulfovibrio vulgaris* (Fauque et al., 1988; Caffrey et al., 2007). Smith et al. present a mathematical model of the growth and metabolism of this bacterium, whereas Löffler et al. investigate the kinetic isotope fractionation associated with its H_2 oxidation activity. A comprehensive review led by Schuchmann et al. covers recent advances in understanding clostridial H_2 metabolism; it details the discovery and characterization of multimeric electron-bifurcating [FeFe]-hydrogenases, including those associated with formate dehydrogenases (Schut and Adams, 2009; Schuchmann and Müller, 2012, 2013; Buckel and Thauer, 2018). Another article led by Dragomirova et al. focuses on heterologous expression of a [NiFe]-hydrogenase from dehalogenating Chloroflexi (Kublik et al., 2016; Hartwig et al., 2017), reporting another unexpected association with formate dehydrogenase activity. Pinske explores a third type of formate dehydrogenase-linked hydrogenase, namely the classical formate hydrogenlyase complex of Enterobacteriaceae (McDowall et al., 2014), and its association with two novel iron-sulfur proteins.

Several articles also investigate aerobic H_2 metabolism. Islam et al. report two other novel iron-sulfur proteins in mycobacteria, demonstrating that they are essential for the activity of the two high-affinity hydrogenases described in this lineage (Greening et al., 2014). Carere et al. meanwhile, build on the recent discovery that verrucomicrobial methanotrophs are facultative mixotrophs (Carere et al., 2017; Mohammadi et al., 2017) by showing resource allocation of *Methylacidiphilum* varies depending on H_2 availability. Three articles also explore H_2 metabolism at the ecosystem level. Adam and Perner explore the diversity of aerobic and anaerobic H_2 metabolism in deep-sea hydrothermal vent systems, whereas Meyer-Dombard et al. investigate the influence of H_2 on biogeochemical cycling in serpentinizing springs in the Philippines. Teng et al. review the previously underexplored area of H_2 metabolism in bioremediation, including in the reduction of organohalides, nitroaromatic compounds, and heavy metals (Chardin et al., 2003; Hong et al., 2008; Schubert et al., 2018).

In summary, this special Research Topic sheds light on the diverse role of H_2 in microbial metabolism and uncovers novel enzymes and pathways that mediate this process. This body of work highlights the intricate linkages between H_2 cycling and the cycling of various other compounds, including methane, formate, carbon dioxide, sulfate, and organohalides, among others. In turn, these findings pave way for future studies on the biochemistry, physiology, ecology, and industrial applications of microbial H_2 metabolism.

AUTHOR CONTRIBUTIONS

CG and EB drafted this editorial together and approve its submission.

FUNDING

This work was supported by the U.S. Department of Energy, Office of Science, Basic Energy Sciences under Award DE-SC0020246 (EB).

ACKNOWLEDGMENTS

We would like to acknowledge all authors, peer reviewers, guest editors, and the Frontiers team for their support in developing this Research Topic. The salary of CG is covered by an Australian Research Council DECRA Fellowship (DE170100310) and a National Health & Medical Research Council EL2 Fellowship (APP1178715).

REFERENCES

Amenabar, M. J., Colman, D. R., Poudel, S., Roden, E. E., and Boyd, E. S. (2018). Electron acceptor availability alters carbon and energy metabolism in a thermoacidophile. *Environ. Microbiol.* 20, 2523–2537. doi: 10.1111/1462-2920.14270

Boyd, E. S., Schut, G., Adams, M. W. W., and Peters, J. W. (2014). Hydrogen metabolism and the evolution of respiration. *Microbe* 9, 361–367. doi: 10.1128/microbe.9.361.1

Brazelton, W. J., Nelson, B., and Schrenk, M. O. (2012). Metagenomic evidence for H_2 oxidation and H_2 production by serpentinite-hosted subsurface microbial communities. *Front. Microbiol.* 2:268. doi: 10.3389/fmicb.2011.00268

Buckel, W., and Thauer, R. K. (2018). Flavin-based electron bifurcation, a new mechanism of biological energy coupling. *Chem. Rev.* 118, 3862–3886. doi: 10.1021/acs.chemrev.7b00707

Caffrey, S. M., Park, H.-S., Voordouw, J. K., He, Z., Zhou, J., and Voordouw, G. (2007). Function of periplasmic hydrogenases in the sulfate-reducing bacterium *Desulfovibrio vulgaris* Hildenborough. *J. Bacteriol.* 189, 6159–6167. doi: 10.1128/JB.00747-07

Carere, C. R., Hards, K., Houghton, K. M., Power, J. F., McDonald, B., Collet, C., et al. (2017). Mixotrophy drives niche expansion of verrucomicrobial methanotrophs. *ISME J* 11, 2599–2610. doi: 10.1038/ismej.2017.112

Chardin, B., Giudici-Orticoni, M.-T., De Luca, G., Guigliarelli, B., and Bruschi, M. (2003). Hydrogenases in sulfate-reducing bacteria function as chromium reductase. *Appl. Microbiol. Biotechnol.* 63, 315–321. doi: 10.1007/s00253-003-1390-8

Conrad, R. (1996). Soil microorganisms as controllers of atmospheric trace gases (H_2, CO, CH_4, OCS, N_2O, and NO). *Microbiol. Mol. Biol. Rev.* 60, 609–640. doi: 10.1128/MMBR.60.4.609-640.1996

Constant, P., Chowdhury, S. P., Pratscher, J., and Conrad, R. (2010). Streptomycetes contributing to atmospheric molecular hydrogen soil uptake are widespread and encode a putative high-affinity [NiFe]-hydrogenase. *Environ. Microbiol.* 12, 821–829. doi: 10.1111/j.1462-2920.2009.02130.x

Cordero, P. R. F., Grinter, R., Hards, K., Cryle, M. J., Warr, C. G., Cook, G. M., et al. (2019). Two uptake hydrogenases differentially interact with the aerobic respiratory chain during mycobacterial growth and persistence. *J. Biol. Chem.* 294, 18980–18991. doi: 10.1074/jbc.RA119.011076

Dong, X., Greening, C., Rattray, J. E., Chakraborty, A., Chuvochina, M., Mayumi, D., et al. (2019). Metabolic potential of uncultured bacteria and archaea associated with petroleum seepage in deep-sea sediments. *Nat. Commun.* 10:1816. doi: 10.1038/s41467-019-09747-0

Fauque, G., Peck, H. D., Moura, J. J. G., Huynh, B. H., Berlier, Y., DerVartanian, D. V, et al. (1988). The three classes of hydrogenases from sulfate-reducing bacteria of the genus *Desulfovibrio*. *FEMS Microbiol. Lett.* 54, 299–344. doi: 10.1111/j.1574-6968.1988.tb02748.x

Greening, C., Berney, M., Hards, K., Cook, G. M., and Conrad, R. (2014). A soil actinobacterium scavenges atmospheric H_2 using two membrane-associated, oxygen-dependent [NiFe] hydrogenases. *Proc. Natl. Acad. Sci. U.S.A.* 111, 4257–4261. doi: 10.1073/pnas.1320586111

Greening, C., Biswas, A., Carere, C. R., Jackson, C. J., Taylor, M. C., Stott, M. B., et al. (2016). Genomic and metagenomic surveys of hydrogenase distribution indicate H_2 is a widely utilised energy source for microbial growth and survival. *ISME J.* 10, 761–777. doi: 10.1038/ismej.2015.153

Greening, C., and Cook, G. M. (2014). Integration of hydrogenase expression and hydrogen sensing in bacterial cell physiology. *Curr. Opin. Microbiol.* 18, 30–38. doi: 10.1016/j.mib.2014.02.001

Greening, C., Geier, R., Wang, C., Woods, L. C., Morales, S. E., McDonald, M. J., et al. (2019). Diverse hydrogen production and consumption pathways influence methane production in ruminants. *ISME J.* 13, 2617–2632. doi: 10.1038/s41396-019-0464-2

Hartwig, S., Dragomirova, N., Kublik, A., Türkowsky, D., von Bergen, M., Lechner, U., et al. (2017). A H_2-oxidizing, 1, 2, 3-trichlorobenzene-reducing multienzyme complex isolated from the obligately organohalide-respiring bacterium *Dehalococcoides mccartyi* strain CBDB1. *Environ. Microbiol. Rep.* 9, 618–625. doi: 10.1111/1758-2229.12560

Hong, Y.-G., Guo, J., and Sun, G.-P. (2008). Identification of an uptake hydrogenase for hydrogen-dependent dissimilatory azoreduction by *Shewanella decolorationis* S12. *Appl. Microbiol. Biotechnol.* 80:517. doi: 10.1007/s00253-008-1597-9

Horner, D. S., Foster, P. G., and Embley, T. M. (2000). Iron hydrogenases and the evolution of anaerobic eukaryotes. *Mol. Biol. Evol.* 17, 1695–1709. doi: 10.1093/oxfordjournals.molbev.a026268

Ji, M., Greening, C., Vanwonterghem, I., Carere, C. R., Bay, S. K., Steen, J. A., et al. (2017). Atmospheric trace gases support primary production in Antarctic desert surface soil. *Nature* 552, 400–403. doi: 10.1038/nature25014

Kaji, M., Taniguchi, Y., Matsushita, O., Katayama, S., Miyata, S., Morita, S., et al. (1999). The *hydA* gene encoding the H_2-evolving hydrogenase of *Clostridium perfringens*: molecular characterization and expression of the gene. *FEMS Microbiol. Lett.* 181, 329–336. doi: 10.1111/j.1574-6968.1999.tb08863.x

Kessler, A. J., Chen, Y.-J., Waite, D. W., Hutchinson, T., Koh, S., Popa, M. E., et al. (2019). Bacterial fermentation and respiration processes are uncoupled in permeable sediments. *Nat. Microbiol.* 4, 1014–1023. doi: 10.1038/s41564-019-0391-z

Kim, D.-H., and Kim, M.-S. (2011). Hydrogenases for biological hydrogen production. *Bioresour. Technol.* 102, 8423–8431. doi: 10.1016/j.biortech.2011.02.113

Koch, H., Galushko, A., Albertsen, M., Schintlmeister, A., Gruber-Dorninger, C., Lucker, S., et al. (2014). Growth of nitrite-oxidizing bacteria by aerobic hydrogen oxidation. *Science* 345, 1052–1054. doi: 10.1126/science.1256985

Kovács, K. L., Kovács, Á. T., Maróti, G., Meszaros, L. S., Balogh, J., Latinovics, D., et al. (2005). The hydrogenases of *Thiocapsa roseopersicina*. *Biochem. Soc. Trans.* 33, 61–63. doi: 10.1042/BST0330061

Kublik, A., Deobald, D., Hartwig, S., Schiffmann, C. L., Andrades, A., von Bergen, M., et al. (2016). Identification of a multi-protein reductive dehalogenase complex in *Dehalococcoides mccartyi* strain CBDB 1 suggests a protein-dependent respiratory electron transport chain obviating quinone involvement. *Environ. Microbiol.* 18, 3044–3056. doi: 10.1111/1462-2920.13200

Lane, N., Allen, J. F., and Martin, W. (2010). How did LUCA make a living? Chemiosmosis in the origin of life. *BioEssays* 32, 271–280. doi: 10.1002/bies.200900131

Lindsay, M. R., Colman, D. R., Amenabar, M. J., Fristad, K. E., Fecteau, K. M., Debes, R. V, et al. (2019). Probing the geological source and biological fate of hydrogen in Yellowstone hot springs. *Environ. Microbiol.* 21, 3816–3830. doi: 10.1111/1462-2920.14730

Maier, L., Vyas, R., Cordova, C. D., Lindsay, H., Sebastian, T., Schmidt, B., et al. (2013). Microbiota-derived hydrogen fuels *Salmonella typhimurium* invasion of the gut ecosystem. *Cell Host Microbe* 14, 641–651. doi: 10.1016/j.chom.2013.11.002

Maier, R. J., Olczak, A., Maier, S., Soni, S., and Gunn, J. (2004). Respiratory hydrogen use by *Salmonella enterica* serovar Typhimurium is essential for virulence. *Infect. Immun.* 72, 6294–6299. doi: 10.1128/IAI.72.11.6294-6299.2004

Marreiros, B. C., Batista, A. P., Duarte, A. M. S., and Pereira, M. M. (2013). A missing link between complex I and group 4 membrane-bound [NiFe] hydrogenases. *Biochim. Biophys. Acta* 1827, 198–209. doi: 10.1016/j.bbabio.2012.09.012

McDowall, J. S., Murphy, B. J., Haumann, M., Palmer, T., Armstrong, F. A., and Sargent, F. (2014). Bacterial formate hydrogenlyase complex. *Proc. Natl. Acad. Sci. U.S.A.* 111, E3948–E3956. doi: 10.1073/pnas.1407927111

Mohammadi, S., Pol, A., van Alen, T. A., Jetten, M. S. M., and Op den Camp, H. J. M. (2017). *Methylacidiphilum fumariolicum* SolV, a thermoacidophilic "Knallgas" methanotroph with both an oxygen-sensitive and -insensitive hydrogenase. *ISME J.* 11, 945–958. doi: 10.1038/ismej.2016.171

Mulder, D. M., Boyd, E. S., Sarma, R., Endrizzi, J. A., Lange, R., Broderick J. B., et al. (2010). Stepwise [FeFe]-hydrogenase H-cluster assembly revealed in the structure of $HydA^{\Delta EFG}$. *Nature* 465, 248–252. doi: 10.1038/nature08993

Olson, J. W., and Maier, R. J. (2002). Molecular hydrogen as an energy source for *Helicobacter pylori*. *Science* 298, 1788–1790. doi: 10.1126/science.1077123

Peters, J. W., Lanzilotta, W. N., Lemon, B. J., and Seefeldt, L. C. (1998). X-ray crystal structure of the Fe-only hydrogenase (CpI) from *Clostridium pasteurianum* to 1.8 Angstrom resolution. *Science* 282, 1853–1858. doi: 10.1126/science.282.5395.1853

Peters, J. W., Schut, G. J., Boyd, E. S., Mulder, D. W., Shepard, E. M., Broderick, J. B., et al. (2015). [FeFe]- and [NiFe]-hydrogenase diversity, mechanism, and maturation. *Biochim. Biophys. Acta* 1853, 1350–1369. doi: 10.1016/j.bbamcr.2014.11.021

Petersen, J. M., Zielinski, F. U., Pape, T., Seifert, R., Moraru, C., Amann, R., et al. (2011). Hydrogen is an energy source for hydrothermal vent symbioses. *Nature* 476:176. doi: 10.1038/nature10325

Pinske, C., and Sawers, R. G. (2016). Anaerobic formate and hydrogen metabolism. *EcoSal Plus* 7. doi: 10.1128/ecosalplus.ESP-0011-2016

Schubert, T., Adrian, L., Sawers, R. G., and Diekert, G. (2018). Organohalide respiratory chains: composition, topology and key enzymes. *FEMS Microbiol. Ecol.* 94:fiy035. doi: 10.1093/femsec/fiy035

Schuchmann, K., and Müller, V. (2012). A bacterial electron-bifurcating hydrogenase. *J. Biol. Chem.* 287, 31165–31171. doi: 10.1074/jbc.M112.395038

Schuchmann, K., and Müller, V. (2013). Direct and reversible hydrogenation of CO_2 to formate by a bacterial carbon dioxide reductase. *Science* 342, 1382–1385. doi: 10.1126/science.1244758

Schuchmann, K., and Muller, V. (2014). Autotrophy at the thermodynamic limit of life: a model for energy conservation in acetogenic bacteria. *Nat. Rev. Microbiol.* 12, 809–821. doi: 10.1038/nrmicro3365

Schut, G. J., and Adams, M. W. W. (2009). The iron-hydrogenase of *Thermotoga maritima* utilizes ferredoxin and NADH synergistically: a new perspective on anaerobic hydrogen production. *J. Bacteriol.* 191, 4451–4457. doi: 10.1128/JB.01582-08

Schwartz, E., Fritsch, J., and Friedrich, B. (2013). *H2-Metabolizing Prokaryotes*. eds E. Rosenberg, E. F. DeLong, S. Lory, E. Stackebrandt, and F. Thompson Berlin; Heidelberg: Springer Berlin Heidelberg.

Shima, S., Pilak, O., Vogt, S., Schick, M., Stagni, M. S., Meyer-Klaucke, W., et al. (2008). The crystal structure of [Fe]-Hydrogenase reveals the geometry of the active site. *Science* 321, 572–575. doi: 10.1126/science.1158978

Sørensen, J., Christensen, D., and Jørgensen, B. B. (1981). Volatile fatty acids and hydrogen as substrates for sulfate-reducing bacteria in anaerobic marine sediment. *Appl. Environ. Microbiol.* 42, 5–11. doi: 10.1128/AEM.42.1.5-11.1981

Tamagnini, P., Leitão, E., Oliveira, P., Ferreira, D., Pinto, F., Harris, D. J., et al. (2007). Cyanobacterial hydrogenases: diversity, regulation and applications. *FEMS Microbiol. Rev.* 31, 692–720. doi: 10.1111/j.1574-6976.2007.00085.x

Telling, J., Boyd, E. S., Bone, N., Jones, E. L., Tranter, M., MacFarlane, J. W., et al. (2015). Rock comminution as a source of hydrogen for subglacial ecosystems. *Nat. Geosci.* 8, 851–857. doi: 10.1038/ngeo2533

Thauer, R. K., Kaster, A.-K., Goenrich, M., Schick, M., Hiromoto, T., and Shima, S. (2010). Hydrogenases from methanogenic archaea, nickel, a novel cofactor, and H_2 storage. *Annu. Rev. Biochem.* 79, 507–536. doi: 10.1146/annurev.biochem.030508.152103

Vignais, P. M., and Billoud, B. (2007). Occurrence, classification, and biological function of hydrogenases: an overview. *Chem. Rev.* 107, 4206–4272. doi: 10.1021/cr050196r

Volbeda, A., Charon, M. H., Piras, C., Hatchikian, E. C., Frey, M., and Fontecilla-Camps, J. C. (1995). Crystal structure of the nickel-iron hydrogenase from *Desulfovibrio gigas*. *Nature* 373, 580–587. doi: 10.1038/373580a0

Weiss, M. C., Sousa, F. L., Mrnjavac, N., Neukirchen, S., Roettger, M., Nelson-Sathi, S., et al. (2016). The physiology and habitat of the last universal common ancestor. *Nat. Microbiol.* 1:16116. doi: 10.1038/nmicrobiol.2016.116

Wolf, P. G., Biswas, A., Morales, S. E., Greening, C., and Gaskins, H. R. (2016). H_2 metabolism is widespread and diverse among human colonic microbes. *Gut Microbes* 7, 235–245. doi: 10.1080/19490976.2016.1182288

Wu, L. F., and Mandrand, M. A. (1993). Microbial hydrogenases: primary structure, classification, signatures and phylogeny. *FEMS Microbiol. Rev.* 10, 243–269. doi: 10.1111/j.1574-6968.1993.tb05870.x

Conflict of Interest: The authors declare that the research was conducted in the absence of any commercial or financial relationships that could be construed as a potential conflict of interest.

frontiers in Microbiology

ORIGINAL RESEARCH
published: 11 June 2018
doi: 10.3389/fmicb.2018.01238

The Ferredoxin-Like Proteins HydN and YsaA Enhance Redox Dye-Linked Activity of the Formate Dehydrogenase H Component of the Formate Hydrogenlyase Complex

*Constanze Pinske**

Institute for Biology/Microbiology, Martin-Luther University Halle-Wittenberg, Halle, Germany

Formate dehydrogenase H (FDH-H) and [NiFe]-hydrogenase 3 (Hyd-3) form the catalytic components of the hydrogen-producing formate hydrogenlyase (FHL) complex, which disproportionates formate to H_2 and CO_2 during mixed acid fermentation in enterobacteria. FHL comprises minimally seven proteins and little is understood about how this complex is assembled. Early studies identified a ferredoxin-like protein, HydN, as being involved in FDH-H assembly into the FHL complex. In order to understand how FDH-H and its small subunit HycB, which is also a ferredoxin-like protein, attach to the FHL complex, the possible roles of HydN and its paralogue, YsaA, in FHL complex stability and assembly were investigated. Deletion of the *hycB* gene reduced redox dye-mediated FDH-H activity to approximately 10%, abolished FHL-dependent H_2-production, and reduced Hyd-3 activity. These data are consistent with HycB being an essential electron transfer component of the FHL complex. The FDH-H activity of the *hydN* and the *ysaA* deletion strains was reduced to 59 and 57% of the parental, while the double deletion reduced activity of FDH-H to 28% and the triple deletion with *hycB* to 1%. Remarkably, and in contrast to the *hycB* deletion, the absence of HydN and YsaA was without significant effect on FHL-dependent H_2-production or total Hyd-3 activity; FDH-H protein levels were also unaltered. This is the first description of a phenotype for the *E. coli ysaA* deletion strain and identifies it as a novel factor required for optimal redox dye-linked FDH-H activity. A *ysaA* deletion strain could be complemented for FDH-H activity by *hydN* and *ysaA*, but the *hydN* deletion strain could not be complemented. Introduction of these plasmids did not affect H_2 production. Bacterial two-hybrid interactions showed that YsaA, HydN, and HycB interact with each other and with the FDH-H protein. Further novel anaerobic cross-interactions of 10 ferredoxin-like proteins in *E. coli* were also discovered and described. Together, these data indicate that FDH-H activity measured with the redox dye benzyl viologen is the sum of the FDH-H protein interacting with three independent small subunits and suggest that FDH-H can associate with different redox-protein complexes in the anaerobic cell to supply electrons from formate oxidation.

Keywords: [NiFe]-hydrogenase, formate hydrogenlyase, YsaA, HydN, formate dehydrogenase H, FDH-H, ferredoxin, FeS-cluster proteins

OPEN ACCESS

Edited by:
Chris Greening,
Monash University, Australia

Reviewed by:
Robert Maier,
University of Georgia, United States
William Thomas Self,
University of Central Florida, United States

***Correspondence:**
Constanze Pinske
constanze.pinske@mikrobiologie.uni-halle.de

Specialty section:
This article was submitted to Microbial Physiology and Metabolism, a section of the journal Frontiers in Microbiology

Received: *29 March 2018*
Accepted: *23 May 2018*
Published: *11 June 2018*

Citation:
Pinske C (2018) The Ferredoxin-Like Proteins HydN and YsaA Enhance Redox Dye-Linked Activity of the Formate Dehydrogenase H Component of the Formate Hydrogenlyase Complex. Front. Microbiol. 9:1238. doi: 10.3389/fmicb.2018.01238

INTRODUCTION

Ferredoxins are small proteins containing non-heme iron as iron-sulfur (FeS) clusters and they serve as electron carriers within the cell (Bruschi and Guerlesquin, 1988; Beinert, 1990). The group of ferredoxin proteins is ubiquitously distributed, very diverse and different classes can be distinguished based on the FeS cluster type (Bruschi and Guerlesquin, 1988; Beinert et al., 1997). They have typical cysteine motifs in common that co-ordinate the FeS clusters. In addition to the ferredoxin protein itself, Fdx, which is involved in FeS cluster synthesis, ferredoxin-like proteins often have functions as small or β-subunits of modular respiratory complexes like the *E. coli* proteins NarH of the nitrate reductase, HybA of the H_2-oxidizing hydrogenase 2, FdoH and FdnH of the formate dehydrogenases O and N, respectively, NrfC of the periplasmic nitrite reductase, HycB and HycF of the H_2-producing formate hydrogenlyase (FHL) complex and HyfA of the FHL-homologous complex, FHL-2. These proteins are predicted to have a similar core-fold with alpha-antiparallel beta sandwiches to hold the FeS-clusters (Pfam domain Fer4). In addition to the above, a number of other ferredoxin-like proteins are known in *E. coli*. Occasionally, these proteins are required for full activity of a particular respiratory enzyme, but are not essential components of the final enzyme. Among those are the NapF, G and H proteins, which are required for the full activity of the periplasmic nitrate reductase, and HydN, which is required for full formate dehydrogenase H activity (FDH-H) (Maier et al., 1996; Brondijk et al., 2002; Nilavongse et al., 2006). Other ferredoxin-like proteins like AegA and YsaA are not located within or close to an operon encoding an enzyme with predicted oxidoreductase activity and no phenotype has yet been described for mutants lacking these genes (Cavicchioli et al., 1996).

The FHL complex in *E. coli* is the main route of H_2 production under fermentative growth conditions (Pinske and Sawers, 2016). The complex comprises a bis-molybdopterin guanine dinucleotide (Mo-bis-PGD)-dependent FDH-H that oxidizes formate to electrons and CO_2. FDH-H is physically linked to the [NiFe]-hydrogenase protein HycE by 3 iron-sulfur (FeS) proteins. These are the FDH-H small subunit HycB, which has a ferredoxin-like fold and carries 4 FeS clusters, the ferredoxin-type protein HycF with 2 predicted FeS clusters, and the hydrogenase small subunit, HycG with a single FeS cluster. These five subunits are attached to the cytoplasmic side of the membrane by the HycC and HycD proteins. Notably, the *fdhF* gene, which encodes FDH-H, is located separately on the chromosome from the FHL-encoding *hyc*-operon, but it belongs to the same regulon (Sawers, 2005; Pinske and Sawers, 2016). Furthermore, it was established that FDH-H is the most loosely attached protein component of the FHL complex (McDowall et al., 2015). In addition to the Mo-bis-PGD cofactor, the FDH-H protein contains a selenocysteine and a FeS cluster, the latter of which requires insertion prior to attachment of FDH-H to the FHL complex (Boyington et al., 1997). A further function for FDH-H has been proposed as part of an alternative FHL-2 complex, encoded by the *hyf*-operon and expressed under different growth conditions in *E. coli* (Andrews et al., 1997; Trchounian et al., 2012). While FDH-H activity is associated with fermentative growth, the other formate dehydrogenases in *E. coli*, FDH-N and FDH-O, are associated with respiratory formate oxidation. FDH-N is active during nitrate respiration while FDH-O is active in the presence of both oxygen and nitrate (Sawers et al., 1991).

It has been suggested that HydN forms an additional pool of small subunits for FDH-H when it is not incorporated into the FHL complex (Sargent, 2016). Due to a high similarity with YfrA from *Proteus vulgaris*, the probable FeS subunit of fumarate reductase, it was further suggested that HydN could be involved in the electron transfer from formate to fumarate. However, a Δ*hydN* strain was investigated for its ability to transfer electrons from formate to fumarate, and proved to be unimpaired (Maier, 1997). Notably, the *hydN* gene is in an operon with the *hypF* gene (Maier et al., 1996) and HypF is one of the universal maturases that assemble the [NiFe]-cofactor. Due to its co-expression with *hypF*, the product of *hydN* was also suggested to be involved in H_2-metabolism of the cell. Nevertheless, the co-occurrence of *hydN* and *hypF* is negligible in other organisms, while on the other hand *hydN* scores highly in its co-occurrence with *hycB* (0.778) and with *fdhF* (0.572) (Szklarczyk et al., 2015), suggesting a tight functional linkage.

HydN is predicted to harbor four [4Fe-4S] clusters and resembles a formate dehydrogenase small subunit similar to HycB of the FHL complex with which it shares 39% amino acid identity (52% similarity). Although both proteins share the same ferredoxin-like fold, suggesting a function in electron transfer, they cannot functionally replace one another (Maier, 1997). Interestingly, the *hydN* gene forms a transcriptional unit with the *fdhF* gene in the opportunistic pathogen *Serratia liquefaciens*. This FDH-H is similar to the *E. coli* protein, but it harbors a cysteine instead of the catalytic selenocysteine in its active site. A respective *E. coli* Cys variant is 20-fold less active than the SeCys protein (Pinske and Sawers, 2016). Nevertheless, fermentative gas production from glucose has been observed in *S. liquefaciens* (Brenner et al., 2006), but it was not yet identified whether this gas is CO_2 or H_2.

Due to the weak phenotype of the *hydN* deletion strain (Maier et al., 1996), a new homology search was conducted to identify other possible homologs, and revealed the ferredoxin-type protein YsaA (synonym YiaI) in *E. coli,* which shares 62% amino acid identity (72% similarity) with HydN and is therefore even more closely related to HydN than HycB. The *ysaA* gene co-occurrence with *fdhF* is 0.545 and thus in the same range as the *hydN-fdhF* co-occurrence (Szklarczyk et al., 2015). Therefore, the presence of YsaA might exhibit functional redundancy with HydN. Nothing is known about the *ysaA* gene and it is not located near any hydrogenase-associated genes. However, an interaction with NuoE, a protein of the closely to FHL related respiratory Complex I, which is required for the association of the diaphorase subunit, and with RclA (synonym YkgC) has been reported (Arifuzzaman et al., 2006). Furthermore, expression of the gene is 2.7 fold up-regulated under anoxic conditions (Kang

Abbreviations: FHL, formate hydrogenlyase; Mo-bis-PGD, molybdopterin guanine dinucleotide; BV, benzyl viologen; FDH-H, formate dehydrogenase H; MU, Miller Units.

et al., 2005). Therefore, we wanted to investigate the role of YsaA in H_2 metabolism and to establish the interaction network of these ferredoxin-like proteins based on the hypothesis described above.

MATERIALS AND METHODS

Growth Conditions and Strain Construction

Strains and plasmids used in this study are listed in **Table 1**. Strains were routinely grown in liquid LB medium in a shaking incubator or on LB agar plates. For determination of enzyme activities and bacterial two hybrid interactions, the bacteria were grown in buffered TGYEP medium supplemented with glucose: 1% (w/v) trypton, 0.5% (w/v) yeast extract, 0.8% (w/v) glucose, 0.1 M potassium buffer, pH 6.5; according to Begg et al. (1977). The medium was supplemented with 100 μg ml^{-1} ampicillin to ensure plasmid maintenance. Furthermore, when required, chloramphenicol was used at 12.5 μg ml^{-1} and kanamycin at 50 μg ml^{-1}. The strain DHD-N was used as Δ*hydN* mutant and was previously described (Maier et al., 1996). The *ysaA* deletion was constructed in BW25113 transformed with the lambda red recombinase plasmid pKD46 according to Datsenko and Wanner (2000) by using the oligonucleotides ysaA_5'KO 5′-CTCTGGCACTCTGCTGTTTTAGTGCAA AGGAGTGATCATG CCATGGTCCATATGAATATCCTCC-3′ and ysaA_3′KO 5′-CGCACTGTTCCGGCGTTGAGAAAC GCCGGAAAACGTTTCA GCGATTGTGTAGGCTGGA GCT-3′ to amplify the *cat* gene from pKD3. The mutation was subsequently moved to MC4100, DHD-N and JW2694 (Δ*hycB*) by $P1_{vir}$ phage transduction (Miller, 1972). The resistance cassette was eliminated using the pCP20 plasmid as described (Cherepanov and Wackernagel, 1995). The deletion of *aegA* was introduced by the method of Hamilton et al. (1989) by cloning the upstream region as KpnI/BamHI fragment with the oligonucleotides DaegA1_KpnI 5′-GCGGGTACCGCCTGA TACCACGGCAAATC-3′ and DaegA2_BamHI 5′-GCGGGA TCC CATAATAAAACGATTCATAAC-3′ and the downstream region as BamHI/HindIII fragment with the oligonucleotides DaegA3_BamHI 5′-GCGGGATCCCAGTCAAATCTCACT GATAG-3′ and DaegA4_HindIII 5′-GCGAAGCTTCGCCGG TTTTGATCATCTCC-3′ into pMAK705 and recombining with the desired target strain as described. Introduction of the Δ*hycB* deletion in DHD-N backgrounds or *vice versa* has been done according to Datsenko and Wanner (2000) by introducing the lambda red recombinase on the pKD46 plasmid, growing competent cells and inducing them with 10 mM L-arabinose before electroporation of a PCR fragment containing a kanamycin resistance cassette and the upstream and downstream regions of the gene. These PCR fragments were obtained after amplification of the corresponding regions from strain JW2694 (Δ*hycB*) or JW2683 (Δ*hydN*). All clones were verified using colony PCR.

TABLE 1 | Strains and plasmids.

Strain	Genotype	Reference/source
MC4100	F^- *araD139* Δ(*argF-lac*)*U169 ptsF25 deoC1 relA1 flbB150*$^-$ *rspL150*$^-$	Casadaban, 1976
BW25113	F^- Δ (*araD-araB*)*567* Δ *lacZ4787*(::*rrnB-3*) λ^- *rph-1* Δ (*rhaD-rhaB*)*568 hsdR514*	Baba et al., 2006
DHD-N	As MC4100, but Δ*hydN*	Maier et al., 1996
JW2683	As BW25113, but Δ*hydN*::*kan*	Baba et al., 2006
JW2694	As BW25113, but Δ*hycB*::*kan*	Baba et al., 2006
CPH090	As BW25113, but Δ*ysaA*	This work
CPH010	As MC4100, but Δ*ysaA*	This work
CPH011	As MC4100, but Δ*hydN* Δ*ysaA*	This work
CPH012	As MC4100, but Δ*aegA*	This work
CPH013	As DHD-N (Δ*hydN*), but Δ*aegA*	This work
CPH014	As CPH010 (Δ*ysaA*), but Δ*aegA*	This work
CPH015	As JW2694 (Δ*hycB*), but Δ*ysaA*	This work
CPH016	As CPH015 (Δ*hycB* Δ*ysaA*), but Δ*aegA*	This work
CPH017	As JW2694 (Δ*hycB*), but Δ*aegA*	This work
CPH018	As DHD-N (Δ*hydN*), but Δ*hycB*	This work
CPH019	As CPH015 (Δ*hycB* Δ*ysaA*), but Δ*hydN*	This work
CPH020	As MC4100, but Δ*hyaB* Δ*hybC* Δ*hycAI* Δ*fdhF*	This work
RM102	As MC4100, but Δ (*srl-recA*)*306*::Tn*10 fnr zci*::Tn*10*	Birkmann et al., 1987
BTH101	F′, *cya*-99, *araD*139, *galE*15, *galK*16, *rpsL*1(Str^R), *hsdR*2, *mcrA*1, *mcrB*1	Karimova et al., 1998
PLASMIDS[a]		
pCP20	*FLP*$^+$, λcI857$^+$, λp_R Rep^{ts}, Amp^R, Cm^R	Cherepanov and Wackernagel, 1995
pKD46	Contains λ Red genes γ, β and *exo*; Amp^R	Datsenko and Wanner, 2000
pJET1.2	Commercially available cloning vector; Amp^R	Thermo Fisher Scientific
phydN	pBluescriptSK(+) containing *hydN* in BamHI and EcoRI site; Amp^R	This work
pysaA	pJET1.2 containing *ysaA* in MCS; Amp^R	This work
pT25	Bacterial two hybrid plasmid expressing the T25 fragment and a MCS at the 3′ end of T25; Cm^R	Karimova et al., 1998
pT25-zip	pT25, Leucine zipper fused to T25 fragment (1–224 amino acids of CyaA)	Karimova et al., 1998
pT18	Bacterial two hybrid plasmid expressing the T18 fragment and a MCS at the 5′ end of T18; Amp^R	Karimova et al., 1998
pT18-zip	pT18, Leucine zipper fused to T18 fragment (225–399 amino acids of CyaA)	Karimova et al., 1998

[a] *Further plasmids from the bacterial two hybrid system that were constructed here can be found in Table S2.*

Cloning of *ysaA* and *hydN*

Cloning of *ysaA* gene in the pJET1.2 cloning vector (commercially available from Thermo Fisher Scientific) was done by using the T18-ysaAFW_HindIII 5′-GCGAAG CTTGATGAACCGGTTTATTATTGCG-3′ and T18C/T25-ysaARW_KpnI 5′-GCGGGTACCTTATCAAACAGGCTG CTGCCGTAGC-3′ oligonucleotides for amplification from

chromosomal DNA of MC4100 by the Q5-DNA polymerase (NEB) according to the manufacturer's instructions. The *hydN* gene was cloned into pBluescriptSK(+) by using the oligonucleotides HydN_FW_BamHI 5′-CGCGGATCCATG AACCGTTTCATCATTGC-3′ and HydN_RW_EcoRI 5′-CGC GAATTCTTAGAACATCAGCGCCGT-3′, digestion of both vector and PCR product with BamHI and EcoRI and subsequent ligation. All cloning products were verified by sequencing.

Bacterial Two Hybrid Interactions

The bacterial two-hybrid system (Karimova et al., 1998) was used to clone constructs by amplifying the respective gene fragment from chromosomal DNA of MC4100 and digesting both the pUT18 or the pT25 target vectors and the insert with the same restriction enzymes before ligation. The bacterial two hybrid vectors were constructed to yield functional in-frame fusion proteins and all inserts were verified by sequencing. The oligonucleotides used are listed in Table S1, where the restriction sites are given as part of the oligonucleotide name. Generally, the entire orf was amplified except for the start codons (T25 fusions) or stop codons (T18 fusions) and all newly generated constructs are listed in Table S2. Plasmids of pT25 origin were transformed together with a pUT18 plasmid into BTH101 and grown as anaerobic culture in TGYEP, pH 6.5 at 30°C for 16h containing both ampicillin and chloramphenicol as antibiotics. Determination and calculation of β-galactosidase activity was done according to Miller (1972). Each experiment was performed three times independently, and the activity for each sample was determined in triplicate. Alternatively, a volume of 5 μl of the culture was spotted on McConkey plates containing 0.5% (w/v) maltose, the antibiotics ampicillin and chloramphenicol. The plates were then aerobically incubated at 30°C for 16 h.

Enzymatic Assays

For determination of protein activities, the cells were grown in TGYEP medium, pH 6.5 as standing liquid cultures in 50 ml reaction tubes at 30°C for 16 h. For induction of NAR and FDH-N enzyme synthesis, sodium nitrate was added to the anaerobic cultures to a final concentration of 1% (w/v). The cells were harvested by centrifugation, sonicated (20 W, 0.5 s pulses, 3 min) and the extracts used directly. Activities of the soluble formate dehydrogenase and total hydrogenase were measured as formate-dependent benzyl viologen (BV) reduction (FDH-H) and H_2-dependent BV reduction (hydrogenase), respectively at 600 nm as described in Pinske et al. (2011a). Detection of NAR and FDH-N activities by in-gel activity staining was done as described (Pinske and Sawers, 2012). Immunoblotting against FDH-H (1:3000) polypeptides was done after denaturing gel electrophoresis as described (Pinske et al., 2011a).

GC Analysis of Gases in Culture Headspace

For assessing the activity of the intact FHL complex, the H_2 content of the gas headspace was quantified. The H_2 content of the 10 ml gas phase of an overnight culture was measured by sampling 200 μl in a GC-2010. The system was equipped with a packed column (Shin Carbon Micropacked column ST80/100). The carrier gas was N_2 with a flow rate of 13.9 ml min^{-1}, the injector was kept at 140°C, the column at 110°C and the TCD detector at 150°C and 40 mA. Quantification was done with a calibration curve of known amounts of H_2.

Bioinformatics

The unrooted tree was created based on an alignment conducted within Uniprot (Clustal Omega) and visualized with iTOL (Sievers and Higgins, 2013; Letunic and Bork, 2016).

RESULTS AND DISCUSSION

HydN has Paralogues in *E. coli*

A phylogenetic tree shows that YsaA and HydN are most closely related among all known ferredoxin-like proteins in *E. coli* (**Figure 1**). Together with the two proteins HycB and HyfA, the small subunits of the FHL and FHL-2 complexes, respectively, and the AegA, YgfS, and YgfT proteins of unknown function, they form a group of paralogous proteins (see Figure S1 for alignment). In contrast, the HycF proteins represents the FeS-protein that provides an electron relay between the small subunit HycB of FDH-H and Hyd-3; however, HycF is more distantly related to HydN and YsaA. It is located in the tree together with proteins that are known to be required for full activity of respiratory complexes like NapF and NapG, but also with the *E. coli* ferredoxin protein Fer and the pyruvate formate-lyase activator PflA, which is required to introduce a radical into pyruvate formate-lyase (Knappe et al., 1969). The more classical β-subunits of multi-subunit respiratory enzymes like hydrogenase 2 (HybA), formate dehydrogenases N and O (subunits FdnH and FdoH, respectively), and nitrate reductases (NarH and NarY) cluster separately. Proteins of unknown function can be found clustered together both with the β-subunits and with the HydN paralogues. Due to the characteristic architecture of these proteins and the incorporation of one or more FeS clusters, it seems probable that these proteins also have a role in electron transfer within the cell.

The Δ*ysaA* Mutant has a Similar Phenotype to the Δ*hydN* Mutant

Previous research from the Böck group had identified a *hydN* deletion strain, that resulted in reduced FDH-H activity to 38% compared to the parental, while total hydrogenase activity remained at approximately 80% (Maier et al., 1996). These findings could be reproduced in this study using both the same strain (DHD-N) used previously (Maier et al., 1996), as well as the Δ*hydN* strain (JW2683) of the Keio collection (**Table 2**). The FDH-H activity was reduced to 59 and 34%, while total hydrogenase activity was reduced only to 74% in the Δ*hydN* strains DHD-N and JW2683, respectively. Having an influence on the activity of an enzyme, but not completely abolishing it suggested that HydN exhibits some redundancy with another unknown protein. Therefore, the gene coding for the most similar protein YsaA was deleted by the Datsenko and Wanner method (Datsenko and Wanner, 2000) and the deletion moved into the MC4100 and DHD-N backgrounds, resulting in strains CPH010 and CPH011 (see **Table 1**). The strain CPH010 phenocopied the

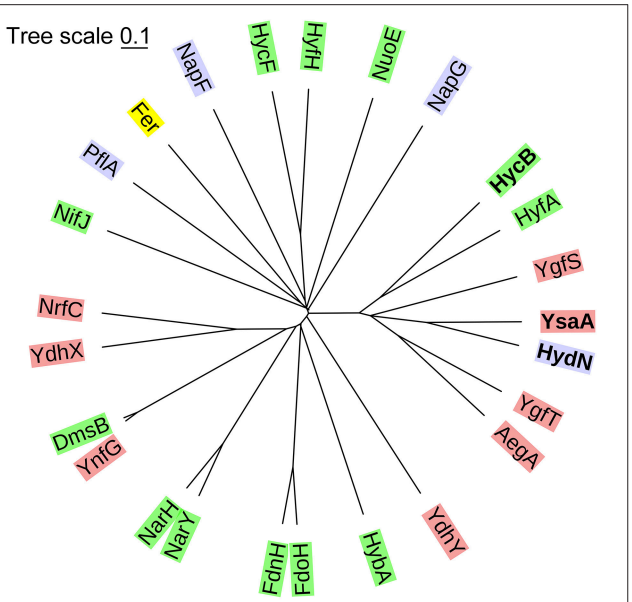

FIGURE 1 | Phylogenetic tree classifying the ferredoxin-like proteins of *E. coli*. The proteins were classified based on a Clustal Omega alignment. The evolutionary distances were computed with a mBed algorithm (Sievers and Higgins, 2013) and visualized with iTOL (Letunic and Bork, 2016). The green background shows known β-subunits of respiratory complexes, in red are proteins that have no known function, blue are the proteins that are known to be required for the activity of a certain protein, but not part of the catalytically active complex and yellow is the electron carrier protein ferredoxin.

Δ*hydN* strains and had reduced FDH-H activity to 57% of the parental while total hydrogenase activity was comparable with the MC4100 parental (**Table 2**). Remarkably, the double deletion strain had a reduction in FDH-H activity to 28% demonstrating that the effect of the *hydN* and *ysaA* deletion was additive.

Only 10% of FDH-H activity measured anaerobically as formate-dependent BV reduction remained detectable when *hycB* was deleted (**Table 2**). The formate-dependent BV reduction was not detectable in an *fdhF* deletion strain and therefore highly specific for FDH-H [data not shown and (Pecher et al., 1983)]. This is in agreement with a previous finding that the HycB, HycE, HycF, and HycG are equally required for full FDH-H activity (Sauter et al., 1992). In contrast to the *hydN* and *ysaA* deletion strains, the *hycB* deletion disrupted electron flow from FDH-H to hydrogenase 3 and the strain retained only residual hydrogenase activity due to hydrogenases 1 and 2 activities, and thus had a total hydrogenase activity that was reduced by more than 90% (Pinske et al., 2011b). The strain consequently failed to produce H_2. The effect of the *hycB* deletion on FDH-H activity was even more dramatic when the *hycB* and *ysaA* deletions were combined, which resulted in a residual 3% FDH-H activity (**Table 2**). The same could be observed when the *hycB* and *hydN* deletions were combined in strain CPH018, which showed 2% remaining FDH-H activity and total hydrogenase activity as low as in the Δ*hycB* strain JW2694. Most strikingly, the combination of all three deletions in strain CPH019 resulted still in a detectable FDH-H activity of about 1% compared to the parental.

Electron transfer from formate to BV is thought to occur via the FeS cluster in the FDH-H polypeptide, which is located within 15 Å from the protein's surface (Boyington et al., 1997). The isolated enzyme without the small subunit was also shown to be electrochemically active in both directions on an electrode (Bassegoda et al., 2014) and in the BV assay (Axley et al., 1990). The findings in the present study, however, strongly suggest that in extracts FDH-H activity requires the presence of the ferredoxin-like proteins and in the absence of these only 1% of the FDH-H activity can be assayed directly from the enzyme.

FDH-H delivers the electrons from formate oxidation that are required for H_2 production by the FHL complex. Alternative electron donors other than formate are not known for the FHL complex, but synthetic protein-fusion experiments with *Thermotoga maritima* ferredoxin have shown that HycB can receive electrons from other sources like pyruvate:ferredoxin oxidoreductase to some extent (Lamont et al., 2017). When cultures are grown on glucose, the H_2 from the FHL complex accumulates in a closed growth vessel and can partially be re-oxidized by hydrogenase 1 and 2 in *E. coli*. However, in our experience the amount of accumulated H_2 also roughly corresponds to the activity of the FHL complex and therefore is a good indicator of FHL activity (Lindenstrauß et al., 2017). By sampling the gas headspace it became clear that the *hydN* deletion reduced the FHL activity to 86% of the wild-type level, while the *ysaA hydN* double deletion retained 91% H_2 production and the *ysaA* deletion alone had no influence on the amount of H_2 produced (**Table 2**). Thus, the reduced FDH-H activity as measured by BV reduction in the *hydN* and *ysaA* deletion strains does not correlate with FHL activity as quantified by H_2 production, perhaps suggesting that this reduced activity might be derived from FDH-H associated with another complex or complexes.

To test whether the effect of deleting the *ysaA* or *hydN* on FDH-H activity is specific, a further candidate AegA from the HydN-YsaA family of proteins was targeted and its corresponding gene *aegA* was deleted. The *aegA* gene was deleted alone and in combination with *hydN*, *ysaA* or *hycB*, but the effect on FDH-H activity was not greater than in the respective strains without *aegA* deletion (**Table 2**). Similarly, the *aegA* deletion had no influence on H_2 production and total hydrogenase activity. This indicates that FDH-H cannot transfer electrons from formate via AegA to the redox dye BV.

Previous experiments also showed that the complementation of the *hydN* deletion did not restore full FDH-H activity (Maier et al., 1996), which could be confirmed here regardless of whether strain DHD-N or strain JW2683 was used. The Δ*hydN* Δ*ysaA* double deletion strain showed the same behavior like the two Δ*hydN* mutants after complementation with phydN. Somewhat surprisingly, restoration of almost parental FDH-H activity could be achieved when the Δ*ysaA* deletion strain was transformed with phydN (**Table 2**), which further substantiates at least partial redundancy of function between these proteins. The Δ*ysaA* mutant could also be complemented with pysaA to parental levels of FDH-H activity. Notably, however, introduction of the pysaA

TABLE 2 | Influence of YsaA and HydN on formate dehydrogenase H, hydrogenase, and H_2-production activities.

Strain (genotype)	FDH-H (U * mg protein^{-1})	% FDH-H activity of MC4100	Total hydrogenase (U * mg protein^{-1})	H_2-headspace (μmol * ml culture^{-1} * $OD_{600\ nm}^{-1}$)
MC4100	2.81 ± 0.03	100	6.06 ± 0.05	9.7 ± 0.6
DHD-N (Δ*hydN*)	1.67 ± 0.24	59	5.87 ± 0.41	8.3 ± 0.2
JW2683 (Δ*hydN*)	0.95 ± 0.06	34	4.50 ± 0.70	9.4 ± 4.5
Δ*ysaA*	1.60 ± 0.06	57	5.93 ± 0.69	9.5 ± 0.8
Δ*aegA*	2.14 ± 0.40	76	4.18 ± 0.30	11.6 ± 2.0
Δ*hycB*	0.27 ± 0.09	10	0.25 ± 0.03	n.d.
Δ*hydN* Δ*ysaA*	0.80 ± 0.22	28	5.00 ± 0.55	8.8 ± 0.5
Δ*hydN* Δ*aegA*	0.76 ± 0.34	27	2.31 ± 0.89	10.1 ± 2.8
Δ*hydN* Δ*hycB*	0.06 ± 0.03	2	0.21 ± 0.02	n.d.
Δ*ysaA* Δ*aegA*	2.25 ± 0.15	80	4.34 ± 1.12	11.9 ± 1.9
Δ*hycB* Δ*ysaA*	0.09 ± 0.03	3	0.21 ± 0.10	n.d.
Δ*hycB* Δ*aegA*	0.11 ± 0.01	4	0.21 ± 0.05	n.d.
Δ*hycB* Δ*ysaA* Δ*aegA*	0.12 ± 0.05	4	0.19 ± 0.01	n.d.
Δ*hycB* Δ*ysaA* Δ*hydN*	0.03 ± 0.02	1	0.28 ± 0.01	n.d.
JW2683 + phydN	1.05 ± 0.18	37	2.79 ± 0.51	10.2 ± 1.9
JW2683 + pysaA	0.85 ± 0.15	30	3.52 ± 0.35	10.4 ± 1.6
DHD-N + phydN	0.97 ± 0.08	35	4.40 ± 0.39	10.1 ± 0.1
DHD-N + pysaA	0.86 ± 0.11	31	3.76 ± 0.23	8.4 ± 0.9
Δ*ysaA* + phydN	2.47 ± 0.85	88	5.71 ± 1.57	11.4 ± 0.5
Δ*ysaA* + pysaA	2.55 ± 0.60	91	5.06 ± 0.63	9.7 ± 0.4
Δ*hydN* Δ*ysaA* + phydN	1.09 ± 0.33	39	3.79 ± 0.86	10.9 ± 0.6
Δ*hydN* Δ*ysaA* + pysaA	0.77 ± 0.15	27	3.70 ± 0.14	8.3 ± 0.2

The strains indicated were grown in TGYEP, pH 6.5 and assayed as described in the Materials and Methods section. The values are given for three independent biological replicates with standard deviations. n.d., not determined.

plasmid into the Δ*hydN* strain caused a further reduction of FDH-H activity. This shows that although the effect of the *hydN* and *ysaA* deletions on FDH-H activity is additive, the functions of the gene products are not identical. The use of two independent Δ*hydN* strains indicates that the lack of complementation is not strain-specific and therefore is unlikely due to additional mutations. The *hycB* deletion cannot be complemented for H_2 production by plasmid-encoded HydN (Maier, 1997).

Based on the observation that *ysaA* and *hydN* had little influence on total hydrogenase activity and H_2-production, the addition *in trans* of these genes was not expected to cause significant differences in these activities. The complementation with either phydN or pysaA caused a slight reduction in total hydrogenase activity in all strains tested. Another interesting effect of the complementation was visible with the GC-headspace H_2-quantification. While the addition of pysaA had no influence on the amount of H_2 produced by the cells in comparison to the respective plasmid-free strains, the addition of phydN increased the H_2 amount slightly in all strains.

Interaction Network of YsaA and HydN

In vivo protein interactions can be monitored by the bacterial two-hybrid system (Karimova et al., 1998). Generally, a T18 and a T25 domain of the adenylate cyclase is fused to the target proteins *C*-terminally or *N*-terminally, respectively, and any interaction can be quantified by measurement of β-galactosidase activity. Growth of the cells under the conditions where proteins under investigation are also normally synthesized ensures that a protein interaction that requires a further unknown interaction partner can be identified. Therefore, the reporter strain was grown under anoxic conditions with glucose, where proteins of the mixed-acid fermentation are synthesized. These conditions show that empty pT25 and pUT18 plasmids yielded 217 ± 11 Miller units (MU) of activity while the zip positive control resulted in 3,619 ± 548 MU. An activity of more than 600 MU generally reflects a real interaction (Karimova et al., 1998). As additional control the empty pT25 and pT18 plasmids were co-transformed with each of the pT18 or pT25 protein fusions constructed here, respectively. They showed that the empty pT18 plasmid is not able to activate β-galactosidase in combination with any pT25 fusions. However, the empty pT25 plasmid gave a signal of more than 800 MU for the T18-HydN and T18-HyfA constructs while the other constructs showed interactions with less than the 600 MU threshold established here. Semi-aerobic interactions were additionally assessed qualitatively by spotting the colonies on McConkey-Maltose plates and showed that not all interactions identified anaerobically are detectable aerobically (**Figure 2**).

Initially, the interaction of FDH-H and its predicted small subunit HycB was determined. Because the *N*-terminus of this 80 kDa FDH-H protein (encoded by *fdhF*) is located at a distance of 20 Å from the FeS cluster (Boyington et al., 1997) it is therefore likely to be able to interact with its cognate small

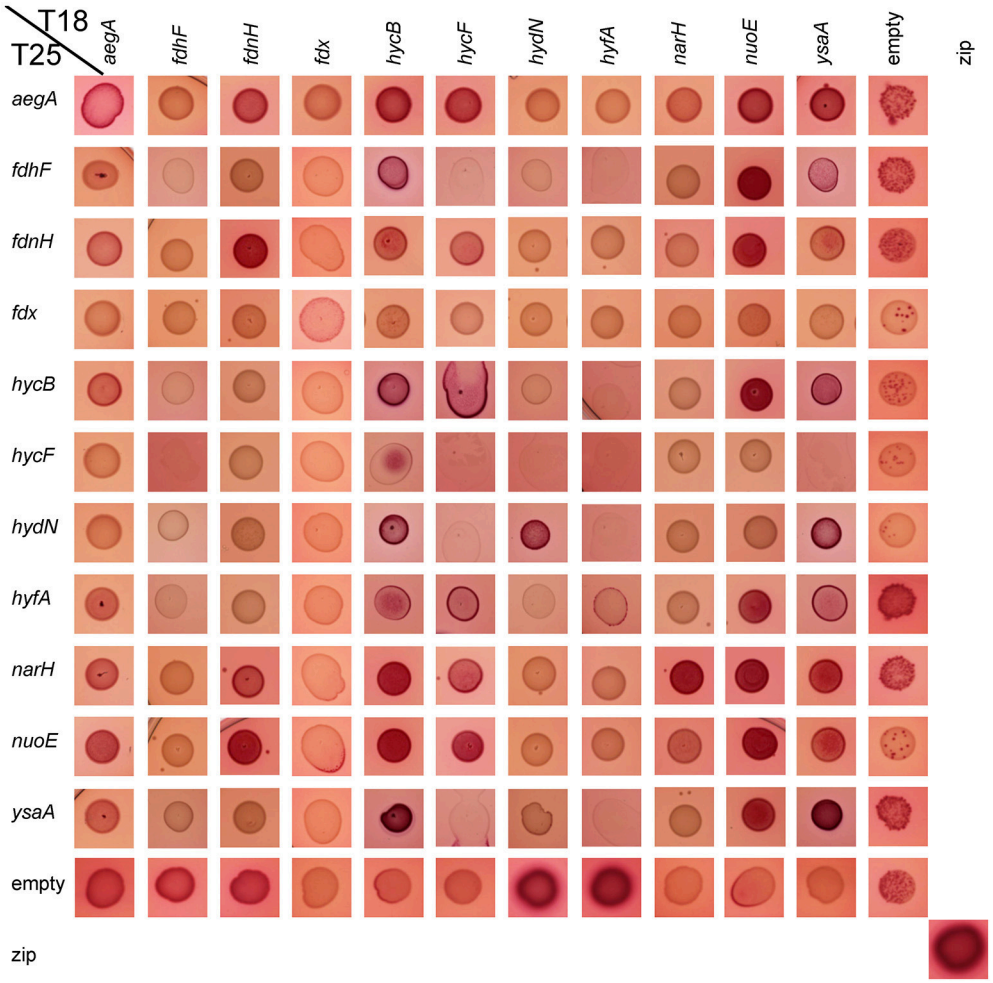

FIGURE 2 | Qualitative aerobic assessment of bacterial two hybrid interactions. The respective combinations of pT18 and pT25 plasmids in strain BTH101 as given on the edges were spotted with a volume of 5 μl from liquid culture on McConkey-Agar containing 0.5% (w/v) maltose, ampicillin, and chloramphenicol and grown over night at 30°C. The red color indicates an interaction, while pale yellowish colors show a lack of interaction.

subunit. Therefore, a T25-FdhF fusion, in which the entire FDH-H protein was fused to the *C*-terminus of the T25 fragment, was constructed. The interaction with the *C*-terminal fusion of HycB (fused to T18) showed an activity of 800 MU, which was also within the same order of magnitude as the interaction with T18-HydN (728 MU) and T18-YsaA (694 MU) with T25-FdhF (**Table 3**). No other positive interactions of the FdhF protein were detectable here (**Figure 3**). The T18-HydN fusion, however, showed also an interaction with the empty T25 plasmid in this order of magnitude (892 MU) and the interaction will need to be evaluated carefully by additional methods. Although, the *C*-terminal fusion between FDH-H and HycB was previously shown to be successful in transferring electrons into the FHL complex (McDowall et al., 2015), the T18-FdhF showed neither an interaction with HycB nor with the other tested protein fusions. This could indicate that HydN and YsaA only transiently interact with FdhF before it assembles into the FHL complex, as we could show recently for the HycH protein interaction with the hydrogenase 3 of the FHL complex on the pathway of assembly into the complex (Lindenstrauß et al., 2017). But instead of a temporal order of interactions, these results could also be interpreted to indicate that FDH-H interacts with other protein complexes.

The strong interaction between the *N*-terminal fusions of HydN, YsaA and the HycB proteins and their corresponding *C*-terminal fusions favors the latter hypothesis (**Table 3**). These range between 2,413 MU for the HycB self-interaction and 4,608 MU for the T25-YsaA × T18-HydN interaction. Interestingly, the AegA protein participates in this interaction network by showing strong interactions with itself, HycB, HydN, and YsaA. The close proximity of the second ferredoxin-like protein in the FHL complex HycF to HycB is probably the reason this protein interacts with the same partners as HycB, with the exception of FDH-H. It is striking that no interaction between the HycB homolog, HyfA, of the FHL-2 complex and the FDH-H can be detected here. Although a missing bacterial two hybrid

TABLE 3 | Beta-galactosidase activities of bacterial two hybrid interactions.

	T18-AegA	T18-FdhF	T18-FdnH	T18-Fdx	T18-HycB	T18-HycF	T18-HydN	T18-HyfA	T18-NarH	T18-NuoE	T18-YsaA	T18
T25-AegA	982 ± 88	164 ± 19	392 ± 44	125 ± 10	1,877 ± 164	1,157 ± 202	2,247 ± 336	2,956 ± 350	164 ± 17	413 ± 27	5,867 ± 431	62 ± 11
T25-FdhF	511 ± 153	451 ± 11	446 ± 51	132 ± 4	800 ± 37	305 ± 24	728 ± 62	338 ± 25	311 ± 149	321 ± 50	694 ± 37	40 ± 3
T25-FdnH	230 ± 39	182 ± 16	1,282 ± 116	139 ± 19	1,139 ± 48	1,116 ± 45	211 ± 55	223 ± 16	278 ± 18	518 ± 37	905 ± 59	39 ± 16
T25-Fdx	107 ± 18	188 ± 27	421 ± 174	134 ± 13	500 ± 182	241 ± 166	197 ± 13	225 ± 18	267 ± 17	333 ± 112	194 ± 24	57 ± 13
T25-HycB	6,482 ± 771	421 ± 12	1,111 ± 37	127 ± 9	2,413 ± 176	3,973 ± 420	4,544 ± 115	265 ± 19	429 ± 252	1,334 ± 50	4,215 ± 303	30 ± 15
T25-HycF	1,555 ± 175	300 ± 125	1,109 ± 68	141 ± 11	2,174 ± 155	2,505 ± 375	1,683 ± 191	341 ± 141	448 ± 127	311 ± 45	2,188 ± 185	41 ± 14
T25-HydN	4,581 ± 788	401 ± 23	450 ± 52	141 ± 10	3,131 ± 146	2,120 ± 286	3,172 ± 116	317 ± 20	282 ± 22	363 ± 182	3,072 ± 116	17 ± 10
T25-HyfA	1,773 ± 277	272 ± 8	423 ± 21	152 ± 25	1,066 ± 54	2,567 ± 219	449 ± 44	296 ± 12	491 ± 194	537 ± 59	2,660 ± 96	48 ± 9
T25-NarH	257 ± 24	195 ± 33	1,255 ± 77	140 ± 7	1,283 ± 148	1,211 ± 89	186 ± 15	206 ± 21	1,084 ± 137	1,481 ± 166	927 ± 220	29 ± 6
T25-NuoE	417 ± 45	183 ± 16	512 ± 38	158 ± 19	1,546 ± 97	1,273 ± 153	194 ± 22	243 ± 137	472 ± 136	1,450 ± 84	618 ± 66	65 ± 6
T25-YsaA	6,150 ± 1,172	410 ± 18	446 ± 61	150 ± 14	3,896 ± 194	2,370 ± 180	4,608 ± 519	944 ± 30	297 ± 26	308 ± 22	4,237 ± 268	63 ± 8
T25	400 ± 62	590 ± 70	330 ± 26	244 ± 8	161 ± 12	341 ± 45	892 ± 39	821 ± 60	336 ± 17	148 ± 11	146 ± 18	217 ± 11

[a]*Shown are the mean Miller Units (MU) from 3 independent biological samples measured in duplicates to triplicates with their respective standard deviations. Cells were grown anaerobically in TGYEP, pH 6.5 until stationary phase. The zip plasmids and empty plasmids served as positive and negative controls, respectively (Karimova et al., 1998). The positive control yielded an activity of 3,619 ± 548 MU and empty pUT18 and pT25 vectors as negative control had an activity of 217 ± 11 MU Strong interactions (> 1,000 MU) are highlighted by an orange color, weak interactions (600–1,000 MU) are shown with a yellow background.*

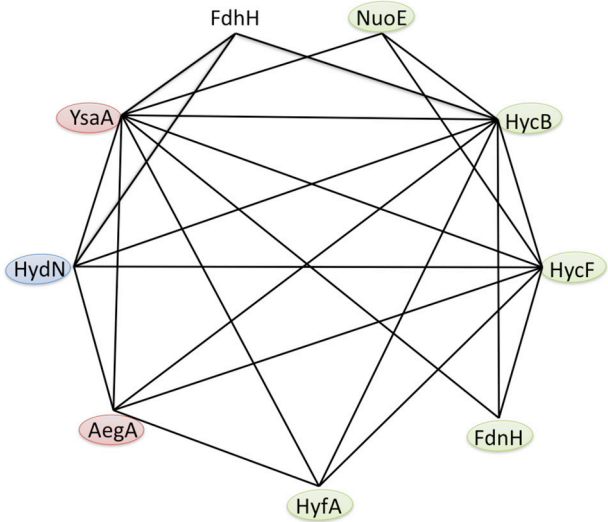

FIGURE 3 | Protein interaction network of the *E. coli* ferredoxin-like family. Based on the results of the bacterial two hybrid interaction studies in **Table 3**, the anaerobic interactions of FDH-H and the ferredoxin-like proteins AegA, FdnH, HycB, HycF, HydN, HyfA, NuoE and YsaA are shown. Self-interactions are not visualized and the colors indicate known β-subunits (green), proteins that are required for full activity of a respiratory protein (blue) and those proteins with unknown function (red).

interaction does not necessarily reflect the absence of a true interaction, the similarity of the HycB and HyfA proteins and the detectable interaction of the former, is a strong indication and these initial findings do not support the proposed interaction (Bagramyan and Trchounian, 2003) between FDH-H with the HyfA subunit of the FHL-2 complex. It should be noted, however, that AegA and YsaA interact in only one orientation with HycB and HycF of the FHL complex. Thus, further fusion constructs need to be tested.

It is noteworthy that YsaA also showed an interaction with FdnH and NarH, the two β-subunits of nitrate-dependent formate dehydrogenase (FDH-N) and nitrate reductase (NAR), respectively. The genes encoding these enzymes are transcribed at only a low level (Walker and DeMoss, 1991; Li and Stewart, 1992), therefore these subunits of FDH-N and NAR complexes are likely to be present in the assay. The HydN and AegA proteins do not interact with these nitrate-dependent proteins, supporting the specificity for the YsaA interaction. The FdnH and NarH proteins furthermore show a self-interaction as well as a cross-interaction, which can be explained for FdnH because the enzyme complex FdnGHI exists as a trimer of trimers (Jormakka et al., 2003) and although primarily coupled by a Q-cycle the special co-localisation of FDH-N and NAR activities was shown to be highly organized and proximal to each other in the membrane (Alberge et al., 2015).

The previously identified interaction between YsaA with NuoE, a subunit of Complex I, using Tap-tag technology could also be verified here (Arifuzzaman et al., 2006). Further interactions of NuoE with itself and NarH, as well as of

NuoE with the FHL subunits HycB and HycF were also detected here. However, the Fdx protein did not show any interaction with the protein fusions tested here, showing that its interaction with the proteins of the FeS-insertion machinery of the cell is highly specific (Tokumoto et al., 2002). This further indicates that it is not the general fold of the protein that is important for the interaction, but particular residues on the surface of the respective protein. Moreover, there are significant differences in length in a loop region between the third and the fourth Cys-rich ($Cx_2Cx_{2-8}Cx_3C$) motif and the *C*-terminal region of the HycB, HydN, and YsaA proteins, the former lies at the expected interface with the interaction partner and this loop could also play a role in discrimination of the correct target. All identified interactions are summarized in **Figure 3**.

FDH-H Protein Pattern Remains Unaltered

Remarkably, although the activity of FDH-H varies among the Δ*hydN* and Δ*ysaA* strains, western blot analysis of the polypeptide showed that both the migration pattern and the protein amount appear similar in the *ysaA*, *hydN*, and *ysaA hydN* deletion mutants when compared to the protein in the MC4100 parental strain; the same is the case for strains carrying the plasmids pysaA or phydN (**Figure 4A**). Therefore, the transcription or translation of the *fdhF* gene is not altered in the mutants.

A native PAGE showing the activities of hydrogenases 1 and 2 (**Figure 4B**) reveals that the migration pattern and in-gel enzyme activities are similar regardless of the presence or absence of either HydN or YsaA. These hydrogenases harbor the same [NiFe]-cofactor as HycE, the hydrogenase of the FHL complex. Thus the influence is strictly limited to FDH-H and not the hydrogenases in general.

The *hydN* and *ysaA* Deletions Have no Influence on Other Mo-bis-PGD–Dependent Activities

In order to investigate whether the influence of the *hydN* and *ysaA* mutations on FDH-H is generally related to Mo-bis-PGD cofactor insertion, the cytoplasmic NAR and periplasmic FDH-N activities, which are both Mo-bis-PGD-dependent, were analyzed. **Figures 4C,D** show that the amount and migration patterns of the nitrate reductase and formate dehydrogenase N activities were comparable to those in the wild type strain, regardless of whether HydN and YsaA are present or not. Both activities are strictly dependent on Fnr for gene expression, hence the Δ*fnr* mutant RM102 served as a negative control.

CONCLUSIONS

Of the three formate dehydrogenases encoded in the *E. coli* genome, FDH-H is the only cytoplasmic enzyme. An early mutant study by Mandrand-Berthelot showed that differences in the requirements for maturation of the cytoplasmic and periplasmic formate dehydrogenases exist (Mandrand-Berthelot et al., 1988). One of the isolated mutants had a mutation in *fdhE* and was deficient in the respiratory formate dehydrogenases N and O only; this mutation was without effect on transcription (Stewart et al., 1991). The mutation in another mutant was located in *fdhD* and had an effect on all three formate dehydrogenases, because FdhD, as was shown recently (Thomé et al., 2012; Arnoux et al., 2015), is involved in donating a sulfur

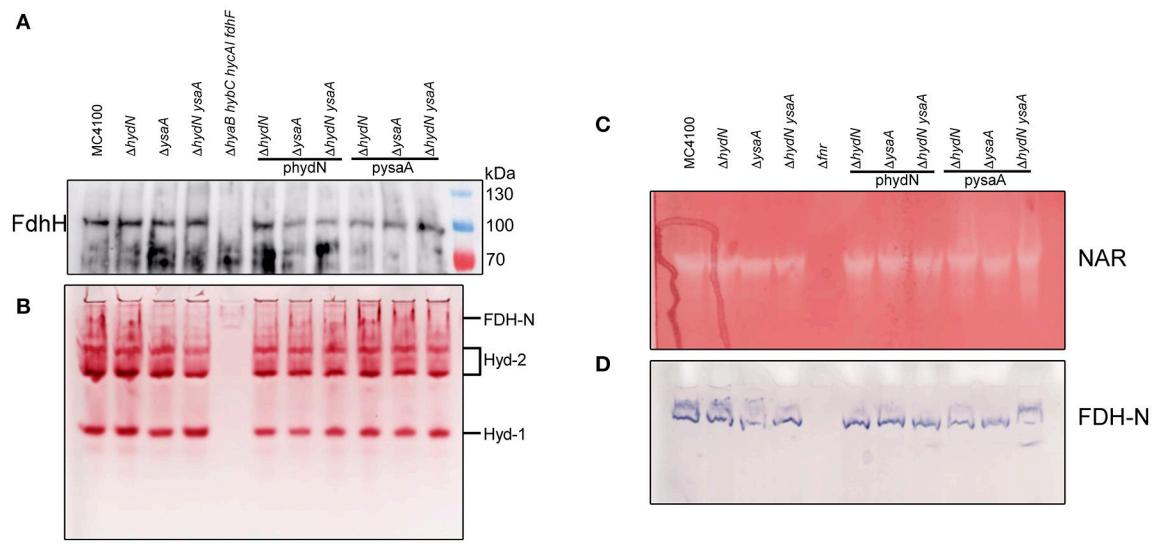

FIGURE 4 | Influence of HydN and YsaA on activities and polypeptides. **(A)** Shows a western blot of anaerobically grown cells as indicated by their genotype after separation of 25 μg protein in a SDS-PAGE, transfer to nitrocellulose and challenge with antibodies against FDH-H. **(B)** Shows identical samples but non-denatured and separated in a native-PAGE and stained for hydrogenase activity with H_2/BV and TTC. **(C,D)** Show a native-PAGE of cells as indicated by their genotype on top after anaerobic growth with 1% nitrate and staining for NAR (nitrate, BV, TTC, dithionite) and FDH-N (PMS, NBT, formate) activities, respectively.

ligand to the Mo-bis-PGD. It is conceivable that HydN and YsaA could contribute specifically to the cofactor activation of the FDH-H protein, since NAR and FDH-N activities are not impaired in the mutant; however, it would be expected that a more pronounced phenotype of the individual mutants would be observed, making this explanation unlikely.

Based on the observation of reduced, but not completely abolished FDH-H activity in the *ysaA, hydN, hycB* and the double and triple deletion mutants, it appears that full redox dye-reducing activity of FDH-H can only be measured when all three proteins are present simultaneously. Therefore, either all three proteins are involved as components of the FHL complex, although only HycB is essential (Sauter et al., 1992; **Table 2)** or HydN and YsaA could represent alternative β-subunits of the FDH-H enzyme, linking formate oxidation to other protein complexes. Neither HydN nor YsaA could be identified as components of the purified FHL complex (McDowall et al., 2014). If HydN and YsaA were transient components of FHL, then it would be anticipated that additional copies of *hydN in trans* should compete for FDH-H protein with HycB and reduce the H_2-production by the FHL complex. However, H_2 production by the FHL complex remained essentially unaffected by all these mutations, which renders this hypothesis improbable. The data currently suggest, therefore, that HydN/YsaA provide alternative electron transfer routes for FDH-H to non-hydrogen producing electron acceptor complexes.

The phylogenetic analysis shows that AegA and YgfST are closely related to YsaA and HydN. Although AegA interacts with the ferredoxin-like proteins, the lack of interaction with FDH-H reflects an absence of influence on FDH-H activity. The AegA protein is a fusion of two domains; an *N*-terminal ferredoxin-like domain and a *C*-terminal glutamate synthase domain (Cavicchioli et al., 1996). Identifying its role within the network of ferredoxin-like proteins will require further experiments.

Generally, these interaction data have to be carefully evaluated because some proteins require interaction partners and if the physiological partner is not present, they seem to interact non-specifically with a number of other proteins. Therefore, future protein-protein interaction experiments will have to be performed *in vitro*. So far, HydN has proved recalcitrant to over-production and alternative purification strategies will have to be established to allow full biochemical characterization of this protein family.

AUTHOR CONTRIBUTIONS

CP planned and performed the experiments. CP has drafted and written the manuscript.

ACKNOWLEDGMENTS

Financial support for the publication came from the Open Access Publication Fund of the Martin-Luther-University Halle-Wittenberg. The project was funded by the Deutsche Forschungsgemeinschaft project PI 1252/2. Special acknowledgement goes to R. Gary Sawers for critical and helpful discussions and to Ute Lindenstrauß for valuable technical assistance.

SUPPLEMENTARY MATERIAL

The Supplementary Material for this article can be found online at: https://www.frontiersin.org/articles/10.3389/fmicb.2018.01238/full#supplementary-material

REFERENCES

Alberge, F., Espinosa, L., Seduk, F., Sylvi, L., Toci, R., Walburger, A., et al. (2015). Dynamic subcellular localization of a respiratory complex controls bacterial respiration. *Elife* 4:e05357. doi: 10.7554/eLife.05357

Andrews, S. C., Berks, B. C., McClay, J., Ambler, A., Quail, M. A., Golby, P., et al. (1997). A 12-cistron *Escherichia coli* operon (hyf) encoding a putative proton-translocating formate hydrogenlyase system. *Microbiology* 143 (Pt 11), 3633–3647. doi: 10.1099/00221287-143-11-3633

Arifuzzaman, M., Maeda, M., Itoh, A., Nishikata, K., Takita, C., Saito, R., et al. (2006). Large-scale identification of protein-protein interaction of *Escherichia coli* K-12. *Genome Res.* 16, 686–691. doi: 10.1101/gr.4527806

Arnoux, P., Ruppelt, C., Oudouhou, F., Lavergne, J., Siponen, M. I., Toci, R., et al. (2015). Sulphur shuttling across a chaperone during molybdenum cofactor maturation. *Nat. Commun.* 6:6148. doi: 10.1038/ncomms7148

Axley, M. J., Grahame, D., and Stadtman, T. (1990). *Escherichia coli* formate-hydrogen lyase. Purification and properties of the selenium-dependent formate dehydrogenase component. *J. Biol. Chem.* 265, 18213–18218.

Baba, T., Ara, T., Hasegawa, M., Takai, Y., Okumura, Y., Baba, M., et al. (2006). Construction of *Escherichia coli* K-12 in-frame, single-gene knockout mutants: the Keio collection. *Mol. Syst. Biol.* 2:2006.02008. doi: 10.1038/msb4100050

Bagramyan, K., and Trchounian, A. (2003). Structural and functional features of formate hydrogen lyase, an enzyme of mixed-acid fermentation from *Escherichia coli*. *Biochemistry* 68, 1159–1170. doi: 10.1023/B:BIRY.0000009129.18714.a4

Bassegoda, A., Madden, C., Wakerley, D. W., Reisner, E., and Hirst, J. (2014). Reversible interconversion of CO2 and formate by a molybdenum-containing formate dehydrogenase. *J. Am. Chem. Soc.* 136, 15473–15476. doi: 10.1021/ja508647u

Begg, Y., Whyte, J., and Haddock, B. (1977). The identification of mutants of *Escherichia coli* deficient in formate dehydrogenase and nitrate reductase activities using dye indicator plates. *FEMS Microbiol. Lett.* 2, 47–50. doi: 10.1111/j.1574-6968.1977.tb00905.x

Beinert, H. (1990). Recent developments in the field of iron-sulfur proteins. *FASEB J.* 4, 2483–2491. doi: 10.1096/fasebj.4.8.2185975

Beinert, H., Holm, R. H., and Münck, E. (1997). Iron-sulfur clusters: nature's modular, multipurpose structures. *Science* 277, 653–659. doi: 10.1126/science.277.5326.653

Birkmann, A., Sawers, R. G., and Böck, A. (1987). Involvement of the ntrA gene product in the anaerobic metabolism of *Escherichia coli*. *Mol. Gen. Genet.* 210, 535–542. doi: 10.1007/BF00327209

Boyington, J. C., Gladyshev, V. N., Khangulov, S. V., Stadtman, T. C., and Sun, P. D. (1997). Crystal structure of formate dehydrogenase H: catalysis involving Mo, molybdopterin, selenocysteine, and an Fe4S4 cluster. *Science* 275, 1305–1308. doi: 10.1126/science.275.5304.1305

Brenner, D. J., Krieg, N. R., Staley, J. T., and Garrity, G. M. (2006). *Bergey's Manual® of Systematic Bacteriology, 2nd Edn.* New York, NY: Springer.

Brondijk, T. H., Fiegen, D., Richardson, D. J., and Cole, J. A. (2002). Roles of NapF, NapG and NapH, subunits of the *Escherichia coli* periplasmic

nitrate reductase, in ubiquinol oxidation. *Mol. Microbiol.* 44, 245–255. doi: 10.1046/j.1365-2958.2002.02875.x

Bruschi, M., and Guerlesquin, F. (1988). Structure, function and evolution of bacterial ferredoxins. *FEMS Microbiol. Rev.* 4, 155–175. doi: 10.1111/j.1574-6968.1988.tb02741.x

Casadaban, M. J. (1976). Transposition and fusion of the lac genes to selected promoters in *Escherichia coli* using bacteriophage lambda and Mu. *J. Mol. Biol.* 104, 541–555. doi: 10.1016/0022-2836(76)90119-4

Cavicchioli, R., Kolesnikow, T., Chiang, R. C., and Gunsalus, R. P. (1996). Characterization of the aegA locus of *Escherichia coli*: control of gene expression in response to anaerobiosis and nitrate. *J. Bacteriol.* 178, 6968–6974. doi: 10.1128/jb.178.23.6968-6974.1996

Cherepanov, P. P., and Wackernagel, W. (1995). Gene disruption in *Escherichia coli*: TcR and KmR cassettes with the option of Flp-catalyzed excision of the antibiotic-resistance determinant. *Gene* 158, 9–14. doi: 10.1016/0378-1119(95)00193-A

Datsenko, K. A., and Wanner, B. L. (2000). One-step inactivation of chromosomal genes in *Escherichia coli* K-12 using PCR products. *Proc. Natl. Acad. Sci. U.S.A.* 97, 6640–6645. doi: 10.1073/pnas.120163297

Hamilton, C. M., Aldea, M., Washburn, B. K., Babitzke, P., and Kushner, S. R. (1989). New method for generating deletions and gene replacements in *Escherichia coli*. *J. Bacteriol.* 171, 4617–4622. doi: 10.1128/jb.171.9.4617-4622.1989

Jormakka, M., Byrne, B., and Iwata, S. (2003). Formate dehydrogenase-a versatile enzyme in changing environments. *Curr. Opin. Struct. Biol.* 13, 418–423. doi: 10.1016/S0959-440X(03)00098-8

Kang, Y., Weber, K. D., Qiu, Y., Kiley, P. J., and Blattner, F. R. (2005). Genome-wide expression analysis indicates that FNR of *Escherichia coli* K-12 regulates a large number of genes of unknown function. *J. Bacteriol.* 187, 1135–1160. doi: 10.1128/JB.187.3.1135-1160.2005

Karimova, G., Pidoux, J., Ullmann, A., and Ladant, D. (1998). A bacterial two-hybrid system based on a reconstituted signal transduction pathway. *Proc. Natl. Acad. Sci. U.S.A.* 95, 5752–5756. doi: 10.1073/pnas.95.10.5752

Knappe, J., Schacht, J., Möckel, W., Höpner, T., Vetter, H., and Edenharder, R. (1969). Pyruvate formate-lyase reaction in *Escherichia coli*. The enzymatic system converting an inactive form of the lyase into the catalytically active enzyme. *Eur. J. Biochem.* 11, 316–327. doi: 10.1111/j.1432-1033.1969.tb00775.x

Lamont, C. M., Kelly, C. L., Pinske, C., Buchanan, G., Palmer, T., and Sargent, F. (2017). Expanding the substrates for a bacterial hydrogenlyase reaction. *Microbiology* 163, 649–653. doi: 10.1099/mic.0.000471

Letunic, I., and Bork, P. (2016). Interactive tree of life (iTOL) v3: an online tool for the display and annotation of phylogenetic and other trees. *Nucleic Acids Res.* 44, W242–W245. doi: 10.1093/nar/gkw290

Li, J., and Stewart, V. (1992). Localization of upstream sequence elements required for nitrate and anaerobic induction of fdn (formate dehydrogenase-N) operon expression in *Escherichia coli* K-12. *J. Bacteriol.* 174, 4935–4942. doi: 10.1128/jb.174.15.4935-4942.1992

Lindenstrauß, U., Skorupa, P., McDowall, J. S., Sargent, F., and Pinske, C. (2017). The dual-function chaperone HycH improves assembly of the formate hydrogenlyase complex. *Biochem. J.* 474, 2937–2950. doi: 10.1042/BCJ20170431

Maier, T., Binder, U., and Böck, A. (1996). Analysis of the hydA locus of *Escherichia coli*: two genes (hydN and hypF) involved in formate and hydrogen metabolism. *Arch. Microbiol.* 165, 333–341. doi: 10.1007/s002030050335

Maier, T. H. P. (1997). *Katalysierter Metall-Einbau in Proteine: Biosynthese von [NiFe]-Hydrogenasen in Escherichia coli*. Dissertation, Ludwig-Maximilian University Munich, Munich, Germany.

Mandrand-Berthelot, M. A., Couchoux-Luthaud, G., Santini, C. L., and Giordano, G. (1988). Mutants of *Escherichia coli* specifically deficient in respiratory formate dehydrogenase activity. *J. Gen. Microbiol.* 134, 3129–3139. doi: 10.1099/00221287-134-12-3129

McDowall, J. S., Hjersing, M. C., Palmer, T., and Sargent, F. (2015). Dissection and engineering of the *Escherichia coli* formate hydrogenlyase complex. *FEBS Lett.* 589, 3141–3147. doi: 10.1016/j.febslet.2015.08.043

McDowall, J. S., Murphy, B. J., Haumann, M., Palmer, T., Armstrong, F. A., and Sargent, F. (2014). Bacterial formate hydrogenlyase complex. *Proc. Natl. Acad. Sci. U.S.A.* 111, E3948–E3956. doi: 10.1073/pnas.1407927111

Miller, J. (1972). *Experiments in Molecular Genetics*. Cold Spring Harbor, NY: Cold Spring Harbor Laboratory.

Nilavongse, A., Brondijk, T. H., Overton, T. W., Richardson, D. J., Leach, E. R., and Cole, J. A. (2006). The NapF protein of the *Escherichia coli* periplasmic nitrate reductase system: demonstration of a cytoplasmic location and interaction with the catalytic subunit, NapA. *Microbiology* 152, 3227–3237. doi: 10.1099/mic.0.29157-0

Pecher, A., Zinoni, F., Jatisatienr, C., Wirth, R., Hennecke, H., and Böck, A. (1983). On the redox control of synthesis of anaerobically induced enzymes in enterobacteriaceae. *Arch. Microbiol.* 136, 131–136. doi: 10.1007/BF00404787

Pinske, C., Bönn, M., Krüger, S., Lindenstrauß, U., and Sawers, R. G. (2011a). Metabolic deficiences revealed in the biotechnologically important model bacterium *Escherichia coli* BL21(DE3). *PLoS ONE* 6:e22830. doi: 10.1371/journal.pone.0022830

Pinske, C., Krüger, S., Soboh, B., Ihling, C., Kuhns, M., Braussemann, M., et al. (2011b). Efficient electron transfer from hydrogen to benzyl viologen by the [NiFe]-hydrogenases of *Escherichia coli* is dependent on the coexpression of the iron-sulfur cluster-containing small subunit. *Arch. Microbiol.* 193, 893–903. doi: 10.1007/s00203-011-0726-5

Pinske, C., and Sawers, R. G. (2012). A-type carrier protein ErpA is essential for formation of an active formate-nitrate respiratory pathway in *Escherichia coli* K-12. *J. Bacteriol.* 194, 346–353. doi: 10.1128/JB.06024-11

Pinske, C., and Sawers, R. G. (2016). Anaerobic formate and hydrogen metabolism. *EcoSal Plus* 7:ESP—0011–2016. doi: 10.1128/ecosalplus.ESP-0011-2016

Sargent, F. (2016). The model [NiFe]-hydrogenases of *Escherichia coli*. *Adv. Microb. Physiol.* 68, 433–507. doi: 10.1016/bs.ampbs.2016.02.008

Sauter, M., Böhm, R., and Böck, A. (1992). Mutational analysis of the operon (hyc) determining hydrogenase 3 formation in *Escherichia coli*. *Mol. Microbiol.* 6, 1523–1532. doi: 10.1111/j.1365-2958.1992.tb00873.x

Sawers, R. G. (2005). Formate and its role in hydrogen production in *Escherichia coli*. *Biochem. Soc. Trans.* 33, 42–46. doi: 10.1042/BST0330042

Sawers, G., Heider, J., Zehelein, E., and Böck, A. (1991). Expression and operon structure of the sel genes of *Escherichia coli* and identification of a third selenium-containing formate dehydrogenase isoenzyme. *J. Bacteriol.* 173, 4983–4993. doi: 10.1128/jb.173.16.4983-4993.1991

Sievers, F., and Higgins, D. G. (2013). "Clustal omega, accurate alignment of very large numbers of sequences," in *Protein Chromatography Methods in Molecular Biology*, ed D. J. Russell (Totowa, NJ: Humana Press), 105–116.

Stewart, V., Lin, J. T., and Berg, B. L. (1991). Genetic evidence that genes fdhD and fdhE do not control synthesis of formate dehydrogenase-N in *Escherichia coli* K-12. *J. Bacteriol.* 173, 4417–4423. doi: 10.1128/jb.173.14.4417-4423.1991

Szklarczyk, D., Franceschini, A., Wyder, S., Forslund, K., Heller, D., Huerta-Cepas, J., et al. (2015). STRING v10: protein-protein interaction networks, integrated over the tree of life. *Nucleic Acids Res.* 43, D447–D452. doi: 10.1093/nar/gku1003

Thomé, R., Gust, A., Toci, R., Mendel, R., Bittner, F., Magalon, A., et al. (2012). A sulfurtransferase is essential for activity of formate dehydrogenases in *Escherichia coli*. *J. Biol. Chem.* 287, 4671–4678. doi: 10.1074/jbc.M111.327122

Tokumoto, U., Nomura, S., Minami, Y., Mihara, H., Kato, S.-I., Kurihara, T., et al. (2002). Network of protein-protein interactions among iron-sulfur cluster assembly proteins in *Escherichia coli*. *J. Biochem.* 131, 713–719. doi: 10.1093/oxfordjournals.jbchem.a003156

Trchounian, K., Poladyan, A., Vassilian, A., and Trchounian, A. (2012). Multiple and reversible hydrogenases for hydrogen production by *Escherichia coli*: dependence on fermentation substrate, pH and the F0F1-ATPase. *Crit. Rev. Biochem. Mol. Biol.* 47, 236–249. doi: 10.3109/10409238.2012.655375

Walker, M. S., and DeMoss, J. A. (1991). Promoter sequence requirements for Fnr-dependent activation of transcription of the narGHJI operon. *Mol. Microbiol.* 5, 353–360. doi: 10.1111/j.1365-2958.1991.tb02116.x

Conflict of Interest Statement: The author declares that the research was conducted in the absence of any commercial or financial relationships that could be construed as a potential conflict of interest.

frontiers in Microbiology

ORIGINAL RESEARCH
published: 21 November 2018
doi: 10.3389/fmicb.2018.02837

Insights Into the Redox Sensitivity of *Chloroflexi* Hup-Hydrogenase Derived From Studies in *Escherichia coli*: Merits and Pitfalls of Heterologous [NiFe]-Hydrogenase Synthesis

Nadya Dragomirova, Patricia Rothe, Stefan Schwoch, Stefanie Hartwig, Constanze Pinske and R. Gary Sawers**

Institute of Microbiology, Martin-Luther University Halle-Wittenberg, Halle, Germany

OPEN ACCESS

Edited by:
Chris Greening, Monash University, Australia

Reviewed by:
Bat-Erdene Jugder, Harvard Medical School, United States
Rhiannon Mari Evans, University of Oxford, United Kingdom

***Correspondence:**
Constanze Pinske
constanze.pinske@mikrobiologie.uni-halle.de
R. Gary Sawers
gary.sawers@mikrobiologie.uni-halle.de

Specialty section:
This article was submitted to Microbial Physiology and Metabolism, a section of the journal Frontiers in Microbiology

Received: *19 September 2018*
Accepted: *05 November 2018*
Published: *21 November 2018*

Citation:
Dragomirova N, Rothe P, Schwoch S, Hartwig S, Pinske C and Sawers RG (2018) Insights Into the Redox Sensitivity of Chloroflexi Hup-Hydrogenase Derived From Studies in Escherichia coli: Merits and Pitfalls of Heterologous [NiFe]-Hydrogenase Synthesis. Front. Microbiol. 9:2837. doi: 10.3389/fmicb.2018.02837

The highly oxygen-sensitive hydrogen uptake (Hup) hydrogenase from *Dehalococcoides mccartyi* forms part of a protein-based respiratory chain coupling hydrogen oxidation with organohalide reduction on the outside of the cell. The HupXSL proteins were previously shown to be synthesized and enzymatically active in *Escherichia coli*. Here we examined the growth conditions that deliver active Hup enzyme that couples H_2 oxidation to benzyl viologen (BV) reduction, and identified host factors important for this process. In a genetic background lacking the three main hydrogenases of *E. coli* we could show that additional deletion of genes necessary for selenocysteine biosynthesis resulted in inactive Hup enzyme, suggesting requirement of a formate dehydrogenase for Hup activity. Hup activity proved to be dependent on the presence of formate dehydrogenase (Fdh-H), which is typically associated with the H_2-evolving formate hydrogenlyase (FHL) complex in the cytoplasm. Further analyses revealed that heterologous Hup activity could be recovered if the genes encoding the ferredoxin-like electron-transfer protein HupX, as well as the related HycB small subunit of Fdh-H were also deleted. These findings indicated that the catalytic HupL and electron-transferring HupS subunits were sufficient for enzyme activity with BV. The presence of the HupX or HycB proteins in the absence of Fdh-H therefore appears to cause inactivation of the HupSL enzyme. This is possibly because HupX or HycB aided transfer of electrons to the quinone pool or other oxidoreductase complexes, thus maintaining the HupSL heterodimer in a continuously oxidized state causing its inactivation. This proposal was supported by the observation that growth under either aerobic or anaerobic respiratory conditions did not yield an active HupSL. These studies thus provide a system to understand the redox sensitivity of this heterologously synthesized hydrogenase.

Keywords: hydrogen, formate, ferredoxin-like proteins, electron transfer, uptake hydrogenase, heterologous expression

INTRODUCTION

The bacterial genus *Dehalococcoides* belongs to the phylum *Chloroflexi* and the type species *D. mccartyi* is completely dependent on hydrogen for growth (Löffler et al., 2013; Schubert et al., 2018). *D. mccartyi* synthesizes several types of [NiFe]-hydrogenase (Hyd), and the hydrogen-uptake (Hup) hydrogenase is thought to be the main enzyme involved in H_2-driven organohalide respiration. As *D. mccartyi* lacks quinones (Kube et al., 2005; Schipp et al., 2013), a direct transfer of the electrons derived from H_2 oxidation by Hup via protein–protein interaction has been implicated (Kublik et al., 2016; Hartwig et al., 2017; Seidel et al., 2018). The Hup enzyme is found in a respiratory supercomplex comprising a two-subunit complex iron-sulfur molybdoprotein, OmeAB (organohalide molybdoenzyme) and one of a number of reductive dehalogenases (Rdh), which catalyze the reduction of particular organohalides that function as electron acceptors for the bacterium (Fincker and Spormann, 2017; Schubert et al., 2018). In addition, the ferredoxin-like protein HupX, which resembles electron-transferring subunits of oxidoreductases, is associated with the complex.

Hup comprises two structural components: the catalytic subunit HupL, containing the $NiFe(CN)_2CO$ cofactor and HupS, the small electron-transferring subunit, which is predicted to have three iron-sulfur clusters. The membrane-associated, ferredoxin-like protein HupX is encoded within the operon of the Hup hydrogenase, but seems to associate more tightly with the core OmeAB-Rdh complex (Hartwig et al., 2017; Seidel et al., 2018), suggesting that it is the main mediator of electron transfer and acts as a "connector" protein between HupSL and the rest of the complex. HupX is homologous to HybA, a component of the Hyd-2 H_2-oxidizing hydrogenase of *Escherichia coli* (Sargent et al., 1998; Beaton et al., 2018) and recent studies have provided strong evidence indicating that HybA is responsible for coupling electron transfer to the quinone pool, as Hyd-2 has no membrane subunit with a recognized heme cofactor, necessary for electron transfer into the membrane (Dubini et al., 2002; Pinske et al., 2015; Beaton et al., 2018).

The ferredoxin-like family of electron–transfer proteins harbors four [4Fe-4S] clusters and an interaction network of several members of this family has been uncovered recently in *E. coli* (Pinske, 2018). One member is HycB, the small subunit of the formate dehydrogenase (Fdh-H) that forms one of the two catalytic centers of the formate hydrogenlyase (FHL) complex, and another is the related protein HydN, which is proposed to be involved in FHL complex assembly (Pinske, 2018). Generally, however, the physiological function of most members of this emerging superfamily of iron-sulfur-containing electron transfer proteins is not understood.

Due to the fact that *D. mccartyi* grows extremely slowly and produces limited amounts of biomass, making biochemical studies challenging, we have established a heterologous expression system for the synthesis of a functional Hup enzyme in *E. coli* (Hartwig et al., 2015b). It is hoped that this system will facilitate a detailed biochemical characterization of Hup. Despite the significant phylogenetic distance between *D. mccartyi* and *E. coli*, the Hyp maturation system responsible for [NiFe]-cofactor biosynthesis and insertion (Böck et al., 2006) is capable of recognizing the HupL apoprotein and generating an active enzyme when the complete operon encoding Hup is expressed under anaerobic conditions (Hartwig et al., 2015b).

As well as the three structural genes, the *hupXSL-hoxM* operon (**Figure 1A**) also encodes a HupL-specific maturation endoprotease (HoxM). Initial characterization of the heterologously synthesized Hup enzyme identified a fast-migrating complex, mainly comprising HupS and HupL after native-PAGE, which migrated at a similar position as the complex present in crude extracts of *D. mccartyi* that contained HupSL and minor amounts of HupX (Hartwig et al., 2015b). This suggests that HupSL alone is capable of catalyzing H_2-dependent reduction of the redox dye BV. The activity of the complex was oxygen-sensitive, even when synthesized anaerobically in the heterologous host (Hartwig et al., 2015b), suggesting that a cofactor in the enzyme is redox-sensitive. Whether this redox-sensitive cofactor is in HupL, HupS or HupX is unclear. Therefore, to address these questions, in the current study we decided to determine the conditions necessary for heterologous production of HupSL activity and whether any other components of the host's metabolism, other than the Hyp proteins, are required for activity to be visualized. Surprisingly, we found a strong dependence for HupSL activity on the Fdh-H enzyme of the FHL complex. This dependence on Fdh-H for activity proved to be linked to an involvement of ferredoxin-like electron transfer proteins and to the redox sensitivity of the HupSL heterodimer.

MATERIALS AND METHODS

Strains and Growth Conditions

The strains listed in **Table 1** were used in this study. For routine molecular biology studies, growth was on LB-agar plates or in LB-broth at 37°C (Miller, 1972). Anaerobic growths were performed at 37°C as standing liquid cultures and cells were usually grown in M9 minimal medium (47.6 mM $Na_2HPO_4 \times 2\ H_2O$, 22 mM KH_2PO_4, 8.4 mM NaCl, 20 mM NH_4Cl, 2 mM $MgSO_4$, 0.1 mM $CaCl_2$, 0.1 mM thiamin dichloride, 0.2% w/v casamino acids) containing 0.8% (w/v) glucose, or 0.4% (v/v) glycerol plus 15 mM fumarate, or 0.8% (w/v) glucose plus 1% (w/v) nitrate, where indicated, as described (Sambrook et al., 1989). When growth in rich medium was performed, buffered TGYEP (1% w/v tryptone, 0.5% w/v yeast extract, 0.8% w/v glucose, 100 mM potassium phosphate, pH 6.5) was used (Begg et al., 1977). The growth medium was supplemented with trace element solution SLA (Hormann and Andreesen, 1989). When required, the antibiotic kanamycin or chloramphenicol was added to a final concentration of 50 or 25 $\mu g\ ml^{-1}$, respectively. Cells were harvested anaerobically by centrifugation at 5,000 *g* for 15 min at 4°C when cultures had reached an $OD_{600\ nm}$ of between 0.8 and 1.2. Cell pellets were used immediately or stored at −20°C until use.

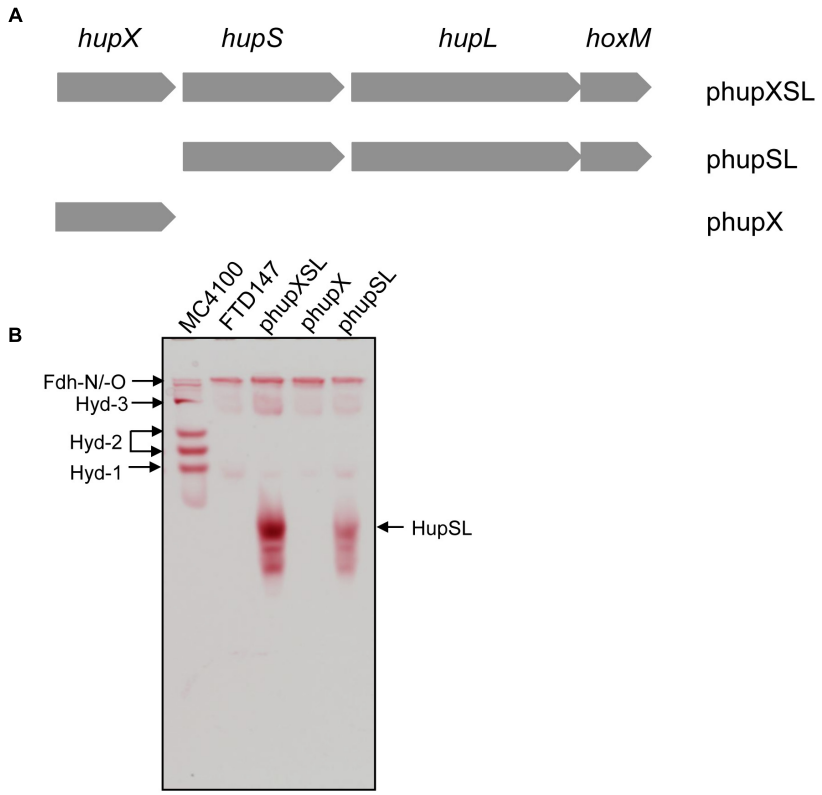

FIGURE 1 | HupX is not required for heterologous HupSL activity. **(A)** Schematic representation of the plasmids used in this study is shown. The plasmid inserts are not drawn to scale but the complete *hupXSLhoxM* region encompasses 4216 bp (Hartwig et al., 2015b). **(B)** An in-gel activity stain for hydrogen-oxidizing activity is shown. Crude extracts (70 μg of protein; 30 μg in the case of wild type MC4100) derived from FTD147 (Δ*hyaB* Δ*hybC* Δ*hycE*) carrying the indicated plasmids were applied to a native polyacrylamide gel (7.5% w/v polyacrylamide). The migration positions of HupSL and the *E. coli* hydrogenases are indicated. The formate dehydrogenases Fdh-N and Fdh-O (Fdh-N/O) have a weak hydrogen-oxidizing activity (Soboh et al., 2011), which is also indicated and was used as an internal loading control for the experiment.

Plasmid and Strain Construction

The *hupX* gene (*cbdbA131*) was amplified as a 1212 bp DNA fragment from chromosomal DNA isolated from *D. mccartyi* strain CBDB1 using Pfu DNA polymerase and the oligonucleotides hupX_fw (5′-GGGGCATATGCCTAATGGAATGCTGATTG-3′) and hupX_re (5′-GGGGCTCGAGCTAGTGCTTGCCAGCCTTG-3′) and cloned in plasmid pACYC-Duet-I. Plasmid phupSL was constructed by using pSHH18 (referred to as phupXSL throughout this study) as template in a PCR mutagenesis employing the Q5® Site-Directed Mutagenesis Kit (New England Biolabs, NEB). Care was taken when deleting the *hupX* gene to ensure that the ribosome binding site for the downstream *hupS* gene remained intact by using the oligonucleotides hupSLhoxM_fw (5′-ATGGAGTAGGAAAAATGTTTAATAC-3′) and hupSLhoxM_re (5′-TCCTGTTGCCCCCCTTGT-3′) and by following the instructions given in the Q5® Site-Directed Mutagenesis Kit.

E. coli strains were constructed using P1*kc*-mediated phage transduction (Miller, 1972) to introduce the respective defined deletion mutation from the appropriate donor strain obtained from the Keio collection (Baba et al., 2006) to generate the series of FTD147 mutants lacking the structural genes encoding the three formate dehydrogenases of *E. coli*. When multiple gene knock-outs were constructed, the plasmid pCP20 was used to remove the kanamycin antibiotic resistance cassette as described (Cherepanov and Wackernagel, 1995).

Preparation of Crude Cell Extracts and Cell Fractionation

Unless otherwise stated, all experiments were performed in an anaerobic Coy^{TM} chamber under an atmosphere of 95% nitrogen/5% hydrogen. For standard hydrogenase enzyme activity determination, *E. coli* cell paste was re-suspended at a ratio of 1 g cell wet weight to 3 ml 50 mM MOPS buffer, pH 7. Cells were disrupted by sonication (30 W power for 5 min with 0.5 s pulses). Unbroken cells and cell debris were removed by centrifugation for 30 min at 50,000 *g* and 4°C. The resulting crude extract, unless otherwise stated, was used for all studies reported herein.

In order to perform sub-cellular fractionation, periplasmic, soluble and membrane fractions were isolated as described (Sawers et al., 1985).

TABLE 1 | Strains and plasmids used in this study.

Strain or plasmid	Relevant genotype or characteristic(s)	Reference or source
STRAIN		
MC4100	F$^-$ *araD139* (*argF-lac*)*U169 ptsF25 deoC1 relA1 flbB5301 rspL150*	Casadaban, 1976
RM220	As MC4100, but Δ*pflAB*	Kaiser and Sawers, 1994
FTD147	As MC4100, but Δ*hyaB*Δ*hybC*Δ*hycE*	Redwood et al., 2008
FTD147Δ*fdnG*	As [a]FTD147, but Δ*fdnG*	This work
FTD147Δ*fdoG*	As [a]FTD147, but Δ*fdoG*	This work
FTD147Δ*fdhF*	As [a]FTD147, but Δ*fdhF*	This work
FTD147Δ*fdnG*Δ*fdoG*	As [a]FTD147, but Δ*fdnG* Δ*fdoG*	This work
FTD147Δ*fdnG*Δ*fdhF*	As [a]FTD147, but Δ*fdnG* Δ*fdhF*	This work
FTD147Δ*fdoG*Δ*fdhF*	As [a]FTD147, but Δ*fdoG* Δ*fdhF*	This work
FTD147Δ*fdnG*Δ*fdoG*Δ*fdhF*	As [a]FTD147, but Δ*fdnG* Δ*fdoG* Δ*fdhF*	This work
FTD147 Δ*selC*	As FTD147, but Δ*selC* Kan^R	This work
FTD150	As MC4100, but Δ*hyaB*Δ*hybC*Δ*hycE* Δ*hyfG*	Redwood et al., 2008
FTD150Δ*selB*	As FTD150, but Δ*selB* Kan^R	This work
CP1170	As MC4100, but Δ*hyaB*Δ*hybC*Δ*hycA-I*	This work
CPH008	As MC4100, but Δ*hycA-I* Δ*fdhF*	This work
CPH020	As MC4100, but Δ*hyaB*Δ*hybC*Δ*hycA-I*Δ*fdhF*	Pinske, 2018
CPH021	As MC4100, but Δ*hyaB*Δ*hybC*Δ*hycA-I*Δ*fdhE*	This work
RT2	As MC4100, but Δ*hyaB*Δ*hybC*Δ*hycA-I*Δ*fdhE* Δ*pflA*	Pinske and Sargent, 2016
PLASMIDS		
pCP20	*FLP*$^+$, λ*cI857*$^+$, λp_R Rep^{ts}, Amp^R, Cm^R	Cherepanov and Wackernagel, 1995
[b]pSHH18	pACYC-Duet-I, *hupXSLhoxM*$^+$ Cm^R = phupXSL	Hartwig et al., 2015b
phupSL	pACYC-Duet-I, *hupSLhoxM*$^+$, Cm^R	This work
phupX	pACYC-Duet-I, *hupX*$^+$, Cm^R	This work

[a] *The series of FTD147 mutants with different combinations of Fdh gene mutations was constructed by transduction of mutations from the corresponding Keio collection of mutants (see Materials and Methods).* [b] *Note that for reasons of clarity, this plasmid was referred to as phupXSL throughout this study.*

Determination of protein concentration was done as described (Lowry et al., 1951).

Non-denaturing Polyacrylamide Gel Electrophoresis and Activity-Staining

Unless otherwise specified, non-denaturing polyacrylamide gel electrophoresis (PAGE) was performed anaerobically. Separating gels included 0.1% (w/v) Triton X-100 as described (Ballantine and Boxer, 1985). The crude extracts, or sub-cellular fractions, were incubated with a final concentration of 4% (w/v) Triton X-100 prior to application (usually 50 μg of protein) to the gel, which included 6% (w/v) polyacrylamide. Hydrogenase activity-staining was done in 50 mM MOPS buffer pH 7.0, as described (Sawers et al., 1985; Pinske et al., 2012), and included 0.5 mM BV and 1 mM 2,3,5-triphenyltetrazolium chloride (TTC). Gels were incubated under an atmosphere of 100% hydrogen gas.

Hydrogenase Activity Assay

Measurement of hydrogenase enzyme activity using BV as electron acceptor was performed as described (Ballantine and Boxer, 1985; Pinske et al., 2011). Briefly, anaerobically prepared cuvettes (1.6 ml) were filled with 0.8 ml of H_2-saturated, anaerobic 50 mM MOPS buffer, pH 7.0, including 4 mM BV and placed under a H_2 atmosphere. After baseline determination, the assay was initiated by adding enzyme sample (approximately 150 μg of protein). All assays were performed at 25°C. The wavelength used was 600 nm and an ε_M value of 7400 M^{-1} cm^{-1} was assumed for reduced BV. One million unit of enzyme activity corresponded to the reduction of 1 nmol of substrate min^{-1}. Enzyme assays were performed in triplicate using three biological replicates.

Denaturing Polyacrylamide Gel Electrophoresis (PAGE) and Western Blotting

Polypeptides in crude extracts were separated by 12.5% (w/v) sodium dodecyl sulfate (SDS)-PAGE (Laemmli, 1970) and gels were either stained with Coomassie Brilliant Blue R or transferred to nitrocellulose membranes for western blotting, which was performed as described (Towbin et al., 1979). The antibodies used were either anti-Strep-tag (IBA Life Sciences), anti-Hyd-2 (Sargent et al., 1998), anti-HupL or anti-HupX peptide antibodies (Hartwig et al., 2017).

RESULTS

HupL and HupS Are Sufficient for BV Reduction Activity

The *hupXSLhoxM* operon has been shown to be functional in anaerobically grown *E. coli* (Hartwig et al., 2015b). In order to determine whether all three structural components

(HupSL and HupX) are essential for the manifestation of the H_2:BV oxidoreductase activity observed in that study, we constructed two additional plasmid derivatives, one of which carried only the *hupX* gene, while the other included *hupSLhoxM* but lacked *hupX* (**Figure 1A**). These plasmids, along with pSHH18 (*hupXSLhoxM*$^+$; Hartwig et al., 2015b; here referred to as phupXSL in the aid of clarity), were introduced into FTD147, which lacks the genes encoding the catalytic subunits of Hyd-1, Hyd-2, and Hyd-3 (Redwood et al., 2008). After fermentative growth, crude extracts were separated in native-PAGE and stained for hydrogenase enzyme activity (**Figure 1B**). As anticipated, the plasmid encoding only HupX showed no hydrogenase enzyme activity in extracts of strain FTD147 (Δ*hyaB*Δ*hybC*Δ*hycE*), while both of the other plasmids resulted in a fast-migrating activity band corresponding to the HupSL heterodimer (**Figure 1B**). Notably, although the activity resulting from introduction of the plasmid lacking the *hupX* gene (phupSL in **Figure 1B**) was apparently weaker than that resulting from introduction of phupXSL, both enzyme activities showed very similar migration characteristics, indicating that HupX is neither necessary for the ability of the enzyme to reduce BV nor seems to co-migrate with HupSL in this particular activity band. This result correlates well with earlier mass spectrometric analyses of heterologously expressed enzyme, which identified mainly the HupL protein (Hartwig et al., 2015b).

Manifestation of Heterologous HupSL Enzyme Activity Requires Fermentative Growth Conditions

In order to optimize conditions for the analysis of heterologously produced HupSL activity, we tested different anaerobic growth conditions using FTD147 (Δ*hyaB*Δ*hybC*Δ*hycE*) transformed with either phupXSL or phupSL (**Figure 2A**). The activity band was slightly more intense when cells were grown with 0.8% w/v glucose compared with half that glucose concentration (0.4% w/v). Suprisingly, however, no HupSL activity could be detected when cells were grown under anaerobic respiratory conditions, with either glycerol and fumarate or glucose and nitrate. Western blot analysis of the extracts derived from anaerobically grown strains after separation by SDS-PAGE using peptide antibodies raised against HupL revealed that the HupL polypeptide could be detected in each extract (**Figure 2B**). This indicates that a lack of transcription of the *hup* genes under respiratory conditions was not the reason for absence of HupSL enzyme activity. Surprisingly, it was not possible to restore *in vitro* HupSL enzyme activity to these extracts, even by incubating the extracts under reducing conditions. This suggests that the HupSL enzyme was irreversibly inhibited under the oxidizing conditions that prevailed within the cells grown under these conditions.

Quantitative assessment of H_2-dependent BV reduction activity in anaerobically prepared, concentrated crude extracts of FTD147 (Δ*hyaB,* Δ*hybC*, Δ*hycE*) transformed with phupXSL measured a low but detectable hydrogenase activity of approximately 60 mU/mg (**Table 2**), which is in good agreement with previously determined HupSL activity in *E. coli* extracts (Hartwig et al., 2015b). The phenotypically identical strain CP1170 (Δ*hyaB,* Δ*hybC*, Δ*hycE*) had a background activity of 10 mU/mg. Brief incubation of the extract from FTD147 + phupXSL in the presence of oxygen resulted in a reduction of the HupSL activity by 50% (**Table 2**).

HupSL Activity in *E. coli* Requires a Functional Selenocysteine-Insertion Machinery

The lack of HupSL enzyme activity after respiratory growth is reminiscent of the effects of these growth conditions on

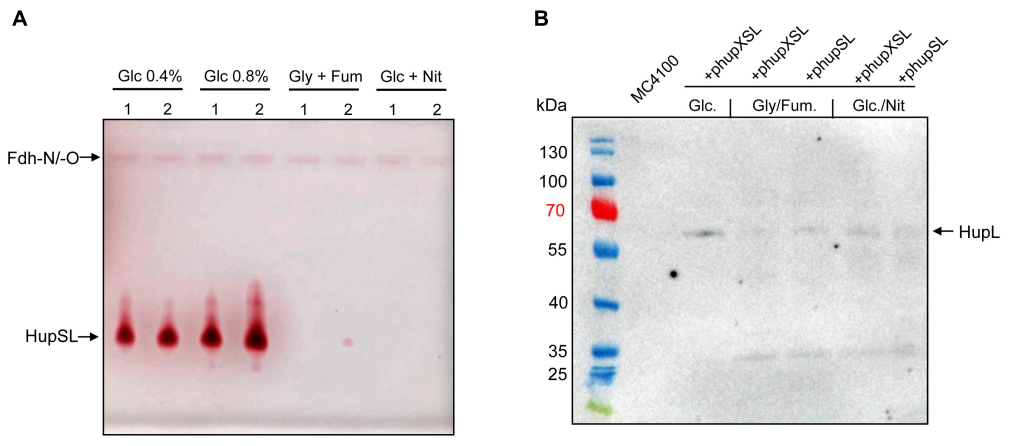

FIGURE 2 | Heterologous HupSL enzyme activity is only detectable in fermentatively growing *E. coli* cells. **(A)** Crude extracts derived from FTD147 (Δ*hyaB*Δ*hybC*Δ*hycE*) transformed with plasmid phupXSL (1) or phupSL (2) after growth in M9 minimal medium with the indicated carbon sources were separated in native-PAGE and stained for hydrogenase enzyme activity, as described in the legend to **Figure 1**. **(B)** A western blot using peptide antibodies raised against HupL (Hartwig et al., 2017) is shown in which the same extracts used in part A were separated in 10% (w/v) SDS-PAGE. The molecular mass marker proteins are presented in kDa. MC4100 was the wild type strain.

TABLE 2 | H_2:BV oxidoreductase activities of *E. coli* strains carrying phupXSL.

Strain	Anaerobic hydrogenase activity (mU mg protein^{-1})	Activity after O_2 exposure (mU mg protein^{-1})[a]
CP1170 (Δ*hyaB*, Δ*hybC*, Δ*hycA-I*)	10 ± 3[b]	n.d[c]
FTD147 (Δ*hyaB*, Δ*hybC*, Δ*hycE*) + phupXSL	58 ± 18	29 ± 9
FTD147 Δ*fdnG*, Δ*fdoG*	26 ± 13	n.d.
FTD147 Δ*fdnG*, Δ*fdoG* + phupXSL	59 ± 1	22 ± 1
FTD147 Δ*fdhF*	4 ± 2	n.d.
FTD147 Δ*fdhF* + phupXSL	11 ± 1	n.d

[a]*Crude extracts were exposed to air for 15 min prior to determination of hydrogenase activity.* [b]*Assays were performed in triplicate from 3 independent growth experiments. The activity is shown together with the standard deviation.* [c]*n.d, not determined.*

appearance of *E. coli* Hyd-3 and Fdh-H enzyme activities (Sawers et al., 1985), with the exception that the effect on synthesis of the *E. coli* enzymes is at the transcriptional level due to depletion of the regulatory metabolite formate (Rossmann et al., 1991). Due to the fact that HupSL is naturally associated with a formate dehydrogenase-like enzyme, OmeAB (Kublik et al., 2016; Hartwig et al., 2017), we wished to examine the influence of the Fdh-O and Fdh-N enzymes, which are phylogenetically related to OmeAB, on HupSL enzyme activity. Initially, we introduced into strain FTD147 a mutation in the *selC* gene, which encodes the selenocysteinyl-$tRNA_{Sec}$ necessary for translation of special UGA codons as selenocyteine, and which, when deleted, renders all Fdhs inactive (Leinfelder et al., 1988). This would provide information on whether HupSL enzyme activity was influenced by defects in formate metabolism. The left panel shown in **Figure 3** shows a control for HupSL activity revealing that is was readily detectable in strain FTD150 (Δ*hyaB*Δ*hybC*Δ*hycE*Δ*hyfG*), which is identical to strain FTD147 with the exception that the gene encoding the catalytic subunit of Hyd-4 (Andrews et al., 1997) is also deleted (Redwood et al., 2008). Thus, both FTD150 and FTD147 yield an identical phenotype with regard to the heterologous HupSL activity (see also below). Analysis of an extract of the FTD147 Δ*selC* mutant revealed that no HupSL activity was detectable (**Figure 3** right panel). The lack of *selC* was confirmed by the absence of the H_2:BV oxidoreductase activity associated with Fdh-N/O in the strain (Soboh et al., 2011). This result confirms that HupSL enzyme activity is linked to formate metabolism, most likely through one of the formate dehydrogenases (Fdh) the bacterium synthesizes under anaerobic conditions. Introduction of a mutation in *selB*, which encodes the special translation factor required to decode the UGA codon as selenocysteine (Forchhammer et al., 1989), into FTD150 also revealed a similar lack of HupSL activity (data not shown), confirming that the phenotype was due to a lack of selenocysteine incorporation.

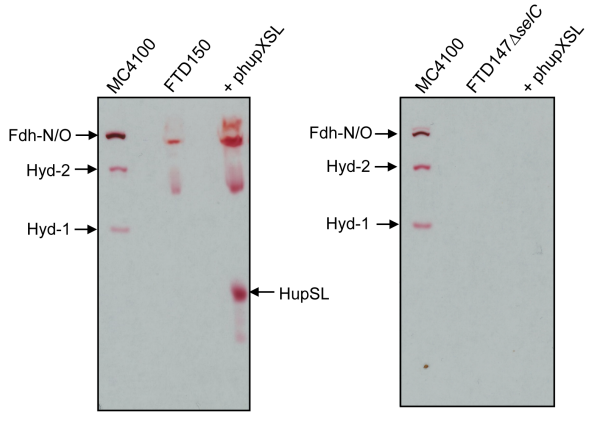

FIGURE 3 | Appearance of HupSL enzyme activity is dependent on a functional selenocysteine biosynthetic apparatus. Crude extracts (100 μg of protein, except M4100 where 30 μg of protein were applied) of the indicated strains were separated in native-PAGE and stained for hydrogenase enzyme activity as described in the legend to **Figure 1**. Strains used include: MC4100 (wild type); FTD150 (Δ*hyaB*Δ*hybC*Δ*hycE* Δ*hyfG*); FTD147Δ*selC* (Δ*hyaB*Δ*hybC*Δ*hycE* Δ*selC*).

In-Gel HupSL Activity Depends on the Fdh-H Enzyme

Dependence on the selenocysteine biosynthetic machinery for appearance of HupSL enzyme activity suggests an involvement of one or more of the three Fdhs present in *E. coli*. To determine which of the three Fdhs is required for the appearance of heterologous HupSL activity, we constructed a series of strains (see **Table 1**) lacking one or more of the genes encoding the catalytic subunit of FdnG (of Fdh-N), FdoG (of Fdh-O), or FdhF (of Fdh-H) (Pinske and Sawers, 2016; **Figure 4**). Strain FTD150, which lacked all four hydrogenases and the quadruple and quintuple mutants of FTD147, which lacked Hyd-1, Hyd-2, Hyd-3 as well as either or both respiratory Fdhs (Fdh-N and Fdh-O), retained fully active HupSL (**Figure 4**). Hydrogenase activity in extracts derived from FTD147Δ*fdnG*Δ*fdoG* with plasmid phupXSL was approximately 60 mU, while the strain without plasmid had approximately half this activity (**Table 2**). Exposure of the crude extract from FTD147Δ*fdnG*Δ*fdoG* transformed with phupXSL to air resulted in a similar 50–60% reduction in hydrogenase activity as was observed with FTD147 containing phupXSL (**Table 2**). This result confirms that HupSL is oxygen-labile (Hartwig et al., 2015b).

The only strains that lacked a detectable HupSL enzyme activity band were those that lacked the *fdhF* gene, which encodes the Fdh-H component of the FHL complex (**Figure 4**). Assay of hydrogenase activity in extracts derived from FTD147Δ*fdhF* + phupXSL failed to show HupSL-dependent hydrogenase activity

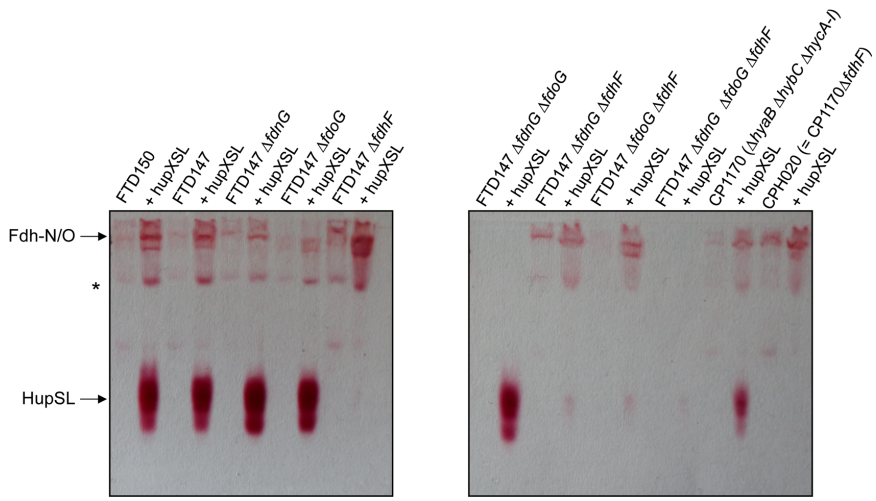

FIGURE 4 | Only strains lacking Fdh-H, the product of the *fdhF* gene, failed to show HupSL enzyme activity. Crude extracts (90 μg of protein) of the indicated strains were separated in native-PAGE and stained for hydrogenase enzyme activity as described in the legend to **Figure 1**. The asterisk denotes a fast-migrating form of the Fdh-O enzyme (Hartwig et al., 2015a). Strains used include: FTD147 (Δ*hyaB*Δ*hybC*Δ*hycE*), plus its deletion derivatives; FTD150 (Δ*hyaB*Δ*hybC*Δ*hycE* Δ*hyfG*); CP1170 (Δ*hyaB*Δ*hybC*Δ*hycA-I*); CPH020 (Δ*hyaB*Δ*hybC*Δ*hycA-I*Δ*fdhF*).

(**Table 2**). These findings indicate that for full HupSL activity to be manifested, an active Fdh-H enzyme is required.

In order to determine what the link between the appearance of HupSL enzyme activity and Fdh-H might be, we first performed a western blot using anti-HupX antibodies and with crude extracts derived from some of the strains shown in **Figure 4**. Surprisingly, HupX was only detectable in extracts of strains lacking *fdhF*, which encodes the Fdh-H enzyme, and, as expected, only in those strains carrying the phupXSL plasmid (**Figure 5**). This suggests that when Fdh-H was absent, HupX was stably synthesized and

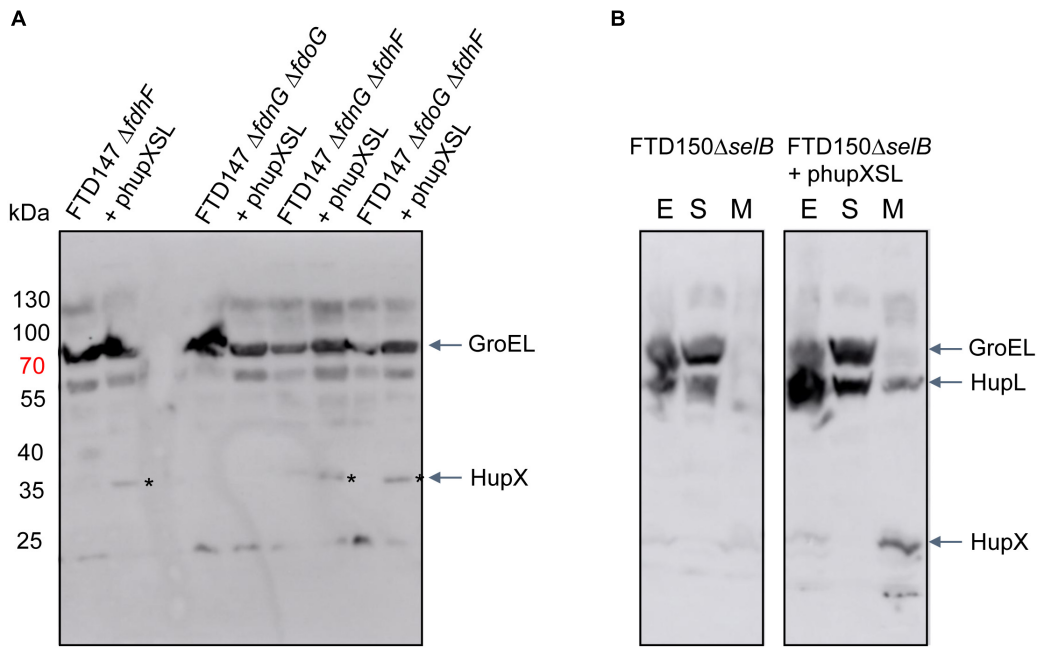

FIGURE 5 | HupX is only detectable in extracts of strains lacking the *fdhF* gene. Western blots using peptide antibodies raised against HupX or HupL are shown in which 50 μg of crude extracts **(A)** or subcellular fractions **(B)** were separated in 10% (w/v) SDS-PAGE. The migration positions of molecular mass marker proteins are shown in kDa. The strong signal migrating around 70 kDa represents GroEL, which cross-reacted with the HupX antibodies, and acted as a protein loading control. The asterisks denote the HupX polypeptide. In **(B)**, the letters E, S, and M represent crude extract, soluble cytoplasmic fraction and membrane fraction, respectively. Strain used include: deletion derivatives of FTD147 (Δ*hyaB*Δ*hybC*Δ*hycE*); and deletion derivatives of FTD150 (Δ*hyaB*Δ*hybC*Δ*hycE* Δ*hyfG*).

when Fdh-H was present in the cells, HupX became unstable and was presumably degraded.

The Influence of Fdh-H on HupSL Activity Is Indirect via the Ferredoxin-Like Proteins HupX and HycB

To examine whether HupX might influence HupSL activity, plasmids phupSL and phupXSL, both encoding HupL, HupS and the endoprotease HoxM, but only the latter also encoding HupX (**Figure 1A**), were introduced into strains FTD147 and FTD147Δ*fdhF* and enzyme activity was compared after anaerobic growth with glucose (**Figure 6A**). The products of both plasmids in strain FTD147Δ*fdhF* showed a strongly reduced activity of HupSL compared with the *fdhF*$^+$ strain FTD147. This result indicates that the dependence on Fdh-H for HupSL activity was retained in the absence of HupX.

A recent study in *E. coli* identified a flexible interaction network of ferredoxin-like proteins with Fdh-H, including its small, electron-transferring subunit, HycB (Pinske, 2018). HycB and HupX belong to this family but share only 24% amino acid identity (38% similarity) in a MuscleWS alignment. The HupX protein, however, cannot functionally replace HycB in formate-dependent BV reduction (data not shown). Due to the link between HupSL activity and Fdh-H demonstrated above, we therefore examined whether the presence of HycB influenced HupSL's ability to reduce BV. To do this, we analyzed HupSL activity in strain CP1170 (Δ*hyaB,* Δ*hybC,* Δ*hycA-I*), which is similar to FTD147 (Δ*hyaB,* Δ*hybC,* Δ*hycE*) with the exception that the complete *hyc* operon is deleted in CP1170, rather than only the *hycE* gene (**Table 1**). Introduction of plasmid phupXSL into CP1170 and its Δ*fdhF* derivative CPH020 (Δ*hyaB*Δ*hybC*Δ*hycA-I*Δ*fdhF*) (**Table 1**), revealed that the dependence on Fdh-H for HupSL activity was retained (**Figure 4**, right side of right panel). However, introduction of plasmid phupSL (lacking *hupX*) into CPH020 (CP1170 Δ*fdhF*) revealed that HupSL activity in native PAGE was no longer reduced in the absence of Fdh-H (**Figure 6B**, lane 1, right panel). Introduction of phupSL into strain CPH008 (Δ*hycA-I,* Δ*fdhF*) in which Hyd-1 and Hyd-2 are still active, but all structural components of the FHL complex are missing, demonstrated that HupSL activity was retained, and even slightly more intense (**Figure 6B**, lane 2 left panel). As a final control, we analyzed HupSL activity after introduction of phupSL into strain RT2 (Δ*hyaB*Δ*hybC*Δ*hycA-I*Δ*fdhE*Δ*pflA*), which lacks Hyd-1, Hyd-2 and Hyd-3, as well as Fdh-N/O (through the *fdhE* mutation; Mandrand-Berthelot et al., 1988; Lüke et al., 2008) and the formate-inducible Fdh-H, due to the lack of active PflB (due to the *pflA* mutation), which is required for formate production (Sawers and Böck, 1988; Rossmann et al., 1991). This strain was chosen because it uses a different combination of mutations to generate the same phenotype, i.e., no hydrogenase or formate dehydrogenase enzymes, and no HycB protein. HupSL activity was also retained in this genetic background confirming that strains devoid of HupX and HycB exhibit HupSL- and H_2-dependent reduction of BV (**Figure 6B**, lane 1).

Surprisingly, however, when phupSL was introduced into strain RM220 (Δ*pflAB*), which generates considerably reduced levels of formate under respiratory conditions (Suppmann and

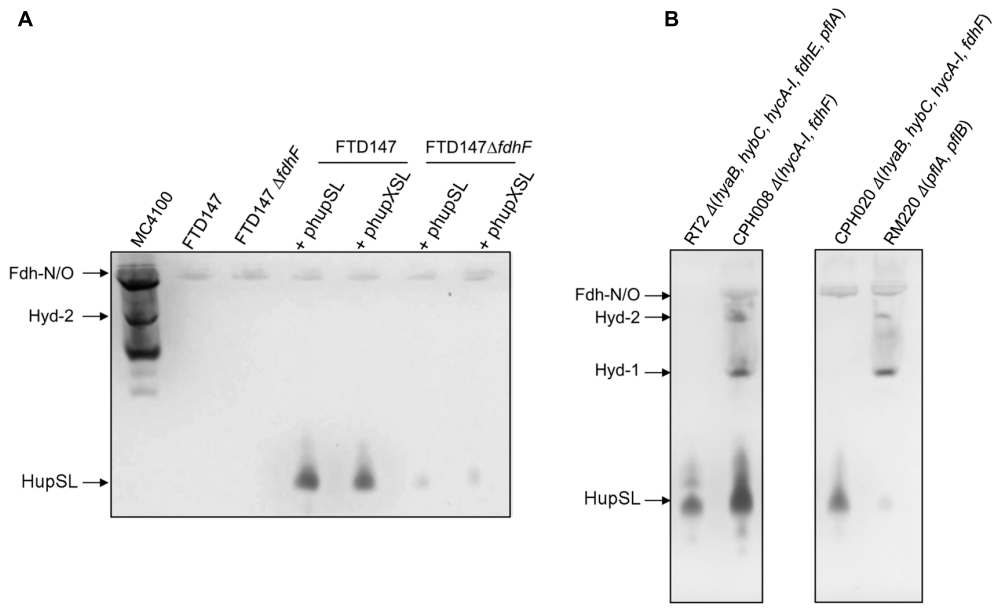

FIGURE 6 | Deletion of the *hycA-I* operon restores HupSL activity in a *fdhF* mutant. **(A)** Crude extracts derived (approximately 60 μg of protein) from the indicated strains after growth in M9 minimal medium with 0.8% (w/v) glucose were separated in native-PAGE and stained for hydrogenase enzyme activity, as described in the legend to **Figure 1**. In **(B)**, strains were transformed with plasmid phupSL. The migration positions of the respective hydrogen-oxidizing enzymes are indicated. Strain used include: MC4100 represents wild type; FTD147 (Δ*hyaB*Δ*hybC*Δ*hycE*); FTD147 Δ*fdhF*; RT2 (Δ*hyaB*Δ*hybC*Δ*hycA-I*Δ*fdhE*Δ*pflA*); CPH008 (Δ*hycA-I* Δ*fdhF*); CPH020 (Δ*hyaB*Δ*hybC*Δ*hycA-I*Δ*fdhF*); RM220 (Δ*pflA*Δ*pflB*).

Sawers, 1994), and thus expresses only low levels of the formate-inducible *hyc* operon (Rossmann et al., 1991), the anticipated high activity of HupSL was not observed (**Figure 6B**, lane 4). This result indicates that even the low levels of HycB produced in this strain (Rossmann et al., 1991) are likely sufficient to inhibit HupSL activity.

DISCUSSION

In this study, we analyzed how the fermentative metabolism of the *E. coli* host influenced the redox dye-reducing activity of a heterologously synthesized hydrogen-uptake [NiFe]-hydrogenase from the *Chloroflexi* phylum. We had previously demonstrated that the host's Hyp-maturation machinery was capable of recognizing the large subunit precursor pre-HupL and of successfully introducing the bimetallic [NiFe]-cofactor, generating active enzyme (Hartwig et al., 2015b). We also showed in that particular study that the HupSL hydrogenase had H_2:BV oxidoreductase activity, which could be identified after anaerobic native-PAGE. Here we made the surprising discovery that the appearance of this HupSL enzyme activity was apparently dependent on whether the host's Fdh-H enzyme was synthesized or not. Under conditions favoring synthesis of Fdh-H, HupSL activity was observed, while in strains unable to synthesize Fdh-H, due to a deletion of the *fdhF* structural gene or the selenocysteine insertion machinery, no, or substantially reduced, activity was detected. Notably, however, this lack of enzyme activity did not result from a lack of synthesis of the HupSL enzyme, but rather appears to be due to an inactivation of the enzyme.

A recent study revealed that Fdh-H interacts with at least three electron-transferring small subunits, all of which belong to the ferredoxin-like family of electron-transfer proteins and possibly facilitate the coupling of Fdh-H with different enzyme complexes (Pinske, 2018). We currently interpret our data to indicate that the apparent dependence on Fdh-H for HupSL activity is, in fact, indirect and likely due to Fdh-H sequestering these small subunits, in particular HycB of the FHL complex. Notably, the HupX protein, which is presumed to mediate electron transfer within the Hup-Ome-Rdh supercomplex in the natural host *D. mccartyi* (Schubert et al., 2018), also belongs to the ferredoxin-like superfamily and this protein's ability to interact with the HupSL heterodimer also appears to be influenced by the presence of Fdh-H. If Fdh-H is either genotypically or phenotypically (e.g., through strongly reduced formate synthesis; Rossmann et al., 1991) absent, the ferredoxin-like proteins HupX or HycB remain consequently unbound within the cell. We suggest that if HupX is also absent, HycB can transiently interact with or modulate the HupSL enzyme within the cell prior to separation in the native-PAGE, rendering the enzyme inactive. This inactivity could result from a loss of the ability of the heterodimer to reduce or interact with BV in the presence of H_2. Alternatively, these ferredoxin-like proteins might act by sequestering the HupSL complex resulting in an inactive complex in the native-PAGE; or indeed a combination of both effects might be the cause (**Figure 7**). The consequence would be that HupSL activity becomes visible in the absence of HycB despite simultaneous absence of Fdh-H. The redox-potentials of the ferredoxin-like proteins have not yet been determined.

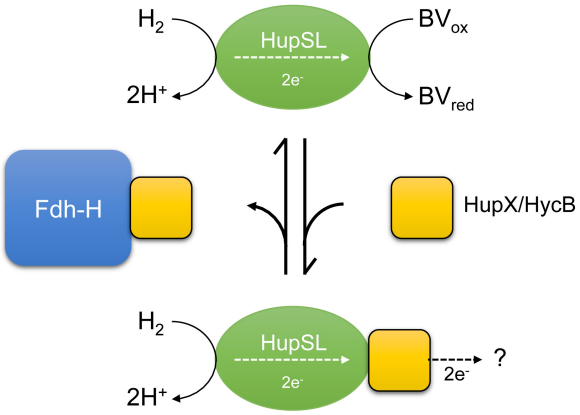

FIGURE 7 | A schematic depiction of the current interpretation of our data is shown. The hypothesis states that the HupSL heterodimer is capable of interacting with and reducing BV and if HupX or HycB are free and not sequestered by Fdh-H they prevent HupSL transferring electrons to BV and instead deliver them to currently unknown acceptor complexes, or possibly to the quinone pool (?). HupX has been shown to interact with HupSL (Hartwig et al., 2017; Seidel et al., 2018), while this has not been so far shown for HycB.

The model shown in **Figure 7** presents a working hypothesis for how we currently interpret our data. Under fermentative growth conditions Fdh-H is present and is available to interact with HycB. The presence of Fdh-H also prevents HupX interacting with HupSL, possibly forming an interaction with HupX, allowing the HupSL heterodimer to interact with and reduce BV.

How does an ability to interact with HupX, and possibly HycB, interfere with electron transfer to BV by HupSL? The redox dye BV can accept electrons directly from the electron-transferring subunit HupS, as evidenced by the fact that deletion of the *hupX* gene does not significantly affect H_2-dependent reduction of BV by HupSL. Moreover, previous mass spectrometric analysis of the Hup activity band isolated after native-PAGE revealed mainly HupL and HupS to be present, suggesting that HupX's interaction with the heterodimer is weak or transient (Hartwig et al., 2015b). Moreover, in the natural host *D. mccartyi*, HupX preferentially associates with OmeAB, the formate dehydrogenase homolog, and reductive dehydrogenases rather than with HupSL (Hartwig et al., 2015b; Seidel et al., 2018; Dragomirova and Sawers, unpublished observations), which supports the suggestion that the affinity of HupX for HupSL is low. We also observed using antibodies raised against HupX that it is only readily detectable in the membrane fraction of cells that lack Fdh-H, suggesting that when Fdh-H is present it is more readily degraded. How this apparent degradation is controlled is currently unclear.

The HupS subunit encodes a functional Tat-signal peptide allowing its transport across the cytoplasmic membrane (Hartwig et al., 2015b). Together with HupX, the HupSL complex could be sufficiently anchored in the membrane to transfer the electrons

derived from oxidation of H_2 to the quinone pool, which is also the function of another HupX homolog, the HybA protein of *E. coli* Hyd-2 (Pinske et al., 2015; Beaton et al., 2018).

Support for the oxidative inactivation of HupSL was provided by the demonstration of inactivation of the enzyme complex after growth of the *E. coli* host under respiratory conditions, with either O_2 ($E^{o\prime}$ = +830 mV), NO_3^- ($E^{o\prime}$ = +420 mV), or fumarate ($E^{o\prime}$ = 0 mV) as electron acceptor. We have only been able to detect HupSL activity after fermentative growth ($E^{o\prime}$ = -415 mV), strongly suggesting that the enzyme retains activity only under strongly reducing conditions, which are also likely to be those prevailing in the environmental conditions where *D. mccartyi* is found (Löffler et al., 2013).

These studies thus provide a platform to study how heterologously synthesized hydrogenases can be integrated into the host's anaerobic metabolism. Clearly, this work is at an early stage but one of the next steps will be to examine whether electrons derived from H_2 oxidation can be coupled to reduction of *E. coli*-typical electron acceptors, e.g., fumarate. Initial studies examining hydrogen-driven fumarate reduction by HupXLS yielded first indications that a weak, but unfortunately so far irreproducible, activity was detectable (Schwoch et al., unpublished data). Optimization of Hup enzyme synthesis and membrane integration will likely be required for this approach to be fruitful.

Because *D. mccartyi* species are not amenable to large-scale biochemical analysis, and are currently genetically intractable, using the *E. coli* Hyd- and Fdh-negative host strains developed here will provide a means of studying the biochemical mechanism(s) underlying the loss of HupSL activity in response to oxidizing redox conditions and whether this effect is linked to a particular iron-sulfur cluster, or clusters, in HupS, or whether the bimetallic cofactor in HupL is the target of irreversible inactivation. A recent study by Hartmann et al. (2018) indicates that, at least for certain [NiFe]-hydrogenases, the $NiFe(CN)_2CO$ cofactor is not sensitive to oxidative conditions, suggesting that it might indeed be the electron-transfer pathway that is disrupted by non-reducing redox potentials.

AUTHOR CONTRIBUTIONS

ND, PR, SS, SH, and CP designed and performed the experiments and analyzed the data. CP and RS conceived the study, interpreted the data and drafted the manuscript. All authors read and approved the manuscript.

FUNDING

This work was funded by the Deutsche Forschungsgemeinschaft as part of the research unit FOR1530: "Anaerobic Biological Dehalogenation: Organisms, Biochemistry, and (Eco)physiology" granted to RS and by the priority program SPP1927 "Iron Sulfur for Life" granted to both CP and RS. We acknowledge the financial support of the Open Access Publication Fund of the Martin Luther University Halle-Wittenberg.

REFERENCES

Andrews, S. C., Berks, B. C., McClay, J., Ambler, A., Quail, M. A., Golby, P., et al. (1997). A 12-cistron *Escherichia coli* operon (*hyf*) encoding a putative proton-translocating formate hydrogenlyase system. *Microbiology* 143, 3633–3647. doi: 10.1099/00221287-143-11-3633

Baba, T., Ara, T., Hasegawa, M., Takai, Y., Okumura, Y., Baba, M., et al. (2006). Construction of *Escherichia coli* K-12 in-frame, single-gene knockout mutants: the Keio collection. *Mol. Syst. Biol.* 2:0008. doi: 10.1038/msb4100050

Ballantine, S. P., and Boxer, D. H. (1985). Nickel-containing hydrogenase isoenzymes from anaerobically grown *Escherichia coli* K-12. *J. Bacteriol.* 163, 454–459.

Beaton, S. E., Evans, R. M., Finney, A. J., Lamont, C. M., Armstrong, F. A., Sargent, F., et al. (2018). The structure of hydrogenase-2 from *Escherichia coli*: implications for H2-driven proton pumping. *Biochem. J.* 475, 1353–1370. doi: 10.1042/BCJ20180053

Begg, Y., Whyte, J., and Haddock, B. A. (1977). The identification of mutants of *Escherichia coli* deficient in formate dehydrogenase and nitrate reductase activities using dye indicator plates. *FEMS Microbiol. Lett.* 2, 47–50. doi: 10.1111/j.1574-6968.1977.tb00905.x

Böck, A., King, P., Blokesch, M., and Posewitz, M. (2006). Maturation of hydrogenases. *Adv. Microb. Physiol.* 51, 1–71. doi: 10.1016/S0065-2911(06)51001-X

Casadaban, M. J. (1976). Transposition and fusion of the *lac* genes to selected promoters in *Escherichia coli* using bacteriophage lambda and Mu. *J. Mol. Biol.* 104, 541–555. doi: 10.1016/0022-2836(76)90119-4

Cherepanov, P. P., and Wackernagel, W. (1995). Gene disruption in *Escherichia coli*: TcR and KmR cassettes with the option of Flp-catalyzed excision of the antibiotic-resistance determinant. *Gene* 158, 9–14. doi: 10.1016/0378-1119(95)00193-A

Dubini, A., Pye, R., Jack, R., Palmer, T., and Sargent, F. (2002). How bacteria get energy from hydrogen: a genetic analysis of periplasmic hydrogen oxidation in *Escherichia coli*. *Int. J. Hydrogen Energy* 27, 1413–1420. doi: 10.1016/S0360-3199(02)00112-X

Fincker, M., and Spormann, A. M. (2017). Biochemistry of catabolic reductive dehalogenation. *Annu. Rev. Biochem.* 86, 357–386. doi: 10.1146/annurev-biochem-061516-044829

Forchhammer, K., Leinfelder, W., and Böck, A. (1989). Identification of a novel translation factor necessary for the incorporation of selenocysteine into protein. *Nature* 342, 453–456. doi: 10.1038/342453a0

Hartmann, S., Frielingsdorf, S., Ciaccafava, A., Lorent, C., Fritsch, J., Siebert, E., et al. (2018). O2-tolerant H2 activation by a solitary large subunit of a [NiFe] hydrogenase. *Biochemistry* 57, 5339–5349. doi: 10.1021/acs.biochem.8b00760

Hartwig, S., Dragomirova, N., Kublik, A., Türkowsky, D., von Bergen, M., Lechner, U., et al. (2017). A H2-oxidizing, 1,2,3-trichlorobenzene-reducing multienzyme complex isolated from the obligately organohalide-respiring bacterium *Dehalococcoides mccartyi* strain CBDB1. *Environ. Microbiol. Rep.* 9, 618–625. doi: 10.1111/1758-2229.12560

Hartwig, S., Pinske, P., and Sawers, R. G. (2015a). Chromogenic assessment of the three molybdo-selenoprotein formate dehydrogenases in *Escherichia coli*. *Biochem. Biophys. Rep.* 1, 62–67. doi: 10.1016/j.bbrep.2015.03.006

Hartwig, S., Thomas, C., Krumova, N., Quitzke, V., Türkowsky, D., Jehmlich, N., et al. (2015b). Heterologous complementation studies in *Escherichia coli* with the Hyp accessory protein machinery from *Chloroflexi* provide insight into [NiFe]-hydrogenase large subunit recognition by the HypC protein family. *Microbiology* 161, 2204–2219. doi: 10.1099/mic.0.000177

Hormann, K., and Andreesen, J. R. (1989). Reductive cleavage of sarcosine and betaine by *Eubaterium acidaminophilum* via enzyme systems different from glycine reductase. *Arch. Microbiol.* 153, 50–59. doi: 10.1007/BF00277541

Kaiser, M., and Sawers, G. (1994). Pyruvate formate-lyase is not essential for nitrate respiration by *Escherichia coli*. *FEMS Microbiol. Lett.* 117, 163–168. doi: 10.1111/j.1574-6968.1994.tb06759.x

Kube, M., Beck, A., Zinder, S. H., Kuhl, H., Reinhardt, R., and Adrian, L. (2005). Genome sequence of the chlorinated compound-respiring bacterium *Dehalococcoides* species strain CBDB1. *Nat. Biotechnol.* 23, 1269–1273. doi: 10.1038/nbt1131

Kublik, A., Deobald, D., Hartwig, S., Schiffmann, C. L., Andrades, A., von Bergen, M., et al. (2016). Identification of a multiprotein reductive dehalogenase complex in *Dehalococcoides mccartyi* strain CBDB1 suggests a protein-dependent respiratory electron transport chain obviating quinone involvement. *Environ. Microbiol.* 18, 3044–3056. doi: 10.1111/1462-2920.13200

Laemmli, U. (1970). Cleavage of structural proteins during the assembly of the head of bacteriophage T4. *Nature* 227, 680–685. doi: 10.1038/227680a0

Leinfelder, W., Zehelein, E., Mandrand-Berthelot, M.-A., and Böck, A. (1988). Gene for a novel tRNA species that accepts L-serine and cotranslationally inserts selenocysteine. *Nature* 331, 723–725. doi: 10.1038/331723a0

Löffler, F. E., Yan, J., Ritalahti, K. M., Adrian, L., Edwards, E. A., Konstantinidis, K. T., et al. (2013). *Dehalococcoides mccartyi* gen. nov., sp. nov., obligately organohalide-respiring anaerobic bacteria relevant to halogen cycling and bioremediation, belong to a novel bacterial class, *Dehalococcoidia* classis nov., order *Dehalococcoidales ord*. nov. and family *Dehalococcoidaceae fam*. nov., within the phylum *Chloroflexi*. *Int. J. Syst. Evol. Microbiol.* 63, 625–635. doi: 10.1099/ijs.0.034926-0

Lowry, O., Rosebrough, N., Farr, A., and Randall, R. (1951). Protein measurement with the Folin phenol reagent. *J. Biol. Chem.* 193, 265–275.

Lüke, I., Butland, G., Moore, K., Buchanan, G., Lyall, V., Fairhurst, S. A., et al. (2008). Biosynthesis of the respiratory formate dehydrogenases from *Escherichia coli*: characterization of the FdhE protein. *Arch. Microbiol.* 90, 685–696. doi: 10.1007/s00203-008-0420-4

Mandrand-Berthelot, M.-A., Couchoux-Luthaud, G., Santini, C.-L., and Giordano, G. (1988). Mutants of *Escherichia coli* specifically defective in respiratory formate dehydrogenase activity. *J. Gen. Microbiol.* 134, 3129–3139.

Miller, J. (1972). *Experiments in Molecular Genetics*. Cold Spring Harbor, NY: Cold Spring Harbor Laboratory.

Pinske, C. (2018). The ferredoxin-like proteins HydN and YsaA enhance redox dye-linked activity of the formate dehydrogenase H component of the formate hydrogenlyase complex. *Front. Microbiol.* 9:1238. doi: 10.3389/fmicb.2018.01238

Pinske, C., Jaroschinsky, M., Linek, S., Kelly, C. L., Sargent, F., and Sawers, R. G. (2015). Physiology and bioenergetics of [NiFe]-hydrogenase 2-catalyzed H2-consuming and H2-producing reactions in *Escherichia coli*. *J. Bacteriol.* 197, 296–306. doi: 10.1128/JB.02335-14

Pinske, C., Jaroschinsky, M., Sargent, F., and Sawers, G. (2012). Zymographic differentiation of [NiFe]-hydrogenases 1, 2 and 3 of *Escherichia coli* K-12. *BMC Microbiol.* 12:134. doi: 10.1186/1471-2180-12-134

Pinske, C., Krüger, S., Soboh, B., Ihling, C., Kuhns, M., Braussemann, M., et al. (2011). Efficient electron transfer from hydrogen to benzyl viologen by the [NiFe]-hydrogenases of *Escherichia coli* is dependent on the coexpression of the iron-sulfur cluster-containing small subunit. *Arch. Microbiol.* 193, 893–903. doi: 10.1007/s00203-011-0726-5

Pinske, C., and Sargent, F. (2016). Exploring the directionality of *Escherichia coli* formate hydrogenlyase: a membrane-bound enzyme capable of fixing carbon dioxide to organic acid. *Microbiologyopen* 9:1238. doi: 10.1002/mbo3.365

Pinske, C., and Sawers, R. G. (2016). Anaerobic formate and hydrogen metabolism. *EcoSal Plus*. doi: 10.1128/ecosalplus.ESP-0011-2016

Redwood, M. D., Mikheenko, I., Sargent, F., and Macaskie, L. (2008). Dissecting the roles of *Escherichia coli* hydrogenases in biohydrogen production. *FEMS Microbiol. Lett.* 278, 48–55. doi: 10.1111/j.1574-6968.2007.00966.x

Rossmann, R., Sawers, G., and Böck, A. (1991). Mechanism of regulation of the formate-hydrogenlyase pathway by oxygen, nitrate and pH: definition of the formate regulon. *Mol. Microbiol.* 5, 2807–2814. doi: 10.1111/j.1365-2958.1991.tb01989.x

Sambrook, J., Fritsch, E. F., and Maniatis, T. (1989). *Molecular Cloning: A Laboratory Manual*, 2nd Edn. Cold Spring Harbor, NY: Cold Spring Harbor Laboratory.

Sargent, F., Ballantine, S. P., Rugman, P. A., Palmer, T., and Boxer, D. H. (1998). Reassignment of the gene encoding the *Escherichia coli* hydrogenase 2 small subunit: identification of a soluble precursor of the small subunit in a hypB mutant. *Eur. J. Biochem.* 255, 746–754. doi: 10.1046/j.1432-1327.1998.2550746.x

Sawers, G., and Böck, A. (1988). Anaerobic regulation of pyruvate formate-lyase from *Escherichia coli* K-12. *J. Bacteriol.* 170, 5330–5336. doi: 10.1128/jb.170.11.5330-5336.1988

Sawers, R. G., Ballantine, S. P., and Boxer, D. H. (1985). Differential expression of hydrogenase isoenzymes in *Escherichia coli* K-12: evidence for a third isoenzyme. *J. Bacteriol.* 164, 1324–1331.

Schipp, C. J., Marco-Urrea, E., Kublik, A., Seifert, J., and Adrian, L. (2013). Organic cofactors in the metabolism of *Dehalococcoides mccartyi* strains. *Philos. Trans. R. Soc. Lond. B Biol. Sci.* 368:20120321. doi: 10.1098/rstb.2012.0321

Schubert, T., Adrian, L., Sawers, R. G., and Diekert, G. (2018). Organohalide respiratory chains: composition, topology, and key enzymes. *FEMS Microbiol. Ecol.* 94:4. doi: 10.1093/femsec/fiy035

Seidel, K., Kühnert, J., and Adrian, L. (2018). The complexome of *Dehalococcoides mccartyi* reveals its organohalide respiration-complex is modular. *Front. Microbiol.* 9:1130. doi: 10.3389/fmicb.2018.01130

Soboh, B., Pinske, C., Kuhns, M., Waclawek, M., Ihling, C., Trchounian, K., et al. (2011). The respiratory molybdo-selenoprotein formate dehydrogenases of *Escherichia coli* have hydrogen: benzyl viologen oxidoreductase activity. *BMC Microbiol.* 11:173. doi: 10.1186/1471-2180-11-173

Suppmann, B., and Sawers, G. (1994). Isolation and characterisation of hypophosphite-resistant mutants of *Escherichia coli*: identification of the FocA protein, encoded by the *pfl* operon, as a putative formate transporter. *Mol. Microbiol.* 11, 965–982. doi: 10.1111/j.1365-2958.1994.tb00375.x

Towbin, H., Staehelin, T., and Gordon, J. (1979). Electrophoretic transfer of proteins from polyacrylamide gels to nitrocellulose sheets: procedure and some applications. *Proc. Natl. Acad. Sci. U.S.A.* 76, 4350–4354. doi: 10.1073/pnas.76.9.4350

Conflict of Interest Statement: The authors declare that the research was conducted in the absence of any commercial or financial relationships that could be construed as a potential conflict of interest.

frontiers in Microbiology

REVIEW
published: 23 November 2018
doi: 10.3389/fmicb.2018.02873

Microbially Mediated Hydrogen Cycling in Deep-Sea Hydrothermal Vents

*Nicole Adam and Mirjam Perner**

Geomicrobiology, GEOMAR Helmholtz Centre for Ocean Research Kiel, Kiel, Germany

Deep-sea hydrothermal vents may provide one of the largest reservoirs on Earth for hydrogen-oxidizing microorganisms. Depending on the type of geological setting, hydrothermal environments can be considerably enriched in hydrogen (up to millimolar concentrations). As hot, reduced hydrothermal fluids ascend to the seafloor they mix with entrained cold, oxygenated seawater, forming thermal and chemical gradients along their fluid pathways. Consequently, in these thermally and chemically dynamic habitats biochemically distinct hydrogenases (adapted to various temperature regimes, oxygen and hydrogen concentrations) from physiologically and phylogenetically diverse Bacteria and Archaea can be expected. Hydrogen oxidation is one of the important inorganic energy sources in these habitats, capable of providing relatively large amounts of energy (237 kJ/mol H_2) for driving ATP synthesis and autotrophic CO_2 fixation. Therefore, hydrogen-oxidizing organisms play a key role in deep-sea hydrothermal vent ecosystems as they can be considerably involved in light-independent primary biomass production. So far, the specific role of hydrogen-utilizing microorganisms in deep-sea hydrothermal ecosystems has been investigated by isolating hydrogen-oxidizers, measuring hydrogen consumption (*ex situ*), studying hydrogenase gene distribution and more recently by analyzing metatranscriptomic and metaproteomic data. Here we summarize this available knowledge and discuss the advent of new techniques for the identification of novel hydrogen-uptake and -evolving enzymes from hydrothermal vent microorganisms.

Keywords: hydrogen cycling, hydrogen consumption, hydrogenases, hydrogen oxidizers, hydrothermal vent

OPEN ACCESS

Edited by:
Chris Greening,
Monash University, Australia

Reviewed by:
Xiyang Dong,
University of Calgary, Canada
Carlo Robert Carere,
University of Canterbury, New Zealand

***Correspondence:**
Mirjam Perner
mperner@geomar.de

Specialty section:
This article was submitted to Microbial Physiology and Metabolism, a section of the journal Frontiers in Microbiology

Received: *03 August 2018*
Accepted: *08 November 2018*
Published: *23 November 2018*

Citation:
Adam N and Perner M (2018) Microbially Mediated Hydrogen Cycling in Deep-Sea Hydrothermal Vents. Front. Microbiol. 9:2873. doi: 10.3389/fmicb.2018.02873

INTRODUCTION

Hydrogen conversion, the reversible reaction of molecular hydrogen (H_2) to protons and electrons, plays a major role for metabolic processes in microbial cells: generally, energy conservation and the recycling of reducing equivalents (in microbial fermentation or light-dependent photosynthesis) is accomplished by enzymatic hydrogen evolution (Vignais and Billoud, 2007; Hallenbeck, 2009). Enzymatically catalyzed hydrogen oxidation is widely distributed among prokaryotes, and can power the synthesis of energy-rich ATP, which is needed for autotrophic carbon fixation (Dilling and Cypionka, 1990; Bothe et al., 2010; Greening et al., 2016).

The thermal (4°C to several 100s °C) and chemical (e.g., oxidized to reduced) gradients hallmarking deep-sea hydrothermal vent habitats have the potential to host one of the largest reservoirs of physiologically and phylogenetically diverse hydrogen-converting microorganisms

(**Figure 1**, Kelley et al., 2002; Perner et al., 2013b). As the fluids pass through the subsurface, they get enriched in various inorganic compounds, such as reduced minerals, sulfide and hydrogen (**Figure 1**). The actual hydrogen and sulfide concentrations of the emanating fluids strongly depend on the type of host rock underlying the respective vent system and the mixing ratio of seawater and fluids. Hydrothermal end-member fluids of basalt-hosted systems are usually characterized by greater sulfide than hydrogen concentrations, resulting from magma degassing and high-temperature-leaching from enclosing host rocks. In contrast, due to serpentinization processes, end-member fluids of ultramafic-hosted vent systems usually exhibit greater hydrogen (up to 1–10 M) and methane (on mM levels) concentrations than sulfide concentrations (Charlou et al., 2002; Kelley et al., 2005; Haase et al., 2007; Perner et al., 2013b). Correspondingly, sulfide oxidation in the sulfide-rich basalt-hosted and hydrogen oxidation and methanotrophy in the hydrogen-rich ultramafic-hosted systems are estimated to be the predominant sources of metabolic energy available in venting habitats (McCollom, 2007).

Since the discovery of hydrothermal vents in the late 70s (Corliss et al., 1979), numerous hydrogen-oxidizers have been isolated from thermally and chemically distinct deep-sea vent habitats (e.g., Campbell et al., 2006; Miroshnichenko and Bonch-Osmolovskaya, 2006; Nakagawa and Takai, 2008; Hansen and Perner, 2015; Nagata et al., 2017). Although considerable efforts have been undertaken to promote our understanding of the distribution and role of hydrogen-oxidizing organisms in these environments (Nealson et al., 2005; Campbell et al., 2006; Perner et al., 2010, 2013b; Petersen et al., 2011; Adam and Perner, 2018), our knowledge of the overall hydrogen utilization potential and microbial hydrogen pathways still remains limited. This review summarizes the work that has been done on hydrogen-metabolizing microorganisms colonizing hydrothermally influenced environments with respect to their diversity, hydrogen consumption rates in incubation experiments and protein biochemistry. Recent findings in the context of culture-independent metagenomic and metatranscriptomic approaches for the identification of novel hydrogen-converting enzymes are included. Finally, an outlook is given which techniques (e.g., *in situ* experiments) and work are needed to

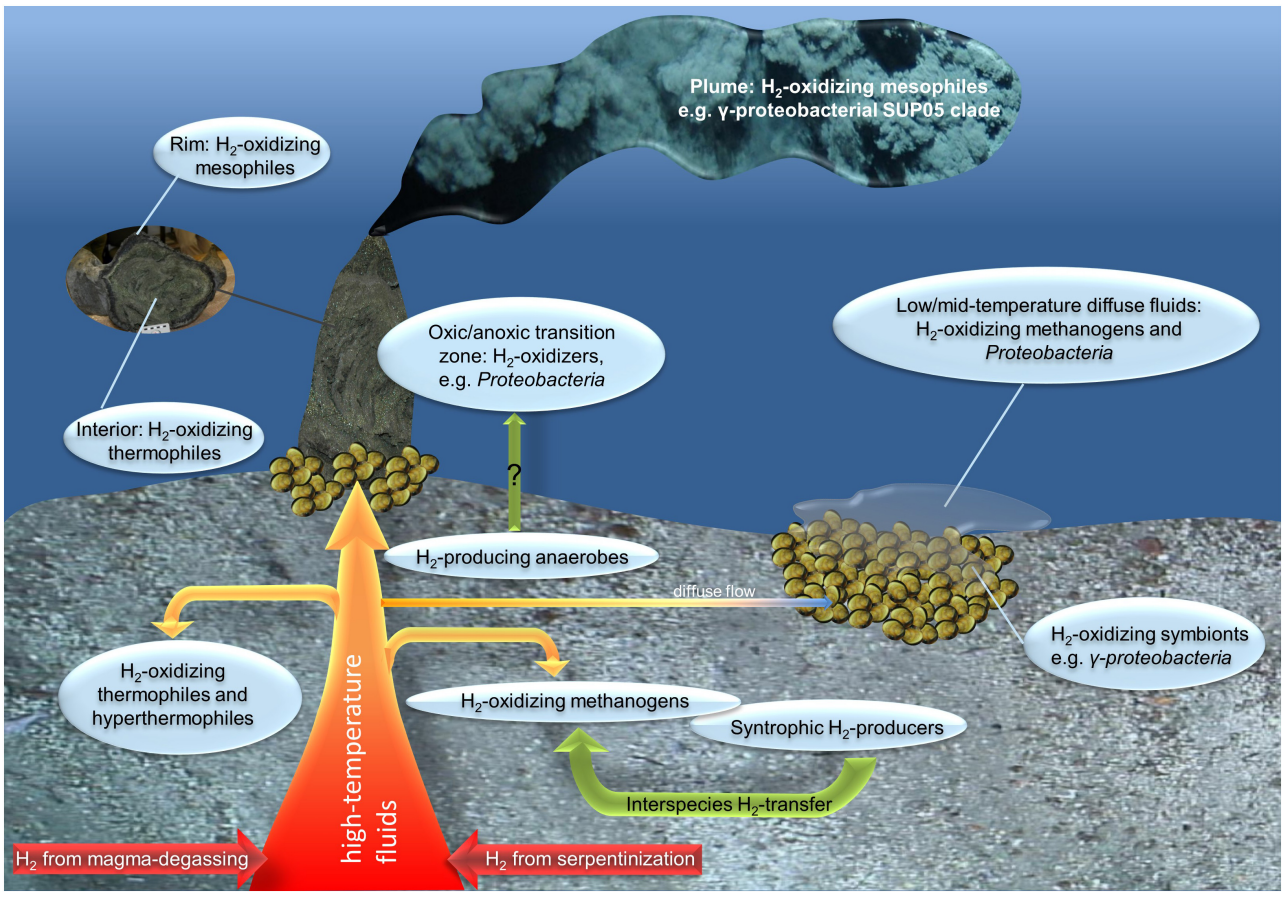

FIGURE 1 | Overview of possible (microbially mediated) hydrogen cycling in hydrothermal vent systems. Hydrothermal emissions emanate from the subsurface either as high-temperature focused fluids causing the typical black or white smoker structures or low- to mid-temperature diffuse fluids (for example from mussel beds). Abiogenic hydrogen sources are displayed in red and orange (hydrothermal fluids) and biogenic hydrogen sources in the shape of green arrows.

advance our understanding of the role that hydrogen-cycling microorganisms play in hydrothermal vents.

HYDROGEN-PRODUCING AND -OXIDIZING MICROORGANISMS

It is well known that hydrogen-producing and -oxidizing microorganisms can coexist or even interact in a variety of anoxic habitats like sediments or intestinal tracts (Chassard and Bernalier-Donadille, 2006). At low hydrogen partial pressures (e.g., <100 Pa), hydrogen can be produced in the course of microbial fermentation processes (Kraemer, 2007; Hallenbeck, 2009) which is then oxidized by hydrogenotrophic microorganisms, especially methanogens. This interspecies hydrogen transfer thereby forms so-called syntrophic communities (hydrogen-producers and –consumers thrive in close proximity) and most likely represents an important hydrogen source in hydrogen-poor habitats (Bryant et al., 1977; Chassard and Bernalier-Donadille, 2006). Since fermentative hydrogen production can already be inhibited at relatively low hydrogen concentrations (i.e., on a nM level) (Wolin, 1976; Hoehler et al., 1998; Hallenbeck, 2009), the role, that microbially produced hydrogen plays in hydrothermal vent systems, remains enigmatic. Even the hydrogen levels of hydrogen-poor hydrothermal vent systems easily exceed those of habitats known to harbor fermentative bacteria like sediments (which are typically below 60 nM) (Novelli et al., 1987; Hoehler et al., 1998; Charlou et al., 2002; Perner et al., 2013b) and thus are likely above the inhibitory limit for biological hydrogen production. This may explain why studies on microbial hydrogen production in deep-sea hydrothermal vent systems have been largely neglected so far. However, hydrogen-evolving heterotrophic Archaea and Bacteria have been identified in hydrothermal fluid incubation experiments (Topcuoglu et al., 2016). The authors posited that in some of the micro niches represented by the culturing conditions, hyperthermophilic *Euryarchaeota* and thermophilic *Firmicutes* produced hydrogen as a waste product during fermentation which was consumed by hydrogenotrophic sulfate-reducing Bacteria or methanogenic Archaea (under distinct temperature regimes) (Topcuoglu et al., 2016). Hydrogenotrophic methanogens can use hydrogen to reduce CO_2 via the reductive acetyl-CoA pathway (Wood-Ljungdahl pathway), thereby forming methane (Ladapo and Whitman, 1990; Thauer, 1998). Acetogenic Bacteria (producing acetate from CO_2) can compete with hydrogenotrophic methanogens in anoxic, hydrogen-rich habitats using the same electron donor (hydrogen) and carbon fixation pathway (Wood Ljungdahl pathway) (Chassard and Bernalier-Donadille, 2006). Due to a lower hydrogen threshold (minimum hydrogen concentration required for hydrogenotrophic growth) and a greater overall energy yield from the conversion of CO_2 to methane, methanogenic Archaea are usually the dominating group in this competition (Ragsdale and Pierce, 2008 and references therein). Moreover, acetogens (and methanogens) can be outcompeted by Bacteria with an even lower hydrogen threshold than methanogens, such as *Campylobacterota*, which are highly abundant at hydrothermal vent sites and take advantage of their versatile metabolisms (for details see below). Therefore, active acetogenic Bacteria are presumably less abundant in venting biotopes and have so far not been the focus of research related to hydrogen utilization in deep-sea hydrothermal vent environments.

Overall, sulfide and thiosulfate oxidation as well as hydrogen oxidation are among the chemosynthetic reactions which provide the greatest energy yields in hydrothermal vent biotopes (Amend and Shock, 2001; Fuchs et al., 2007). Although considerably more energy is yielded through oxidation of sulfide or thiosulfate than through hydrogen oxidation (free standard enthalpies are −797 kJ/mol H_2S vs. −237 kJ/mol H_2 with O_2 as electron acceptor) (**Table 1**, Fuchs et al., 2007), the latter reaction is favorable for autotrophic carbon fixation. Since the redox-potential of hydrogen is more negative than that of the reducing equivalent NAD(P)/H, in contrast to sulfide, a reverse electron transport is not required in conjunction with hydrogen oxidation. Thus, only a third of the energy is required for fixing 1 mol of carbon when oxidizing hydrogen compared to sulfide (1060 kJ for hydrogen vs. 3500 kJ for sulfide) (Heijnen and Van Dijken, 1992). The individual fluid compositions of different hydrothermal systems may even increase this effect:

TABLE 1 | Overall reactions and standard free reaction enthalpies of hydrogen oxidation coupled to different electron acceptors.

Reaction	$\Delta G'^0$	Reference
$2\ H_2 + \mathbf{O_2} \rightarrow 2\ H_2O$	−297 kJ/mol H_2	Fuchs et al., 2007
$5\ H_2 + 2\ \mathbf{NO_3^-} + 2\ H^+ \rightarrow N_2 + 6\ H_2O$	−224.2 kJ/mol H_2	
$H_2 + \mathbf{MnO_2} \rightarrow Mn^{2+} + 2\ OH^-$	−166 kJ/mol H_2	Konhauser, 2006
$0.5\ H_2 + \mathbf{Fe(OH)_3} \rightarrow Fe^{2+} + 2\ OH^- + H_2O$	−110 kJ/mol H_2	
$H_2 + \mathbf{(2/3)CrO_4^{2-}} + (4/3)H^+ \rightarrow (2/3)Cr(OH)_3 + (2/3)\ H_2O$	−98.35 kJ/mol H_2	Liu et al., 2002
$H_2 + \mathbf{UO_2^{2+}} \rightarrow 2H_+ + UO_2$	−92 kJ/mol H_2	Konhauser, 2006
$H_2 + 2\ \mathbf{Co(III)EDTA^-} \rightarrow 2\ Co(II)EDTA^{2-} + 2\ H^+$	−68.5 kJ/mol H_2	Liu et al., 2002
$H_2 + (2/3)\mathbf{TcO4^-} \rightarrow (2/3)TcO2 + (4/3)H_2O$	−66.99 kJ/mol H_2	
$4\ H_2 + \mathbf{SO4^{2-}} \rightarrow H_2S + 2\ OH^- + 2\ H_2O$	−38 kJ/mol H_2	Konhauser, 2006
$4\ H_2 + \mathbf{CO_2} \rightarrow CH_4 + H_2O$	−32.75 kJ/mol H_2	Fuchs et al., 2007
$H_2 + \mathbf{S^0} \rightarrow H_2S$	−28 kJ/mol H_2	Konhauser, 2006

Electron acceptors are indicated by bold letters.

depending on hydrogen and sulfide concentrations as well as other abiotic factors, such as temperature and pressure, thermodynamic models for fluids of ultramafic vent fields predict that between 10 to 18 times more energy per kg of fluid can be yielded by hydrogen oxidation compared to sulfide oxidation (McCollom and Shock, 1997; McCollom, 2007; Petersen et al., 2011). The actual energy yields of the respective oxidation reactions strongly depend on the type of terminal electron acceptor used in the metabolism, where coupled to oxygen reduction the greatest energy amount is gained (**Table 1**, Conrad, 1996). Alternative electron acceptors commonly used by hydrogen-oxidizing microorganisms are sulfate, Fe (III) and nitrate (Vignais and Billoud, 2007), but also elemental sulfur and CO_2 as well as different metals, e.g., Mn (III/IV), U (VI), Cr (VI), Co (III) and Tc (VII), can be reduced by hydrogen-consumers (**Table 1**, Liu et al., 2002; Nakagawa and Takai, 2008). Due to mixing processes with oxygenated, ambient seawater, deep-sea hydrothermal fluids may contain numerous possible electron acceptors (primarily oxygen, nitrate, sulfate, elemental sulfur and iron). Their individual concentrations may vary strongly, depending on the geological setting of the vent system and the seawater mixing ratio.

Since covering all aspects of microbial hydrogen conversion at hydrothermal vents in detail would go beyond the scope of this review, we will here primarily focus on autotrophic hydrogen-oxidizers. Genes encoding hydrogen-oxidizing (or producing) enzymes have been identified via (meta-)genomic approaches in *Alpha-*, *Beta-*, *Gamma-*, and *Deltaproteobacteria*, *Epsilonproteobacteria* (in the following referred to as Campylobacterota as recently proposed by Waite, 2018), *Firmicutes*, *Actinobacteria*, *Bacteroidetes*, *Aquificales* and other, (less abundant) bacterial and also archaeal phyla in diverse habitats (cf. **Figure 2** and Greening et al., 2016). Consistent with the generally great abundance of *Campylobacterota* at hydrothermal vents (often constituting more than 90% of the microbial vent communities in incubation experiments or metagenomic studies) (e.g., Dahle et al., 2013; Perner et al., 2013a; McNichol et al., 2018), a large part of the hydrothermal vent-derived hydrogen oxidizing, autotrophic isolates are related to this class. They are characterized by versatile metabolisms and only a few isolates are strict hydrogen oxidizers (i.e., they are not capable of using any other tested organic or inorganic electron donor), such as the mesophilic *Sulfurovum aggregans* (Mino et al., 2014) or the thermophilic *Caminibacter hydrogeniphilus* (Alain et al., 2002). Overall, there is a trend in the use of alternative electron donors with respect to the thermal preferences: while thermophilic members of the order *Nautiliales* tend to use formate (e.g., Nagata et al., 2017), mesophilic *Campylobacterota* like *Sulfurimonas paralvinellae* have the ability to use different reduced sulfur species such as thiosulfate or elemental sulfur as energy sources (Takai et al., 2006). Based on their metabolic and physiological versatility, *Campylobacterota* occupy diverse niches and can dominate microbial communities in hydrothermal vent environments. The frequent isolation of H_2-oxidizing *Campylobacterota* from deep-sea vents further emphasizes that this class may play a major role in hydrogen conversion and hydrogen-based primary production within hydrothermal habitats (Corre et al., 2001; Nakagawa et al., 2005; Campbell et al., 2006).

Hydrogen-oxidizing *Deltaproteobacteria* isolated from deep-sea vents – like *Desulfonauticus submarinus* – are commonly heterotrophic (Audiffrin et al., 2003), albeit representatives of this class were isolated from deep-sea vents that can couple hydrogen oxidation to autotrophic growth. Up to now, the vent-derived autotrophic, hydrogen-oxidizing *Deltaproteobacteria* are nearly all characterized as thermophiles with temperature optima between 50 and 61°C, with the so far only exception being a *Desulfobulbus* species with a mesophilic temperature optimum (Sievert and Kuever, 2000; Slobodkin et al., 2013; Slobodkina et al., 2016; Han et al., unpublished). Notably, among them the thermophilic *Desulfacinum hydrothermale* belongs to the group of Sulfate Reducing Bacteria (SRB). Most members of the SRB (which are ubiquitously found in anoxic habitats) belong to the *Deltaproteobacteria* and the group of SRB is known for comprising autotrophs that couple the oxidation of hydrogen to the reduction of sulfate or other electron acceptors as thiosulfate or elemental sulfur (Sievert and Kuever, 2000; Muyzer and Stams, 2008). As the substrates for hydrogenotrophic growth of SRB are readily available in hydrothermal vent systems, deltaproteobacterial SRB may contribute to hydrogen consumption in anoxic hydrothermal vent habitats to a greater extent than previously thought. Still, this hypothesis needs to be proven by the continuing identification of such microorganisms. So far, further evidence for the presence of hydrogen-converting *Deltaproteobacteria* in hydrothermal fluids stems from metatranscriptomic data, where deltaproteobacterial genes encoding hydrogen-converting enzymes were identified (Fortunato and Huber, 2016). *Gammaproteobacteria* are also demonstrated to be relevant for microbially mediated hydrogen cycling. The gammaproteobacterial *Thiomicrospira/Hydrogenovibrio/Thiomicrorhabdus* genera (recently reclassified by Boden et al., 2017) can be significantly enriched in bacterial vent communities with relative abundances of up to 37% based on 16S rRNA sequencing (Brazelton and Baross, 2010; Brazelton et al., 2010; Perner et al., 2011a). For many years isolates of the *Thiomicrospira* group (some of which are regrouped into the *Hydrogenovibrio* genus) were described as conventional sulfur oxidizers (Brinkhoff et al., 1999; Takai et al., 2004a; Knittel et al., 2005), until the first sequenced genome of this group indicated genes encoding hydrogen-converting enzymes (Scott et al., 2006) and strains of this group were shown to use hydrogen (Hansen and Perner, 2015, 2016). Although other hydrogen-oxidizing, autotrophic, gammaproteobacterial isolates have not been recovered yet, there is evidence for the hydrogen-converting ability among this group, based on classical sulfur-oxidizing symbionts (Petersen et al., 2011) and widespread deep-sea bacteria of the SUP 05 clade (Anantharaman et al., 2016).

Besides members of the Proteobacteria, other Bacteria and also Archaea contribute to the hydrogen-oxidizing communities in deep-sea vents. Particularly (among the Bacteria) the deeply branching order of *Aquificales* hosts a wide range of hydrogen-oxidizing organisms of different families and genera (e.g., *Desulfurobacteriaceae*) that have been isolated from

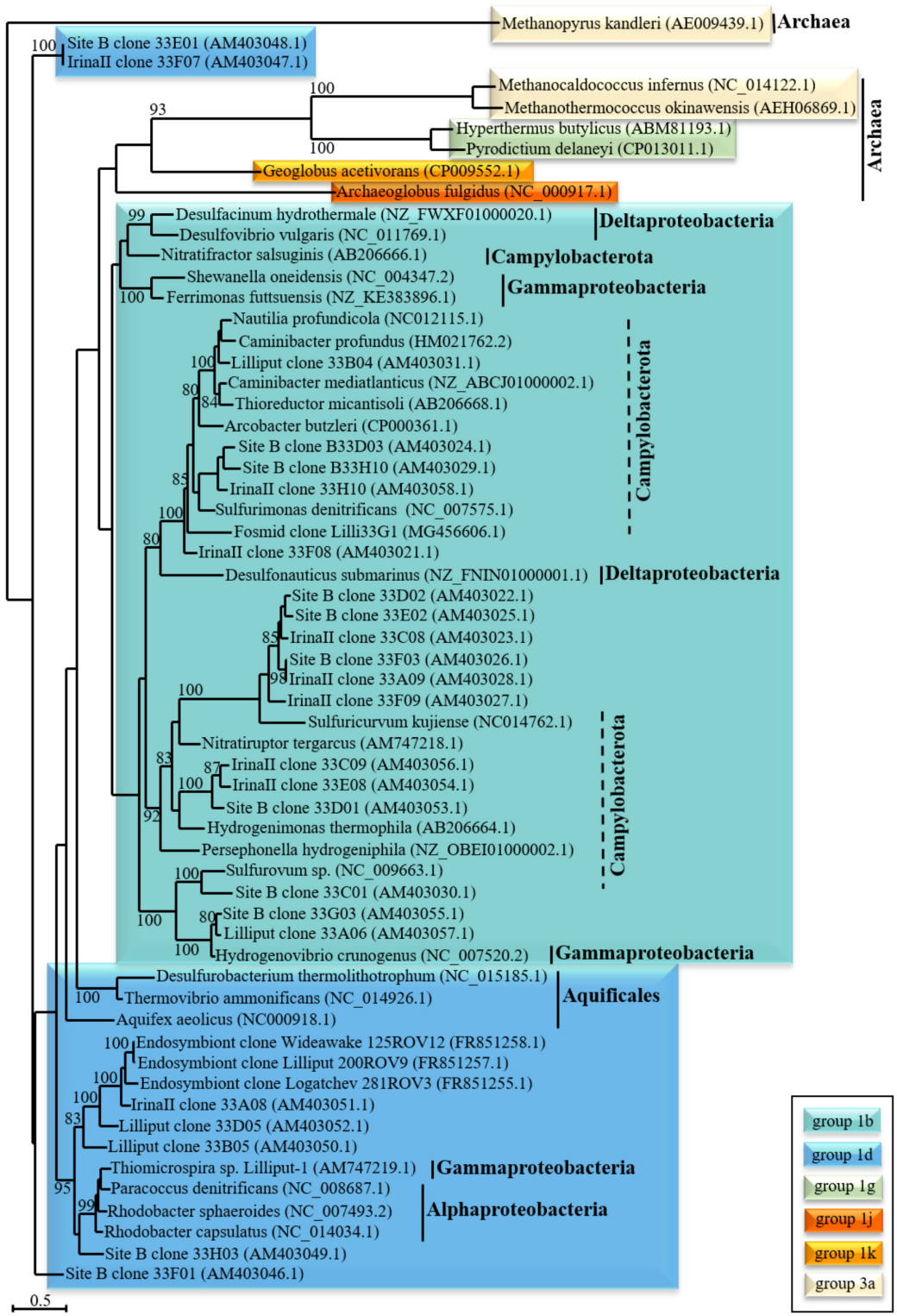

FIGURE 2 | Phylogenetic relationship of "uptake" [NiFe]-hydrogenase large subunit structural genes. The phylogenetic tree was calculated for nucleotide sequences of the large subunit [NiFe]-hydrogenase genes of (primarily vent-derived) phylogenetically diverse Bacteria and Archaea. The scale bar denotes the number of substitutions per nucleotide position and bootstrap values are only indicated if greater than 80%. ClustalW alignments were performed prior to tree calculation using BioEdit (Hall, 1999) with the standard settings. The tree was calculated using seaview (Gouy et al., 2010) with maximum likelihood analysis (four rate classes) and bootstrap values were calculated with 100 replicates. The classification of the [NiFe]-hydrogenase genes was determined using the HydDB web tool (Sondergaard et al., 2016).

hydrothermal fields around the globe (L'Haridon et al., 2006; Ferrera et al., 2014). Although they differ in their specific growth requirements (e.g., temperature, pH, electron acceptors), they are all described as strict chemolithoautotrophs and thermophiles (Nakagawa et al., 2003; L'Haridon et al., 2006). The strictly anaerobic, vent-derived *Desulfurobacterium thermolithotrophum* from the family of the *Desulfobacteraceae* was the first known thermophilic bacterial isolate with the ability to act as a primary producer in the temperature range of 45–70°C (L'Haridon et al., 1998). Notably, most members of the *Aquificales*, such as *Thermovibrio ammonificans* or *Balnearium lithotrophicum*, use hydrogen as the only energy source for autotrophic growth (Takai et al., 2003; Vetriani et al., 2004). Another thermophile-comprising phylum, *Thermodesulfobacteria*, usually is not considered as an important contributor of hydrogen-oxidizing vent-derived bacteria. Nonetheless, two of its five genera comprise thermophilic SRB isolated from hydrothermal vents, which share the ability to use hydrogen as the sole energy source for autotrophic growth (Jeanthon et al., 2002; Moussard et al., 2004; Alain et al., 2010).

Among the Archaea, thermophilic and hyperthermophilic methanogens are supposed to be the numerically largest and (in terms of the hydrogen consumption ability) most important group of hydrogen-oxidizers in hotter temperature regimes (Huber et al., 2002; Topcuoglu et al., 2016; Fortunato et al., 2018). Starting from the 1980's, shortly after the first discovery of hydrothermal vent systems, methanogenic isolates were repeatedly drawn from hydrothermal vents (e.g., Huber et al., 1982, 1989; Jones et al., 1989), some of them using hydrogen as the sole energy source for autotrophic CO_2 fixation and methane production (e.g., Huber et al., 1982; Jeanthon et al., 1998; L'Haridon et al., 2003; Takai et al., 2004b). As mentioned above, the hydrogen can stem from an abiogenic source (e.g., resulting from serpentinization processes) or be produced by hydrogen-evolving microorganisms (**Figure 1**, Ver Eecke et al., 2012; Toki et al., 2016; Topcuoglu et al., 2016). Methanogenic communities require greater hydrogen concentrations (e.g., $\geq$17 μM according to experiments with hyperthermophilic *Methanocaldococcus* species) to support chemolithoautotrophic growth than organisms coupling hydrogen oxidation to alternative electron acceptors, e.g., oxygen, nitrate, ferric iron and sulfate (Lovley and Goodwin, 1988; Hoehler et al., 1998; Ver Eecke et al., 2012). Besides methanogens, other hydrogen-oxidizing, autotrophs also exist among the Archaea: Fe(III)-reducing, hydrogen-oxidizing hyperthermophiles are encountered among the *Euryarchaeota* and *Crenarchaeota* (Slobodkina et al., 2009; Lin et al., 2016). These hydrogenotrophic Archaea thrive at lesser hydrogen concentrations than methanogens (Ver Eecke et al., 2009). Thus, they may be important contributors to microbial hydrogen consumption in venting environments that are characterized by elevated temperatures but lesser hydrogen levels. Nonetheless, the biogeochemical and ecological impact of these two groups still needs to be resolved.

Despite the large difficulties typically associated with taking samples from deep-sea hydrothermal vents and the culturing of vent-derived microorganisms, a large number of hydrogen-oxidizers has been isolated so far. However, a decreasing trend can be observed regarding the number of novel isolates from hydrothermal vent environments, which may be caused by insuperable obstacles in defining the appropriate culture conditions. More likely though, the laborious efforts in isolating (extremophilic) slow-growing microorganisms from hydrothermal vents have lessened due to the advent of cost-effective culture-independent techniques. For now, we have only gained a small-scale insight into the great diversity of microbial hydrogen uptake taking place at hydrothermal vents (see further discussions below).

HYDROGENASE GENES

The interconversion of molecular hydrogen to protons and electrons ($H_2 \leftrightarrow 2H^+ + 2e^-$) is catalyzed by hydrogenase enzymes, which are widely distributed among Bacteria and Archaea. Hydrogenases are classified according to their catalytic center and to date three different types are known: (i) [NiFe]-hydrogenases, (ii) [FeFe]-hydrogenases and (iii) [Fe]-hydrogenases (Vignais and Billoud, 2007). [NiFe]-hydrogenases are usually involved in hydrogen sensing and consumption, [FeFe]-hydrogenases are the so-called "hydrogen-evolving" (producing) hydrogenases and [Fe]-hydrogenases play a key role in methanogenesis (Thauer, 1998; Vignais and Billoud, 2007). Among the [NiFe]-hydrogenases four groups are distinguished, that each can be further divided into several subgroups based on different parameters concerning the catalytic subunit like amino acid sequence phylogeny and reported biochemical properties. Group 1 and group 4 [NiFe]-hydrogenases are termed membrane-bound "H_2-uptake" (consuming) and "hydrogen-evolving" hydrogenases, respectively, which are involved in energy metabolism. The group 2 encompasses mainly cytosolic hydrogen-sensing hydrogenases and some with so far unknown function and localization, while the cytosolic group 3 includes the F_{420}-reducing hydrogenases from methanogens, the bifunctional NADP-coupled hydrogenases and the bifurcating, heterodisulphide-linked hydrogenases (Greening et al., 2016; Sondergaard et al., 2016).

The [FeFe]-hydrogenases can also be further distinguished in three groups (A-C), of which groups A and C are additionally subdivided into four and three subgroups, respectively. Notably, only group A1 hosts the prototypical "hydrogen-evolving" [FeFe]-hydrogenases (other group A hydrogenases are involved in electron bifurcation or have unknown functions). [FeFe]-hydrogenases of groups B and C are currently only assigned to putative functions involved in hydrogen sensing and hydrogen production (Sondergaard et al., 2016).

While [NiFe]- and [FeFe]-hydrogenases are present in diverse prokaryotes, [Fe]-hydrogenases are only found in methanogenic Archaea and cannot be subdivided into distinct groups (Greening et al., 2016; Sondergaard et al., 2016). In contrast to [NiFe]- and [FeFe]-hydrogensaes, they do not contain FeS-clusters and couple the oxidation of hydrogen to the reduction of methenyltetrahydromethanopterin.

This intermediary step is only required in the reduction of CO_2 to methane under nickel limiting conditions when [NiFe]-hydrogenases cannot be synthesized (Vignais and Billoud, 2007). Due to the habitat-specific conditions, "uptake" [NiFe]-hydrogenases (and primarily those of the prototypical group 1b, see **Figure 2**) likely are the most common and (concerning primary biomass production) important hydrogenase type in deep-sea hydrothermal vent systems. As hydrothermal fluids usually contain various minerals and metals, nickel (central component of the active center in [NiFe]-hydrogenases) limitation should not occur in these habitats. Moreover, given the elevated hydrogen concentrations (>μM levels), fermentative hydrogen production is likely limited or inhibited in hydrothermal vent systems, leading to the assumption that microbial hydrogen oxidation (catalyzed by [NiFe]-hydrogenases) may be the dominating process in these environments.

Hydrogenase genes (and those of [NiFe]-hydrogenases in particular) are usually arranged in gene clusters that differ in their size and gene patterns (**Figure 3**). Due to the highly specific and complex maturation processes involved in the biosynthesis of hydrogenases, the clusters (in addition to the catalytic subunits) commonly also comprise genes encoding proteins for electron transfer, regulation factors and maturation factors, but also hypothetical proteins and partner enzymes (Casalot and Rousset, 2001; Bock et al., 2006; Greening et al., 2016). Commonly, the heterologous expression of (hydrogenase) enzymes (i.e., the expression in a foreign host) is limited by promoter recognition, diverging codon-usage, translation and the incompatibility or a lack of the respective maturation and assembly apparatus (cf. Perner et al., 2011b). In *E. coli* for example, the exchange of a carboxy-terminal extension of the large subunit of a [NiFe]-hydrogenase with that from an isoenzyme resulted in the abortion of the protein maturation. This indicates the great specificity of the proteolytic cleavage by the endopeptidase HybD, which is a necessity to form an active hydrogenase (Theodoratou et al., 2000; Casalot and Rousset, 2001). Furthermore, nickel incorporation proteins (HypA) or the carbamoyltransferase HypF (involved in the formation of the active site) are of vital importance for the formation of a functional protein (**Figure 3**, Casalot and Rousset, 2001). Nevertheless, heterologous expression of [NiFe]-hydrogenases has successfully been demonstrated in the past: not only with genes of (phylogenetically) closely related organisms (Rousset et al., 1998) but also in a setup where the insert hydrogenase and the host stem from different bacterial classes (Adam and Perner, 2018).

Hydrogenase genes from hydrothermal vents have been targeted by PCR amplification (group 1 and F_{420}-reducing [NiFe]-hydrogenases) (Takai et al., 2005; Perner et al., 2010; Petersen et al., 2011) or by direct sequencing of metagenomes (Perner et al., 2014; Pjevac et al., 2018) and metatranscriptomes (Dahle et al., 2013; Fortunato and Huber, 2016) (consisting of the whole genetic information) of vent-derived samples. However, compared to some enzymes like esterases, which are considered as one of the most important industrial biocatalysts (cf. Perner et al., 2011b), hydrogenases have only rarely been in the focus of metagenomic studies. Moreover, in most cases the metagenomic datasets were merely screened for the presence of [NiFe]-hydrogenase genes (e.g., Brazelton et al., 2012; Dahle et al., 2013; Perner et al., 2014; Fortunato and Huber, 2016). The majority of the identifiable [NiFe]-hydrogenase genes of these studies can be phylogenetically related to members of the *Campylobacterota* (see phylogenetic tree, **Figure 2**), other proteobacterial and also archaeal phyla. The frequent identification of *Campylobacterota* may be a consequence of the specific primer sets and the database entries that are available to identify hydrogenase genes. As only those genes can be identified that share sequence homologies to known hydrogenase sequences (or specific groups), it cannot be excluded that by applying PCR- and other sequence-based techniques an unintentional selection occurred. Still, the large number of campylobacterotal isolates also emphasizes the importance for primary biomass production and large abundance of this group in hydrothermal vent systems.

However, examples exist where no campylobacterotal genes could be identified: the [NiFe]-hydrogenase genes identified in the metagenome of a chimney sample from the hydrogen-rich, ultramafic Lost City hydrothermal field were primarily affiliated with betaproteobacterial [NiFe]-hydrogenase genes, showing the greatest resemblance to the *Ralstonia eutropha* hydrogenase (Brazelton et al., 2012). Since *R. eutropha* and other *Betaproteobacteria* closely related to the hydrogenases found in the Lost City metagenome are aerobic or facultatively anaerobic, the authors assume that the respective hydrogen oxidizers thrive in the oxic-anoxic transition zone of the chimney. Surprisingly, in addition to these [NiFe]-hydrogenases, "hydrogen-evolving" [FeFe]-hydrogenases related to *Clostridiales* were identified, which are most likely associated with fermentation of organic compounds. Given that fermentative hydrogen production can be inhibited even at nM hydrogen concentrations (discussed earlier), microbial hydrogen production technically does not seem feasible in a hydrogen-rich vent environment like the Lost City hydrothermal field. Furthermore, the origin of the organic fermentation substrates has not been resolved yet. Still, there are indications that in the course of serpentinization processes abiogenic organic carbon might evolve that can be used in microbial fermentation. As most fermentation processes require anoxic conditions, it is proposed that anaerobic *Clostridia* colonize the anoxic, deep-subsurface of the Lost City vent system (eventually entrained to the surface as the fluids pass by). It may also be possible that the hydrogen produced by *Clostridia* is later consumed by the hydrogen oxidizing *Betaproteobacteria* (Brazelton et al., 2012 and references therein). Despite the metagenomic indications, clear evidence for hydrogen pathways (including the oxidation of microbially produced hydrogen) in this habitat is still missing (cf. **Figure 1**). So far, it remains unclear if the respective genes actually belong to living organisms and are transcribed and expressed as functioning enzymes. Recently, Pjevac et al. (2018) stated a large discrepancy in the hydrogenase frequency of metagenomes and metaproteomes of two distinct chimneys of the Roman Ruins vent field: From 160 phylogenetically diverse hydrogenase genes identified in the metagenomes only

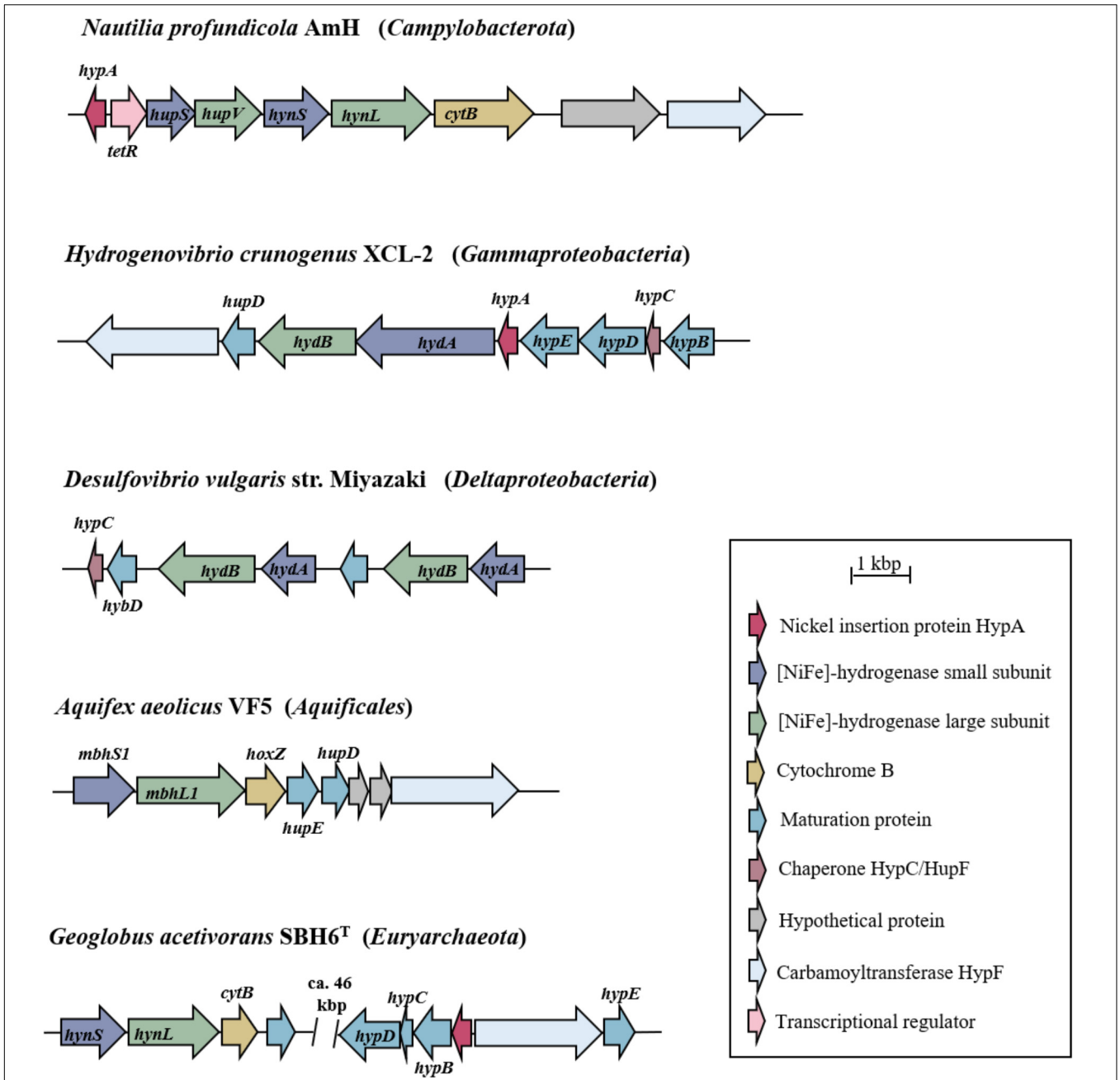

FIGURE 3 | Hydrogenase gene clusters of bacterial and archaeal representatives. Only the gene clusters containing the structural genes for the large and small subunit of the [NiFe]-hydrogenases and the corresponding maturation proteins are shown. According to the classification of Sondergaard et al. (2016) the [NiFe]-hydrogenases of *N. profundicola*, *H. crunogenus*, and *D. vulgaris* belong to group 1b, that of *A. aeolicus* to group 1d and that of *G. acetivorans* to group 1k (cf. **Figure 2**). Genes are pictured as arrows in the direction of transcription. Arrows of the same color indicate the same function of the encoded protein as explained by the key legend. Gene (and protein) abbreviations follow the respective annotations in the publicly available databases.

five proteins were found in the respective metaproteomes, all belonging to campylobacterotal representatives. Accordingly, the great phylogenetic diversity (in general but also of the hydrogenase genes) does not coincide with the actual metabolic diversity of the microbial communities. This phenomenon may in part be explained by the fact that due to the great microbial diversity, protein quantities of hydrogenases probably lay below the detection threshold of the experimental setup. Additionally, many of the "uptake" hydrogenases are membrane-associated and a bias of the isolation method against such membrane-bound proteins has to be considered. Still, it cannot be excluded that a significant part of the hydrogenase genes present in the metagenome are not expressed and are therefore missing in the metaproteome (Pjevac et al., 2018).

A deepened insight into putatively active metabolic processes – and microbial hydrogen utilization – as well as possible regulating factors can also be gained by metaproteomic approaches (Anantharaman et al., 2013; Fortunato et al., 2018). A comparison of the metatranscriptomes of a plume and a background sample of the Guaymas basin demonstrated site-specific (up-regulated) transcript abundances of distinct [NiFe]-hydrogenase genes of plume-derived and epipelagic members of the sulfur-oxidizing SUP05 group of the *Gammaproteobacteria*. Combined with transcript abundances of other genes related to chemoautotrophy like a form II ribulose-1,5-bisphosphate carboxylase-oxygenase (RubisCO) and other genes of the Calvin-Benson-Bassham (CBB) cycle, the hydrogenase expression levels indicate that hydrogen oxidation strongly contributes to the energy budget of the SUP05 group thriving in deep-ocean habitats (Anantharaman et al., 2013). Gammaproteobacterial [NiFe]-hydrogenase genes and transcripts were – in addition to those of *Deltaproteobacteria* and *Campylobacterota* as well as the methanogenic F_{420}-reducing hydrogenase - also detected in metagenomes and metatranscriptomes of low-temperature diffuse fluid samples derived from the Axial Seamount hydrothermal field (Fortunato and Huber, 2016). In this study meta-omics were coupled to additional, hydrogen-enriched, RNA stable isotope probing incubation experiments at different temperatures, integrating the influence of a thermal gradient on the chemoautotrophic microbial community. This thermal gradient was reflected by the hydrogen-oxidizing communities of the incubation experiments: while at 30°C exclusively (mesophilic) *Campylobacterota* were found, at 55°C thermophilic *Campylobacterota* and (to a lesser extent) methanogens dominated. The 80°C incubations, however, were dominated by hyperthermophilic methanogens, indicating that methanogenesis was the main metabolism at this temperature and may play a significant role for primary production in subsurface habitats, characterized by greater temperatures and greater hydrogen concentrations (Fortunato and Huber, 2016). In a more recent metaproteomic study, Fortunato and co-workers compared the fluid communities of three hydrothermal vents of the Axial Seamount field, sampled on an annual basis over a period of 3 years. Fluids from Marker 33 and Marker 113 exhibited 10 to 30 times lesser hydrogen concentrations than that of the Anemone vent. However, the hydrogen-poor fluids exhibited greater abundances and expression levels of hydrogenase genes and a greater percentage of hydrogen-utilizing *Campylobacterota*, *Aquificae* and methanogens. Notably, methanogenic transcripts at Marker 113 ranged from 30 to 56% of all annotated transcripts, with a large portion of hydrogenase genes. Therefore, the lesser hydrogen concentrations are likely caused by a draw-down of hydrogen through microbial hydrogen oxidation. Overall, more than 90% of the intra- and inter-vent changes in the community compositions observed within this study could be explained with the geochemical variables determined for the different fluid, plume and background samples (e.g., temperature, pH, hydrogen, sulfide and nitrate concentrations) (Fortunato et al., 2018).

Yet, such clear-cut, proportional relations between abiotic environmental parameters and the corresponding microbial (metabolic) diversity are often difficult to draw. In particular, differing hydrogen-concentrations are often not directly reflected by the microbial community: varying hydrogen concentrations, for example, do not necessarily lead to differences in the diversity and abundance of hydrogenase genes. The hydrogenase distribution across differing hydrogen concentrations indicates that other environmental parameters also play a central role in the distribution of hydrogen oxidizing microorganisms (Perner et al., 2010, 2014). Other factors putatively influencing the diversity and abundance of hydrogenase genes observed in hydrothermal vent environments might be the kinetics and affinities of the respective enzymes. The K_m values of [NiFe]-hydrogenases reported in the past show a great diversity ranging from 0.06 to 140 μM (Léger et al., 2004; van Haaster et al., 2005 and references therein). It may be assumed that organisms harboring high-affinity hydrogenases exhibiting low K_m values can suppress hydrogen oxidizers that harbor hydrogenases with greater K_m values, leading to a reduced diversity. However, the high-affinity, oxygen-tolerant [NiFe]-hydrogenases of group 1 h/5, which are widely distributed in soils (Constant et al., 2011), have not been identified in hydrothermal vent environments yet.

Furthermore, a metatranscriptomic study showed that increased hydrogenase gene expression is not limited to hydrothermal emission zones with elevated hydrogen concentrations but can also be observed at similar levels in intra-field water samples. The latter are not directly hydrothermally influenced but located in the vicinity of diffuse venting sites (Olins et al., 2017). Compared to background water samples, in most diffuse fluids and intra-field water samples the hydrogenase transcript levels were significantly enriched (Olins et al., 2017). The frequent identification of hydrogenase genes and elevated hydrogenase transcript abundances in hydrothermal vents and intra-field waters give evidence that hydrogen oxidation is of particular importance for primary biomass production in the different habitats surrounding hydrothermal vent orifices.

HYDROGEN CONSUMPTION MEASUREMENTS

Despite influences of individual fluid composition and seawater mixing ratios, compared to hydrogen-poor basalt-hosted systems, microbial hydrogen consumption rates of hydrogen-rich, ultramafic-hosted vent systems generally are expected to be greater. In fact, *ex situ* incubation experiments with symbiont-hosting mussel tissue from distinct vent systems revealed a 20- to 30-fold greater hydrogen consumption potential of symbionts from the hydrogen-rich ultramafic vent system relative to the hydrogen-poor basalt-hosted system (**Table 2**, Petersen et al., 2011). The respective CO_2-fixation rates confirmed that hydrogen oxidation fueled autotrophy (**Table 2**, Petersen et al., 2011). *Ex situ* incubations with diverse hydrothermal fluids (and free-living microorganisms), however, could not confirm the thermodynamic estimates.

TABLE 2 | Hydrogen consumption rates of different *ex situ* measurements performed with hydrothermal fluid samples or bacterial strains isolated from hydrothermal environments.

Sample type or strain	T	O_2	H_2 addition	Other incubation characteristics	H_2 consumption rate	CO_2-fixation rate	Reference
Wideawake diffuse fluids, basalt-hosted, MAR	18°C	+	+ 2% in head space		13.9 ± 1.7 – 18.9 ± 3.1 [fmol H_2 $cell^{-1}$ h^{-1}]	0.1 – 0.2 [fmol CO_2 $cell^{-1}$ h^{-1}]	Perner et al., 2013a
		–			63.7 ± 24.0 – 89.0 ± 25.9 [fmol H_2 $cell^{-1}$ h^{-1}]	0.1 – 0.2 [fmol CO_2 $cell^{-1}$ h^{-1}]	
Clueless diffuse fluids, basalt-hosted, MAR	18°C	+	+ 2% in head space		0.1 ± 0.08 [fmol H_2 $cell^{-1}$ h^{-1}]	0.004 [fmol CO_2 $cell^{-1}$ h^{-1}]	
		–			0.01 ± 0.004 [fmol H_2 $cell^{-1}$ h^{-1}]	<0.0001 [fmol CO_2 $cell^{-1}$ h^{-1}]	
Desperate diffuse fluids, basalt-hosted, MAR	18°C	+	+ 2% in head space		0.2 ± 0.1 [fmol H_2 $cell^{-1}$ h^{-1}]	0.0002 [fmol CO_2 $cell^{-1}$ h^{-1}]	
		–			0.09 ± 0.02 [fmol H_2 $cell^{-1}$ h^{-1}]	0.0005 [fmol CO_2 $cell^{-1}$ h^{-1}]	
Sisters Peak diffuse fluids, basalt-hosted, MAR	18°C	+	+ 2% in head space		0.8 ± 0.05 [fmol H_2 $cell^{-1}$ h^{-1}]	<0.001 [fmol CO_2 $cell^{-1}$ h^{-1}]	
		–			49.3 ± 6.1 [fmol H_2 $cell^{-1}$ h^{-1}]	0.2 ± 0.1 [fmol CO_2 $cell^{-1}$ h^{-1}]	
Foggy Corner diffuse fluids, basalt-hosted, MAR	18°C	+	+ 2% in head space		82.0 ± 10.0 [fmol H_2 $cell^{-1}$ h^{-1}]	0.003 ± 0.001 [fmol CO_2 $cell^{-1}$ h^{-1}]	
		–			92.0 ± 11.0 [fmol H_2 $cell^{-1}$ h^{-1}]	0.006 ± 0.001 [fmol CO_2 $cell^{-1}$ h^{-1}]	
Lilliput diffuse fluids, basalt-hosted, MAR	18°C	+	+ 2% in head space		0.3 ± 0.06 [fmol H_2 $cell^{-1}$ h^{-1}]	0.01 [fmol CO_2 $cell^{-1}$ h^{-1}]	
		–			0.3 ± 0.004 [fmol H_2 $cell^{-1}$ h^{-1}]	0.01 [fmol CO_2 $cell^{-1}$ h^{-1}]	
Quest diffuse fluids, ultramafic-hosted, MAR	18°C	+	+ 2% in head space		<0.002 [fmol H_2 $cell^{-1}$ h^{-1}]	0.002 ± 0.001 [fmol CO_2 $cell^{-1}$ h^{-1}]	
		–			<0.02 [fmol H_2 $cell^{-1}$ h^{-1}]	0.002 ± 0.001 [fmol CO_2 $cell^{-1}$ h^{-1}]	
Irina II diffuse fluids, ultramafic-hosted, MAR	18°C	+	+ 2% in head space		17.0 ± 17.1 [fmol H_2 $cell^{-1}$ h^{-1}]	0.02 [fmol CO_2 $cell^{-1}$ h^{-1}]	
		–			1.6 ± 1.9 [fmol H_2 $cell^{-1}$ h^{-1}]	0.02 [fmol CO_2 $cell^{-1}$ h^{-1}]	
Irina II plume, ultramafic-hosted, MAR	18°C	+	+ 2% in head space		50.5 ± 14.6 [fmol H_2 $cell^{-1}$ h^{-1}]	0.001 [fmol CO_2 $cell^{-1}$ h^{-1}]	
		–			2.6 ± 2.0 [fmol H_2 $cell^{-1}$ h^{-1}]	0.001 [fmol CO_2 $cell^{-1}$ h^{-1}]	
Nibelungen hot fluids, ultramafic-hosted, MAR	18°C	+	+ 2% in head space		0.2 ± 0.1 [fmol H_2 $cell^{-1}$ h^{-1}]	0.003 [fmol CO_2 $cell^{-1}$ h^{-1}]	
		–			0.7 ± 0.04 [fmol H_2 $cell^{-1}$ h^{-1}]	0.003 [fmol CO_2 $cell^{-1}$ h^{-1}]	

(Continued)

TABLE 2 | Continued

Sample type or strain	T	O_2	H_2 addition	Other incubation characteristics	H_2 consumption rate	CO_2-fixation rate	Reference
Crab Spa diffuse fluids, basalt-hosted, EPR	24°C	Not added	150 μM dissolved H_2	25 MPa pressure	3.66 – 5.77 [fmol H_2 $cell^{-1}$ h^{-1}]	n.d.	McNichol et al., 2016
Crab Spa diffuse fluids, basalt-hosted, EPR	24°C	Not added	150 μM dissolved H_2	25 MPa pressure + 100 μM nitrate	14.65 – 21.18 [fmol H_2 cell-1 h^{-1}]	n.d.	
Crab Spa diffuse fluids, basalt-hosted, EPR	50°C	Not added	150 μM dissolved H_2	25 MPa pressure + 100 μM nitrate	41.24 – 63.97 [fmol H_2 $cell^{-1}$ h^{-1}]	n.d.	
Symbiont-hosting *Bathimodiolus* tissue from ultramafic Logatchev field, MAR	4°C	+	100 ppm in head space		656 ± 207 [nmol H_2 h^{-1} (g wet weight)$^{-1}$]	∼ 67 [^{14}C Bq (g wet weight)$^{-1}$]	Petersen et al., 2011
Symbiont-hosting *Bathimodiolus* tissue from ultramafic Logatchev field, MAR	4°C	+	100–1783 ppm in head space		656 ± 207 – 2945 ± 201 [nmol H_2 h^{-1} (g wet weight)$^{-1}$]	n.d.	
Symbiont-hosting *Bathimodiolus* tissue from basalt-hosted Comfortless Cove field, MAR	4°C	+	95–938 ppm in head space		30 ± 25 – 208 ± 67 [nmol H_2 h^{-1} (g wet weight)$^{-1}$]	n.d.	
Symbiont-hosting *Bathimodiolus* tissue from basalt-hosted Lilliput field, MAR	4°C	+	93–2916 ppm in head space		20 ± 9 – 316 ± 100 [nmol H_2 h^{-1} (g wet weight)$^{-1}$]	n.d.	
Janssand sediments, German Wadden Sea	14°C	–	220 μM in head space		0.46 [fmol H_2 $cell^{-1}$ h^{-1}]	n.d.	Dyksma et al., 2018
Hydrogenovibrio SP-41*	28°C	+	2% in head space	Different growth media were tested	1.47 – 6.1 [fmol H_2 $cell^{-1}$ h^{-1}]	n.d.	Hansen and Perner, 2015
H. crunogenus TH-55*	28°C	+	2% in head space		0.73 [fmol H_2 $cell^{-1}$ h^{-1}]	n.d.	

*T states the incubation temperature during the experiments and O_2 indicates whether the experiments were conducted under oxic (+) or anoxic (–) conditions. For comparison, a non-hydrothermal sample (Janssand sediments) is also included. *Previously Thiomicrospira (crunogena).*

In most incubations, hydrogen consumption rates and biomass production were greater in the tested fluids from basaltic than from ultramafic systems. These observations may result from the specific conditions provided with the experimental setup, i.e., oxic and anoxic conditions, addition of 12–14 μM hydrogen (in solution) and incubation at 18°C (Perner et al., 2010, 2011a, 2013b). Accordingly, altered incubation conditions may exhibit quite different hydrogen consumption rates. Similar incubation experiments, performed with only basalt-hosted hydrothermal emissions, were advanced by mimicking *in situ* pressure and temperature in gas-tight samplers (McNichol et al., 2016). Nitrate availability had a stimulating effect on the respective hydrogen consumption rates, ranging from 3.66 to 63.97 fmol H_2 $cell^{-1}$ h^{-1} (**Table 2**, McNichol et al., 2016), comparable to those of previous *ex situ* measurements ranging from 0.2 to 92.0 fmol H_2 $cell^{-1}$ h^{-1} (Perner et al., 2013b). Despite the efforts made to reproduce *in situ* conditions in *ex situ* incubations, it is impossible to simulate the dynamic nature of the (micro) habitats present in the hydrothermal vent systems. These are hallmarked by vast thermal and chemical gradients in venting habitats, ranging from several 100 s to 4°C water temperature and from highly reduced to fully oxic, respectively. Therefore, incubations with more conditions than manageable would have to be set up to cover all the micro niches present in a hydrothermal venting biotope (Perner et al., 2010). Other methods to determine the microbial hydrogen oxidation potential, e.g., the tritium-based hydrogenase assay applied to subsurface sediments also show a great potential for hydrogen oxidation (Adhikari et al., 2016). Yet, they suffer from similar limitations as the hydrogen consumption measurements of hydrothermal vent samples: the incubation experiments are not conducted under *in situ* conditions and freezing of the samples prior to the assay cause additional deviation (Adhikari et al., 2016). Against this background, the development of *in situ* techniques for the determination of microbial hydrogen consumption rates is inevitable.

In situ measurements of hydrogen concentrations are already being done by employing *in situ* mass spectrometry (Wankel et al., 2011; Perner et al., 2013a) and has been used to draw conclusions on the impact of subsurface microbial activity on hydrogen concentrations of diffuse hydrothermal fluids. A discrepancy between the calculated and actually measured hydrogen concentrations of hydrothermal fluids, ranging from 50 to 80%, was attributed to microbial activity taking place below the seafloor (Wankel et al., 2011). Yet, a link to the microorganisms responsible for the presumable hydrogen consumption is missing. To provide this link, the existing measurement techniques could be amended by the recently established *in situ* fixation of fluids for later nucleotide extraction and metatranscriptomic and/or metagenomic analysis (Fortunato and Huber, 2016; Olins et al., 2017). Therefore, future *in situ* hydrogen measurements and consumption experiments would ideally combine monitoring of hydrogen and CO_2 concentrations, cell counting and fixation of (fluid) samples for metagenomic and metatranscriptomic analysis to cover the full hydrogen consumption potential of vent-associated microbial communities.

So far, *ex situ* hydrogen consumption measurements have been linked to unspecified *Campylobacterota* (McNichol et al., 2016), mesophilic *Alpha-, Beta-* and *Gammaproteobacteria*, mesophilic *Campylobacterota*, methanogens (Perner et al., 2010, 2011a) as well as a typically sulfur-oxidizing gammaproteobacterial symbiont (Petersen et al., 2011). First hints that another vent-inhabiting, sulfur-oxidizing *Gammaproteobacterium* might be able to oxidize hydrogen were gained from sequencing the hydrogenase gene cluster containing genome of *Thiomicrospira crunogena* (Scott et al., 2006) (now *Hydrogenovibrio crunogenus*) (Boden et al., 2017). Additionally, in some oxic, H_2-amended incubation experiments, genes related to the sulfur-oxidizing gammaproteobacterial *Hydrogenovibrio crunogenus* were highly (8 to 23-fold) enriched compared to sulfide-spiked incubations of the same vent sample (Perner et al., 2011a). Still, it remained unclear whether *Thiomicrospira* strains actually express functional hydrogenases until *Thiomicrospira* SP-41's hydrogen consumption ability was discovered (Hansen and Perner, 2015). Further hydrogen consuming (previously classified as) *Thiomicrospira* strains were detected after offering diverse growth conditions and supplements (Hansen and Perner, 2016), demonstrating an unexpected potential for hydrogen consumption among these sulfur-oxidizing *Gammaproteobacteria*. The flexibility to use hydrogen as an alternative electron donor might also be a key to the success and dominance of (other) sulfur-oxidizing *Gammaproteobacteria* as observed in a variety of hydrothermal fluids (Perner et al., 2010; Olins et al., 2017).

A similar hydrogen consumption potential can also be expected for sulfur-oxidizing representatives of the order *Campylobacterales*: for example, the growth of a sulfur-oxidizing *Sulfurimonas denitrificans* isolate was significantly improved by the addition of hydrogen in growth experiments and hydrogen consumption measurements confirmed the utilization as electron donor (Han and Perner, 2014). Although *S. denitrificans* was originally isolated from Wadden Sea sediments (Timmer-Ten Hoor, 1975), numerous strains have also been identified in hydrothermally influenced habitats (cf e.g., Perner et al., 2013a). Furthermore, hydrogenase genes of a *S. denitrificans* strains were found in vent-derived metatranscriptomes (Fortunato and Huber, 2016). Given the great abundances of *Sulfurimonas* and other *Campylobacterales* genera like *Arcobacter* in hydrothermal fluids or plumes (Perner et al., 2010, 2013a; Fortunato and Huber, 2016), members of the *Campylobacterales* may contribute significantly to overall hydrogen consumption in deep-sea vent systems.

Although diverse archaeal hydrogen-consuming representatives have been isolated, much of the archaeal hydrogen consumption in hydrothermal vents can likely be assigned to methanogens, evidenced by incubation experiments and sequencing (Perner et al., 2010; Ver Eecke et al., 2012; Fortunato and Huber, 2016). The full potential of methanogenic hydrogen-based primary production, however, may be even greater than current incubation experiments suggest, occurring over a wider temperature and pressure range. By applying elevated (*in situ*) hydrostatic pressure of 20 MPa, the growth range of the hyperthermophilic vent-derived *Methanopyrus*

kandleri was expanded from 116°C up to 122°C and the temperature optimum was increased by 5°C to 105°C (compared to the standard 0.4 MPa incubations), while the carbon isotope fractionation of generated methane decreased (Takai et al., 2008). The small carbon isotope fractionation of biogenic methane could lead to a misinterpretation of data from hydrothermal vent environments: it could be identified as isotopically "heavy" methane from a magmatic source, thus diminishing the estimated methanogenic contribution (Takai et al., 2008 and references therein).

So far, incubation experiments with hydrothermal fluid samples have been performed with temperatures up to 80°C (Fortunato and Huber, 2016), thus the conditions might not have been ideal for hyperthermophiles in the existing incubations and their abundances were underestimated.

Before genomic analyses and incubation experiments could link hydrogen consumption to the putatively responsible organisms, for many species such as *Thiomicrospira* sp. no hints for a potential hydrogen utilization were obvious. Matched with the still existing difficulties in the cultivation of vent inhabitants, a need for the implementation of culture-independent approaches becomes evident in order to identify novel hydrogen-oxidizing or -producing microorganisms and respective enzymes.

ACCESSING THE UNCULTURED MAJORITY AND THEIR HYDROGEN-CONVERTING POTENTIAL

Hydrogenase genes have been frequently identified in metagenomic deep-sea hydrothermal vent data sets. The [NiFe]-hydrogenase hit rate (i.e., the number of identified hydrogenase genes relative to all other genes in the data set) from a hydrothermal vent metagenome can be up to 40-fold higher than in metagenomes from other habitat types (Brazelton et al., 2012; Perner et al., 2014), revealing the importance of hydrogen-uptake in venting biotopes. However, these sequence-based approaches only indicate potential hydrogenase encoding genes. The functionality of the putative hydrogen-converting enzymes remains unclear, until hydrogen-uptake or –evolution is experimentally confirmed. Furthermore, hydrogen-converting enzymes lacking sequence homologies to known hydrogenases cannot be identified by sequence-based metagenomic approaches. Up to now, truly novel enzymes can only be found by screening metagenomes with activity-based approaches (Handelsman, 2004).

Until recently no activity-based screen existed, that could seek hydrogen-converting enzymes from the environment. However, a newly developed screen enables the search for environmental hydrogenases: It is based on the recombinant expression of metagenome-derived genes in a [NiFe]-hydrogenase deletion mutant of *Shewanella oneidensis* MR-1 (Adam and Perner, 2017). By applying this screen to metagenomic libraries of hydrothermal vent environments, hydrogen-converting clones were identified, whose metagenomic inserts largely do not share any sequence homology with known hydrogenases. Hydrogen-uptake activities of the clones exhibited up to 258 ± 19 nmol $H_2{*}min^{-1}{*}mg^{-1}$ of partially purified proteins at 55°C, exceeding those of some cultured organisms (Adam and Perner, 2018). Given the difficulties and drawbacks associated with heterologous (hydrogenase) enzyme expression, a limitation in the hydrogenase detection ability of this screen is not surprising. For example, hydrogenases of *Escherichia coli*, *Hydrogenovibrio* sp., *Thiobacillus denitrificans*, *Desulfovibrio vulgaris,* and *Aquifex aeolicus* (and thus likely those of uncultured relatives from the environment) could not be identified with this host-vector system. Nevertheless, the [NiFe]-hydrogenases from *Photobacterium leiognathi*, *Rhodobacter capsulatus*, *Sulfurimonas denitrificans* and *Wolinella succinogenes* were successfully expressed and exhibited measurable activities that were up to 2.6-fold higher than that of the host's own hydrogenase (Adam and Perner, 2018). Still, it can be assumed that by establishing other hosts with varying growth optima for the activity-based screen, the detection range may be significantly improved. Given specific hydrogen-uptake activities of up to $48{,}700 \pm 4{,}000$ nmol $H_2{*}min^{-1}{*}mg^{-1}$ for the vent isolate *Thioreductor micantisoli* (Takai et al., 2005), the large potential for the discovery of (highly) active hydrogenases present in the enzymatic pool of vent environments is apparent.

The possibility of successfully expressing vent-derived hydrogen-converting enzymes in an "easily" culturable host may also open the door to biotechnological applications of these enzymes. Hydrogen-converting enzymes are of particular interest for the use in hydrogen production as a clean energy carrier and energy generation in biofuel cells (Armstrong et al., 2009; Chenevier et al., 2013). As shown for *Escherichia coli*'s hydrogenases for example, these enzymes can be used for enhanced hydrogen production on surface-enlarged nanofiber electrodes (Schlicht et al., 2016). Due to the steep thermal and chemical gradients prevailing in vent environments, enzymes of exceptional stability under various conditions (e.g., temperature or oxygen contents) can be expected to be found. These would be the ideal candidates for biotechnological applications in the field of hydrogen production or energy generation in biofuel cells.

CONCLUSION

Hydrogen oxidation, catalyzed by phylogenetically diverse Bacteria and Archaea with versatile metabolic pathways, plays a major role for primary biomass production in chemically distinct deep-sea hydrothermal vent systems. However, the metabolic processes and biogeochemical interactions involved in hydrogen conversion are still not fully understood. Assessing the full hydrogen consumption potential of microbial vent communities has often proved to be difficult as incubation experiments but also metagenomic and metatranscriptomic approaches have their particular limitations: i.e., either in the reproducibility of optimal growth and hydrogen consumption conditions or in the lack of functional proof for the putative hydrogen conversion ability. The development of *in situ* hydrogen consumption measurement techniques that include sampling for subsequent molecular analyses would therefore considerably improve the exploration of hydrogen-converting communities in deep-sea vents.

Since the culture-dependent and –independent approaches all exhibit individual limitations in identifying novel mechanisms of hydrogen-based metabolisms, the currently available techniques should ideally be combined to elucidate the full hydrogen utilization potential among the yet uncultured majority.

AUTHOR CONTRIBUTIONS

NA and MP wrote the manuscript.

FUNDING

This work was supported by the research grant DFG PE1549-6/1 and PE1549-6/3 from the German Science Foundation.

ACKNOWLEDGMENTS

We greatly appreciate the funding of the DFG in the framework of the research grants PE1549-6/1 and PE1549-6/3.

REFERENCES

Adam, N., and Perner, M. (2017). "Activity-based screening of metagenomic libraries for hydrogenase enzymes," in *Metagenomics – Methods and Protocols*, eds W. Streit and R. Daniel (Berlin: Springer).

Adam, N., and Perner, M. (2018). Novel hydrogenases from deep-sea hydrothermal vent metagenomes identified by a recently developed activity-based screen. *ISME J.* 12, 1225–1236. doi: 10.1038/s41396-017-0040-6

Adhikari, R. R., Glombitza, C., Nickel, J. C., Anderson, C. H., Dunlea, A. G., Spivack, A. J., et al. (2016). Hydrogen utilization potential in subsurface sediments. *Front. Microbiol.* 7:8. doi: 10.3389/fmicb.2016.00008

Alain, K., Postec, A., Grinsard, E., Lesongeur, F., Prieur, D., and Godfroy, A. (2010). *Thermodesulfatator atlanticus* sp. nov., a thermophilic, chemolithoautotrophic, sulfate-reducing bacterium isolated from a mid-atlantic ridge hydrothermal vent. *Int. J. Syst. Evolut. Microbiol.* 60, 33–38. doi: 10.1099/ijs.0.009449-0

Alain, K., Querellou, J., Lesongeur, F., Pignet, P., Crassous, P., Raguenes, G., et al. (2002). *Caminibacter hydrogeniphilus* gen. nov., sp. nov., a novel thermophilic, hydrogen-oxidizing bacterium isolated from an east pacific rise hydrothermal vent. *Int. J. Syst. Evolut. Microbiol.* 52, 1317–1323.

Amend, J. P., and Shock, E. L. (2001). Energetics of overall metabolic reactions of thermophilic and hyperthermophilic Archaea and Bacteria. *FEMS Microbiol. Rev.* 25, 175–243. doi: 10.1111/j.1574-6976.2001.tb00576.x

Anantharaman, K., Breier, J. A., and Dick, G. J. (2016). Metagenomic resolution of microbial functions in deep-sea hydrothermal plumes across the Eastern Lau Spreading Center. *ISME J.* 10, 225–239. doi: 10.1038/ismej.2015.81

Anantharaman, K., Breier, J. A., Sheik, C. S., and Dick, G. J. (2013). Evidence for hydrogen oxidation and metabolic plasticity in widespread deep-sea sulfur-oxidizing bacteria. *Proc. Natl. Acad. Sci. U.S.A.* 110, 330–335. doi: 10.1073/pnas.1215340110

Armstrong, F. A., Belsey, N. A., Cracknell, J. A., Goldet, G., Parkin, A., Reisner, E., et al. (2009). Dynamic electrochemical investigations of hydrogen oxidation and production by enzymes and implications for future technology. *Chem. Soc. Rev.* 38, 36–51. doi: 10.1039/B801144N

Audiffrin, C., Cayol, J. L., Joulian, C., Casalot, L., Thomas, P., Garcia, J. L., et al. (2003). *Desulfonauticus submarinus* gen. nov., sp. nov., a novel sulfate-reducing bacterium isolated from a deep-sea hydrothermal vent. *Int. J. Syst. Evolut. Microbiol.* 53, 1585–1590. doi: 10.1099/ijs.0.02551-0

Bock, A., King, P. W., Blokesch, M., and Posewitz, M. C. (2006). Maturation of hydrogenases. *Adv. Microb. Physiol.* 51, 1–71. doi: 10.1016/S0065-2911(06)51001-X

Boden, R., Scott, K. M., Williams, J., Russel, S., Antonen, K., Rae, A. W., et al. (2017). An evaluation of *Thiomicrospira*, *Hydrogenovibrio* and *Thioalkalimicrobium*: reclassification of four species of *Thiomicrospira* to each thiomicrorhabdus gen. nov. and *Hydrogenovibrio*, and reclassification of all four species of *Thioalkalimicrobium* to *Thiomicrospira*. *ISME J.* 67, 1140–1151.

Bothe, H., Schmitz, O., Yates, M. G., and Newton, W. E. (2010). Nitrogen fixation and hydrogen metabolism in cyanobacteria. *Microbiol. Mol. Biol. Rev.* 74, 529–551. doi: 10.1128/MMBR.00033-10

Brazelton, W. J., and Baross, J. A. (2010). Metagenomic comparison of two *Thiomicrospira* lineages inhabiting contrasting deep-sea hydrothermal environments. *PLoS One* 5:e13530. doi: 10.1371/journal.pone.0013530

Brazelton, W. J., Ludwig, K. A., Sogin, M. L., Andreishcheva, E. N., Kelley, D. S., Shen, C. C., et al. (2010). Archaea and bacteria with surprising microdiversity show shifts in dominance over 1,000-year time scales in hydrothermal chimneys. *Proc. Natl. Acad. Sci. U.S.A.* 107, 1612–1617. doi: 10.1073/pnas.0905369107

Brazelton, W. J., Nelson, B., and Schrenk, M. O. (2012). Metagenomic evidence for H2 oxidation and H2 production by serpentinite-hosted subsurface microbial communities. *Front. Microbiol.* 2:268. doi: 10.3389/fmicb.2011.00268

Brinkhoff, T., Muyzer, G., Wirsen, C. O., and Kuever, J. (1999). *Thiomicrospira kuenenii* sp. nov. and *Thiomicrospira frisia* sp. nov., two mesophilic obligately chemolithoautotrophic sulfur-oxidizing bacteria isolated from an intertidal mud flat. *Int. J. Syst. Bacteriol.* 49(Pt 2), 385–392. doi: 10.1099/00207713-49-2-385

Bryant, M. P., Campbell, L. L., Reddy, C. A., and Crabill, M. R. (1977). Growth of desulfovibrio in lactate or ethanol media low in sulfate in association with H2-utilizing methanogenic bacteria. *Appl. Environ. Microbiol.* 33, 1162–1169.

Campbell, B. J., Engel, A. S., Porter, M. L., and Takai, K. (2006). The versatile e-proteobacteria: key players in sulphidic habitats. *Nat. Rev. Microbiol.* 4, 458–468. doi: 10.1038/nrmicro1414

Casalot, L., and Rousset, M. (2001). Maturation of the [NiFe] hydrogenases. *Trends Microbiol.* 9, 228–237. doi: 10.1016/S0966-842X(01)02009-1

Charlou, J. L., Donval, J. P., Fouquet, Y., Jean-Baptiste, P., and Holm, N. (2002). Geochemistry of high H2 and CH4 vent fluids issuing from ultramafic rocks at the Rainbow hydrothermal field (36°14'N, MAR). *Chem. Geol.* 191, 345–359. doi: 10.1016/S0009-2541(02)00134-1

Chassard, C., and Bernalier-Donadille, A. (2006). H2 and acetate transfers during xylan fermentation between a butyrate-producing xylanolytic species and hydrogenotrophic microorganisms from the human gut. *FEMS Microbiol. Lett.* 254, 116–122. doi: 10.1111/j.1574-6968.2005.00016.x

Chenevier, P., Mugherli, L., Darbe, S., Darchy, L., Dimanno, S., Tran, P. D., et al. (2013). Hydrogenase enzymes: application in biofuel cells and inspiration for the design of noble-metal free catalysts for H2 oxidation. *C. R. Chim.* 16, 491–505. doi: 10.1016/j.crci.2012.11.006

Conrad, R. (1996). Soil microorganisms as controllers of atmospheric trace gases (H2, CO, CH4, OCS, N2O, and NO). *Microbiol. Rev.* 60, 609–640.

Constant, P., Chowdhury, S. P., Hesse, L., Pratscher, J., and Conrad, R. (2011). Genome data mining and soil survey for the novel group 5 [NiFe]-hydrogenase to explore the diversity and ecological importance of presumptive high-affinity H2-oxidizing bacteria. *Appl. Environ. Microbiol.* 77, 6027–6035. doi: 10.1128/AEM.00673-11

Corliss, J. B., Dymond, J., Gordon, L. I., Edmond, J. M., Von Herzen, R. P., Ballard, R. D., et al. (1979). Submarine thermal springs on the galapagos rift. *Science* 203, 1073–1083. doi: 10.1126/science.203.4385.1073

Corre, E., Reysenbach, A. L., and Prieur, D. (2001). Epsilon-proteobacterial diversity from a deep-sea hydrothermal vent on the mid-atlantic ridge. *FEMS Microbiol. Lett.* 205, 329–335.

Dahle, H., Roalkvam, I., Thorseth, I. H., Pedersen, R. B., and Steen, I. H. (2013). The versatile in situ gene expression of an Epsilon*proteobacteria*-dominated biofilm from a hydrothermal chimney. *Environ. Microbiol. Rep.* 5, 282–290. doi: 10.1111/1758-2229.12016

Dilling, W., and Cypionka, H. (1990). Aerobic respiration in sulfate-reducing bacteria. *FEMS Microbiol. Lett.* 71, 123–127.

Dyksma, S., Pjevac, P., Ovanesov, K., and Mussmann, M. (2018). Evidence for H2 consumption by uncultured Desulfobacterales in coastal sediments. *Environ. Microbiol.* 20, 450–461. doi: 10.1111/1462-2920.13880

Ferrera, I., Banta, A. B., and Reysenbach, A. L. (2014). Spatial patterns of aquificales in deep-sea vents along the eastern lau spreading center (SW pacific). *Syst. Appl. Microbiol.* 37, 442–448. doi: 10.1016/j.syapm.2014.04.002

Fortunato, C. S., and Huber, J. A. (2016). Coupled RNA-SIP and metatranscriptomics of active chemolithoautotrophic communities at a deep-sea hydrothermal vent. *ISME J.* 10, 1925–1938. doi: 10.1038/ismej.2015.258

Fortunato, C. S., Larson, B., Butterfield, D. A., and Huber, J. A. (2018). Spatially distinct, temporally stable microbial populations mediate biogeochemical cycling at and below the seafloor in hydrothermal vent fluids. *Environ. Microbiol.* 20, 769–784. doi: 10.1111/1462-2920.14011

Fuchs, G., Eitinger, T., Heider, J., Kemper, B., Kothe, E., Schink, B., et al. (2007). *Allgemeine Mikrobiologie*. Stuttgart: Georg Thieme Verlag. doi: 10.1055/b-002-44938

Gouy, M., Guindon, S., and Gascuel, O. (2010). SeaView version 4: a multiplatform graphical user interface for sequence alignment and phylogenetic tree building. *Mol. Biol. Evol.* 27, 221–224. doi: 10.1093/molbev/msp259

Greening, C., Biswas, A., Carere, C. R., Jackson, C. J., Taylor, M. C., Stott, M. B., et al. (2016). Genomic and metagenomic surveys of hydrogenase distribution indicate H2 is a widely utilised energy source for microbial growth and survival. *ISME J.* 10, 761–777. doi: 10.1038/ismej.2015.153

Haase, K. M., Petersen, S., Koschinsky, A., Seifert, R., Devey, C. W., Keir, R., et al. (2007). Young volcanism and related hydrothermal activity at 5°S on the slow-spreading southern Mid-Atlantic Ridge. *Geochem. Geophys. Geosyst.* 8, 1–17. doi: 10.1029/2006GC001509

Hall, T. A. (1999). BioEdit: a user-friendly biological sequence alignment editor and analysis program for Windows 95/98/NT. *Nucleic Acids Sympos. Ser.* 41, 95–98.

Hallenbeck, P. C. (2009). Fermentative hydrogen production: principles, progress, and prognosis. *Int. J. Hydr. Energy* 34, 7379–7389. doi: 10.1016/j.ijhydene.2008.12.080

Han, Y., and Perner, M. (2014). The role of hydrogen for sulfurimonas denitrificans' metabolism. *PLoS One* 9:e106218. doi: 10.1371/journal.pone.0106218

Handelsman, J. (2004). Metagenomics: application of genomics to uncultured microorganisms. *Microbiol. Mol. Biol. Rev.* 68, 669–685. doi: 10.1128/MMBR.68.4.669-685.2004

Hansen, M., and Perner, M. (2015). A novel hydrogen oxidizer amidst the sulfur-oxidizing *Thiomicrospira* lineage. *ISME J.* 9, 696–707. doi: 10.1038/ismej.2014.173

Hansen, M., and Perner, M. (2016). Hydrogenase gene distribution and H2 consumption ability within the *Thiomicrospira* lineage. *Front. Microbiol.* 7:99. doi: 10.3389/fmicb.2016.00099

Heijnen, J. J., and Van Dijken, J. P. (1992). In search of a thermodynamic description of biomass yields for the chemotrophic growth of microorganisms. *Biotechnol. Bioeng.* 39, 833–858. doi: 10.1002/bit.260390806

Hoehler, T. M., Alperin, M. J., Albert, D. B., and Martens, C. S. (1998). Thermodynamic control on hydrogen concentrations in anoxic sediments. *Geochim. Cosmochim. Acta* 62, 1745–1756. doi: 10.1016/S0016-7037(98)00106-9

Huber, H., Thomm, M., König, H., Thies, G., and Stetter, K. O. (1982). Methanococcus thermolithotrophicus, a novel thermophilic lithotrophic methanogen. *Arch. Microbiol.* 132, 47–50. doi: 10.1007/BF00690816

Huber, J. A., Butterfield, D. A., and Baross, J. A. (2002). Temporal changes in archaeal diversity and chemistry in a mid-ocean ridge subseafloor habitat. *Appl. Environ. Microbiol.* 68, 1585–1594. doi: 10.1128/AEM.68.4.1585-1594.2002

Huber, R., Kurr, M., Jannasch, H. W., and Stetter, K. O. (1989). A novel group of abyssal methanogenic archaebacteria (*Methanopyrus*) growing at 110 °C. *Nature* 342:833. doi: 10.1038/342833a0

Jeanthon, C., L'haridon, S., Cueff, V., Banta, A., Reysenbach, A. L., and Prieur, D. (2002). *Thermodesulfobacterium hydrogeniphilum* sp. nov., a thermophilic, chemolithoautotrophic, sulfate-reducing bacterium isolated from a deep-sea hydrothermal vent at guaymas basin, and emendation of the genus *Thermodesulfobacterium*. *Int. J. Syst. Evolut. Microbiol.* 52, 765–772.

Jeanthon, C., L'haridon, S., Reysenbach, A. L., Vernet, M., Messner, P., Sleytr, U. B., et al. (1998). *Methanococcus infernus* sp. nov., a novel hyperthermophilic lithotrophic methanogen isolated from a deep-sea hydrothermal vent. *Int. J. Syst. Evolut. Microbiol.* 48(Pt 3), 913–919.

Jones, W. J., Stugard, C. E., and Jannasch, H. W. (1989). Comparison of thermophilic methanogens from submarine hydrothermal vents. *Arch. Microbiol.* 151, 314–318. doi: 10.1007/BF00406557

Kelley, D. S., Baross, J. A., and Delaney, J. R. (2002). Volcanoes, fluids, and life at mid-ocean ridge spreading centers. *Annu. Rev. Earth Planet. Sci.* 30, 385–491. doi: 10.1146/annurev.earth.30.091201.141331

Kelley, D. S., Karson, J. A., Fruh-Green, G. L., Yoerger, D. R., Shank, T. M., Butterfield, D. A., et al. (2005). A serpentinite-hosted ecosystem: the lost city hydrothermal field. *Science* 307, 1428–1434. doi: 10.1126/science.1102556

Knittel, K., Kuever, J., Meyerdierks, A., Meinke, R., Amann, R., and Brinkhoff, T. (2005). *Thiomicrospira arctica* sp. nov. and *Thiomicrospira psychrophila* sp. nov., psychrophilic, obligately chemolithoautotrophic, sulfur-oxidizing bacteria isolated from marine arctic sediments. *Int. J. Syst. Evolut. Microbiol.* 55, 781–786. doi: 10.1099/ijs.0.63362-0

Konhauser, K. O. (2006). *Introduction to Geomicrobiology*. Hoboken, NJ: Wiley-Blackwell.

Kraemer, J. T. (2007). Improving the yield from fermentative hydrogen production. *Biotechnol. Lett.* 29, 685–695. doi: 10.1007/s10529-006-9299-9

Ladapo, J., and Whitman, W. B. (1990). Method for isolation of auxotrophs in the methanogenic archaebacteria: role of the acetyl-CoA pathway of autotrophic CO2 fixation in *Methanococcus maripaludis*. *Proc. Natl. Acad. Sci. U.S.A.* 87, 5598–5602. doi: 10.1073/pnas.87.15.5598

Léger, C., Dementin, S., Bertrand, P., Rousset, M., and Guigliarelli, B. (2004). Inhibition and aerobic inactivation kinetics of *Desulfovibrio* fructosovorans NiFe hydrogenase studied by protein film voltammetry. *J. Am. Chem. Soc.* 126, 12162–12172. doi: 10.1021/ja046548d

L'Haridon, S., Cilia, V., Messner, P., Raguenes, G., Gambacorta, A., Sleytr, U. B., et al. (1998). *Desulfurobacterium thermolithotrophum* gen. nov., sp. nov., a novel autotrophic, sulphur-reducing bacterium isolated from a deep-sea hydrothermal vent. *Int. J. Syst. Bacteriol.* 48(Pt 3), 701–711. doi: 10.1099/00207713-48-3-701

L'Haridon, S., Reysenbach, A. L., Banta, A., Messner, P., Schumann, P., Stackebrandt, E., et al. (2003). *Methanocaldococcus indicus* sp. nov., a novel hyperthermophilic methanogen isolated from the Central Indian Ridge. *Int. J. Syst. Evolut. Microbiol.* 53, 1931–1935. doi: 10.1099/ijs.0.02700-0

L'Haridon, S., Reysenbach, A. L., Tindall, B. J., Schonheit, P., Banta, A., Johnsen, U., et al. (2006). *Desulfurobacterium atlanticum* sp. nov., *Desulfurobacterium pacificum* sp. nov. and *Thermovibrio guaymasensis sp.* nov., three thermophilic members of the *Desulfurobacteriaceae fam.* nov., a deep branching lineage within the Bacteria. *Int. J. Syst. Evolut. Microbiol.* 56, 2843–2852. doi: 10.1099/ijs.0.63994-0

Lin, T. J., El Sebae, G., Jung, J. H., Jung, D. H., Park, C. S., and Holden, J. F. (2016). *Pyrodictium delaneyi* sp. nov., a hyperthermophilic autotrophic archaeon that reduces Fe(III) oxide and nitrate. *Int. J. Syst. Evolut. Microbiol.* 66, 3372–3376. doi: 10.1099/ijsem.0.001201

Liu, C., Gorby, Y. A., Zachara, J. M., Fredrickson, J. K., and Brown, C. F. (2002). Reduction kinetics of Fe(III), Co(III), U(VI), Cr(VI), and Tc(VII) in cultures of dissimilatory metal-reducing bacteria. *Biotechnol. Bioeng.* 80, 637–649. doi: 10.1002/bit.10430

Lovley, D. R., and Goodwin, S. (1988). Hydrogen concentrations as an indicator of the predominant terminal electron-accepting reactions in aquatic sediments. *Geochim. Cosmochim. Acta* 52, 2993–3003. doi: 10.1016/0016-7037(88)90163-9

McCollom, T. M. (2007). Geochemical constraints on source of metabolic energy for chemolithoautotrophy in ultramafic-hosted deep-sea hydrothermal systems. *Astrobiology* 7, 933–950. doi: 10.1089/ast.2006.0119

McCollom, T. M., and Shock, E. L. (1997). Geochemical constraints on chemolithoautotrophic metabolism by microorganisms in seafloor hydrothermal systems. *Geochim. Cosmochim. Acta* 61, 4375–4391. doi: 10.1016/S0016-7037(97)00241-X

McNichol, J., Stryhanyuk, H., Sylva, S. P., Thomas, F., Musat, N., Seewald, J. S., et al. (2018). Primary productivity below the seafloor at deep-sea hot springs. *Proc. Natl. Acad. Sci. U.S.A.* 115, 6756–6761. doi: 10.1073/pnas.1804351115

McNichol, J., Sylva, S. P., Thomas, F., Taylor, C. D., Sievert, S. M., and Seewald, J. S. (2016). Assessing microbial processes in deep-sea hydrothermal systems by incubation at in situ temperature and pressure. *Deep Sea Res. Part I: Oceanogr. Res. Papers* 115, 221–232. doi: 10.1016/j.dsr.2016.06.011

Mino, S., Kudo, H., Arai, T., Sawabe, T., Takai, K., and Nakagawa, S. (2014). *Sulfurovum aggregans* sp. nov., a hydrogen-oxidizing, thiosulfate-reducing

chemolithoautotroph within the epsilonproteobacteria isolated from a deep-sea hydrothermal vent chimney, and an emended description of the genus Sulfurovum. *Int. J. Syst. Evolut. Microbiol.* 64, 3195–3201. doi: 10.1099/ijs.0.065094-0

Miroshnichenko, M. L., and Bonch-Osmolovskaya, E. A. (2006). Recent developments in the thermophilic microbiology of deep-sea hydrothermal vents. *Extremophiles* 10, 85–96. doi: 10.1007/s00792-005-0489-5

Moussard, H., L'haridon, S., Tindall, B. J., Banta, A., Schumann, P., Stackebrandt, E., et al. (2004). *Thermodesulfatator indicus* gen. nov., sp. nov., a novel thermophilic chemolithoautotrophic sulfate-reducing bacterium isolated from the Central Indian Ridge. *Int. J. Syst. Evolut. Microbiol.* 54, 227–233. doi: 10.1099/ijs.0.02669-0

Muyzer, G., and Stams, A. J. (2008). The ecology and biotechnology of sulphate-reducing bacteria. *Nat. Rev. Microbiol.* 6, 441–454. doi: 10.1038/nrmicro1892

Nagata, R., Takaki, Y., Tame, A., Nunoura, T., Muto, H., Mino, S., et al. (2017). *Lebetimonas natsushimae* sp. nov., a novel strictly anaerobic, moderately thermophilic chemoautotroph isolated from a deep-sea hydrothermal vent polychaete nest in the Mid-Okinawa Trough. *Syst. Appl. Microbiol.* 40, 352–356. doi: 10.1016/j.syapm.2017.06.002

Nakagawa, S., and Takai, K. (2008). Deep-sea vent chemoautotrophs: diversity, biochemistry and ecological significance. *FEMS Microbiol. Ecol.* 65, 1–14. doi: 10.1111/j.1574-6941.2008.00502.x

Nakagawa, S., Takai, K., Horikoshi, K., and Sako, Y. (2003). *Persephonella hydrogeniphila* sp. nov., a novel thermophilic, hydrogen-oxidizing bacterium from a deep-sea hydrothermal vent chimney. *Int. J. Syst. Evolut. Microbiol.* 53, 863–869. doi: 10.1099/ijs.0.02505-0

Nakagawa, S., Takai, K., Inagaki, F., Hirayama, H., Nunoura, T., Horikoshi, K., et al. (2005). Distribution, phylogenetic diversity and physiological characteristics of epsilonproteobacteria in a deep-sea hydrothermal field. *Environ. Microbiol.* 7, 1619–1632. doi: 10.1111/j.1462-2920.2005.00856.x

Nealson, K. H., Inagaki, F., and Takai, K. (2005). Hydrogen-driven subsurface lithoautotrophic microbial ecosystems (SLiMEs): do they exist and why should we care? *Trends Microbiol.* 13, 405–410. doi: 10.1016/j.tim.2005.07.010

Novelli, P. C., Scranton, M. I., and Michener, R. H. (1987). Hydrogen distributions in marine sediments 1,2. *Limnol. Oceanogr.* 32, 565–576. doi: 10.4319/lo.1987.32.3.0565

Olins, H. C., Rogers, D. R., Preston, C., Ussler, W., Pargett, D., Jensen, S., et al. (2017). Co-registered geochemistry and metatranscriptomics reveal unexpected distributions of microbial activity within a hydrothermal vent field. *Front. Microbiol.* 8:1042. doi: 10.3389/fmicb.2017.01042

Perner, M., Gonnella, G., Hourdez, S., Bohnke, S., Kurtz, S., and Girguis, P. (2013a). In situ chemistry and microbial community compositions in five deep-sea hydrothermal fluid samples from Irina II in the Logatchev field. *Environ. Microbiol.* 15, 1551–1560. doi: 10.1111/1462-2920.12038

Perner, M., Hansen, M., Seifert, R., Strauss, H., Koschinsky, A., and Petersen, S. (2013b). Linking geology, fluid chemistry, and microbial activity of basalt- and ultramafic-hosted deep-sea hydrothermal vent environments. *Geobiology* 11, 340–355. doi: 10.1111/gbi.12039

Perner, M., Gonnella, G., Kurtz, S., and Laroche, J. (2014). Handling temperature bursts reaching 464°C: different microbial strategies in the Sisters Peak hydrothermal chimney. *Appl. Environ. Microbiol.* 80, 4585–4598. doi: 10.1128/AEM.01460-14

Perner, M., Hentscher, M., Rychlik, N., Seifert, R., Strauss, H., and Bach, W. (2011a). Driving forces behind the biotope structures in two low-temperature hydrothermal venting sites on the southern Mid-Atlantic Ridge. *Environ. Microbiol. Rep.* 3, 727–737. doi: 10.1111/j.1758-2229.2011.00291.x

Perner, M., Ilmberger, N., Köhler, H. U., Chow, J., and Streit, W. R. (2011b). "Emerging fields in functional metagenomics and its industrial relevance: overcoming limitations and redirecting the search for novel biocatalysts," in *Handbook of Molecular Microbial Ecology II*, ed. F. J. de Bruijn (Hoboken, NJ: John Wiley & Sons, Inc.), 481–498.

Perner, M., Petersen, J. M., Zielinski, F., Gennerich, H. H., and Seifert, R. (2010). Geochemical constraints on the diversity and activity of H2 -oxidizing microorganisms in diffuse hydrothermal fluids from a basalt- and an ultramafic-hosted vent. *FEMS Microbiol. Ecol.* 74, 55–71. doi: 10.1111/j.1574-6941.2010.00940.x

Petersen, J. M., Zielinski, F. U., Pape, T., Seifert, R., Moraru, C., Amann, R., et al. (2011). Hydrogen is an energy source for hydrothermal vent symbioses. *Nature* 476, 176–180. doi: 10.1038/nature10325

Pjevac, P., Meier, D. V., Markert, S., Hentschker, C., Schweder, T., Becher, D., et al. (2018). Metaproteogenomic profiling of microbial communities colonizing actively venting hydrothermal chimneys. *Front. Microbiol.* 9:680. doi: 10.3389/fmicb.2018.00680

Ragsdale, S. W., and Pierce, E. (2008). Acetogenesis and the wood-Ljungdahl pathway of CO(2) fixation. *Biochim. Biophys. Acta* 1784, 1873–1898. doi: 10.1016/j.bbapap.2008.08.012

Rousset, M., Magro, V., Forget, N., Guigliarelli, J., and Hatchikian, E. C. (1998). Heterologous expression of the *Desulfovibrio gigas* [NiFe] hydrogenase in *Desulfovibrio* fructososvorans MR400. *J. Bacteriol.* 180, 4982–4986.

Schlicht, S., Assaud, L., Hansen, M., Lickleder, M., Bechelany, M., Perner, M., et al. (2016). An electrochemically functional layer of hydrogenase extract on an electrode of large and tunable specific surface area. *J. Mater. Chem. A* 4, 6487–6494. doi: 10.1039/C6TA00392C

Scott, K. M., Sievert, S. M., Abril, F. N., Ball, L. A., Barrett, C. J., Blake, R. A., et al. (2006). The genome of deep-sea vent chemolithoautotroph *Thiomicrospira crunogena* XCL-2. *PLoS Biol.* 4:e383. doi: 10.1371/journal.pbio.0040383

Sievert, S. M., and Kuever, J. (2000). *Desulfacinum hydrothermale* sp. nov., a thermophilic, sulfate-reducing bacterium from geothermally heated sediments near Milos Island (Greece). *Int. J. Syst. Evolut. Microbiol.* 50(Pt 3), 1239–1246. doi: 10.1099/00207713-50-3-1239

Slobodkin, A. I., Reysenbach, A. L., Slobodkina, G. B., Kolganova, T. V., Kostrikina, N. A., and Bonch-Osmolovskaya, E. A. (2013). *Dissulfuribacter thermophilus* gen. nov., sp. nov., a thermophilic, autotrophic, sulfur-disproportionating, deeply branching deltaproteobacterium from a deep-sea hydrothermal vent. *Int. J. Syst. Evolut. Microbiol.* 63, 1967–1971. doi: 10.1099/ijs.0.046938-0

Slobodkina, G. B., Kolganova, T. V., Kopitsyn, D. S., Viryasov, M. B., Bonch-Osmolovskaya, E. A., and Slobodkin, A. I. (2016). *Dissulfurirhabdus thermomarina* gen. nov., sp. nov., a thermophilic, autotrophic, sulfite-reducing and disproportionating deltaproteobacterium isolated from a shallow-sea hydrothermal vent. *Int. J. Syst. Evolut. Microbiol.* 66, 2515–2519. doi: 10.1099/ijsem.0.001083

Slobodkina, G. B., Kolganova, T. V., Querellou, J., Bonch-Osmolovskaya, E. A., and Slobodkin, A. I. (2009). *Geoglobus acetivorans* sp. nov., an iron(III)-reducing archaeon from a deep-sea hydrothermal vent. *Int. J. Syst. Evolut. Microbiol.* 59, 2880–2883. doi: 10.1099/ijs.0.011080-0

Sondergaard, D., Pedersen, C. N., and Greening, C. (2016). HydDB: a web tool for hydrogenase classification and analysis. *Sci. Rep.* 6:34212. doi: 10.1038/srep34212

Takai, K., Campbell, B. J., Cary, S. C., Suzuki, M., Oida, H., Nunoura, T., et al. (2005). Enzymatic and genetic characterization of carbon and energy metabolisms by deep-sea hydrothermal chemolithoautotrophic isolates of epsilonproteobacteria. *Appl. Environ. Microbiol.* 71, 7310–7320. doi: 10.1128/AEM.71.11.7310-7320.2005

Takai, K., Hirayama, H., Nakagawa, T., Suzuki, Y., Nealson, K. H., and Horikoshi, K. (2004a). *Thiomicrospira thermophila* sp. nov., a novel microaerobic, thermotolerant, sulfur-oxidizing chemolithomixotroph isolated from a deep-sea hydrothermal fumarole in the TOTO caldera, Mariana Arc, Western Pacific. *Int. J. Syst. Evolut. Microbiol.* 54, 2325–2333. doi: 10.1099/ijs.0.63284-0

Takai, K., Nealson, K. H., and Horikoshi, K. (2004b). *Methanotorris formicicus* sp. nov., a novel extremely thermophilic, methane-producing archaeon isolated from a black smoker chimney in the Central Indian Ridge. *Int. J. Syst. Evolut. Microbiol.* 54, 1095–1100. doi: 10.1099/ijs.0.02887-0

Takai, K., Nakagawa, S., Sako, Y., and Horikoshi, K. (2003). *Balnearium lithotrophicum* gen. nov., sp. nov., a novel thermophilic, strictly anaerobic, hydrogen-oxidizing chemolithoautotroph isolated from a black smoker chimney in the Suiyo Seamount hydrothermal system. *Int. J. Syst. Evolut. Microbiol.* 53, 1947–1954. doi: 10.1099/ijs.0.02773-0

Takai, K., Nakamura, K., Toki, T., Tsunogai, U., Miyazaki, M., Miyazaki, J., et al. (2008). Cell proliferation at 122 degrees C and isotopically heavy CH4 production by a hyperthermophilic methanogen under high-pressure cultivation. *Proc. Natl. Acad. Sci. U.S.A.* 105, 10949–10954. doi: 10.1073/pnas.0712334105

Takai, K., Suzuki, M., Nakagawa, S., Miyazaki, M., Suzuki, Y., Inagaki, F., et al. (2006). *Sulfurimonas paralvinellae* sp. nov., a novel mesophilic, hydrogen- and sulfur-oxidizing chemolithoautotroph within the *Epsilonproteobacteria* isolated from a deep-sea hydrothermal vent polychaete nest, reclassification of *Thiomicrospira denitrificans* as *Sulfurimonas denitrificans* comb. nov. and emended description of the genus *Sulfurimonas*. *Int. J. Syst. Evolut. Microbiol.* 56, 1725–1733. doi: 10.1099/ijs.0.64255-0

Thauer, R. K. (1998). Biochemistry of methanogenesis: a tribute to marjory Stephenson. *Microbiology* 144(Pt 9), 2377–2406. doi: 10.1099/00221287-144-9-2377

Theodoratou, E., Paschos, A., Mintz-Weber, S., and Böck, A. (2000). Analysis of the cleavage site specificity of the endopeptidase involved in the maturation of the large subunit of hydrogenase 3 from *Escherichia coli*. *Arch. Microbiol.* 173, 110–116. doi: 10.1007/s002039900116

Timmer-Ten Hoor, A. (1975). A new type of thiosulphate oxidizing, nitrate reducing microorganism: *Thiomicrospira denitrificans* sp. nov. *Netherl. J. Sea Res.* 9, 344–350. doi: 10.1016/0077-7579(75)90008-3

Toki, T., Hamamoto, A., Tawata, M., Miyazaki, J., Nakamura, K., Abe, M., et al. (2016). Methanogens in H2 -rich hydrothermal fluids resulting from phase separation in a sediment-starved, basalt-hosted hydrothermal system. *Chem. Geol.* 447, 208–218. doi: 10.1016/j.chemgeo.2016.11.004

Topcuoglu, B. D., Stewart, L. C., Morrison, H. G., Butterfield, D. A., Huber, J. A., and Holden, J. F. (2016). Hydrogen limitation and syntrophic growth among natural assemblages of thermophilic methanogens at deep-sea hydrothermal vents. *Front. Microbiol.* 7:1240. doi: 10.3389/fmicb.2016.01240

van Haaster, D. J., Hagedoorn, P. L., Jongejan, J. A., and Hagen, W. R. (2005). On the relationship between affinity for molecular hydrogen and the physiological directionality of hydrogenases. *Biochem. Soc. Trans.* 33, 12–14. doi: 10.1042/BST0330012

Ver Eecke, H. C., Butterfield, D. A., Huber, J. A., Lilley, M. D., Olson, E. J., Roe, K. K., et al. (2012). Hydrogen-limited growth of hyperthermophilic methanogens at deep-sea hydrothermal vents. *Proc. Natl. Acad. Sci. U.S.A.* 109, 13674–13679. doi: 10.1073/pnas.1206632109

Ver Eecke, H. C., Kelley, D. S., and Holden, J. F. (2009). Abundances of hyperthermophilic autotrophic Fe(III) oxide reducers and heterotrophs in hydrothermal sulfide chimneys of the northeastern Pacific Ocean. *Appl. Environ. Microbiol.* 75, 242–245. doi: 10.1128/AEM.01462-08

Vetriani, C., Speck, M. D., Ellor, S. V., Lutz, R. A., and Starovoytov, V. (2004). *Thermovibrio ammonificans* sp. nov., a thermophilic, chemolithotrophic, nitrate-ammonifying bacterium from deep-sea hydrothermal vents. *Int. J. Syst. Evolut. Microbiol.* 54, 175–181. doi: 10.1099/ijs.0.02781-0

Vignais, P. M., and Billoud, B. (2007). Occurrence, classification, and biological function of hydrogenases: an overview. *Chem. Rev.* 107, 4206–4272. doi: 10.1021/cr050196r

Waite, D. W. (2018). Erratum: addendum: comparative genomic analysis of the class epsilonproteobacteria and proposed reclassification to *Epsilonbacteraeota* (phyl. nov.). *Front. Microbiol.* 9:772. doi: 10.3389/fmicb.2018.00772

Wankel, S. D., Germanovich, L. N., Lilley, M. D., Genc, G., Diperna, C. J., Bradley, A. S., et al. (2011). Influence of subsurface biosphere on geochemical fluxes from diffuse hydrothermal fluids. *Nat. Geosci.* 4, 461–468. doi: 10.1038/ngeo1183

Wolin, M. J. (1976). "Interactions between H2-producing and methane-producing species," in *Microbial Formation and Utilization of Gases*, eds H. G. Schlegel, G. Gottschalk, and N. Pfennig (Göttingen: Goltze), 141–150.

Conflict of Interest Statement: The authors declare that the research was conducted in the absence of any commercial or financial relationships that could be construed as a potential conflict of interest.

frontiers in Microbiology

REVIEW
published: 04 December 2018
doi: 10.3389/fmicb.2018.02911

Complex Multimeric [FeFe] Hydrogenases: Biochemistry, Physiology and New Opportunities for the Hydrogen Economy

*Kai Schuchmann, Nilanjan Pal Chowdhury and Volker Müller**

Molecular Microbiology and Bioenergetics, Institute of Molecular Biosciences, Johann Wolfgang Goethe University, Frankfurt am Main, Germany

Hydrogenases are key enzymes of the energy metabolism of many microorganisms. Especially in anoxic habitats where molecular hydrogen (H_2) is an important intermediate, these enzymes are used to expel excess reducing power by reducing protons or they are used for the oxidation of H_2 as energy and electron source. Despite the fact that hydrogenases catalyze the simplest chemical reaction of reducing two protons with two electrons it turned out that they are often parts of multimeric enzyme complexes catalyzing complex chemical reactions with a multitude of functions in the metabolism. Recent findings revealed multimeric hydrogenases with so far unknown functions particularly in bacteria from the class Clostridia. The discovery of [FeFe] hydrogenases coupled to electron bifurcating subunits solved the enigma of how the otherwise highly endergonic reduction of the electron carrier ferredoxin can be carried out and how H_2 production from NADH is possible. Complexes of [FeFe] hydrogenases with formate dehydrogenases revealed a novel enzymatic coupling of the two electron carriers H_2 and formate. These novel hydrogenase enzyme complex could also contribute to biotechnological H_2 production and H_2 storage, both processes essential for an envisaged economy based on H_2 as energy carrier.

Keywords: hydrogenase, formate dehydrogenase, CO_2 reduction, electron bifurcation, hydrogen production, acetogenesis, clostridia, hydrogen storage

OPEN ACCESS

Edited by:
Chris Greening,
Monash University, Australia

Reviewed by:
Armen Trchounian,
Yerevan State University, Armenia
Kyle Costa,
University of Minnesota Twin Cities, United States

***Correspondence:**
Volker Müller
vmueller@bio.uni-frankfurt.de

Specialty section:
This article was submitted to Microbial Physiology and Metabolism, a section of the journal Frontiers in Microbiology

Received: *30 August 2018*
Accepted: *13 November 2018*
Published: *04 December 2018*

Citation:
Schuchmann K, Chowdhury NP and Müller V (2018) Complex Multimeric [FeFe] Hydrogenases: Biochemistry, Physiology and New Opportunities for the Hydrogen Economy. Front. Microbiol. 9:2911. doi: 10.3389/fmicb.2018.02911

INTRODUCTION

Molecular hydrogen (H_2) is only present in trace concentrations (550 parts per billion) in the Earth's lower atmosphere (Novelli et al., 1999). Nevertheless, it plays an essential part in the biogeochemical cycles of other elements such as carbon and is a major constituent of the microbial metabolism. For example, H_2 is an important electron donor for methane formation in anoxic environments (Schink, 1997; Thauer et al., 2008). Here, too, steady state concentrations are very low ($pH_2 < 10$ Pa) but the turnover of H_2 is very high (150 million tons of H_2 of biological origin are estimated to be produced in anoxic ecosystem annually to fuel methanogenesis) (Thauer et al., 2008, 2010). In anoxic ecosystems, the major role of H_2 is electron transfer between the different participants of the food chain, e.g., transfer of electrons generated by primary fermenters to methanogens (Stams and Plugge, 2009; Schink et al., 2017). To produce or consume H_2 nature has evolved complex metalloenzymes, hydrogenases, which catalyze one of the simplest chemical reaction, reversible

oxidation of H_2 into two protons and two electrons:

$$H_2 \rightleftharpoons 2H^+ + 2e^- \quad (1)$$

Hydrogenases are widespread in nature and can be found in all domains of life. Based on their phylogeny, they can be classified into three distinct classes that are named by the metal ions contained in their active sites as [NiFe]-, [FeFe]-, and [Fe] hydrogenases (Vignais et al., 2001; Vignais and Colbeau, 2004). [NiFe] hydrogenases have been found in bacteria and archaea, [FeFe] hydrogenases in bacteria and some eukaryotes, and [Fe] hydrogenases only in archaea (Vignais and Billoud, 2007). Even though [NiFe]- and [FeFe] hydrogenases have evolved independently, the complex metal centers responsible for catalysis share many features. The metal ions are ligated by inorganic CO and CN^- ligands and are bridged by sulfur atoms. H_2 can reach the active sites that are buried within the enzymes by a hydrophobic gas channel and the electrons that result from H_2 oxidation are in both enzyme classes transferred to an [4Fe–4S] cluster adjacent to the metal center (Happe et al., 1997; Pierik et al., 1998; Fontecilla-Camps and Ragsdale, 1999). The third class of hydrogenases, the [Fe] hydrogenases which are only found in methanogenic archaea differ not only by their architecture of the active site, but also by the catalyzed reaction that does not result in the release of electrons to an iron–sulfur cluster, but the direct transfer to the cosubstrate methenyltetrahydromethanopterin (Shima and Thauer, 2007; Shima et al., 2008). In this review, we will mainly focus on hydrogenases of the [FeFe] class. Enzymes from this class are widespread in anaerobic prokaryotes and play important roles in the energy and carbon metabolism in anoxic ecosystems. Crystal structures have been reported for three enzymes, namely from *Clostridium pasteurianum* (Peters et al., 1998), *Desulfovibrio desulfuricans* (Nicolet et al., 1999) and the eukaryotic algae *Chlamydomonas reinhardtii* (Mulder et al., 2010) and show high similarity in the overall structure and the architecture of the active site. Details on the crystal structures and the reaction mechanism have been described in excellent and comprehensive reviews elsewhere and will therefore not been repeated here except for the architecture of the cofactors in the *C. pasteurianum* enzyme that we will discuss in the context of electron bifurcation later (Vignais and Colbeau, 2004; Thauer et al., 2010; Lubitz et al., 2014). Interestingly, despite the apparent high similarity of the "core" hydrogenase subunit responsible for H_2 oxidation and production, [FeFe] hydrogenases show a remarkable diversity with respect to the auxiliary subunits that can be found in most enzymes and an even higher diversity can be predicted from genome sequence data. The auxiliary subunits follow a very modular structure and add multiple functions to the core subunit. These functions can include electron transfer to soluble electron carriers, coupling of H_2 oxidation/production to other chemical reactions, coupling to energy conservation by coupling the electron transfer to the generation of a transmembrane ion potential, or utilization of the novel energetic coupling mechanism of flavin-based electron bifurcation (FBEB) to overcome energetic limitations of the electron transfer (Buckel and Thauer, 2018a,b; Müller et al., 2018). A notable diversity of multimeric [FeFe] hydrogenases can be found especially in the strictly anaerobic Gram-positive bacteria of the class Clostridia within the phylum Firmicutes (Calusinska et al., 2010; Schmidt et al., 2010). Recent discoveries have revealed multimeric hydrogenases with remarkable and so far undescribed functions and catalytic properties, solving important questions of the metabolism and ecosystem functioning in anoxic environment. In addition, recently described multimeric hydrogenases provide interesting opportunities for biotechnological applications. H_2 is a candidate energy carrier that could replace fossil fuels for storage and transportation of energy generated from renewable sources such as wind or solar power (Dunn, 2002; Brandon and Kurban, 2017). However, for an economically viable H_2 economy many obstacles need to be overcome such as efficient methods for H_2 production and technologies for storage and transportation of the volatile and explosive gas (Service, 2004; Preuster et al., 2017a).

Here, we review the recent findings of novel complex multimeric hydrogenases and especially their function in the microbial H_2 metabolism. These include enzymes using the novel energy coupling mechanism of FBEB enabling otherwise endergonic H_2 production from NADH or the otherwise endergonic electron transfer from H_2 to the iron–sulfur protein ferredoxin. The second part will focus on the recently discovered formate dehydrogenase coupled hydrogenases enabling direct CO_2 reduction with H_2 or H_2 evolution from formate. In addition, both hydrogenase types will be discussed in the context of their biotechnological potential for the H_2 economy.

H_2 FUNCTIONING AS ELECTRON CARRIER IN ANOXIC ECOSYSTEMS

H_2 can be utilized by many organisms as electron donor. Recently, it has been reported that microorganisms are even capable of utilizing the low atmospheric concentrations of H_2 (Greening et al., 2014a,b). Nevertheless, the most prominent functions of H_2 are found in anoxic ecosystems where it is rapidly produced and consumed by microorganisms resulting in a large turnover. H_2 connects different parts of the food web to allow full remineralization of organic material. When complex polymeric organic material (polysaccharides, proteins, nucleic acids, lipids) enter anoxic ecosystems it is typically first hydrolyzed by exoenzymes followed by the partial oxidation by primary fermenting microorganisms into different fermentation products such as lactate, alcohols, short chain fatty acids, acetate, formate, CO_2 and H_2. In the absence of suitable external electron acceptors, the latter compounds (acetate, formate, CO_2 and H_2) can be directly converted by methanogenic archaea into methane (Schink, 1997; Thauer et al., 2008). Further oxidation of the other compounds leads to an energetic problem that can only be solved by the concerted cooperation of secondary fermenting organisms with methanogens in a process call syntrophy (Schink, 2002; Sieber et al., 2012; Morris et al., 2013). Secondary fermenters oxidize their substrates typically to acetate as end product coupled to oxidation of protons to H_2 to reoxidize their electron carriers. However, under standard conditions these reactions are endergonic and do not provide

energy for the cell. During substrate oxidation, electrons are typically transferred to either ferredoxin, a small iron–sulfur cluster containing protein with a very negative redox potential ($E°'$ = −400 to −500 mV), or NAD^+ with a more positive redox potential ($E°'[NAD^+/NADH]$ = −320 mV) (Thauer et al., 1977). Proton reduction can be used to recycle these electron carriers. The redox potential of the H^+/H_2 couple is, under standard conditions, −414 mV. Therefore, while H_2 production from reduced ferredoxin is an exergonic reaction, H_2 formation from NADH represents a strong energetic barrier for the cells since it is a highly endergonic reaction (Thauer et al., 1977). Two possible mechanisms have evolved to overcome this problem and allow H_2 formation from NADH. In the classical view, H_2 oxidizing methanogens lower the H_2 partial pressure to very low values (1–10 Pa H_2) resulting in a more positive redox potential of the H^+/H_2 couple (above −300 mV) thus rendering H_2 formation from NADH an exergonic reaction (Schink, 2002; Sieber et al., 2012; Morris et al., 2013). Recently, another mechanism has been discovered that solves the problem of NADH reoxidation with protons as acceptor within one enzyme. Complex multimeric hydrogenases are necessary to catalyze this reaction that solves the energetic problem by energetically coupling the endergonic electron transfer to a second exergonic redox reaction, a process called FBEB. As we will see later, these enzymes not only participate in the metabolism of secondary fermenting organisms but can also be found in primary fermenters, thereby increasing the energy yield that can be conserved from a given substrate, or, in the reverse, be found in acetogenic bacteria to allow ferredoxin reduction with H_2 as electron donor.

THE CONCEPT OF FLAVIN-BASED ELECTRON BIFURCATION

In 2008 a new energy coupling mechanism called FBEB was first discovered in an enzyme complex of an electron-transferring flavoprotein and a butyryl-CoA dehydrogenase (Etf/Bcd) (Herrmann et al., 2008; Li et al., 2008). In FBEB, an electron pair from an electron donor such as NADH is split toward two different one-electron acceptors, one with a more positive redox potential and another with a much lower redox potential than that of the electron donor. It was proposed and later proven that electron transfer to a positive redox potential (exergonic reaction) sustains the movement of an electron to a more negative redox potential (endergonic reaction). In case of Etf/Bcd, the positive electron redox potential acceptor was crotonyl-CoA ($E^{0'}$ = −10 mV) and the negative redox potential acceptor was ferredoxin ($E^{0'}$ = −420 mV). NADH ($E^{0'}$ = −320 mV) is the electron donor. The complete reaction catalyzed by the protein complex is

$$\begin{aligned} &\text{Crotonyl}-\text{CoA} + 2\,\text{NADH} + \text{Fd}_{ox} \\ \rightarrow\ &\text{Butyryl}-\text{CoA} + 2\,\text{NAD}^+ + \text{Fd}_{red} \end{aligned} \quad (2)$$

The enzyme complex contained FAD as the only cofactor that was essential for the activity (Chowdhury et al., 2014; Demmer et al., 2017). Hence, the name originated as FBEB. FBEB was drawn in analogy to the quinone-based electron bifurcation (QBEB) of the cytochrome bc_1 complex of the respiratory chain, which was discovered 43 years ago by Peter Mitchell, in which the oxidation of reduced ubiquinone (UQH_2) by the high potential cytochrome c_1 by one electron allows the reduction of low-potential cytochrome b_L and further UQ inside the membrane (Mitchell, 1975). The process is repeated twice that allows four protons to be released outside of the cell and doubling the amount of energy conserved and electrons finally flow down to oxygen (terminal electron acceptor) to reduce oxygen to water.

H_2 PRODUCTION FROM NADH: ELECTRON-BIFURCATING HYDROGENASES FOR H_2 EVOLUTION

Soon after the discovery of FBEB in Clostridia, the first hydrogenase was reported that utilizes the mechanism of FBEB, however, in the physiological context in the reverse direction (named electron confurcation) (Schut and Adams, 2009). The enzyme was discovered in the hyperthermophilic and anaerobic bacterium *Thermotoga maritima.* The bacterium ferments one mole of glucose by the classical Embden–Meyerhof–Parnas pathway to two moles of CO_2, two acetate and four moles of H_2 (Schroder et al., 1994). During its metabolism, both NADH and reduced ferredoxin are generated, however, for decades the link to the oxidation of these electron carriers to H_2 production remained obscure (Wrba et al., 1990; Blamey and Adams, 1993). The trimeric [FeFe] hydrogenase was isolated and could be assayed by coupling reduction of viologen dyes with H_2. However, the enzyme did not use either reduced ferredoxin or NADH as sole electron donor (Verhagen et al., 1999). Though reduced clostridial ferredoxin ($E^{0'}$ = −420 mV) alone can reduce protons to H_2 ($E^{0'}$ = −414 mV), NADH cannot. It was an enigma since the discovery of fermentative H_2 production to how H_2 is produced from NADH. The solution was FBEB: exergonic electron flow from reduced ferredoxin to H^+ that drives endergonic electron flow from NADH to H^+, according to:

$$\text{NADH} + \text{Fd}_{red} + 3\,\text{H}^+ \rightleftharpoons \text{NAD}^+ + \text{Fd}_{ox} + 2\,\text{H}_2 \quad (3)$$

The hydrogenase of *T. maritima* is now the classic example where reduced ferredoxin drives H_2 evolution from NADH. The enzyme oxidizes NADH and ferredoxin simultaneously in a 1:1 ratio to produce H_2. In this case both electrons from NADH and reduced ferredoxin are converged to reduce protons to H_2. This mode of electron converging from different sources of electron donor (NADH and Fd_{red}) to a single electron acceptor (protons) is now called electron confurcation. A similar lifestyle and metabolic pathway is also observed in the rumen bacterium *Ruminococcus albus* (Zheng et al., 2014). Similar to *T. maritima*, when grown in continuous culture the bacterium produces the same amounts of H_2 and acetate from glucose (**Figure 1A**). Also, the acetogenic model bacterium *Acetobacterium woodii* is suggested to use a confurcating hydrogenase to evolve H_2 from organic substrates (Schuchmann and Müller, 2012; Bertsch et al., 2015; Kremp et al., 2018). This mode of H_2 evolution

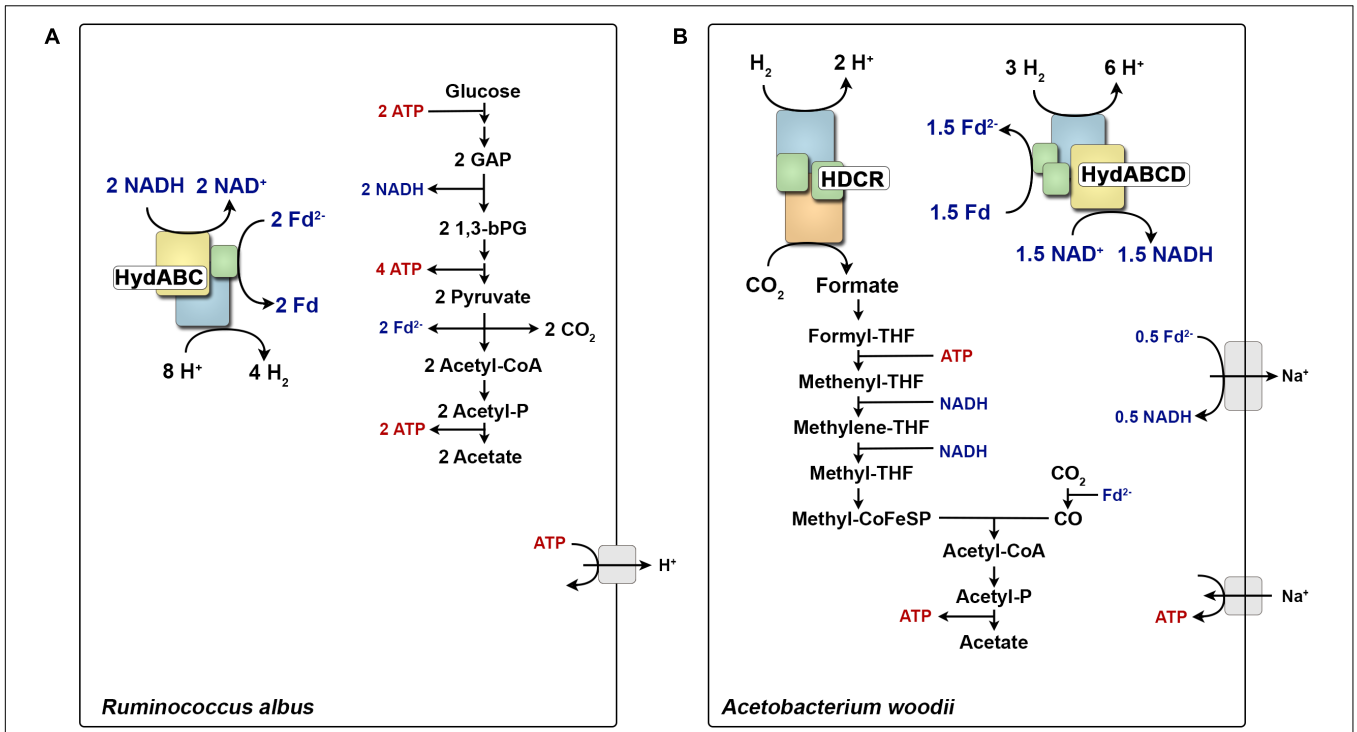

FIGURE 1 | Role of multimeric hydrogenases in the energy metabolism of *Ruminococcus albus* **(A)** and *Acetobacterium woodii* **(B)**. During glucose fermentation, *R. albus* oxidizes glucose to two molecules acetate. All generated reducing equivalents are reoxidized by the electron confurcating hydrogenase HydABC. In contrast, *A. woodii* can grow with H_2 + CO_2 as substrates and forms acetate as major end product. HDCR catalyzes the first step of the WLP from CO_2 to formate. All reducing equivalents are provided from H_2 oxidation catalyzed by the electron bifurcating hydrogenase HydABCD. Fd^{2-}, reduced ferredoxin; CoA, coenzyme-A; THF, tetrahydrofolate; CoFeSP, corrinoid–iron–sulfur protein; GAP, glyceraldehyde 3-phosphate; 1,3-bPG, 1,3-bisphosphoglycerate.

by electron confurcating hydrogenases is important for energy conservation in these fermenting bacteria. ATP is synthesized by substrate level phosphorylation at the phosphoglycerate kinase and pyruvate kinase reactions and NADH is formed by NAD-specific glycerinaldehyde-3-phosphate-dehydrogenase. The redox pool could for example be balanced by reducing pyruvate to lactate, where 2 NADH will be consumed. However, this pathway will produce 2 ATP less. Rather the bacteria maintain its redox balance by producing two moles of acetyl-CoA *via* the pyruvate-ferredoxin oxidoreductase and finally releases 2 ATP catalyzed by the acetate kinase. This mode of metabolism leaves 2 NADH and 2 reduced ferredoxin that are converted to H_2 by FBEB hydrogenase. Hence, the presence of FBEB hydrogenases allows NADH and ferredoxin to be reoxidized with H^+ as electron acceptor and thus increasing the ATP yield (Müller et al., 2018).

ELECTRON-BIFURCATING UPTAKE HYDROGENASES

In the autotrophic mode of life, organisms can synthesize most of their carbon compounds from CO_2 using H_2 or another electron donor as reductant. One such group are the acetogenic bacteria that are capable of producing acetate from two molecules of CO_2 with H_2 as the reductant *via* the reductive acetyl-CoA pathway (also known as Wood–Ljungdahl pathway, WLP) (Wood, 1991; Wood and Ljungdahl, 1991). Three model organisms that have been studied in detail are *Moorella thermoacetica, A. woodii,* and *Clostridium ljungdahlii.* As these bacteria grow simply on CO_2 and H_2 without any external carbon source added, this mode of metabolism must be coupled to net ATP formation.

A. woodii as a model organism has been studied in detail to answer how energy is conserved during acetogenesis (Schuchmann and Müller, 2014). This unearthed surprising enzyme complexes that are unique in their diversity of the reactions they catalyze as well as their working mechanisms. Three such enzyme complexes are the Rnf complex, an FBEB hydrogenase and a H_2-dependent CO_2 reductase. *A. woodii* employs a sodium ion-dependent ferredoxin: NAD-oxidoreductase (Rnf complex) that couples the exergonic oxidation of reduced ferredoxin ($E^{0'} \sim -450$ mV) with NAD^+ ($E^{0'} = -320$ mV) to the generation of a transmembrane electrochemical Na^+ gradient (**Figure 1B**). The difference in the redox potential of ferredoxin and NAD^+/NADH allows the pumping of Na^+ over the cytoplasmic membrane resulting in a Na^+ gradient that then drives the synthesis of ATP *via* the well-characterized Na^+ F_1F_O-ATP synthase (Spruth et al., 1995). Therefore, to drive energy conservation catalyzed by the Rnf complex, ferredoxin needs to be reduced. *A. woodii* solves this problem by using a FBEB uptake hydrogenase (Schuchmann and Müller, 2012) which is quite similar to the electron confurcating hydrogenases from *T. maritima* or *R. albus* (Zheng et al., 2014).

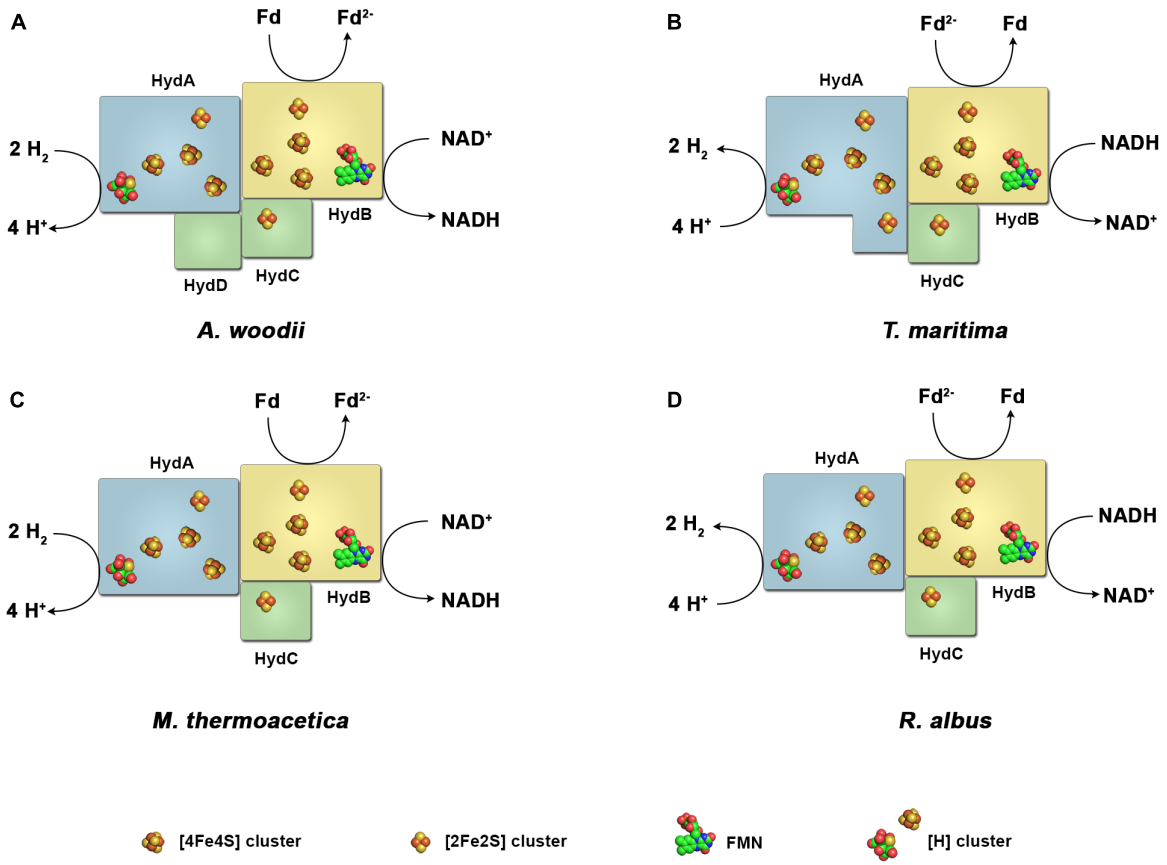

FIGURE 2 | Diversity of the subunit architecture and cofactor content of electron bifurcating and confurcating hydrogenases. Enzymes of this class have been isolated and characterized from *A. woodii* **(A)**, *T. maritima* **(B)**, *M. thermoacetica* **(C)** and *R. albus* **(D)**. All enzymes contain the subunits HydA, harboring the active site, the putative flavin-containing and NAD-binding subunit HydB, and the putative electron-transferring subunit HydC. *A. woodii* contains the additional subunit HydD. The arrangement of the iron–sulfur clusters and the binding site for ferredoxin are chosen arbitrary. Fd, ferredoxin.

However, in case of chemolitotrophic growth, H_2 is oxidized to reduce both NAD^+ and ferredoxin. The hydrogenase couples the exergonic oxidation of H_2 ($E^{0'} = -414$ mV) with NAD^+ ($E^{0'} = -320$ mV) to the endergonic reduction of ferredoxin ($E^{0'} \sim -450$ mV). Reduced ferredoxin is used in two different reactions, one to reduce CO_2 to CO ($E^{0'} = -520$ mV) in the WLP and secondly to transfer electrons *via* the Rnf to NAD^+, resulting in a Na^+ gradient (Biegel and Müller, 2010, 2011; Biegel et al., 2011). However, reaching the very low reduction potential for CO_2 to CO reduction is difficult even at very high H_2 partial pressure (10^5 Pa). FBEB provides an elegant solution by providing reduced ferredoxin with a more negative redox potential than the initial electron donor H_2. The same is true when *A. woodii* is grown on methanol, where FBEB hydrogenase provides the extra reduced ferredoxin which is then used for CO_2 reduction (Kremp et al., 2018).

The hydrogenase of *A. woodii* has been studied in the context of the autotrophic metabolism where its function is H_2 oxidation. Besides, further insights into the non-autotrophic metabolism of *A. woodii* have revealed that the enzyme may function as a H_2-evolving (electron bifurcating) hydrogenase as well. For example, when *A. woodii* grows on ethanol, only NADH is produced when ethanol is oxidized to acetyl-CoA. One part of the NADH is oxidized at the Rnf complex reducing ferredoxin. This reduced ferredoxin is then used with the other part of NADH by the hydrogenase to produce H_2 for the first step of the WLP (**Figure 1B**) (Bertsch et al., 2015). So, the electron-bifurcating/confurcating hydrogenase from *A. woodii* provides a nice example how anaerobes have evolved their metabolic enzymes which serves the purpose of both uptake and evolving H_2 when needed in two different modes of energy metabolism.

COFACTOR AND SUBUNIT ARCHITECTURE OF FBEB HYDROGENASES

The H_2 forming hydrogenases from *T. maritima*, *R. albus*, and *M. thermoacetica* (Wang et al., 2013b) and the H_2 uptake/forming hydrogenase from *A. woodii* possess quite similar subunit compositions (**Figure 2**). All four enzymes are composed of the three subunits Hyd A (~64 kDa), Hyd B (~65 kDa) and Hyd C (~14 kDa). HydA from *T. maritima* is larger compared to its counterpart by having a size of 73 kDa putatively containing

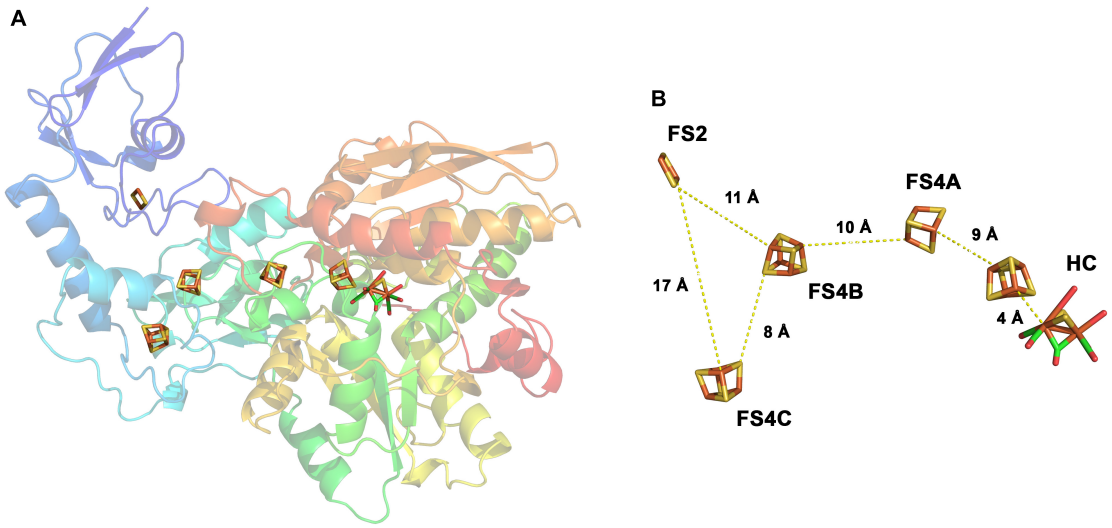

FIGURE 3 | Structure of the monomeric ferredoxin-dependent hydrogenase of *C. pasteurianum*. The 3D structure has been solved at 1.8 Å resolution (1FEH, RSCB PDB database). The monomeric enzyme contains the H-cluster typical for [FeFe] hydrogenases including the auxiliary [4Fe–4S] cluster. In addition, one [2Fe–2S]- and three [4Fe–4S] clusters are bound in the enzyme **(A)**. The iron–sulfur centers are arranged in a forked architecture with cluster FS2 being too far away from FS4C for direct electron transfer **(B)**. FS2 and FS4C are both close enough to FS4B for electron transfer. HC, H-cluster. Modified from Peters et al. (1998).

an additional [2Fe–2S] cluster. Another exception is that the *A. woodii* hydrogenase has an extra subunit HydD (∼15 kDa) which is predicted to contain no cofactor (Schuchmann and Müller, 2012, 2014). On amino acid sequence comparison, HydA finds the closest similarity to the monomeric [FeFe] hydrogenase from *C. pasteurianum* (**Figure 3**). The first crystal structure of the [FeFe] hydrogenase from *C. pasteurianum* CpI was reported by Peters et al. (1998). The overall structure of the core domain consists of the H-cluster (the active site of [FeFe] hydrogenases catalyzing H_2 oxidation) including a diiron subcluster and one [4Fe–4S] cluster connected *via* a cysteine residue as found conserved in most of the [FeFe] hydrogenases. The diiron metals are coordinated by CN^- and CO, while the proximal Fe is linked to a cubane [4Fe–4S] cluster *via* a cysteine. The [4Fe–4S] is around 4 Å apart from the di-iron center. Apart from the H_2-activating domain the domain interacting with the active-site domain contains two [4Fe–4S] clusters named as FS4A and FS4B (**Figure 3**). FS4A is 9 Å apart from the H-cluster thus the direct electron carrier to or from the H-cluster. FS4A is around 10 Å apart from FS4B cluster and thus in line to the putative electron transfer pathway. There are two additional domains, one containing a [2Fe–2S] cluster named FS2 (11 Å from FS4B), the other contains a single [4Fe–4S] cluster called FS4C. FS4C has an unusual three cysteine and one histidine ligation. The two clusters FS4C and FS2 exhibit a forked architecture, where FS2 is far away from the direct line of electron transfer from FS4C. Most probably, FS4C directly gets electron from FS4B and finally transfers electrons to ferredoxin. A recent study using protein–protein docking modeling and NMR studies of electron transfer complex formation between the photosynthetic electron-transfer ferredoxin (PetF) containing a [2Fe–2S] cluster and the hydrogenase HydA1 from the microalga *C. reinhardtii* revealed PetF to interact with HydA1 near to FS4C (Chang et al., 2007; Rumpel et al., 2015). The function of FS2 and the forked orientation of the possible electron transfer chains is puzzling, especially in the context of an electron bifurcating enzyme.

Assuming a similar structural organization and cofactor content in the FBEB hydrogenases, HydA is predicted as the catalytic subunit for H_2 oxidation. It contains the H-cluster which is the site for H_2 activation, one [2Fe–2S] and three [4Fe–4S] clusters. HydB has closest similarity to the NADH binding subunit NuoF of NADH-quinone oxidoreductase from *E. coli*, and is predicted to contain one FMN, one [2Fe–2S] and three [4Fe–4S] clusters. HydC, which is related to NuoE, contains only one [2Fe–2S] cluster.

A POSSIBLE ELECTRON PATHWAY IN FBEB HYDROGENASES

How can the electron flow from H_2 to NAD^+ and H_2 to ferredoxin be energetically coupled within these multimeric hydrogenases? Until now the basis of FBEB has been revealed in other enzyme complexes like the Etf/Bcd complex from *Acidaminococcus fermentans* (Chowdhury et al., 2014, 2016), *C. difficile* (Demmer et al., 2017) and *Megasphaera elsdenii* (Chowdhury et al., 2015), LctBCD and CarCDE of *A. woodii* (Bertsch et al., 2013; Weghoff et al., 2015) and the Nfn transhydrogenase from *T. maritima* (Demmer et al., 2015), *Pyrococcus furiosus* (Lubner et al., 2017), FixABCX of *Azotobacter vinelandii* (Ledbetter et al., 2017) and HdrABC-MvhAGD from the thermophilic methanogenic archaeon *Methanothermococcus thermolithotrophicus* (Wagner et al., 2017). However, FBEB hydrogenases represent a very special case. FBEB enzymes so far all are proposed to contain a flavin having special redox properties. Flavins have three different redox potentials for the

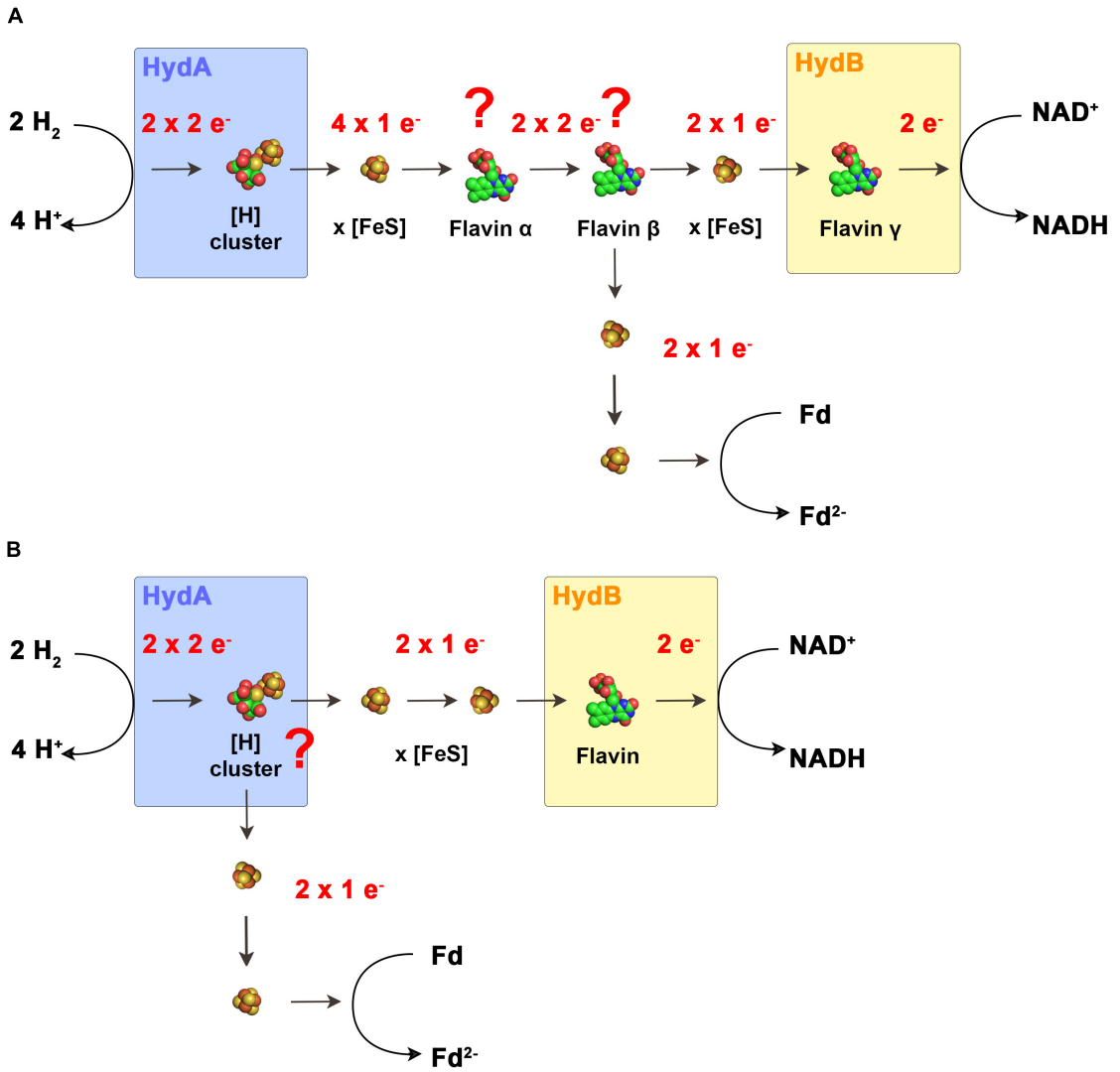

FIGURE 4 | Models for the electron flow in electron bifurcating hydrogenases. In the scenario that electron-bifurcation is facilitated by a flavin **(A)** according to the standard model of FBEB, the enzymes would have to contain two additional flavins that cannot be predicted from the primary structure. Flavin α functions as switch from one electron transferring iron–sulfur clusters to the actual bifurcating flavin β. Here, the two electrons are bifurcated to other iron–sulfur clusters and to the final acceptors. Flavin γ functions as switch from the one electron transferring iron–sulfur clusters to NAD^+. In the second scenario **(B)**. The H-cluster is the site of electron bifurcation. Here only one flavin is required for the switch from the one electron transferring iron–sulfur clusters to NAD^+. Fd, ferredoxin.

three possible redox reactions:

$$FMN + 1\ e^- \rightleftharpoons\ FMN^{\circ -}\quad (E_1) \tag{4}$$

$$FMN^{\circ -} + 1\ e^- + 2\ H^+ \rightleftharpoons FMNH_2\quad (E_2) \tag{5}$$

$$FMN + 2\ e^- + 2\ H^+ \rightleftharpoons FMNH_2\quad (E_3) \tag{6}$$

In "standard" flavins the midpoint potential of E_1 is more positive than E_2. In FBEB enzymes the flavin is supposed to have a "crossed" redox potential meaning that E_1 is more negative than E_2 (Nitschke and Russell, 2012). The two-electron redox potential (E_3) is supposed to be between, meaning the average, of E_1 and E_2. Therefore, the flavin can be reduced in a two-electron transfer reaction by the electron donor (E_3) followed by the first electron being transferred to the more positive electron acceptor (e.g., NAD^+) (E_2) leaving behind a highly reactive $FMN^{\circ -}$ that can now transfer the second electron to the more negative electron acceptor (e.g., ferredoxin) (E_1) (Demmer et al., 2017; Baymann et al., 2018; Buckel and Thauer, 2018a).

Based on the current knowledge, FBEB hydrogenases have only one predicted flavin in HydB which is required for the switch from a two-electron carrier (NADH) to a one electron carrier (iron–sulfur cluster), a typical function of "standard" flavins. Therefore, Buckel and Thauer (2013) proposed that FBEB hydrogenases need to have an additional "special" flavin to perform the electron bifurcation reaction. To function in

accordance to the standard model of FBEB, the electron flow would look like the following (**Figure 4A**): H_2 is oxidized at the H-cluster followed by the electron transfer to the iron–sulfur clusters. H_2 has a redox potential in between NAD^+ and ferredoxin, therefore, it must reduce the flavin with a two-electron transfer reaction to reach the flavin redox potential E_3. However, since iron sulfur clusters can only transfer one electron at a time we therefore speculate that in this model a second flavin (flavin α) would be required for the additional one electron/two electron switch. Then, the "special" flavin (flavin β) can transfer the first electron to the iron sulfur cluster leading to NAD^+ leaving behind a highly reactive flavin radical that transfers the second electron to the iron–sulfur clusters leading to ferredoxin. The third flavin (flavin γ) is then needed for the second one electron/two electron switch from the iron sulfur clusters to NAD^+.

Of the characterized FBEB enzymes HdrABC-MvhAGD from *M. thermolithotrophicus*, a complex of a multimeric heterodisulfide reductase and a [NiFe] hydrogenase represents a special case (Wagner et al., 2017). The flavin proposed to be responsible for electron bifurcation is assumed to receive both electrons from H_2 in two single electron transfer steps in contrast to a two electron transfer from a hydride donor. This is in contrast to the current model of the energetic landscape required for electron bifurcating flavins. However, if electron bifurcation is possible by a flavin connected to three one electron donors/acceptors in the form of iron–sulfur clusters, this could also be the case in FBEB [FeFe] hydrogenases and would render the presence of the hypothetically proposed flavin α redundant.

The aforementioned model assumes the presence of additional flavin binding sites that are not predicted by the amino acid sequence. The flavin content of all isolated FBEB hydrogenases could not be determined or not reported since the flavins are only loosely attached and must be added to the buffers for activity and got immediately lost when left out of the buffers. Assuming that the additional flavins do not exist, a completely new mechanism of FBEB must be present in FBEB hydrogenases. First Nitschke and Russell (2012) raised the possibility that also some metal centers could have crossed redox potentials and could potentially catalyze the same reaction as catalyzed by the flavin cofactor. Peters et al. (2018) took up this exciting possibility and proposed for electron bifurcating hydrogenases that since the FMN cannot be the site for electron bifurcation, the H-cluster could be the possible site for the electron bifurcation reaction. In their proposal, the electrons flow from the H-cluster directly to two different accepting iron–sulfur clusters with different redox potentials. The first string of Fe–S clusters transfers the electrons from the H-cluster to ferredoxin. The other string of iron–sulfur clusters plus the single flavin transfers the electrons from the H-cluster to NAD^+ (**Figure 4B**). However, so far no metal center has been shown to accommodate the special properties necessary for electron bifurcation, therefore, this model would lead to a completely new field of enzyme mechanism catalyzed by metal centers.

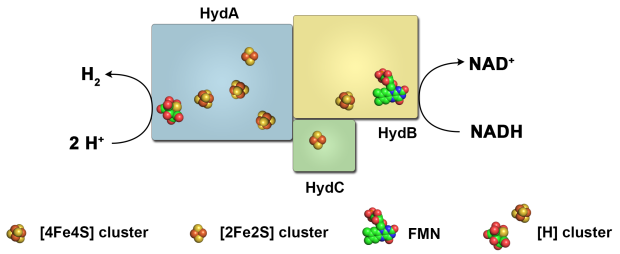

FIGURE 5 | Subunit architecture and cofactor content of the NADH-dependent hydrogenase of *S. wolfei*. This enzyme resembles in the overall subunit architecture electron bifurcating/confurcating hydrogenases that utilize NADH and reduced ferredoxin in an energetically coupled reaction to produce H_2 (or *vice versa*). The hydrogenase of *S. wolfei* putatively lacks three iron–sulfur clusters in the subunit HydB and utilizes NADH alone for H_2 production, thus not using FBEB.

THE CURIOUS CASE OF THE NAD^+-DEPENDENT HYDROGENASE FROM *Syntrophomonas wolfei*

Recently, a hydrogenase has been purified from the syntrophic bacterium *S. wolfei* that very much resembles all known FBEB hydrogenases discussed so far, however, does not show FBEB (Losey et al., 2017). Therefore, comparison of this enzyme to the other ones might be helpful to unravel the mechanism of FBEB hydrogenases. The purified recombinant hydrogenase (Hyd1ABC) of *S. wolfei* showed H_2 production from NADH alone, uncoupled to ferredoxin. The recombinant enzyme had a very high H_2-dependent: methyl-viologen reducing activity (3,340 U/mg), H_2-dependent NAD^+ reducing activity (94.5 U/mg) and catalyzed H_2 production from NADH with a specific activity of 6.6 U/mg. The enzyme is a trimeric protein complex composed of HydA1 (63 kDa), HydB1 (43 kDa), and HydC1 (17.5 kDa) (**Figure 5**). It contains five [4Fe–4S], two [2Fe–2S] clusters, and one H-cluster. The flavin content was determined to be 0.7 mol of FMN per mole of enzyme. The Hyd1ABC subunits share close similarity to those of the earlier discussed FBEB hydrogenases. HydA1 is, again, similar to the monomeric *C. pasteurianum* hydrogenase, putatively containing the H-cluster, 3 [4Fe–4S] clusters and one [2Fe–2S] cluster and is the site for H_2 formation. HydC1 has been predicted to contain one [2Fe–2S] cluster. Nevertheless, the question arose why this enzyme Hyd1ABC of *S. wolfei*, though having the same organization of subunits like FBEB hydrogenases, does not oxidize/reduce ferredoxin. One reason that the authors discuss is the lack of one [2Fe–2S] cluster putatively bound in a N-terminal domain of HydB of FBEB hydrogenases as well as the lack of one [4Fe–4S] cluster putatively bound in the C-terminal domain of HydB of FBEB hydrogenases. In fact, *S. wolfei* HydB1 is much smaller than HydB of other FBEB hydrogenases (43 kDa compared to 63 kDa). Electrons are supposed to be transferred from NADH *via* the FMN to the proximal [4Fe–4S] cluster, and further transferred *via* the [Fe–S] clusters in HydA1 to the H-cluster to reduce protons to H_2. The *S. wolfei* hydrogenase

might be a step in evolution away from FBEB hydrogenases to "standard" hydrogenases or, possibly, the other way around. In any case, solving the structure of this enzyme and comparing it to a bifurcating hydrogenase might unravel factors essential for the energetic coupling within the bifurcating enzymes.

FORMATE DEHYDROGENASE COUPLED HYDROGENASES

Protons can be used by microorganisms as ubiquitously available electron acceptor to get rid of excess reducing equivalents. A similar function is played by CO_2. In anoxic environments, CO_2 or HCO_3^- is ubiquitously available (50–100 mM HCO_3^- in lake sediments, 200-400 mM HCO_3^- in biogas reactors) and can be used as electron acceptor yielding formic acid/formate (Crable et al., 2011; Schink et al., 2017). Interestingly, the redox potential of the CO_2/formate couple of −432 mV is very close to the H^+/H_2 couple rendering both electron acceptors energetically very similar. Therefore, it is not surprising that both H_2 and formate have been observed as important electron carriers in anoxic environments with often interchangeable functions (Thiele and Zeikus, 1988; Stams and Plugge, 2009; Schink et al., 2017; Montag and Schink, 2018). However, for a long time little was known on how the two pools of high energy redox mediators are connected with each other. In the past years these two compounds gained increasing interest due to their potential as electron donors for biofuel production, as energy carriers for mobile applications or issues like H_2 storage. This has led to discoveries of novel enzymes but also so far unknown organisms that connect and utilize these two redox mediators.

FORMATE HYDROGEN LYASE OF *E. coli*

Already in 1932 Stephenson and Stickland discovered that whole cells of *E. coli* grown in the presence of formate decompose formate into $H_2 + CO_2$ (Stephenson and Stickland, 1931, 1932). They named the supposed enzyme system formate hydrogen lyase (FHL). When growing under anoxic conditions in the absence of an alternative electron acceptor *E. coli* produces formic acid during mixed acid fermentation from pyruvate catalyzed by pyruvate-formate lyase which is then exported from the cytoplasm by the channels FocA and/or FocB (Clark, 1989; Sawers et al., 2004; Wang et al., 2009; Lu et al., 2011; Trchounian and Trchounian, 2014; Hakobyan et al., 2018). Formic acid (pK_S = 3.7) dissociates to formate and leads to an acidification of the environment. A drop in the pH together with the accumulation of formate leads to subsequent import of formate again and the induction of expression of the genes coding for the FHL enzyme. FHL then oxidizes formate to $H_2 + CO_2$ followed by reoxidation of H_2 by other membrane bound hydrogenases of *E. coli* that transfer the electrons to the quinone pool (Rossmann et al., 1991; Sawers, 1994; Sawers, 2005; Pinske and Sawers, 2016).

Stephenson and Stickland assumed the enzymes to be a combination of formate dehydrogenase and hydrogenase. Genetic and physiological studies have confirmed this assumption and shown that the FHL of *E. coli* consist of a formate dehydrogenase bound to a membrane integral multimeric hydrogenase located in the cytoplasmic membrane (Zinoni et al., 1986; Böhm et al., 1990; Rossmann et al., 1991; Sauter et al., 1992). However, isolation of the whole FHL complex was achieved only recently by McDowall et al. (2014). The enzyme complex consists of two membrane integral subunits and five soluble subunits. The soluble subunits HycE and HycG represent the large (65 kDa) and small (20 kDa) subunits of the [NiFe]-hydrogenase termed *E. coli* hydrogenase-3 (Hyd-3) (**Figure 6A**). Formate is oxidized by the subunit FdhF (also called formate dehydrogenase H) (Axley et al., 1990; Gladyshev et al., 1996; Boyington et al., 1997).

The FHL complex shows high similarity to a group of similar membrane bound hydrogenases now called energy-converting hydrogenases (Ech). These enzymes are found in many anaerobic and facultative anaerobic bacteria and H_2 formation is coupled to different electron donors such as reduced ferredoxin or CO, facilitated by auxiliary subunits (Fox et al., 1996; Künkel et al., 1998; Meuer et al., 1999; Sapra et al., 2000; Soboh et al., 2002). It has been assumed that Ech hydrogenases couple H_2 formation to the translocation of ions across the membrane. Experimental proof for this concept was established using inverted membrane vesicles of the methanogenic archaeon *Methanosarcina mazei* (Welte et al., 2010a,b). However, whether the FHL complex of *E. coli* is also coupled to energy conservation has been a matter of debate for many years (Bagramyan and Martirosov, 1989; Trchounian et al., 1997, 2000, 2011; Hakobyan et al., 2005; McDowall et al., 2014; Trchounian and Sawers, 2014; Pinske and Sargent, 2016).

FHL couples the two half reactions

$$formate + H^+ \rightleftharpoons CO_2 + 2\ e^- + 2\ H^+ \qquad E^{0'} = -432\ mV \quad (7)$$

and

$$2\ H^+ + 2\ e^- \rightleftharpoons H_2 \qquad E^{0'} = -414\ mV \quad (8)$$

resulting in the net reaction

$$formate + H^+ \rightleftharpoons H_2 + CO_2 \quad (9)$$

Under standard conditions, the free energy change of Eq. (9) is only −3.5 kJ mol^{-1} (Thauer et al., 1977). Thus, based on the $\Delta G^{0'}$ value, the FHL reaction should be fully reversible under physiological conditions, however, the enzyme shows a strong bias toward formate oxidation. Values for *in vitro* turnover frequency (TOF) for FHL activity was reported between 1,200 h^{-1} and 1,920 h^{-1} (McDowall et al., 2014; Pinske and Sargent, 2016) whereas the reverse reaction, formate formation from $H_2 + CO_2$ was only observed with an apparent TOFs of only 202 h^{-1} (measured in a discontinuous one point assay and reported as 3.25 μmol formate produced after 5 h with 370 μg of enzyme) (Pinske and Sargent, 2016). This bias could not be explained by the catalytic properties of FdhF and Hyd-3 that have been analyzed separately and show high activities in both reaction directions (Bassegoda et al., 2014; McDowall et al., 2014). In addition to both active sites a factor determining the bias in one or the other direction could be the thermodynamic landscape

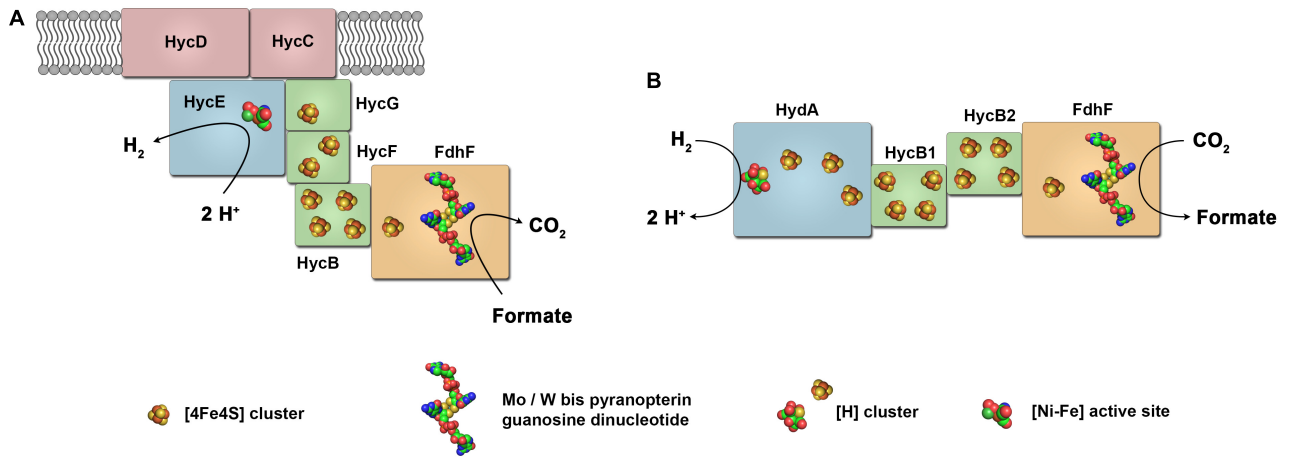

FIGURE 6 | Model of the structure of formate dehydrogenase coupled hydrogenases. FHL of *E. coli* **(A)** has the physiological function of formate oxidation coupled to H_2 formation. The FHL consist of a [NiFe] hydrogenase coupled to a formate dehydrogenase and membrane integral subunits. In contrast, the HDCR of *A. woodii* **(B)** is composed of a [FeFe] hydrogenase coupled to a formate dehydrogenase and catalyzes reversible CO_2 reduction with H_2 as electron donor.

of the connecting iron–sulfur clusters. In addition, the membrane attachment of this enzyme complex and the connection to the enzyme activity is still puzzling (Bagramyan and Martirosov, 1989; Trchounian et al., 1997, 2000, 2011; Hakobyan et al., 2005; McDowall et al., 2014; Trchounian and Sawers, 2014; Pinske and Sargent, 2016). From a physiological point of view, the bias could be a remnant of evolution since there is no physiological situation where *E. coli* would use the reverse reaction to produce formate from CO_2 since this organism is not able to utilize formate further in the metabolism.

HYDROGEN-DEPENDENT CO_2 REDUCTASES

For many years, FHL was the only enzyme complex known that connects the electron carriers H_2 and formate but this enzyme shows a strong bias toward formate oxidation. Did evolution also bring up enzymes adapted for the reverse reaction? Efficient catalysts for hydrogenation of CO_2 are highly sought-after (Appel et al., 2013; Beller and Bornscheuer, 2014; Wang et al., 2015). These could be used for CO_2 conversion technologies for carbon capture, for CO_2-based synthesis or for H_2 storage (Yishai et al., 2016; Preuster et al., 2017b; Bulushev and Ross, 2018). Many homogeneous and heterogenous chemical catalyst have been developed, however, often requiring high temperatures and pressures (Fujita et al., 2013; Wang et al., 2015). In biological systems, of the six pathways known for CO_2 fixation, only the WLP proceeds *via* direct reduction of CO_2 to formate catalyzed by formate dehydrogenases (Fuchs, 2011). In 2013, a formate dehydrogenase was isolated from the acetogenic bacterium *A. woodii* that was in complex with a hydrogenase, on first glance resembling the FHL of *E. coli* (Schuchmann and Müller, 2013). However, in contrast to FHL, the enzyme was lacking membrane integral subunits. When isolated, the enzyme contained only four subunits, one formate dehydrogenase, one hydrogenase and two iron–sulfur cluster rich subunits, identified as being encoded by genes found in one gene cluster (**Figure 6B**). The gene clusters contains in addition a gene coding for a second formate dehydrogenase, a gene for a third iron–sulfur cluster rich subunits and a gene designated as *fdhD* (Poehlein et al., 2012; Schuchmann and Müller, 2013). The formate dehydrogenase FdhF2 as found in the isolated enzyme is a 80.1 kDa protein with 59% identity to FdhH of the *E. coli* FHL aligning over the whole sequence of 713 amino acids. It has one predicted [4Fe–4S] cluster and a bis-PGD cofactor. ICP-MS identified 0.6 mol molybdenum but no tungsten per mol of isolated enzyme preparation agreeing with a mononuclear molybdenum bound to the bis-PGD cofactor thus classifying this enzyme as member of the dimethylsulfoxide reductase family within the Mo/W-bis PGD super-family (Schuchmann and Müller, 2013). At amino acid position 139, a selenocysteine is predicted which is in agreement with the determined selenium in the preparation. In contrast to *E. coli* FHL, the [NiFe] hydrogenase subunits of FHL are substituted by the [FeFe] hydrogenase subunit HydA2 (50.2 kDa). The sequence of this subunit contains the conserved regions typical for H-cluster binding and aligns to amino acid region 201–572 of the monomeric ferredoxin-dependent [FeFe] hydrogenase of *C. pasteurianum* (**Figure 3**). In contrast to the *C. pasteurianum* enzyme, the N-terminus containing one [2Fe–2S]- and one [4Fe–4S] cluster is missing. In addition to the H-cluster including the adjacent [4Fe–4S] cluster, the enzyme is predicted to contain two additional [4Fe–4S] clusters. HydA2 and FdhF2 are supposed to be connected by the two small electron transferring subunits HycB2 and HycB3 (18.9 and 20.1 kDa, respectively) containing 4 [4Fe–4S] clusters each (**Figure 6B**).

Enzymatic assays utilizing methyl viologen demonstrated that both FdhF2 as well as HydA2 were highly active in the isolated enzyme. H_2 oxidation was catalyzed with a TOF of 30,474 s^{-1} (Schuchmann and Müller, 2013). The formate dehydrogenase subunit catalyzed formate oxidation with 1,693 s^{-1} and CO_2 reduction with 372 s^{-1} also showing a bias for formate oxidation,

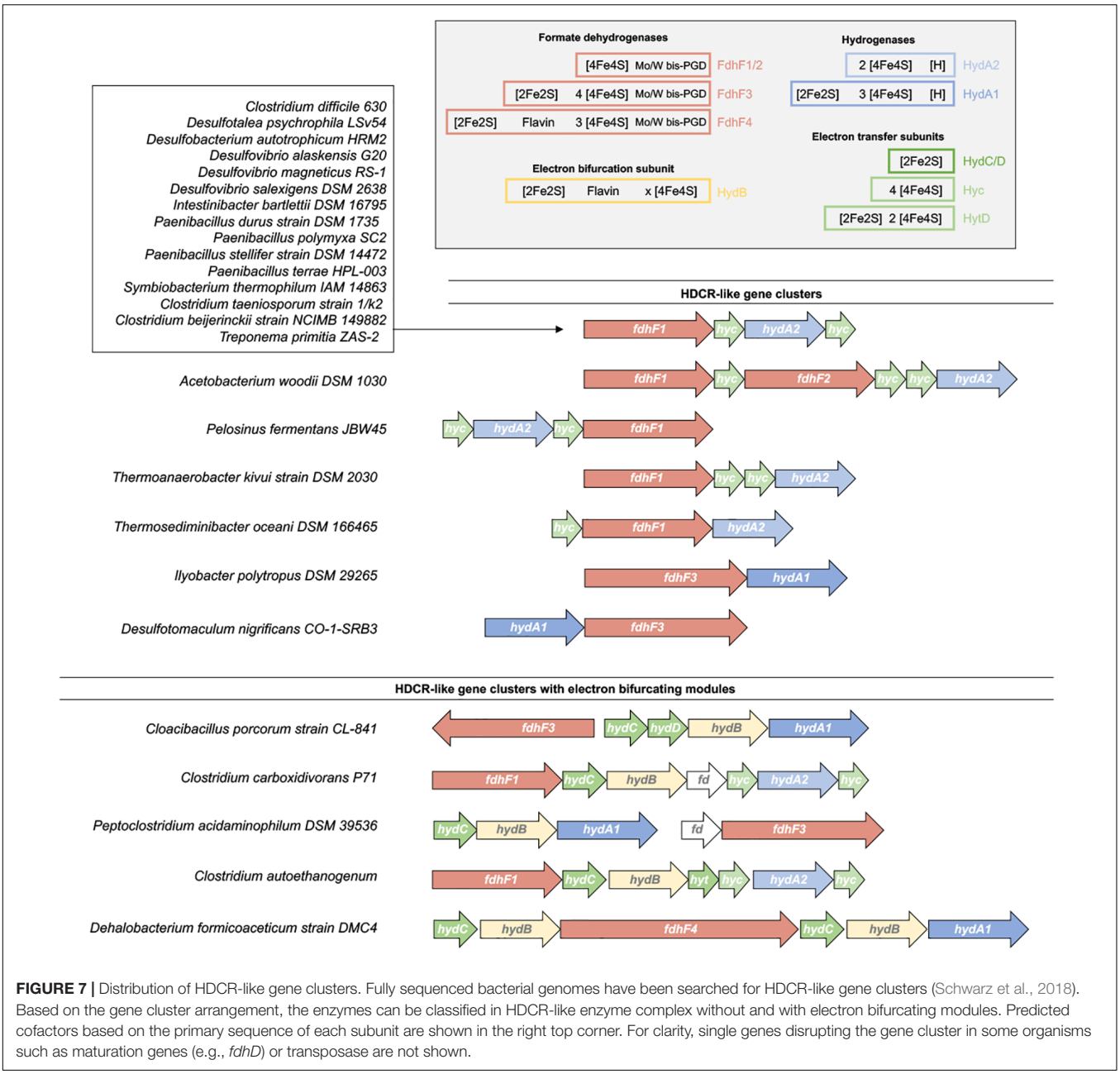

FIGURE 7 | Distribution of HDCR-like gene clusters. Fully sequenced bacterial genomes have been searched for HDCR-like gene clusters (Schwarz et al., 2018). Based on the gene cluster arrangement, the enzymes can be classified in HDCR-like enzyme complex without and with electron bifurcating modules. Predicted cofactors based on the primary sequence of each subunit are shown in the right top corner. For clarity, single genes disrupting the gene cluster in some organisms such as maturation genes (e.g., *fdhD*) or transposase are not shown.

however, not as severe as reported for FdhH of the FHL that showed no measurable CO_2 reduction activity with soluble electron carriers. HydA2 has been analyzed by catalytic protein film electrochemistry by adsorbing the whole enzyme complex to an electrode (Ceccaldi et al., 2017). The hydrogenase is biased for proton reduction oxidizing H_2 10 times slower than it reduces protons at pH 6 as is typical for [FeFe] hydrogenases. However, this ratio defining the bias decreases with increasing pH.

K_M for H_2 was determined to 0.24 atm [K_i (H_2) = 6.4 atm], being three times lower than reported values for *C. reinhardtii* and *Clostridium acetobutylicum* and thus showing the highest affinity ever reported for a [FeFe] hydrogenase (Fourmond et al., 2013; Ceccaldi et al., 2017). In addition, HydA2 showed the surprising characteristic of being the first completely CO tolerant [FeFe] hydrogenase. Even though the enzyme is strongly inhibited by CO [K_i(CO) = 0.11 μM], it fully reactivates upon removal of CO which is in contrast to other [FeFe] hydrogenases where CO provokes irreversible damage to the H-cluster (Goldet et al., 2009; Baffert et al., 2011; Foster et al., 2012). This feature could be a result of the metabolism of *A. woodii* where CO is an intermediate of the reductive acetyl-CoA pathway (Schuchmann and Müller, 2014; Bertsch and Müller, 2015b).

Coupling of the formate dehydrogenase/hydrogenase complex of *A. woodii* was analyzed by incubating the isolated enzyme in the presence of formate. This lead to H_2 production with a TOF of 142,212 h^{-1} (Schuchmann and Müller, 2013). Interestingly,

this enzyme is fully reversible also catalyzing hydrogenation of CO_2 at 30°C and 0.8 bar of H_2 and 0.2 bar of CO_2 with a TOF of 101,600 h^{-1} being significantly faster than the currently best known chemical catalysts (Hull et al., 2012; Jeletic et al., 2013; Wang et al., 2015; Eppinger and Huang, 2017). To distinguish the soluble enzyme complex from membrane bound FHL complexes that are weak catalysts for CO_2 hydrogenation the enzyme was named hydrogen-dependent CO_2 reductase (HDCR). As mentioned before, CO is a strong inhibitor of the hydrogenase activity (Goldet et al., 2009). Interestingly, the HDCR has an alternative electron entry site and can use reduced ferredoxin as electron donor to allow CO_2 reduction even in the presence of 1 atm CO. However, this activity is 17 times slower than the hydrogen-dependent activity with a TOF of only 6,095 h^{-1} (Schuchmann and Müller, 2013). Noteworthy, further characterization of the HDCR revealed another interesting property of the enzyme. *In vitro* the HDCR of *A. woodii* reversibly polymerized into ordered filamentous structures of more than 0.1 μM in length (Schuchmann et al., 2016). Divalent cations could be identified to promote the polymerization process and it was observed that the polymerized form of the enzyme was more active. The *in vivo* significance of this observation is unresolved.

As described before, the HDCR gene cluster of *A. woodii* contains a gene, *fdhF1*, for a second formate dehydrogenase subunit with the corresponding electron transferring subunit *hycB1*. The deduced amino acid sequence of FdhF1 is to 80% identical to FdhF2 with the major exception being a cysteine in FdhF1 at position 139 where a selenocysteine is encoded in FdhF2. Metal-dependent formate dehydrogenases have been described with either selenocysteine or cysteine in the active site (Axley et al., 1990; Friedebold and Bowien, 1993; Raaijmakers et al., 2002; de Bok et al., 2003; Laukel et al., 2003). The lower pK_a value of selenocysteine compared to cysteine is typically connected to a higher reactivity (Stadtman, 1996; Böck et al., 2005; Stock and Rother, 2009). Exchanging selenocysteine by cysteine in FdhH of *E. coli* let to a decrease in turnover number by over two orders of magnitude. However, the affinity for the substrate was increased in the cysteine variant as reflected by a lower K_M value (Axley et al., 1991). There is no data on the different properties of FdhF1 and FdhF2 of *A. woodii*, however, the assumption is that in dependence on the presence of selenium in the environment the two subunits are produced differentially with the selenocysteine containing variant being the more active one. In another acetogenic bacterium, a spirochete from the termite gut, *Treponema primitia*, a gene cluster with similarity to the HDCR gene cluster was identified (Matson et al., 2010). It consists of the genes $fdhF_{cys}$, two *hycB* genes, *fdhD* and *hydA*. Separated by 14 genes, a second *fdhF* gene is encoded, containing a putative selenocysteine codon and a SECIS element ($fdhF_{sec}$). Transcript analysis revealed a differential expression of $fdhF_{cys}$ and $fdhF_{sec}$ in dependence of selenium availability with up to 40-fold change in transcript levels. Half-maximum decrease in transcript level of $fdhF_{cys}$ was observed with less than 50 pM sodium selenite, whereas 1.5 nM sodium selenite were required for half-maximum increase in $fdhF_{sec}$ transcript levels. Interestingly, only transcript levels downstream of the SECIS element were differentially expressed, whereas transcript upstream of the SECIS element did not show differential regulation (Matson et al., 2010).

PHYSIOLOGY AND DIVERSITY OF HDCR COMPLEXES

The first HDCR complex has been identified in the acetogenic bacterium *A. woodii*. Acetogenic bacteria utilize the WLP for energy conservation and carbon fixation, the only carbon fixation pathway that utilizes CO_2 by direct reduction to formate. Therefore, this first reduction step of CO_2 is essential for the metabolism of these bacteria. The redox potential of CO_2/formate of −432 mV limits the number of possible electron donors for this reaction. The first formate dehydrogenase characterized in an acetogenic bacterium was isolated from *Moorella thermoacetica* (Yamamoto et al., 1983). This heterotetrameric enzyme was the first enzyme described to contain tungsten and catalyzes CO_2 reduction coupled to NADPH oxidation. The standard redox potential of $NADP^+$/NADPH of −340 mV is too positive for CO_2 reduction, however, in anaerobes the intracellular ratio of $NADP^+$/NADPH is 1/40 resulting in a redox potential of −370 mV (Sauer et al., 2004; Bennett et al., 2009). Insights into an increasing number of sequenced genomes of acetogenic bacteria has revealed that the genes encoding enzymes for the first reaction step of the WLP show a large diversity (Schuchmann and Müller, 2014; Bertsch and Müller, 2015a; Bengelsdorf et al., 2016). Therefore, the knowledge of the enzymes of *M. thermoacetica* could not be transferred to other acetogens. Characterization of *A. woodii* has revealed that it does not use NADPH but H_2 as electron donor for CO_2 reduction catalyzed by the HDCR. Energetically, the difference between NADPH and H_2 is very small under physiological conditions. H_2 is a stronger reductant under standard conditions ($E^{0'} = -414$ mV), however, at the minimum H_2 pressures required by *A. woodii* to perform acetogenesis (250 Pa) the redox potential is only −340 mV (Poehlein et al., 2012). Under these conditions, the equilibrium concentration of formate is 0.1 mM (CO_2 at 0.2×10^5 Pa, 30°C), in the range of the K_M value of next enzyme of the pathway, the formyl-THF synthetase (Poehlein et al., 2012). Coupling CO_2 reduction directly to H_2 oxidation also energetically couples it directly to the external H_2 partial pressure. A H_2 pressure of 250 Pa is very high compared to the values observed in methanogenic environments of 1 to 10 Pa H_2 (Conrad et al., 1986; Seitz et al., 1990). Therefore, CO_2 reduction by HDCR enzymes seems to be not competitive in methanogenic environments. However, the observation of reduced ferredoxin as alternative electron carrier could be a mechanism to overcome this limitation (in addition to the proposed bypass for CO inhibition of the hydrogenase as discussed before). On the other hand, utilizing reduced ferredoxin instead of H_2 would result, in *A. woodii*, in less ATP conserved (Schuchmann and Müller, 2013). The physiological relevance of the ferredoxin entry site of the HDCR has, however, not been studied yet.

The complete reversibility of the HDCR, as opposed to membrane bound FHL complexes, is a direct reflection of its physiological function. Besides $H_2 + CO_2$, *A. woodii* can grow

for example with formate or methanol as sole carbon and energy sources (Schuchmann and Müller, 2016; Kremp et al., 2018). To convert these compounds, part of the substrate must be oxidized to CO_2 to provide reducing equivalents. In these scenarios, the HDCR must operate in reverse to oxidize formate to $H_2 + CO_2$ since it is the only formate dehydrogenase found in *A. woodii* (Poehlein et al., 2012).

H_2 and formate are widely used electron carriers in anoxic ecosystems and are product or substrate of many microorganisms. The discovery of the HDCR enzyme as soluble, not energetically coupled enzyme complex that connects these two pools raised the question of the distribution of similar enzymes in other organisms. When searching for gene clusters containing homologs of *fdhF1, hycB1/3* and *hydA2* of *A. woodii* we found 18 organisms encoding gene clusters encoding putative HDCRs (**Figure 7**), see also Schwarz et al. (2018). Of these putative enzymes only one from the acetogen *Thermoanaerobacter kivui* has been isolated and characterized (Schwarz et al., 2018). Of the 18 organisms, three are acetogenic bacteria that can grow with $H_2 + CO_2$ as substrates [*Clostridium difficile* (Köpke et al., 2013), *T. primitia* (Graber and Breznak, 2004), *T. kivui* (Leigh et al., 1981)] and 5 belong to the sulfate reducers [*Desulfotalea psychrophila* (Knoblauch et al., 1999), *Desulfobacterium autotrophicum* (Brysch et al., 1987), *Desulfovibrio alaskensis* (Feio et al., 2004), *Desulfovibrio magneticus* (Sakaguchi et al., 2002), *Desulfovibrio salexigens* (Postgate and Campbell, 1966)]. In these organisms the HDCRs could play a role in the WLP as in *A. woodii* to reduce CO_2 to formate either for carbon fixation alone (sulfate reducers) or for carbon fixation and energy conservation (acetogens). Many organisms from the genus *Paenibacillus* have putative HDCR gene clusters. Paenibacilli are found in many environments from polar to tropic regions, often found in soil where they have been reported to be associated with plant roots promoting plant growth, some species are pathogenic to honeybees or invertebrates and some are opportunistic pathogenic to humans (Grady et al., 2016). Species such as *Paenibacillus polymyxa* are facultative anaerobes and can ferment glucose under anoxic conditions by mixed acid fermentation to a mixture of products such as acetate, ethanol, lactate, formate, H_2 and CO_2 (Marwoto et al., 2004). Cell free extracts of *P. polymyxa* have been shown to contain hydrogenase activity and catalyze H_2 evolution from formate (Grau and Wilson, 1962). We conclude, that in Paenibacilli the HDCR could take over the function of the FHL complex as used by *E. coli* to detoxify formate produced during fermentation by oxidizing it to $H_2 + CO_2$.

We identified two gene clusters that show notable differences to the standard HDCR gene cluster. In this case, the hydrogenase subunit resembles the hydrogenase subunit of electron bifurcating hydrogenases by containing two additional iron–sulfur clusters. The formate dehydrogenase subunit also contains three putative additional iron–sulfur clusters whereas genes for the Hyc proteins are missing (**Figure 7**). The additional iron–sulfur clusters in the Hyd and Fdh subunit could take over the function of electron transfer otherwise catalyzed by the Hyc proteins. In contrast, in five other organisms we identified putative HDCR gene cluster that are more complex than the "standard" HDCR and that have, in the case of *Clostridium autoethanogenum*, been shown to combine features of HDCR-like enzyme complexes and electron bifurcating hydrogenases (Wang et al., 2013a).

RAISING THE COMPLEXITY: FORMATE DEHYDROGENASE COUPLED ELECTRON BIFURCATING HYDROGENASES

In the acetogenic bacterium *C. autoethanogenum* a very complex enzyme has been isolated that indeed combines the features of the HDCR enzyme complex and hydrogenases utilizing FBEB (Wang et al., 2013a). This complex is encoded by seven genes found in one cluster on the chromosome. It putatively contains 19 iron–sulfur clusters that could connect the active site of a [FeFe] hydrogenase and a selenocysteine containing bis-PGD containing formate dehydrogenase (**Figure 8**). In addition, a flavin is predicted to be bound to the complex. Chemical analysis of the isolated complex confirmed the presence of FMN, selenium, tungsten and 60 mol iron of 76 predicted mol iron per complex. Molybdenum and FAD were not detected. The enzyme complex showed very interesting catalytic properties. When incubated with $H_2 + CO_2$ it catalyzed formate formation with 41 U mg^{-1} and the reverse reaction, H_2 formation from formate with 40 U mg^{-1} thus showing the typical reversible reaction of HDCR enzymes. However, when incubated with H_2, $NADP^+$, and oxidized ferredoxin the enzyme oxidized H_2 and reduced $NADP^+$ and ferredoxin simultaneously (32 U mg^{-1}). $NADP^+$, NAD^+ or ferredoxin alone in the presence of H_2 are not reduced. H_2 could also be formed only in the presence of NADPH and reduced ferredoxin together (27 U mg^{-1}). In addition, $NADP^+$ and oxidized ferredoxin could also be reduced with formate, again only in the presence of both electron acceptors (15 U mg^{-1}). The same was true for the reverse reaction, CO_2 reduction with NADPH and reduced ferredoxin (7 U mg^{-1}). It has been further demonstrated that the electron-bifurcating reactions with two electron acceptors are strictly energetically coupled (Wang et al., 2013a). Taking these results together, the enzyme represents a combination of formate dehydrogenase coupled hydrogenase as in the case of the HDCR and subunits facilitating FBEB. Interestingly, electron bifurcation to $NADP^+$ and oxidized ferredoxin is catalyzed with two alternative electron donors, H_2 or formate. Puzzling as well is the observation that CO inhibits not only the hydrogenase activity but also reduction of $NADP^+$ and ferredoxin with formate, even though CO is not known to inhibit formate dehydrogenases. The physiological function is complex as well. The enzyme is highly produced in cells grown with syngas as substrate (42% CO, 36% N_2, 20% CO_2, and 2% H_2) even though already CO concentrations of around 0.1% inhibit most activities of the enzyme complex to 50%. Wang et al. (2013a) propose that during balanced growth on CO the steady state concentration within the cell is much lower than external CO concentrations thus not inhibiting the enzyme completely. The authors propose the enzyme utilizes NADPH

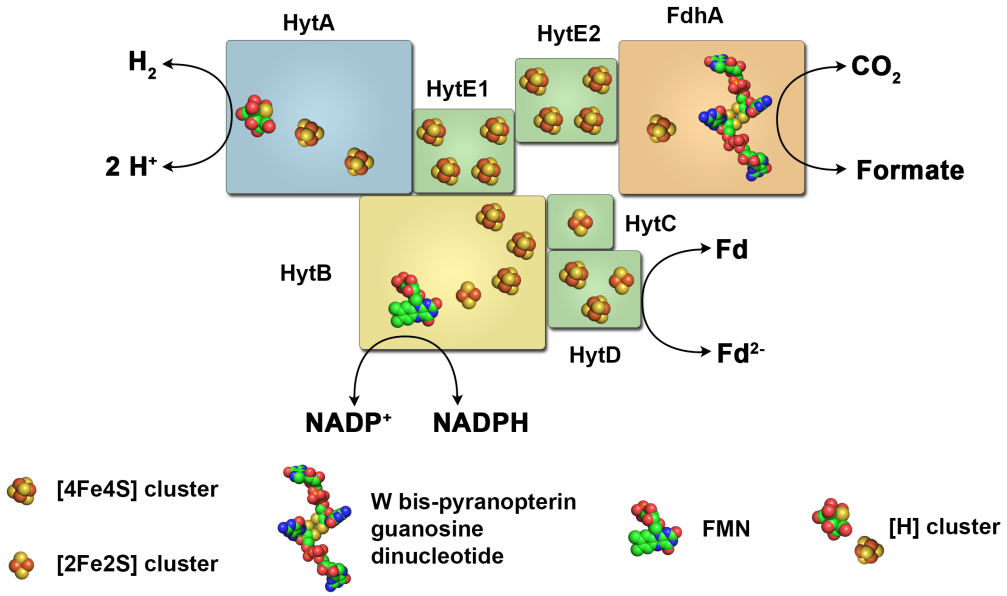

FIGURE 8 | The electron-bifurcating formate dehydrogenase/hydrogenase complex of *C. autoethanogenum*. The enzyme complex of the acetogenic bacterium *C. autoethanogenum* consists of a [FeFe] hydrogenase, a formate dehydrogenase and subunits typical for electron bifurcating hydrogenases. It catalyzes electron transfer from H_2 or formate to $NADP^+$ and ferredoxin (energetically coupled) and *vice versa*, or from H_2 to CO_2 forming formate and *vice versa*. Fd, ferredoxin.

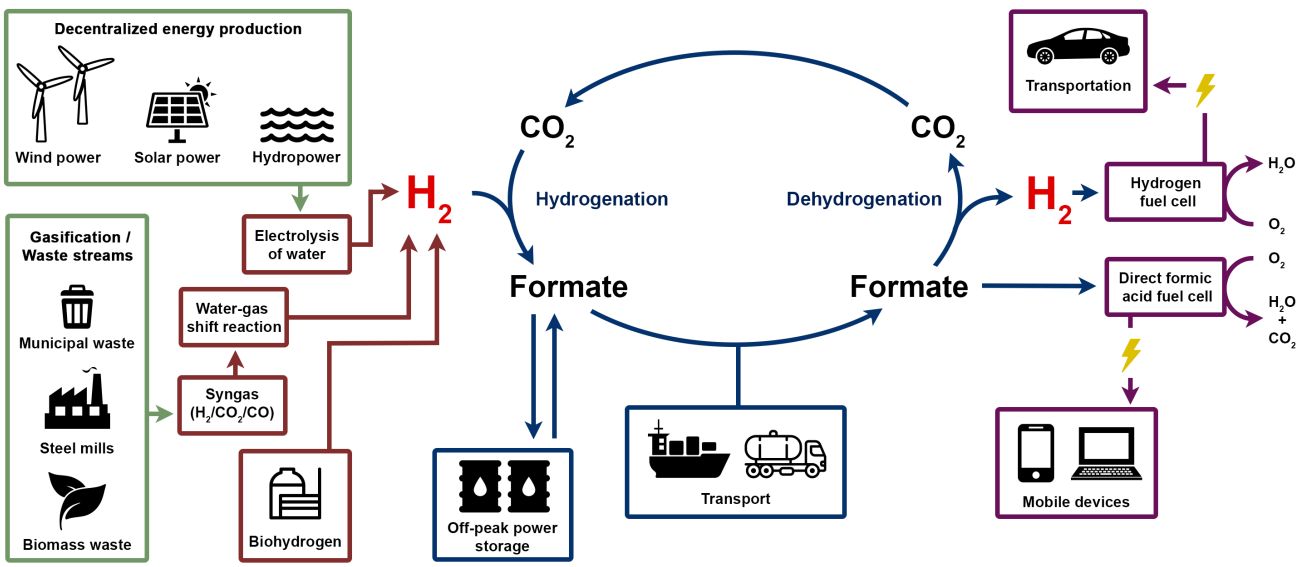

FIGURE 9 | Formate storage and the H_2 economy and envisioned H_2 economy could use sustainably produced electricity, biohydrogen or gasified waste as sources for H_2 gas. Hydrogenation of CO_2 leads to formic acid/formate which can be stored and transported easier, safer and in a more compact form compared to gaseous H_2. Formic acid can serve as fuel directly in a direct formic acid fuel cell or formate is dehydrogenated to release H_2 again to be used in a H_2 fuel cell in, e.g., fuel cell powered cars.

and reduced ferredoxin for CO_2 reduction when cells grown on CO and the hydrogenase module has the function to protect the cells from over-reduction when $NADP^+$ and ferredoxin get too reduced during growth of *C. autoethanogenum* on CO. For a detailed discussion of this function we refer the reader to the original work of Wang et al. (2013a) since it is beyond the scope of this review.

In four other organisms, we identified gene clusters that encode for putative enzyme complexes resembling the electron-bifurcating formate dehydrogenase/hydrogenase complex of *C. autoethanogenum*. These include the acetogen *Clostridium carboxidivorans* that can, as *C. autoethanogenum* utilize CO as carbon and energy source (Liou et al., 2005) and the amino acid fermenting bacteria *Cloacibacillus porcorum* (Looft

et al., 2013) and *Peptoclostridium acidaminophilum* (formerly *Eubacterium acidaminophilum*) (Zindel et al., 1988) (**Figure 7**). *P. acidaminophilum* uses formate as electron donor to reduce glycine, sarcosine, or betaine to acetyl phosphate (Hormann and Andreesen, 1989; Andreesen, 1994). In addition, it is able to grow in syntrophic culture on, e.g., alanine, valine, leucine or malate if a hydrogen- or formate-consuming bacterium is also present (Zindel et al., 1988). The genome encodes for two putative formate dehydrogenases of which one has been isolated and characterized (Graentzdoerffer et al., 2003). The purified enzyme contained the subunits FdhF (selenocysteine and tungsten bis-PGD cofactor containing formate dehydrogenase), two iron–sulfur cluster containing subunits and the flavin- and NAD(P) binding subunit HydB. The corresponding gene cluster encodes for a [FeFe] hydrogenase, however, hydrogenase activity was lost during purification and a hydrogenase subunit or hydrogenase activity could not be detected in the isolated enzyme. On the other hand, formate dehydrogenase activity was present and showed reversible catalysis of formate oxidation/CO_2 reduction (43 U mg^{-1}/12 U mg^{-1}, methyl viologen as electron donor/acceptor).

BIOTECHNOLOGICAL H_2 PRODUCTION AND STORAGE

H_2 has been considered for a long time to replace fossil fuels in the future to tackle the climate problem by decreasing emission of CO_2 (Ball and Wietschel, 2010). H_2 is a very simple molecule that can be produced by various methods including splitting of water that, if the energy is provided by renewable energy sources like solar or wind power does not lead to CO_2 emission. Consumption of H_2 for energy generation either by thermal combustion or H_2 fuel cells at the site of use does not release CO_2 as well. On the other hand, significant challenges are connected with a switch to the H_2 economy. Currently, 95% of world-wide H_2 is produced from fossil fuels by coal gasification or by steam reforming of natural gas followed by further processing to increase the H_2 yield (water-gas shift reaction) (Brandon and Kurban, 2017). These processes emit large quantities of CO_2 and are not sustainable. Another major drawback of H_2 is its very low density. On a gravimetric basis, the energy content of 33.3 kWh/kg H_2 is three times higher than that of gasoline. On a volumetric basis this situation is dramatically reversed to 3 Wh/L for gaseous H_2 versus 8,600 Wh/L to 9800 Wh/L for gasoline or diesel, respectively (Preuster et al., 2017a). Therefore, methods need to be developed for on-board storage of H_2 in mobile applications such as cars and large-scale storage of H_2, e.g., for storing energy produced by wind or solar power at off peak times. Another challenge of H_2 concerns safety issues with respect to the high volatility and the formation of highly explosive gas mixtures if getting in contact with air.

A key technology to sustainably produce H_2 without carbon emission is electrolysis of water driven by electricity generated from renewable sources (Ursua et al., 2012). Electrocatalytic splitting of water releases only H_2 and O_2 thus generating H_2 free of contaminations such as CO which is important for H_2 fuel cell applications. This process has been used already in large scale, however, the low price of fossil fuels has rendered it uneconomic. In the near future, process efficiencies of 85–95% are expected with the current price of H_2 produced by electrolysis being approximately at 3 € per kg (Tremel et al., 2015).

Biological catalysis provides another alternative method for H_2 production. These processes can currently not be considered as the major technology to provide H_2 for the H_2 economy but could provide small but significant contributions to exploit other H_2 sources as well. H_2 production by biological systems can be classified into four general mechanisms, namely direct and indirect biophotolysis, photofermentation, and dark fermentation which have been extensively reviewed elsewhere (Manish and Banerjee, 2008; van Niel, 2016; Kumar et al., 2018). We want to focus here on dark fermentation which has shown the highest H_2 evolution rates so far (Rittmann and Herwig, 2012), biological alternatives to store H_2 and the new opportunities provided by the recent discoveries of novel types of hydrogenases.

Dark fermentation can be catalyzed by single organisms or complex consortia to extract energy from multiple substrates such as waste biomass. This process has been used successfully for many years in biogas plants that convert waste biomass to methane. Within this process, H_2 is produced by fermenting organisms but immediately consumed by methanogens. Selective inhibition of methanogens can stop H_2 consumption leading to H_2 accumulation (Schink, 1997; Catal et al., 2015). Alternatives are single organisms capable of producing large quantities of H_2 either naturally or by metabolic engineering. In nature, most H_2 is produced from the fermentation of carbohydrates (Thauer et al., 2008). Complete oxidation of 1 mole of hexoses such as glucose would yield a maximum of 12 moles of H_2

$$C_6H_{12}O_6 + 12\ H_2O \rightleftharpoons 12\ H_2 + \ 12\ HCO_3^- \qquad (10)$$

This reaction is endergonic [$\Delta G^{0'}$ = 13.6 kJ mol^{-1} (Flamholz et al., 2012)] and thus not feasible *in vivo*. The maximum H_2 that can be produced from glucose by microorganisms is limited to 4 mol H_2 per mol of glucose known as the Thauer limit (Thauer et al., 1977). In practice, most H_2 yields of microorganisms are far below this theoretical limit due to thermodynamic reasons. Oxidation of glucose to 2 pyruvate by the Embden–Meyerhof–Parnas pathway transfers all electrons to NAD^+ producing in total 2 NADH. In contrast, oxidative decarboxylation of 2 pyruvate to acetyl-CoA and CO_2 can be used to reduce 2 ferredoxins as electron carrier. H_2 production from ferredoxin is exergonic whereas H_2 production from NADH is endergonic as described above. Thus, without a H_2 consuming partner organism, H_2 can only be produced from reduced ferredoxin resulting in a maximum of 2 H_2 produced per mol of glucose. The solution to this problem is provided by the new class of electron-bifurcating hydrogenases that can produce H_2 from NADH as well, driven by the coupled production of H_2 from reduced ferredoxin (Buckel and Thauer, 2013). Organisms that harbor such enzymes such as *T. maritima* (Selig et al., 1997; Frock et al., 2012) or *R. albus* (Zheng et al., 2014) are able to reach the Thauer

limit by fermenting glucose according to

$$Glucose + 2\ H_2O \rightleftharpoons 4\ H_2 + 2\ Acetate^- + 2\ CO_2 \qquad (11)$$

with a $\Delta G^{0'}$ value of −250 kJ mol^{-1} at 90°C (growth temperature of *T. maritima*) and −215 kJ mol^{-1} at 25°C. An alternative strategy to reach these high H_2 yields has been observed in the hyperthermophilic archaeon *Pyrococcus furiosus* growing at 100°C. In this organism the NAD^+-dependent glyceraldehyde-3-phosphate dehydrogenase is replaced by a ferredoxin-dependent enzyme at the expense of this enzyme not being couple to ATP formation (Mukund and Adams, 1995). Thus, glucose oxidation results only in generation of reduced ferredoxin allowing full reoxidation by formation of H_2.

Because of the good understanding of the metabolism and the well-established genetic tools, *E. coli* is the prime candidate for biotechnological applications. However, *E. coli* does not harbor an FBEB hydrogenase and is limited to producing 2 mol H_2 per mol glucose. Recently, it has been demonstrated for the first time that heterologous expression of an FBEB hydrogenase in *E. coli* is possible (Kelly et al., 2015). Since *E. coli* lacks pyruvate:ferredoxin oxidoreductase (PFO), this enzyme from *T. maritima* as well as ferredoxin from *T. maritima* had to be produced additionally in *E. coli* to achieve H_2 production. The amounts and rates of H_2 production were very low therefore this study can be seen as mere proof of principle that such a complex hydrogenase can be produced in *E. coli*, however, future studies need to prove that this approach indeed can significantly improve the H_2 yields of *E. coli*.

The recently discovered formate dehydrogenase coupled hydrogenases could also contribute to the H_2 economy in the part of H_2 storage and transportation. To overcome the very low volumetric energy density of gaseous H_2 many technologies are tested to store H_2 in a more compact form (Schlapbach and Zuttel, 2001; Preuster et al., 2017a,b). Physical options are compression and storage in high pressure tanks above 200 bar or storage of H_2 in its liquid form present at −253°C, both technologies requiring high energy input reducing the efficiency of H_2 as energy carrier. A chemical alternative is reacting H_2 with other compounds to produce liquid organic H_2 carriers (LOHCs). For example, hydrogenation of CO_2 leads to formic acid that contains 4.4 wt % of H_2. This is close to the 2017 H_2 storage target of 5.5 wt % in gravimetric energy density set by the United States Department of Energy at temperatures from −40 to 60°C at a maximum pressure of 100 atm (Enthaler et al., 2010; Laurenczy, 2011; Kawanami et al., 2017). The volumetric capacity is 53 g H_2/L formic acid thus one liter formic acid can store roughly 600 liter of gaseous H_2. Formic acid is non-toxic and non-explosive, however, its corrosive nature requires special consideration for tanks and equipment. Formic acid can be decomposed to H_2 + CO_2 before H_2 is then used in a H_2 fuel cell. Chemical catalysts have been developed that catalyze this dehydrogenation with high activity and stability at ambient temperatures below 100°C (Boddien et al., 2008, 2009). However, the initial hydrogenation of CO_2 still represents a challenge. Many homogenous and heterogenous chemical catalyst have been developed but are depending on either high temperatures and pressures, expensive bases or special media for high efficiencies (Hull et al., 2012; Jeletic et al., 2013; Wang et al., 2015; Eppinger and Huang, 2017). Highest rates for CO_2 hydrogenation (TOF 3,400 h^{-1}) with chemical catalyst at ambient conditions have been achieved with cobalt based catalysts in the presence of a special and expensive base (Verkade's base) (Jeletic et al., 2013). The newly discovered HDCR complexes could provide a biotechnological alternative or could serve as model to design more efficient catalysts. HDCR of *A. woodii* catalyzes CO_2 hydrogenation with a TOF of 101,600 h^{-1} at 30°C and 1 bar of pressure (Schuchmann and Müller, 2013). In contrast to other CO_2 reductases the enzyme directly utilizes H_2 thus not requiring soluble electron carriers. In addition, with even higher TOFs it catalyzes the reverse reaction as well, closing the cycle for a H_2 storage process. By coupling the HDCR with a ferredoxin dependent CO dehydrogenase, conversion of syngas (H_2, CO, CO_2) or CO alone to formate was achieved (Schuchmann and Müller, 2013). This is advantageous since CO is very toxic to H_2 fuel cells and can be removed by intermittent conversion of the gases to formate. Major drawbacks are the high oxygen sensitivity and inherent stability issues typical for biocatalysts such as narrow pH and temperature range. To overcome the requirement of enzyme isolation, a whole cell system has been established using *A. woodii* as catalyst for reversible H_2 storage (Schuchmann and Müller, 2013). Genetic manipulations were not required since competing pathways for product formation were inhibited by addition of a sodium ionophore that makes the cytoplasmic membrane permeable for sodium ions thus inhibiting energy conservation and ATP synthesis. Using this system, formate could be specifically produced from H_2 + CO_2 reaching final concentrations (up to ∼0.25 M formate) that where only limited by the thermodynamics of the reaction. Formate was produced with a rate of 120 mmol formate h^{-1} g^{-1}. Formate decomposition was catalyzed by whole cells with activities up to 71 mmol H_2 h^{-1} g^{-1} (Kottenhahn et al., 2018). Yields of 1 mol H_2 per mol of formate were demonstrated. Recently, the first HDCR from a thermophile, namely the acetogen *T. kivui,* was isolated (Schwarz et al., 2018). This enzyme showed surprising activities with TOFs for CO_2 hydrogenation of 9,556,000 h^{-1} at 60°C and still 1,856,000 h^{-1} at 30°C. Formate dehydrogenation was catalyzed with a TOF of 9,892,000 h^{-1}. This enzyme contained in contrast to the HDCR of *A. woodii* tungsten instead of molybdenum and no selenocysteine in the formate dehydrogenase subunit. Future insights into the structure and biochemistry of this enzyme will hopefully unravel the factors determining this tremendous CO_2 reductase activities not observed for other apparently very similar formate dehydrogenases.

One alternative for HDCR catalysis of CO_2 hydrogenation is the FHL enzyme complex as found in *E. coli*. For many years thought to work efficiently only in direction of formate oxidation, recent work has demonstrated the reversibility. Even though CO_2 reductase activity of the isolated enzyme are orders

of magnitude slower compared to HDCR enzymes, whole cell catalysis under high pressure showed promising results (Roger et al., 2018). Utilizing a genetically modified strain that is deficient in competing formate dehydrogenases, hydrogenases and pyruvate formate lyase that are otherwise present in *E. coli* and using 10 bar of H_2 + CO_2 (H_2:CO_2 ratio 1:1) at 37°C approximately 500 mM formate could be produced over a time course of 23 h. Yields reached 100% (produced formate per consumed CO_2) and initial rates of 36 mmol formate produced h^{-1} g^{-1} were demonstrated. Even though the FHL enzyme has less advantageous catalytic properties in the isolated form and has the disadvantage of being a membrane integral enzyme complex, the catalytic rates observed with whole cells of *E. coli* in the high-pressure system are in the same order of magnitude as whole cell catalysis with *A. woodii*, however, the latter being performed at ambient pressures.

How could formic acid be integrated in the H_2 economy? As shown in **Figure 9**, energy production from renewable sources such as solar or wind power will be more decentralized. Electricity produced could be converted electrochemically by water splitting into H_2. Alternative H_2 sources can be biohydrogen produced for example from waste biomass and multiple sources of synthesis gas such as industrial off-gas or gasification of municipal waste or biomass. H_2 production from syngas are well established technologies utilized already as major pathway for H_2 production. In the next step, H_2 could be bound to CO_2 at decentralized facilities producing formic acid that could then be stored in bulk amounts for energy storage or distributed to the final customer. Formic acid could be used directly for energy generation in direct formic acid fuel cells (DFAFCs) that are potential power sources for portable devices (Aslama et al., 2012). DFAFCs are less well developed compared to H_2 fuel cells. Therefore, for utilization in H_2 fuel cells, H_2 must be generated first by dehydrogenation of formic acid again at the site of use. Combustion of formic acid directly or H_2 after formic acid dehydrogenation results in release of water and CO_2 only. CO_2 can be used for the next H_2 storage cycle; therefore, no net CO_2 is generated.

CONCLUSION

Enzymes utilizing H_2 are known for almost a century and since the first crystal structure of a hydrogenase in 1995 (Volbeda et al., 1995) a very large number of studies revealed many facets of the biochemistry, reaction mechanism and evolution of hydrogenases. Most knowledge has been gained about the core subunit of hydrogenases that harbors the active site for H_2 oxidation/H^+ reduction, however, in recent years more and more hydrogenases have been discovered that are part of large and very complex multimeric enzymes connecting H_2 oxidation to multiple functions. One of the major breakthroughs in (anaerobic) microbiology within the last decade was the discovery of the novel enzyme mechanisms of FBEB. This discovery solved many thermodynamic enigmas within the physiology of anaerobic microorganisms. Concerning H_2 production, unraveling of hydrogenases utilizing FBEB finally solved the long-standing questions how H_2 production from NADH is possible and, the other way around, how H_2 can be used to reduce ferredoxin, both highly endergonic reactions without energetic coupling to other redox reactions. These enzymes follow a modular architecture with the large subunit of [FeFe] hydrogenases HydA being coupled to other functional subunits. The same is true for hydrogenases coupled to formate dehydrogenases or the combination of hydrogenase, formate dehydrogenase and electron bifurcation. All these enzymes contain a large number of iron–sulfur clusters that are supposed to accomplish the electrical connection of the different active sites or the active sites and multiple electron acceptors. The biochemical characterization of all these enzymes needs now to be followed by detail insights into the structure and reaction mechanisms. FBEB hydrogenases constitute a fascinating puzzle on how the splitting and energetic coupling of the two electrons is achieved since the flavin to take over this function in other characterized FBEB enzymes is apparently missing. The idea that indeed a metal center can take over this function is a compelling thought. On the other hand, a detailed understanding of H_2-dependent CO_2 reductases would not only be important from a biochemical point of view but could also help to provide better catalysts for economic problems such as H_2 storage. After more than two decades focusing on the major subunit of hydrogenases the next decade might reveal the fascinating complexity of the auxiliary subunits of this still highly important class of enzymes.

AUTHOR CONTRIBUTIONS

All authors listed have made a substantial, direct and intellectual contribution to the work, and approved it for publication.

FUNDING

Work from the authors laboratory was funded by the Deutsche Forschungsgemeinschaft and the European Research Council (ERC) under the European Union's Horizon 2020 Research and Innovation Programme (Grant Agreement No. 741791).

REFERENCES

Andreesen, J. R. (1994). "Glycine metabolism in anaerobes," in *Acetogenesis*, ed. H. L. Drake (New York, NY: Chapman and Hall), 568–629. doi: 10.1007/978-1-4615-1777-1_23

Appel, A. M., Bercaw, J. E., Bocarsly, A. B., Dobbek, H., DuBois, D. L., Dupuis, M., et al. (2013). Frontiers, opportunities, and challenges in biochemical and chemical catalysis of CO_2 fixation. *Chem. Rev.* 113, 6621–6658. doi: 10.1021/cr300463y

Aslama, N. M., Masdara, M. S., Kamarudina, S. K., and Dauda, W. R. W. (2012). Overview on direct formic acid fuel cells (DFAFCs) as an energy sources. *APCBEE Procedia* 3, 33–39. doi: 10.1016/j.apcbee.2012.06.042

Axley, M. J., Bock, A., and Stadtman, T. C. (1991). Catalytic properties of an *Escherichia coli* formate dehydrogenase mutant in which sulfur replaces

selenium. *Proc. Natl. Acad. Sci. U.S.A.* 88, 8450–8454. doi: 10.1073/pnas.88.19.8450

Axley, M. J., Grahame, D. A., and Stadtman, T. C. (1990). *Escherichia coli* formate-hydrogen lyase - purification and properties of the selenium-dependent formate dehydrogenase component. *J. Biol. Chem.* 265, 18213–18218.

Baffert, C., Bertini, L., Lautier, T., Greco, C., Sybirna, K., Ezanno, P., et al. (2011). CO disrupts the reduced H-cluster of FeFe hydrogenase. A combined DFT and protein film voltammetry study. *J. Am. Chem. Soc.* 133, 2096–2099. doi: 10.1021/ja110627b

Bagramyan, K. A., and Martirosov, S. M. (1989). Formation of an ion transport supercomplex in *Escherichia coli*. An experimental model of direct transduction of energy. *FEBS Lett.* 246, 149–152. doi: 10.1016/0014-5793(89)80272-8

Ball, M., and Wietschel, M. (2010). *The Hydrogen Economy: Opportunities and Challenges*. Cambridge: Cambridge University Press.

Bassegoda, A., Madden, C., Wakerley, D. W., Reisner, E., and Hirst, J. (2014). Reversible interconversion of CO_2 and formate by a molybdenum-containing formate dehydrogenase. *J. Am. Chem. Soc.* 136, 15473–15476. doi: 10.1021/ja508647u

Baymann, F., Schoepp-Cothenet, B., Duval, S., Guiral, M., Brugna, M., Baffert, C., et al. (2018). On the natural history of flavin-based electron bifurcation. *Front. Microbiol.* 9:1357. doi: 10.3389/fmicb.2018.01357

Beller, M., and Bornscheuer, U. T. (2014). CO_2 fixation through hydrogenation by chemical or enzymatic methods. *Angew. Chem. Int. Ed. Engl.* 53, 4527–4528. doi: 10.1002/anie.201402963

Bengelsdorf, F. R., Poehlein, A., Linder, S., Erz, C., Hummel, T., Hoffmeister, S., et al. (2016). Industrial acetogenic biocatalysts: a comparative metabolic and genomic analysis. *Front. Microbiol.* 7:1036. doi: 10.3389/fmicb.2016.01036

Bennett, B. D., Kimball, E. H., Gao, M., Osterhout, R., Van Dien, S. J., and Rabinowitz, J. D. (2009). Absolute metabolite concentrations and implied enzyme active site occupancy in *Escherichia coli*. *Nat. Chem. Biol.* 5, 593–599. doi: 10.1038/nchembio.186

Bertsch, J., and Müller, V. (2015a). Bioenergetic constraints for conversion of syngas to biofuels in acetogenic bacteria. *Biotechnol. Biofuels* 8, 1–12. doi: 10.1186/s13068-015-0393-x

Bertsch, J., and Müller, V. (2015b). CO metabolism in the acetogen *Acetobacterium woodii*. *Appl. Environ. Microbiol.* 81, 5949–5956. doi: 10.1128/AEM.01772-15

Bertsch, J., Parthasarathy, A., Buckel, W., and Müller, V. (2013). An electron-bifurcating caffeyl-CoA reductase. *J. Biol. Chem.* 288, 11304–11311. doi: 10.1074/jbc.M112.444919

Bertsch, J., Siemund, A. L., Kremp, F., and Muller, V. (2015). A novel route for ethanol oxidation in the acetogenic bacterium *Acetobacterium woodii*: the AdhE pathway. *Environ. Microbiol.* 18, 2913–2922. doi: 10.1111/1462-2920.13082

Biegel, E., and Müller, V. (2010). Bacterial Na^+-translocating ferredoxin:NAD^+ oxidoreductase. *Proc. Natl. Acad. Sci. U.S.A.* 107, 18138–18142. doi: 10.1073/pnas.1010318107

Biegel, E., and Müller, V. (2011). A Na^+-translocating pyrophosphatase in the acetogenic bacterium *Acetobacterium woodii*. *J. Biol. Chem.* 286, 6080–6084. doi: 10.1074/jbc.M110.192823

Biegel, E., Schmidt, S., González, J. M., and Müller, V. (2011). Biochemistry, evolution and physiological function of the Rnf complex, a novel ion-motive electron transport complex in prokaryotes. *Cell. Mol. Life Sci.* 68, 613–634. doi: 10.1007/s00018-010-0555-8

Blamey, J. M., and Adams, M. W. (1993). Purification and characterization of pyruvate ferredoxin oxidoreductase from the hyperthermophilic archaeon *Pyrococcus furiosus*. *Biochim. Biophys. Acta* 1161, 19–27. doi: 10.1016/0167-4838(93)90190-3

Böck, A., Thanbichler, M., Rother, M., and Resch, A. (2005). "Selenocysteine," in *The Aminoacyl-tRNA Synthetases*, eds M. Ibba, C. Fancklyn, and S. Cusack (Georgetown: Landes Bioscience), 320–327.

Boddien, A., Loges, B., Junge, H., and Beller, M. (2008). Hydrogen generation at ambient conditions: application in fuel cells. *ChemSusChem* 1, 751–758. doi: 10.1002/cssc.200800093

Boddien, A., Loges, B., Junge, H., Gartner, F., Noyes, J. R., and Beller, M. (2009). Continuous hydrogen generation from formic acid: highly active and stable ruthenium catalysts. *Adv. Synth. Catal.* 351, 2517–2520. doi: 10.1002/adsc.200900431

Böhm, R., Sauter, M., and Böck, A. (1990). Nucleotide sequence and expression of an operon in *Escherichia coli* coding for formate hydrogen lyase components. *Mol. Microbiol.* 4, 231–243. doi: 10.1111/j.1365-2958.1990.tb00590.x

Boyington, J. C., Gladyshev, V. N., Khangulov, S. V., Stadtman, T. C., and Sun, P. D. (1997). Crystal structure of formate dehydrogenase H: catalysis involving Mo, molybdopterin, selenocysteine, and an Fe4S4 cluster. *Science* 275, 1305–1308. doi: 10.1126/science.275.5304.1305

Brandon, N. P., and Kurban, Z. (2017). Clean energy and the hydrogen economy. *Philos. Trans. R. Soc. A* 375:20160400. doi: 10.1098/rsta.2016.0400

Brysch, K., Schneider, C., Fuchs, G., and Widdel, F. (1987). Lithoautotrophic growth of sulfate-reducing bacteria, and description of *Desulfobacterium autotrophicum* gen. nov., sp. nov. *Arch. Microbiol.* 148, 264–274. doi: 10.1007/BF00456703

Buckel, W., and Thauer, R. K. (2013). Energy conservation via electron bifurcating ferredoxin reduction and proton/Na^+ translocating ferredoxin oxidation. *Biochim. Biophys. Acta* 1827, 94–113. doi: 10.1016/j.bbabio.2012.07.002

Buckel, W., and Thauer, R. K. (2018a). Flavin-based electron bifurcation, a new mechanism of biological energy coupling. *Chem. Rev.* 118, 3862–3886. doi: 10.1021/acs.chemrev.7b00707

Buckel, W., and Thauer, R. K. (2018b). Flavin-based electron bifurcation, ferredoxin, flavodoxin, and anaerobic respiration with protons (Ech) or NAD^+ (Rnf) as electron acceptors: a historical review. *Front. Microbiol.* 9:401. doi: 10.3389/fmicb.2018.00401

Bulushev, D. A., and Ross, J. R. H. (2018). Towards sustainable production of formic acid. *Chemsuschem* 11, 821–836. doi: 10.1002/cssc.201702075

Calusinska, M., Happe, T., Joris, B., and Wilmotte, A. (2010). The surprising diversity of clostridial hydrogenases: a comparative genomic perspective. *Microbiology* 156, 1575–1588. doi: 10.1099/mic.0.032771-0

Catal, T., Lesnik, K. L., and Liu, H. (2015). Suppression of methanogenesis for hydrogen production in single chamber microbial electrolysis cells using various antibiotics. *Bioresour. Technol.* 187, 77–83. doi: 10.1016/j.biortech.2015.03.099

Ceccaldi, P., Schuchmann, K., Müller, V., and Elliott, S. J. (2017). The hydrogen dependent CO_2 reductase: the first completely CO tolerant FeFe-hydrogenase. *Energy. Environm. Sci.* 10, 503–508. doi: 10.1039/C6EE02494G

Chang, C. H., King, P. W., Ghirardi, M. L., and Kim, K. (2007). Atomic resolution modeling of the ferredoxin:[FeFe] hydrogenase complex from *Chlamydomonas reinhardtii*. *Biophys. J.* 93, 3034–3045. doi: 10.1529/biophysj.107.108589

Chowdhury, N. P., Kahnt, J., and Buckel, W. (2015). Reduction of ferredoxin or oxygen by flavin-based electron bifurcation in *Megasphaera elsdenii*. *FEBS J.* 282, 3149–3160. doi: 10.1111/febs.13308

Chowdhury, N. P., Klomann, K., Seubert, A., and Buckel, W. (2016). Reduction of flavodoxin by electron bifurcation and sodium ion-dependent reoxidation by NAD^+ catalyzed by ferredoxin-NAD^+ reductase (Rnf). *J. Biol. Chem.* 291, 11993–12002. doi: 10.1074/jbc.M116.726299

Chowdhury, N. P., Mowafy, A. M., Demmer, J. K., Upadhyay, V., Koelzer, S., Jayamani, E., et al. (2014). Studies on the mechanism of electron bifurcation catalyzed by electron transferring flavoprotein (Etf) and butyryl-CoA dehydrogenase (Bcd) of *Acidaminococcus fermentans*. *J. Biol. Chem.* 289, 5145–5157. doi: 10.1074/jbc.M113.521013

Clark, D. P. (1989). The fermentation pathways of *Escherichia coli*. *FEMS Microbiol. Rev.* 5, 223–234. doi: 10.1016/0168-6445(89)90033-8

Conrad, R., Schink, B., and Phelps, T. J. (1986). Thermodynamics of H_2-consuming and H_2-producing metabolic reactions in diverse methanogenic environments under in situ conditions. *FEMS Microbiol. Ecol.* 38, 353–360. doi: 10.1111/j.1574-6968.1986.tb01748.x

Crable, B. R., Plugge, C. M., McInerney, M. J., and Stams, A. J. (2011). Formate formation and formate conversion in biological fuels production. *Enzyme Res.* 2011:532536. doi: 10.4061/2011/532536

de Bok, F. A., Hagedoorn, P. L., Silva, P. J., Hagen, W. R., Schiltz, E., Fritsche, K., et al. (2003). Two W-containing formate dehydrogenases (CO_2-reductases) involved in syntrophic propionate oxidation by *Syntrophobacter fumaroxidans*. *Eur. J. Biochem.* 270, 2476–2485. doi: 10.1046/j.1432-1033.2003.03619.x

Demmer, J. K., Huang, H., Wang, S., Demmer, U., Thauer, R. K., and Ermler, U. (2015). Insights into flavin-based electron bifurcation via the NADH-dependent reduced ferredoxin:$NADP^+$ oxidoreductase structure. *J. Biol. Chem.* 290, 21985–21995. doi: 10.1074/jbc.M115.656520

Demmer, J. K., Pal Chowdhury, N., Selmer, T., Ermler, U., and Buckel, W. (2017). The semiquinone swing in the bifurcating electron transferring flavoprotein/butyryl-CoA dehydrogenase complex from *Clostridium difficile*. *Nat. Commun.* 8:1577. doi: 10.1038/s41467-017-01746-3

Dunn, S. (2002). Hydrogen futures: toward a sustainable energy system. *Int. J. Hydrogen Energy* 27, 235–264. doi: 10.1016/S0360-3199(01)00131-8

Enthaler, S., von Langermann, J., and Schmidt, T. (2010). Carbon dioxide and formic acid-the couple for environmental-friendly hydrogen storage? *Energy Environ. Sci.* 3, 1207–1217. doi: 10.1039/b907569k

Eppinger, J., and Huang, K. W. (2017). Formic acid as a hydrogen energy carrier. *ACS Energy Lett.* 2, 188–195. doi: 10.1021/acsenergylett.6b00574

Feio, M. J., Zinkevich, V., Beech, I. B., Llobet-Brossa, E., Eaton, P., Schmitt, J., et al. (2004). *Desulfovibrio alaskensis* sp. nov., a sulphate-reducing bacterium from a soured oil reservoir. *Int. J. Syst. Evol. Microbiol.* 54, 1747–1752. doi: 10.1099/ijs.0.63118-0

Flamholz, A., Noor, E., Bar-Even, A., and Milo, R. (2012). eQuilibrator–the biochemical thermodynamics calculator. *Nucleic Acids Res.* 40, D770–D775. doi: 10.1093/nar/gkr874

Fontecilla-Camps, J. C., and Ragsdale, S. W. (1999). Nickel-iron-sulfur active sites: hydrogenase and CO dehydrogenase. *Adv. Inorg. Chem.* 47, 283–333. doi: 10.1016/S0898-8838(08)60081-1

Foster, C. E., Kramer, T., Wait, A. F., Parkin, A., Jennings, D. P., Happe, T., et al. (2012). Inhibition of [FeFe]-hydrogenases by formaldehyde and wider mechanistic implications for biohydrogen activation. *J. Am. Chem. Soc.* 134, 7553–7557. doi: 10.1021/ja302096r

Fourmond, V., Baffert, C., Sybirna, K., Dementin, S., Abou-Hamdan, A., Meynial-Salles, I., et al. (2013). The mechanism of inhibition by H_2 of H_2-evolution by hydrogenases. *Chem. Commun.* 49, 6840–6842. doi: 10.1039/c3cc43297a

Fox, J. D., He, Y., Shelver, D., Roberts, G. P., and Ludden, P. W. (1996). Characterization of the region encoding the CO-induced hydrogenase of *Rhodospirillum rubrum*. *J. Bacteriol.* 178, 6200–6208. doi: 10.1128/jb.178.21.6200-6208.1996

Friedebold, J., and Bowien, B. (1993). Physiological and biochemical characterization of the soluble formate dehydrogenase, a molybdoenzyme from *Alcaligenes eutrophus*. *J. Bacteriol.* 175, 4719–4728. doi: 10.1128/jb.175.15.4719-4728.1993

Frock, A. D., Gray, S. R., and Kelly, R. M. (2012). Hyperthermophilic *Thermotoga* species differ with respect to specific carbohydrate transporters and glycoside hydrolases. *Appl. Environ. Microbiol.* 78, 1978–1986. doi: 10.1128/AEM.07069-11

Fuchs, G. (2011). Alternative pathways of carbon dioxide fixation: insights into the early evolution of life? *Annu. Rev. Microbiol.* 65, 631–658. doi: 10.1146/annurev-micro-090110-102801

Fujita, E., Muckerman, J. T., and Himeda, Y. (2013). Interconversion of CO_2 and formic acid by bio-inspired Ir complexes with pendent bases. *Biochim. Biophys. Acta* 1827, 1031–1038. doi: 10.1016/j.bbabio.2012.11.004

Gladyshev, V. N., Boyington, J. C., Khangulov, S. V., Grahame, D. A., Stadtman, T. C., and Sun, P. D. (1996). Characterization of crystalline formate dehydrogenase H from *Escherichia coli*. Stabilization, EPR spectroscopy, and preliminary crystallographic analysis. *J. Biol. Chem.* 271, 8095–8100. doi: 10.1074/jbc.271.14.8095

Goldet, G., Brandmayr, C., Stripp, S. T., Happe, T., Cavazza, C., Fontecilla-Camps, J. C., et al. (2009). Electrochemical kinetic investigations of the reactions of [FeFe]-hydrogenases with carbon monoxide and oxygen: comparing the importance of gas tunnels and active-site electronic/redox effects. *J. Am. Chem. Soc.* 131, 14979–14989. doi: 10.1021/ja905388j

Graber, J. R., and Breznak, J. A. (2004). Physiology and nutrition of *Treponema primitia*, an H_2/CO_2-acetogenic spirochete from termite hindguts. *Appl. Environ. Microbiol.* 70, 1307–1314. doi: 10.1128/AEM.70.3.1307-1314.2004

Grady, E. N., MacDonald, J., Liu, L., Richman, A., and Yuan, Z. C. (2016). Current knowledge and perspectives of *Paenibacillus*: a review. *Microb. Cell Fact.* 15:203. doi: 10.1186/s12934-016-0603-7

Graentzdoerffer, A., Rauh, D., Pich, A., and Andreesen, J. R. (2003). Molecular and biochemical characterization of two tungsten- and selenium-containing formate dehydrogenases from *Eubacterium acidaminophilum* that are associated with components of an iron-only hydrogenase. *Arch. Microbiol.* 179, 116–130. doi: 10.1007/s00203-002-0508-1

Grau, F. H., and Wilson, P. W. (1962). Physiology of nitrogen fixation by Bacillus polymyxa. *J. Bacteriol.* 83, 490–496.

Greening, C., Berney, M., Hards, K., Cook, G. M., and Conrad, R. (2014a). A soil actinobacterium scavenges atmospheric H_2 using two membrane-associated, oxygen-dependent [NiFe] hydrogenases. *Proc. Natl. Acad. Sci. U.S.A.* 111, 4257–4261. doi: 10.1073/pnas.1320586111

Greening, C., Constant, P., Hards, K., Morales, S., Oakeshott, J. G., Russell, R. J., et al. (2014b). Atmospheric hydrogen scavenging: from enzymes to ecosystems. *Appl. Environ. Microbiol.* 81, 1190–1199.

Hakobyan, B., Pinske, C., Sawers, G., Trchounian, A., and Trchounian, K. (2018). pH and a mixed carbon-substrate spectrum influence FocA- and FocB-dependent, formate-driven H_2 production in *Escherichia coli*. *FEMS Microbiol. Lett.* 365:fny233. doi: 10.1093/femsle/fny233

Hakobyan, M., Sargsyan, H., and Bagramyan, K. (2005). Proton translocation coupled to formate oxidation in anaerobically grown fermenting *Escherichia coli*. *Biophys. Chem.* 115, 55–61. doi: 10.1016/j.bpc.2005.01.002

Happe, R. P., Roseboom, W., Pierik, A. J., Albracht, S. P. J., and Bagley, K. A. (1997). Biological activation of hydrogen. *Nature* 385, 126–126. doi: 10.1038/385126a0

Herrmann, G., Jayamani, E., Mai, G., and Buckel, W. (2008). Energy conservation via electron-transferring flavoprotein in anaerobic bacteria. *J. Bacteriol.* 190, 784–791. doi: 10.1128/JB.01422-07

Hormann, K., and Andreesen, J. R. (1989). Reductive cleavage of sarcosine and betaine by *Eubacterium acidaminophilum* via enzyme systems different from glycine reductase. *Arch. Microbiol.* 153, 50–59. doi: 10.1007/BF00277541

Hull, J. F., Himeda, Y., Wang, W. H., Hashiguchi, B., Periana, R., Szalda, D. J., et al. (2012). Reversible hydrogen storage using CO_2 and a proton-switchable iridium catalyst in aqueous media under mild temperatures and pressures. *Nat. Chem.* 4, 383–388. doi: 10.1038/nchem.1295

Jeletic, M. S., Mock, M. T., Appel, A. M., and Linehan, J. C. (2013). A cobalt-based catalyst for the hydrogenation of CO_2 under ambient conditions. *J. Am. Chem. Soc.* 135, 11533–11536. doi: 10.1021/ja406601v

Kawanami, H., Himeda, Y., and Laurenczy, G. (2017). Formic acid as a hydrogen carrier for fuel cells toward a sustainable energy system. *Adv. Inorg. Chem.* 70, 395–427. doi: 10.1016/bs.adioch.2017.04.002

Kelly, C. L., Pinske, C., Murphy, B. J., Parkin, A., Armstrong, F., Palmer, T., et al. (2015). Integration of an [FeFe]-hydrogenase into the anaerobic metabolism of *Escherichia coli*. *Biotechnol. Rep.* 8, 94–104. doi: 10.1016/j.btre.2015.10.002

Knoblauch, C., Sahm, K., and Jorgensen, B. B. (1999). Psychrophilic sulfate-reducing bacteria isolated from permanently cold arctic marine sediments: description of *Desulfofrigus oceanense* gen. nov., sp. nov., *Desulfofrigus fragile* sp. nov., *Desulfofaba gelida gen.* nov., sp. nov., *Desulfotalea psychrophila* gen. nov., sp. nov. and *Desulfotalea arctica* sp. nov. *Int. J. Syst. Bacteriol.* 49(Pt 4), 1631–1643.

Köpke, M., Straub, M., and Dürre, P. (2013). *Clostridium difficile* is an autotrophic bacterial pathogen. *PLoS One* 8:e62157. doi: 10.1371/journal.pone.0062157

Kottenhahn, P., Schuchmann, K., and Müller, V. (2018). Efficient whole cell biocatalyst for formate-based hydrogen production. *Biotechnol. Biofuels.* 11:93. doi: 10.1186/s13068-018-1082-3

Kremp, F., Poehlein, A., Daniel, R., and Müller, V. (2018). Methanol metabolism in the acetogenic bacterium *Acetobacterium woodii*. *Environ. Microbiol.* doi: 10.1111/1462-2920.14356 [Epub ahead of print].

Kumar, G., Shobana, S., Nagarajan, D., Lee, D. J., Lee, K. S., Lin, C. Y., et al. (2018). Biomass based hydrogen production by dark fermentation - recent trends and opportunities for greener processes. *Curr. Opin. Biotechnol.* 50, 136–145. doi: 10.1016/j.copbio.2017.12.024

Künkel, A., Vorholt, J. A., Thauer, R. K., and Hedderich, R. (1998). An *Escherichia coli* hydrogenase-3-type hydrogenase in methanogenic archaea. *Eur. J. Biochem.* 252, 467–476. doi: 10.1046/j.1432-1327.1998.2520467.x

Laukel, M., Chistoserdova, L., Lidstrom, M. E., and Vorholt, J. A. (2003). The tungsten-containing formate dehydrogenase from *Methylobacterium extorquens* AM1: purification and properties. *Eur. J. Biochem.* 270, 325–333. doi: 10.1046/j.1432-1033.2003.03391.x

Laurenczy, G. (2011). Hydrogen storage and delivery: the carbon dioxide – formic acid couple. *Chimia* 65, 663–666. doi: 10.2533/chimia.2011.663

Ledbetter, R. N., Garcia Costas, A. M., Lubner, C. E., Mulder, D. W., Tokmina-Lukaszewska, M., Artz, J. H., et al. (2017). The electron bifurcating FixABCX protein complex from *Azotobacter vinelandii*: generation of low-potential

reducing equivalents for nitrogenase catalysis. *Biochemistry* 56, 4177–4190. doi: 10.1021/acs.biochem.7b00389

Leigh, J. A., Mayer, F., and Wolfe, R. S. (1981). *Acetogenium kivui*, a new thermophilic hydrogen-oxidizing, acetogenic bacterium. *Arch. Microbiol.* 129, 275–280. doi: 10.1007/BF00414697

Li, F., Hinderberger, J., Seedorf, H., Zhang, J., Buckel, W., and Thauer, R. K. (2008). Coupled ferredoxin and crotonyl coenzyme A (CoA) reduction with NADH catalyzed by the butyryl-CoA dehydrogenase/Etf complex from *Clostridium kluyveri*. *J. Bacteriol.* 190, 843–850. doi: 10.1128/JB.01417-07

Liou, J. S., Balkwill, D. L., Drake, G. R., and Tanner, R. S. (2005). *Clostridium carboxidivorans* sp. nov., a solvent-producing clostridium isolated from an agricultural settling lagoon, and reclassification of the acetogen *Clostridium scatologenes* strain SL1 as *Clostridium drakei* sp. nov. *Int. J. Syst. Evol. Microbiol.* 55, 2085–2091. doi: 10.1099/ijs.0.63482-0

Looft, T., Levine, U. Y., and Stanton, T. B. (2013). *Cloacibacillus porcorum* sp. nov., a mucin-degrading bacterium from the swine intestinal tract and emended description of the genus *Cloacibacillus*. *Int. J. Syst. Evol. Microbiol.* 63, 1960–1966. doi: 10.1099/ijs.0.044719-0

Losey, N. A., Mus, F., Peters, J. W., Le, H. M., and McInerney, M. J. (2017). *Syntrophomonas wolfei* uses an NADH-dependent, ferredoxin-independent [FeFe]-hydrogenase to reoxidize NADH. *Appl. Environ. Microbiol.* 83. doi: 10.1128/AEM.01335-17

Lu, W., Du, J., Wacker, T., Gerbig-Smentek, E., Andrade, S. L., and Einsle, O. (2011). pH-dependent gating in a FocA formate channel. *Science* 332, 352–354. doi: 10.1126/science.1199098

Lubitz, W., Ogata, H., Rüdiger, O., and Reijerse, E. (2014). Hydrogenases. *Chem. Rev.* 114, 4081–4148. doi: 10.1021/cr4005814

Lubner, C. E., Jennings, D. P., Mulder, D. W., Schut, G. J., Zadvornyy, O. A., Hoben, J. P., et al. (2017). Mechanistic insights into energy conservation by flavin-based electron bifurcation. *Nat. Chem. Biol.* 13, 655–659. doi: 10.1038/nchembio.2348

Manish, S., and Banerjee, R. (2008). Comparison of biohydrogen production processes. *Int. J. Hydrogen Energy* 33, 279–286. doi: 10.1016/j.ijhydene.2007.07.026

Marwoto, B., Nakashimada, Y., Kakizono, T., and Nishio, N. (2004). Metabolic analysis of acetate accumulation during xylose consumption by *Paenibacillus polymyxa*. *Appl. Microbiol. Biotechnol.* 64, 112–119. doi: 10.1007/s00253-003-1435-z

Matson, E. G., Zhang, X., and Leadbetter, J. R. (2010). Selenium controls transcription of paralogous formate dehydrogenase genes in the termite gut acetogen, *Treponema primitia*. *Environ. Microbiol. Rep.* 12, 2245–2258. doi: 10.1111/j.1462-2920.2010.02188.x

McDowall, J. S., Murphy, B. J., Haumann, M., Palmer, T., Armstrong, F. A., and Sargent, F. (2014). Bacterial formate hydrogenlyase complex. *Proc. Natl. Acad. Sci. U.S.A.* 111, E3948–E3956. doi: 10.1073/pnas.1407927111

Meuer, J., Bartoschek, S., Koch, J., Künkel, A., and Hedderich, R. (1999). Purification and catalytic properties of Ech hydrogenase from Methanosarcina barkeri. *Eur. J. Biochem.* 265, 325–335. doi: 10.1046/j.1432-1327.1999.00738.x

Mitchell, P. (1975). The protonmotive Q cycle: a general formulation. *FEBS Lett.* 59, 137–139. doi: 10.1016/0014-5793(75)80359-0

Montag, D., and Schink, B. (2018). Comparison of formate and hydrogen as electron shuttles in terminal fermentations in an oligotrophic freshwater lake sediment. *Appl. Environ. Microbiol.* 84:AEM.01572-18. doi: 10.1128/AEM.01572-18

Morris, B. E., Henneberger, R., Huber, H., and Moissl-Eichinger, C. (2013). Microbial syntrophy: interaction for the common good. *FEMS Microbiol. Rev.* 37, 384–406. doi: 10.1111/1574-6976.12019

Mukund, S., and Adams, M. W. (1995). Glyceraldehyde-3-phosphate ferredoxin oxidoreductase, a novel tungsten-containing enzyme with a potential glycolytic role in the hyperthermophilic archaeon *Pyrococcus furiosus*. *J. Biol. Chem.* 270, 8389–8392. doi: 10.1074/jbc.270.15.8389

Mulder, D. W., Boyd, E. S., Sarma, R., Lange, R. K., Endrizzi, J. A., Broderick, J. B., et al. (2010). Stepwise [FeFe]-hydrogenase H-cluster assembly revealed in the structure of HydA(DeltaEFG). *Nature* 465, 248–251. doi: 10.1038/nature08993

Müller, V., Chowdhury, N. P., and Basen, M. (2018). Electron bifurcation: a long-hidden energy-coupling mechanism. *Annu. Rev. Microbiol.* 72, 331–353. doi: 10.1146/annurev-micro-090816-093440

Nicolet, Y., Piras, C., Legrand, P., Hatchikian, C. E., and Fontecilla-Camps, J. C. (1999). *Desulfovibrio desulfuricans* iron hydrogenase: the structure shows unusual coordination to an active site Fe binuclear center. *Structure* 7, 13–23. doi: 10.1016/S0969-2126(99)80005-7

Nitschke, W., and Russell, M. J. (2012). Redox bifurcations: mechanisms and importance to life now, and at its origin: a widespread means of energy conversion in biology unfolds. *Bioessays* 34, 106–109. doi: 10.1002/bies.201100134

Novelli, P. C., Lang, P. M., Masarie, K. A., Hurst, D. F., Myers, R., and Elkins, J. W. (1999). Molecular hydrogen in the troposphere: global distribution and budget. *J. Geophys. Res.* 104, 30427–30444. doi: 10.1029/1999JD900788

Peters, J. W., Beratan, D. N., Schut, G. J., and Adams, M. W. W. (2018). On the nature of organic and inorganic centers that bifurcate electrons, coupling exergonic and endergonic oxidation-reduction reactions. *Chem. Commun.* 54, 4091–4099. doi: 10.1039/c8cc01530a

Peters, J. W., Lanzilotta, W. N., Lemon, B. J., and Seefeldt, L. C. (1998). X-ray crystal structure of the Fe-only hydrogenase (Cpl) from *Clostridium pasteurianum* to 1.8 angstrom resolution. *Science* 282, 1853–1858. doi: 10.1126/science.282.5395.1853

Pierik, A. J., Hulstein, M., Hagen, W. R., and Albracht, S. P. J. (1998). A low-spin iron with CN and CO as intrinsic ligands forms the core of the active site in [Fe]-hydrogenases. *Eur. J. Biochem.* 258, 572–578. doi: 10.1046/j.1432-1327.1998.2580572.x

Pinske, C., and Sargent, F. (2016). Exploring the directionality of *Escherichia coli* formate hydrogenlyase: a membrane-bound enzyme capable of fixing carbon dioxide to organic acid. *MicrobiologyOpen* 5, 721–737. doi: 10.1002/mbo3.365

Pinske, C., and Sawers, R. G. (2016). Anaerobic formate and hydrogen metabolism. *EcoSal Plus* 7, doi: 10.1128/ecosalplus.ESP-0011-2016

Poehlein, A., Schmidt, S., Kaster, A.-K., Goenrich, M., Vollmers, J., Thürmer, A., et al. (2012). An ancient pathway combining carbon dioxide fixation with the generation and utilization of a sodium ion gradient for ATP synthesis. *PLoS One* 7:e33439. doi: 10.1371/journal.pone.0033439

Postgate, J. R., and Campbell, L. L. (1966). Classification of *Desulfovibrio* species, the nonsporulating sulfate-reducing bacteria. *Bacteriol. Rev.* 30, 732–738.

Preuster, P., Alekseev, A., and Wasserscheid, P. (2017a). Hydrogen storage technologies for future energy systems. *Annu. Rev. Chem. Biomol. Eng.* 8, 445–471. doi: 10.1146/annurev-chembioeng-060816-101334

Preuster, P., Papp, C., and Wasserscheid, P. (2017b). Liquid organic hydrogen carriers (LOHCs): toward a hydrogen-free hydrogen economy. *Acc. Chem. Res.* 50, 74–85. doi: 10.1021/acs.accounts.6b00474

Raaijmakers, H., Macieira, S., Dias, J. M., Teixeira, S., Bursakov, S., Huber, R., et al. (2002). Gene sequence and the 1.8 *angstrom crystal structure of the tungsten-containing formate dehydrogenase from Desulfolvibrio gigas*. *Structure* 10, 1261–1272. doi: 10.1016/S0969-2126(02)00826-2

Rittmann, S., and Herwig, C. (2012). A comprehensive and quantitative review of dark fermentative biohydrogen production. *Microb. Cell Fact.* 11:1. doi: 10.1186/1475-2859-11-115

Roger, M., Brown, F., Gabrielli, W., and Sargent, F. (2018). Efficient hydrogen-dependent carbon dioxide reduction by *Escherichia coli*. *Curr. Biol.* 28, 140–145. doi: 10.1016/j.cub.2017.11.050

Rossmann, R., Sawers, G., and Böck, A. (1991). Mechanism of regulation of the formate-hydrogenlyase pathway by oxygen, nitrate, and pH: definition of the formate regulon. *Mol. Microbiol.* 5, 2807–2814. doi: 10.1111/j.1365-2958.1991.tb01989.x

Rumpel, S., Siebel, J. F., Diallo, M., Fares, C., Reijerse, E. J., and Lubitz, W. (2015). Structural insight into the complex of ferredoxin and [FeFe] hydrogenase from *Chlamydomonas reinhardtii*. *Chembiochem* 16, 1663–1669. doi: 10.1002/cbic.201500130

Sakaguchi, T., Arakaki, A., and Matsunaga, T. (2002). *Desulfovibrio magneticus* sp. nov., a novel sulfate-reducing bacterium that produces intracellular single-domain-sized magnetite particles. *Int. J. Syst. Evol. Microbiol.* 52, 215–221. doi: 10.1099/00207713-52-1-215

Sapra, R., Verhagen, M. F., and Adams, M. W. (2000). Purification and characterization of a membrane-bound hydrogenase from the hyperthermophilic archaeon *Pyrococcus furiosus*. *J. Bacteriol.* 182, 3423–3428. doi: 10.1128/JB.182.12.3423-3428.2000

Sauer, U., Canonaco, F., Heri, S., Perrenoud, A., and Fischer, E. (2004). The soluble and membrane-bound transhydrogenases UdhA and PntAB have divergent functions in NADPH metabolism of *Escherichia coli*. *J. Biol. Chem.* 279, 6613–6619. doi: 10.1074/jbc.M311657200

Sauter, M., Böhm, R., and Böck, A. (1992). Mutational analysis of the operon (hyc) determining hydrogenase 3 formation in *Escherichia coli*. *Mol. Microbiol.* 6, 1523–1532. doi: 10.1111/j.1365-2958.1992.tb00873.x

Sawers, G. (1994). The hydrogenases and formate dehydrogenases of *Escherichia coli*. *Antonie Van Leeuwenhoek* 66, 57–88. doi: 10.1007/BF00871633

Sawers, R. G. (2005). Formate and its role in hydrogen production in *Escherichia coli*. *Biochem. Soc. Trans.* 33, 42–46. doi: 10.1042/BST0330042

Sawers, R. G., Blokesch, M., and Böck, A. (2004). Anaerobic formate and hydrogen metabolism. *EcoSal Plus* 1, doi: 10.1128/ecosalplus.3.5.4

Schink, B. (1997). Energetics of syntrophic cooperation in methanogenic degradation. *Microbiol. Mol. Biol. Rev.* 61, 262–280.

Schink, B. (2002). Synergistic interactions in the microbial world. *Antonie Van Leeuwenhoek* 81, 257–261. doi: 10.1023/A:1020579004534

Schink, B., Montag, D., Keller, A., and Müller, N. (2017). Hydrogen or formate: alternative key players in methanogenic degradation. *Environ. Microbiol. Rep.* 9, 189–202. doi: 10.1111/1758-2229.12524

Schlapbach, L., and Zuttel, A. (2001). Hydrogen-storage materials for mobile applications. *Nature* 414, 353–358. doi: 10.1038/35104634

Schmidt, O., Drake, H. L., and Horn, M. A. (2010). Hitherto unknown [Fe-Fe]-hydrogenase gene diversity in anaerobes and anoxic enrichments from a moderately acidic fen. *Appl. Environ. Microbiol.* 76, 2027–2031. doi: 10.1128/AEM.02895-09

Schroder, C., Selig, M., and Schonheit, P. (1994). Glucose fermentation to acetate, CO_2 and H_2 in the anaerobic hyperthermophilic eubacterium *Thermotoga maritima* – involvement of the Embden-Meyerhof pathway. *Arch. Microbiol.* 161, 460–470.

Schuchmann, K., and Müller, V. (2012). A bacterial electron bifurcating hydrogenase. *J. Biol. Chem.* 287, 31165–31171. doi: 10.1074/jbc.M112.395038

Schuchmann, K., and Müller, V. (2013). Direct and reversible hydrogenation of CO_2 to formate by a bacterial carbon dioxide reductase. *Science* 342, 1382–1385. doi: 10.1126/science.1244758

Schuchmann, K., and Müller, V. (2014). Autotrophy at the thermodynamic limit of life: a model for energy conservation in acetogenic bacteria. *Nat. Rev. Microbiol.* 12, 809–821. doi: 10.1038/nrmicro3365

Schuchmann, K., and Müller, V. (2016). Energetics and application of heterotrophy in acetogenic bacteria. *Appl. Environ. Microbiol.* 82, 4056–4069. doi: 10.1128/AEM.00882-16

Schuchmann, K., Vonck, J., and Müller, V. (2016). A bacterial hydrogen-dependent CO_2 reductase forms filamentous structures. *FEBS J.* 283, 1311–1322. doi: 10.1111/febs.13670

Schut, G. J., and Adams, M. W. (2009). The iron-hydrogenase of Thermotoga maritima utilizes ferredoxin and NADH synergistically: a new perspective on anaerobic hydrogen production. *J. Bacteriol.* 191, 4451–4457. doi: 10.1128/JB.01582-08

Schwarz, F. M., Schuchmann, K., and Müller, V. (2018). Hydrogenation of CO_2 at ambient pressure catalyzed by a highly active thermostable biocatalyst. *Biotechnol. Biofuels* 11:237. doi: 10.1186/s13068-018-1236-3

Seitz, H. J., Schink, B., Pfennig, N., and Conrad, R. (1990). Energetics of syntrophic ethanol oxidation in defined chemostat cocultures.2. Energy sharing in biomass production. *Arch. Microbiol.* 155, 89–93. doi: 10.1007/BF00291280

Selig, M., Xavier, K. B., Santos, H., and Schönheit, P. (1997). Comparative analysis of Embden-Meyerhof and Entner-Doudoroff glycolytic pathways in hyperthermophilic archaea and the bacterium thermotoga. *Arch. Microbiol.* 167, 217–232. doi: 10.1007/BF03356097

Service, R. F. (2004). The hydrogen backlash. *Science* 305, 958–961. doi: 10.1126/science.305.5686.958

Shima, S., Pilak, O., Vogt, S., Schick, M., Stagni, M. S., Meyer-Klaucke, W., et al. (2008). The crystal structure of [Fe]-hydrogenase reveals the geometry of the active site. *Science* 321, 572–575. doi: 10.1126/science.1158978

Shima, S., and Thauer, R. K. (2007). A third type of hydrogenase catalyzing H_2 activation. *Chem. Rec.* 7, 37–46. doi: 10.1002/tcr.20111

Sieber, J. R., McInerney, M. J., and Gunsalus, R. P. (2012). Genomic insights into syntrophy: the paradigm for anaerobic metabolic cooperation. *Ann. Rev. Microbiol.* 66, 429–452. doi: 10.1146/annurev-micro-090110-102844

Soboh, B., Linder, D., and Hedderich, R. (2002). Purification and catalytic properties of a CO-oxidizing:H_2-evolving enzyme complex from *Carboxydothermus hydrogenoformans*. *Eur. J. Biochem.* 269, 5712–5721. doi: 10.1046/j.1432-1033.2002.03282.x

Spruth, M., Reidlinger, J., and Muller, V. (1995). Sodium-ion dependence of inhibition of the Na^+-translocating F_1F_0-ATPase from *Acetobacterium woodii* – probing the site(S) involved in ion-transport. *BBA-Bioenerg.* 1229, 96–102. doi: 10.1016/0005-2728(94)00192-8

Stadtman, T. C. (1996). Selenocysteine. *Annu. Rev. Biochem.* 65, 83–100. doi: 10.1146/annurev.bi.65.070196.000503

Stams, A. J., and Plugge, C. M. (2009). Electron transfer in syntrophic communities of anaerobic bacteria and archaea. *Nat. Rev. Microbiol.* 7, 568–577. doi: 10.1038/nrmicro2166

Stephenson, M., and Stickland, L. H. (1931). Hydrogenase: a bacterial enzyme activating molecular hydrogen: the properties of the enzyme. *Biochem. J.* 25, 205–214. doi: 10.1042/bj0250205

Stephenson, M., and Stickland, L. H. (1932). Hydrogenlyases: bacterial enzymes liberating molecular hydrogen. *Biochem. J.* 26, 712–724. doi: 10.1042/bj0260712

Stock, T., and Rother, M. (2009). Selenoproteins in archaea and Gram-positive bacteria. *Biochim. Biophys. Acta* 1790, 1520–1532. doi: 10.1016/j.bbagen.2009.03.022

Thauer, R. K., Jungermann, K., and Decker, K. (1977). Energy conservation in chemotrophic anaerobic bacteria. *Bacteriol. Rev.* 41, 100–180.

Thauer, R. K., Kaster, A. K., Goenrich, M., Schick, M., Hiromoto, T., and Shima, S. (2010). Hydrogenases from methanogenic archaea, nickel, a novel cofactor, and H_2 storage. *Annu. Rev. Biochem.* 79, 507–536. doi: 10.1146/annurev.biochem.030508.152103

Thauer, R. K., Kaster, A. K., Seedorf, H., Buckel, W., and Hedderich, R. (2008). Methanogenic archaea: ecologically relevant differences in energy conservation. *Nat. Rev. Microbiol.* 6, 579–591. doi: 10.1038/nrmicro1931

Thiele, J. H., and Zeikus, J. G. (1988). Control of interspecies electron flow during anaerobic digestion: significance of formate transfer versus hydrogen transfer during syntrophic methanogenesis in flocs. *Appl. Environ. Microbiol.* 54, 20–29.

Trchounian, A., Bagramyan, K., and Poladian, A. (1997). Formate hydrogenlyase is needed for proton-potassium exchange through the F_0F_1-ATPase and the TrkA system in anaerobically grown and glycolysing *Escherichia coli*. *Curr. Microbiol.* 35, 201–206. doi: 10.1007/s002849900239

Trchounian, A., and Sawers, R. G. (2014). Novel insights into the bioenergetics of mixed-acid fermentation: can hydrogen and proton cycles combine to help maintain a proton motive force? *IUBMB Life* 66, 1–7. doi: 10.1002/iub.1236

Trchounian, A. A., Bagramyan, K. A., Vassilian, A. V., and Poladian, A. A. (2000). Relationship between formate hydrogen lyase and proton-potassium pump under heterolactic fermentation in *Escherichia coli*: functional multienzyme associations in the cell membrane. *Membr. Cell Biol.* 13, 511–526.

Trchounian, K., Pinske, C., Sawers, R. G., and Trchounian, A. (2011). Dependence on the F_0F_1-ATP synthase for the activities of the hydrogen-oxidizing hydrogenases 1 and 2 during glucose and glycerol fermentation at high and low pH in *Escherichia coli*. *J. Bioenerg. Biomembr.* 43, 645–650. doi: 10.1007/s10863-011-9397-9

Trchounian, K., and Trchounian, A. (2014). Different role of *focA* and *focB* encoding formate channels for hydrogen production by *Escherichia coli* during glucose or glycerol fermentation. *Int. J. Hydrogen Energy* 39, 20987–20991. doi: 10.1016/j.ijhydene.2014.10.074

Tremel, A., Wasserscheid, P., Baldauf, M., and Hammer, T. (2015). Techno-economic analysis for the synthesis of liquid and gaseous fuels based on hydrogen production via electrolysis. *Int. J. Hydrogen Energy* 40, 11457–11464. doi: 10.1016/j.ijhydene.2015.01.097

Ursua, A., Gandia, L. M., and Sanchis, P. (2012). Hydrogen production from water electrolysis: current status and future trends. *Proc. IEEE* 100, 410–426. doi: 10.1109/JPROC.2011.2156750

van Niel, E. W. (2016). Biological processes for hydrogen production. *Adv. Biochem. Eng. Biotechnol.* 156, 155–193. doi: 10.1007/10_2016_11

Verhagen, M. F. J. M., O'Rourke, T., and Adams, M. W. W. (1999). The hyperthermophilic bacterium, *Thermotoga maritima*, contains an unusually complex iron-hydrogenase: amino acid sequence analyses *versus* biochemical characterization. *Biochim. Biophys. Acta* 1412, 212–229. doi: 10.1016/S0005-2728(99)00062-6

Vignais, P. M., and Billoud, B. (2007). Occurrence, classification, and biological function of hydrogenases: an overview. *Chem. Rev.* 107, 4206–4272. doi: 10.1021/cr050196r

Vignais, P. M., Billoud, B., and Meyer, J. (2001). Classification and phylogeny of hydrogenases. *FEMS Microbiol. Rev.* 25, 455–501. doi: 10.1111/j.1574-6976.2001.tb00587.x

Vignais, P. M., and Colbeau, A. (2004). Molecular biology of microbial hydrogenases. *Curr. Issues Mol. Biol.* 6, 159–188.

Volbeda, A., Charon, M. H., Piras, C., Hatchikian, E. C., Frey, M., and Fontecilla-Camps, J. C. (1995). Crystal structure of the nickel-iron hydrogenase from *Desulfovibrio gigas*. *Nature* 373, 580–587. doi: 10.1038/373580a0

Wagner, T., Koch, J., Ermler, U., and Shima, S. (2017). Methanogenic heterodisulfide reductase (HdrABC-MvhAGD) uses two noncubane [4Fe-4S] clusters for reduction. *Science* 357, 699–703. doi: 10.1126/science.aan0425

Wang, S., Huang, H., Kahnt, J., Mueller, A. P., Köpke, M., and Thauer, R. K. (2013a). NADP-specific electron-bifurcating [FeFe]-hydrogenase in a functional complex with formate dehydrogenase in *Clostridium autoethanogenum* grown on CO. *J. Bacteriol.* 195, 4373–4386. doi: 10.1128/JB.00678-13

Wang, S., Huang, H., Kahnt, J., and Thauer, R. K. (2013b). A reversible electron-bifurcating ferredoxin- and NAD-dependent [FeFe]-hydrogenase (HydABC) in *Moorella thermoacetica*. *J. Bacteriol.* 195, 1267–1275. doi: 10.1128/JB.02158-12

Wang, W. H., Himeda, Y., Muckerman, J. T., Manbeck, G. F., and Fujita, E. (2015). CO_2 hydrogenation to formate and methanol as an alternative to photo- and electrochemical CO_2 reduction. *Chem. Rev.* 115, 12936–12973. doi: 10.1021/acs.chemrev.5b00197

Wang, Y., Huang, Y., Wang, J., Cheng, C., Huang, W., Lu, P., et al. (2009). Structure of the formate transporter FocA reveals a pentameric aquaporin-like channel. *Nature* 462, 467–472. doi: 10.1038/nature08610

Weghoff, M. C., Bertsch, J., and Müller, V. (2015). A novel mode of lactate metabolism in strictly anaerobic bacteria. *Environ. Microbiol.* 17, 670–677. doi: 10.1111/1462-2920.12493

Welte, C., Kallnik, V., Grapp, M., Bender, G., Ragsdale, S., and Deppenmeier, U. (2010a). Function of Ech hydrogenase in ferredoxin-dependent, membrane-bound electron transport in *Methanosarcina mazei*. *J. Bacteriol.* 192, 674–678. doi: 10.1128/JB.01307-09

Welte, C., Krätzer, C., and Deppenmeier, U. (2010b). Involvement of Ech hydrogenase in energy conservation of *Methanosarcina mazei*. *FEBS J.* 277, 3396–3403. doi: 10.1111/j.1742-4658.2010.07744.x

Wood, H. G. (1991). Life with CO or CO_2 and H_2 as a source of carbon and energy. *FASEB J.* 5, 156–163. doi: 10.1096/fasebj.5.2.1900793

Wood, H. G., and Ljungdahl, L. G. (1991). "Autotrophic character of the acetogenic bacteria," in *Variations in Autotrophic Life*, eds J. M. Shively and L. L. Barton (San Diego: Academic press), 201–250.

Wrba, A., Jaenicke, R., Huber, R., and Stetter, K. O. (1990). Lactate dehydrogenase from the extreme thermophile *Thermotoga maritima*. *Eur. J. Biochem.* 188, 195–201. doi: 10.1111/j.1432-1033.1990.tb15388.x

Yamamoto, I., Saiki, T., Liu, S. M., and Ljungdahl, L. G. (1983). Purification and properties of NADP-dependent formate dehydrogenase from *Clostridium thermoaceticum*, a tungsten-selenium-iron protein. *J. Biol. Chem.* 258, 1826–1832.

Yishai, O., Lindner, S. N., Gonzalez de la Cruz, J., Tenenboim, H., and Bar-Even, A. (2016). The formate bio-economy. *Curr. Opin. Chem. Biol.* 35, 1–9. doi: 10.1016/j.cbpa.2016.07.005

Zheng, Y., Kahnt, J., Kwon, I. H., Mackie, R. I., and Thauer, R. K. (2014). Hydrogen formation and its regulation in *Ruminococcus albus*: involvement of an electron-bifurcating [FeFe]-hydrogenase, of a non-electron-bifurcating [FeFe]-hydrogenase, and of a putative hydrogen-sensing [FeFe]-hydrogenase. *J. Bacteriol.* 196, 3840–3852. doi: 10.1128/JB.02070-14

Zindel, U., Freudenberg, W., Rieth, M., Andreesen, J. R., Schnell, J., and Widdel, F. (1988). *Eubacterium acidaminophilum* sp. nov., a versatile amino acid-degrading anaerobe producing or utilizing H_2 or formate. Description and enzymatic studies. *Arch. Microbiol.* 150, 254–266. doi: 10.1007/BF00407789

Zinoni, F., Birkmann, A., Stadtman, T. C., and Böck, A. (1986). Nucleotide sequence and expression of the selenocysteine-containing polypeptide of formate dehydrogenase (formate-hydrogen-lyase-linked) from *Escherichia coli*. *Proc. Natl. Acad. Sci. U.S.A.* 83, 4650–4654. doi: 10.1073/pnas.83.13.4650

Conflict of Interest Statement: The authors declare that the research was conducted in the absence of any commercial or financial relationships that could be construed as a potential conflict of interest.

frontiers in Microbiology

REVIEW
published: 14 February 2019
doi: 10.3389/fmicb.2019.00106

Function of Biohydrogen Metabolism and Related Microbial Communities in Environmental Bioremediation

Ying Teng[1], Yongfeng Xu[1,2], Xiaomi Wang[1] and Peter Christie[1]*

[1] Key Laboratory of Soil Environment and Pollution Remediation, Institute of Soil Science, Chinese Academy of Sciences, Nanjing, China, [2] College of Resources and Environment, University of Chinese Academy of Sciences, Beijing, China

Hydrogen (H_2) metabolism has attracted considerable interest because the activities of H_2-producing and consuming microbes shape the global H_2 cycle and may have vital relationships with the global cycling of other elements. There are many pathways of microbial H_2 emission and consumption which may affect the structure and function of microbial communities. A wide range of microbial groups employ H_2 as an electron donor to catalyze the reduction of pollutants such as organohalides, azo compounds, and trace metals. Syntrophy coupled mutualistic interaction between H_2-producing and H_2-consuming microorganisms can transfer H_2 and be accompanied by the removal of toxic compounds. Moreover, hydrogenases have been gradually recognized to have a key role in the progress of pollutant degradation. This paper reviews recent advances in elucidating role of H_2 metabolism involved in syntrophy and hydrogenases in environmental bioremediation. Further investigations should focus on the application of bioenergy in bioremediation to make microbiological H_2 metabolism a promising remediation strategy.

Keywords: bioremediation, hydrogenase, H_2 consumption, H_2 metabolism, H_2 production

OPEN ACCESS

Edited by:
Eric Boyd,
Montana State University,
United States

Reviewed by:
Karen Trchounian,
Yerevan State University, Armenia
Philippe Constant,
Institut National de la Recherche Scientifique (INRS), Canada

****Correspondence:***
Ying Teng
yteng@issas.ac.cn

Specialty section:
This article was submitted to Microbial Physiology and Metabolism, a section of the journal Frontiers in Microbiology

Received: *31 October 2018*
Accepted: *17 January 2019*
Published: *14 February 2019*

Citation:
Teng Y, Xu Y, Wang X and Christie P (2019) Function of Biohydrogen Metabolism and Related Microbial Communities in Environmental Bioremediation. Front. Microbiol. 10:106. doi: 10.3389/fmicb.2019.00106

INTRODUCTION

It is well established that the main sources of molecular hydrogen (H_2) are geochemical and anthropogenic activities and the main sink is the biological consumption of H_2 in soil ecosystems. The H_2 cycle can influence air quality and climate indirectly via effects on the oxidative capacity of the atmosphere (Ehhalt and Rohrer, 2009). In addition, the H_2 cycle plays an important role in microbial metabolism due to numerous microbial processes that depend on H_2 production and consumption (Vignais and Billoud, 2007; Greening et al., 2015b). For example, most of the tropospheric H_2 is consumed by soils due to the capacity of the majority of H_2-oxidizing bacteria displaying high affinity for H_2 in soils to recycle it (Constant et al., 2010). H_2 is also a key metabolic compound in many anoxic ecosystems and its oxidation may support deep subsurface lithoautotrophic microbial ecosystems (Chivian et al., 2008; Nyyssonen et al., 2014; Wu et al., 2015; Bagnoud et al., 2016). The activities of H_2-producing and consuming microbes therefore shape the global H_2 cycle and may have vital relationships with the global cycling of other elements including carbon, sulfur, and nitrogen.

The first H_2-oxidizing microorganisms were discovered in the 1900s (Kaserer, 1905; Stephenson and Stickland, 1931). The physical properties of H_2 (e.g., its diffusion coefficient, 4×10^{-9} m^2 s^{-1}, and redox potential, $E^{0'} = -0.42$ V, make it relatively active in biological processes

(Greening et al., 2016). H_2 has dual physiological functions in microorganisms. Firstly, microbial fermentation of H_2 produced by facultative or obligate fermenters can disperse excess reductant from fermentative metabolism, for example in *Escherichia coli* and *Clostridium* spp. (Trchounian et al., 2012, 2017a,b). Secondly, prokaryotic microorganisms with different metabolic processes such as hydrogen-oxidizing bacteria, methanogens and anoxygenic phototrophic bacteria can exploit H_2 as an energy source and reductant (Schwartz et al., 2013). There are also a wide range of microorganisms with the ability to metabolize H_2 such as aerobes and anaerobes and lithotrophs and phototrophs (Vignais and Billoud, 2007; Schwartz et al., 2013; Peters et al., 2015; Greening et al., 2016). Furthermore, recent studies show that some aerobic soil acidobacteria and actinobacteria can exploit low levels of H_2 for survival in addition to growth, which challenges the traditional belief that H_2 metabolism is restricted to high-H_2 and low-O_2 environments (Constant et al., 2010; Osborne et al., 2010; Greening et al., 2014, 2015a,b; Liot and Constant, 2016).

Hydrogenases catalyze microbial H_2 production and consumption and are reversible enzymes responsible for reversible or partial catalytic reactions as follows (Equation 1).

$$H_2 \Leftrightarrow H^- + H^+ \Leftrightarrow 2H^+ + 2e^- \quad (1)$$

On the basis of the metal cofactors of their H_2-binding sites, these hydrogenases can be divided into three categories, namely the [NiFe]−, [FeFe]−, and [Fe]-hydrogenases (Vignais and Billoud, 2007; Schilter et al., 2016). [NiFe]-hydrogenases are closely related to both H_2 production and consumption, while [FeFe]-hydrogenases are responsible mainly for the production of H_2 owing to their higher turnover rate and activity compared with [NiFe]-hydrogenases (Marshall et al., 2012). However, [Fe]-hydrogenases have so far only been found in methanogenic archaea without cytochromes (Thauer et al., 2010). A recent study shows that the three different types of hydrogenase contain many subgroups based on the properties of metalloenzymes (such as metal-binding motifs, amino acid sequence phylogeny, reported biochemical characteristics and predicted genetic organization), and hydrogenase-encoding genes have also been identified in many microorganisms indicating a broad ecological distribution (Trchounian et al., 2011; Greening et al., 2016). Although the contribution of H_2 metabolism to the entire ecosystem function is recognized in several environments such as hydrothermal vents, anoxic sediments and animal guts (Vignais and Billoud, 2007; Schwartz et al., 2013; Greening et al., 2016), the functions of hydrogenases in ecosystems in general remain largely unknown.

H_2 metabolism plays a vital role in stability and performance in many microbial biotopes at ecosystem level (Marshall et al., 2012). It has been gradually recognized that hydrogenases may be used in bioremediation (Vignais and Billoud, 2007; Jugder et al., 2013). Numerous studies have shown that H_2 can be utilized as an electron donor for reductive dehalogenation by many microorganisms and the occurrence of hydrogenases involved has been reported in dehalogenated bacteria (Seshadri et al., 2005; Rahm et al., 2006; Vignais and Billoud, 2007). In addition, microbial hydrogenases have been used in the remediation of metal-containing industrial wastes for the reduction of potentially toxic metals (Li et al., 2018). Under the impact of hydrogenases, microbial metabolic activities can influence the cycling of belowground minerals and organic matter and play a positive role in the bioremediation of both organic and inorganic pollutants (Lovley, 1993, 2008; Lovley and Coates, 2000; Vignais and Billoud, 2007). Thus, the use of hydrogenases for the remediation of polluted soils might be a promising strategy. In this review we attempt to integrate our understanding of the role of H_2 metabolism in environment and environmental bioremediation processes and summarize the knowledge of H_2 metabolism and hydrogenases involved in bioremediation.

MICROBIAL H_2-PRODUCING PROCESSES AND THEIR IMPACT ON THE ENVIRONMENT

Fermentative Hydrogen Production From Organic Compounds

H_2 is a key compound in the metabolism of many anaerobes, as well as a few aerobes, which owed the capacity to use this energy-rich molecule when it is available in the environment and derive electrons from its oxidation to drive energy generation. In the absence of external electron acceptors, many anaerobic bacteria can exploit carbohydrate rich substrates to produce H_2 by reducing protons continuously. As described previously (Das and Veziroğlu, 2001; Das and Veziroglu, 2008; Hallenbeck, 2009), the fermentative process generating H_2 comprises two major pathways. In the first, butane 2,3 diol fermentation or mixed acid fermentation produces H_2 via formate decomposition where glucose is transformed to pyruvate and then releases electrons to produce H_2 under hydrogenase through a series of oxidation and reduction reactions (**Figure 1A**). The second is an NADH pathway in which H_2 is produced by the re-oxidation of NADH (**Figure 1B**). In the various pyruvate metabolic pathways, H_2 is usually produced by butyric acid fermentation, mixed acid fermentation, and bacterial ethanol fermentation (Ren et al., 2005). Fermentative microorganisms such as *Clostridium* spp. (e.g., *C. butyricum* and *C. acetobutylicum*) (Fang et al., 2006; Zhang et al., 2006), rumen flora (e.g., *Butyrivibrio fibrisolvens, Eubacterium limosum, Megasphaera elsdenii, Ruminococcus flavefaciens,* and *Ruminococcus albus*) (Miller and Wolin, 1973; Joyner et al., 1977; Miller and Wolin, 1979; Chaucheyras-Durand et al., 2010), *Enterobacter* spp. (e.g., *E. cloacae* and *E. aerogenes*) (Kumar and Das, 2000; Fabiano and Perego, 2002), *Pyrococcus furiosus* and *Thermococcus litoralis* (Malik et al., 1989; Rákhely et al., 1999; Schwartz et al., 2013) have been found to effectively produce H_2 via different pyruvate metabolic pathways. Hydrogenase enzymes also play an important role in fermentative H_2 production (Woodward et al., 2000; Trchounian et al., 2012). In general, H_2 production could be catalyzed by a soluble [FeFe]-hydrogenase or a special class of membrane bound [NiFe]-hydrogenase (Ech). For example, *Escherichia coli* can transform intermediary fermentation products to the gaseous products H_2 and CO_2 by formate hydrogenlyase reaction

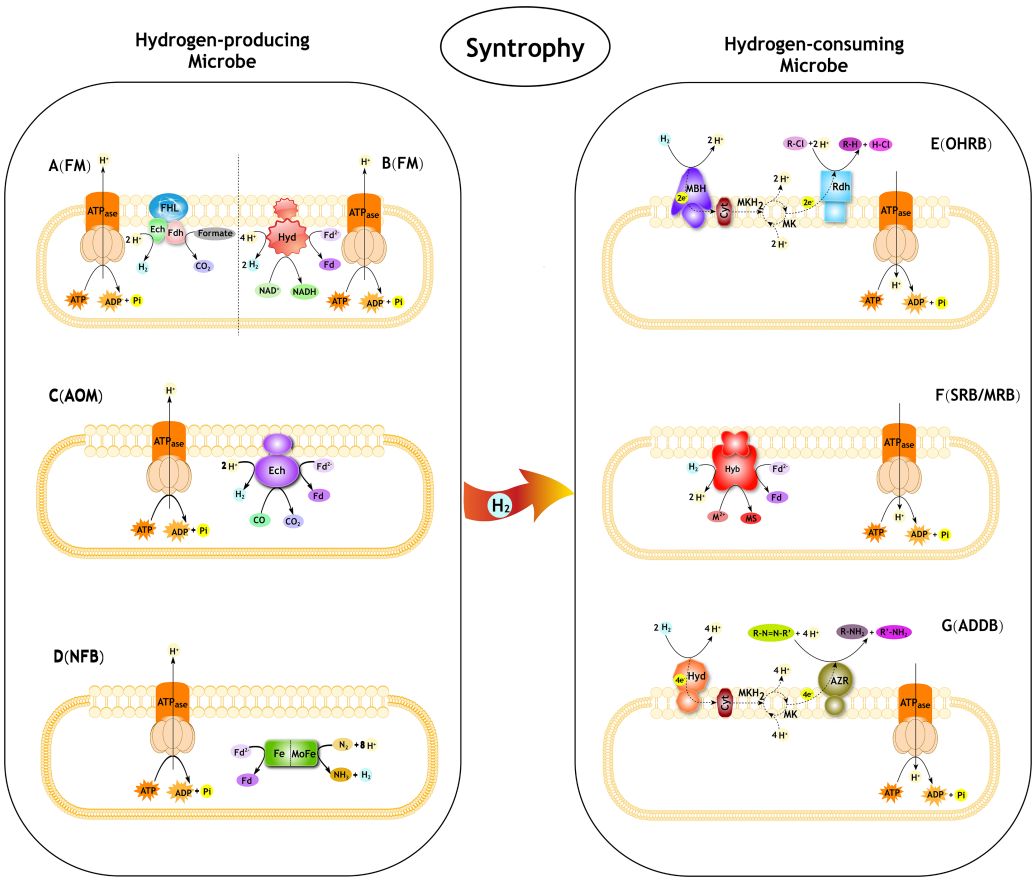

FIGURE 1 | Syntrophic interactions between hydrogen-producing and hydrogen-consuming microbes in pollutant degradation. FM, Fermentative microbe; AOM, Anaerobic CO oxidation microbe; NFB, Nitrogen-fixing bacteria; OHRB, Organohalide-respiring bacteria; SRB, Sulfate-reducing bacteria; MRB, Metal-reducing bacteria; ADDB, Azo dyes decolorization bacteria. **(A)** The progress of formate oxidation coupled to H_2 formation in *E. coli* (derived from Sawers, 1994; Hallenbeck, 2009; Trchounian et al., 2012). The FHL complex consist of a Ech type membrane-bound H_2-evolving [NiFe] hydrogenase coupled to a formate dehydrogenase (Fdh) and membrane integral subunits. **(B)** The progress of re-oxidation of NADH coupled to H_2 formation in *T. roseopersicina* (derived from Jenney and Adams, 2008; Maróti et al., 2010). The Hyd is a membrane-bound H_2-evolving [FeFe] hydrogenase. Fd, ferredoxin. **(C)** The progress of anaerobic CO oxidation coupled to H_2 formation in *C. hydrogenoformans* (derived from Svetlichny et al., 1991; Soboh et al., 2002). The Ech is a membrane-bound H_2-evolving [NiFe] hydrogenase. Fd, ferredoxin. **(D)** The progress of producing H_2 as a byproduct of N_2 fixation. The nitrogenase complex consist of a Fe protein and MoFe protein. **(E)** The role of H_2 in reductive dechlorination in *Dehalococcoides* spp. (derived from Jugder et al., 2016). MBH, membrane-bound uptake hydrogenase. Cyt, cytochrome. MK, menaquinone; MKH_2, dihydromenaquinone. Rdh, reductive dehalogenase. R-Cl, organohalide. **(F)** The role of H_2 in reductive PTEs in *Desulfovibrio fructosovorans* (derived from Chardin et al., 2003; Cao et al., 2014). Hyb is a membrane-bound H_2-uptake [NiFe] hydrogenase. Fd, ferredoxin. M, PTEs. MS, metal sulfides. **(G)** The role of H_2 in reductive azo compounds in *Shewanella decolorationis* (derived from Hong et al., 2007, 2008). Hya, membrane-bound uptake [NiFe]-hydrogenase. Cyt, cytochrome. MK, menaquinone; MKH_2, dihydromenaquinone. AZR, azo reductase.R-N = N-R', azo compounds.

(**Figure 1A**) (Sawers, 1994). Soboh et al. (2004) report that a ferredoxin-dependent [NiFe]-hydrogenase and a NADH-dependent [Fe]-hydrogenase may catalyze H_2 evolution from NADH in *Thermoanaerobacter tengcongensis*. Production of H_2 by fermentation in *Thermotoga maritima* is catalyzed by a heterotrimeric [FeFe]-hydrogenase and two cytoplasmic [NiFe]-hydrogenases have been identified in *Thiocapsa roseopersicina* (**Figure 1B**) (Jenney and Adams, 2008; Maróti et al., 2010).

Anaerobic Carbonic Monoxide (CO) Oxidation

There are several microbes owing different types of hydrogenogens that grow anaerobically in the dark and can unitize CO as the sole energy source to produce H_2 (**Figure 1C**). Uffen (1976) and Fox et al. (1996a,b) showed that *Rhodospirillum rubrum* can produce H_2 by oxidation of CO with the reduction of protons under the catalysis of a complex enzyme consisting of a CO-insensitive [NiFe]-hydrogenase and carbon monoxide dehydrogenase. A typical example of this group is the strictly anaerobic *Carboxydothermus hydrogenoformans* which contains a multienzyme membrane-bound [NiFe]-hydrogenase (Ech) complex (**Figure 1C**) (Svetlichny et al., 1991; Soboh et al., 2002). These enzymes together can oxidize CO and subsequently reduce the protons derived from H_2O to form molecular H_2. *Carboxydocella thermautotrophica* (Sokolova et al., 2002), *Thermosinus carboxydivorans* (Sokolova et al., 2004), *Thermincola carboxydiphila* (Sokolova et al., 2005), and

Thermolithobacter carboxydivorans (Sokolova et al., 2007) are also thermophilic hydrogenogens.

Production of H_2 as a Byproduct of N_2 Fixation

Nitrogen fixation is one of the main processes of biogenic H_2 production and is catalyzed by nitrogenase (**Figure 1D**). Approximately 30–50% of the entire reduction power consumed by nitrogenase is laterally tracked to H_2 evolution (Brewin, 1984; Evans et al., 1987). However, H_2 is not both a competitive inhibitor of N_2 fixation and also represents a net loss of energy unless the H_2 can be reprocessed by means of the uptake hydrogenase (Kosourov et al., 2014). Many H_2-utilizing microorganisms such as the aerobic H_2-oxidizing bacteria in soils reduce the loss of energy (Stein et al., 2005; Maimaiti et al., 2007; Constant et al., 2008; Osborne et al., 2010; Annan et al., 2012; Greening et al., 2015b). Many rhizobia can symbiotically fix dinitrogen in the root nodules of legumes and produce H_2 concomitantly. The most-studied symbiotic nitrogen-fixing bacteria in legumes include *Bradyrhizobium japonicum*, *Mesorhizobium mediterraneum*, *Sinorhizobium meliloti,* and *Rhizobium leguminosarum* (Nour et al., 1995; Spaink, 2000; Laranjo et al., 2014). In addition, strains of *Azotobacter* (Cocking, 2003) and various cyanobacteria (e.g., *Anabaena cylindrica, Nostoc muscorum,* and *Westiellopsis prolica*) (Bulen et al., 1965; Fay, 1992; Nandi and Sengupta, 1998; Das and Veziroğlu, 2001; Das and Veziroglu, 2008) can produce hydrogen through the nitrogen fixation process. Gest and Kamen (1949) report that *Rhodospirillum rubrum* can evolve significant amounts of H_2 in the light and this is termed the photoproduction of H_2 caused by nitrogenase-catalyzed reduction of protons (Bulen et al., 1965). Photoproduction of H_2 was subsequently discovered in other phototrophic bacteria such as *Rhodobater capsulatus*, *Rhodobater sphaeroides*, *Rhodobater palustris*, *Thiocapsa roseopersicina,* and *Halobacterium halobium* (Vincenzini et al., 1982; Gogotov et al., 1991; Khan and Bhatt, 1991; Krahn et al., 1996; Fascetti et al., 1998).

Effects of Microbial Hydrogen Production on Environment

Atmospheric H_2 is derived mainly from anthropogenic activities and oxidation of atmospheric methane (CH_4) and non-methane hydrocarbons. An H_2 mixing ratio of 0.53 ppmv is typically found in the global atmosphere (Novelli et al., 1999) and participates in atmospheric chemical cycles of H_2O and greenhouse gasses as well as various pollutants (Schlegel et al., 1976; Crutzen and Fishman, 1977; Salvi and Subramanian, 2015; Talibi et al., 2017). In addition, H_2 is a potential future energy carrier that may significantly affect the atmospheric H_2 budget when used on a large scale (Brenninkmeijer et al., 2003; Petersen et al., 2011). It has been estimated that the total amount of H_2 emissions into the troposphere each year is approximately 107 Tg (Rhee et al., 2006). Tromp et al. (2003) reported that the concentrations of stratospheric H_2O and ozone and stratospheric temperatures would be affected by these H_2 emissions. Moreover, the potential impacts of an increase in anthropogenic H_2 emissions on the concentration of other trace gasses such as CH_4 and CO) are also proposed.

About 7–11% of the global H_2 pool is contributed by all oceanic, lake, and soil organisms (Schwartz et al., 2013). 'Hot spots' can be found in hypersaline cyanobacterial mats, with the release of H_2 concentrations between 16,000 and 90,000 ppmv (Nielsen et al., 2015), which might be the main source of H_2 emission from lake surface waters to the atmosphere. Numerous studies show that both cell counts of cyanobacteria and their N_2 fixation rates are correlated with the H_2 concentration of lake water (Conrad et al., 1983; Schütz et al., 1988; Schmidt and Conrad, 1993). Furthermore, the production of fermentation H_2 and organic acids is a key component in the biogeochemistry of microbial mats, which promotes close interactions between anoxygenic phototrophs, cyanobacteria and heterotrophic bacteria (Otaki et al., 2012; Lee et al., 2014; Nielsen et al., 2015). However, almost all of the H_2 produced from hypoxic sediments is also consumed by the sediments (Schwartz et al., 2013). The effects of hydrogen consumption on microbial communities in sediments therefore deserve further study.

The contribution of soils to the atmospheric H_2 reservoir is more complex because soils are the main sink of the global H_2 cycle, accounting for about 75 to 80% of atmospheric absorption (Constant et al., 2009; Ehhalt and Rohrer, 2009). However, nitrogen-fixing bacteria that form symbioses with legumes or free-living N_2 fixing bacteria can generate large amounts of H_2 as a by-product during N_2 fixation (Orr et al., 2011; Mus et al., 2016). It has been estimated that H_2 concentrations inside N_2-fixing legume nodules range from 9,000 to 27,000 ppmv (Hunt et al., 1988; Witty, 1991; Witty and Minchin, 1998), so that diffusion losses during the growing season might reach 240,000 L H_2 (Dong et al., 2003). Thus, the intensity of these H_2 emissions to soils is determined by the hydrogen-metabolic capabilities of rhizobacterial symbionts (Hup^+ or Hup^- genotypes) in nodules through an uptake [NiFe]-hydrogenase (Evans et al., 1988; Annan et al., 2012). In the Hup^+ legume rhizosphere the energy of H_2 can be recycled by the [NiFe]-hydrogenase, while H_2 is released into the surrounding soil in the Hup^- legume rhizosphere. There is thus increasing evidence that H_2 released into surrounding soils plays a key role in increasing plant biomass via the enrichment of aerobic H_2-oxidizing bacteria (HOB), or plant growth-promoting rhizobacteria (PGPR) in both legumes and non-legumes (Dong et al., 2003; Maimaiti et al., 2007). Different H_2 mixing ratios found in natural ecosystems may indeed lead to changes in soil microbial community structure and coordinated feedback of community functions. Constant et al. (2008) found that soil actinomycetes (such as *Streptomyces* sp. PCB7) are the main users of trace level of H_2 in soils and might be key contributors to the function of soils as a sink in the global H_2 cycle. Subsequently, Khdhiri et al. (2017) validated their own hypothesis by showing that the taxonomic response of the soil microbial community composition to H_2 exposure is inconsistent across land use types. Piché-Choquette et al. (2018) revealed that H_2 supports metabolic and energetic flexibility in microorganisms supplying a variety of ecosystem services via dose-response relationships between environmentally relevant

H_2 concentrations and the biological sinks of H_2, CH_4, and CO in soils.

ROLE OF H_2 IN ENVIRONMENTAL BIOREMEDIATION

The H_2 produced both biogenically and abiogenically can be released and provided to support for the growth and metabolism of hydrogenotrophic prokaryotes (Karyakin et al., 2007). H_2 metabolism fulfills a critical role in the ecosystems of many microbial biotopes (Vignais and Billoud, 2007; Schwartz et al., 2013; Greening et al., 2016). It is currently considered that a wide range of microbial groups employ H_2 as an electron donor to catalyze the reduction of pollutants such as organohalides, azo compounds and potentially toxic elements.

Organohalides

Organohalides are recalcitrant, toxic, highly persistent, globally prevalent, and carcinogenic environmental contaminants. Organohalide-respiring bacteria (OHRB) have been isolated from polluted soils, sludges, sediments, aquifers, freshwaters, and marine habitats, and they are of considerable importance in bioremediation processes and natural halogen cycles (Zanaroli et al., 2015). Most OHRB discovered to date belong to *Desulfomonile*, *Dehalococcoides*, *Dehalobacter*, *Desulfitobacterium*, *Desulfuromonas*, and *Sulfurospirillum* (formerly *Dehalospirillum*) as reviewed by Jugder et al. (2015). Reductive dechlorination is an anaerobic respiration process that utilizes H_2 as electron donor to dehalorespire these halogenated organics (**Figure 1E**) (Zanaroli et al., 2015; Agarwal et al., 2017). The process of electron via electron transport phosphorylation from the oxidation of the H_2 to reductive dechlorination of organohalides involving membrane associated oxidoreductases (**Figure 1E**) (Jugder et al., 2016). Membrane-bound hydrogenases (MBH) are the initial oxidizers to take up the electrons released from molecular H_2, which play a vital role in organohalide respiration (Jugder et al., 2013, 2015, 2016). The reductive dehalogenation of organohalides is typically catalyzed by dehalogenating enzyme systems coupled to ATP synthesis, reductive dehalogenases (Rdases) replace the halogen substituent with a hydrogen atom, reducing the toxicity and recalcitrance to biodegradation (**Figure 1E**) (Adrian and Loeffler, 2016; Gevorgyan et al., 2018). Sequencing data of genomes reveal that OHRB possess as many as 36 putative Rdases. After transformation to lower halogenated organics under anaerobic conditions, these toxic compounds can subsequently be mineralized by aerobic bacteria (Jugder et al., 2015).*Desulfomonile tiedjei* strain DCB-1 is one of the best-described dechlorinating anaerobes. The strain, first discovered by Suflita et al. (1982), reductively dechlorinates 3-chlorobenzoate while replacing the chlorine atom with hydrogen from H_2, whereby providing energy for bacterial growth (Shelton and Tiedje, 1984; Dolfing and Tiedje, 1986; Dolfing and Tiedje, 1987). The strain was then noted to consume H_2 with 3-chloro-, 3-bromo-, 3-iodobenzoate, tetrachloroethene (PCE), trichloroethene (TCE) (Cole et al., 1995), and chlorophenols (Mohn and Kennedy, 1992) as electron acceptors (DeWeerd et al., 1991). During the dehalogenation of 3-chlorobenzoate, formate was the most effective electron donor, followed by H_2, pyruvate, and acetate.

Dehalococcoides strains are also some of the best known species capable of reductively dechlorinating a wide range of haloorganics including chlorinated benzenes, biphenyls, dioxins, ethenes, naphthalenes, and brominated diphenyl ethers. For example, tetrachloroethene is a commonly used solvent that possesses high toxicity and is a suspect carcinogen. The complete reductive dechlorination of tetrachloroethylene (PCE) and trichloroethylene (TCE) to non-toxic ethylene was first observed under methanogenic conditions by mixed cultures (Freedman and Gossett, 1989). Although H_2 also served as the electron donor, methanol was more effective in sustaining the reductive dechlorination process. Holliger et al. (1993) isolated an anaerobic bacterial culture, previously named as PER-K23, from an anaerobic packed-bed column. By using H_2 and formate as the only electron donors, PCE or TCE was reductively transformed to ethane via *cis*-1,2-dichloroethene (*cis*-1,2-DCE), chloroethene, and ethene, which was coupled to bacterial growth. The key role of hydrogenases in metabolizing these pollutants is underscored by the fact that both uptake (Hup type) and energy-conserving hydrogenases (Hyc or Ech type) were found in the genome of *Dehalobacter restrictus* PER-K23 (Rupakula et al., 2013). Maymó-Gatell et al. (1997) then isolated a dehalogenator, strain 195, and characterized it as *Dehalococcoides ethenogenes*. To date, *Dehalococcoides* species are the only bacteria known to be capable of completely dechlorinating chloroethylene. Genomic analysis of *Dehalococcoides ethenogenes* 195 showed that several hydrogenase genes including the membrane-bound periplasmic Hup, cytoplasmic Vhu, and membrane-bound Ech and Hyc [NiFe]-hydrogenases (Groups 1, 3, 4, and 4, respectively), and a membrane-bound Hym [Fe]-hydrogenases has potential roles in electron transport, which are capable of completing anaerobic dechlorination of the solvents PCE and TCE to vinyl chloride (VC) and ethane (Vignais et al., 2001; Morris et al., 2006).

Unlike other halorespiring bacteria, *Dehalococcoides* spp. use only H_2 as an obligate electron donor for the dechlorination reaction, and no other electron acceptors support growth. For example, *D. ethenogenes* strain 195 grew only on H_2 as electron donor for both bacterial growth and PCE reduction rather than formate, lactate, methanol, ethanol, glucose, pyruvate, or yeast extract (Maymó-Gatell et al., 1997). In addition, *Dehalococcoides* sp. CBDB1 was the first purified isolate of a bacterium relying on the energy obtained from stoichiometrical dehalorespiration of chlorobenzenes (CB) such as 1,2,3-trichlorobenzene (TCB) and 1,2,3,4-tetrachlorobenzene (TeCB) (Adrian et al., 2000). Both *Dehalococcoides* sp. 195 and CBDB1 exhibit reductive dehalogenation of chlorophenols (Adrian et al., 2007). Kube et al. (2005) compared the genome sequence of *Dehalococcoides* sp. CBDB1 with *Dehalococcoides ethenogenes* strain 195 and revealed that the hydrogenases previously described for strain

195 are also present in strain CBDB1. Chloroform (CF, $CHCl_3$) is a non-polar solvent that is ubiquitous and is toxic to humans. The biodegradation of CF involves two processes, (1) dehalorespiration in which CF is dechlorinated to dichloromethane (DCM, CH_2Cl_2) by employing H_2 as electron donor under the action of uptake hydrogenase, and (2) a fermentative process in which DCM is transformed to H_2, acetate and carbon dioxide. Lee et al. (2012) report the involvement of *Dehalobacter* in dehalorespiration of CF [Equation (2)].

$$CHCl_3 + H_2 \rightarrow CH_2Cl_2 + H^+ + Cl^- \quad (2)$$

Despite these findings in respiration of organohalides, there is no real consensus on the involvement of various membrane associated components.

Potentially Toxic Elements (PTEs)

Potentially toxic elements display environmental durability, biological accumulation, and potential biological toxicity. The remediation of PTEs can be achieved by sulfate-reducing bacteria (SRB) or metal-reducing bacteria that can utilize H_2 or other organic compounds as terminal electron donors to reduce the PTEs. Tebo and Obraztsova (1998) isolated the first sulfate-reducing bacterium from PTE-polluted sediments named *Desulfotomaculum reducens* sp. nov. strain MI-1, which can utilize H_2 as terminal electron donor and metals [such as Cr(VI), Mn(IV), Fe(III), and U(VI)] as electron acceptors accompanied by bacterial growth. Thus far, more than 40 SRB species have been identified, including *Desulfobacter*, *Desulfovibrio*, *Desulfotomaculum* and *Desulfomicrobium,* and others (Leloup et al., 2009; Mizuno et al., 2012; Hussain et al., 2016; Li et al., 2018). Subsequently, due to the advantages of SRB (no secondary pollution and strong adaptability), they have been used in the bioremediation of PTEs (Li et al., 2018). Generally speaking, there are two steps involved in the mechanism of SRB removal of PTEs from wastewaters: (i) SRB utilize sulfate as electron acceptor to oxidize simple organic compounds to generate bicarbonate ion and hydrogen sulfide under anaerobic conditions [Equation (3)], and (ii) the hydrogen sulfide generated reacts with dissolved PTE to form insoluble metal sulfide precipitates [Equation (4)] (Kieu et al., 2011; Singh et al., 2011; Li et al., 2017).

$$2CH_2O + SO_4^{2-} \rightarrow 2HCO_3^- + H_2S \quad (3)$$

$$H_2S + M^{2+} \rightarrow 2H^+ + MS(S) \quad (4)$$

Where CH_2O represents simple organic compounds (such as acetate and lactate), M represents PTEs, and MS represents metal sulfides. Because of their special characteristics with the corresponding metal sulfides readily forming precipitates, SRBs have been used to treat PTE-polluted wastewaters (e.g., uranium-containing, chromium-containing and antimony-containing wastewaters, organochlorines, and other pollutants) (Li et al., 2018). Lovley and Phillips (1994) showed that the bioremediation effect of *Desulfovibrio vulgaris* which utilizes H_2 as the electron donor catalyzed by the c_3 cytochrome functions as a Cr(VI) reductase in Cr(VI)-contaminated waters was superior to the previously described Cr(VI) reductive microorganisms. Kieu et al. (2011) reported that the PTE removal efficiencies of Cu^{2+}, Ni^{2+}, Zn^{2+}, and Cr^{6+} in anaerobic semi-continuous stirred tank reactors containing a consortium of SRB reached 94–100% after 4 weeks under experimental conditions. In addition, several microbial genera reduced uranium to form easily precipitated reduced U(IV) species, and this has been used successfully in soil remediation (Phillips et al., 1995; Fredrickson et al., 2000; Valls and De Lorenzo, 2002).

Several uptake hydrogenases were considered to have potential application in the bioremediation of PTEs. The [NiFe] uptake hydrogenases in group 1 including membrane-bound respiratory uptake hydrogenases that couple H_2 oxidation to catalyze metal reduction (**Figure 1F**). For example, [NiFe]-uptake hydrogenase from SRB can reduce toxic chromate VI to form a less toxic product (Chardin et al., 2003). In addition, technetium VII is reduced by *Desulfovibrio fructosovorans* through this mechanism (Tabak et al., 2005), and hydrogenases involving in metal reduction have also been observed in other metals including ferrum (Fe) (Coppi et al., 2004), platinum (Riddin et al., 2009), and lead (Deplanche et al., 2010). A comprehensive analysis of the genome sequence of the metal-reducing bacterium (*Shewanella oneidensis*) has been conducted, and has predicted that an [Fe]-hydrogenase and several cytochromes are involved in the electron transport and metal reduction processes (Heidelberg et al., 2002). However, the potential application of microbes with different subgroup hydrogenases for PTE respiration is not enough, requiring further study including the biochemical investigations of these different subgroup hydrogenases.

Other Pollutants

Azo compounds undergo dissimilatory azoreduction by *Shewanella decolorationis* S12 under anaerobic conditions. This strain utilized azo compounds as carbon source for growth by azo reductase which is sustained by the H_2 supply. The strain also catalyzed H_2-dependent reduction of Fe(III) and humic substances (Coppi et al., 2004; Hong et al., 2008). Brigé et al. (2008) show that *Shewanella decolorationis* MR-1 utilized azo dye amaranth as electron acceptor for microbial energy conservation. Mutambanengwe et al. (2007) show the decolorization of a wide range of azo dyes with sulfate-reducing microbes (SRM) and hydrogenases might be involved in the degradation process. A multicomponent electron transfer chain has been proposed to be involved in the extracellular reduction of azo compounds. The electron transfer components consist of the cytoplasm/outer membrane, periplasm, c-type cytochromes, and menaquinone (Hong et al., 2007; Brigé et al., 2008). Hya type [NiFe]-hydrogenase or Hyd type [Fe]- hydrogenase act as a critical hub mediating the oxidization of H_2 to provide electrons for azoreduction metabolism (**Figure 1G**) (Hong et al., 2008).

H_2-dependent reduction has been reported in nitroaromatic compounds (Watrous et al., 2003). In a strict anaerobe, *Clostridium acetobotulinicum*, an [Fe]-hydrogenase is responsible for the reduction of nitro substituents of 2,4,6-trinitrotoluene

(TNT) to the corresponding hydroxylamine in an acidogenic environment.

Factors Affecting the Utilization of Hydrogen by Degrading Bacteria in the Environment

There are many factors affecting the utilization of H_2 by degrading bacteria in the environment such as H_2 source, H_2 transfer process and other environmental factors (including trophic hierarchies, external pH, osmotic coditions, concentration of carbon sources and their mixtures and microbial community and other physicochemical factors).

Methanogens were found to affect the interspecies H_2 transfer of dehalorespiring bacteria, which might promote or inhibit the dechlorination process (Smatlak et al., 1996; Fennell et al., 1997; Yang and McCarty, 1998). Johnson et al. (2008) demonstrated the dechlorination of stress-related net cell growth by *Dehalococcoides ethenogenes* strain 195 (DE195) which was isolated and then transited to a smooth phase. Although *Methanobacterium congolense* (MC) can compete with DE195 for hydrogen, adverse effects of the dechlorination rate were not observed (Men et al., 2012). This is mainly because the H_2 threshold required for dechlorination is very low, so that even though methane production consumes a large amount of H_2, it does not compete for dechlorination (Yang and McCarty, 1998; Men et al., 2012). In syntrophic communities, H_2-producing bacteria and H_2-consuming methanogens perceive the redox conditions and affect each other's metabolism (Stams and Plugge, 2009). Several studies have shown that the reduction dechlorination can be promoted in some communities in the presence of methanogens (Vogel and McCARTY, 1985; Heimann et al., 2006; Kong et al., 2014). In addition, a recent study found that *Methylobacter* seemed to be tolerant to TCE and may play a vital role in TCE degradation (Kong et al., 2014). Although many studies have assessed the association between methanogens and dechlorination bacteria, the mechanism by which methanogens affect dechlorinating communities remains unclear.

The process of forming compact aggregates involves both physicochemical and biological interactions (Stams and Plugge, 2009). When the compact aggregates are formed in anaerobic bacteria and methanogenic archaea, the rate of H_2 transfer between two species increases significantly (Lettinga et al., 1988; Stams and Plugge, 2009). Several studies have also shown that the inter-microbial distances affect both their specific growth rates and biodegradation rates (Ishii et al., 2005; Stams et al., 2006; Stams and Plugge, 2009). Thus, forming compact aggregates might be an important factor influencing the biodegradation rates of degrading bacteria.

It is well known that trophic hierarchies occur because different functional members of the community provide each other with a matrix and basic cofactors, and eliminate inhibitory metabolites (Schink, 1997; Rittmann and McCarty, 2012). DeWeerd et al. (1991) reported that acetylene, molybdate, selenate, and metronidazole can inhibit dehalogenation, sulfite reduction and H_2 metabolism, indicating that the reduction of sulfite and dehalogenation may share part of the same electron transport chain. However, some environmental factors might accelerate the degradation of pollutants by promoting H_2 utilization. For example, cobalamin has a positive effect on the dechlorination process as a co-factor of the reductive dehalogenases (Yan et al., 2012). *Desulfovibrio vulgaris* Hildenborough (DVH) possesses the full set of genes required for the biosynthesis of adenosylcobalamin, a derivative of vitamin B12 which might result in an increased concentration of the corrinoid co-factor (vitamin B12) in co-cultures, taken up and utilized immediately by *Dehalococcoides* species (Rodionov et al., 2004). In addition, the main factors influencing H_2 utilization such as external pH, osmotic conditions, concentration of carbon sources and their mixtures, microbial community and other physicochemical factors mainly affected growth and the physiological activity including uptake hydrogenase and pollutant degrading enzymes of the degrading bacteria (Richter and Gescher, 2014; Trchounian and Trchounian, 2014, 2015; Trchounian et al., 2017a).

INTERSPECIES HYDROGEN TRANSFER DURING SYNTROPHIC GROWTH

Syntrophy coupling mutualistic interactions between hydrogen-/formate-producing and hydrogen-/formate-consuming microorganisms is essential for biofuel production, pollutant degradation, and global carbon cycling (Kleinsteuber et al., 2012; Sieber et al., 2012; Morris et al., 2013). When sulfate is limited or unavailable, SRBs can also mediate the transfer of H_2 between species, which provides the bacterial species with a very versatile metabolism adapted to complex ecological environments. Odom and Peck (1981) first documented the transfer of the redundant H_2 evolved from substrate fermentation by SRBs to other H_2 consuming bacteria. Using a defined two-member continuous culture, Drzyzga et al. (2001) demonstrated that the sulfate reducer *Desulfovibrio* sp. strain SULF1 can use the dehalorespiring *Desulfitobacterium frappieri* TCE1 as a 'biological electron acceptor' to sustain growth. They also noted that dehalogenation of tetrachloroethene (PCE) was inhibited at sulfate concentrations above 2.5 mM, while PCE was completely dehalogenated to *cis*-dichloroethene (*cis*-DCE) with 1 mM sulfate or without sulfate addition (Drzyzga and Gottschal, 2002). In this community, *Desulfovibrio vulgaris* Hildenborough (DVH) can grow syntrophically with *Dehalococcoides ethenogenes* strain 195 (DE195), thus enhancing the robustness of bacterial growth and the dechlorination activity of trichloroethene (Men et al., 2012). The syntrophical interaction with sulfate reducers has been shown to result in more effective transfer of H_2, thereby facilitating faster dechlorination and more rubust growth of dehalogenating strains compared with gaseous H_2 (Men et al., 2012). The syntrophic relationship between methanogens and archaea also involves interspecies H_2 transfer in the process of converting long-chain fatty acids (Stams and Plugge, 2009). Subsequently, Ziels et al. (2017) found several formate hydrogenases and dehydrogenases in the enriched genome bins (GBs) of both their codigesters. In the process of CF dechlorination, interspecies H_2 transfer was observed in the

form of acetogenesis and methanogenesis by Lee et al. (2012), which required syntrophic partners to maintain low H_2 partial pressures.

The possible processes of syntrophic interactions between H_2-producing and H_2-consuming microbes in pollutant degradation are shown in **Figure 1**. Previous studies have shown that H_2-forming bacteria and H_2-utilizing bacteria sense redox conditions, influencing each other's metabolism in syntrophic communities (Stams and Plugge, 2009). Interspecies electron transfer mechanisms underlie thermodynamically favorable syntrophic processes (Gieg et al., 2014). In anoxic environments, butyrate oxidations involving energy-dependent reactions were possible to be applied in syntrophic degradation of organohalides. For example, the standard free reaction enthalpies ($\Delta G^{o\prime}$) of butyrate oxidations and organohalide degradations were as follows [Equation (5) Müller et al., 2010; Equation (6) Jugder et al., 2016]:

$$\mathrm{Butyrate}^- + 2\mathrm{H_2O} \rightarrow 2\mathrm{Acetate}^- + \mathrm{H}^+ + 2\mathrm{H_2} (\Delta G^{o'} = +48.3 KJ/mol) \quad (5)$$

$$\mathrm{H_2} + \mathrm{R-Cl} \rightarrow \mathrm{R-H} + \mathrm{HCl} (\Delta G^{o'} = -131 to -192 KJ/mol) \quad (6)$$

Based on energy balance toward H_2 production and consumption analysis, we propose that the energy-transforming reactions between H_2 production and organohalide degradations might be involved in syntrophic H_2 production and consumption microorganisms. Dehalogenating microorganisms (such as *Dehalococcoides* sp. strain BAV1 and *Dehalococcoides ethenogenes* strain 195) can utilize acetate as carbon source and H_2 as electron donor when grown in isolation, exhibiting limited dechlorination activity and low growth rates (He et al., 2003a,b). Thus, a promising method might be to develop improved bioremediation strategies by enhancing the strong growth and dechlorination activity of dehalogenating microorganisms (Men et al., 2012). However, many interspecies H_2 transfer interactions are syntrophic, and thus only present in complex microbial communities but not in pure cultures. In complex microbial consortia, H_2 indirectly mediates electron shuttle between electron donors and acceptors. Hydrogenotrophic bacteria can profit from the H_2 produced from their syntrophic partners, thereby transforming pollutants. Thus, both H_2-producing and H_2-consuming microorganisms are essential for their own growth and might also promote the degradation of pollutants (Stams and Plugge, 2009).

CONCLUSION AND PERSPECTIVES

Metabolism of H_2 including H_2 production and H_2 consumption have been recognized as a potential driving force affecting the structure of microbial communities and may even change community functions. Although the contribution of H_2 metabolism to entire ecosystem processes is recognized in hydrothermal vents, anoxic sediments and animal guts (Vignais and Billoud, 2007; Schwartz et al., 2013), the role of H_2 metabolism and hydrogenases in ecosystems are not fully elucidated. Further advances in exploiting the function of biohydrogen metabolism and related microbial communities in environmental bioremediation are expected to result from (i) using metagenome sequencing, single-gene fluorescence *in situ* hybridization, the functional gene arrays (GeoChip) and *in situ* mass spectrometry to track the dynamics of pollutant-degrading bacteria involving in H_2 metabolism and the interplay between pollutant-degrading bacteria and H_2-metabolism bacteria in degradation process; (ii) effects of soil conditions on H_2-consuming microorganisms degrading pollutants; (iii) structural studies of hydrogenases or the synergistic action of other enzymes (such as ATPase and Rdase) involving in the process of environmental bioremediation and enhancing these enzymes activity through protein engineering; (iv) integrative analyses of genomic, transcriptomic, and epigenomic data in these environmental bioremediation process.

To date, environmentally friendly management techniques named "3B" techniques (biological carbon sequestration, bioenergy, and bioremediation) have been proposed to further enhance biodiversity and mitigate environmental stressors (Teng et al., 2012). Environmental H_2 is an energy source for aerobic H_2 oxidizers, sulfate reducers, acetogens and methanogens and is also a source of reducing power for anaerobic bacteria and anoxygenic phototrophs (Schwartz et al., 2013). Syntrophy coupling mutualistic interactions between H_2-producing and H_2-consuming microorganisms is not restricted to the transfer of reducing agents such as H_2 or formate, but can also involve the exchange of organic, sulfurous and nitrogenous compounds or the removal of toxic compounds. Nevertheless, there is still a considerable need for appropriate research initiatives to apply those microbial groups to the bioremediation of contaminated soils. However, soil is a complex and dynamic biological system. From the soil to the microorganism, bioavailability of pollutants involves a full process of adsorption and desorption, transport, and uptake by microorganisms which are also affected by the soil conditions such as soil organic matter, soil minerals, soil moisture, soil aggregates and so on (Ren et al., 2018; Teng and Chen, 2019).

Proton ATPase or other membrane bound secondary transporters affect hydrogenase activity and thus H_2 metabolism (Trchounian et al., 2011; Gevorgyan et al., 2018). So, structural studies of hydrogenases or other synergistic enzymes (such as ATPase and Rdase) involving in the process of environmental bioremediation are vital important in directing protein engineering, for example, in rendering these enzymes activity to promote the degradation efficiency of pollutants via identification of factors linked to the protein environment of the active site. Studies of H_2 metabolism and regulation will also be important in engineering microorganisms at the cellular level to maximize the degradation efficiency of pollutants. Since hydrogenases and other synergistic enzymes have been shown to play an important role in the degradation of pollutants, it is also tempting to consider that analysis of genomic, transcriptomic,

and epigenomic data of these enzymes in environmental bioremediation process will likely provide vital insights into the hydrogenase participates in degradation mechanism of pollutants.

In conclusion, this review provides a comprehensive framework for H_2 production and H_2 consumption in environmental bioremediation processes. The syntrophy coupling mutualistic interaction between H_2-producing and H_2-consuming microorganisms could be applied to the removal of toxic compounds. In addition, several uptake hydrogenases are also considered to have potential application in the bioremediation of those toxic compounds. The use of this bioenergy may provide a low-input and ecologically friendly bioremediation strategy for the future.

AUTHOR CONTRIBUTIONS

YT, YX, and XW collected the data. YT and YX drafted the article. YT, XW, and PC critically revised the article.

FUNDING

This study was funded by the Outstanding Youth Fund of Jiangsu Province (No. BK20150049), the National Natural Science Foundation of China (Grant Nos. 41671327 and 41571308), and the Special Project on the Basis of the National Science and Technology of China (2015FY110700).

REFERENCES

Adrian, L., Hansen, S. K., Fung, J. M., Görisch, H., and Zinder, S. H. (2007). Growth of *Dehalococcoides* strains with chlorophenols as electron acceptors. *Environ. Sci. Technol.* 41, 2318–2323. doi: 10.1021/es062076m

Adrian, L., and Loeffler, F. E. (2016). *Organohalide-Respiring Bacteria*. Berlin: Springer. doi: 10.1007/978-3-662-49875-0

Adrian, L., Szewzyk, U., Wecke, J., and Görisch, H. (2000). Bacterial dehalorespiration with chlorinated benzenes. *Nature* 408, 580–583. doi: 10.1038/35046063

Agarwal, V., Miles, Z. D., Winter, J. M., Eustáquio, A. S., El Gamal, A. A., and Moore, B. S. (2017). Enzymatic halogenation and dehalogenation reactions: pervasive and mechanistically diverse. *Chem. Rev.* 117, 5619–5674. doi: 10.1021/acs.chemrev.6b00571

Annan, H., Golding, A. L., Zhao, Y., and Dong, Z. (2012). Choice of hydrogen uptake (Hup) status in legume-rhizobia symbioses. *Ecol. Evol.* 2, 2285–2290. doi: 10.1002/ece3.325

Bagnoud, A., Chourey, K., Hettich, R. L., de Bruijn, I., Andersson, A. F., Leupin, O. X., et al. (2016). Reconstructing a hydrogen-driven microbial metabolic network in Opalinus Clay rock. *Nat. Commun.* 7:12770. doi: 10.1038/ncomms12770

Brenninkmeijer, C. A., Janssen, C., Kaiser, J., Röckmann, T., Rhee, T., and Assonov, S. (2003). Isotope effects in the chemistry of atmospheric trace compounds. *Chem. Rev.* 103, 5125–5162. doi: 10.1021/cr020644k

Brewin, N. (1984). "Hydrogenase and energy efficiency in nitrogen fixing symbionts," in *Genes Involved in Microbe-Plant Interactions*, eds D. P. S. Verma and T. Hohn (Vienna: Springer), 179–203.

Brigé, A., Motte, B., Borloo, J., Buysschaert, G., Devreese, B., and Van Beeumen, J. J. (2008). Bacterial decolorization of textile dyes is an extracellular process requiring a multicomponent electron transfer pathway. *Microb. Biotechnol.* 1, 40–52. doi: 10.1111/j.1751-7915.2007.00005.x

Bulen, W., Burns, R., and LeComte, J. (1965). Nitrogen fixation: hydrosulfite as electron donor with cell-free preparations of *Azotobacter vinelandii* and *Rhodospirillum rubrum*. *Proc. Natl. Acad. Sci. U.S.A.* 53, 532–593. doi: 10.1073/pnas.53.3.532

Cao, H., Wang, Y., Lee, O. O., Zeng, X., Shao, Z., and Qian, P. Y. (2014). Microbial sulfur cycle in two hydrothermal chimneys on the Southwest Indian Ridge. *mBio* 5:e00980-13. doi: 10.1128/mBio.00980-13

Chardin, B., Giudici-Orticoni, M. T., De Luca, G., Guigliarelli, B., and Bruschi, M. (2003). Hydrogenases in sulfate-reducing bacteria function as chromium reductase. *Appl. Microbiol. Biotechnol.* 63, 315–321. doi: 10.1007/s00253-003-1390-8

Chaucheyras-Durand, F., Masseglia, S., Fonty, G., and Forano, E. (2010). Influence of the composition of the cellulolytic flora on the development of hydrogenotrophic microorganisms, hydrogen utilization, and methane production in the rumens of gnotobiotically reared lambs. *Appl. Environ. Microbiol.* 76, 7931–7937.doi: 10.1128/aem.01784-10

Chivian, D., Brodie, E. L., Alm, E. J., Culley, D. E., Dehal, P. S., DeSantis, T. Z., et al. (2008). Environmental genomics reveals a single-species ecosystem deep within earth. *Science* 322, 275–278. doi: 10.1126/science.1155495

Cocking, E. C. (2003). Endophytic colonization of plant roots by nitrogen-fixing bacteria. *Plant Soil* 252, 169–175. doi: 10.1023/A:1024106605806

Cole, J. R., Fathepure, B. Z., and Tiedje, J. M. (1995). Tetrachloroethene and 3-chlorobenzoate dechlorination activities are co-induced in *Desulfomonile tiedjei* DCB-1. *Biodegradation* 6, 167–172. doi: 10.1007/BF00695347

Conrad, R., Aragno, M., and Seiler, W. (1983). Production and consumption of hydrogen in a eutrophic lake. *Appl. Environ. Microbiol.* 45, 502–510.

Constant, P., Chowdhury, S. P., Pratscher, J., and Conrad, R. (2010). Streptomycetes contributing to atmospheric molecular hydrogen soil uptake are widespread and encode a putative high-affinity [NiFe]-hydrogenase. *Environ. Microbiol.* 12, 821–829. doi: 10.1111/j.1462-2920.2009.02130.x

Constant, P., Poissant, L., and Villemur, R. (2008). Isolation of *Streptomyces sp. PCB7*, the first microorganism demonstrating high-affinity uptake of tropospheric H2. *ISME J.* 2, 1066–1076. doi: 10.1038/ismej.2008.59

Constant, P., Poissant, L., and Villemur, R. (2009). Tropospheric H2 budget and the response of its soil uptake under the changing environment. *Sci. Total Environ.* 407, 1809–1823. doi: 10.1016/j.scitotenv.2008.10.064

Coppi, M. V., O'Neil, R. A., and Lovley, D. R. (2004). Identification of an uptake hydrogenase required for hydrogen-dependent reduction of Fe (III) and other electron acceptors by *Geobacter sulfurreducens*. *J. Bacteriol.* 186, 3022–3028. doi: 10.1128/JB.186.10.3022-3028.2004

Crutzen, P. J., and Fishman, J. (1977). Average concentrations of OH in the troposphere, and the budgets of CH4, CO, H2 and CH3CCl3. *Geophys. Res. Lett.* 4, 321–324. doi: 10.1029/GL004i008p00321

Das, D., and Veziroglu, T. N. (2008). Advances in biological hydrogen production processes. *Int. J. Hydrogen Energ.* 33, 6046–6057. doi: 10.1016/j.ijhydene.2008.07.098

Das, D., and Veziroğlu, T. N. (2001). Hydrogen production by biological processes: a survey of literature. *Int. J. Hydrogen Energ.* 26, 13–28. doi: 10.1016/S0360-3199(00)00058-6

Deplanche, K., Caldelari, I., Mikheenko, I. P., Sargent, F., and Macaskie, L. E. (2010). Involvement of hydrogenases in the formation of highly catalytic Pd (0) nanoparticles by bioreduction of Pd (II) using *Escherichia coli* mutant strains. *Microbiology* 156, 2630–2640. doi: 10.1099/mic.0.036681-0

DeWeerd, K., Concannon, F., and Suflita, J. M. (1991). Relationship between hydrogen consumption, dehalogenation, and the reduction of sulfur oxyanions by *Desulfomonile tiedjei*. *Appl. Environl. Microbiol.* 57, 1929–1934.

Dolfing, J., and Tiedje, J. M. (1986). Hydrogen cycling in a three-tiered food web growing on the methanogenic conversion of 3-chlorobenzoate. *FEMS Microbiol. Ecol.* 2, 293–298. doi: 10.1111/j.1574-6968.1986.tb01740.x

Dolfing, J., and Tiedje, J. M. (1987). Growth yield increase linked to reductive dechlorination in a defined 3-chlorobenzoate degrading methanogenic coculture. *Arch. Microbiol.* 149, 102–105. doi: 10.1007/BF00425073

Dong, Z., Wu, L., Kettlewell, B., Caldwell, C., and Layzell, D. (2003). Hydrogen fertilization of soils–is this a benefit of legumes in rotation? *Plant Cell Environ.* 26, 1875–1879. doi: 10.1046/j.1365-3040.2003.01103.x

Drzyzga, O., Gerritse, J., Dijk, J. A., Elissen, H., and Gottschal, J. C. (2001). Coexistence of a sulphate-reducing *Desulfovibrio* species and the dehalorespiring *Desulfitobacterium frappieri* TCE1 in defined chemostat cultures grown with various combinations of sulphate and tetrachloroethene. *Environ. Microbiol.* 3, 92–99. doi: 10.1046/j.1462-2920.2001.00157.x

Drzyzga, O., and Gottschal, J. C. (2002). Tetrachloroethene dehalorespiration and growth of *Desulfitobacterium frappieri* TCE1 in strict dependence on the activity of *Desulfovibrio fructosivorans*. *Appl. Environ. Microbiol.* 68, 642–649. doi: 10.1128/AEM.68.2.642-649.2002

Ehhalt, D. H., and Rohrer, F. (2009). The tropospheric cycle of H2: a critical review. *Tellus B* 61, 500–535. doi: 10.1111/j.1600-0889.2009.00416.x

Evans, H., Russell, S., Hanus, F., and Ruiz-Argueso, T. (1988). "The importance of hydrogen recycling in nitrogen fixation by legumes," in *World Crops: Cool Season Food Legumes*, ed. R. J. Summerfield (Dordrecht: Springer), 777–791. doi: 10.1007/978-94-009-2764-3_62

Evans, H. J., Harker, A., Papen, H., Russell, S. A., Hanus, F., and Zuber, M. (1987). Physiology, biochemistry, and genetics of the uptake hydrogenase in rhizobia. *Annu. Rev. Microbiol.* 41, 335–361. doi: 10.1146/annurev.mi.41.100187.002003

Fabiano, B., and Perego, P. (2002). Thermodynamic study and optimization of hydrogen production by *Enterobacter aerogenes*. *Int. J. Hydrogen Energ.* 27, 149–156. doi: 10.1016/S0360-3199(01)00102-1

Fang, H. H., Zhu, H., and Zhang, T. (2006). Phototrophic hydrogen production from glucose by pure and co-cultures of *Clostridium butyricum* and *Rhodobacter sphaeroides*. *Int. J. Hydrogen Energ.* 31, 2223–2230. doi: 10.1016/j.ijhydene.2006.03.005

Fascetti, E., D'addario, E., Todini, O., and Robertiello, A. (1998). Photosynthetic hydrogen evolution with volatile organic acids derived from the fermentation of source selected municipal solid wastes. *Int. J. Hydrogen Energ.* 23, 753–760. doi: 10.1016/S0360-3199(97)00123-7

Fay, P. (1992). Oxygen relations of nitrogen fixation in cyanobacteria. *Microbiol. Rev.* 56, 340–373.

Fennell, D. E., Gossett, J. M., and Zinder, S. H. (1997). Comparison of butyric acid, ethanol, lactic acid, and propionic acid as hydrogen donors for the reductive dechlorination of tetrachloroethene. *Environ. Sci. Technol.* 31, 918–926. doi: 10.1021/es960756r

Fox, J. D., He, Y., Shelver, D., Roberts, G. P., and Ludden, P. W. (1996a). Characterization of the region encoding the CO-induced hydrogenase of *Rhodospirillum rubrum*. *J. Bacteriol.* 178, 6200–6208.

Fox, J. D., Kerby, R. L., Roberts, G. P., and Ludden, P. W. (1996b). Characterization of the CO-induced, CO-tolerant hydrogenase from *Rhodospirillum rubrum* and the gene encoding the large subunit of the enzyme. *J. Bacteriol.* 178, 1515–1524.

Fredrickson, J. K., Zachara, J. M., Kennedy, D. W., Duff, M. C., Gorby, Y. A., Shu-mei, W. L., et al. (2000). Reduction of U (VI) in goethite (α-FeOOH) suspensions by a dissimilatory metal-reducing bacterium. *Geochim. Cosmochim. Acta* 64, 3085–3098. doi: 10.1016/S0016-7037(00)00397-5

Freedman, D. L., and Gossett, J. M. (1989). Biological reductive dechlorination of tetrachloroethylene and trichloroethylene to ethylene under methanogenic conditions. *Appl. Environ. Microbiol.* 55, 2144–2151.

Gest, H., and Kamen, M. D. (1949). Photoproduction of molecular hydrogen by *Rhodospirillum rubrum*. *Science* 109, 558–559. doi: 10.1126/science.109.2840.558

Gevorgyan, H., Trchounian, A., and Trchounian, K. (2018). Understanding the role of *Escherichia coli* hydrogenases and formate dehydrogenases in the F0F1-ATPase activity during the mixed acid fermentation of mixture of carbon sources. *IUBMB Life* 70, 1040–1047. doi: 10.1002/iub.1915

Gieg, L. M., Fowler, S. J., and Berdugo-Clavijo, C. (2014). Syntrophic biodegradation of hydrocarbon contaminants. *Curr. Opin. Biotechnol.* 27, 21–29. doi: 10.1016/j.copbio.2013.09.002

Gogotov, I., Zorin, N., and Serebriakova, L. (1991). Hydrogen production by model systems including hydrogenases from phototrophic bacteria. *Int. J. Hydrogen Energ.* 16, 393–396. doi: 10.1016/0360-3199(91)90137-8

Greening, C., Berney, M., Hards, K., Cook, G. M., and Conrad, R. (2014). A soil actinobacterium scavenges atmospheric H2 using two membrane-associated, oxygen-dependent [NiFe] hydrogenases. *Proc. Natl. Acad. Sci. U.S.A.* 111, 4257–4261. doi: 10.1073/pnas.1320586111

Greening, C., Biswas, A., Carere, C. R., Jackson, C. J., Taylor, M. C., Stott, M. B., et al. (2016). Genomic and metagenomic surveys of hydrogenase distribution indicate H2 is a widely utilised energy source for microbial growth and survival. *ISME J.* 10, 761–777. doi: 10.1038/ismej.2015.153

Greening, C., Carere, C. R., Rushton-Green, R., Harold, L. K., Hards, K., Taylor, M. C., et al. (2015a). Persistence of the dominant soil phylum Acidobacteria by trace gas scavenging. *Proc. Natl. Acad. Sci. U.S.A.* 112, 10497–10502. doi: 10.1073/pnas.1508385112

Greening, C., Constant, P., Hards, K., Morales, S. E., Oakeshott, J. G., Russell, R. J., et al. (2015b). Atmospheric hydrogen scavenging: from enzymes to ecosystems. *Appl. Environ. Microbiol.* 81, 1190–1199. doi: 10.1128/aem.03364-14

Hallenbeck, P. C. (2009). Fermentative hydrogen production: principles, progress, and prognosis. *Int. J. Hydrogen Energ.* 34, 7379–7389. doi: 10.1016/j.ijhydene.2008.12.080

He, J., Ritalahti, K. M., Aiello, M. R., and Löffler, F. E. (2003a). Complete detoxification of vinyl chloride by an anaerobic enrichment culture and identification of the reductively dechlorinating population as a *Dehalococcoides* species. *Appl. Environ. Microbiol.* 69, 996–1003.

He, J., Ritalahti, K. M., Yang, K.-L., Koenigsberg, S. S., and Löffler, F. E. (2003b). Detoxification of vinyl chloride to ethene coupled to growth of an anaerobic bacterium. *Nature* 424, 62–65.

Heidelberg, J. F., Paulsen, I. T., Nelson, K. E., Gaidos, E. J., Nelson, W. C., Read, T. D., et al. (2002). Genome sequence of the dissimilatory metal ion-reducing bacterium *Shewanella oneidensis*. *Nat. Biotechnol.* 20, 1118–1123. doi: 10.1038/nbt749

Heimann, A. C., Batstone, D. J., and Jakobsen, R. (2006). *Methanosarcina* spp. Drive vinyl chloride dechlorination via interspecies hydrogen transfer. *Appl. Environ. Microbiol.* 72, 2942–2949. doi: 10.1128/AEM.72.4.2942-2949.2006

Holliger, C., Schraa, G., Stams, A., and Zehnder, A. (1993). A highly purified enrichment culture couples the reductive dechlorination of tetrachloroethene to growth. *Appl. Environ. Microbiol.* 59, 2991–2997.

Hong, Y., Guo, J., and Sun, G. (2008). Identification of an uptake hydrogenase for hydrogen-dependent dissimilatory azoreduction by *Shewanella decolorationis* S12. *Appl. Microbiol. Biotechnol.* 80, 517–524. doi: 10.1007/s00253-008-1597-9

Hong, Y. G., Xu, M. Y., Guo, J., Xu, Z. C., Chen, X. J., and Sun, G. P. (2007). Respiration and growth of *Shewanella decolorationis* S12 with an azo compound as the sole electron acceptor. *Appl. Environ. Microbiol.* 73, 64–72. doi: 10.1128/AEM.01415-06

Hunt, S., Gaito, S. T., and Layzell, D. B. (1988). Model of gas exchange and diffusion in legume nodules. *Planta* 173, 128–141. doi: 10.1007/BF00394497

Hussain, A., Hasan, A., Javid, A., and Qazi, J. I. (2016). Exploited application of sulfate-reducing bacteria for concomitant treatment of metallic and non-metallic wastes: a mini review. *3 Biotech* 6:119. doi: 10.1007/s13205-016-0437-3

Ishii, S., Kosaka, T., Hori, K., Hotta, Y., and Watanabe, K. (2005). Coaggregation facilitates interspecies hydrogen transfer between *Pelotomaculum thermopropionicum* and *Methanothermobacter thermautotrophicus*. *Appl. Environ. Microbiol.* 71, 7838–7845. doi: 10.1128/AEM.71.12.7838-7845.2005

Jenney, F. E., and Adams, M. W. (2008). Hydrogenases of the model hyperthermophiles. *Ann. N. Y. Acad. Sci.* 1125, 252–266. doi: 10.1196/annals.1419.013

Johnson, D. R., Brodie, E. L., Hubbard, A. E., Andersen, G. L., Zinder, S. H., and Alvarez-Cohen, L. (2008). Temporal transcriptomic microarray analysis of "*Dehalococcoides ethenogenes*" strain 195 during the transition into stationary phase. *Appl. Environ. Microbiol.* 74, 2864–2872. doi: 10.1128/AEM.02208-07

Joyner, A., Winter, W., and Godbout, D. (1977). Studies on some characteristics of hydrogen production by cell-free extracts of rumen anaerobic bacteria. *Can. J. Microbiol.* 23, 346–353. doi: 10.1139/m77-051

Jugder, B., Ertan, H., Lee, M., Manefield, M., and Marquis, C. P. (2015). Reductive dehalogenases come of age in biological destruction of organohalides. *Trends Biotechnol.* 33, 595–610. doi: 10.1016/j.tibtech.2015.07.004

Jugder, B., Welch, J., Aguey-Zinsou, K., and Marquis, C. P. (2013). Fundamentals and electrochemical applications of [Ni-Fe]-uptake hydrogenases. *RSC Adv.* 3, 8142–8159. doi: 10.1039/c3ra22668a

Jugder, B. E., Ertan, H., Bohl, S., Lee, M., Marquis, C. P., and Manefield, M. (2016). Organohalide respiring bacteria and reductive dehalogenases: key tools in organohalide bioremediation. *Front. Microbiol.* 7:249. doi: 10.3389/fmicb.2016.00249

Karyakin, A. A., Morozov, S. V., Voronin, O. G., Zorin, N. A., Karyakina, E. E., Fateyev, V. N., et al. (2007). The limiting performance characteristics in bioelectrocatalysis of hydrogenase enzymes. *Angew. Chem. Int. Ed. Engl.* 46, 7244–7246. doi: 10.1002/anie.200701096

Kaserer, H. (1905). *Über die Oxydation des Wasserstoffes und des Methans durch Mikroorganismen*. Berlin: Hartleben.

Khan, M. T., and Bhatt, J. (1991). Polyethylene glycol mediated fusion of *Halobacterium halobium* MMT22 and *Escherichia coli* for enhancement of hydrogen production. *Int. J. Hydrogen Energ.* 16, 683–685. doi: 10.1016/0360-3199(91)90191-K

Khdhiri, M., Piché-Choquette, S., Tremblay, J., Tringe, S. G., and Constant, P. (2017). The tale of a neglected energy source: elevated hydrogen exposure affects both microbial diversity and function in soil. *Appl. Environ. Microbiol.* 83:e00275-17. doi: 10.1128/AEM.00275-17

Kieu, H. T., Müller, E., and Horn, H. (2011). Heavy metal removal in anaerobic semi-continuous stirred tank reactors by a consortium of sulfate-reducing bacteria. *Water Res.* 45, 3863–3870. doi: 10.1016/j.watres.2011.04.043

Kleinsteuber, S., Schleinitz, K. M., and Vogt, C. (2012). Key players and team play: anaerobic microbial communities in hydrocarbon-contaminated aquifers. *Appl. Microbiol. Biotechnol.* 94, 851–873. doi: 10.1007/s00253-012-4025-0

Kong, J. Y., Bai, Y., Su, Y., Yao, Y., and He, R. (2014). Effects of trichloroethylene on community structure and activity of methanotrophs in landfill cover soils. *Soil Biol. Biochem.* 78, 118–127. doi: 10.1016/j.soilbio.2014.07.018

Kosourov, S., Leino, H., Murukesan, G., Lynch, F., Sivonen, K., Tsygankov, A. A., et al. (2014). Hydrogen photoproduction by immobilized N2-fixing cyanobacteria: understanding the role of uptake hydrogenase in the long-term process. *Appl. Environ. Microbiol.* 80, 5807–5817. doi: 10.1128/AEM.01776-14

Krahn, E., Schneider, K., and Müller, A. (1996). Comparative characterization of H2 production by the conventional Mo nitrogenase and the alternative "iron-only" nitrogenase of *Rhodobacter capsulatus* hup- mutants. *Appl. Microbiol. Biotechnol.* 46, 285–290. doi: 10.1007/s002530050818

Kube, M., Beck, A., Zinder, S. H., Kuhl, H., Reinhardt, R., and Adrian, L. (2005). Genome sequence of the chlorinated compound–respiring bacterium *Dehalococcoides* species strain CBDB1. *Nat. Biotechnol.* 23, 1269–1273. doi: 10.1038/nbt1131

Kumar, N., and Das, D. (2000). Enhancement of hydrogen production by *Enterobacter cloacae* IIT-BT 08. *Proc. Biochem.* 35, 589–593. doi: 10.1016/S0032-9592(99)00109-0

Laranjo, M., Alexandre, A., and Oliveira, S. (2014). Legume growth-promoting rhizobia: an overview on the *Mesorhizobium* genus. *Microbiol. Res.* 169, 2–17. doi: 10.1016/j.micres.2013.09.012

Lee, J. Z., Burow, L. C., Woebken, D., Everroad, R. C., Kubo, M. D., Spormann, A. M., et al. (2014). Fermentation couples *Chloroflexi* and sulfate-reducing bacteria to *Cyanobacteria* in hypersaline microbial mats. *Front. Microbiol.* 5:61. doi: 10.3389/fmicb.2014.00061

Lee, M., Low, A., Zemb, O., Koenig, J., Michaelsen, A., and Manefield, M. (2012). Complete chloroform dechlorination by organochlorine respiration and fermentation. *Environ. Microbiol.* 14, 883–894. doi: 10.1111/j.1462-2920.2011.02656.x

Leloup, J., Fossing, H., Kohls, K., Holmkvist, L., Borowski, C., and Jørgensen, B. B. (2009). Sulfate-reducing bacteria in marine sediment (Aarhus Bay, Denmark): abundance and diversity related to geochemical zonation. *Environ. Microbiol.* 11, 1278–1291. doi: 10.1111/j.1462-2920.2008.01855.x

Lettinga, G., Zehnder, A., Grotenhuis, J., and Hulshoff Pol, L. (1988). "Granular anaerobic sludge; microbiology and technology," in *Proceedings of the GASMAT-Workshop*, Lunteren.

Li, X., Dai, L., Zhang, C., Zeng, G., Liu, Y., Zhou, C., et al. (2017). Enhanced biological stabilization of heavy metals in sediment using immobilized sulfate reducing bacteria beads with inner cohesive nutrient. *J. Hazard. Mater.* 324, 340–347. doi: 10.1016/j.jhazmat.2016.10.067

Li, X., Lan, S. M., Zhu, Z. P., Zhang, C., Zeng, G. M., Liu, Y. G., et al. (2018). The bioenergetics mechanisms and applications of sulfate-reducing bacteria in remediation of pollutants in drainage: a review. *Ecotoxicol. Environ. Saf.* 158, 162–170. doi: 10.1016/j.ecoenv.2018.04.025

Liot, Q., and Constant, P. (2016). Breathing air to save energy–new insights into the ecophysiological role of high-affinity [NiFe]-hydrogenase in *Streptomyces avermitilis*. *Microbiol. Open* 5, 47–59. doi: 10.1002/mbo3.310

Lovley, D. R. (1993). Dissimilatory metal reduction. *Annu. Rev. Microbiol.* 47, 263–290. doi: 10.1146/annurev.mi.47.100193.001403

Lovley, D. R. (2008). The microbe electric: conversion of organic matter to electricity. *Curr. Opin. Biotechnol.* 19, 564–571. doi: 10.1016/j.copbio.2008.10.005

Lovley, D. R., and Coates, J. D. (2000). Novel forms of anaerobic respiration of environmental relevance. *Curr. Opin. Microbiol.* 3, 252–256. doi: 10.1016/S1369-5274(00)00085-0

Lovley, D. R., and Phillips, E. J. (1994). Reduction of chromate by *Desulfovibrio vulgaris* and its c3 cytochrome. *Appl. Environ. Microbiol.* 60, 726–728.

Maimaiti, J., Zhang, Y., Yang, J., Cen, Y. P., Layzell, D. B., Peoples, M., et al. (2007). Isolation and characterization of hydrogen-oxidizing bacteria induced following exposure of soil to hydrogen gas and their impact on plant growth. *Environ. Microbiol.* 9, 435–444. doi: 10.1111/j.1462-2920.2006.01155.x

Malik, B., Su, W. W., Wald, H., Blumentals, I., and Kelly, R. (1989). Growth and gas production for hyperthermophilic archaebacterium, *Pyrococcus furiosus*. *Biotechnol. Bioeng.* 34, 1050–1057. doi: 10.1002/bit.260340805

Maróti, J., Farkas, A., Nagy, I. K., Maróti, G., Kondorosi, É., Rákhely, G., et al. (2010). A second soluble Hox-type NiFe enzyme completes the hydrogenase set in *Thiocapsa roseopersicina* BBS. *Appl. Environ. Microbiol.* 76, 5113–5123. doi: 10.1128/AEM.00351-10

Marshall, I. P., Berggren, D. R., Azizian, M. F., Burow, L. C., Semprini, L., and Spormann, A. M. (2012). The Hydrogenase Chip: a tiling oligonucleotide DNA microarray technique for characterizing hydrogen-producing and-consuming microbes in microbial communities. *ISME J.* 6, 814–826. doi: 10.1038/ismej.2011.136

Maymó-Gatell, X., Chien, Y.-T., Gossett, J. M., and Zinder, S. H. (1997). Isolation of a bacterium that reductively dechlorinates tetrachloroethene to ethene. *Science* 276, 1568–1571. doi: 10.1126/science.276.5318.1568

Men, Y., Feil, H., VerBerkmoes, N. C., Shah, M. B., Johnson, D. R., Lee, P. K., et al. (2012). Sustainable syntrophic growth of *Dehalococcoides ethenogenes* strain 195 with *Desulfovibrio vulgaris* Hildenborough and *Methanobacterium congolense*: global transcriptomic and proteomic analyses. *ISME J.* 6, 410–421. doi: 10.1038/ismej.2011.111

Miller, T. L., and Wolin, M. (1973). Formation of hydrogen and formate by *Ruminococcus albus*. *J. Bacteriol.* 116, 836–846.

Miller, T. L., and Wolin, M. (1979). Fermentations by saccharolytic intestinal bacteria. *Am. J. Clin. Nutr.* 32, 164–172. doi: 10.1093/ajcn/32.1.164

Mizuno, K., Morishita, Y., Ando, A., Tsuchiya, N., Hirata, M., and Tanaka, K. (2012). Genus-specific and phase-dependent effects of nitrate on a sulfate-reducing bacterial community as revealed by dsrB-based DGGE analyses of wastewater reactors. *World J. Microbiol. Biotechnol.* 28, 677–686. doi: 10.1007/s11274-011-0862-8

Mohn, W. W., and Kennedy, K. J. (1992). Reductive dehalogenation of chlorophenols by *Desulfomonile tiedjei* DCB-1. *Appl. Environ. Microbiol.* 58, 1367–1370.

Morris, B. E., Henneberger, R., Huber, H., and Moissl-Eichinger, C. (2013). Microbial syntrophy: interaction for the common good. *FEMS Microbiol. Rev.* 37, 384–406. doi: 10.1111/1574-6976.12019

Morris, R. M., Sowell, S., Barofsky, D., Zinder, S., and Richardson, R. (2006). Transcription and mass-spectroscopic proteomic studies of electron transport oxidoreductases in *Dehalococcoides ethenogenes*. *Environ. Microbiol.* 8, 1499–1509. doi: 10.1111/j.1462-2920.2006.01090.x

Müller, N., Worm, P., Schink, B., Stams, A. J., and Plugge, C. M. (2010). Syntrophic butyrate and propionate oxidation processes: from genomes to reaction mechanisms. *Environ. Microbiol. Rep.* 2, 489–499. doi: 10.1111/j.1758-2229.2010.00147.x

Mus, F., Crook, M. B., Garcia, K., Costas, A. G., Geddes, B. A., Kouri, E. D., et al. (2016). Symbiotic nitrogen fixation and the challenges to its extending to nonlegumes. *Appl. Environ. Microbiol.* 82, 3698–3710. doi: 10.1128/AEM.01055-16

Mutambanengwe, C., Togo, C., and Whiteley, C. (2007). Decolorization and degradation of textile dyes with biosulfidogenic hydrogenases. *Biotechnol. Prog.* 23, 1095–1100. doi: 10.1021/bp070147v

Nandi, R., and Sengupta, S. (1998). Microbial production of hydrogen: an overview. *Crit. Rev. Microbiol.* 24, 61–84. doi: 10.1080/10408419891294181

Nielsen, M., Revsbech, N. P., and Kühl, M. (2015). Microsensor measurements of hydrogen gas dynamics in cyanobacterial microbial mats. *Front. Microbiol.* 6:726. doi: 10.3389/fmicb.2015.00726

Nour, S. M., Cleyet-Marel, J.-C., Normand, P., and Fernandez, M. P. (1995). Genomic heterogeneity of strains nodulating chickpeas (*Cicer arietinum* L.) and description of *Rhizobium mediterraneum* sp. nov. *Int. J. Syst. Bacteriol.* 45, 640–648. doi: 10.1099/00207713-45-4-640

Novelli, P. C., Lang, P. M., Masarie, K. A., Hurst, D. F., Myers, R., and Elkins, J. W. (1999). Molecular hydrogen in the troposphere: global distribution and budget. *J. Geophys. Res.* 104, 30427–30444. doi: 10.1029/1999JD900788

Nyyssonen, M., Hultman, J., Ahonen, L., Kukkonen, I., Paulin, L., Laine, P., et al. (2014). Taxonomically and functionally diverse microbial communities in deep crystalline rocks of the Fennoscandian shield. *ISME J.* 8, 126–138. doi: 10.1038/ismej.2013.125

Odom, J., and Peck, H. Jr. (1981). Hydrogen cycling as a general mechanism for energy coupling in the sulfate-reducing bacteria, *Desulfovibrio* sp. *FEMS Microbiol. Lett.* 12, 47–50. doi: 10.1111/j.1574-6968.1981.tb07609.x

Orr, C. H., James, A., Leifert, C., Cooper, J. M., and Cummings, S. P. (2011). Diversity and activity of free-living nitrogen-fixing bacteria and total bacteria in organic and conventionally managed soils. *Appl. Environ. Microbiol.* 77, 911–919. doi: 10.1128/AEM.01250-10

Osborne, C. A., Peoples, M. B., and Janssen, P. H. (2010). Detection of a reproducible, single-member shift in soil bacterial communities exposed to low levels of hydrogen. *Appl. Environ. Microbiol.* 76, 1471–1479. doi: 10.1128/AEM.02072-09

Otaki, H., Everroad, R. C., Matsuura, K., and Haruta, S. (2012). Production and consumption of hydrogen in hot spring microbial mats dominated by a filamentous anoxygenic photosynthetic bacterium. *Microbes Environ.* 27, 293–299. doi: 10.1264/jsme2.ME11348

Peters, J. W., Schut, G. J., Boyd, E. S., Mulder, D. W., Shepard, E. M., Broderick, J. B., et al. (2015). [FeFe]-and [NiFe]-hydrogenase diversity, mechanism, and maturation. *Biochim. Biophys. Acta* 1853, 1350–1369. doi: 10.1016/j.bbamcr.2014.11.021

Petersen, J. M., Zielinski, F. U., Pape, T., Seifert, R., Moraru, C., Amann, R., et al. (2011). Hydrogen is an energy source for hydrothermal vent symbioses. *Nature* 476, 176–180. doi: 10.1038/nature10325

Phillips, E. J., Landa, E. R., and Lovley, D. R. (1995). Remediation of uranium contaminated soils with bicarbonate extraction and microbial U (VI) reduction. *J. Ind. Microbiol.* 14, 203–207. doi: 10.1007/BF01569928

Piché-Choquette, S., Khdhiri, M., and Constant, P. (2018). Dose-response relationships between environmentally-relevant H2 concentrations and the biological sinks of H2, CH4 and CO in soil. *Soil Biol. Biochem.* 123, 190–199. doi: 10.1016/j.soilbio.2018.05.008

Rahm, B. G., Morris, R. M., and Richardson, R. E. (2006). Temporal expression of respiratory genes in an enrichment culture containing *Dehalococcoides ethenogenes*. *Appl. Environ. Microbiol.* 72, 5486–5491. doi: 10.1128/AEM.00855-06

Rákhely, G., Zhou, Z. H., Adams, M. W., and Kovács, K. L. (1999). Biochemical and molecular characterization of the [NiFe] hydrogenase from the hyperthermophilic archaeon, *Thermococcus litoralis*. *Eur. J. Biochem.* 266, 1158–1165. doi: 10.1046/j.1432-1327.1999.00969.x

Ren, N., Wang, A., and Ma, F. (2005). *Physiological Ecology of Acid-Producing Fermentative Microbiology*. Beijing: Science Press.

Ren, X. Y., Zeng, G. M., Tang, L., Wang, J. J., Wan, J., Liu, Y., et al. (2018). Sorption, transport and biodegradation-an insight into bioavailability of persistent organic pollutants in soil. *Sci. Total Environ.* 610, 1154–1163. doi: 10.1016/j.scitotenv.2017.08.089

Rhee, T., Brenninkmeijer, C., and Röckmann, T. (2006). The overwhelming role of soils in the global atmospheric hydrogen cycle. *Atmos. Chem. Phys.* 6, 1611–1625. doi: 10.5194/acp-6-1611-2006

Richter, K., and Gescher, J. (2014). Accelerated glycerol fermentation in *Escherichia coli* using methanogenic formate consumption. *Bioresour. Technol.* 162, 389–391. doi: 10.1016/j.biortech.2014.04.011

Riddin, T., Govender, Y., Gericke, M., and Whiteley, C. (2009). Two different hydrogenase enzymes from sulphate-reducing bacteria are responsible for the bioreductive mechanism of platinum into nanoparticles. *Enzyme Microb. Technol.* 45, 267–273. doi: 10.1016/j.enzmictec.2009.06.006

Rittmann, B. E., and McCarty, P. L. (2012). *Environmental Biotechnology: Principles and Applications*. New York, NY: Tata McGraw-Hill Education.

Rodionov, D. A., Dubchak, I., Arkin, A., Alm, E., and Gelfand, M. S. (2004). Reconstruction of regulatory and metabolic pathways in metal-reducing δ-proteobacteria. *Genome Biol.* 5:R90. doi: 10.1186/gb-2004-5-11-r90

Rupakula, A., Kruse, T., Boeren, S., Holliger, C., Smidt, H., and Maillard, J. (2013). The restricted metabolism of the obligate organohalide respiring bacterium *Dehalobacter restrictus*: lessons from tiered functional genomics. *Philos. Trans. R. Soc. Lond. B Biol. Sci.* 368:20120325. doi: 10.1098/rstb.2012.0325

Salvi, B., and Subramanian, K. (2015). Sustainable development of road transportation sector using hydrogen energy system. *Renew. Sustain. Energy Rev.* 51, 1132–1155. doi: 10.1016/j.rser.2015.07.030

Sawers, G. (1994). The hydrogenases and formate dehydrogenases of *Escherichia coli*. *Antonie Van Leeuwenhoek* 66, 57–88. doi: 10.1007/BF00871633

Schilter, D., Camara, J. M., Huynh, M. T., Hammes-Schiffer, S., and Rauchfuss, T. B. (2016). Hydrogenase enzymes and their synthetic models: the role of metal hydrides. *Chem. Rev.* 116, 8693–8749. doi: 10.1021/acs.chemrev.6b00180

Schink, B. (1997). Energetics of syntrophic cooperation in methanogenic degradation. *Microbiol. Mol. Biol. Rev.* 61, 262–280.

Schlegel, H. G., Gottschalk, G., and Pfenning, N. (1976). "Symposium on Microbial production and utilization of gases (H2, CH4, CO)," in *Proceedings of the Symposium on Microbial Production and Utilization of Gases (H2, CH4, CO)*, (Göttingen: Akademie der Wissenschaften).

Schmidt, U., and Conrad, R. (1993). Hydrogen, carbon monoxide, and methane dynamics in Lake Constance. *Limnol. Oceanogr.* 38, 1214–1226. doi: 10.4319/lo.1993.38.6.1214

Schütz, H., Conrad, R., Goodwin, S., and Seiler, W. (1988). Emission of hydrogen from deep and shallow freshwater environments. *Biogeochemistry* 5, 295–311. doi: 10.1007/BF02180069

Schwartz, E., Fritsch, J., and Friedrich, B. (2013). "H2-metabolizing prokaryotes," in *The Prokaryotes*, eds M. Dworkin, S. Falkow, E. Rosenberg, K. H. Schleifer, and E. Stackebrandt (New York, NY: Springer), 119–199.

Seshadri, R., Adrian, L., Fouts, D. E., Eisen, J. A., Phillippy, A. M., Methe, B. A., et al. (2005). Genome sequence of the PCE-dechlorinating bacterium *Dehalococcoides ethenogenes*. *Science* 307, 105–108. doi: 10.1126/science.1102226

Shelton, D. R., and Tiedje, J. M. (1984). Isolation and partial characterization of bacteria in an anaerobic consortium that mineralizes 3-chlorobenzoic acid. *Appl. Environ. Microbiol.* 48, 840–848.

Sieber, J. R., McInerney, M. J., and Gunsalus, R. P. (2012). Genomic insights into syntrophy: the paradigm for anaerobic metabolic cooperation. *Annu. Rev. Microbiol.* 66, 429–452. doi: 10.1146/annurev-micro-090110-102844

Singh, R., Kumar, A., Kirrolia, A., Kumar, R., Yadav, N., Bishnoi, N. R., et al. (2011). Removal of sulphate, COD and Cr (VI) in simulated and real wastewater by sulphate reducing bacteria enrichment in small bioreactor and FTIR study. *Bioresour. Technol.* 102, 677–682. doi: 10.1016/j.biortech.2010.08.041

Smatlak, C. R., Gossett, J. M., and Zinder, S. H. (1996). Comparative kinetics of hydrogen utilization for reductive dechlorination of tetrachloroethene and methanogenesis in an anaerobic enrichment culture. *Environ. Sci. Technol.* 30, 2850–2858. doi: 10.1021/es9602455

Soboh, B., Linder, D., and Hedderich, R. (2002). Purification and catalytic properties of a CO-oxidizing: H2-evolving enzyme complex from *Carboxydothermus hydrogenoformans*. *Eur. J. Biochem.* 269, 5712–5721. doi: 10.1046/j.1432-1033.2002.03282.x

Soboh, B., Linder, D., and Hedderich, R. (2004). A multisubunit membrane-bound [NiFe] hydrogenase and an NADH-dependent Fe-only hydrogenase in the fermenting bacterium *Thermoanaerobacter tengcongensis*. *Microbiol.* 150, 2451–2463. doi: 10.1099/mic.0.27159-0

Sokolova, T., Hanel, J., Onyenwoke, R., Reysenbach, A.-L., Banta, A., Geyer, R., et al. (2007). Novel chemolithotrophic, thermophilic, anaerobic bacteria *Thermolithobacter ferrireducens* gen. nov., sp. nov. and *Thermolithobacter carboxydivorans* sp. nov. *Extremophiles* 11, 145–157. doi: 10.1007/s00792-006-0022-5

Sokolova, T., Kostrikina, N., Chernyh, N., Tourova, T., Kolganova, T., and Bonch-Osmolovskaya, E. (2002). Carboxydocella thermautotrophica gen. nov., sp. nov., a novel anaerobic, CO-utilizing thermophile from a Kamchatkan hot spring. *Int. J. Syst. Evol. Microbiol.* 52, 1961–1967.

Sokolova, T. G., Gonzalez, J. M., Kostrikina, N. A., Chernyh, N. A., Slepova, T. V., Bonch-Osmolovskaya, E. A., et al. (2004). *Thermosinus carboxydivorans* gen. nov., sp. nov., a new anaerobic, thermophilic, carbon-monoxide-oxidizing, hydrogenogenic bacterium from a hot pool of Yellowstone National Park. *Int. J. Syst. Evol. Microbiol.* 54, 2353–2359. doi: 10.1099/ijs.0.63186-0

Sokolova, T. G., Kostrikina, N. A., Chernyh, N. A., Kolganova, T. V., Tourova, T. P., and Bonch-Osmolovskaya, E. A. (2005). *Thermincola carboxydiphila* gen. nov., sp. nov., a novel anaerobic, carboxydotrophic, hydrogenogenic bacterium from a hot spring of the Lake Baikal area. *Int. J. Syst. Evol. Microbiol.* 55, 2069–2073. doi: 10.1099/ijs.0.63299-0

Spaink, H. P. (2000). Root nodulation and infection factors produced by rhizobial bacteria. *Annu. Rev. Microbiol.* 54, 257–288. doi: 10.1146/annurev.micro.54.1.257

Stams, A. J., De Bok, F. A., Plugge, C. M., Van Eekert, M. H., Dolfing, J., and Schraa, G. (2006). Exocellular electron transfer in anaerobic microbial communities. *Environ. Microbiol.* 8, 371–382. doi: 10.1111/j.1462-2920.2006.00989.x

Stams, A. J., and Plugge, C. M. (2009). Electron transfer in syntrophic communities of anaerobic bacteria and archaea. *Nat. Rev. Microbiol.* 7, 568–577. doi: 10.1038/nrmicro2166

Stein, S., Selesi, D., Schilling, R., Pattis, I., Schmid, M., and Hartmann, A. (2005). Microbial activity and bacterial composition of H2-treated soils with net CO2 fixation. *Soil Biol. Biochem.* 37, 1938–1945. doi: 10.1016/j.soilbio.2005.02.035

Stephenson, M., and Stickland, L. H. (1931). Hydrogenase: a bacterial enzyme activating molecular hydrogen: the properties of the enzyme. *Biochem. J.* 25, 205–214. doi: 10.1042/bj0250205

Suflita, J. M., Horowitz, A., Shelton, D. R., and Tiedje, J. M. (1982). Dehalogenation: a novel pathway for the anaerobic biodegradation of haloaromatic compounds. *Science* 218, 1115–1117. doi: 10.1126/science.218.4577.1115

Svetlichny, V., Sokolova, T., Gerhardt, M., Ringpfeil, M., Kostrikina, N., and Zavarzin, G. (1991). *Carboxydothermus hydrogenoformans* gen. nov., sp. nov., a CO-utilizing thermophilic anaerobic bacterium from hydrothermal environments of Kunashir Island. *Syst. Appl. Microbiol.* 14, 254–260. doi: 10.1016/S0723-2020(11)80377-2

Tabak, H. H., Lens, P., van Hullebusch, E. D., and Dejonghe, W. (2005). Developments in bioremediation of soils and sediments polluted with metals and radionuclides–1. Microbial processes and mechanisms affecting bioremediation of metal contamination and influencing metal toxicity and transport. *Rev. Environ. Sci. Biotechnol.* 4, 115–156. doi: 10.1007/s11157-005-2169-4

Talibi, M., Hellier, P., and Ladommatos, N. (2017). The effect of varying EGR and intake air boost on hydrogen-diesel co-combustion in CI engines. *Int. J. Hydrogen Energy* 42, 6369–6383. doi: 10.1016/j.ijhydene.2016.11.207

Tebo, B. M., and Obraztsova, A. Y. (1998). Sulfate-reducing bacterium grows with Cr (VI), U (VI), Mn (IV), and Fe (III) as electron acceptors. *FEMS Microbiol. Lett.* 162, 193–199. doi: 10.1111/j.1574-6968.1998.tb12998.x

Teng, Y., and Chen, W. (2019). Soil microbiome: a promising strategy for contaminated soil remediation. *Pedosphere*. doi: 10.1016/S1002-0160(18)60061-X

Teng, Y., Xu, Z., Luo, Y., and Reverchon, F. (2012). How do persistent organic pollutants be coupled with biogeochemical cycles of carbon and nutrients in terrestrial ecosystems under global climate change? *J. Soil Sediments* 12, 411–419. doi: 10.1007/s11368-011-0462-0

Thauer, R. K., Kaster, A. K., Goenrich, M., Schick, M., Hiromoto, T., and Shima, S. (2010). Hydrogenases from methanogenic archaea, nickel, a novel cofactor, and H2 storage. *Annu. Rev. Biochem.* 79, 507–536. doi: 10.1146/annurev.biochem.030508.152103

Trchounian, K., Müller, N., Schink, B., and Trchounian, A. (2017a). Glycerol and mixture of carbon sources conversion to hydrogen by *Clostridium beijerinckii* DSM791 and effects of various heavy metals on hydrogenase activity. *Int. J. Hydrogen Energy* 42, 7875–7882. doi: 10.1016/j.ijhydene.2017.01.011

Trchounian, K., Sawers, R. G., and Trchounian, A. (2017b). Improving biohydrogen productivity by microbial dark-and photo-fermentations: novel data and future approaches. *Renew. Sustain. Energy Rev.* 80, 1201–1216. doi: 10.1016/j.rser.2017.05.149

Trchounian, K., Pinske, C., Sawers, R. G., and Trchounian, A. (2011). Dependence on the F0F1-ATP synthase for the activities of the hydrogen-oxidizing hydrogenases 1 and 2 during glucose and glycerol fermentation at high and low pH in *Escherichia coli*. *J. Bioenerg. Biomembr.* 43, 645–650. doi: 10.1007/s10863-011-9397-9

Trchounian, K., Poladyan, A., Vassilian, A., and Trchounian, A. (2012). Multiple and reversible hydrogenases for hydrogen production by *Escherichia coli*: dependence on fermentation substrate, pH and the F0F1-ATPase. *Crit. Rev. Biochem. Mol.* 47, 236–249. doi: 10.3109/10409238.2012.655375

Trchounian, K., and Trchounian, A. (2014). Hydrogen producing activity by *Escherichia coli* hydrogenase 4 (*hyf*) depends on glucose concentration. *Int. J. Hydrogen Energy* 39, 16914–16918. doi: 10.1016/j.ijhydene.2014.08.059

Trchounian, K., and Trchounian, A. (2015). *Escherichia coli* hydrogen gas production from glycerol: effects of external formate. *Renew. Energy* 83, 345–351. doi: 10.1016/j.renene.2015.04.052

Tromp, T. K., Shia, R.-L., Allen, M., Eiler, J. M., and Yung, Y. L. (2003). Potential environmental impact of a hydrogen economy on the stratosphere. *Science* 300, 1740–1742. doi: 10.1126/science.1085169

Uffen, R. L. (1976). Anaerobic growth of a Rhodopseudomonas species in the dark with carbon monoxide as sole carbon and energy substrate. *Proc. Natl. Acad. Sci. U.S.A.* 73, 3298–3302. doi: 10.1073/pnas.73.9.3298

Valls, M., and De Lorenzo, V. (2002). Exploiting the genetic and biochemical capacities of bacteria for the remediation of heavy metal pollution. *FEMS Microbiol. Rev.* 26, 327–338. doi: 10.1111/j.1574-6976.2002.tb00618.x

Vignais, P. M., and Billoud, B. (2007). Occurrence, classification, and biological function of hydrogenases: an overview. *Chem. Rev.* 107, 4206–4272. doi: 10.1021/cr050196r

Vignais, P. M., Billoud, B., and Meyer, J. (2001). Classification and phylogeny of hydrogenases. *FEMS Microbiol. Rev.* 25, 455–501. doi: 10.1111/j.1574-6976.2001.tb00587.x

Vincenzini, M., Materassi, R., Tredici, M., and Florenzano, G. (1982). Hydrogen production by immobilized cells—I. light dependent dissimilation of organic substances by *Rhodopseudomonas palustris*. *Int. J. Hydrogen Energy* 7, 231–236. doi: 10.1016/0360-3199(82)90086-6

Vogel, T. M., and McCARTY, P. L. (1985). Biotransformation of tetrachloroethylene to trichloroethylene, dichloroethylene, vinyl chloride, and carbon dioxide under methanogenic conditions. *Appl. Environ. Microbiol.* 49, 1080–1083.

Watrous, M. M., Clark, S., Kutty, R., Huang, S., Rudolph, F. B., Hughes, J. B., et al. (2003). 2, 4, 6-Trinitrotoluene reduction by an Fe-only hydrogenase in *Clostridium acetobutylicum*. *Appl. Environ. Microbiol.* 69, 1542–1547. doi: 10.1128/AEM.69.3.1542-1547.2003

Witty, J. F. (1991). Microelectrode measurements of hydrogen concentrations and gradients in legume nodules. *J. Exp. Bot.* 42, 765–771. doi: 10.1093/jxb/42.6.765

Witty, J. F., and Minchin, F. R. (1998). Hydrogen measurements provide direct evidence for a variable physical barrier to gas diffusion in legume nodules. *J. Exp. Bot.* 49, 1015–1020. doi: 10.1093/jxb/49.323.1015

Woodward, J., Orr, M., Cordray, K., and Greenbaum, E. (2000). Biotechnology: enzymatic production of biohydrogen. *Nature* 405, 1014–1015. doi: 10.1038/35016633

Wu, X., Holmfeldt, K., Hubalek, V., Lundin, D., Åström, M., Bertilsson, S., et al. (2015). Microbial metagenomes from three aquifers in the Fennoscandian shield terrestrial deep biosphere reveal metabolic partitioning among populations. *ISME J.* 10, 1192–1203. doi: 10.1038/ismej.2015.185

Yan, J., Ritalahti, K. M., Wagner, D. D., and Löffler, F. E. (2012). Unexpected specificity of interspecies cobamide transfer from *Geobacter* spp. to organohalide-respiring *Dehalococcoides mccartyi* strains. *Appl. Environ. Microbiol.* 78, 6630–6636. doi: 10.1128/AEM.01535-12

Yang, Y., and McCarty, P. L. (1998). Competition for hydrogen within a chlorinated solvent dehalogenating anaerobic mixed culture. *Environ. Sci. Technol.* 32, 3591–3597. doi: 10.1021/es980363n

Zanaroli, G., Negroni, A., Häggblom, M. M., and Fava, F. (2015). Microbial dehalogenation of organohalides in marine and estuarine environments. *Curr. Opin. Biotechnol.* 33, 287–295. doi: 10.1016/j.copbio.2015.03.013

Zhang, H., Bruns, M. A., and Logan, B. E. (2006). Biological hydrogen production by *Clostridium acetobutylicum* in an unsaturated flow reactor. *Water Res.* 40, 728–734. doi: 10.1016/j.watres.2005.11.041

Ziels, R. M., Sousa, D. Z., Stensel, H. D., and Beck, D. A. (2017). DNA-SIP based genome-centric metagenomics identifies key long-chain fatty acid-degrading populations in anaerobic digesters with different feeding frequencies. *ISME J.* 12, 112–123. doi: 10.1038/ismej.2017.143

Conflict of Interest Statement: The authors declare that the research was conducted in the absence of any commercial or financial relationships that could be construed as a potential conflict of interest.

frontiers in Microbiology

ORIGINAL RESEARCH
published: 01 May 2019
doi: 10.3389/fmicb.2019.00761

The Effect of a Tropical Climate on Available Nutrient Resources to Springs in Ophiolite-Hosted, Deep Biosphere Ecosystems in the Philippines

D'Arcy R. Meyer-Dombard[1], Magdelena R. Osburn[2], Dawn Cardace[3] and Carlo A. Arcilla[4]*

[1] Department of Earth and Environmental Sciences, The University of Illinois at Chicago, Chicago, IL, United States, [2] Department of Earth and Planetary Sciences, Northwestern University, Evanston, IL, United States, [3] Department of Geosciences, The University of Rhode Island, Kingston, RI, United States, [4] Director of Science and Technology-Philippine Nuclear Research Institute, Manilla, Philippines

OPEN ACCESS

Edited by:
Eric Boyd, Montana State University, United States

Reviewed by:
Ruth Hindshaw, University of Cambridge, United Kingdom
Piyali Chanda, University of Wisconsin–Madison, United States

***Correspondence:**
D'Arcy R. Meyer-Dombard
drmd@uic.edu

Specialty section:
This article was submitted to Microbial Physiology and Metabolism, a section of the journal Frontiers in Microbiology

Received: *02 October 2018*
Accepted: *26 March 2019*
Published: *01 May 2019*

Citation:
Meyer-Dombard DR, Osburn MR, Cardace D and Arcilla CA (2019) The Effect of a Tropical Climate on Available Nutrient Resources to Springs in Ophiolite-Hosted, Deep Biosphere Ecosystems in the Philippines. Front. Microbiol. 10:761. doi: 10.3389/fmicb.2019.00761

Springs hosted in ophiolites are often affected by serpentinization processes. The characteristically low DIC and high CH_4 and H_2 gas concentrations of serpentinizing ecosystems have led to interest in hydrogen based metabolisms in these subsurface biomes. However, a true subsurface signature can be difficult to identify in surface expressions such as serpentinizing springs. Here, we explore carbon and nitrogen resources in serpentinization impacted springs in the tropical climate of the Zambales and Palawan ophiolites in the Philippines, with a focus on surface vs. subsurface processes and exogenous vs. endogenous nutrient input. Isotopic signatures in spring fluids, biomass, and carbonates were examined to identify sources and sinks of carbon and nitrogen, carbonate geochemistry, and the effect of seasonal precipitation. Seasonality affected biomass production in both low flow and high flow spring systems. Changes in meteorological precipitation affected $\delta^{13}C_{DIC}$ and $\delta^{13}C_{DOC}$ values of the spring fluids, which reflected seasonal gain/loss of atmospheric influence and changes in exogenous DOC input. The primary carbon source in high flow systems was variable, with DOC contributing to biomass in many springs, and a mix of DIC and carbonates contributing to biomass in select locations. However, primary carbon resources in low flow systems may depend more on endogenous than exogenous carbon, even in high precipitation seasons. Isotopic evidence for nitrogen fixation was identified, with seasonal influence only seen in low flow systems. Carbonate formation was found to occur as a mixture of recrystallization/recycling of older carbonates and rapid mineral precipitation (depending on the system), with highly $\delta^{13}C$ and $\delta^{18}O$ depleted carbonates occurring in many locations. Subsurface signatures (e.g., low DOC influence on $C_{biomass}$) were most apparent in the driest seasons and lowest flow systems, indicating locations where metabolic processes divorced from surface influences (including hydrogen based metabolisms) are most likely to be occurring.

Keywords: serpentinization, carbon isotopes, carbonates, carbon cycling, nitrogen cycling, deep biosphere

INTRODUCTION

Recent interest in the terrestrial deep biosphere has been fueled by estimates of biomass (Kallmeyer et al., 2012; Lomstein et al., 2012; McMahon and Parnell, 2014) and reports of unique microbial communities and ecosystem functions (Biddle et al., 2012; Parkes et al., 2014; Solden et al., 2016). The overall impact of the deep biosphere on global biogeochemical cycling remains unknown (Menez et al., 2012), and direct access remains expensive with non-trivial logistics. Surface connected expressions of the terrestrial deep biosphere such as caves, wells, and springs are convenient and less expensive (compared to drilling based endeavors), but elicit questions about authenticity of a subsurface signature. Evidence of subsurface biosphere diversity and function may be overprinted or masked by the oxygenated, photosynthesis-driven, surface biosphere to an unknown degree.

Several studies have attempted to isolate a subsurface signature from terrestrial locations. Arguably the most success has come from studies with direct access to subsurface sampling. These works have relied on comparative metagenomics (e.g., Lau et al., 2014), geochemical modeling integrated with statistical analyses (e.g., Osburn et al., 2014), and innovative culturing techniques (e.g., Rowe et al., 2017) to distinguish subsurface contributions to nutrients, energy, diversity, and biomass. Isolating a subsurface signature when samples are obtained within the surface biome (i.e., springs and seeps) poses additional challenge. More frequently, only individual processes can be linked to the subsurface. For example, the widespread ability to fix nitrogen (Hamilton et al., 2011) or carbon (Osburn et al., 2011; Urschel et al., 2015) using non-photosynthetic pathways in terrestrial hydrothermal systems suggests these traits are maintained due to a general lack of reliable nutrient input from the surface biome.

Stable isotope chemistry of nutrient pools and resident biomass is a useful tool for deep subsurface biosphere applications. Kinetic isotope fractionation associated with biosynthetic machinery discriminates broadly against heavy isotopes, producing ^{13}C and ^{15}N- depleted biomass relative to sources. Fractionation varies by process for both carbon and nitrogen isotopes and much can be learned or inferred by comparing isotopic ratios of sources and resulting biomass. For example, it has been shown that different carbon fixation pathways fractionate carbon to differing degrees (Berg et al., 2010; Pearson et al., 2016), and the isotopic composition of nitrogen in biomass is affected by how the organism participates in the nitrogen cycle (Brunner et al., 2013; Mobius, 2013; Frey et al., 2014; Zhang et al., 2014). While there is still much to learn concerning the fractionation of carbon or nitrogen by specific groups of organisms under varying environmental conditions, as well as abiotic considerations (McCollom et al., 2010; Li et al., 2012; Wunderlich et al., 2012; Schrenk and Brazelton, 2013; Zhang et al., 2014) a holistic approach of comparing isotopic ratios of bulk carbon, nitrogen, and biomass can reveal broad ecosystem patterns.

This study focuses specifically on surface expressions (springs and seeps) of the deep biosphere sourced in ultramafic rock units in the Philippines. Springs and seeps emanating from ophiolites represent subsurface fluids produced from the process of "serpentinization" that are mixed with fluids of other sources. Briefly, serpentinization is the aqueous alteration of ultramafic rocks (part of the ophiolite body). In terrestrial ophiolites, the process is often recharged by groundwaters, and provides alteration products including mineralogically altered solids, fluids of distinctive geochemistry, gasses such as H_2 (and possibly CH_4), and chemical energy abundant enough to fuel chemosynthetic metabolism. Other resources have thoroughly described and reviewed this process and the resulting potential subsurface habitats (McCollom and Bach, 2009; Schrenk and Brazelton, 2013). Serpentinization has been discussed as a possible process fueling life on other planetary bodies (e.g., Mars and icy ocean worlds – Ehlmann et al., 2010; Vance et al., 2016; Deamer and Damer, 2017), as well as a potential platform for the development of life on Earth (Sleep et al., 2011; Russell et al., 2014). In both of these extensions, it is assumed that serpentinization-driven life support is divorced from potential carbon and energy sources supplied from photosynthetic processes. Further, serpentinizing springs and seeps are often noted to have low dissolved organic or inorganic carbon (e.g., Morrill et al., 2013; Szponar et al., 2013). The production of H_2 gas from the serpentinization process has indicated the potential for hydrogen driven metabolic processes in impacted environments, with an overlying assumption that the presence of hydrogen gas may indicate a more subsurface "signal." Therefore, separating a true subsurface signal from complicating surface influence at modern, terrestrial, serpentinizing seeps is essential for understanding their utility as a "portal" into the deep subsurface biosphere of modern, ancient, and astrobiological environments.

The isotopic ratios of carbon in total or dissolved inorganic carbon (TIC/DIC) and dissolved organic carbon (DOC) can be compared to that of biomass, allowing conclusions concerning the source of the carbon fueling the biomass production. This approach has been used many times in other terrestrial environments (e.g., Lang et al., 2012; Schubotz et al., 2013; Pearson et al., 2016). There have been several reports from terrestrial serpentinizing seeps and springs that highlight potential carbon and nutrient sources. Both DOC and TIC have been reported in low concentrations in springs located in the Tablelands (Newfoundland, Canada) and The Cedars (CA, United States) areas, with $\delta^{13}C_{DOC}$ ranging from -22 to $-13‰$, and $\delta^{13}C_{TIC}$ ranging from -33 to $-2‰$ (Brazelton et al., 2013; Morrill et al., 2013; Szponar et al., 2013). Isotopic composition of carbon from both DIC and DOC in the Yanartaş/Chimera site in Turkey are comparable, although concentrations of both are higher than other reported locations (50 and ∼5 ppmC, respectively, Meyer-Dombard et al., 2015). Carbon isotopic compositions of biomass are seldom reported in general for these locations (however, see Meyer-Dombard et al., 2015), but that of the carbonates found in these systems has been widely reported and summarized. The comparison of $\delta^{13}C_{carbonate}$ and $\delta^{18}O_{carbonate}$ is useful for determining the sources of carbon and oxygen

that formed the carbonates as well as processes involved in that mineral precipitation, and several reports give useful comparisons of carbonates found in serpentinizing seeps from Oman, Costa Rica, Italy, and the western United States (e.g., Szponar et al., 2013; Mervine et al., 2014; Sanchez-Murillo et al., 2014; Falk et al., 2016). The $\delta^{13}C_{carbonate}$ and $\delta^{18}O_{carbonate}$ in carbonates from serpentinizing seeps range from ∼ −33 to ∼ +3‰ $\delta^{13}C$ and ∼ −20 to ∼ +5‰ $\delta^{18}O$. This wide range of isotopic compositions makes it clear that the formation and history of carbonates in serpentinizing systems can follow a varied path, which can sometimes be clarified using "clumped isotope" techniques (e.g., Eiler, 2007).

Among the studied examples of terrestrial serpentinizing seeps, few data are from tropical biomes (Beccaluva et al., 1999; Sanchez-Murillo et al., 2014; Cardace et al., 2015; Woycheese et al., 2015). Tropical surface biomes that deliver significant meteorological precipitation and cover field locations in dense foliage may complicate the isolation of the deep subsurface signal from surficial components. Frequent or heavy precipitation may facilitate the incorporation of exogenous nutrients into the surface exposed seeps and springs, and impact the nutrient availability to the subsurface biosphere. Conversely, addition of meteoric water to the serpentinizing fluids associated with the seeps and springs may locally dilute endogenous nutrient or energy resources, changing the fluid-rock interactions happening in the subsurface. Either scenario could cause fluctuations in sources of energy and carbon between seasons, ultimately affecting the ability to identify true subsurface-driven processes such as hydrogen based metabolisms. While this may incur difficulty in separating a "true" subsurface signal in serpentinizing systems hosted in ophiolites located in tropical biomes, it also provides an opportunity to explore a largely unrecognized exchange between the surface and subsurface biosphere.

TABLE 1 | Fluid geochemistry including DIC and DOC concentrations and carbon isotopic ratios from 2017 samples during the very dry season.

Sample	Location	Notes (outflow distance, m)	Fluid depth sampled	Season	Temp. °C	pH	DIC, ppmC	$\delta^{13}C$, DIC ‰	DOC, ppmC	$\delta^{13}C$, DOC ‰
ML1	Manleluag	Cistern pool (0 m)	80 cm	2012, dry	34.36	10.89	0.6	−12.8	0.85	−26.8
				2013, wet	34.35	10.86	0.9	−15.42	0.34	−29.63
		January 26th		2017, v. dry	34.39	11.11	0.2	−14.74	0.1	−23.6
		January 27th		2017, v. dry	34.37	10.69	0.2	−11.23	0.2	−23.9
ML2	Manleluag	Source pool (0 m)	30 cm	2012, dry	34.45	10.85	0.5	−16.5	0.4	−26.0
				2013, wet	34.44	10.83	0.4	−11.0	0.12	−26.0
				2017, v. dry	34.45	10.08	0.4	−17.66	0.6	−28.2
		Spill Pool (1.5 m)	20 cm	2012, dry	34.31	10.85	0.8	−15.0	0.81	−25.5
				2017, v. dry	34.22	10.12	0.3	−14.81	bdl	−20.8
		Outflow (10 m)	10 cm	2012, dry	33.84	10.81	1.5	−18.7	0.5	−27.0
				2017, v. dry	33.51	10.25	nd	nd	0.1	−22.1
		Outflow (18.3 m)	5 cm	2013, wet	32.55	10.23	4.4	−21.13	0.73	−29.14
				2017, v. dry	31.29	10.58	1.7	−20.71	0.7	−27.4
PB1	Poon Bato	Pool 1, main (0 m)	10 cm	2012, dry	31.46	11.27	1.3	−25.4	0.3	−23.0
				2013, wet	30.38	11.25	3.0	−13.0	0.3	−27.0
PB2	Poon Bato	Pool 2, "ice cube"	30 cm	2012, dry	26.76	10.43	6.0	−17.5	1.15	−24.4
		Pool 2, "waterfall"	2 cm	2013, wet	29.68	8.74	22.5	−13.76	1.2	−25.8
PB3	Poon Bato	Pool 3, minor	5 cm	2012, dry	28.58	11.31	nd	nd	0.2	−21.0
PBR	Poon Bato	River*	50 cm	2012, dry	27.88	8.64	18.5	−12.1	0.28	−27.8
		River*	50 cm	2013, wet	26.36	8.3	21.3	−8.15	0.61	−23.55
MF1	Mainit Falls	Source (0 m)	5 cm	2012, dry	40.56	9.68	28.1	−15.3	0.29	−26.4
SS1	San Isidro	Cistern pool (0 m)	147 cm	2017, v. dry	48.0	10.53	0.08	−7.48	bdl	−20.9
GS	Governor's Sp.	Source (0 m)	15 cm	2017, v. dry	38.83	11.08	0.2	−14.5	bdl	−19.3
		Outflow (5 m)	2 cm	2017, v. dry	38.14	11.13	0.4	−17.4	bdl	−19.5
		Outflow (10.3 m)	2 cm	2017, v. dry	37.8	11.13	0.6	−19.99	2.7	−50.8
NWD	NW Dugout	Main pool (0 m)	30 cm	2017, v. dry	29.27	9.91	2.2	−22.52	1.1	−25.7
DH-4		NWD, well*	200 cm	2017, v. dry	32.78	9.50	10.9	−14.78	7.8	−24.8
PF1	Pinaduguan Falls	'"Pig" pool (0 m)	10 cm	2017, v. dry	35.66	10.95	0.2	−11.45	bdl	−21.6
PF2		"Apron" pool (0 m)	25 cm	2017, v. dry	35.62	10.8	1.3	−20.83	0.2	−23.7
PFR		River*	50 cm	2017, v. dry	30.0	8.4	81.3	−18.85	1.1	−28.8

*Data for samples during the dry (2012) and wet (2013) seasons have been previously reported (Cardace et al., 2015; Table 2), and are repeated here for seasonal comparison. Carbon isotope ratios expressed as compared to VPDB. nd, not determined; bdl, below detection limit. *Data for rivers and well are provided as points of reference to the local water table. The rivers are immediately proximal to the sample locations, in both cases. The well "DH-4" was drilled ∼200 m from the NWD pool.*

Our interest lies in investigating the effect of seasonal meteorological precipitation on the deep subsurface signature from spring locations in the Zambales and Palawan ophiolites in the Philippines. Geologic and geochemical descriptions of both ophiolite exposures and springs have been reported previously (Abrajano et al., 1989; Abrajano and Sturchio, 1990; Cardace et al., 2015; Ilao et al., 2018). Here, we look at carbon isotopic signatures in fluids and solid materials (sediments, biomass, and carbonates), and nitrogen isotopic signatures of biomass, over three precipitation-defined periods. Both the Zambales and Palawan ophiolites are located in Monsoon climatic regimes, with defined wet and dry seasons. In addition, we categorize our sample locations based on the flow rate of subsurface fluids emanating from the springs. The driving questions in this work concern whether increased seasonal precipitation will increase exogenous nutrient input to the surface expressions [springs], or conversely, dilute the available metabolic resources derived from subsurface processes. We hypothesized that seasonal precipitation would differentially impact systems with low flow vs. high flow of subsurface fluids, which is supported by the results given here.

MATERIALS AND METHODS

Description of Field Locations

Both field locations are within the monsoon climate zone of the Philippines. Locations were visited in October 2012 during the beginning of the dry season (193 mm/month average precipitation), September 2013 at the end of the wet season (346 mm/month average precipitation), and January 2017 when the least precipitation is received in our field areas (<20 mm/month average precipitation). Several sites in the Zambales and Palawan ophiolites were sampled, although not all sites were sampled in all three seasons. **Table 1** notes the season each location was sampled, and **Tables 1**, **2** note the depth below fluid surface and distance down the outflow channel, where applicable. In general, both fluids and solids were sampled when they were both accessible/removable. Solids included loose sediments, obvious biofilms, or carbonate features (not all were available at every sample location). **Table 2** also provides details on sample name and the type of sample collected. For example, at 10m down the outflow at site ML2, three different solid materials were collected in 2012; "gray sediment," "carbonate mound," and "rimstone" (**Table 2**). Samples with identical names and notations between multiple sample years were taken from the same location, as exactly as possible, based on photographic records of previous sampling efforts. We were unable to sample precipitation during the time that we were in the field.

Images of the sampling areas are provided in **Figure 1** with more detailed images and descriptions given in **Supplementary Figure S1** for reference. Discharge was estimated by catching runoff into a 500 ml wide mouthed bottle over a 30 s interval, repeated in triplicate and averaged. Where relevant, discharge was measured at multiple points. Sample sites are regarded as being high flow (>2 L/min), with discrete pools and runoff channels, or low flow (<2 L/min) with individual pools or a series of pools and associated carbonate terraces and similar features, but run off channels limited or not present. All locations featuring actively flowing run off channels were estimated to have a discharge rate of >2 L/min. In addition, low flow areas are also designated as "capped" or "uncapped," where "capped" refers to the presence of a carbonate film on the top of the pool. In such cases, the bottom of the pool is not visible, although the caps may be transient and potentially broken by meteorological precipitation or animal (including human) interaction. Examples of capped and uncapped pools are shown in **Figure 1**. High flow systems are expected to have an abundance of input from subsurface fluid and gas, and increasing interaction with surface conditions and atmospheric exchange as the fluids progress down the outflow channel. Low flow systems are expected to have slower fluid and gas input from the subsurface, and the degree of interaction with surface conditions depends on the presence of absence of a carbonate cap. We expect that pools with carbonate caps will have more limited atmospheric exchange, as the cap functions as a physical barrier at the surface of the pool.

Concentration and Isotopic Analysis of Dissolved Inorganic Carbon (DIC) and Dissolved Organic Carbon (DOC) in Spring Fluids

Amber I-CHEM vials and septa were pre-washed and pre-treated as previously described (Cardace et al., 2015). A glass media bottle was used to collect sample from the springs, after being triple rinsed with sample. Once collected, sample was filtered through a Millipore Sterivex GV 0.22 μm filter unit for sterilizing aqueous solutions (Cat. No. SVGVL10RC/Lot No. 1515/00631) into the sample bottle. Some samples required pumping for efficient collection, and a Geotech Environmental Geopump peristaltic pump was used to fill the glass collection bottle. Viton Masterflex tubing (Cole Parmer, Vernon Hills, IL, United States) was used for pumping when collecting DIC samples, at a slow pumping rate of <100 ml/min and as short a pumping distance as possible to minimize gas loss. DOC bottles were filled only after the filter was conditioned with several liters of sample. Both DIC and DOC bottles were filled to the top with sample to exclude air bubbles, and were stored at 4°C.

Samples were analyzed by the University of California, Davis, Stable Isotope Laboratory. Carbon isotopic ratios of carbon in DOC was analyzed with a O.I. Analytical Model 1030 TOC analyzer (Xylem Analytics, College Station, TX, United States), interfaced to a PDZ Europa 20–20 isotope ratio mass spectrometer (Sercon Ltd., Cheshire, United Kingdom) with a GD-100 Gas Trap Interface (Graden Instruments). Several replicates of reference materials were interspersed with samples, including IAEA-600, USGS-40, USGS-41, and Elemental Microanalysis reference materials.

Dissolved inorganic carbon samples were analyzed on a GasBench II system interfaced to a Delta V Plus IRMS (Thermo Fisher Scientific, Bremen, Germany). The fluids were added to

TABLE 2 | Isotopic ratios and wt% of carbon, nitrogen, and oxygen from solid materials (mineral, sediment, biofilm) collected in all three field seasons.

				Inorganic chemistry (carbonates)			Calculated		Organic chemistry (post acidification remnants)				Calculated	
Name, outflow distance	**Depth below fluid surface**	**Notes, sample description[a]**	**year**	**wt% C, $CaCO_3$**	**$\delta^{13}C$ (VPDB)‰**	**$\delta^{18}O$ (VSMOW)‰**	**$\delta^{13}C$ $CO_2(g)$[b]‰**	**$\delta^{18}O$ $CaCO_3$[c]‰**	**wt% C, organic**	**$\delta^{13}C$ (VPDB)‰**	**wt% N**	**$\delta^{15}N$ (Air)‰**	**$\Delta^{13}C$ rel. to DIC**	**$\Delta^{13}C$ rel. to DOC**
ML1 0 m	80 cm	Source sedi.	2012	93.93	−17.09	−13.38	−25.94	−9.35	0.74	−28.29	0.061	1.987	−15.51	−1.48
0 m	80 cm	Source sedi.	2013	0.31	−13.58	−12.82	−22.46	nd	0.1	−27.24	0.005	3.096	−11.82	2.38
0 m	80 cm	Source sedi.	2017	13.0	−17.6	−10.8	−26.44	−9.11	0.07	−24.7	0.008	−3.303	−13.49	−0.82
ML2 0 m	30 cm	Source sedi.	2012	0.28	−12.79	−15.53	−21.67	−9.25	0.49	−26.72	0.023	1.17	−10.24	−0.25
1.5 m	20 cm	Spill pool	2012	0.9	−18.84	−18.12	−27.68	−9.25	0.21	−26.57	0.015	2.29	−11.53	−1.03
10 m	10 cm	Gray sedi.	2012	4.76	−19.82	−16.76	−28.70	nd	0.34	−26.52	0.024	1.007	−7.86	0.31
10 m	10 cm	Carb. mound	2012	8.61	−18.87	−15.20	−27.75	nd	0.15	−22.98	0.011	1.911	−4.32*	3.84*
10 m	10 cm	Rimstone	2012	84.06	−19.58	−14.97	−28.45	nd	1.94	−25.01	0.167	0.813	−6.36*	1.80*
0 m	30 cm	Source sedi.	2013	0.21	−12.24	−14.45	−21.46	nd	0.63	−27.50	0.033	1.139	−16.69	−1.99
1.5 m	20 cm	Spill pool	2013	0.14	−14.52	−13.71	nd	nd	0.2	−26.96	0.015	−0.798	−16.2*	−1.45*
10 m	10 cm	Gray sedi.	2013	16.75	−20.48	−18.50	−29.47	nd	0.37	−26.02	0.028	2.001	nd	nd
10 m	10 cm	Rimstone	2013	91.15	−19.66	−15.28	−28.66	nd	14.33	−28.29	1.086	0.463	nd	nd
17.7 m	5 cm	Above apron	2013	61.23	−19.20	−16.83	nd	nd	1.35	−21.40	0.121	1.248	−0.27*	7.74*
18.3 m	5 cm	Apron	2013	108.79	−20.11	−15.87	nd	nd	10.22	−27.10	0.836	0.334	−5.97*	2.04*
19.5 m	5 cm	Below apron	2013	2.68	−19.62	−15.64	−28.62	nd	29.91	−28.03	3.257	−2.231	−6.9	1.11
0 m	30 cm	Source sedi.	2017	2.0	−11.8	−14.9	−20.70	−9.15	0.13	−27.0	0.009	1.494	−9.32	1.22
1.5 m	20 cm	Spill pool	2017	3.0	−19.7	−17.1	−28.52	nd	0.14	−28.0	0.01	0.272	−13.18	−7.19
10 m	10 cm	Gray sedi.	2017	72.0	−19.5	−10.3	−28.42	nd	0.16	−26.9	0.014	−0.214	−8.22*	−4.78*
10 m	10 cm	Rimstone	2017	97.0	−19.5	−11.3	−28.43	nd	0.17	−25.9	0.019	0.139	−7.2*	−3.76*
PB1	10 cm	Main pool	2012	14.0	−20.4	−17.5	−29.48	−8.40	0.13	−27.6	0.009	−1.809	−2.12	−4.63
	2 cm	Minor pool	2012	12.0	−19.1	−15.6	nd	nd	0.11	−28.9	0.009	1.433	−3.49*	−6.00*
	0.25 cm	Terrace	2012	99.5	−25.2	−18.6	nd	nd	0.11	−22.8	0.01	−2.034	2.67*	0.16*
	10 cm	Main pool	2013	103.43	−23.30	−18.30	−32.48	nd	0.35	−25.43	0.025	2.385	−12.63	1.42
	2 cm	Minor pool	2013	68.78	−19.96	−15.46	nd	nd	7.96	−25.56	0.736	−0.314	−12.8*	1.28*
	0.25 cm	Micro-terracette	2013	86.18	−19.68	−13.81	nd	nd	26.57	−25.28	2.632	1.601	−12.5*	1.57*
	0.25 cm	Terrace	2013	99.29	−27.75	−21.89	nd	nd	13.45	−27.14	1.592	−0.395	−14.3*	−0.29*
	2 cm	Muddy pot	2013	59.15	−23.56	−18.99	nd	nd	4.23	−28.09	0.405	−1.137	nd	nd
PB2	25 cm	"Star pool" terraces	2012	92.96	−15.46	−9.37	−25.04	−8.31	6.58	−31.23	0.453	2.101	−13.78	−6.82
	2 cm	"Waterfall"	2012	66.0	−16.5	−10.2	−26.08	−8.31	5.30	−30.3	0.235	0.97	−16.49	−4.45
	30 cm	"Ice cube"	2012	99.0	−14.8	−4.8	−24.40	−8.3	0.17	−30.1	0.009	0.324	−12.6*	−5.65*
	N/A	Litter ref.	2012	28.0	−24.6	−21.10	nd	nd	27.13	−31.4	0.364	0.022	nd	nd
	N/A	Soil ref.	2012	16.0	−14.7	−13.3	nd	nd	0.59	−31.8	0.007	0.685	nd	nd

(Continued)

TABLE 2 | Continued

				Inorganic chemistry (carbonates)			Calculated		Organic chemistry (post acidification remnants)				Calculated	
Name, outflow distance	**Depth below fluid surface**	**Notes, sample description[a]**	**year**	**wt% C, $CaCO_3$**	**$\delta^{13}C$ (VPDB)‰**	**$\delta^{18}O$ (VSMOW)‰**	**$\delta^{13}C$ $CO_2(g)$[b]‰**	**$\delta^{18}O$ $CaCO_3$[c]‰**	**wt% C, organic**	**$\delta^{13}C$ (VPDB)‰**	**wt% N**	**$\delta^{15}N$ (Air)‰**	**$\Delta^{13}C$ rel. to DIC**	**$\Delta^{13}C$ rel. to DOC**
PB3	5 cm	Main pool, red sedi.	2012	1.07	−18.17	−14.80	−27.36	nd	0.59	−25.80	0.043	2.067	−8.3*	−4.36*
	3 cm	Minor seep, white sedi.	2012	68.14	−13.11	−9.41	−22.60	nd	4.62	−28.48	0.091	2.375	−10.9*	−7.04
MF 0 m	5 cm	Source sedi.	2012	25.0	−10.5	−11.2	−19.64	−6.8	0.11	−26.7	0.016	−3.21	−11.46	−0.35
60 cm	0.5 cm	Outflow	2012	3.0	−13.6	−12.4	nd	nd	0.13	−27.1	0.016	−0.32	−11.8*	−0.69*
2.2 m	0.5 cm	Outflow	2012	99.5	−9.3	−12.5	nd	nd	*bdl*	−26.9	0.0001	0.492	−11.7*	−0.56*
4.3 m	0.5 cm	Outflow	2012	2.03	−16.29	−15.39	nd	nd	0.30	−27.46	0.031	1.136	−12.2*	−1.07*
PF1	10 cm	"Pig" pool	2017	56.0	−19.8	−11.4	−28.46	−7.21	0.22	−26.5	0.029	6.075	−15.04	−4.89
PF2	25 cm	"Apron" pool	2017	99.5	−13.5	−7.3	−22.23	−7.20	0.05	−29.6	0.003	2.555	−8.73	−5.86
GS 0 m	15 cm	Source exit	2017	17.0	−11.8	−17.4	−20.29	−7.39	0.21	−18.4	0.014	3.892	−3.95	−0.85
0.5 m	10 cm	Spill pool	2017	29.0	−21.7	−17.1	−30.05	−0.03	0.79	−24.2	0.07	3.831	−9.73*	−4.93*
4.5 m	3 cm	Outflow	2017	85.0	−28.1	−24.6	−36.49	−7.21	0.3	−26.2	0.025	2.008	−8.76*	−6.66*
5.0 m	2 cm	Outflow	2017	49.0	−25.6	−20.6	−34.02	−0.02	0.71	−26.1	0.057	2.86	−8.73	−6.63
10.3 m	2 cm	Outflow	2017	74.0	−22.8	−19.9	−31.30	−7.20	0.93	−26.7	0.056	3.306	−6.74	24.07
NWD	30 cm	Source pool carbonate	2017	99.0	−16.5	−10.3	−25.86	−7.20	0.28	−22.3	0.019	−0.675	0.19	3.37
5 m	4 cm	Outflow	2017	99.5	−18.5	−13.5	−27.68	nd	0.17	−22.3	0.009	−0.245	0.17	3.35
12 m	1 cm	Outflow	2017	95.0	−17.1	−11.9	nd	nd	1.71	−20.6	0.042	−1.58	1.92	5.10
12 m	1 cm	Black biofilm	2017	82.0	−11.6	−10.8	nd	nd	11.19	−27.7	0.354	0.769	−5.18	−2.00

Inorganic chemistry of solids (e.g., carbonates) and organic chemistry are presented separately. In addition, calculated equilibrium carbon enrichment between calcite and $CO_{2(g)}$, equilibrium $\delta^{13}C$ $CO_{2(g)}$, equilibrium carbonate oxygen isotope composition, and the δ fractionation between organic carbon and DIC and DOC are given. Equilibrium constants can be found in ***Supplementary Table S1****.* [a]*Abbreviations in this column are as follows: sedi., sediment; ref., reference; carb., carbonate.* [b]*Calculated – equilibrium $\delta^{13}C_{CO2\ (g)}$ using $\varepsilon_{\ calcite\text{-}CO2(g)}$ and measured $\delta^{13}C_{CaCO3}$ (Bottinga, 1969).* [c]*Calculated – equilibrium carbonate $\delta^{18}O$ (O'Neil et al., 1969; Friedman and O'Neil, 1977).* **Estimated using $\delta^{13}C$ DIC or $\delta^{13}C$ DOC from a proximal and directly related location.*

FIGURE 1 | General locations and images of select sample areas. Additional sample area images and site descriptions can be found in **Supplementary Figure S1**. **(a)** Map of the Philippines with sample regions. Marine Geoscience Data System (MGDS; www.marine-geo.org). **(b)** Cistern pool ML1, Manleluag area. Images of location ML2 and associated outflow sites can be found in **Supplementary Figure S1**. **(c)** Source pool of "Governor's Spring." Small white scale bar noted. White arrow at top right indicates flow direction. **(d)** North West Dugout Pool. White arrow indicates location of spring in **(c)**. **(e)** Pinaduguan Falls. Inset shows close up of "Pig Pool" (PF1). **(f)** Poon Bato "PB2" location, with major features noted. Car battery for scale. **(g)** Poon Bato "PB1" location. Note calcite "cap" on top of the low flow pool (arrow). **(h)** Close up image of "Star Pool" in **(f)**. Note lack of calcite "cap" (bottom of pool is visible).

a sealed, He-purged exetainer, and acidified to liberate all of the DIC as CO_2. Reference materials for DIC analyses were lithium carbonate (Acros-1, Acros-2 Li_2CO_3, lots measuring $\delta^{13}C$ −13.4 and −3.85, respectively, Thermo Fisher Scientific, St. Louis, MO, United States) dissolved in degassed deionized water and a deep seawater (both calibrated against NIST 8545). Final $\delta^{13}C$ values are expressed relative to the international standard VPDB (Vienna PeeDee Belemnite).

Determination of Endmember Composition and Contributions

An estimation of subsurface endmember $\delta^{13}C_{DIC}$ was calculated following the method of Miller and Tans (2003), where $\delta^{13}C_{DIC}$ *[DIC] is plotted as a function of [DIC], for each field area, and the slope of the resulting linear regression indicates an estimated $\delta^{13}C_{DIC}$ for the endmember fluid at that field site. These endmember values of $\delta^{13}C_{DIC}$ were then used to estimate the fraction of the subsurface endmember remaining following select microbial metabolic processes on the measured $\delta^{13}C_{DIC}$ pool. Here, a Rayleigh distillation model was used;

$$\delta^{13}C_{observed} = \delta^{13}C_{source} + 10^3(\alpha - 1)\ln(f)$$

Where $\delta^{13}C_{observed}$ is the measured $\delta^{13}C_{DIC}$ in the samples, and $\delta^{13}C_{source}$ is either the estimated $\delta^{13}C_{DIC-subsurface}$, or $\delta^{13}C_{DOC}$, as specified below. Fractionation factors, α, were chosen for individual microbial processes. For chemoautotrophic

pathways, namely the acetyl Co-A and rTCA cycles, a range of α = 0.964–0.996 as reported in Hayes, 2001 was used. For bacterial photoautotrophy, a range of α = 0.978–0.99 as reported in Hayes, 2001 was used. For hydrogenotrophic methanogenesis, α = 0.945 from carbonate to methane (Waldron et al., 1998) and α = 0.942 from CO_2 to methane (Krzycki et al., 1987) were used. For each of the above processes utilizing the DIC pool as a carbon source, the $\delta^{13}C_{source}$ used was the estimated subsurface endmember $\delta^{13}C_{DIC}$ as calculated for each location as in Miller and Tans, 2003. Processes that produce CO_2, such as acetoclastic methanogenesis (α = 0.976, Waldron et al., 1998) and methanol methanogenesis (α = 0.932, Rosenfeld and Silvermann, 1959; Silverman and Oyama, 1968) were also considered. For these latter processes, the $\delta^{13}C_{source}$ used was the measured $\delta^{13}C_{DOC}$.

Carbon and Nitrogen Isotopic Ratios in Solid Materials

Solid samples, consisting of sediments, carbonate terrace materials, and any resident microbiota or biofilms, were collected using sterile technique into Whirlpac bags, and kept frozen at −20°C until analysis. Samples were freeze dried, and then ground to a fine powder in glass or agate mortars. Mortars and Pestles were baked at 550°C overnight prior to use. Samples were analyzed in the Osburn Isotope Geobiology Laboratory at Northwestern University.

Carbonate content, assayed as mg CO_2 and its respective $\delta^{13}C$ value (hereafter $\delta^{13}C_{CO3}$) was determined simultaneously via continuous flow on a Thermo Fisher Scientific GasBench II, coupled to a Delta V Plus isotope ratio mass-spectrometer (CF-IRMS) at the Northwestern Stable Isotope Facility. Prior determination of the CO_3^{2-} content from gravimetric quantification guided the sample amount used for analysis, aiming for ∼10 μmol CO_2. Samples were weighed into 12 mL Exetainer® vials, which were subsequently septum-sealed and purged with UHP He for 7 min. Approximately 200 μL of 103% H_3PO_4 was injected into each vial, and the samples placed into a thermos-stated block at 70°C to allow CO_2 to evolve overnight. The isotopic composition, $\delta^{13}C_{CO3}$ is corrected using the periodic sampling of CO_2 from the H_3PO_4-acidified $CaCO_3$ standards NBS18 ($\delta^{13}C_{VPDB}$ = −5.014‰) and NBS19 ($\delta^{13}C_{VPDB}$ = 1.95‰), and samples reported on the VPDB scale. Estimated precision (1 s.d.) on $\delta^{13}C_{CO3}$ is ± 0.06‰.

For the determination of wt% organic C and organic N, acidified and decarbonated samples were weighed into tin capsules and combusted online in a Costech 4010 Elemental Analyzer, coupled to a Thermo Fisher Scientific Delta V Plus mass-spectrometer via a ConFloIV. Briefly, ∼10–30 mg of powdered decarbonated samples were weighed, then combusted online in a column containing chromium (III) oxide and silvered cobaltous chloride, held at 980°C. Product gasses were carried over hot Cu reduction column held at 705°C to removed excess O_2 and convert nitrogen oxides to N_2. Product CO_2 and N_2 were separated by a molecular sieve 5A GC column. The gasses were analyzed via CF-irms, and size corrected. Tank corrections were done by regular calibration against organic standards supplied by Indiana Biogeochemical laboratories (IU acetanilide and IU urea), and placed on the $\delta^{13}C_{VPDB}$ and $\delta^{15}N_{AIR}$ scales respectively.

Carbonate Mineralogy

An Olympus Terra X-ray diffractometer[1], with the specifications equivalent to the CheMin tool developed for Mars exploration as described in Blake et al. (2012), was used for X-ray diffraction (XRD) analysis. The Terra engages a Co X-ray source and a cooled charge-coupled device (CCD) detector arranged in transmission geometry with the sample, with angular range of 5° to 50° 2θ with <0.35° 2θ resolution (Blake et al., 2012). X-ray tube voltage is typically 30 kV, with a power of 10 W, a step size of 0.05°, and an exposure time of 10 s per step. A minimum of 250 exposures were recorded prior to diffractogram interpretation.

Dry samples were powdered using an agate mortar and pestle, cleaned with isopropyl alcohol between samples. Powder was passed through a standard 150 μm sieve (100-mesh) prior to analysis. Powdered, sieved material was transferred with a spatula to the input hopper of the vibration chamber sample cell, and shaken into the space between two mylar window, to be agitated during analysis, presenting all planes with the mineral sample to the x-ray beam.

The resulting diffractogram was interpreted using XPowder software[2], which is a commercially available peak search-and-match program that queries the PDF2 database for reference mineral peak information (see text footnote 2). XPowder allows for identification of major minerals; trace minerals can be missed or masked by peaks of other minerals. Diffractograms convey mineral fingerprint information customarily by plotting of diffracted signal intensity on the *y*-axis against °2θ on the *x*-axis. An intensity peak is the result of constructive interference when Bragg's law ($n\lambda = 2d \sin\theta$, where n is the "order" of reflection, λ is the incident X-rays wavelength, *d* is spacing between atomic planes in a crystal structure, and θ is the incidence angle) is fulfilled by the incoming x-rays. For reference, for data collected using a Co x-ray tube, the three most prominent *d*-values for minerals of interest are as follows: serpentine (var. lizardite) $Mg_3Si_2O_5(OH)_4$, D1: 7.12 Å, D2: 2.379 Å, D3: 3.56 Å; serpentine (var. antigorite) $(Mg,Fe{+}{+})_3Si_2O_5(OH)_4$, D1: 7.29 Å, D2: 2.53 Å, D3: 3.61 Å; brucite $Mg(OH)_2$, D1: 2.365 Å, D2: 4.77 Å, D3: 1.794 Å; hydrotalcite $Mg_6Al_2(CO_3)(OH)_{16}{\cdot}4(H_2O)$, D1: 7.69 Å, D2: 3.88 Å, D3: 2.58 Å; portlandite $Ca(OH)_2$, D1: 2.628 Å, D2: 4.9 Å, D3: 1.927 Å; calcite $CaCO_3$, D1: 3.035 Å, D2: 2.285 Å, D3: 2.095 Å; magnesite $MgCO_3$, D1: 2.742 Å, D2: 2.102 Å, D3: 1.700 Å; artinite $Mg_2(CO_3)(OH)_2{\cdot}3(H_2O)$, D1: 2.736 Å, D2: 5.34 Å, D3: 3.69 Å; chlorite (var clinochlore) $(Mg,Fe{+}{+})_5Al(Si_3Al)O_{10}(OH)_8$, D1: 7.16 Å, D2; 4.77 Å, D3: 3.58 Å; and smectite (var beidellite) $Na_{0.5}Al_2(Si_{3.5}Al_{0.5})O_{10}(OH)_2{\cdot}n(H_2O)$, D1: 2.55 Å, D2: 2.61 Å, D3: 4.52 Å.

In order to interpret co-occurring minerals in association with spring water, an Eh-pH diagram was constructed in Geochemist's Workbench Act 2. The system was modeled at a temperature

[1]https://www.olympus-ims.com/en/xrf-xrd/mobile-benchtop-xrd/terra/#!

[2]http://www.xpowder.com/

of 25°C, at a pressure of 1.013 bars, with log activity HCO_3^- set at −2.699, log activity Ca^{2+} set at 2, log activity Fe^{2+} set at −3, and unit activity of Mg^{2+} and water. The log activity HCO_3^- is based on high CO_2 in to water mixture as low DIC spring water encounters high DIC surface water. The log activity Ca^{2+} set at 2 represents generally observed molalities of $[Ca^{2+}]$ near 100 m, which correspond to activities of ∼100, thus log 100 = 2. The log activity Fe^{2+} set at −3 represents generally observed molalities of $[Fe^{2+}]$ near 1 mmolal, which correspond to activities of ∼0.001, thus log 0.001 = −3. Unit activity of Mg^{2+} conveys the Ca dominance of the aqueous system, about two orders of magnitude greater than Mg, thus Mg activity taken as one. Unit activity of water is appropriate for most lower salinity, low temperature waters (activity coefficients not impacted by high levels of solutes).

RESULTS

Dissolved Carbon (DIC and DOC)

Results of the analysis of DIC and DOC can be found in **Table 1**. **Figures 2**, **3** display the carbon isotopic ratios and concentrations of DIC and DOC, separated by flow regime (high flow in **Figure 1**, low flow in **Figure 2**) and season. Data are grouped in **Figure 2** by samples that are in or near the source pools, vs. those that are part of the extended outflow channel. Calculated estimates of potential subsurface endmember $\delta^{13}C_{DIC}$ are shown in **Supplementary Figure S3**, and are ∼ −21.8‰ for ML, ∼ −22.7‰ for GS, ∼ −12.8‰ for NWD, ∼ −13.26‰ for PB, and ∼ −22.5‰ for PF locations. The ratio of DOC:DIC at each major field area is considered in **Supplementary Figure S4**. We are lacking $\delta^{13}C_{DIC}$ from precipitation during the time periods that we were in the field, so estimates of input from this source of DIC were not considered.

DIC in High Flow Systems (ML, GS, MF)

General trends in DIC (**Figure 2**) in high flow systems include low concentrations of DIC (e.g., <1 ppmC) in source pools, continuing downstream to end with an often higher concentration signal (1–10 ppmC). The $\delta^{13}C_{DIC}$ at the source pools was more enriched relative to downstream locations at all sites and varied between −11 to ∼ −18‰ at ML, but ∼ −14 to −22‰ in high flow Palawan ophiolite locations. At the high flow system ML2, a sample was taken 1.5 m beyond the mouth of the source pool in 2012 and 2017, and the $\delta^{13}C_{DIC}$ became briefly more enriched than the source pool across that distance. Discrete source pools associated within a larger spring system [e.g., ML1-ML2 or GS-NWD] had highly variable $\delta^{13}C_{DIC}$, with as much as a 7–8‰ difference in $\delta^{13}C$ between them (**Figure 2**). Precipitation (meteorological) did not influence DIC concentration, but may influence the $\delta^{13}C_{DIC}$ in the high flow ML systems (the only high flow systems where data from multiple seasons are available). The $\delta^{13}C_{DIC}$ at ML1 was more ^{13}C enriched in drier seasons relative to the wet season, while the $\delta^{13}C_{DIC}$ at ML2 became more ^{13}C depleted in drier seasons relative to the wet season. The highest concentration of DIC in a high flow system was found in MF (dry season). It was concluded previously that this site is influenced in part by non-serpentinizing hydrothermal fluids (Cardace et al., 2015).

Subsurface endmember $\delta^{13}C_{DIC}$ for sites at ML and GS are depleted by ∼13‰ relative to atmospheric DIC. A Rayleigh distillation model (**Supplementary Table S3**) predicts a wide range of potential $\delta^{13}C_{DIC}$ from the subsurface endmember for both areas (∼6–91%) after fractionation by microbial processes that consume DIC, after DIC production and fractionation by acetoclastic and methanol methanogenesis (54–93%). In contrast, the predicted remaining subsurface endmember at NWD is 0% for DIC consuming microbial processes, but 28–86% for acetoclastic and methanol methanogenesis.

DIC in Low Flow Systems (PB, PF)

Two DIC datapoints are available for each of the two low flow, uncapped sites (**Figure 3**). The data range from <1 to ∼ 30 ppmC, and $\delta^{13}C_{DIC}$ ∼ −11 to −21‰. This isotopic signature is comparable to that of the high flow systems, although DIC was more abundant in these lower flow, uncapped pools.

While limited data availability makes it difficult to identify broad patterns, there was a notable difference in the $\delta^{13}C_{DIC}$ between the wet (∼ −13‰) and dry season (∼ −25‰) in the low flow, capped systems (**Figure 3**). This was the most negative $\delta^{13}C_{DIC}$ found. Concentrations of DIC for both low flow, capped samples was 1–10 ppmC.

The subsurface endmember sources of $\delta^{13}C_{DIC}$ were predicted to be −13.26‰ to the PB area, and −22.5‰ to the PF area. These calculated endmembers are considered with caution, as they are based on very few data.

DOC in High Flow Systems (ML, GS, MF)

DOC concentrations in the high flow systems were highly variable and range from 0 to 2.7 ppmC (**Figure 2**). Carbon isotopic signatures were typically <−25‰ although several samples taken in the very dry season had more positive values (see ML and GS, **Figure 2**). Notable outliers to these general trends included a groundwater well associated with site NWD with 7.8 ppmC, and the highly ^{13}C depleted DOC (−50.8‰, relative to the DOC at all other locations) found 10.3 m down the outflow of GS. There was little apparent effect of meteorological precipitation on the concentration of DOC in the high flow systems, however, lack of rain may be linked to the most positive $\delta^{13}C_{DOC}$ values found (−19 to −22‰) which occurred in the very dry season in both ML and GS systems.

DOC in Low Flow Systems (PB, PF)

The DOC in the fluids of the low flow, uncapped systems (**Figure 3**) had a more narrow isotopic range than that in the high flow systems. However, the DOC was ^{13}C enriched relative to that of many sites (−21 to −26‰), resembling the range for the very dry season samples at high flow ML and GS. No direct seasonal comparison could be made for these sites, due to lack of data from multiple seasons for identical locations. However, the spring systems sampled in the very dry season (PF) had an order of magnitude less DOC than the spring system sampled in the dry season (PB).

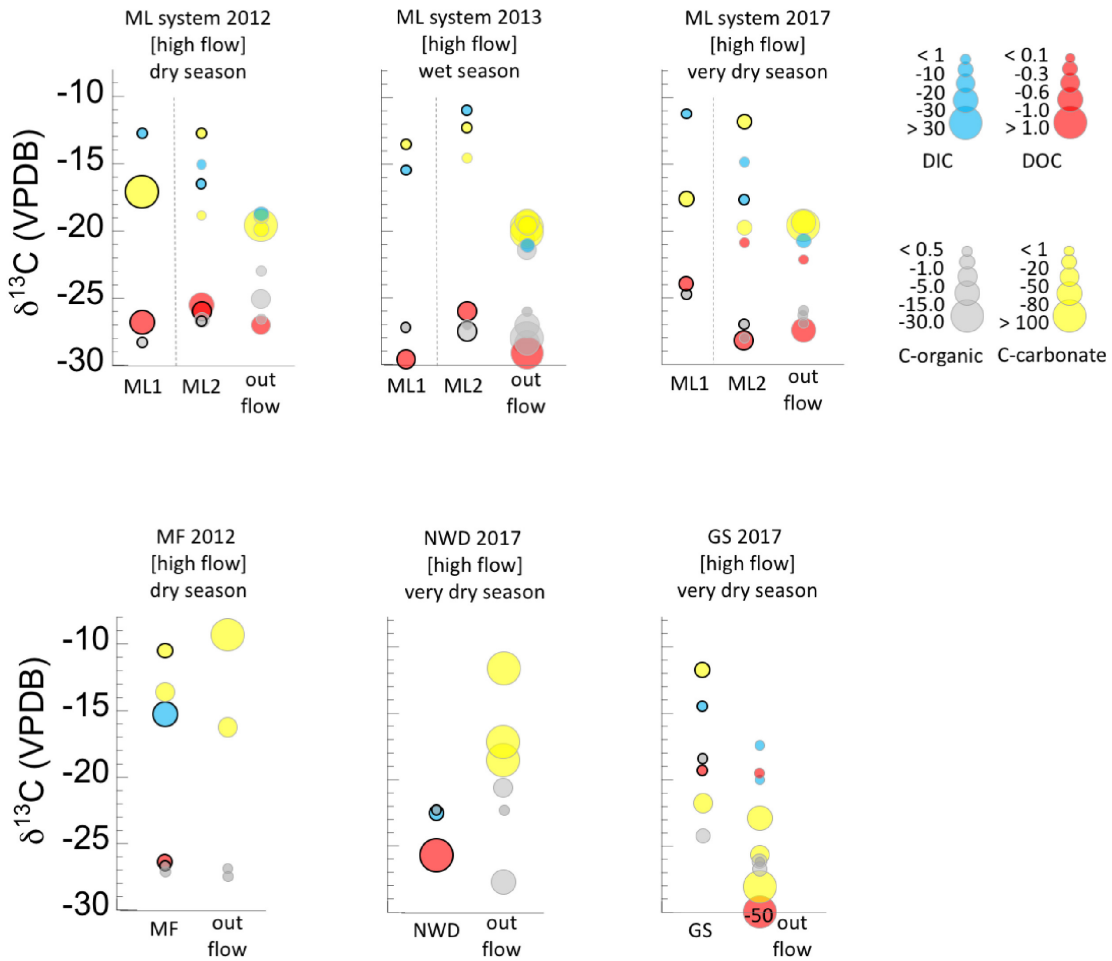

FIGURE 2 | Ranges of concentrations and $\delta^{13}C$ isotopic composition of dissolved carbon (DIC, DOC), and solid carbon (C-org, C-carbonate) in the high flow systems. Concentration ranges are given by the size of the circle for each value (key at right). Samples are grouped as pool sources plus sample locations within 2 m in one vertical column, and samples farther down the outflow channel are given as a second vertical column. The pool source is distinguished from the other samples by a bold outline around the circle. Refer to **Table 1** for full sample names and distances along the outflow. Circles are offset along the horizontal for clarity only. Data are also separated by seasonal sampling, and sample names correspond to the names in the sample location pictures (**Figure 1** and **Supplementary Figure S1**) and **Table 1**. Dashed lines separate discrete samples within a season. Data can also be found separated by discrete samples in **Supplementary Figure S2**.

Concentrations of DOC from the low flow, capped systems were between 0.1 and 0.3 ppmC, and the $\delta^{13}C$ was −23 to −27‰ (**Figure 3**), more ^{13}C depleted than the uncapped, low flow counterparts. In the dry season, DOC was more ^{13}C enriched than in the wet season, possibly representing the "leftover" pool in the reservoir, which was not refreshed by new material brought in by meteorological precipitation.

Geochemistry of Solids/Mineralogy

Organic Carbon (Biomass) in High Flow Systems (ML, GS, NWD, MF)

The carbon isotopic signature of organic carbon in solids (biomass) from high flow systems was in the range of ∼ −21 to −28‰, across all seasons and locations (**Figure 2** and **Table 2**). The samples from high flow systems also had the largest range in fractionation between biomass, DIC, and DOC (**Figure 4**) of all the systems investigated. Biomass in the high flow systems was slightly ^{13}C depleted relative to DOC (**Table 2** and **Figures 2**, **4**). There were exceptions, usually from samples near the end of the runoff channel which broaden the range of fractionation from DOC. The biomass samples in these systems were the most ^{13}C enriched relative to DOC of all the systems considered (**Figure 4**). In general, the abundance of biomass increased downstream. In addition, biomass was far less abundant in the very dry season, and more abundant in the wet season (**Figure 2**). The GS system outflow channel presented an atypical case compared to other high flow systems. While the relationship between the biomass and the DOC in the source pool at GS was similar to the other high flow systems, the biomass was as much as 10‰ ^{13}C enriched relative to other sites. In addition, the $\delta^{13}C_{biomass}$ and $\delta^{13}C_{DOC}$ in the outflow channel of GS were dissimilar, casting doubt that DOC was the source of the carbon for the biomass in the outflow sites.

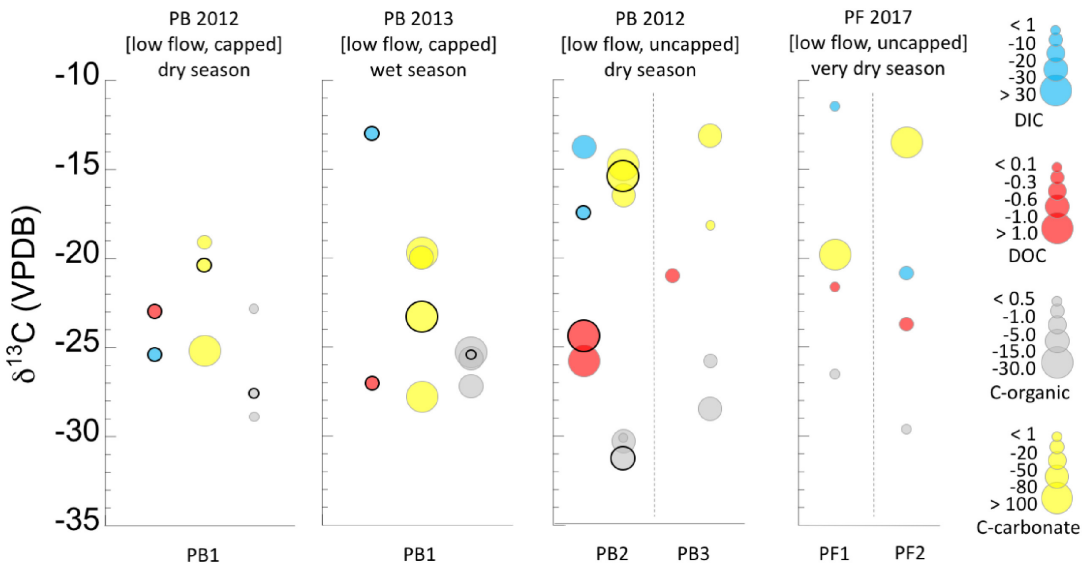

FIGURE 3 | Ranges of concentrations and $\delta^{13}C$ isotopic compositions of dissolved carbon (DIC, DOC), and solid carbon (C-org, C-carbonate) in the low flow systems. Concentration ranges are given by the size of the circle for each value (key at right). In locations where samples included both a pool source and addition samples in and around the same pool, the pool source is distinguished from the other samples by a bold outline around the circle. Refer to **Table 1** for full sample names. Circles are offset along the horizontal for clarity only. Data are also separated by seasonal sampling, and sample names correspond to the names in the sample location pictures (**Figure 1** and **Supplementary Figure S1**) and **Table 1**. Dashed lines separate discrete samples within a season. Data can also be found separated by discrete samples in **Supplementary Figure S2**.

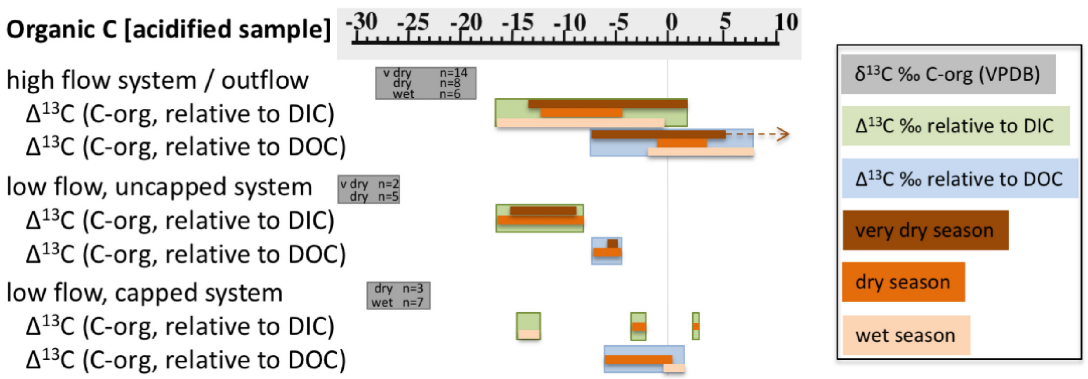

FIGURE 4 | Ranges of measured $\delta^{13}C_{organic}$ in each of the three types of sample systems (vs. VPDB), and calculated $\Delta^{13}C$ of organic carbon in solids relative to DIC and DOC. Gray bars note the $\delta^{13}C_{organic}$ range, and number of analyses per sample type. The sample types are also broken into seasons, key at right. The brown arrow indicates a single outlier data point of ~ + 24‰.

Organic Carbon (Biomass) in Low Flow Systems (PB, PF)

The $\delta^{13}C_{biomass}$ with the most negative values were found in the low flow, uncapped systems. All samples were >4‰ ^{13}C depleted relative to the DOC, and there was very little seasonal variability (**Figures 3**, **4**). These samples also had the most depleted $\delta^{13}C_{biomass}$ relative to DIC of all the systems sampled, with samples from the very dry season as much as ~ −18‰ depleted relative to DIC (**Figure 4**). Biomass from the low flow, capped systems had a similar $\delta^{13}C_{biomass}$ as that from the high flow systems (between ~ −24 to −29‰), with the more negative $\delta^{13}C_{biomass}$ in samples from the dry season.

Carbonates

In the pH range of the spring locations, speciation of DIC is expected to vary as a function of pH; at pH ~10.3 we can expect about equal proportions of bicarbonate and carbonate components of DIC, below pH = 10.3 bicarbonate will dominate over carbonate, and above pH = 10.3 carbonate is the dominant ion. Fractionation between the two species occurs, but is expected to be small across the temperature and pH ranges studied here. Fractionation as carbonate minerals precipitate will also vary with precipitation rate. Fractionations due to pH and temperature differences between samples/seasons are expected to be minimal, on the order of <2‰ when considering fractionation between

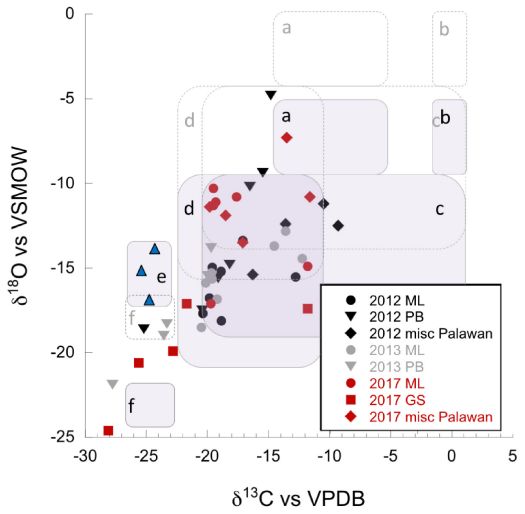

FIGURE 5 | $\delta^{13}C$ (vs. VPDB), and $\delta^{18}O$ (vs. VPDB) of carbonates, given in ‰. Black symbols = dry 2012 season, gray symbols = wet 2013 season, and red symbols = very dry 2017 season. Data are found in **Table 2**. Fields indicate formation and fractionation processes discussed in Clark et al. (1992) and Falk et al. (2016). Dashed boxes indicate the position of fields outlining formation and fractionation processes as discussed in Clark et al. (1992) and Falk et al. (2016) for Oman serpentinization-associated carbonates. Shaded boxes show adjusted positions accounting for the up to ~5‰ difference in $\delta^{18}O$ of seasonal and annual rainfall for our study areas. Isotopic data for precipitation were obtained from the Online Isotopes in Precipitation Calculator and are found in **Supplementary Table S2** (Bowen and Revenaugh, 2003; Bowen et al., 2005; Bowen, 2019). **(a,b)** These fields represent the expected isotopic ranges for carbonates formed in equilibrium with soil CO_2, and atmospheric CO_2, respectively (purposefully no data in the "**b**" fields). **(c)** This field is interpreted by Falk et al. (2016) as containing carbonates that result from mixing of endmember fluids, or recrystallization and/or isotopic exchange in older carbonates. **(d)** Fossil travertine crusts from Oman (Clark et al., 1992), interpreted as shifting toward equilibrium values during secondary recrystallization of more depleted travertine. **(e)** Field containing modern crusts from Oman (Clark et al., 1992), blue triangles, provided for reference. **(f)** Carbonates potentially formed by the CO_2 hydroxylation process.

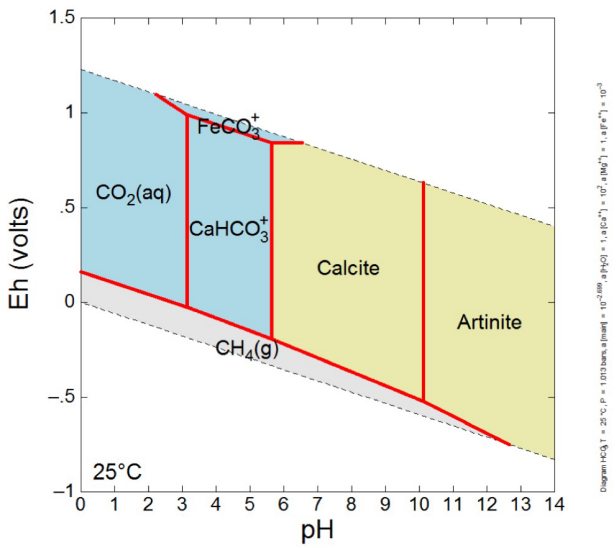

FIGURE 6 | Eh-pH diagram illustrating likely carbonate mineralogy of GS area spring waters, which are Ca-dominated waters with near surface DIC values due to interaction with atmosphere, and bear low concentrations of dissolved Mg and very low concentrations of dissolved Fe. The system was modeled at a temperature of 25°C, at a pressure of 1.013 bars, with log activity HCO_3^- set at –2.699, log activity Ca^{2+} set at 2, log activity Fe^{2+} set at –3, and unit activity of Mg^{2+} and water. Note that artinite is a hydrated magnesium carbonate mineral [$Mg_2(CO_3)(OH)_2{\cdot}3H_2O$], and calcite is taken to be pure $CaCO_3$. For relevant high pH, low Eh environmental conditions (lower right plotted area), one expects mineral precipitation of artinite, grading to calcite as pH drops (possibly due to organic acid production by microbiology or influx of atmospheric CO_2).

H_2O and CO_2 due to pH (Halas et al., 1997, **Table 4**), and <1 to ~2‰ between bicarbonate and carbonate in our temperature range (Emrich et al., 1970; **Table 1**). The fractionation due to precipitation rates is also expected to be <1‰ (Turner, 1982). There are no reports that consider all three of these variables on fractionation of DIC or carbonate minerals in the range of conditions of our study sites.

The $\delta^{13}C$ of solid inorganic carbon (carbonates) were typically only slightly fractionated relative to DIC, showing the most similarity in the wet season and the most fractionation from DIC in the dry and very dry seasons (**Table 2** and **Figures 2**, **3**). Again, there were exceptions to this pattern. For example, the carbonates in wet season samples from the PB location (2013), which was low flow and capped, were nearly 15‰ ^{13}C depleted relative to the DIC (**Figure 3**). In these samples, $\delta^{13}C_{carbonate}$ was more isotopically similar to the $\delta^{13}C_{biomass}$ and $\delta^{13}C_{DOC}$. A similar landscape of carbonates ^{13}C depleted relative to DIC was found at the GS site, both near the source and farther down the outflow (**Figure 2**).

Carbonates from the Philippines had some of the most depleted $\delta^{13}C$ and $\delta^{18}O$ values reported from terrestrial serpentinizing environments (**Table 2** and **Figure 5**). Values of $\delta^{13}C$ in our carbonates range from −28.1 to −9.3‰ VPDB, and values of $\delta^{18}O$ range from −24.6 to −4.8‰ VPDB (5.5–23.4‰ VSMOW). Equilibrium considerations in the formation of carbonates were calculated and are available in **Table 2**, including a starting $\delta^{13}C_{CO2}$ and $\delta^{18}O_{CO2}$. The difference between the measured $\delta^{18}O_{carbonate}$ and the expected (calculated) $\delta^{18}O_{carbonate}$ is shown in **Figure 7**, for samples for which a $\delta^{18}O_{water}$ was available. In all samples except one (from PB2), the measured $\delta^{18}O_{carbonate}$ was depleted in ^{18}O relative to the calculated, expected value for $\delta^{18}O_{carbonate}$, with up to −17.39‰ difference. Carbonates depleted in ^{18}O relative to equilibrium with water indicate rapid mineral precipitation or precipitation far out of equilibrium.

Because the most negative $\delta^{13}C$ carbonates were primarily from the GS area, the mineralogy of solid samples from those locations was further explored. The expected carbonate mineralogy is shown in the Eh/pH diagram in **Figure 6**; measured carbonate mineralogy is given in **Figure 8**. The model for carbonate stability for a Ca-dominated water with low Mg, low Fe, and near surface DIC values suggests that at the pH and Eh of GS locations, the expected stable magnesium and calcium carbonate minerals are artinite and calcite.

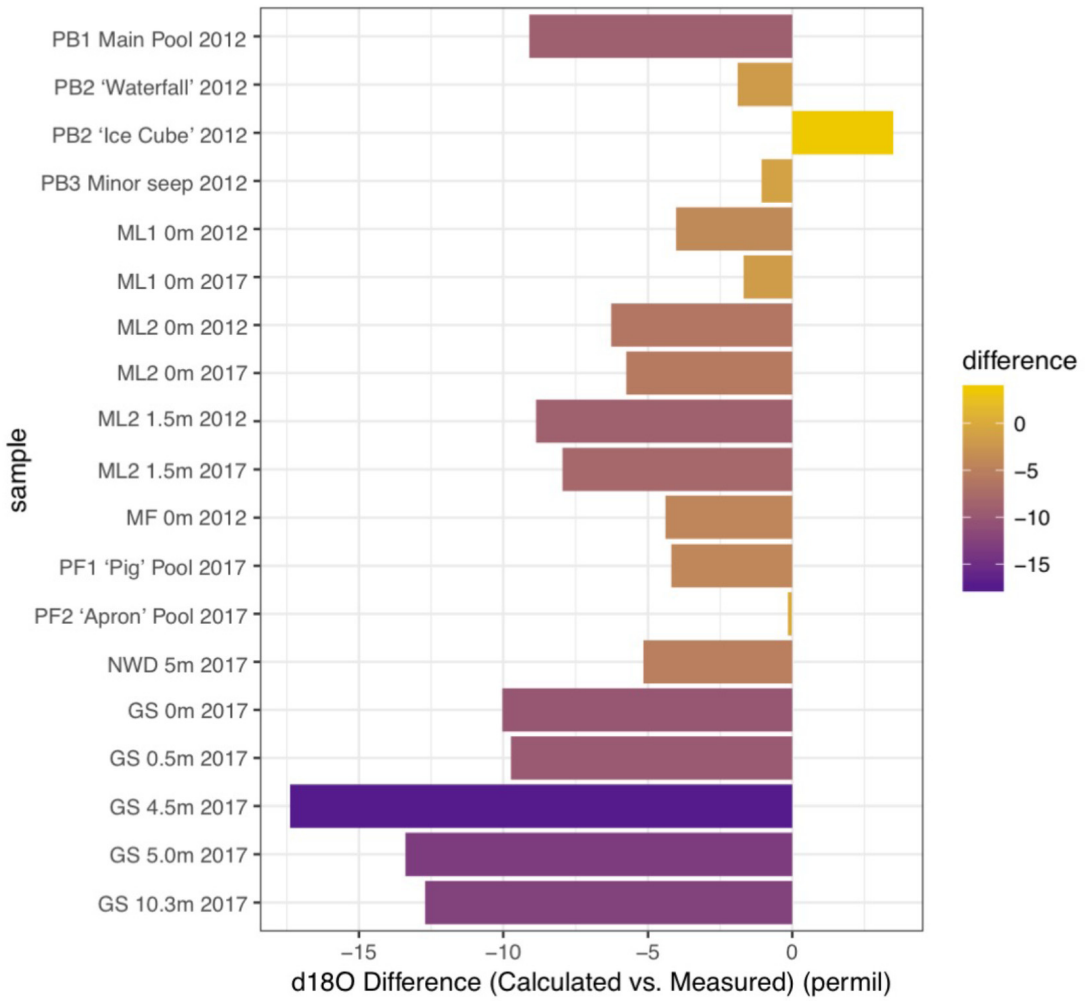

FIGURE 7 | Differences in the values measured for $\delta^{18}O$ in carbonates and values expected for $\delta^{18}O$ in carbonates (calculated) in samples from 2012 (dry season) and 2017 (very dry season). Data (see **Table 2**) are compared for the Poon Bato (PB), Manleluag (ML), Mainit Falls (MF), and San Isidro area springs (PF, NWD, and GS). Positive values are enriched in ^{18}O relative to equilibrium, and negative values are depleted relative to equilibrium with water.

XRD analysis of GS location carbonates (**Figure 8**) showed that the outflow sites between 4.5 and 10.3 m are dominated by calcite, serpentinite, clay minerals such as smectite and chlorite, and other smaller proportions of carbonates such as aragonite, magnesite, and artinite, with possible portlandite [$Ca(OH)_2$], suggested by variable right-side shoulder near the serpentine peak at ∼42.5 °2-theta. At the source pool alone, brucite [$Mg(OH)_2$] and hydrotalcite [$Mg_6Al_2CO_3(OH)_{16}{\cdot}4H_2O$] are indicated in XRD results, giving evidence for mineral precipitation of hydroxide phases from this OH^- dominated spring water where it emerges from the subsurface.

Nitrogen

The $\delta^{15}N$ in solid samples (presumably from biomass) compared to the ratio of total carbon to total nitrogen (both as wt.%) are given in **Figure 9**, broken down by flow system type and season. A relationship between the abundance of nitrogen in biomass and a depleted ^{15}N isotopic signature relative to atmospheric may indicate diazotrophic activity, supplying freshly fixed nitrogen to the biomass (e.g., Loiacono et al., 2012 and sources within). In contrast, nitrogen limitation or an ^{15}N enriched nitrogen isotopic signature relative to atmospheric may indicate nutrient recycling, exogenous nitrogen addition from eukaryotic surface systems, or microbial nitrogen cycling functions such as nitrification or denitrification. A poorly fit relationship was present between the C:N and $\delta^{15}N$ in the high flow systems during the seasons with more meteorological precipitation (**Figure 9A**), but not in the very dry season (**Figure 9B**). While there were fewer data points available for the lower flow systems (**Figure 9C**), data cluster according to the season the samples were obtained in. Very dry season samples had the most positive $\delta^{15}N$, with high nitrogen biomass (**Figure 9C**, blue field), dry season samples had the lowest wt% nitrogen in biomass, and $\delta^{15}N$ data fall between $\pm$ 2.3‰ (yellow field), while wet season samples were primarily $\delta^{15}N < 0$‰ and low C:N (red field).

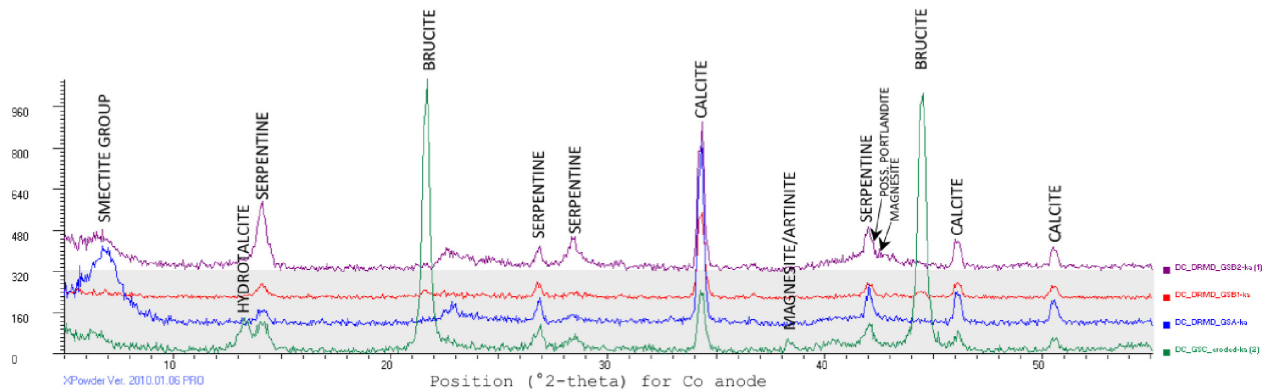

FIGURE 8 | X-ray diffractograms convey mineralogical differences between representative samples of Governor's Spring solids, collected at spring source (green), two locations along the outflow path (red, purple), and at the base of the main flow channel (blue). Data were collected using an Olympus Terra XRD unit outfitted with Co tube (https://www.olympus-ims.com/en/xrf-xrd/mobile-benchtop-xrd/terra/#!), and peaks were identified using Xpowder (http://www.xpowder.com/). Peaks (intensity on the *y*-axis) indicate strongly diffracted x-rays. Peaks correspond to specific angles (°2-theta, on *x*-axis) at which x-rays are diffracted by specific planes of atoms present in the mineral sample. At spring source (green diffractogram), serpentine peaks co-occur with strong brucite peaks, and associated hydrotalcite. Along outflow path (red and purple diffractograms), carbonate and serpentine minerals dominate, with possible minor brucite, portlandite, and magnesite. The lowest elevation site (blue diffractogram) shows carbonate minerals with a smectite group clay (broad peak, far left).

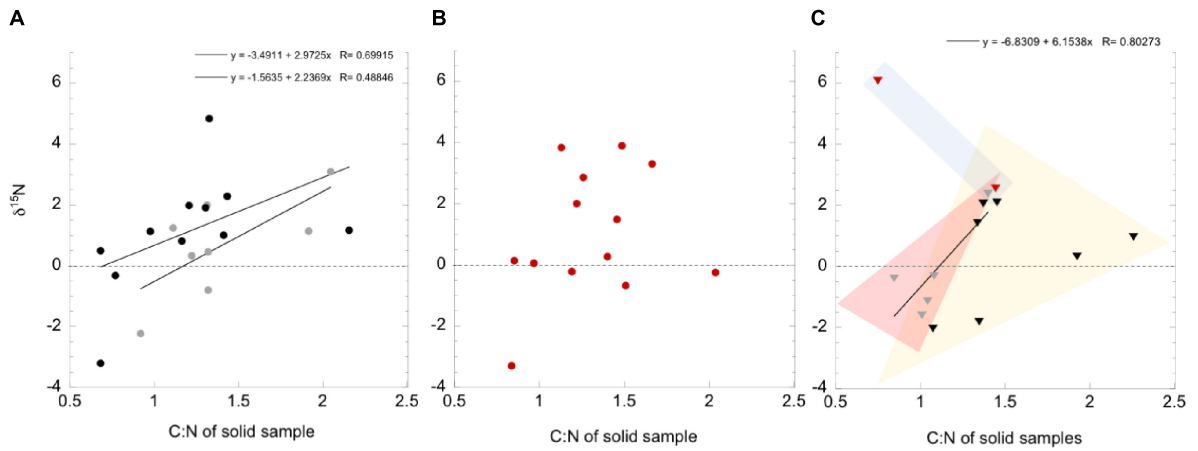

FIGURE 9 | Ranges of measured $\delta^{15}N$ within organic fraction of solid samples, as a function of the C/N ratio in the samples, divided by 10. Data are found in **Table 2**. Three sampling seasons are shown; 2013 wet (gray), 2012 dry (black), and 2017 very dry (red) seasons. Circles indicate high flow systems, Triangles indicate low flow systems. The dashed line indicates the expected $\delta^{15}N$ of atmospheric N_2. Values below this line are interpreted as produced by fractionation during nitrogen fixation processes, and values above are likely influenced by other nitrogen cycling reactions and nitrogen recycling. **(A)** High flow systems, during the wet and dry seasons. **(B)** High flow systems during the very dry season. **(C)** Low flow systems, all seasons.

DISCUSSION

Surface derived carbon, such as DOC picked up from plant, animal, or soil sources during overland flow, is characteristically depleted in $\delta^{13}C$ relative to atmospheric CO_2. Examples of surface derived carbon can be found in **Table 2** – samples from PB1 ("Muddy pot, 2013") and PB2 (leaf litter and soil reference material, 2012), which range from $\delta^{13}C = -14.7$ to $-24.6‰$. When such biomass is carried into the sample locations after being dissolved or transported as solids, it provides organic carbon with $\delta^{13}C$ depleted with respect to atmospheric CO_2. Microbial heterotrophy of organic carbon for biomass production results in very little fractionation of carbon (e.g., Hayes, 1993). In these systems, when the $\delta^{13}C_{biomass}$ is only barely fractionated with respect to $\delta^{13}C_{DOC}$ the assumption can be made that DOC was utilized to produce the biomass. Further, it is logical that the source of the DOC is likely primarily from surface environments, rather than produced within the pools, especially during periods of high precipitation. Care needs to be taken when interpreting DOC-biomass relationships in the low precipitation seasons. Measured $\delta^{13}C_{DOC}$ or $\delta^{13}C_{biomass}$ values with a large enrichment relative to source DOC are likely products of microbial carbon fixation, a result of recycling of carbon in a closed or semi-closed system, or a mix of heterotrophic and autotrophic growth.

The measured $\delta^{13}C_{DIC}$ can be the product of multiple processes, including fluid mixing, fractionation following biological activity, and kinetic effects to name a few. Removal of DIC from the source (whether subsurface or surface) by microbial carbon fixation or methanogenesis will change both the concentration of DIC and the $\delta^{13}C_{DIC}$ in the remaining DIC pool. Some autotrophic organisms are known to fractionate DIC by as much as 36‰ with specific carbon fixation pathways at 25–40°C (Hayes, 2001; House et al., 2003). Likewise, the production of DIC by heterotrophic processes, or acetoclastic methanogenesis will supply DIC to the available pool that is fractionated relative to the source DOC.

Nitrogen fixation fractionates N_2 only slightly from atmospheric values, and $\delta^{15}N_{biomass}$ close to 0‰ can be inferred to be a product of nitrogen fixation (Delwiche and Steyn, 1970). Other nitrogen cycle processes produce more negative $\delta^{15}N_{biomass}$, and values of $\delta^{15}N_{biomas}$ that are enriched relative to atmospheric N_2 can result from recycling fixed N_2 in a closed or partially closed system (e.g., Havig et al., 2011).

The climate of the Philippines affects the primary carbon sources for biomass in serpentinizing spring fluids in the Zambales and Palawan ophiolites. Our goal was to determine the primary carbon source for biomass in both the source pools (where a greater "subsurface" fingerprint might be presumed) and runoff channel locations. Our data indicate that factors that impact the primary carbon source include flow rate of the fluids, and degree of exogenous carbon input from meteorological precipitation-derived DIC and DOC.

Seasonal low meteorological precipitation affects the quantity of biomass present in the sediments at all field locations where multiple seasons were sampled (ML, PB1) – measured biomass was less abundant in the dry and very dry seasons (**Figures 2**, **3**). This decrease in biomass production can not be directly linked to a decrease in DOC concentrations within our sample set. With few exceptions (ML1, and some outflow channel sites of ML2), there is not an apparent decrease of DOC with decreased meteorological precipitation and the highest DOC:DIC ratios are found in very dry season samples (**Supplementary Figure S4**). However, as discussed below, in a few cases (such as ML during the very dry season) there is evidence of DOC recycling during the drier seasons relative to the wet season. A possible explanation is that biomass does increase in response to an increase in delivery of DOC via overland flow, and the DOC measured during the wet season is "leftover" DOC that has not been consumed. The dynamics of population and metabolic shifts that might be tied to DOC have not been studied previously in these systems.

High Flow Systems (ML, GS, NWD, MF)

Our results indicate that the primary source of carbon for microbial communities in high flow systems was variable with location and affected by season. Evidence for carbon limitation was found during the very dry season, and the best indication of mixotrophic communities (i.e., indication of both heterotrophic and autotrophic processes) was found at distance down outflow channels where $\delta^{13}C_{biomass}$ relative to DOC was the most positive (**Figure 4**). Both DIC and DOC were <1 ppmC in the source pools of most high flow systems (with the exception of MF and NWD). The DOC:DIC of high flow sites was <1 (with only three exceptions), and these represent the highest DOC:DIC ratios found in each sampling season (**Supplementary Figure S4**).

The carbon isotopic ratio data indicate the primary carbon source incorporated into biomass in the ML1 and ML2 systems was likely DOC. The $\delta^{13}C_{biomass}$ (**Figure 2**) in these two springs was only slightly depleted or slightly enriched with respect to DOC (**Figure 4**); in cases of $\delta^{13}C_{biomass}$ enrichment relative to DOC, a secondary carbon source of DIC from atmospheric influence or from microbial metabolic byproducts may be invoked. Sampling during the very dry season in the Manleluag area revealed a $\delta^{13}C_{DOC}$ more enriched than that in other seasons, suggesting carbon recycling in the outflow channel due to lower flow rates and less exogenous carbon delivered by meteorological precipitation, resulting in the residual DOC pool harboring more ^{13}C. Modeling of the degree of input from the subsurface $\delta^{13}C_{DIC}$ was inconclusive with a broad range of incorporation of subsurface source $\delta^{13}C_{DIC}$ possible (6–93% incorporation). Given that the measured $\delta^{13}C_{DIC}$ in the ML system is influenced by a wide range of processes we feel the approach used was insufficient to model these dynamics. Our available evidence indicates that carbonate production in the ML systems required a mix of carbon from DIC and atmospheric CO_2. Carbonates analyzed from the source pools of ML1 and ML2 had enriched $\delta^{18}O$ and $\delta^{13}C$ compared to other samples (field "c," **Figure 5**). Carbonates in this range of $\delta^{18}O$ and $\delta^{13}C$ have been interpreted by others as carbonates formed by remineralization or resulting from mixing of endmember fluids. Farther down the outflow at ML2, carbonates are a mix of "fossil" carbonates and freshly formed carbonates with more depleted $\delta^{13}C$ and $\delta^{18}O$ than at the source pools (**Figure 5**, field "d").

The other major high flow system, the GS area and associated NWD, was only sampled in the very dry season and the source of carbon for biomass was variable by location. In the source pool of GS, both $\delta^{13}C_{DOC}$ and $\delta^{13}C_{biomass}$ were enriched compared to all other sample locations (**Figure 2**), and the DOC:DIC was the lowest observed (**Supplementary Figure S4**). The microbial community in the source pool of GS may build biomass from carbon fixation processes, thus producing organic acid byproducts that are ^{13}C enriched relative to the DOC or subsurface DIC endmember (**Supplementary Figure S3**), contributing to the measured $\delta^{13}C_{DOC}$. Alternatively, the measured $\delta^{13}C_{DOC}$ may also be a consequence of the very dry season sample time, similar to that observed in the ML systems described above – a comparison with wet season $\delta^{13}C_{DOC}$ is not available for the GS system. As the fluid at GS flowed downstream, DIC and DOC did not become more abundant (in contrast to the outflow of ML2), and the $\delta^{13}C_{biomass}$ became more depleted relative to the source pool biomass. Rayleigh modeling of the potential input from a subsurface source of DIC was largely inconclusive for the GS system. DIC at NWD is only slightly enriched relative to DOC. Carbonates produced in and near the source pool at GS occur with brucite [$Mg(OH)_2$], and are more ^{13}C

enriched than other samples (and ∼10‰ ^{13}C enriched relative to the next site downstream), possibly representing mixing with endmember fluids or recrystallization of carbonates rather than freshly precipitated carbonates (**Figure 5**, fields "c, d"). However, **Figure 7** shows that the carbonates found in the GS system have the largest difference between the expected $\delta^{18}O$ and the measured $\delta^{18}O$, indicating that rapid carbonate deposition is occurring at this location, even in the source pool. Biomass carbon at the bottom of the outflow channel of GS either incorporated carbon from the carbonates, or influenced the $\delta^{13}C_{carbonates}$. These carbonates had the most negative ^{13}C found in our high flow systems, and there was only <1–4‰ difference between $\delta^{13}C_{biomass}$ and $\delta^{13}C_{carbonate}$. This could indicate that carbonate formed quickly in the outflow and microbial waste product DIC was a key source of carbon used to form the carbonate. Another possibility is that the microbial community utilized carbon from the carbonate to build biomass. There is precedent for this latter concept. In high pH serpentinizing systems found at The Cedars (United States), it has been shown that *Serpentimonas* isolates use $CaCO_3$ in carbon fixation (Suzuki et al., 2014). Future work will be needed to determine if this is a phenomenon is restricted to the low meteorological precipitation season at GS. Regardless, by 4.5 m down the outflow channel, rapid carbonate deposition has resulted in carbonates with some of the most depleted $\delta^{13}C$ and $\delta^{18}O$ relative to other carbonates reported from terrestrial serpentinizing systems.

Evidence for nitrogen fixation in the high flow systems (**Figures 9A,B**) was limited to the MF site (only sampled in the dry season), the source pool of ML1 in the very dry season, and the distant outflow points of ML2 (but excluding the 2012 dry season samples). These results indicate that the ML system communities have potential for nitrogen fixation under some environmental conditions, and more investigation is needed to determine which members of the community are capable of nitrogen fixation and what conditions enable the process. The MF location is slightly higher temperature than ML, with a likely hydrothermal mixing member (Cardace et al., 2015) and nitrogen fixation processes could be attributed to thermophilic members of the community (e.g., Hamilton et al., 2011; Loiacono et al., 2012).

Low Flow, Uncapped Systems (PB2, PB3, PF)

While few data are available for low flow systems in general, those data presented in **Figure 3** indicate that there may be a relationship between more seasonal meteorological precipitation and an increase in concentrations and volume of DIC, DOC, and biomass in the uncapped systems.

Low flow systems have some of the lowest DOC:DIC ratios of all the samples examined (**Supplementary Figure S4**), with little variability between seasons. While few data are available for low flow systems, the uncapped pools featured the most depleted $\delta^{13}C_{biomass}$, relative to DOC, with the largest fractionation from DOC (up to 7‰), regardless of season of sampling. To produce biomass depleted in ^{13}C relative to both DOC and DIC, microorganisms either have to use an unidentified, very $\delta^{13}C$ negative source of carbon, or a large fractionation from DIC needs to occur. These results indicate that even when carbon from surface processes was available in the drier seasons, it is possible that the lower flow, uncapped systems received enough fluid and gas from the subsurface to support a microbial community that engaged in metabolic activities independent from exogenous carbon. During the dry season, these systems may depend on methane or other carbon-bearing gasses sourced from depth. Estimation of the subsurface endmember $\delta^{13}C_{DIC}$ does not produce results that support this hypothesis. However, it is possible that the estimation of the subsurface source $\delta^{13}C_{DIC}$ is inaccurate (**Supplementary Figure S3**) – only a few samples were available for each pool and the Miller-Tans analysis was performed with the PB area samples (capped and uncapped combined) considered as one "site," rather than separate locations that may have differing endmembers in reality. Alternatively, when exogenous carbon was less abundant in the very dry season, the low flow, uncapped systems may recycle carbon similarly as described above for the high flow systems – metagenomic/metatranscriptomic data could help to clarify the carbon flow for the very dry season.

Regardless of the season of sampling, the nitrogen cycle was dependent on surface-sourced nitrogen as no direct evidence from geochemistry points to active subsurface nitrogen fixation (**Figure 9**). The low flow, uncapped systems form carbonates slowly and are enriched in $\delta^{13}C$ and $\delta^{18}O$ relative to other carbonates sampled, suggesting that they have opportunity to undergo recrystallization as they shift toward equilibrium values (fields "c, d," **Figure 5**).

Low Flow, Capped Systems (PB1)

Seasonality affected the carbon isotopic ratio of DIC and DOC in the "capped" low flow pools, the abundance of biomass present, and possibly the source of carbon for the biomass. In the dry season, the pool fluid is separated from atmospheric and most surface influence by the physical barrier of the carbonate skin on the pool surface (**Figure 1g**). The low flow, capped systems appear to be forming carbonates at a rapid rate, both on the bottom of the pools and across the surface of the pool. Some of these data fall outside of identified fields in **Figure 5**, or near field "f," identified as potentially forming via a CO_2 hydroxylation process (Falk et al., 2016). Along with the high flow GS locations, these low flow capped carbonates are the most depleted in $\delta^{13}C$ and $\delta^{18}O$ of the samples, indicating fresh, fast formation. Under these conditions, new carbon and nutrients can only be obtained from slowly flowing gas and fluid from depth, or from solids already present in the pool. **Figure 3** shows how this impacted the DIC, which was more $\delta^{13}C$ depleted than DOC. The DIC pool was likely influenced by metabolic byproducts from microbial metabolism depleted in ^{13}C relative to DIC from surface sources, which were trapped in the fluids under the carbonate cap. The residual DOC pool was also more ^{13}C enriched than in the wet season, indicating that heavier $\delta^{13}C_{DOC}$ was left behind in the DOC pool, non-replenished by surface DOC.

The carbon isotopic signature of the biomass was more ^{13}C depleted than both DIC and DOC, and could be influenced by incorporation of carbon-bearing gasses from depth, such as in the low flow, uncapped pools. We interpret the wet season $\delta^{13}C_{DIC}$ as incorporating atmospheric sources, indicating that the cap was at least periodically washed away by precipitation. Biomass in both the wet and dry season carried a nitrogen isotopic signature indicative of nitrogen fixation (**Figure 9C** and **Table 2**), in contrast to the uncapped low flow systems. It is unclear why the capacity for nitrogen fixation would be more prevalent in these low flow capped systems than the uncapped systems.

CONCLUSION

Our results allow us to broadly characterize the effect of climate and fluid flow on the carbon and nutrient sources of several serpentinization-driven ecosystems in the Zambales and Palawan ophiolites. Increased meteorological precipitation during wetter seasons neither significantly diluted nor added to the DOC and DIC concentrations in the source pools of high flow systems ML1 and ML2, or capped, low flow pool PB1 (the only sample locations where such a direct comparison is possible). Samples farther down outflow channels at ML did have higher concentrations of DOC in the wet season, suggesting that climate may have a larger impact on downstream systems than source pools of high flow systems. However, changes in meteorological precipitation did impact the carbon isotopic ratio of both DIC and DOC in ML and PB1 fluids, which reflected seasonal gain/loss of atmospheric influence on the $\delta^{13}C$ of DIC, and changes in exogenous DOC input.

The primary carbon source in high flow systems was variable, with DOC contributing more to biomass in the ML system, and a mix of DIC and carbonates contributing to biomass in the GS system. Primary carbon resources in the low flow systems may depend more on endogenous than exogenous carbon. Partially, this may be due to smaller "footprints" of the lower flow systems, affecting the surface area available to receive exogenous materials either washed or dropped into the systems. Carbonate "caps" on the very lowest flow systems seasonally isolate the pools from both organic and inorganic exogenous carbon.

The search for a true "subsurface" signature in the Zambales and Palawan serpentinizing systems has concluded that the highest degree of subsurface influence is found in the low flow systems, and in select source pools of the high flow systems (namely GS). Rapid mineral precipitation of carbonate, and $\delta^{13}C_{biomass}$ that was depleted relative to $\delta^{13}C_{DOC}$ highlights potential true subsurface signals. Biomass can not be produced from surface derived $\delta^{13}C_{DOC}$ with a resulting depleted $\delta^{13}C$ relative to that source – therefore a subsurface process can be assumed. The drier the climate, the more the subsurface carbon signature is apparent, making it more likely that processes such as hydrogen based metabolisms (methanogenesis or sulfate reduction, for example) are key in ecosystem functioning. In the very dry season, evidence for $^{13}C_{DOC}$ pool enrichment relative to source DOC, without subsequent $^{13}C_{biomass}$ enrichment indicates that more autotrophy and/or methane-driven (and hydrogen dependent) metabolic schemes were in action while DOC was limited.

Future sampling will focus on obtaining multi-season samples from all these locations, with endmember sampling, to further explore the validity of this conclusion. Higher flow systems at ML should be considered very carefully with respect to subsurface signatures, and the degree of surface impact on the geochemistry and microbiology. Previous work identified relict subsurface genetic capacity in the ML systems, and future work will focus on separating surface vs. subsurface function in microbial systems, with an eye to identifying populations that are actively using hydrogen-driven vs. $C_{organic}$-driven metabolic processes. High flow GS and lower flowing capped systems, including PB1 should be the focus of future subsurface biosphere investigations. Further consideration of carbon and nitrogen cycling potential will include insight from metagenomic datasets. These will clarify the presence/absence of the genetic capacity for the microbial communities found in these locations to participate in carbon and nitrogen cycling, identify metabolisms that use the abundant hydrogen present in these systems, and allow deeper interpretation of these geochemical data presented here.

AUTHOR CONTRIBUTIONS

All authors contributed to the data collection and interpretation in this manuscript.

FUNDING

This work was supported in part by NSF, grant numbers 1147334 and 114610 to DM-D and DC, respectively. Further funding was awarded to DM-D by the Illinois Space Grant Consortium in support of student research. MO was supported by NASA Exobiology grant #NNX15AM08G. Field support was funded by the Alfred P. Sloan Foundation, Deep Carbon Observatory-Deep Energy award number AWD05445 (UCLA Subaward Number 2090 G UA348) to DC.

ACKNOWLEDGMENTS

Dr. Andrew Masterson of the Northwestern Stable Isotope Facility contributed significantly to the isotope analyses presented here. DM-D would like to acknowledge several undergraduate students who helped with this work; Ester Yim, Michael Tanzillo, Alexandra Guzman Biehl, and Mary Chaudhry. This is EDGE lab contribution #6.

SUPPLEMENTARY MATERIAL

The Supplementary Material for this article can be found online at: https://www.frontiersin.org/articles/10.3389/fmicb.2019.00761/full#supplementary-material

REFERENCES

Abrajano, T. A., Pasteris, J. D., and Bacuta, G. C. (1989). Zambales ophiolite, Philippines, I. geology and petrology of the critical zone of the Acoje massif. *Tectonophysics* 168, 65–100.

Abrajano, T. A., and Sturchio, N. C. (1990). Geochemistry of reduced gas related to serpentinization of the Zambales ophiolite, Philippines. *Appl. Geochem.* 5, 625–630.

Beccaluva, L., Chinchilla-Chaves, A. L., Coltori, M., Giunta, G., Sienna, F., and Vaccaro, C. (1999). Petrological and structural significance of the Santa Elena-Nicoya ophiolitic complex in Costa Rica and geodynamic implications. *Eur. J. Mineral.* 11, 1091–1107.

Berg, I. A., Kockelkorn, D., Ramos-Vera, W. H., Say, R. F., Zarzycki, J., Hugler, M., et al. (2010). Autotrophic carbon fixation in Archaea. *Nat. Rev. Microbiol.* 8, 447–460. doi: 10.1038/nrmicro2365

Biddle, J. F., Sylvan, J. B., Brazelton, W. J., Tully, B. J., Edwards, K. J., Moyer, C. L., et al. (2012). Prospects for the study of evolution in the deep biosphere. *Front. Microbiol.* 2:285. doi: 10.3389/fmicb.2011.00285

Blake, D., Vaniman, D., Achilles, C., Anderson, R., Bish, D., Bristow, T., et al. (2012). Characterization and calibration of the CheMin mineralogical instrument on Mars Science Laboratory. *Space Sci. Rev.* 170, 341–399. doi: 10.1007/s11214-012-9905-1

Bottinga, Y. (1969). Calculated fractionation factors for carbon and hydrogen isotope exchange in the system calcite–carbon dioxide–graphite–methane–hydrogen– water vapor. *Geochim. Cosmochim. Acta* 33, 49–64.

Bowen, G. J. (2019). *The Online Isotopes in Precipitation Calculator*. Available at: http://www.waterisotopes.org (accessed January 20, 2019).

Bowen, G. J., and Revenaugh, J. (2003). Interpolating the isotopic composition of modern and meteoric precipitation. *Water Res. Res.* 39:1299.

Bowen, G. J., Wassenaar, L. I., and Hobson, K. A. (2005). Global application of stable hydrogen and oxygen isotopes to wildlife forensics. *Oecologia* 143, 337–348.

Brazelton, W. J., Morrill, P. L., Szponar, N., and Schrenk, M. O. (2013). Bacterial communities associated with subsurface geochemical processes in continental serpentinite springs. *Appl. Environ. Microbiol.* 79, 3906–3916. doi: 10.1128/AEM.00330-13

Brunner, B., Contreras, S., Lehman, M. F., Matantseva, O., Rollog, M., Kalvelage, T., et al. (2013). Nitrogen isotope effects induced by anammox bacteria. *Proc. Natl. Acad. Sci.* 110, 18994–18999. doi: 10.1073/pnas.1310488110

Cardace, D., Meyer-Dombard, D. R., Woycheese, K. M., and Arcilla, C. A. (2015). Feasible metabolisms in high pH springs of the Philippines. *Front. Microbiol.* 6:10. doi: 10.3389/fmicb.2015.00010

Clark, I. D., Fontes, J. C., and Fritz, P. (1992). Stable isotope disequilibria in travertine from high pH waters: Laboratory investigations and field observations from Oman. *Geochim. Cosmochim. Acta* 56, 2041–2050.

Deamer, D., and Damer, B. (2017). Can life begin on Enceladus? A perspective from hydrothermal chemistry. *Astrobiology* 17, 834–839. doi: 10.1089/ast.2016.1610

Delwiche, C. C., and Steyn, P. L. (1970). Nitrogen isotope fractionation in soils and microbial reactions. *Environ. Sci. Technol.* 4, 929–935.

Ehlmann, B. L., Mustard, J. F., and Murchie, S. L. (2010). Geologic setting of serpentine deposits on Mars. *Geophys. Res. Lett.* 37:L06201.

Eiler, J. M. (2007). "Clumped-isotope" geochemistry – The study of naturally-occurring, multiply-substituted isotopologues. *Earth Planet. Sci. Lett.* 262, 309–327.

Emrich, K., Ehhalt, D. H., and Vogel, J. C. (1970). Carbon isotope fractionation during the precipitation of calcium carbonate. *Earth Planet. Sci. Lett.* 8, 363–371.

Falk, E. S., Gui, W., Paukert, A. N., Matter, J. M., Mervine, E. M., and Kelemen, P. B. (2016). Controls on the stable isotope composition of travertine from hyperalkaline springs in Oman: Insights from clumped isotope measurements. *Geochim. Cosmochim. Acta* 192, 1–28.

Frey, C., Hietanen, S., Jurgens, K., Labrenz, M., and Voss, M. (2014). N and O isotope fractionation in nitrate during chemolithoautotrophic denitrification by *Sulfurimonas gotlandica*. *Environ. Sci. Technol.* 48, 13229–13237. doi: 10.1021/es503456g

Friedman, I., O'Neil, J. R., (1977). Compilation of stable isotope fractionation factors of geochemical interest. In *Data of Geochemistry, U.S. Geological Survey Professional Paper 440-KK*, 6th edn ed. M. Fleischer (Reston VA: U.S.G.S).

Halas, S., Szaran, J., and Niezgoda, H. (1997). Experimental determination of carbon isotope equilibrium fractionation between dissolved carbonate and carbon dioxide. *Geochim. Cosmochim. Acta* 61, 2691–2695.

Hamilton, T. L., Lange, R. K., Boyd, E. S., and Peters, J. W. (2011). Biological nitrogen fixation in acidic high-temperature geothermal springs in Yellowstone National Park, Wyoming. *Environ. Microbiol.* 13, 2204–2215. doi: 10.1111/j.1462-2920.2011.02475.x

Havig, J. R., Raymond, J., Meyer-Dombard, D. R., Zolotova, N., and Shock, E. L. (2011). Merging isotopes and community genomics in a siliceous sinter-depositing hot spring. *J. Geophys. Res.* 116:G001005.

Hayes, J. M. (1993). Factors controlling 13C contents of sedimentary organic compounds: principles and evidence. *Mar. Geol.* 113, 111–125.

Hayes, J. M. (2001). Fractionation of carbon and hydrogen isotopes in bio-synthetic processes. *Rev. Min. Geochem.* 43, 225–278.

House, C. H., Schopf, J. W., and Stetter, K. O. (2003). Carbon isotopic fractionation by archaeans and other thermophilic prokaryotes. *Organ. Geochem.* 34, 345–356.

Ilao, K. A., Morley, C. K., and Aurelio, M. A. (2018). 3D seismic investigation of the structural and stratigraphic characteristics of the Pagasa Wedge, Southwest Palawan Basin, Philippines, and their tectonic implications. *J. Asian Earth Sci.* 154, 213–237.

Kallmeyer, J., Pockalny, R., Adhikari, R. R., Smith, D. C., and D'Hondt, S. (2012). Global distribution of microbial abundance and biomass in subsurface sediment. *Proc. Natl Acad. Sci.* 109, 16213–16216.

Krzycki, J. A., Kenealy, W. R., DeNiro, M. J., and Zeikus, J. G. (1987). Stable carbon isotope fractionation by *Methanosarcina barkeri* during methanogenesis from acetate, methanol or carbon dioxide–hydrogen. *Appl. Environ. Microbiol.* 53, 2597–2599.

Lang, S. Q., Fruh-Green, G. L., Bernasconi, S. M., Lilley, M. D., Proskurowski, G., Mehay, S., et al. (2012). Microbial utilization of abiogenic carbon and hydrogen in a serpentinite-hosted system. *Geochim. Cosmochim. Acta* 92, 82–99.

Lau, M. C. Y., Cameron, C., Magnabosco, C., Brown, C. T., Schilkey, F., Grim, S., et al. (2014). Phylogeny and phylogeography of functional genes shared among seven terrestrial subsurface metagenomes reveal N-cycling and microbial evolutionary relationships. *Front. Microbiol.* 5:531. doi: 10.3389/fmicb.2014.00531

Li, L., Sherwood Lollar, B., Li, H., Wortmann, U. G., and Lacrampe-Couloume, G. (2012). Ammonium stability and nitrogen isotope fractionations for NH+4 – NH3(aq)–NH3(gas) systems at 20–70 °C and pH of 2–13: Applications to habitability and nitrogen cycling in low-temperature hydrothermal systems. *Geochim. Cosmochim. Acta* 84, 280–296.

Loiacono, S., Meyer-Dombard, D. R., Havig, J. R., Poret-Peterson, A., Hartnett, H., and Shock, E. L. (2012). Evidence for high-temperature in situ nifH transcription in an alkaline hot spring of Lower Geyser Basin, Yellowstone National Park. *Environ. Microbiol.* 14, 1272–1283. doi: 10.1111/j.1462-2920.2012.02710.x

Lomstein, B. A., Langerhuus, A. T., D'Hondt, S., Jorgensen, B. B., and Spivack, A. J. (2012). Endospore abundance, microbial growth and necromass turnover in deep sub-seafloor sediment. *Nature* 484, 101–104. doi: 10.1038/nature10905

McCollom, T. M., and Bach, W. (2009). Thermodynamic constraints on hydrogen generation during serpentinization of ultramafic rocks. *Geochim. Cosmochim. Acta* 73, 856–875.

McCollom, T. M., Sherwood Lollar, B., Lacrampe-Couloume, G., and Seewald, J. S. (2010). The influence of carbon source on abiotic organic synthesis and carbon isotope fractionation under hydrothermal conditions. *Geochim. Cosmochim. Acta* 74, 2717–2740.

McMahon, S., and Parnell, J. (2014). Weighing the deep continental biosphere. *FEMS Microbiol. Ecol.* 87, 113–120. doi: 10.1111/1574-6941.12196

Menez, B., Pasini, V., and Brunelli, D. (2012). Life in the hydrated suboceanic mantle. *Nat. Geosci.* 5, 133–137.

Mervine, E. M., Humphris, S. E., Sims, K. W. W., Kelemen, P. B., and Jenkins, W. J. (2014). Carbonation rates of peridotite in the Samail Ophiolite, Sultanate of Oman, constrained through 14C dating and stable isotopes. *Geochim. Cosmochim. Acta* 126, 371–397.

Meyer-Dombard, D. R., Woycheese, K. M., Yargiçoglu, E. N., Cardace, D., Shock, E. L., Güleçal-Pektas, Y., et al. (2015). High pH microbial ecosystems in a newly discovered, ephemeral, serpentinizing fluid seep at Yanartas; (Chimera), Turkey. *Front. Extr. Microbiol.* 5:723. doi: 10.3389/fmicb.2014.00723.

Miller, J. B., and Tans, P. P. (2003). Calculating isotopic fractionation from atmospheric measurements at various scales. *Tellus B* 55, 207–214. doi: 10.1034/j.1600-0889.2003.00020.x.

Mobius, J. (2013). Isotope fractionation during nitrogen remineralization (ammonification): implications for nitrogen isotope biogeochemistry. *Geochim. Cosmochim. Acta* 105, 422–432.

Morrill, P. L., Kuenen, J. G., Johnson, O. J., Suzuki, S., Rietze, A., Sessions, A. L., et al. (2013). Geochemistry and geobiology of a present-day serpentinization site in California: the Cedars. *Geochim. Cosmochim. Acta* 109, 222–240.

O'Neil, J. R., Clayton, R. N., and Mayeda, T. K. (1969). Oxygen isotope fractionation in divalent metal carbonates. *J. Chem. Phys.* 51, 5547–5558.

Osburn, M. R., LaRowe, D. E., Momper, L. M., and Amend, J. P. (2014). Chemolithotrophy in the continental deep subsurface: stanford underground research facility (SURF), USA. *Front. Microbiol.* 5:610. doi: 10.3389/fmicb.2014.00610

Osburn, M. R., Sessions, A. L., Pepe-Ranney, C., and Spear, J. R. (2011). Hydrogen-isotopic variability in fatty acids from Yellowstone National Park hot spring microbial communities. *Geochim. Cosmochim. Acta* 75, 4830–4845.

Parkes, R. J., Cragg, B., Roussel, E., Webster, G., Weightman, A., and Sass, H. (2014). A review of prokaryotic populations and processes in sub-seafloor sediments, including biosphere: geosphere interactions. *Mar. Geol.* 352, 409–425.

Pearson, A., Hurley, S. J., Shah Walter, S. R., Kusch, S., Lichtin, S., and Zhang, Y. G. (2016). Stable carbon isotope ratios of intact GDGTs indicate heterogeneous sources to marine sediments. *Geochim. Cosmochim. Acta* 181, 18–35.

Rosenfeld, W. D., and Silvermann, S. R. (1959). Carbon isotope fractionation in bacterial production of methane. *Science* 130, 1658–1659.

Rowe AR, Yoshimura M, LaRowe DE, Bird LJ, Amend JP, Hashimoto K, Nealson KH, Okamoto A (2017). In situ electrochemical enrichment and isolation of a magnetite-reducing bacterium from a high pH serpentinizing spring. *Environ. Microbiol.* 19, 2272–2285. doi: 10.1111/1462-2920.13723

Russell, M. J., Barge, L. M., Bhartia, R., Bocanegra, D., Bracher, P. J., Branscomb, E., et al. (2014). The drive to life on wet and icy worlds. *Astrobiology* 14, 308–343. doi: 10.1089/ast.2013.1110

Sanchez-Murillo, R., Gazal, E., Schwarzenbach, E. M., Crespo-Medina, M., Schrenk, M. O., Boll, J., et al. (2014). Geochemical evidence for active tropical serpentinization in the Santa Elena Ophiolite, Costa Rica: An analog of a humid early Earth? *Geochem. Geophys. Geosyst.* 15, 1783–1800. doi: 10.1002/2013GC005213

Schrenk, M. O., and Brazelton, W. J. (2013). Serpentinization, carbon, and deep life. *Rev. Mineral. Geochem.* 75, 575–606.

Schubotz, F., Meyer-Dombard, D. R., Bradley, A. S., Fredricks, H. F., Hinrichs, K.-U., Shock, E. L., et al. (2013). Spatial and temporal variability of biomarkers and microbial diversity reveal metabolic and community flexibility in streamer biofilm communities in the lower Geyser Basin, Yellowstone National Park. *Geobiology* 11, 549–569. doi: 10.1111/gbi.12051

Silverman, M. P., and Oyama, V. I. (1968). Automatic apparatus for sampling and preparing gases for mass spectral studies of carbon isotope fractionation during methane metabolism. *Anal. Chem.* 40, 1833–1877.

Sleep, N. H., Bird, D. K., and Pope, E. C. (2011). Serpentinite and the dawn of life. *Philos. Trans. R. Soc.* 366, 2857–2869. doi: 10.1098/rstb.2011.0129

Solden, S., Lloyd, K., and Wrighton, K. (2016). The bright side of microbial dark matter: lessons learned from the uncultivated majority. *Curr. Opin. Microbiol.* 31, 217–226. doi: 10.1016/j.mib.2016.04.020

Suzuki, S., Kuenen, J. G., Schipper, K., van der Velde, S., Ishii, S., Wu, A., et al. (2014). Physiological and genomic features of highly alkaliphilic hydrogen-utilizing Betaproteobacteria from a continental serpentinizing site. *Nat. Commun.* 5:3900 doi: 10.1038/ncomms4900.

Szponar, N., Brazelton, W. J., Schrenk, M. O., Bower, D. M., Steele, A., and Morrill, P. L. (2013). Geochemistry of a continental site of serpentinization, the Tablelands Ophiolite, Gros Morne National Park: a Mars analogue. *Icarus* 224, 286–296.

Turner, J. V. (1982). Kinetic fractionation of carbon-13 during calcium carbonate precipitation. *Geochim. Cosmochim. Acta* 46, 1183–1191.

Urschel, M. R., Kubo, M. D., Hoehler, T. M., Peters, J. W., and Boyd, E. S. (2015). Carbon source preference in chemosynthetic hot spring communities. *Appl. Environ. Microbiol.* 81, 3834–3847. doi: 10.1128/AEM.00511-15

Vance, S. D., Hand, K. P., and Pappalardo, R. T. (2016). Geophysical controls of chemical disequilibria in Europa. *Geophys. Res. Lett.* 43, 4871–4879.

Waldron, S., Fallick, A. E., and Hall, A. J. (1998). Comment on "Spatial distribution of microbial methane production pathways in temperate zone wetland soils: stable carbon and hydrogen isotope evidence" by E. R. C Hornibrook, F. J. Longstaffe and W. S. Fyfe. *Geochim. Cosmochim. Acta* 62, 369–372.

Woycheese, K. M., Meyer-Dombard, D. R., Cardace, D., Argayosa, A. M., and Arcilla, C. A. (2015). Out of the dark: transitional subsurface-to-surface microbial diversity in a terrestrial serpentinizing seep (Manleluag, Pangasinan, the Philippines). *Front. Microbiol.* 6:44. doi: 10.3389/fmicb.2015.00044

Wunderlich, A., Meckenstock, R., and Einsiedl, F. (2012). Effect of different carbon substrates on nitrate stable isotope fractionation during microbial denitrification. *Environ. Sci. Technol.* 46, 4861–4868. doi: 10.1021/es204075b

Zhang, X., Sigman, D. M., Morel, F. M. M., and Kraepiel, A. M. L. (2014). Nitrogen isotope fractionation by alternative nitrogenases and past ocean anoxia. *Proc. Natl. Acad. Sci.* 111, 4782–4787. doi: 10.1073/pnas.1402976111

Conflict of Interest Statement: The authors declare that the research was conducted in the absence of any commercial or financial relationships that could be construed as a potential conflict of interest.

frontiers in Microbiology

ORIGINAL RESEARCH
published: 10 July 2019
doi: 10.3389/fmicb.2019.01545

H_2 Kinetic Isotope Fractionation Superimposed by Equilibrium Isotope Fractionation During Hydrogenase Activity of *D. vulgaris* Strain Miyazaki

Michaela Löffler, Steffen Kümmel, Carsten Vogt and Hans-Hermann Richnow*

Department of Isotope Biogeochemistry, Helmholtz Centre for Environmental Research – UFZ, Leipzig, Germany

We determined ^{2}H stable isotope fractionation at natural abundances associated with hydrogenase activity by whole cells of *Desulfovibrio vulgaris* strain Miyazaki F expressing a NiFe(Se) hydrogenase. Inhibition of sulfate reduction by molybdate inhibited the overall oxidation of hydrogen but still facilitated an equilibrium isotope exchange reaction with water. The theoretical equilibrium isotope exchange δ^2H-values of the chemical exchange reaction were identical to the hydrogenase reaction, as confirmed using three isotopically different waters with δ^2H-values of – 62, +461, and + 1533‰. Expected kinetic isotope fractionation of hydrogen oxidation by non-inhibited cells was also superimposed by an equilibrium isotope exchange. The isotope effects were solely catalyzed biotically as hydrogen isotope signatures did not change in control experiments without cells of *D. vulgaris* Miyazaki.

Keywords: hydrogenase, *D. vulgaris* strain Miyazaki, monitoring, GC-IRMS, equilibrium isotope fractionation, kinetic isotope fractionation, hydrogen isotopes

OPEN ACCESS

Edited by:
Eric Boyd,
Montana State University,
United States

Reviewed by:
Wolfgang Buckel,
University of Marburg, Germany
Christopher L. Hemme,
University of Rhode Island,
United States

****Correspondence:***
Carsten Vogt
carsten.vogt@ufz.de

Specialty section:
This article was submitted to Microbial Physiology and Metabolism, a section of the journal Frontiers in Microbiology

Received: *30 April 2019*
Accepted: *20 June 2019*
Published: *10 July 2019*

Citation:
Löffler M, Kümmel S, Vogt C and Richnow H-H (2019) H_2 Kinetic Isotope Fractionation Superimposed by Equilibrium Isotope Fractionation During Hydrogenase Activity of D. vulgaris Strain Miyazaki. Front. Microbiol. 10:1545. doi: 10.3389/fmicb.2019.01545

INTRODUCTION

Many microorganisms use hydrogen (H_2) or protons (H^+) as electron donors or acceptors, coupled to the oxidation or production of H_2. The enzyme catalyzing H_2 oxidation or production is a metalloenzyme termed hydrogenase, for which several differently structured isoenzymes are known (Vignais and Billoud, 2007; Greening et al., 2016). The most abundant and commonly studied type of hydrogenase contains a NiFe(Se)-active center (Vignais and Billoud, 2007). The reaction catalyzed by hydrogenases can be formulated as follows (Eq. 1).

$$H_2 \Leftrightarrow 2H^+ + 2e^- \quad (1)$$

Such a reaction usually leads to a kinetic isotope fractionation, which is defined as the ratio of the rate constants for light and heavy isotopes within the unidirectional reaction of H_2 to two protons releasing two electrons. The isotope fractionation is a result of the slightly lower activation energy needed to cleave and form bonds of lighter isotopes compared to heavy isotopes in this (bio-) chemical reaction. The kinetic isotope fractionation leads to the predominant reaction of light isotopomers, which implies that the remaining fraction would get heavier during the reaction. For the oxidation of molecular hydrogen at natural abundances, this would result in accumulation of

^2H (deuterium) in the remaining fraction. However, during the oxidation of H_2 (Eq. 1), an isotopic exchange with water (Eq. 2) was observed simultaneously to the kinetic isotope effect (Arp and Burris, 1982; Vignais et al., 1997, 2002; Yang et al., 2012).

$$H^2H + H_2O \Leftrightarrow H_2 + H^2HO \quad (2)$$

During the isotope exchange of gaseous hydrogen with water, the heavy isotopes of molecular hydrogen (^2H) exchange with the light hydrogen isotopes (^1H) of the water, until an equilibrium isotope value for molecular hydrogen is reached. This is an inverse isotope effect compared to kinetic isotope fractionation, where the H_2 will become enriched in deuterium over time and thus, the δ^2H-value will become more positive. If kinetic and equilibrium isotope fractionation take place in parallel, the oxidation and the isotope exchange reaction cannot be separated from each other. In order to understand overall isotope effects during H_2-consumption, the equilibrium isotope fractionation of the isotopic exchange reaction must be studied separately. Therefore we designed experiments to study both H_2-oxidation and isotope exchange with cell suspensions of *Desulfovibrio vulgaris* strain Miyazaki F, which expresses one of the best studied NiFe hydrogenases, as well as a NiFe(Se) suited for H_2 oxidation (Yagi et al., 1976; Deckers et al., 1990; Ogata et al., 2002; Foerster et al., 2003; Fichtner et al., 2006; Pandelia et al., 2010; Nonaka et al., 2013; Riethausen et al., 2013). We hypothesized that the addition of molybdate will inhibit electron flow to sulfate (Peck, 1959; Wolin and Miller, 1980) and thus, only the isotopic exchange reaction would be observable.

The aim of our study was to analyze the equilibrium isotope effect of the isotope exchange reaction and the kinetic isotope effect of the unidirectional oxidation reaction of hydrogen, in order to eventually monitor hydrogenase activity in environmental samples and settings, e.g., during hydrogen underground storage. This method, based on natural abundant stable hydrogen isotopes of gaseous samples, would allow *in situ* assessment of hydrogenase activity without further treatment of samples.

MATERIALS AND METHODS

Chemicals

All chemicals until otherwise stated were purchased from Merck Chemicals GmbH (Darmstadt, Germany). Deuterium-enriched waters were prepared by mixing 1 l sterilized tap water water (Merck Millipore, Germany) with either 250 µl or 100 µl ^2H_2O (99.9%; Merck Chemicals, Germany).

Culture and Cultivation Conditions

Desulfovibrio vulgaris strain Miyazaki F (DSM 19637) was obtained from the DSMZ (Deutsche Sammlung von Mikroorganismen und Zellkulturen, Braunschweig, Germany). The strain was grown in a mineral medium for sulfate-reducers, which consisted of NH_4Cl (0.3 g/l), KH_2PO_4 (0.4 g/l), $CaCl_2$ (0.075 g/l), Na_2SO_4 (2 g/l), $MgSO_4$ * 7 H_2O (1 g/l), 1 ml trace element solution SL-10, 0.1 ml selenite-tungstate solution, 4 ml 50 % Na-DL-lactate, 2 ml vitamin solution, 10 ml 1 M $NaHCO_3$ solution, 2 ml 1 M Na-acetate solution. 1 M L-cysteine solution was used for reduction. 0.1 mg/l resazurin was used as redox indicator. The selenite-tungstate solution contained per 100 ml: 0.5 g/l NaOH, 3 mg/l Na_2SeO_3 * 5 H_2O and 4 mg/l Na_2WO_4 * 2 H_2O. The vitamin solution contained per 100 ml: 1 mg biotin, 1 mg folic acid, 25 mg pyridoxine-HCl, 25 mg thiamine-HCl * 2 H_2O, 5 mg riboflavin, 25 mg nicotinic acid, 25 mg D-Ca-pantothenate, 0.5 mg vitamin B_{12}, 25 mg p-aminobenzoic acid and 25 mg lipoic acid. All components, except the last four, were mixed in sterilized tap water (Merck Millipore, Germany) and purged with 75% N_2 and 25% CO_2 until they became virtually oxygen-free and were autoclaved subsequently. The remaining components were added within an anaerobic glovebox (Toepffer Lab Systems, Germany).

Experiments with cell suspensions were performed with cells pre-grown on 28 mM lactate and 22 mM sulfate at 30°C and 120 rpm on a Multitron incubation shaker (Infors, Germany). At optical densities above 0.2 absorbance with no further increase in cell density, 50 ml each were transferred into 120 ml serum bottles in the glovebox, which was filled with a mixture of N_2 (97–98%) and H_2 (2–3%) and crimped close with PTFE-coated chlorobutyl-isoprene septa (Thermo Fisher Scientific, Germany) before the start of the experiment.

Three sets of isotope fractionation experiments were designed with these cells: one set in which cells were inhibited by molybdate, one in which the headspace had been purged to reduce sulfide load, and one without further treatment. For the inhibited setups, six of the bottles each were treated with 20 mM molybdate. Therefore, 2 ml of a 0.5 M sodium molybdate solution was added to each bottle, yielding yellow-orange molybdo-sulfide-complexes (Wolin and Miller, 1980; Biswas et al., 2009). Both the purged and untreated setups consisted of five bottles of cell suspension each. The headspace in the purged setups was exchanged with N_2 to eliminate H_2S-burden in the headspace and reduce potential inhibition by sulfides.

In all samples 12 ml H_2 were hereafter exchanged with the existing headspace with a syringe and an empty needle while bottles were tilted to remove headspace only. Bottles were kept at 30°C and 120 rpm (Multitron incubation shaker, Infors, Germany). For abiotic controls cell suspensions were inactivated by incubation at 80°C in a water bath for 20 min and subsequent addition of 0.3 ml 10 M NaOH, yielding pH 12.

All experimental setups were performed in two replicates using water at natural abundance (δ^2H-H_2O = −62‰) and water enriched in ^2H by adding 100 µl ^2H_2O resulting in an isotope composition of δ^2H-H_2O = +461‰ One experiment with molybdate for inhibition of sulfate reduction was conducted with enriched water (250 µl ^2H_2O) to yield a final isotope composition of δ^2H-H_2O = + 1533‰. Bottles were sacrificed at different time points in a water bath at 80°C for 20 min and stored upside down after the addition of 10 M NaOH before hydrogen isotopes of H_2 in the headspace were analyzed. The setup with enriched water (δ^2H-H_2O = + 1533‰) was sacrificed in different periods of time than the other experiments, in order to gain insight into the initial reaction. NaOH was added to terminate microbial activity and to remove CO_2 from the

headspace by precipitation of sodium bicarbonate. CO_2-removal was necessary for subsequent isotope analysis, as the column used for gas chromatography (GC) would retain it. 100 to 300 µl sample volume were transferred via syringe into 1 ml 3% (w/v) Zn-acetate and stored at −20°C for downstream processing. Sulfides in the headspace of the bottles were eliminated due to precipitation as ZnS by the addition of 3 ml 3 (w/v) % Zn-acetate.

Analytical Methods

Sulfide Measurements

Sulfides were measured as previously described (Cline, 1969; Kleinsteuber et al., 2008) against a blank control. Previously frozen samples were thawed and mixed with 4 ml water and 0.4 ml of Cline's solution. The mixtures were stored in the dark for 20 min before photometric measurement on an UV-1800 (Shimadzu, Germany) at 670 nm. Due to the high concentrations of sulfides, samples were diluted before measurement. Optical densities of cell suspensions were determined on an UV-1800 (Shimadzu, Germany) at 600 nm. 1 ml culture solution was transferred via syringe into a cuvette filled with a few mg of Na-dithionite, closed with parafilm and shaken until dissolved and then measured using water as control.

Isotope Measurement

Hydrogen isotope measurements were performed on a GC-isotope ratio mass spectrometer (IRMS) system (**Supplementary Figure 1**) (7890A, Agilent Technologies, Germany; GC-IsoLink II Thermo Fisher Scientific, Germany; Conflo IV Thermo Fisher Scientific, Germany; Finnigan MAT 253, Thermo Fisher Scientific, Germany) equipped with a J&W CP-Molsieve 5Å GC Column (50 m, 0.32 mm, 30 µm, Agilent Technologies, Germany). An empty ceramic tube was kept isothermal at 500°C inside the GC-IsoLink and the GC column was kept at 40°C during measurements. An additional cold trap operated with liquid nitrogen was installed after the GC to remove water to keep the water background within the ion source of the IRMS low. After 2 h of runtime, the column was heated to 250°C and held for at least 10 min remove residual water vapor and residual CO_2 from the GC column.

0.2 ml headspace injections were made manually at split-ratio of 1:25 with a gas-tight syringe in an interval of roughly eight minutes needed for elution of H_2 and permanent gases. The analytical system was evaluated for reproducibility and isotope artifacts. It was found to be reproducible and deliver true values within the uncertainty of 0.7 ± 0.4‰.

Both the normal and the δ^2H-enriched waters were measured with an elemental analysis-chromium/high temperature conversion (EA-Cr/HTC)-IRMS system (HEKAtech, Germany) coupled via the Conflo IV (Thermo Fisher Scientific, Germany) to the same IRMS instrument (Gehre et al., 2017). All results are reported in the delta notation (Eq. 3) and according to the guidelines for stable isotope measurements (Coplen, 2011).

$$\delta\,[‰] = \left(\frac{R_{sample}}{R_{standard}} - 1\right) * 1000 \qquad (3)$$

The ratio of heavy to light isotopes (R_{sample}) in a compound is reported in δ-notation; for hydrogen, samples will be compared to Vienna Standard Mean Ocean Water (VSMOW) as standard with an isotope ratio of 155.76 ± 0.1 ppm ($R_{standard}$). A laboratory standard, made of 10% H_2 in N_2, with a δ^2H-value of −205‰ was used for reference. The auto-protonation factor (H_3^+ factor) was determined daily and remained stable at 8.24 ± 0.05. Theoretical equilibrium isotope values, mainly dependent on temperature and the isotope signature of water, were calculated according to a formula previously described (Horibe and Craig, 1995).

Assessment of H_2 Concentrations

The concentration of H_2 was measured with the GC-IRMS. For concentration measurements a defined volume of 10% H_2 was prepared using 120 ml serum bottles which were purged with N_2 before. Twelve ml H_2 were exchanged with the gaseous phase by a syringe and an empty needle while the bottle was held upside down. This sample was prepared daily and used for external calibration of the concentration measurement. Therefore the sample was injected three times at the start of each run, and all following samples were normalized to the average area under the curve of all controls in this measurement period. Intensities of external calibration were stable over 20 days, leading to overall variations in H_2-concentration of ± 1.5%. Initial concentrations of H_2 between setups and replicates varied about 5% of the response, probably dependent on handling speed and temperature in the laboratory during exchange of H_2, as well as gas-tightness of the syringe used for injections.

RESULTS

Measurement of Hydrogen Stable Isotopes

The isotope signatures of the different waters were determined to be δ^2H-H_2O = −62 ± 2‰, +461 ± 1‰, and +1533 ± 2‰, respectively. For the sterilized tap water in Leipzig (δ^2H-H_2O = −62‰), an equilibrium δ^2H-value for H_2 of – 744‰ was calculated. The enriched water setups (δ^2H-H_2O = + 461‰ and δ^2H-H_2O = + 1533‰) were calculated to equilibrate with a theoretical value for H_2 of δ^2H = −606‰ and δ^2H = −317‰, respectively.

Control experiments with H_2 in the headspace and sterilized tap water or culture medium showed no significant change in the isotopic signature over the experimental timeframe of 18 days (**Figure 1**), with stable δ^2H-values of δ^2H = −141.2‰ and δ^2H = −142.2‰. These were identical to the isotope value of the pure H_2 used (δ^2H = −139‰), taking usual uncertainties into account. The δ^2H signature of the hydrogen gas used in the anaerobic glove box was substantially lighter (approx. δ^2H = −645‰) than the signature of the H_2 gas used in the whole cell experiments, leading to a shift of Δ^2H = 65‰ (**Figure 1**) when mixed.

H_2-Oxidation by Non-inhibited Cells

Experiments With Reduced Sulfide Concentration

To reduce concentrations of sulfide which may affect the metabolism of *D. vulgaris*, the headspace of culture bottles were

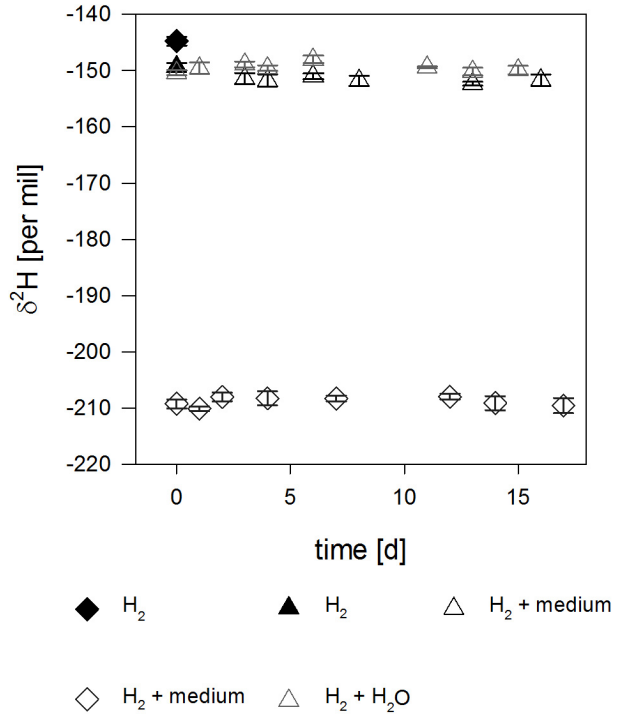

FIGURE 1 | Isotope signal over time in the abiotic controls. Filled symbols correspond to pure H_2 used for the experiment and empty symbols correspond to H_2 in the headspace of serum bottles filled with either water (gray) or medium (black). Please note the depleted δ^2H-values of H_2 (empty diamonds) for the medium prepared in the anaerobe glovebox due to mixing of two isotopically different H_2 sources (see text).

purged with N_2. The sulfide concentrations after purging were typically roughly 6 mM.

13.9 ± 0.7% and 12.2 ± 0.3% H_2 were oxidized within 4 days (**Table 1** and **Figure 2D**). Sulfide concentrations increased from 6.0 ± 2.2 mM and 6.4 ± 0.1 mM to 17.9 mM and 16.7 ± 0.2 mM, respectively, in 3 days (**Figure 2A**). Hydrogen isotope values changed slowly toward depletion in the beginning from $\delta^2H = -309.0 \pm 0.7‰$ and $\delta^2H = -163.2 \pm 0.9‰$, before the reaction gained speed (**Table 2** and **Figure 3**), yielding $\delta^2H = -678.6 \pm 1.5‰$ and $\delta^2H = -475.3 \pm 4.1‰$ after 3 days.

Experiments With High Sulfide Concentration

In the experiments without further treatment to reduce the amount of sulfides present, 20.4 ± 1.0% H_2 and 19.5 ± 0.4% H_2, respectively were consumed within 2 days in normal water (**Table 1** and **Figure 2E**). 17.8 mM and 16.5 mM sulfides were produced starting from 9.48 ± 1.7 mM and 11.2 ± 0.6 mM until day three (**Figure 2B**). The δ^2H of hydrogen in the bottles' headspace was rapidly decreasing from $\delta^2H = -220.4 \pm 0.7‰$ and $\delta^2H = -268.4 \pm 0.5‰$ to $\delta^2H = -702.1 \pm 5.7‰$ and $\delta^2H = -408.1 \pm 2.8‰$ after 1.5 to 2 days (**Table 2** and **Figure 3**). Concentrations at the last measureable time-points were 1.9 ± 0.1% and 1.8 ± 0.1% H_2.

H_2 Isotope Exchange by Cells Inhibited With Molybdate

Molybdate was used to inhibit the electron flow to the electron acceptor sulfate. In molydate-amended cultures, the H_2 concentrations were almost constant with 14.3 ± 1.3%, 13.9 ± 1.7% and 15.8 ± 3.3% H_2. Thus, no consumption of H_2 in the molybdate setups was observed (**Table 1** and **Figure 2F**). Furthermore, the sulfide concentrations did not increase and were stable between 2.5 to 3.5 mM (**Figure 2C**), indicating that sulfate reduction to sulfide was completely inhibited. In all experimental setups inhibited by molybdate, hydrogen isotopes in the headspace were depleting in deuterium starting from $\delta^2H = -246.5 \pm 0.7‰$, $\delta^2H = -223.9 \pm 0.5‰$, and $\delta^2H = -162.4 \pm 1.7‰$ (**Table 2**) and stabilized at $\delta^2H = -735.8 \pm 0.4‰$, $\delta^2H = -599.4 \pm 0.1‰$, and $\delta^2H = -327.3 \pm 0.3‰$ for the differently enriched waters after 6 days (**Figure 3**).

DISCUSSION

No changes in the isotope signature of H_2 for both culture medium and water in the abiotic controls could be observed, even though H_2-concentrations decreased with continuous sampling of the same bottles (**Supplementary Figure 2**). Most studies on hydrogen isotope exchange with water used platinum or palladium as a catalyst and subsequent equilibration times of a few hours were reported at, e.g., 20°C (Crist and Dalin, 1934; Farkas and Farkas, 1934; Horiuti and Polanyi, 1934; Farkas, 1936; Suess, 1949; Rolston et al., 1976). It is therefore reasonable to assume that isotope exchange without a catalyst is too slow to be assessable in the experimental timeframe used in this study. Subsequently, it is unlikely that the isotope signal in environmental samples could be significantly affected by minerals, as catalysts are needed for accelerating the exchange reaction. But sampling itself might lead to bias, as it has been shown that use of steel can lead to the generation of molecular H_2 from water, with which it is equilibrated (Chapelle et al., 1997).

Addition of gaseous hydrogen to water or culture medium leads to an immediate shift in the isotope signature from $\delta^2H = -139.0 \pm 0.8‰$ to $\delta^2H = -141.2 \pm 0.3‰$ for water and $\delta^2H = -142.2 \pm 0.7‰$ for culture medium. This effect is probably due to a relatively higher solubility of ^2H in water, which leads to an isotope fractionation (Muccitelli and Wen, 1978). The observed shift in isotopic signature lies within usual standard deviations for hydrogen isotope measurements, and no further change in the isotope signal was observed after the initial shift (**Figure 1**). Albeit negligible compared to biocatalysis, isotope exchange takes place in abiotic controls within 18 days at 30°C in the absence of a catalyst.

The addition of a cell suspension leads to changes in the isotope signature due to hydrogenase activity. An inverse isotope effect was observed in all three experimental setups. This is consistent with previously reported δ^2H -values for H_2-production from water for *Shewanella oneidensis* MR-1, which can express a NiFe- or a FeFe-hydrogenase (Kreuzer et al., 2014). Upon inhibition of dissimilatory sulfate reduction by molybdate,

TABLE 1 | Concentration of H_2 in all experimental setups: molybdate-inhibited, headspace purged with N_2 to reduce sulfides and without additional treatment.

time	$\delta^2H = -62‰$						$\delta^2H = +461‰$						$\delta^2H = +1533‰$	
	● Molybdate		♦ Purged		▲ Untreated		● Molybdate		♦ Purged		▲ Untreated		● Molybdate	
	C [%]	Stdev [%]	C [%]	Stdev [%]	C [%]	Stdev [%]	C [%]	Stdev [%]	C [%]	Stdev [%]	C [%]	Stdev [%]	C [%]	Stdev [%]
1 min	13.4	0.9	13.9	0.7	20.4	1.0	15.0	0.3	12.2	0.3	19.5	0.4		
29 min													18.2	1.0
55 min													19.1	0.3
88 min													20.0	0.2
3 h 40 min													14.5	0.2
1 day	15.4	1.3	10.9	0.6	4.1	0.2	15.1	0.7	11.7	1.5	2.8	0.1		
1.5 day					1.9	0.1					1.8	0.1		
2 days	13.5	0.7	5.4	0.1	n.d.	n.d.	15.1	0.8	10.3	0.7	n.d.	n.d.		
3 days			1.7	0.1	n.d.	n.d.			0.2	0.0	n.d.	n.d.	13.5	1.0
4 days	15.9	0.1	n.d.	n.d.			14.9	0.6	n.d.	n.d.				
6 days	13.6	0.3											13.4	2.1
9 days							11.8	0.2						
10 days	13.9	0.6											11.6	0.1
11 days							11.6	0.3						
Average	14.3	1.3					13.9	1.7					15.8	3.3

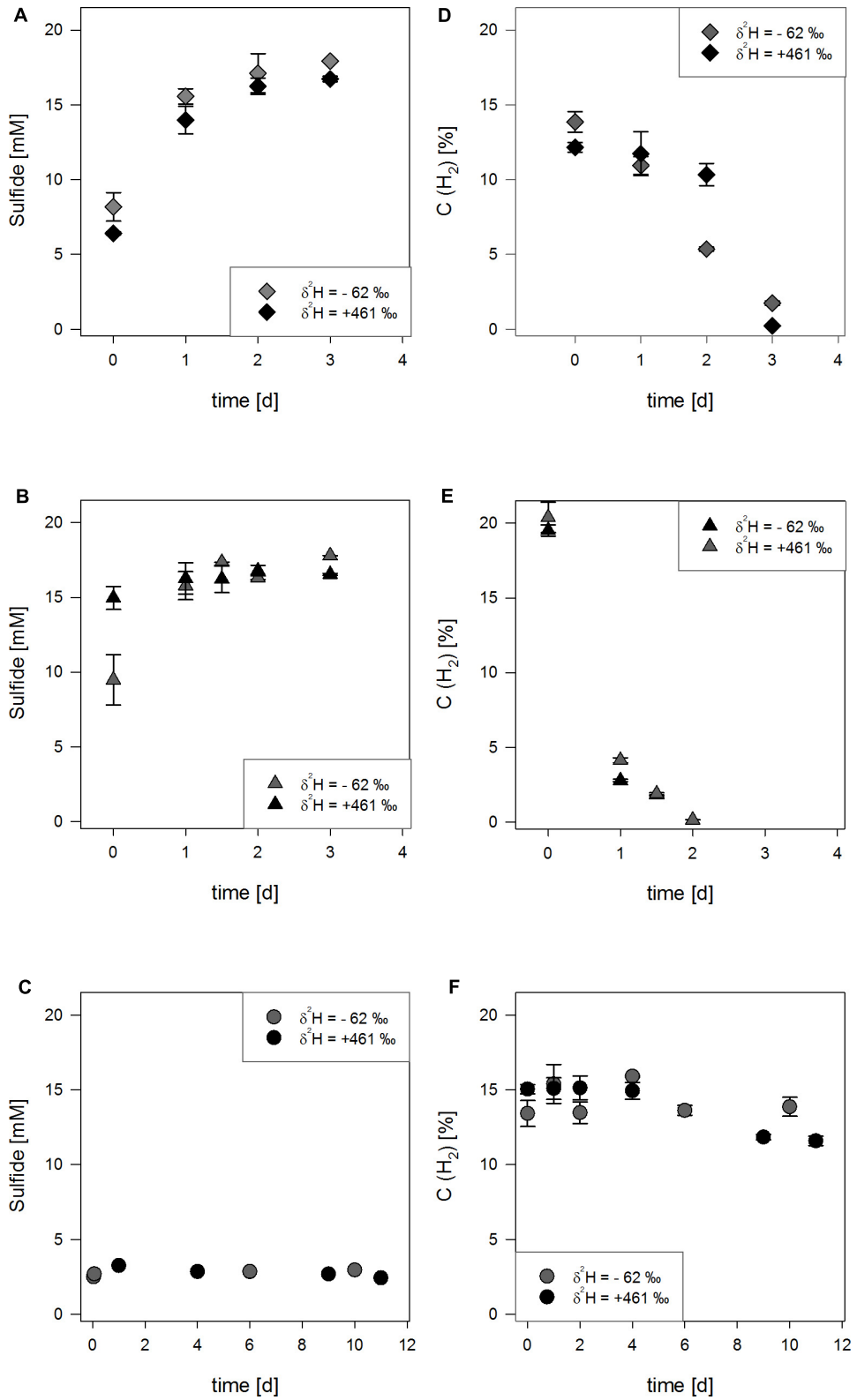

FIGURE 2 | Concentration of H_2 (empty symbols) and sulfides (filled symbols) for three experimental setups **(A,D)**:♦ setups with reduced sulfide burden, **(B,E)**:▲ setups without further treatment, **(C,F)**:● inhibition by molybdate) in either water with $\delta^2H_2O = -62‰$ (gray) or with $\delta^2H_2O = +461‰$ (black). The uncertainty of 2σ is shown.

TABLE 2 | δ^2H-values of H_2 in all experimental setups: molybdate-inhibited, headspace purged with N_2 to reduce sulfides and without additional treatment.

time	δ^2H = −62‰						δ^2H = +461‰				δ^2H = +1532‰	
	● Molybdate		◆ Purged		▲ Untreated		● Molybdate		◆ Purged		▲ Untreated		● Molybdate	
	δ^2H [‰]	Stdev [‰]	δ^2H [‰]	Stdev [‰]	δ^2H [‰]	Stdev [‰]	δ^2H [‰]	Stdev [‰]	δ^2H [‰]	Stdev [‰]	δ^2H [‰]	Stdev [‰]	δ^2H [‰]	Stdev [‰]
1 min	−246.5	0.7	−309.0	0.7	−220.4	0.7	−223.9	0.5	−163.2	0.9	−268.4	0.5		
29 min													−162.4	1.7
55 min													−154.1	0.6
88 min													−154.7	1.0
3 h 40 min													−177.4	1.4
1 day	−624.7	0.3	−341.0	1.0	−463.8	1.2	−405.7	0.3	−203.3	1.0	−377.6	2.3		
1.5 day					−620.2	3.2					−408.1	2.8		
2 days	−722.8	0.4	−593.6	0.8	−702.1	5.7	−524.1	0.3	−280.2	0.4	n.d.	n.d.		
3 days			−678.6	1.5	n.d.	n.d.			−475.3	4.1	n.d.	n.d.	−279.8	0.3
4 days	−733.2	0.3	n.d.	n.d.	n.d.	n.d.	−598.9	0.4	n.d.	n.d.	n.d.	n.d.		
6 days	−733.8	0.3											−328.0	0.7
9 days							−599.6	0.4						
10 days	−735.8	0.3											−327.3	0.3
11 days							−599.4	0.1						

observable isotope effects should be limited to isotope exchange, since H_2 was not consumed. Hydrogenases were previously described to facilitate isotope exchange of $^2H_2$ and H_2O or H_2 and ^2H_2O (Hoberman and Rittenberg, 1943; Jouanneau et al., 1980; Arp and Burris, 1982; Vignais et al., 2000, 2002). We therefore assume that the hydrogenase in our experiments is solely responsible for the isotope exchange.

After four to 6 days the isotope exchange reaction approximately reached equilibrium with differences of Δ^2H = 9‰ and Δ^2H = 6‰ and Δ^2H = 10‰ compared to the theoretical values (**Figure 4**) in cultures inhibited by molybdate addition. Deviations from the theoretical values could be due to the higher measurement error and standard deviations of the water measurements used for calculation, as well as the high sensitivity of the equilibrium equation toward fluctuations in temperature.

It has been shown for the NiFe-hydrogenase from *D. vulgaris* Miyazaki that hydrogen oxidation is a two-step process, during which an enzyme-hydride-state forms (Lubitz et al., 2014). First, H_2 diffuses into the active center. Then, it is heterolytically cleaved, forming a proton and an enzyme-hydride-complex. Afterward, electrons and protons are shuffled out of the protein structure (Lubitz et al., 2014). A study using *D. vulgaris* Hildenborough suggested that H_2 can be caged by the protein structure surrounding the active site when selenocysteine replaces cysteine in the active center of the protein structure (Gutiérrez-Sanz et al., 2013). In this case, substrate and products can accumulate within the protein structure of the NiFeSe-hydrogenase near the catalytic center and the two transfers of protons proceed faster than in NiFe-hydrogenases. The authors suggested that the accumulation and subsequent availability of substrate would correspond to a fast isotope exchange reaction (Gutiérrez-Sanz et al., 2013). This hypothesis connects protein structure and isotope effects. *D. vulgaris* Miyazaki expresses a structurally similar NiFeSe-hydrogenase best suited for hydrogen oxidation (Nonaka et al., 2013; Riethausen et al., 2013), and the corresponding fast isotope exchange reaction was measured in this study, where the isotope equilibrium was reached within 6 days. It might be possible to compare the equilibrium isotope effect of structurally different types of hydrogenases, such as NiFe- and FeFe-hydrogenases, in order to characterize the isotope exchange rate in future studies in more detail. For this, a different inhibition of electron flow might be needed, as molybdo-sulfide-complexes might not work for all microorganisms, as it specifically inhibits sulfate reduction. Even though it has been shown to also inhibit H_2 production from glucose (Wolin and Miller, 1980), it has not been further or sufficiently studied. Information on structurally different hydrogenases is crucial for using stable hydrogen isotopes as a monitoring tool to track *in situ* hydrogenase activity, e.g., during storage of hydrogen in underground reservoirs.

Even though H_2 was consumed in the experiment with purged headspaces, only minimal changes in the δ^2H-values were observed in the beginning. During the substrate consumption, the hydrogen bond is cleaved, which is expected to result in a normal kinetic isotope effect. However, in our experiments,

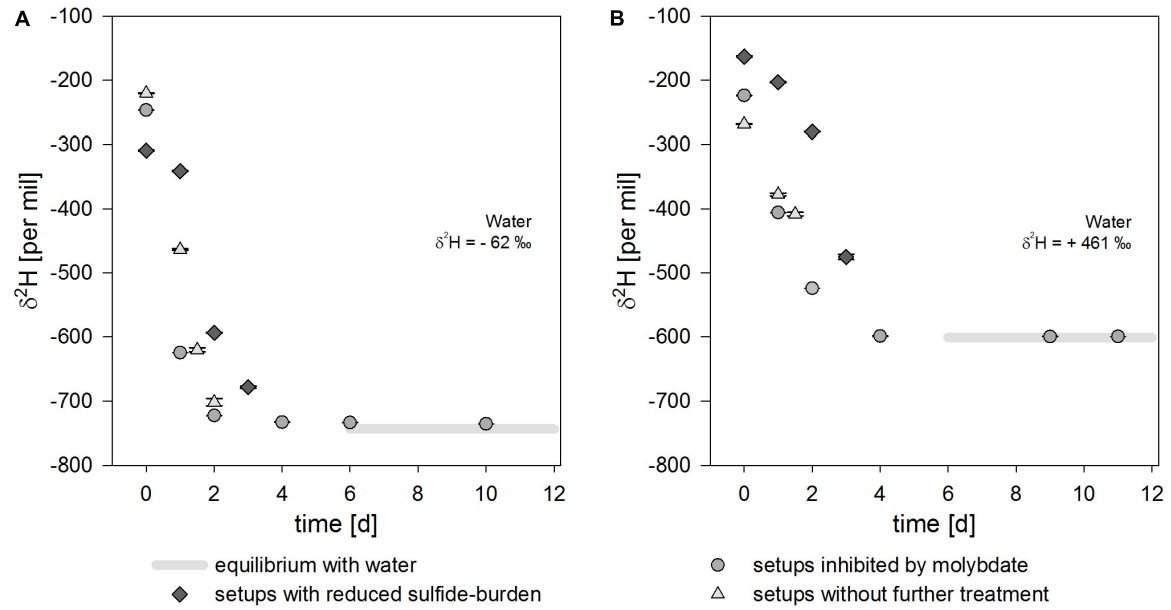

FIGURE 3 | Isotope signal over time for three experimental setups in either water with δ^2 H_2O = –62‰ **(A)** or with δ^2 H_2O = +461‰ **(B)**. The isotope equilibrium is reached after about 6 days and indicated by light gray bars. The uncertainty of 2σ is shown and often smaller than the symbol.

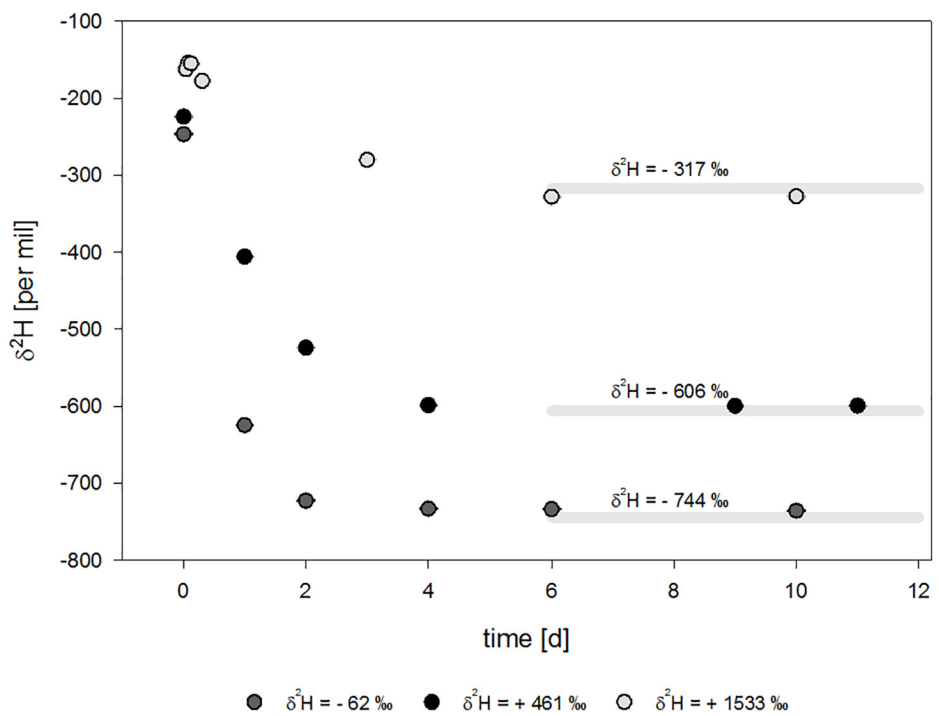

FIGURE 4 | Isotope signature over time for molybdate-inhibited setups with water of different isotope composition. Theoretical equilibrium values ± approx. 5‰ standard deviation are indicated by light gray lines.

the isotope values approximate isotope equilibrium values with increasing time. We therefore suggest that the kinetic isotope effect of the hydrogen bond cleavage is superimposed by the equilibrium isotope exchange reaction. Only in the beginning of hydrogen oxidation, an effect of the kinetic isotope effect can be observed. Here, the equilibrium isotope effect has not yet completely superimposed the isotope signature, which results in seemingly stable isotope values.

The observed kinetic isotope fractionation effects could be due to shuffling of protons into the cell. Hydrogenase and cytochrome complexes are able to translocate protons (Ide et al., 1999; Dolla et al., 2000; Chang et al., 2004). For example, the reduction of sulfate needs two additional protons (Eq. 4).

$$4H_2 + SO_4^{2-} + 2H^+ \rightarrow H_2S + 4H_2O \quad (4)$$

During this process a slight isotope fractionation is expected, due to different diffusivity according to their molecular mass and tunneling effects in the hydrogenase structure (Cukier, 2004). Then, more $^2H^+$ than $^1H^+$ would be released from the hydrogenase, which would equivalent the expected kinetic isotope fractionation. This effect would counteract an equilibrium isotope exchange reaction. Not only the rate of equilibrium isotope exchange, but also the kinetic isotope fractionation could be affected by the protein structure. Therefore, further studies on both kinetic isotope effects and equilibrium isotope effects and their superimposition using structurally different hydrogenases are needed in order to use this concept as a monitoring or diagnostic tool.

Interestingly, cultures containing the highest sulfide concentrations tested in this study (10 mM) showed consumption of H_2, but lacked the "isotopic lag phase" of the purged experiments with 6 mM starting concentration (**Figure 3**). This might be an indication that the amount of sulfides could affect the electron and proton flow, as H_2 is still consumed but the normal kinetic isotope fractionation of the H-H bond cleavage is immediately superimposed by the equilibrium isotope effect of the exchange reaction. During growth on lactate and sulfate, up to 52% of electrons flow into the production of H_2 and the remaining 48 % of electrons are coupled to sulfate reduction in *D. vulgaris*, yielding the potential to reduce approx. 8.9 mM sulfate from lactate and H_2 (Noguera et al., 1998) or 14 mM sulfate from lactate alone before the start of the hydrogen oxidation experiments. And with concentrations of 9.48 up to 11.2 mM sulfide in the setups without further treatment to reduce sulfides at the start of the experiment, inhibition is a consequential hypothesis.

CONCLUSION

The hydrogenase of *Desulfovibrio vulgaris* Miyazaki facilitates an equilibrium isotope exchange when consumption of H_2 is inhibited. Resulting δ^2H-values of H_2 corresponds to theoretical thermodynamic isotope equilibria. During H_2, the kinetic isotope fractionation, which should be observed due to bond-cleavage, is superimposed by the equilibrium isotope exchange. These results might differ for other microorganisms and structurally different hydrogenases. Equilibrium isotope exchange in the experiments with starting concentration of about 10 mM sulfides also indicates a possibility that sulfides could inhibit electron flow. This research is fundamental in nature and aims to build a better understanding of the isotope effects and processes associated with hydrogenases. The results of this study serve as a basis for future research on a simple monitoring tool for environmental, gaseous samples based on stable isotopes of hydrogen.

DATA AVAILABILITY

All datasets generated for this study are included in the manuscript and/or the **Supplementary Files**.

AUTHOR CONTRIBUTIONS

ML planned and performed the experiments and data analyses and wrote the manuscript. SK helped to establish a GC-IRMS method for H_2. CV and H-HR supervised the research and edited the manuscript.

FUNDING

This work was supported by the Federal Ministry for Economic Affairs and Energy (BMWi) within the funding initiative "Energiespeicher," project ANGUS II, Grant Number 03ET6122B.

ACKNOWLEDGMENTS

We would like to acknowledge Florian Tschernikl for help in the cultivation and Matthias Gehre for helpful inputs during method development and work in the isotope lab.

SUPPLEMENTARY MATERIAL

The Supplementary Material for this article can be found online at: https://www.frontiersin.org/articles/10.3389/fmicb.2019.01545/full#supplementary-material

REFERENCES

Arp, D. J., and Burris, R. H. (1982). Isotope exchange and discrimination by the H2-oxidizing hydrogenase from soybean root nodules. *Biochim. Biophys. Acta Protein Struct. Mol. Enzymol.* 700, 7–15. doi: 10.1016/0167-4838(82)90285-0

Biswas, K. C., Woodards, N. A., Xu, H., and Barton, L. L. (2009). Reduction of molybdate by sulfate-reducing bacteria. *BioMetals* 22, 131–139. doi: 10.1007/s10534-008-9198-8

Chang, C. J., Chang, M. C., Damrauer, N. H., and Nocera, D. G. (2004). Proton-coupled electron transfer: a unifying mechanism for biological charge transport, amino acid radical initiation and propagation, and bond making/breaking reactions of water and oxygen. *Biochim. Biophys. Acta Bioenerget.* 1655, 13–28. doi: 10.1016/j.bbabio.2003.08.010

Chapelle, F. H., Vroblesky, D. A., Woodward, J. C., and Lovley, D. R. (1997). Practical considerations for measuring hydrogen concentrations in groundwater. *Environ. Sci. Technol.* 31, 2873–2877. doi: 10.1021/es970085c

Cline, J. D. (1969). Spectrophotometric determination of hydrogen sulfide in natural waters 1. *Limnol. Oceanogr.* 14, 454–458. doi: 10.4319/lo.1969.14.3.0454

Coplen, T. B. (2011). Guidelines and recommended terms for expression of stable-isotope-ratio and gas-ratio measurement results. *Rapid Commun. Mass Spectrom.* 25, 2538–2560. doi: 10.1002/rcm.5129

Crist, R., and Dalin, G. (1934). "Isotopic Equilibria" in the Hydrogen-Hydrogen Oxide system. *J. Chem. Phys.* 2, 735–738. doi: 10.1063/1.1749388

Cukier, R. I. (2004). Theory and simulation of proton-coupled electron transfer, hydrogen-atom transfer, and proton translocation in proteins. *Biochim. Biophys. Acta Bioenerget.* 1655, 37–44. doi: 10.1016/j.bbabio.2003.06.011

Deckers, H. M., Wilson, F. R., and Voordouw, G. (1990). Cloning and sequencing of a [NiFe] hydrogenase operon from *Desulfovibrio vulgaris* Miyazaki F. *Microbiology* 136, 2021–2028. doi: 10.1099/00221287-136-10-2021

Dolla, A., Pohorelic, B. K. J., Voordouw, J. K., and Voordouw, G. (2000). Deletion of the hmc operon of *Desulfovibrio vulgaris* subsp. *vulgaris Hildenborough hampers hydrogen metabolism and low-redox-potential niche establishment*. *Arch. Microbiol.* 174, 143–151. doi: 10.1007/s002030000183

Farkas, A. (1936). The mechanism of the catalytic exchange reaction between deuterium and water. *Trans. Faraday Soc.* 32, 922–932.

Farkas, L., and Farkas, A. (1934). The equilibrium H 2 O+ HD = HDO+ H 2. *Trans. Faraday Soc.* 30, 1071–1079.

Fichtner, C., Laurich, C., Bothe, E., and Lubitz, W. (2006). Spectroelectrochemical characterization of the [NiFe] hydrogenase of *Desulfovibrio vulgaris* miyazaki F. *Biochemistry* 45, 9706–9716.

Foerster, S., Stein, M., Brecht, M., Ogata, H., Higuchi, Y., and Lubitz, W. (2003). Single crystal EPR studies of the reduced active site of [NiFe] Hydrogenase from *Desulfovibrio vulgaris* miyazaki F. *J. Am. Chem. Soc.* 125, 83–93. doi: 10.1021/ja027522u

Gehre, M., Renpenning, J., Geilmann, H., Qi, H., Coplen, T. B., Kümmel, S., et al. (2017). Optimization of on-line hydrogen stable isotope ratio measurements of halogen- and sulfur-bearing organic compounds using elemental analyzer–chromium/high-temperature conversion isotope ratio mass spectrometry (EA-Cr/HTC-IRMS). *Rapid Commun. Mass Spectrom.* 31, 475–484. doi: 10.1002/rcm.7810

Greening, C., Biswas, A., Carere, C. R., Jackson, C. J., Taylor, M. C., Stott, M. B., et al. (2016). Genomic and metagenomic surveys of hydrogenase distribution indicate H 2 is a widely utilised energy source for microbial growth and survival. *ISME J.* 10:761. doi: 10.1038/ismej.2015.153

Gutiérrez-Sanz, O., Marques, M. C., Baltazar, C. S., Fernández, V. M., Soares, C. M., Pereira, I. A., et al. (2013). Influence of the protein structure surrounding the active site on the catalytic activity of [NiFeSe] hydrogenases. *J. Biol. Inorg. Chem.* 18, 419–427. doi: 10.1007/s00775-013-0986-4

Hoberman, H. D., and Rittenberg, D. (1943). Biological catalysis of the exchange reaction between water and hydrogen. *J. Biol. Chem.* 147, 211–227.

Horibe, Y., and Craig, H. (1995). DH fractionation in the system methane-hydrogen-water. *Geochim. Cosmochim. Acta* 59, 5209–5217. doi: 10.1016/0016-7037(95)00391-6

Horiuti, I., and Polanyi, M. (1934). Exchange reactions of hydrogen on metallic catalysts. *Trans. Faraday Soc.* 30, 1164–1172.

Ide, T., Bäumer, S., and Deppenmeier, U. (1999). Energy conservation by the H2: heterodisulfide oxidoreductase from Methanosarcina mazei Gö1: identification of two proton-translocating segments. *J. Bacteriol.* 181, 4076–4080.

Jouanneau, Y., Kelley, B. C., Berlier, Y., Lespinat, P. A., and Vignais, P. M. (1980). Continuous monitoring, by mass spectrometry, of H2 production and recycling in Rhodopseudomonas capsulata. *J. Bacteriol.* 143, 628–636.

Kleinsteuber, S., Schleinitz, K. M., Breitfeld, J., Harms, H., Richnow, H. H., and Vogt, C. (2008). Molecular characterization of bacterial communities mineralizing benzene under sulfate-reducing conditions. *FEMS Microbiol. Ecol.* 66, 143–157. doi: 10.1111/j.1574-6941.2008.00536.x

Kreuzer, H. W., Hill, E. A., Moran, J. J., Bartholomew, R. A., Yang, H., and Hegg, E. L. (2014). Contributions of the [NiFe]-and [FeFe]-hydrogenase to H2 production in Shewanella oneidensis MR-1 as revealed by isotope ratio analysis of evolved H2. *FEMS Microbiol. Lett.* 352, 18–24. doi: 10.1111/1574-6968.12361

Lubitz, W., Ogata, H., Rüdiger, O., and Reijerse, E. (2014). Hydrogenases. *Chem. Rev.* 114, 4081–4148.

Muccitelli, J., and Wen, W.-Y. (1978). Solubilities of hydrogen and deuterium gases in water and their isotope fractionation factor. *J. Solution Chem.* 7, 257–267. doi: 10.1007/bf00644273

Noguera, D. R., Brusseau, G. A., Rittmann, B. E., and Stahl, D. A. (1998). A unified model describing the role of hydrogen in the growth of Desulfovibrio vulgaris under different environmental conditions. *Biotechnol. Bioeng.* 59, 732–746. doi: 10.1002/(sici)1097-0290(19980920)59:6<732::aid-bit10>3.3.co;2-2

Nonaka, K., Nguyen, N. T., Yoon, K.-S., and Ogo, S. (2013). Novel H2-oxidizing [NiFeSe]hydrogenase from *Desulfovibrio vulgaris* Miyazaki F. *J. Biosci. Bioeng.* 115, 366–371. doi: 10.1016/j.jbiosc.2012.10.011

Ogata, H., Mizoguchi, Y., Mizuno, N., Miki, K., Adachi, S.-I., Yasuoka, N., et al. (2002). Structural Studies of the Carbon Monoxide Complex of [NiFe]hydrogenase from *Desulfovibrio vulgaris* Miyazaki F: suggestion for the initial activation site for dihydrogen. *J. Am. Chem. Soc.* 124, 11628–11635. doi: 10.1021/ja012645k

Pandelia, M.-E., Ogata, H., Currell, L. J., Flores, M., and Lubitz, W. (2010). Inhibition of the [NiFe] hydrogenase from *Desulfovibrio vulgaris* Miyazaki F by carbon monoxide: An FTIR and EPR spectroscopic study. *Biochim. Biophys. Acta Bioenerget.* 1797, 304–313. doi: 10.1016/j.bbabio.2009.11.002

Peck, H. D. (1959). The ATP-dependent reduction of sulfate with hydrogen in extracts of Desulfovibrio desulfuricans. *Proc. Natl. Acad. Sci.* 45, 701–708. doi: 10.1073/pnas.45.5.701

Riethausen, J., Rüdiger, O., Gärtner, W., Lubitz, W., and Shafaat, H. S. (2013). Spectroscopic and electrochemical characterization of the [NiFeSe] Hydrogenase from *Desulfovibrio vulgaris* Miyazaki F: reversible redox behavior and interactions between electron transfer centers. *ChemBioChem* 14, 1714–1719. doi: 10.1002/cbic.201300120

Rolston, J., Den Hartog, J., and Butler, J. (1976). The deuterium isotope separation factor between hydrogen and liquid water. *J. Phys. Chem.* 80, 1064–1067. doi: 10.1021/j100551a008

Suess, H. E. (1949). Das Gleichgewicht H2 + HDO ⇌ HD + H2O und die weiteren Austauschgleichgewichte im System H2, D2 und H2O. *Z. Naturforsch. A* 4, 328–332.

Vignais, P. M., and Billoud, B. (2007). Occurrence, classification, and biological function of hydrogenases: an overview. *Chem. Rev.* 107, 4206–4272. doi: 10.1021/cr050196r

Vignais, P. M., Cournac, L., Hatchikian, E. C., Elsen, S., Serebryakova, L., Zorin, N., et al. (2002). Continuous monitoring of the activation and activity of [NiFe]-hydrogenases by membrane-inlet mass spectrometry. *Int. J. Hydrogen Energy* 27, 1441–1448. doi: 10.1016/s0360-3199(02)00114-3

Vignais, P. M., Dimon, B., Zorin, N. A., Colbeau, A., and Elsen, S. (1997). HupUV proteins of Rhodobacter capsulatus can bind H2: evidence from the H-D exchange reaction. *J. Bacteriol.* 179, 290–292. doi: 10.1128/jb.179.1.290-292.1997

Vignais, P. M., Dimon, B., Zorin, N. A., Tomiyama, M., and Colbeau, A. (2000). Characterization of the hydrogen-deuterium exchange activities of the energy-transducing HupSL hydrogenase and H2-signaling HupUV hydrogenase in Rhodobacter capsulatus. *J. Bacteriol.* 182, 5997–6004. doi: 10.1128/jb.182.21.5997-6004.2000

Wolin, M., and Miller, T. L. (1980). Molybdate and sulfide inhibit H2 and increase formate production from glucose by Ruminococcus albus. *Arch. Microbiol.* 124, 137–142. doi: 10.1007/bf00427718

Yagi, T., Kimura, K., Daidoji, H., Sakai, F., Tamura, S., and Inokuchi, H. (1976). Properties of purified hydrogenase from the particulate fraction of *Desulfovibrio vulgaris*, Miyazaki. *J. Biochem.* 79, 661–671. doi: 10.1093/oxfordjournals.jbchem.a131111

Yang, H., Gandhi, H., Shi, L., Kreuzer, H. W., Ostrom, N. E., and Hegg, E. L. (2012). Using gas chromatography/isotope ratio mass spectrometry to determine the fractionation factor for H2 production by hydrogenases. *Rapid Commun. Mass Spectrom.* 26, 61–68. doi: 10.1002/rcm.5298

Conflict of Interest Statement: The authors declare that the research was conducted in the absence of any commercial or financial relationships that could be construed as a potential conflict of interest.

frontiers in Microbiology

ORIGINAL RESEARCH
published: 17 July 2019
doi: 10.3389/fmicb.2019.01652

A Mathematical Model for the Hydrogenotrophic Metabolism of Sulphate-Reducing Bacteria

Nick W. Smith[1,2,3,4], Paul R. Shorten[1,3], Eric Altermann[2,3], Nicole C. Roy[2,3,5] and Warren C. McNabb[3,5]*

[1] AgResearch, Ruakura Research Centre, Hamilton, New Zealand, [2] AgResearch, Grasslands Research Centre, Palmerston North, New Zealand, [3] Riddet Institute, Massey University, Palmerston North, New Zealand, [4] School of Food and Advanced Technology, Massey University, Palmerston North, New Zealand, [5] High-Value Nutrition National Science Challenge, The University of Auckland, Auckland, New Zealand

Sulphate-reducing bacteria (SRB) are studied across a range of scientific fields due to their characteristic ability to metabolise sulphate and produce hydrogen sulphide, which can lead to significant consequences for human activities. Importantly, they are members of the human gastrointestinal microbial population, contributing to the metabolism of dietary and host secreted molecules found in this environment. The role of the microbiota in host digestion is well studied, but the full role of SRB in this process has not been established. Moreover, from a human health perspective, SRB have been implicated in a number of functional gastrointestinal disorders such as Irritable Bowel Syndrome and the development of colorectal cancer. To assist with the study of SRB, we present a mathematical model for the growth and metabolism of the well-studied SRB, *Desulfovibrio vulgaris* in a closed system. Previous attempts to model SRB have resulted in complex or highly specific models that are not easily adapted to the study of SRB in different environments, such as the gastrointestinal tract. We propose a simpler, Monod-based model that allows for easy alteration of both key parameter values and the governing equations to enable model adaptation. To prevent any incorrect assumptions about the nature of SRB metabolic pathways, we structure the model to consider only the concentrations of initial and final metabolites in a pathway, which circumvents the current uncertainty around hydrogen cycling by SRB. We parameterise our model using experiments with varied initial substrate conditions, obtaining parameter values that compare well with experimental estimates in the literature. We then validate our model against four independent experiments involving *D. vulgaris* with further variations to substrate availability. Further use of the model will be possible in a number of settings, notably as part of larger models studying the metabolic interactions between SRB and other hydrogenotrophic microbes in the human gastrointestinal tract and how this relates to functional disorders.

Keywords: hydrogen, gastrointestinal tract, IBS, hydrogen sulphide, mathematical modelling

OPEN ACCESS

Edited by:
Chris Greening,
Monash University, Australia

Reviewed by:
Xiyang Dong,
University of Calgary, Canada
Rafael Muñoz-Tamayo,
Institut National de la Recherche Agronomique (INRA), France

***Correspondence:**
Paul R. Shorten
Paul.shorten@agresearch.co.nz

Specialty section:
This article was submitted to Microbial Physiology and Metabolism, a section of the journal Frontiers in Microbiology

Received: *30 April 2019*
Accepted: *03 July 2019*
Published: *17 July 2019*

Citation:
Smith NW, Shorten PR, Altermann E, Roy NC and McNabb WC (2019) A Mathematical Model for the Hydrogenotrophic Metabolism of Sulphate-Reducing Bacteria. Front. Microbiol. 10:1652. doi: 10.3389/fmicb.2019.01652

INTRODUCTION

Sulphate-reducing bacteria (SRB) play an important role in a variety of ecosystems, from marine sediments and oil fields to the human gastrointestinal tract (Muyzer and Stams, 2008; Carbonero et al., 2012a). The functional group of SRB has been reported to comprise 60 genera (Barton and Fauque, 2009), and is characterised by the ability to utilise sulphate as an electron acceptor during metabolism. The presence of these bacteria has both positive and negative implications on human activities, depending on the context. Much research has been performed on hydrogen sulphide (H_2S) production in oil fields by SRB, which can lead to reduced oil quality and machinery corrosion (Magot et al., 2000), and in the treatment of industrial wastewater, as the sulphides SRB produce facilitate the removal of contaminating heavy metals (Kiran et al., 2017). Less clear are the implications of SRB in the human gastrointestinal tract (GIT). The SRB population size in the GIT has been measured at approximately 10^7 cells per gram of faeces (Doré et al., 1995), but varies between individuals (Nava et al., 2012) and between studies (Smith et al., 2018). These bacteria are widely studied due to their controversial role in a number of functional GIT disorders. Increased levels of colonic SRB and increased H_2S concentrations have been linked to Irritable Bowel Syndrome, Inflammatory Bowel Disease and colorectal cancer [for a review, see Carbonero et al. (2012b)]. However, beneficial effects of H_2S have also been investigated, such as its capacity to stimulate mucus production (Motta et al., 2015) and the potential influence of this molecule on blood pressure regulation (Tomasova et al., 2016). The important connexions between SRB, H_2S and the host justify further research into the metabolism of these bacteria.

Another key molecule in SRB metabolism is elemental hydrogen. Alongside methanogens and reductive acetogens, SRB can metabolise free hydrogen present in the GIT, utilising it in the reduction of sulphate (Smith et al., 2018). The sulphate metabolised by SRB can be dietary or host-derived; cross-feeding by SRB on sulphate released during mucin metabolism by other GIT microbes has been well studied (Willis et al., 1996; Rey et al., 2013). High concentrations of hydrogen in the GIT are known to inhibit the metabolism of saccharolytic members of the microbiota (Wolin and Miller, 1983), therefore the presence of hydrogen cross-feeders is thought to increase the rate of carbohydrate breakdown by the wider microbial population. This has been shown in rodent models and linked to increased energy yield for the host (Samuel and Gordon, 2006; Rey et al., 2010).

Due to the importance of SRB in human health and nutrition, a greater understanding of their metabolism and growth dynamics is sought. To this end, we developed a mathematical model for the metabolite flux and population growth of the human SRB *Desulfovibrio vulgaris*, grown on substrates found in the GIT (Scanlan et al., 2009). Ours is not the first attempt to model SRB metabolism and growth and we compare the predictions of our model with that of the existing mathematical model of Noguera et al. (1998). Many other mathematical models of SRB have been published, but these are almost universally applied to address specific characteristics of SRB or for the investigation of competitive and syntrophic relationships between SRB and methanogens [for example, Robinson and Tiedje (1984), Okabe et al. (1995), Stolyar et al. (2007)]. The model of Noguera et al. (1998) is not targeted to a specific characteristic or environment, therefore is a good benchmark against which to compare our model. The existing model is more complex than that proposed here: it consists of ten ordinary differential equations for aqueous and gaseous metabolite concentrations and microbial growth and is dependent on 20 parameter values that are estimated either from separate experimental work or from model fitting. While the model considers many aspects of the metabolism of *D. vulgaris*, it is computationally intensive and requires greater knowledge of kinetic parameters than is often available in environments such as the GIT. Therefore, its structure is less readily compared or combined with other existing models for the GIT microbiota. We also found that this model shows sensitivity to the initial values for dissolved hydrogen and carbonate concentrations; values that are difficult to determine experimentally and physiologically. As we wish to study SRB in the GIT, we construct a simpler model requiring less inputs to later integrate into a larger microbiota model. Our SRB model considers solely the concentrations of the initial and final metabolites in a metabolic pathway, treating the intermediate metabolites and reactions as a "black box." We calibrate our model using existing experimental data for the monoculture growth of a *D. vulgaris* strain and use it to predict the dynamics of separate independent experiments with both the same bacterium and a different *D. vulgaris* strain.

MATERIALS AND METHODS

Assumptions

For this model it was assumed that the only metabolites involved in the metabolism of *D. vulgaris* are lactate, acetate, hydrogen, sulphate and hydrogen sulphide (H_2S), as these metabolites represent important initial and final metabolites in the major metabolic pathways of *D. vulgaris* (Keller and Wall, 2011). Other metabolic pathways involving fermentation of alternative organic molecules, such as monosaccharides and fatty acids, and reduction of nitrogenous compounds have been studied in *Desulfovibrio* and other SRB genera, but appear to be of lesser importance and not widespread within the functional group (Barton and Fauque, 2009). While formate has been implicated in the metabolism of *Desulfovibrio* species elsewhere (da Silva et al., 2013; Junicke et al., 2015; Martins et al., 2015), here we have assumed that formate may be represented as hydrogen equivalents. This is supported by the similar reduction potentials of formate and hydrogen, allowing for interconversion of the two molecules at low energetic cost to the bacterium (Stams and Plugge, 2009; da Silva et al., 2013; Rabus et al., 2013). Formate concentrations also remained very low (<0.5 mM) in previous experiments with *D. vulgaris* Hildenborough grown on either lactate and sulphate or lactate and hydrogen (da Silva et al., 2013).

We assume that the medium in which *D. vulgaris* is grown contains in abundance all other molecules necessary for growth and that these are not significantly depleted during the

experiment. We further assume that *D. vulgaris* is able to oxidise lactate incompletely to acetate, with concurrent production of hydrogen (Keller and Wall, 2011). This hydrogen may then be utilised in the reduction of sulphate to H_2S. We assume that all metabolites remain in the aqueous phase, with the exception of hydrogen, which may transfer between the aqueous and gaseous phases. We assume that all metabolites in the aqueous phase are available to the bacteria in a well-mixed solution. No spatial component is considered in the model.

The assumed stoichiometries for the two reactions, expressing all protons as hydrogen molecule equivalents, are as follows (Thauer et al., 1977; Noguera et al., 1998; da Silva et al., 2013):

$$\begin{aligned} &CH_3CHOHCOO^- \text{ (Lactate)} + 2\,H_2O \\ &\quad \rightarrow CH_3COO^- \text{ (Acetate)} + 2.5\,H_2 + HCO_3^- \\ &SO_4^{2-} \text{ (Sulphate)} + 5H_2 \rightarrow H_2S + 4\,H_2O \end{aligned}$$

Note that the bicarbonate molecule (HCO_3^-) produced in the oxidation of lactate and the water molecules produced in the reduction of sulphate are not included in the model, as they play no further role in the metabolism of *D. vulgaris*. Moreover, we assume that the culture remains well buffered throughout the experiment, therefore pH is not altered by changing concentrations of bicarbonate or other metabolites. There have been reports of bicarbonate as a growth-limiting molecule for other bacterial strains (Dobay et al., 2018), but there is currently no evidence of this for SRB. We explain this further in the Discussion.

Mathematical Model

The model is based on Monod kinetics for bacterial growth in a batch culture environment (Monod, 1949). Monod kinetics was chosen due to the biological meaning associated with the parameters, as well as the ability to determine these values experimentally if required. The model considers the molar concentration of lactate, acetate, sulphate and H_2S, as well as the molar concentration of hydrogen in the aqueous phase and the partial pressure of hydrogen in the gaseous phase, measured in atmospheres. It also considers the concentration of the bacterial population in the aqueous phase (mg L^{-1}). These units were chosen to align with data sources for both the calibration and validation of the model. **Figure 1** shows the general structure of the model.

Following Monod kinetics, we model the rate of change in lactate concentration (L; mM) by

$$\frac{dL}{dt} = -\frac{\mu_{max,L} X}{Y_L}\left(\frac{L}{K_L + L}\right) \tag{1}$$

where $\mu_{max,L}$ denotes the maximum growth rate (h^{-1}) and Y_L denotes the biomass yield (mg L^{-1} mM^{-1}) of *D. vulgaris* when grown on lactate. K_L is the Monod constant (mM) for this bacterium and substrate, also referred to as the half-saturation constant. This value is the concentration of substrate required for the bacterium to attain half of its maximum growth rate. X is the concentration of bacterial cells in the medium (mg L^{-1}).

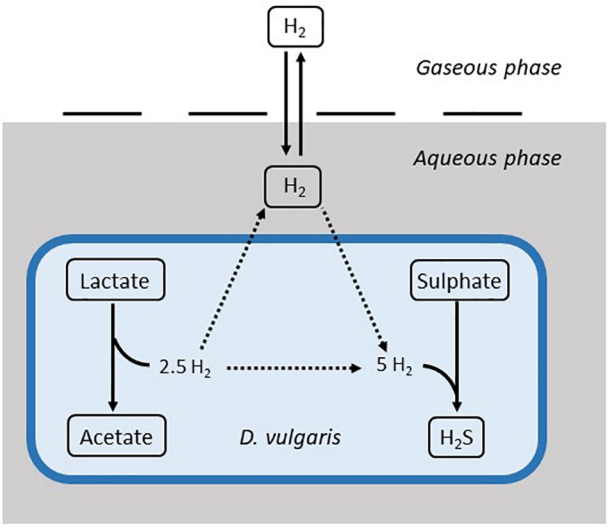

FIGURE 1 | Structure of the mathematical model. Solid arrows denote modelled dynamics. Dotted arrows denote dynamics that are not explicitly modelled. H_2S: hydrogen sulphide.

It is known that high concentrations of hydrogen in the medium inhibit the metabolism of lactate by certain SRB, including *D. vulgaris*, although the mechanism is not clear (Pankhania et al., 1988; Junicke et al., 2015). As such, we add an inhibition term to our model that reduces the rate of lactate metabolism as the aqueous hydrogen concentration, H_{aq} (mM), increases. Equation 1 then becomes

$$\frac{dL}{dt} = -\frac{\mu_{max,L} X}{Y_L}\left(\frac{L}{K_L + L}\right)\left(1 - \frac{H_{aq}}{H_{max}}\right) \tag{2}$$

where H_{max} (mM) is the aqueous hydrogen concentration above which lactate degradation is completely inhibited. This formulation also ensures that the rate of lactate degradation reduces proportionally to the aqueous hydrogen concentration. To ensure that the model is robust to hydrogen concentrations above H_{max}, we add the following condition:

$$\frac{dL}{dt} = 0 \quad \text{when } H_{aq} > H_{max}.$$

The sulphate concentration (S; mM) is given by

$$\frac{dS}{dt} = -\frac{\mu_{max,S} X}{Y_S}\left(\frac{S}{K_S + S}\right)\left(\frac{H_{aq}}{K_H + H_{aq}}\right). \tag{3}$$

Sulphate and hydrogen are both required for the formation of H_2S, hence the inclusion of the aqueous hydrogen concentration in Eq. 3. The equation is adapted from the model equations of Kettle et al. (2015) for multiple essential resources. $\mu_{max,S}$ denotes the maximum growth rate (h^{-1}) and Y_S is the biomass yield (mg L^{-1} mM^{-1}) of *D. vulgaris* during sulphate reduction. K_S and K_H denote the Monod constants (mM) for sulphate and hydrogen, respectively.

We assume that the aqueous hydrogen concentration is influenced by hydrogen production during the oxidation of

lactate, hydrogen consumption in the reduction of sulphate, and liquid-gas transfer of hydrogen. The rate of change in the concentration of aqueous hydrogen is

$$\frac{dH_{aq}}{dt} = -b_{LH}\frac{dL}{dt} + b_{HP}\frac{dS}{dt} - \frac{1}{\rho_H}\frac{dH_g}{dt}\frac{V_g}{V_{aq}} \tag{4}$$

where b_{LH} is the stoichiometric constant for moles of hydrogen produced per mole lactate metabolised and b_{HP} is the stoichiometric constant for moles of hydrogen required to reduce one mole of sulphate. H_g is the gaseous hydrogen concentration, measured in atmospheres, and mass transfer between the aqueous and gaseous phases is assumed to be linear, with

$$\frac{dH_g}{dt} = k_L a\left(\rho_H H_{aq} - H_g\right)\frac{V_{aq}}{V_g} \tag{5}$$

Equation 5 represents a simple mass transfer model as explained in Kadic and Heindel (2014). Briefly, net transfer between the two phases is determined by the concentration gradient, with the rate of transfer determined by the mass transfer coefficient, k_L (calculated from the thickness of the film through which molecules must travel and the diffusivity of the molecule in question) and the surface area, a, across which mass transfer may occur. Although other, more complex models do exist for mass transfer between two phases, as only the gaseous hydrogen concentration data is available here, we are limited in our ability to parameterise a more complex model. Although the simplicity of this representation may result in sub-optimal representation of the hydrogen dynamics, we also seek to minimise the number of fitted parameter values in our model, and thus the film model described here is sufficient for our purposes. $k_L a$ has the unit h^{-1} and V_g and V_{aq} (mL) are the fixed volumes of the gaseous and aqueous phases, respectively. ρ_H (atm mM^{-1}) is the Henry conversion constant for hydrogen. H_g is measured in atmospheres, whereas H_{aq} is given in mM concentration, therefore we adapt the gas transfer equation used in Muñoz-Tamayo et al. (2016) for our model, giving a ρ_H value of 1.364 atm mM^{-1}.

The rates of change in acetate (A) and H_2S (P) concentrations are proportional to the rates of change in the concentrations of lactate and sulphate, respectively.

$$\frac{dA}{dt} = -b_{LA}\frac{dL}{dt} \tag{6}$$

$$\frac{dP}{dt} = -b_{SP}\frac{dS}{dt} \tag{7}$$

where b_{LA} and b_{SP} are constants determined by the stoichiometries of each reaction stated in Section 2.1. Note that we take these stoichiometries directly from the literature and do not include in the model some fraction of substrate being used in the production of cell biomass. This assumption is made as, for the batch culture cases considered here, the experimentally observed stoichiometries of the metabolites closely matched those given in Section 2.1.

Finally, the concentration of bacterial cells in the medium, X (mg L^{-1}), is proportional to the change in lactate and sulphate concentrations, with consideration of the biomass yield terms (assuming the energy requirements for cell maintenance are negligible relative to the growth requirements).

$$\frac{dX}{dt} = -Y_L\frac{dL}{dt} - Y_S\frac{dS}{dt} \tag{8}$$

The system consisting of Eq. 2–8 fully describes the metabolism of *D. vulgaris* under our set of assumptions. A summary of model notation is given in **Table 5**.

Data Capture

Time-course data was captured from the literature using image capturing and graphical input software in MATLAB (The MathWorks[1]). The mathematical model of Noguera et al. (1998) was reconstructed using the information in the original publication. This information was near complete, the only exception being the absence of initial conditions for some of the model variables. We have therefore made some assumptions based on other information given in the paper, which has allowed us to reproduce good representations of the published model fits.

Model Fitting

In order to determine the values of several of the parameters used in the model, model fitting to existing experimental data was performed. Time-course data from Noguera et al. (1998) was collected and used to calibrate the model and estimate parameter values.

The parameter values in **Table 1** were generated by minimising the normalised sum of squared errors between the model prediction and the data. The optimisation was performed using the fminsearch routine in MATLAB (The MathWorks; see text footnote 1).

Statistical Analysis

All statistics were calculated in MATLAB using the captured data and corresponding model prediction. A Markov Chain Monte Carlo (MCMC) technique was implemented over 200,000 MCMC iterations. A non-parametric distribution was then fitted to the MCMC sample for each of the nine parameters estimated. The cumulative density function of this distribution was used to obtain a 95% confidence interval.

To compare the proposed model with the existing model of Noguera et al. (1998), we used the corrected Akaike Information Criterion (AICc) (Akaike, 1974; Hurvich and Tsai, 1989):

$$\text{AICc} = 2K - 2(\log(\mathcal{L}(\theta))) + \frac{2K(K+1)}{n-K-1}$$

where n is the number of data points (63), K is the number of parameters of the model and $\log(\mathcal{L}(\theta))$ is the log likelihood function for the model. Following Burnham and Anderson (2002), we make the substitution

$$\log(\mathcal{L}(\theta)) = -\frac{1}{2}n\log\left(\frac{\text{RSS}}{n}\right)^2$$

where RSS is the normalised residual sum of squares of the model fit to the data. Normalisation, i.e., division by the sample mean in

[1] www.mathworks.com

TABLE 1 | Model parameter values.

Parameter		Notation	Value (Best fit value with 95% confidence interval)	Source	Existing estimates*
Maximum growth rates	Lactate oxidation	$\mu_{max,L}$	0.116 h^{-1} (0.088–1.155)	Model fitting	t_d = 3.7 h (≈0.21 h^{-1}) (Pankhania et al., 1986)
	Sulphate reduction	$\mu_{max,S}$	0.03 h^{-1} (0.023–0.212)	Model fitting	0.057 h^{-1} (Robinson and Tiedje, 1984) 0.15 h^{-1} (strain Marburg) (Badziong and Thauer, 1978) 0.15 h^{-1} (Reis et al., 1992)
Monod constants	Lactate	K_L	4.5 mM (7.3–136.8)	Model fitting	1.4 mM (Pankhania et al., 1988) 29 mM (Noguera et al., 1998)
	Sulphate	K_S	0.05 mM (0.02–0.268)	Model fitting	0.032 mM (Ingvorsen and Jørgensen, 1984) 0.21 mM (Noguera et al., 1998)
	Hydrogen	K_H	1.69×10^{-5} mM (2.5×10^{-4}–3.96×10^{-3})	Model fitting	0.001 mM (Kristjansson et al., 1982) 0.0019 mM (Robinson and Tiedje, 1984) 0.0014 mM (Noguera et al., 1998)
Yield parameters	Lactate	Y_L	5.65 mg L^{-1} mM^{-1} (0.99–9.57)	Model fitting	5.3 mg L^{-1} mM^{-1} (Noguera et al., 1998) 5 mg L^{-1} mM^{-1} (Walker et al., 2009)
	Sulphate	Y_S	4.45 mg L^{-1} mM^{-1} (2.2–19.35)	Model fitting	2.8 mg L^{-1} mM^{-1} (Noguera et al., 1998) 8.3 g mol^{-1} (strain Marburg) (Badziong and Thauer, 1978) 14.3 g cell mol^{-1} (Reis et al., 1992)
Mass transfer parameter		k_La	0.302 h^{-1} (0.182–0.914)	Model fitting	0.29 h^{-1} (Noguera et al., 1998)
Inhibitory hydrogen concentration		H_{max}	0.0216 mM (0.0341–0.0821)	Model fitting	0.001 atm (≈0.0007 mM) (Junicke et al., 2015)
Stoichiometric constants	Moles of hydrogen (H_2) produced per mole lactate oxidised	b_{LH}	2.5	Assumed stoichiometries	2.5 (Thauer et al., 1977; Noguera et al., 1998) 3.5 (Keller and Wall, 2011)
	Moles of hydrogen (H_2) consumed per mole H_2S produced	b_{HP}	5	Assumed stoichiometries	5 (Thauer et al., 1977; Noguera et al., 1998) 4.25 (Keller and Wall, 2011)
	Moles of acetate produced per mole lactate oxidised	b_{LA}	1	Assumed stoichiometries	1 (Thauer et al., 1977; Noguera et al., 1998; Keller and Wall, 2011)
	Moles of H_2S produced per mole sulphate reduced	b_{SP}	1	Assumed stoichiometries	1 (Thauer et al., 1977; Noguera et al., 1998; Keller and Wall, 2011)
Henry constant		ρ_H	1.364	Obtained from literature (Sander, 2015)	

**These estimates are obtained from different models and therefore a direct comparison cannot be made with the parameters estimated in the paper. They are listed here for reference.*

the calculation of the RSS for each data set, was included to ensure the RSS value was not biassed by the scale on which each variable was measured. Finally, we also calculate the Akaike weight, w_i, for each model as follows (Burnham and Anderson, 2002):

$$w_i = \frac{l_i}{l_1 + l_2}$$

where $l_i = \exp\left(-\frac{1}{2}(\mathrm{AICc}_i - \mathrm{AICc}_{min})\right)$. Here, i is the model index (1 for the existing model of Noguera et al. (1998), 2 for the model presented here) and AICc_{min} represents the minimum AICc value of the two models.

RESULTS

Model Calibration

Data from two separate experiments were used simultaneously to obtain parameter values for the model (Noguera et al., 1998). The first experiment involved the growth of *D. vulgaris* in medium supplemented with lactate and sulphate (**Figure 2**), while the second experiment took place in the absence of sulphate (**Figure 3**). Our mathematical model was able to describe the trends in growth and metabolite flux dynamics for both these experiments, giving comparable goodness of fit to the more complex model of Noguera et al. (1998; **Table 2**). The parameter values used are shown in **Table 1**.

The model of Noguera et al. (1998) uses seven model fitted parameters and a total of 20 parameters either fitted or estimated from previous experimentation, whereas our model uses nine fitted parameters and one estimated from previous experimentation, giving a total of 10. This discrepancy is due to the increased complexity of the former model, which additionally models the concentrations and gaseous partial pressures of CO_2, H_2S and bicarbonate, as well as the mass transfer of these molecules between the two phases, and the thermodynamics of each reaction modelled. **Table 3** details the values used for

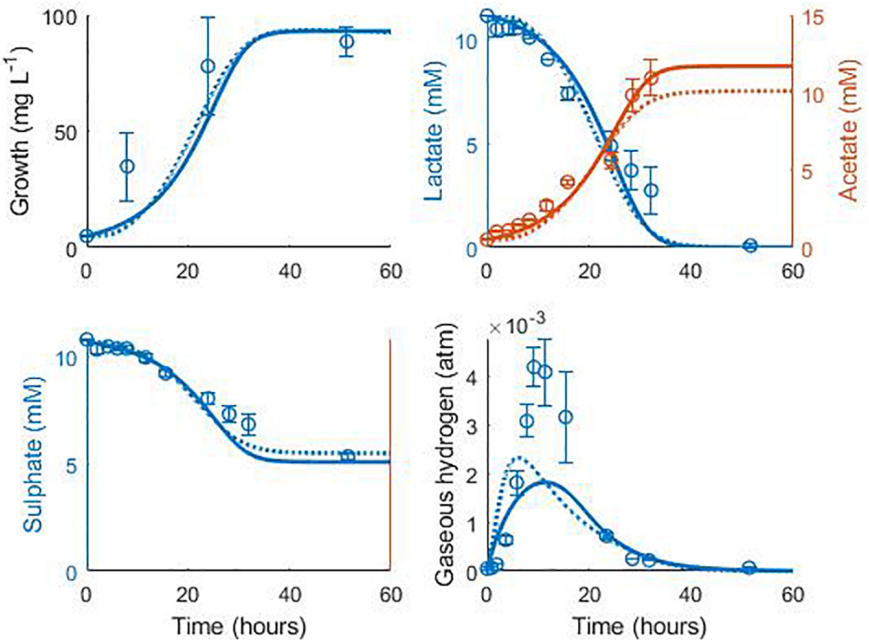

FIGURE 2 | Model fits to data from Noguera et al. (1998): continuous lines display the fit of the current model; dotted lines display the fit of the model described in Noguera et al. (1998). Analysis of model fit is presented in **Table 2**.

the AICc calculation. The AICc value for our model was 263.2 compared to an AICc of 282.8 for the model of Noguera et al. (1998). This indicates the aptness of our model to the data considered, although more complex models may be better suited for larger and more complex data sets.

Some of the parameters shown in **Table 1** were fixed to values taken from the literature. The stoichiometric constants were fixed to correspond with the assumed stoichiometries of the reactions considered and the Henry constant for hydrogen was also obtained from the literature.

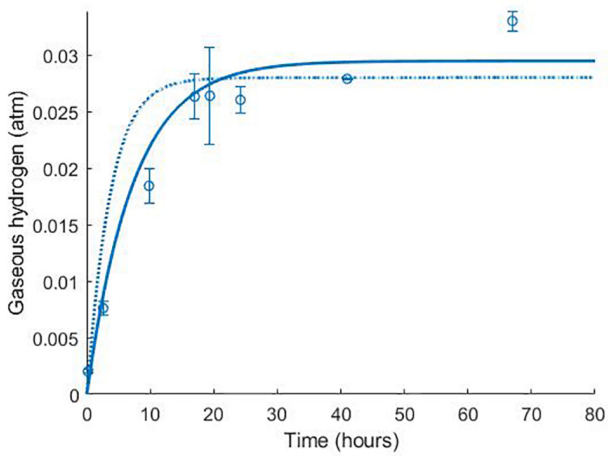

FIGURE 3 | Dynamics of gaseous hydrogen in medium supplemented with 17.3 mM lactate in the absence of sulphate (Noguera et al., 1998): continuous lines display the fit of the current model; dotted lines display the fit of the model described in Noguera et al. (1998). Analysis of model fit is presented in **Table 2**.

It is notable that the best fit parameter values for K_L, K_H and H_{max} lie outside their respective MCMC generated 95% confidence interval. This is likely due to the difficulties in estimating half-saturation constants and maximum growth rates simultaneously, as we observed high correlation between these values. This has been observed in Monod model fitting elsewhere [for example, Muñoz-Tamayo et al. (2016)]. We therefore performed a second MCMC run in which the half-saturation constants were fixed at values obtained from the experimental literature. A comparison of the newly generated confidence intervals for the remaining fitted parameters with the original values is shown in **Table 4**, but the intervals are similar. We therefore analysed the sensitivity of the model prediction to variations in each parameter value (**Supplementary Table S1**). The model prediction for growth in medium with no sulphate, shown in **Figure 3**, was not notably sensitive to small changes in any fitted parameter value except for H_{max}, which determines the final partial pressure of gaseous hydrogen. Contrastingly, the model fit to gaseous hydrogen shown in **Figure 2** showed sensitivity to a number of parameters. Small variations in the maximum growth rates, half-saturation constant for lactate, yield values and the stoichiometric constants b_{LH} and b_{HP}, all resulted in relatively large changes in the quality of fit of the model to the gaseous hydrogen data. The change in the goodness of fit to the other data types was minimal. We also found that the model fit was only slightly sensitive to small changes in the initial conditions for lactate, sulphate and bacterial concentration and

TABLE 2 | Analysis of model fits to the calibration data.

Variable	Noguera et al. (1998) model	Current model			
	R^2	R^2	Pearson's correlation coefficient (95% confidence interval)	CCC†	Mean bias
Figure 2					
Cell concentration	0.83	0.80	0.93 (−0.28, 0.99)	0.84	−10.58 mg L^{-1}
Lactate	0.95	0.96	0.98 (0.95–0.99)	0.96	−0.06 mM
Acetate	0.92	0.97	0.99 (0.94–0.99)	0.97	−0.23 mM
Sulphate	0.94	0.93	0.99 (0.94–0.99)	0.95	−0.26 mM
Gaseous hydrogen	<0	<0	0.93 (0.77–0.98)	0.57	-4.95×10^{-4} atm
Figure 3					
Gaseous hydrogen	0.83	0.96	0.98 (0.89–0.99)	0.96	-4.75×10^{-4} atm

†*CCC: Concordance correlation coefficient (Lin, 1989).*

TABLE 3 | AIC calculation values.

Model	*n*	*K*	RSS	log($\mathcal{L}(\theta)$)	AICc	Akaike weight
Noguera et al. (1998)	63	20	9.6095	−111.4	282.8	0.0001
This model	63	10	8.9861	−119.5	263.2	0.9999

insensitive to such changes in the initial conditions for other metabolites. This was in contrast to the model of Noguera et al. (1998), which we found to be disproportionately sensitive to small changes in the initial conditions for dissolved hydrogen and carbonates: variables less likely to have a strong effect on culture dynamics than lactate, sulphate and bacterial concentrations.

Model Validation

The model was validated against a number of different experimental data sources (Noguera et al., 1998; da Silva et al., 2013). **Figure 4** shows the model simulation for gaseous hydrogen dynamics in medium lacking lactate, where *D. vulgaris* may only perform sulphate reduction, until the available hydrogen is depleted [data from Noguera et al. (1998)].

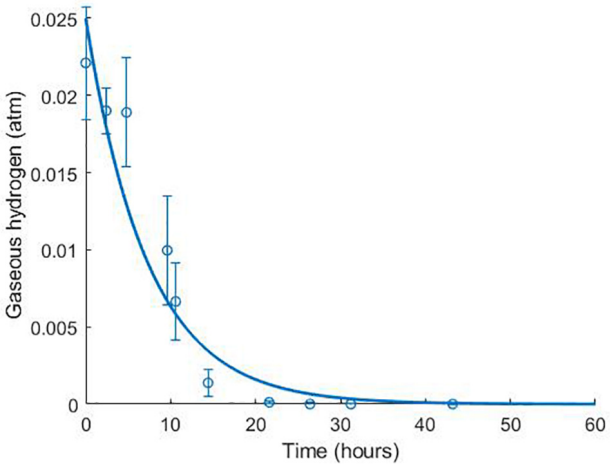

FIGURE 4 | Dynamics of gaseous hydrogen in medium supplemented with 9.3 mM sulphate in the absence of lactate, with an initial hydrogen partial pressure in the gaseous phase of approximately 0.025 atm. 12 mM acetate was added as a carbon source (Noguera et al., 1998). The solid line shows the prediction of the current model. R^2 = 0.91, ρ = 0.96 (0.83, 0.99), CCC = 0.92, mean bias = –0.0003 atm.

Figures 5, **6** show the comparison between the model prediction and experimental data from further validation experiments, with altered initial conditions [data from Noguera et al. (1998)]. Unfortunately, for these and the experiments from which **Figures 3**, **4** were generated, data for aqueous metabolite concentrations and bacterial growth are unavailable, so we cannot verify the model predictions for these variables. We also have no information regarding the concentration of bacteria at the beginning of the experiment, therefore 9.4 mg L^{-1}, the initial bacterial concentration in previous experiments, was assumed.

The model predicts the full utilisation of lactate and only partial consumption of sulphate in **Figure 5**, but is not able to capture the delay in hydrogen accumulation in the headspace observed in the first few hours of the experiment. The same

TABLE 4 | Confidence interval comparisons.

Parameter		Notation	MCMC generated 95% confidence interval	
			Fitted half-saturation parameters	Fixed half-saturation parameters
Maximum growth rates	Lactate oxidation	$\mu_{max,L}$	0.088–1.155	0.02–0.145
	Sulphate reduction	$\mu_{max,S}$	0.023–0.212	0.021–0.171
Monod constants	Lactate	K_L	7.3–136.8	–
	Sulphate	K_S	0.02–0.268	–
	Hydrogen	K_H	2.5×10^{-4}–3.96×10^{-3}	–
Yield parameters	Lactate	Y_L	0.99–9.57	1.18–9.4
	Sulphate	Y_S	2.2–19.35	1.99–17.2
Mass transfer parameter		k_La	0.182–0.914	0.313–3.724
Inhibitory hydrogen concentration		H_{max}	0.0341–0.0821	0.0335–0.0797

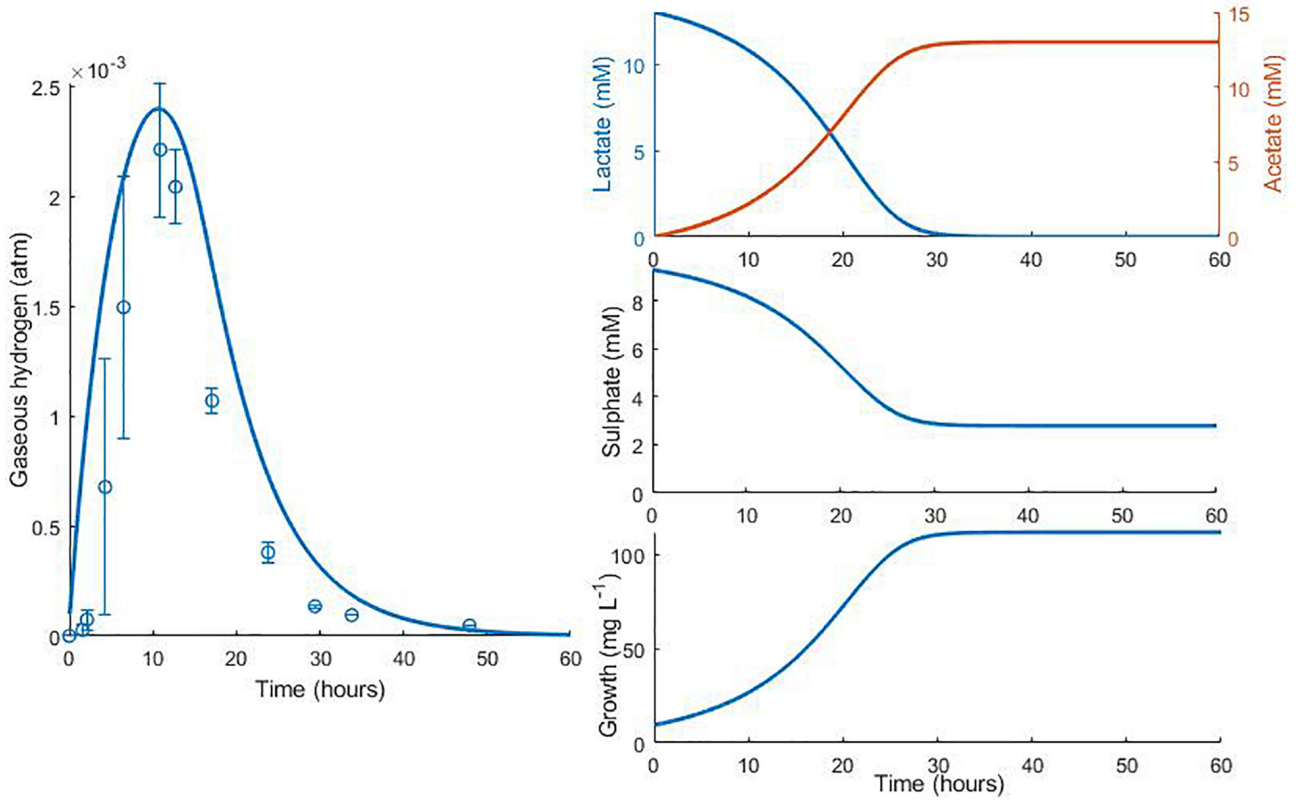

FIGURE 5 | Dynamic changes in gaseous hydrogen with initial metabolite concentrations: 13 mM lactate; 9.3 mM sulphate (Noguera et al., 1998). Solid lines show the prediction of the current model. R^2 = 0.70, ρ = 0.93 (0.76, 0.98), CCC = 0.77, mean bias = 0.0004 atm.

is true of **Figure 6**. Here, the model accurately predicts the final concentration of lactate remaining in the medium at the end of the experiment as 2.98 mM, compared to the observed value of 2.58 mM. However, the model overpredicts the gaseous hydrogen accumulation. Under our model assumptions we expect hydrogen to accumulate to the inhibitory level, whereas in the experiment hydrogen production was far lower. Given that the model accurately predicted the lactate degradation, this would imply that less hydrogen is produced under the conditions shown in **Figure 6** than under the assumed stoichiometry. Hydrogen accumulation was not measured after 48 h in the experiment, therefore it is not possible to know whether and at what point hydrogen accumulation peaks.

Figure 7 shows the validation of the both our model and that of Noguera et al. (1998) against separate experimental data for *D. vulgaris* Hildenborough, taken from da Silva et al. (2013). The experimental starting concentration of bacteria was not stated for this data set, so we fitted this value to the data with all other parameters fixed at their previously determined values. This gave an initial bacterial concentration of 6.75 mg L^{-1} for our model and 0.038 mg L^{-1} for the model of Noguera et al. (1998). As shown in **Figure 7**, the models performed similarly with their respective initial bacterial concentrations, with the exception of the gaseous hydrogen prediction, and both accurately captured the rate of lactate degradation and acetate production with no alteration to the parameter values obtained during model calibration. The large discrepancy between the obtained initial bacterial concentrations for the two models prompted further investigation. The initial optical density (OD) recorded for this experiment was approximately 0.025 (da Silva et al., 2013). No calibration to other units was performed by these authors and few exist in the literature for *Desulfovibrio* strains, but Bernardez and de Andrade Lima (2015) suggested a conversion of: dry weight (mg) = exp (5.12 OD–4.987), which gives an approximate initial bacterial concentration for this experiment of 7.76 mg L^{-1}. Although the conditions under which this conversion was derived differ from the experiment of da Silva et al. (2013), this estimate compares well to that of our model.

The final acetate measurement in **Figure 7** was not predicted by either model, and it is not clear to where the remaining carbon from lactate degradation was directed in this experiment. *D. vulgaris* has the potential to use acetyl-CoA, an intermediate on the lactate oxidation pathway, in the biosynthesis of certain branched-chain amino acids and fatty acids, as well as in an incomplete citric acid cycle (Heidelberg et al., 2004), but only the metabolites shown in **Figure 7** were measured. However, separate experiments by these authors with concentrated cell suspensions found the expected 1:1 ratio of lactate degraded to acetate produced (da Silva et al., 2013).

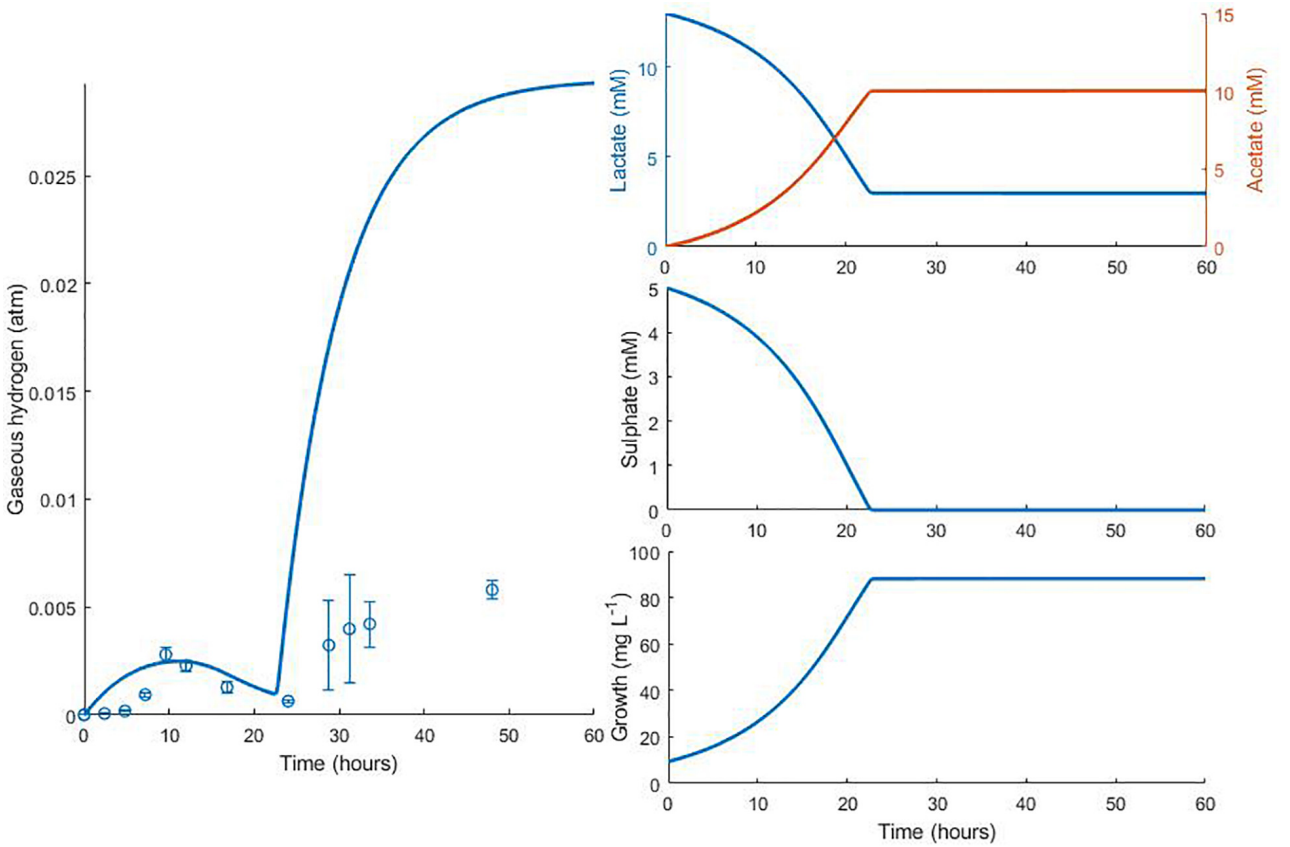

FIGURE 6 | Dynamic changes in gaseous hydrogen with initial metabolite concentrations: 13 mM lactate; 5 mM sulphate (Noguera et al., 1998). Solid lines show the prediction of the current model. R^2 = 0.22, ρ = 0.91 (0.72, 0.97), CCC = 0.22, mean bias = 0.0062 atm.

DISCUSSION

This model provides a simpler mathematical representation of SRB metabolism than is currently available in the literature (Noguera et al., 1998), with similar predictive capability. As such, it can be more easily adapted to specific strains and culture conditions, not limited to SRB of the human GIT. The inclusion of further characteristics of specific SRB strains could be realised with the addition of further terms to existing equations, or the inclusion of further equations if additional metabolites were considered. For example, complete growth inhibition of a SRB strain due to sulphide concentrations above 16.1 mM has been shown previously (Reis et al., 1992). Acetate inhibition has also been investigated for SRB, with approximately 54 mg L^{-1} undissociated acetic acid (≈45.9 mM acetate) resulting in 50% growth inhibition (Reis et al., 1990). Both these concentrations are greater than those measured in the experiments used here, and the H_2S concentration is greater than that reported in faeces (Magee et al., 2000). However, the model could be adjusted to include inhibition terms for acetate and H_2S for application of the model to more extreme environments. These terms could take the form used here for hydrogen inhibition, but alternative inhibition terms could be more appropriate and should be assessed by model fitting (see Han and Levenspiel (1988) for a list of inhibition terms and a generalised form). At present, we are not aware of any time-course data involving such concentrations of these metabolites with which to parameterise the model.

It would also be useful to investigate experimentally the influence of bicarbonate on the growth rate of SRB. Several human-associated bacterial strains have shown reduced growth rates when exposed to 100 mM of bicarbonate in monoculture (Dobay et al., 2018). This molecule was also shown to disrupt biofilm formation in selected strains. *D. vulgaris* is a biofilm forming organism (Clark et al., 2007), but no SRB were studied in the bicarbonate inhibition experiments, so we cannot make any inference about the influence of this molecule on growth rates in our model. However, following the expected stoichiometry of the *D. vulgaris* metabolic pathways, we would anticipate less than 20 mM of bicarbonate could be produced in the experiments of Noguera et al. (1998), and up to 40 mM in the experiments of da Silva et al. (2013), considerably lower than those found to be growth limiting in Dobay et al. (2018). Bicarbonate is secreted into the gastrointestinal lumen in humans, reaching comparable concentrations to those expected in these experiments: bicarbonate concentration at the start of the colon is estimated at around 30 mM (Gennari and Weise, 2008). Further experimental investigation is needed to determine

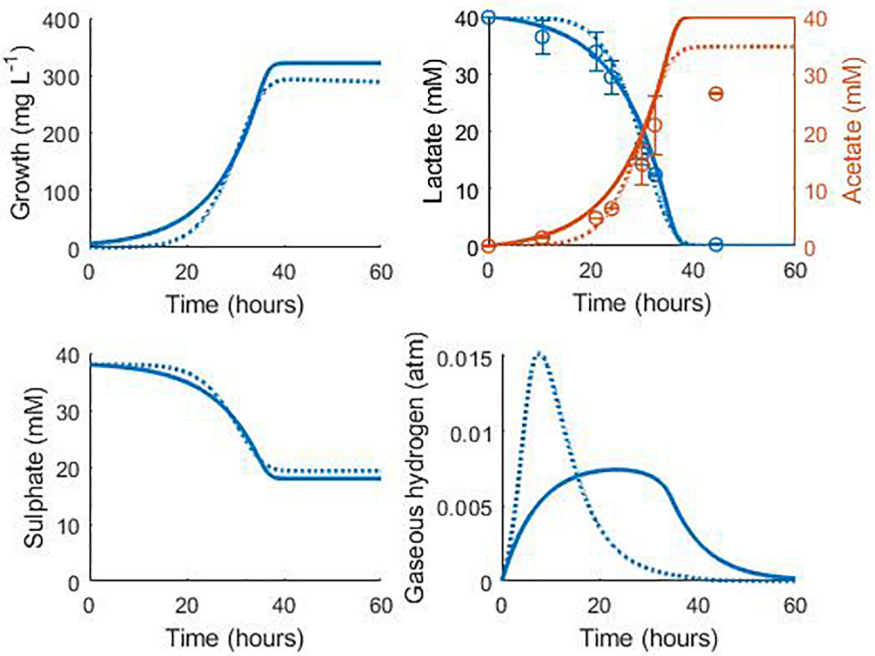

FIGURE 7 | Model prediction for the consumption of lactate and production of acetate in the experimental work of da Silva et al. (2013): continuous lines display the fit of the current model; dotted lines display the fit of the model described in Noguera et al. (1998). See text for full explanation. Continuous line fit: Lactate: R^2 = 0.98, ρ = 0.99 (0.95, 0.99), CCC = 0.98, mean bias = 1.2 mM; Acetate: R^2 = 0.82, ρ = 0.99 (0.93, 0.99), CCC = 0.88, mean bias = 4.12 mM. Dotted line fit: Lactate: R^2 = 0.98, ρ = 0.99 (0.96, 0.99), CCC = 0.98, mean bias = 1.32 mM; Acetate: R^2 = 0.90, ρ = 0.99 (0.97, 0.99), CCC = 0.93, mean bias = 2.08 mM.

whether, and to what extent, bicarbonate may be growth limiting to SRB before it can be included in a model.

Time-course data is also unavailable for the use of acetate as a carbon source by SRB, which has been shown in the absence of lactate [for example, Pankhania et al. (1986)]. We expect that acetate uptake is occurring in the data shown in **Figure 4**, as it is the sole available carbon source in the medium, but this was not measured. Experiments measuring acetate concentrations over time when this is the sole carbon source are required to determine the parameter values of acetate utilisation via model fitting.

Modelling mass transfer in experiments such as those described here is challenging. Due to limited available experimental data, we chose to use a simple mass transfer model to minimise the number of fitting parameters required. Mass transfer is modelled under the assumption of linear dynamics, but without knowledge of the concentration of dissolved hydrogen it is unclear how much this assumption biases the model. The model may be more limited in its ability to accurately capture hydrogen transfer between phases than other, more complex model structures (Kadic and Heindel, 2014). This simple structure may be partially responsible for the sensitivity of the gaseous hydrogen model fit to small changes in some of the parameter values of the model. However, we believe that the model fit to the lactate, acetate and sulphate data are of greater importance than those of gaseous hydrogen and bacterial growth for several reasons. The apparent initial lag phase in the gaseous hydrogen data from the experiments considered here was not captured by our model, despite the good fit to the data for other metabolites. While the inclusion of a lag phase in the model could rectify this aspect, such an addition would complicate a model that we wish to keep parsimonious and we also do not have a probable physiological cause for such a lag. The experimental data shows large variation in gaseous hydrogen pressure between replicates in both the calibration and validation datasets. The data for the concentration of bacterial cells in the medium is similarly limited. Only two measurements were taken during the exponential growth phase in **Figure 2**, and the error on both of these measurements is greater than 25% of the mean value. It is also unclear how reliable the initial value for cell concentration is, since this was assumed from the inoculum rather than measured. Although our model proved only slightly sensitive to certain initial condition values, measuring the initial concentrations of both cells and metabolites would be of great value. The data for lactate, acetate and sulphate concentrations are more complete and more repeatable, encouraging emphasis on the model fit to these data.

Uncertainty remains in the field around the nature of hydrogen production and use by SRB. Previously, there have been arguments both for and against its status as a mandatory intermediate in the simultaneous oxidation of organic compounds and reduction of sulphate, as well as the role of various hydrogenase enzymes (Keller and Wall, 2011; Rabus et al., 2013). The importance of hydrogen in the reduction of sulphate has also been shown differ between SRB species [see review by Rabus et al. (2015)]. We believe that one of the strengths of the model is its avoidance of any biassing assumption about

TABLE 5 | Model notation.

Notation	Description	Unit
$\mu_{max,L}$	Maximum growth rate for lactate	h^{-1}
$\mu_{max,S}$	Maximum growth rate for sulphate	h^{-1}
K_L	Half-saturation constant for lactate	mM
K_S	Half-saturation constant for sulphate	mM
K_H	Half-saturation constant for hydrogen	mM
Y_L	Yield term for lactate oxidation	mg L^{-1} mM^{-1}
Y_S	Yield term for sulphate reduction	mg L^{-1} mM^{-1}
H_{max}	Inhibitory aqueous hydrogen concentration	mM
k_La	Mass transfer coefficient	h^{-1}
b_{LH}	Moles of hydrogen produced per mole lactate oxidised	–
b_{HP}	Moles of hydrogen utilised per mole H_2S produced	–
b_{LA}	Moles of acetate produced per mole lactate oxidised	–
b_{SP}	Moles of H_2S produced per mole sulphate reduced	–
L	Lactate concentration	mM
S	Sulphate concentration	mM
H_{aq}	Aqueous hydrogen concentration	mM
H_g	Gaseous hydrogen concentration	atm
A	Acetate concentration	mM
P	H_2S concentration	mM
X	Bacterial cell concentration	mg L^{-1}
t	Time	h
ρ_H	Henry conversion constant for hydrogen	atm mM^{-1}
V_{aq}	Volume of the aqueous phase [50 mL for the experiments of Noguera et al. (1998), 250 mL for the experiments of da Silva et al. (2013)]	mL
V_g	Volume of the gaseous phase [110 mL for the experiments of Noguera et al. (1998), 250 mL for the experiments of da Silva et al. (2013)]	mL

the nature of these relationships by using our two hydrogen compartments, aqueous and gaseous, as a method to represent hydrogen equivalents that are immediately available for use in sulphate reduction or not, respectively.

The mathematical model presented here is simpler in its construction than previous attempts to capture SRB dynamics. Our model uses nine fitted parameters (10 parameters in total), compared to seven fitted and three experimentally estimated parameters (20 parameters in total) in Noguera et al. (1998), and seven differential equations compared with ten in Noguera et al. (1998). Our model also shows good fits to experimental data as assessed by common measures for model analysis for two *D. vulgaris* strains from several independent experiments under varied conditions. While the model of Noguera et al. (1998) considers more factors, including the thermodynamics of the conversions performed by the bacteria and the concentrations of a greater number of metabolites, these inclusions can be limiting when investigating the metabolism of SRB in environments where knowledge of these factors is not available. For example, application of the model of Noguera et al. (1998) to the human GIT would be challenged by host influences on variables. The applied model would need to consider appropriate representation of bicarbonate and CO_2 when including secretion and absorption by the host, as well as the implications of host metabolite absorption on the modelled thermodynamic inhibition of the metabolic reactions. By contrast, the relative simplicity of our model means it can more easily be adapted to the specific environmental conditions of the GIT and has greater flexibility for the inclusion of additional influences upon the metabolism of these bacteria. In this way the model could be adapted to provide a representative model for the SRB functional group in the GIT.

Regarding dynamics in the GIT, current existing data from rodent models support the increased efficiency of carbohydrate breakdown by saccharolytic bacteria in the presence of either a methanogen or acetogen due to hydrogen metabolism by these microbes (Samuel and Gordon, 2006; Rey et al., 2010). However, there is no such evidence for the SRB, although in theory the same role could be filled by these bacteria (Smith et al., 2018). This may be due to competition for other substrates, which could be investigated using the model presented here in combination with existing models for saccharolytic bacteria [such as Kettle et al. (2015)].

It is our intention to use the SRB model presented here as part of a larger model including other hydrogenotrophic and hydrogenogenic microbes of the human GIT, to examine the role of hydrogen in this environment. Mathematical models for the GIT microbiota are available (Muñoz-Tamayo et al., 2010; Kettle et al., 2015, 2017), but as yet do not consider the action of SRB. The inclusion of this functional group may further enhance their predictive capabilities and could eventually be used to address the role of the SRB in human nutrition and health. Such community modelling should not be limited to the GIT, as the combination of models such as that presented here with similar structures for methanogens and reductive acetogens may reveal information about the cross-feeding and competitive relationships between these hydrogenotrophs in other environments.

DATA AVAILABILITY

The data supporting the conclusions of this manuscript will be made available by the authors, without undue reservation, to any qualified researcher.

AUTHOR CONTRIBUTIONS

NS performed the mathematical modelling and drafted the manuscript. All authors contributed to model and manuscript revision, and read and approved the submitted version.

FUNDING

NS was supported by a Ph.D. fellowship from the Riddet Institute through funding provided by the New Zealand Tertiary Education Commission. We are also grateful to AgResearch for the resources provided to NS.

ACKNOWLEDGMENTS

The authors thank I. Vetharaniam and W. Young at AgResearch for their thoughtful and useful comments on the manuscript.

SUPPLEMENTARY MATERIAL

The Supplementary Material for this article can be found online at: https://www.frontiersin.org/articles/10.3389/fmicb.2019.01652/full#supplementary-material

REFERENCES

Akaike, H. (1974). A new look at the statistical model identification. *IEEE Trans. Automat. Contr.* 19, 716–723. doi: 10.1109/TAC.1974.1100705

Badziong, W., and Thauer, R. K. (1978). Growth yields and growth rates of *Desulfovibrio vulgaris* (Marburg) growing on hydrogen plus sulfate and hydrogen plus thiosulfate as the sole energy sources. *Arch. Microbiol.* 117, 209–214. doi: 10.1007/bf00402310

Barton, L. L., and Fauque, G. D. (2009). Biochemistry, physiology and biotechnology of sulfate-reducing bacteria. *Adv. Appl. Microbiol.* 68, 41–98. doi: 10.1016/S0065-2164(09)01202-7

Bernardez, L. A., and de Andrade Lima, L. R. P. (2015). Improved method for enumerating sulfate-reducing bacteria using optical density. *MethodsX* 2, 249–255. doi: 10.1016/j.mex.2015.04.006

Burnham, K., and Anderson, D. (2002). *Model Selection and Multimodel Inference*. New York, NY: Springer-Verlag.

Carbonero, F., Benefiel, A. C., Alizadeh-Ghamsari, A. H., and Gaskins, H. R. (2012a). Microbial pathways in colonic sulfur metabolism and links with health and disease. *Front. Physiol.* 3:448. doi: 10.3389/fphys.2012.00448

Carbonero, F., Benefiel, A. C., and Gaskins, H. R. (2012b). Contributions of the microbial hydrogen economy to colonic homeostasis. *Nat. Rev. Gastroenterol. Hepatol.* 9:504. doi: 10.1038/nrgastro.2012.85

Clark, M. E., Edelmann, R. E., Duley, M. L., Wall, J. D., and Fields, M. W. (2007). Biofilm formation in *desulfovibrio vulgaris* hildenborough is dependent upon protein filaments. *Environ. Microbiol.* 9, 2844–2854. doi: 10.1111/j.1462-2920.2007.01398.x

da Silva, S. M., Voordouw, J., Leitão, C., Martins, M., Voordouw, G., and Pereira, I. A. C. (2013). Function of formate dehydrogenases in *Desulfovibrio vulgaris* hildenborough energy metabolism. *Microbiology* 159, 1760–1769. doi: 10.1099/mic.0.067868-0

Dobay, O., Laub, K., Stercz, B., Kéri, A., Balázs, B., Tóthpál, A., et al. (2018). Bicarbonate inhibits bacterial growth and biofilm formation of prevalent cystic fibrosis pathogens. *Front. Microbiol.* 9:2245. doi: 10.3389/fmicb.2018.02245

Doré, J., Pochart, P., Bernalier, A., Goderel, I., Morvan, B., and Rambaud, J. C. (1995). Enumeration of H2-utilizing methanogenic archaea, acetogenic and sulfate-reducing bacteria from human feces. *FEMS Microbiol. Ecol.* 17, 279–284. doi: 10.1016/0168-6496(95)00033-7

Gennari, F. J., and Weise, W. J. (2008). Acid-base disturbances in gastrointestinal disease. *Clin. J. Am. Soc. Nephrol.* 3, 1861–1868. doi: 10.2215/CJN.02450508

Han, K., and Levenspiel, O. (1988). Extended monod kinetics for substrate, product, and cell inhibition. *Biotechnol. Bioeng.* 32, 430–447. doi: 10.1002/bit.260320404

Heidelberg, J. F., Seshadri, R., Haveman, S. A., Hemme, C. L., Paulsen, I. T., Kolonay, J. F., et al. (2004). The genome sequence of the anaerobic, sulfate-reducing bacterium *Desulfovibrio vulgaris* hildenborough. *Nat. Biotechnol.* 22:554. doi: 10.1038/nbt959

Hurvich, C. M., and Tsai, C.-L. (1989). Regression and time series model selection in small samples. *Biometrika* 76, 297–307. doi: 10.2307/2336663

Ingvorsen, K., and Jørgensen, B. B. (1984). Kinetics of sulfate uptake by freshwater and marine species of Desulfovibrio. *Arch. Microbiol.* 139, 61–66. doi: 10.1007/bf00692713

Junicke, H., Feldman, H., van Loosdrecht, M. C. M., and Kleerebezem, R. (2015). Impact of the hydrogen partial pressure on lactate degradation in a coculture of Desulfovibrio sp. G11 and *Methanobrevibacter arboriphilus* DH1. *Appl. Microbiol. Biotechnol.* 99, 3599–3608. doi: 10.1007/s00253-014-6241-2

Kadic, E., and Heindel, T. J. (2014). *An Introduction to Bioreactor Hydrodynamics and Gas-Liquid Mass Transfer*. Hoboken NJ: Wiley.

Keller, K., and Wall, J. (2011). Genetics and molecular biology of the electron flow for sulfate respiration in Desulfovibrio. *Front. Microbiol.* 2:135. doi: 10.3389/fmicb.2011.00135

Kettle, H., Holtrop, G., Louis, P., and Flint, H. J. (2017). microPop: modelling microbial populations and communities in R. *Methods Ecol. Evol.* 9, 399–409. doi: 10.1111/2041-210x.12873

Kettle, H., Louis, P., Holtrop, G., Duncan, S. H., and Flint, H. J. (2015). Modelling the emergent dynamics and major metabolites of the human colonic microbiota. *Environ. Microbiol.* 17, 1615–1630. doi: 10.1111/1462-2920.12599

Kiran, M. G., Pakshirajan, K., and Das, G. (2017). An overview of sulfidogenic biological reactors for the simultaneous treatment of sulfate and heavy metal rich wastewater. *Chem. Eng. Sci.* 158, 606–620. doi: 10.1016/j.ces.2016.11.002

Kristjansson, J. K., Schönheit, P., and Thauer, R. K. (1982). Different Ks values for hydrogen of methanogenic bacteria and sulfate reducing bacteria: an explanation for the apparent inhibition of methanogenesis by sulfate. *Arch. Microbiol.* 131, 278–282. doi: 10.1007/bf00405893

Lin, L. I.-K. (1989). A concordance correlation coefficient to evaluate reproducibility. *Biometrics* 45, 255–268.

Magee, E. A., Richardson, C. J., Hughes, R., and Cummings, J. H. (2000). Contribution of dietary protein to sulfide production in the large intestine: an in vitro and a controlled feeding study in humans. *Am. J. Clin. Nutr.* 72, 1488–1494. doi: 10.1093/ajcn/72.6.1488

Magot, M., Ollivier, B., and Patel, B. K. C. (2000). Microbiology of petroleum reservoirs. *Antonie Van Leeuwenhoek* 77, 103–116. doi: 10.1023/a:1002434330514

Martins, M., Mourato, C., and Pereira, I. A. C. (2015). *Desulfovibrio vulgaris* growth coupled to formate-driven H2 production. *Environ. Sci. Technol.* 49, 14655–14662. doi: 10.1021/acs.est.5b02251

Monod, J. (1949). The growth of bacterial cultures. *Annu. Rev. Microbiol.* 3, 371–394. doi: 10.1146/annurev.mi.03.100149.002103

Motta, J.-P., Flannigan, K. L., Agbor, T. A., Beatty, J. K., Blackler, R. W., Workentine, M. L., et al. (2015). Hydrogen sulfide protects from colitis and restores intestinal microbiota biofilm and mucus production. *Inflamm. Bowel Dis.* 21, 1006–1017. doi: 10.1097/MIB.0000000000000345

Muñoz-Tamayo, R., Giger-Reverdin, S., and Sauvant, D. (2016). Mechanistic modelling of in vitro fermentation and methane production by rumen microbiota. *Anim. Feed Sci. Technol.* 220, 1–21. doi: 10.1016/j.anifeedsci.2016.07.005

Muñoz-Tamayo, R., Laroche, B., Walter, T., Doré, J., and Leclerc, M. (2010). Mathematical modelling of carbohydrate degradation by human colonic microbiota. *J. Theor. Biol.* 266, 189–201. doi: 10.1016/j.jtbi.2010.05.040

Muyzer, G., and Stams, A. J. M. (2008). The ecology and biotechnology of sulphate-reducing bacteria. *Nat. Rev. Microbiol.* 6, 441–454. doi: 10.1038/nrmicro1892

Nava, G. M., Carbonero, F., Croix, J. A., Greenberg, E., and Gaskins, H. R. (2012). Abundance and diversity of mucosa-associated hydrogenotrophic microbes in the healthy human colon. *ISME J.* 6, 57–70. doi: 10.1038/ismej.2011.90

Noguera, D. R., Brusseau, G. A., Rittmann, B. E., and Stahl, D. A. (1998). A unified model describing the role of hydrogen in the growth of *Desulfovibrio vulgaris* under different environmental conditions. *Biotechnol. Bioeng.* 59, 732–746. doi: 10.1002/(sici)1097-0290(19980920)59:6<732::aid-bit10>3.3.co;2-2

Okabe, S., Nielsen, P. H., Jones, W. L., and Characklis, W. G. (1995). Sulfide product inhibition of Desulfovibrio desulfuricans in batch and continuous cultures. *Water Res.* 29, 571–578. doi: 10.1016/0043-1354(94)00177-9

Pankhania, I. P., Gow, L. A., and Hamilton, W. A. (1986). The effect of hydrogen on the growth of *Desulfovibrio vulgaris* (Hildenborough) on lactate. *J. Gen. Microbiol.* 132, 3349–3356. doi: 10.1099/00221287-132-12-3349

Pankhania, I. P., Spormann, A. M., Hamilton, W. A., and Thauer, R. K. (1988). Lactate conversion to acetate, CO2 and H2 in cell suspensions of *Desulfovibrio vulgaris* (Marburg): indications for the involvement of an energy driven reaction. *Arch. Microbiol.* 150, 26–31. doi: 10.1007/BF00409713

Rabus, R., Hansen, T. A., and Widdel, F. (2013). *Dissimilatory Sulfate- and Sulfur-Reducing Prokaryotes The Prokaryotes: Prokaryotic Physiology and Biochemistry*. Berlin: Springer, 309–404.

Rabus, R., Venceslau, S. S., Wöhlbrand, L., Voordouw, G., Wall, J. D., and Pereira, I. A. C. (2015). A post-genomic view of the ecophysiology, catabolism and biotechnological relevance of sulphate-reducing prokaryotes. *Adv. Microb. Physiol.* 66, 55–321. doi: 10.1016/bs.ampbs.2015.05.002

Reis, M. A. M., Almeida, J. S., Lemos, P. C., and Carrondo, M. J. T. (1992). Effect of hydrogen sulfide on growth of sulfate reducing bacteria. *Biotechnol. Bioeng.* 40, 593–600. doi: 10.1002/bit.260400506

Reis, M. A. M., Lemos, P. C., Almeida, J. S., and Carrondo, M. J. T. (1990). Influence of produced acetic acid on growth of sulfate reducing bacteria. *Biotechnol. Lett.* 12, 145–148. doi: 10.1007/BF01022432

Rey, F. E., Faith, J. J., Bain, J., Muehlbauer, M. J., Stevens, R. D., Newgard, C. B., et al. (2010). Dissecting the *in vivo* metabolic potential of two human gut acetogens. *J. Biol. Chem.* 285, 22082–22090. doi: 10.1074/jbc.M110.117713

Rey, F. E., Gonzalez, M. D., Cheng, J., Wu, M., Ahern, P. P., and Gordon, J. I. (2013). Metabolic niche of a prominent sulfate-reducing human gut bacterium. *Proc. Natl. Acad. Sci. U.S.A.* 110, 13582–13587. doi: 10.1073/pnas.1312524110

Robinson, J. A., and Tiedje, J. M. (1984). Competition between sulfate-reducing and methanogenic bacteria for H2 under resting and growing conditions. *Arch. Microbiol.* 137, 26–32. doi: 10.1007/BF00425803

Samuel, B. S., and Gordon, J. I. (2006). A humanized gnotobiotic mouse model of host-archaeal-bacterial mutualism. *Proc. Natl. Acad. Sci. U.S.A.* 103, 10011–10016. doi: 10.1073/pnas.0602187103

Sander, R. (2015). Compilation of Henry's law constants (version 4.0) for water as solvent. *Atmos. Chem. Phys.* 15, 4399–4981. doi: 10.5194/acp-15-4399-2015

Scanlan, P. D., Marchesi, J. R., and Shanahan, F. (2009). Culture-independent analysis of desulfovibrios in the human distal colon of healthy, colorectal cancer and polypectomized individuals. *FEMS Microbiol. Ecol.* 69, 213–221. doi: 10.1111/j.1574-6941.2009.00709.x

Smith, N. W., Shorten, P. R., Altermann, E. H., Roy, N. C., and McNabb, W. C. (2018). Hydrogen cross-feeders of the human gastrointestinal tract. *Gut Microbes* 10, 270–288. doi: 10.1080/19490976.2018.1546522

Stams, A. J. M., and Plugge, C. M. (2009). Electron transfer in syntrophic communities of anaerobic bacteria and archaea. *Nat. Rev. Microbiol.* 7, 568–577. doi: 10.1038/nrmicro2166

Stolyar, S., Van Dien, S., Hillesland, K. L., Pinel, N., Lie, T. J., Leigh, J. A., et al. (2007). Metabolic modeling of a mutualistic microbial community. *Mol. Syst. Biol.* 3:92.

Thauer, R. K., Jungermann, K., and Decker, K. (1977). Energy conservation in chemotrophic anaerobic bacteria. *Bacteriol. Rev.* 41, 100–180.

Tomasova, L., Konopelski, P., and Ufnal, M. (2016). Gut bacteria and hydrogen sulfide: the new old players in circulatory system homeostasis. *Molecules* 21:1558. doi: 10.3390/molecules21111558

Walker, C. B., He, Z., Yang, Z. K., Ringbauer, J. A., He, Q., Zhou, J., et al. (2009). The electron transfer system of syntrophically grown *Desulfovibrio vulgaris*. *J. Bacteriol.* 191, 5793–5801. doi: 10.1128/JB.00356-09

Willis, C. L., Cummings, J. H., Neale, G., and Gibson, G. R. (1996). In vitro effects of mucin fermentation on the growth of human colonic sulphate-reducing bacteria. *Anaerobe* 2, 117–122. doi: 10.1006/anae.1996.0015

Wolin, M. J., and Miller, T. L. (1983). Interactions of microbial populations in cellulose fermentation. *Fed. Proc.* 42, 109–113.

Conflict of Interest Statement: The authors declare that the research was conducted in the absence of any commercial or financial relationships that could be construed as a potential conflict of interest.

frontiers in Microbiology

ORIGINAL RESEARCH
published: 16 August 2019
doi: 10.3389/fmicb.2019.01873

Hydrogen Oxidation Influences Glycogen Accumulation in a Verrucomicrobial Methanotroph

Carlo R. Carere[1], Ben McDonald[2], Hanna A. Peach[3], Chris Greening[4], Daniel J. Gapes[2], Christophe Collet[2] and Matthew B. Stott[5]*

[1] Department of Chemical and Process Engineering, University of Canterbury, Christchurch, New Zealand, [2] Scion, Te Papa Tipu Innovation Park, Rotorua, New Zealand, [3] Geomicrobiology Research Group, Department of Geothermal Sciences, GNS Science, Taupō, New Zealand, [4] School of Biological Sciences, Monash University, Clayton, VIC, Australia, [5] School of Biological Sciences, University of Canterbury, Christchurch, New Zealand

OPEN ACCESS

Edited by:
Roland Hatzenpichler, Montana State University, United States

Reviewed by:
Ludmila Chistoserdova, University of Washington, United States
Grayson L. Chadwick, California Institute of Technology, United States
Lisa Y. Stein, University of Alberta, Canada

***Correspondence:**
Carlo R. Carere
carlo.carere@canterbury.ac.nz

Specialty section:
This article was submitted to Microbial Physiology and Metabolism, a section of the journal Frontiers in Microbiology

Received: *06 June 2019*
Accepted: *29 July 2019*
Published: *16 August 2019*

Citation:
Carere CR, McDonald B, Peach HA, Greening C, Gapes DJ, Collet C and Stott MB (2019) Hydrogen Oxidation Influences Glycogen Accumulation in a Verrucomicrobial Methanotroph. Front. Microbiol. 10:1873. doi: 10.3389/fmicb.2019.01873

Metabolic flexibility in aerobic methane oxidizing bacteria (methanotrophs) enhances cell growth and survival in instances where resources are variable or limiting. Examples include the production of intracellular compounds (such as glycogen or polyhydroxyalkanoates) in response to unbalanced growth conditions and the use of some energy substrates, besides methane, when available. Indeed, recent studies show that verrucomicrobial methanotrophs can grow mixotrophically through oxidation of hydrogen and methane gases *via* respiratory membrane-bound group 1d [NiFe] hydrogenases and methane monooxygenases, respectively. Hydrogen metabolism is particularly important for adaptation to methane and oxygen limitation, suggesting this metabolic flexibility may confer growth and survival advantages. In this work, we provide evidence that, in adopting a mixotrophic growth strategy, the thermoacidophilic methanotroph, *Methylacidiphilum* sp. RTK17.1 changes its growth rate, biomass yields and the production of intracellular glycogen reservoirs. Under nitrogen-fixing conditions, removal of hydrogen from the feed-gas resulted in a 14% reduction in observed growth rates and a 144% increase in cellular glycogen content. Concomitant with increases in glycogen content, the total protein content of biomass decreased following the removal of hydrogen. Transcriptome analysis of *Methylacidiphilum* sp. RTK17.1 revealed a 3.5-fold upregulation of the Group 1d [NiFe] hydrogenase in response to oxygen limitation and a 4-fold upregulation of nitrogenase encoding genes (*nifHDKENX*) in response to nitrogen limitation. Genes associated with glycogen synthesis and degradation were expressed constitutively and did not display evidence of transcriptional regulation. Collectively these data further challenge the belief that hydrogen metabolism in methanotrophic bacteria is primarily associated with energy conservation during nitrogen fixation and suggests its utilization provides a competitive growth advantage within hypoxic habitats.

Keywords: methanotroph, hydrogenase, glycogen, extremophile, methylacidiphilum

INTRODUCTION

Aerobic methane oxidizing bacteria (methanotrophs) serve as the primary biological sink for the potent greenhouse gas methane (CH_4) (Kirschke et al., 2013). Methanotrophs grow by oxidizing CH_4 to methanol with a particulate or soluble methane monooxygenase enzyme (pMMO/sMMO) and subsequently yield reducing equivalents (e.g., NADH) for cellular respiration and biosynthesis through the oxidation of methanol to carbon dioxide (CO_2). The gammaproteobacterial (Type I) and alphaproteobacterial (Type II) methanotrophs generate biomass by assimilating the intermediates formaldehyde or formate via the ribulose monophosphate (RuMp) or serine pathways (Hanson and Hanson, 1996) respectively, whereas the verrucomicrobial methanotrophs oxidize methanol directly to formate (Keltjens et al., 2014) and generate biomass by fixing inorganic carbon (CO_2) via the Calvin–Benson–Bassham cycle (Khadem et al., 2012b). Despite the apparent restriction of most methanotrophs to grow on one carbon compounds (C1), they thrive at the interface of various oxic/anoxic habitats (e.g., peat bogs, forest soils, wetlands, rice paddies and geothermal environments) (Dunfield et al., 2007; Singh et al., 2010; Knief, 2015), where the availability of oxidant (O_2), energy and carbon resources for growth is likely to fluctuate. Given the methane monooxygenase reaction ($CH_4 + O_2 + [NAD(P)H + H^+]/QH_2$ $CH_3OH + NAD(P)^+/Q + H_2O$) and the aerobic respiratory chain require a continual source of reductant and oxidant, methanotrophic bacteria must regulate their carbon, energy and resource allocation to fulfill metabolic demands for cellular growth and persistence (Hanson and Hanson, 1996).

Many bacterial species, including methanotrophs, accumulate biopolymers (e.g., glycogen, polyhydroxyalkanoates), phospholipids, and intracellular osmolytes (e.g., ectoine, sucrose) (Strong et al., 2016) in response to unbalanced growth conditions. This allows resources to be strategically conserved for assistance in times of starvation. The biosynthesis of glycogen, a highly branched polysaccharide consisting of α-1,4 bonded glucose residues with additional α-1,6 branched sidechains, is a common metabolic strategy for carbon storage that is shared among evolutionarily distant species (Wilson et al., 2010). Glycogen production has been widely described within Type I methanotroph species (Linton and Cripps, 1978; Eshinimaev et al., 2002) and the production of this compound has recently been reported in the verrucomicrobial methanotroph, *Methylacidiphilum fumarolicum* SolV (Khadem et al., 2012a). The physiological role of glycogen production in methanotrophs is not precisely understood, although it is believed to serve a role in environmental survival during periods of starvation and has been implicated to symbiotic performance, colonization and virulence (Bonafonte et al., 2000; McMeechan et al., 2005; Bourassa and Camilli, 2009; Wilson et al., 2010). Although the accumulation of intracellular glycogen may occur optimally during exponential growth (Gibbons and Kapsimalis, 1963; Eidels and Preiss, 1970), its synthesis is typically associated with entry into stationary phase when growth is limited due to the limitation of some critical nutrient (i.e., nitrogen, phosphate) or in the presence of excess carbon (Wilson et al., 2010). In bacteria, the biosynthesis of glycogen occurs by utilizing ADP-glucose as the glycosyl donor for polymer extension (Preiss, 1984). The precise mechanisms governing glycogen biosynthesis in bacteria, however, remain obscure. It is likely energy availability and redox status play a primary role in regulating glycogen biosynthesis, as ATP acts as substrate for the ADP-glucose producing reaction catalyzed by glucose-1-phosphate adenylyltransferase (Preiss, 1984).

To remain competitive within dynamic environments (Knief et al., 2003; Tavormina et al., 2010), some methanotrophs supplement CH_4 usage with other energy-yielding strategies (Dedysh and Dunfield, 2010). Several recent studies have revealed a few strains, notably *Methylocella silvestris*, utilize a suite of carbon and energy substrates, including simple organic acids, alcohols and short-chain alkane gases (Dedysh et al., 2005; Crombie and Murrell, 2014). Aerobic H_2 metabolism has also been shown in a range of methanotrophs (Chen and Yoch, 1987; Shah et al., 1995; Hanczar et al., 2002) and a wide range of hydrogenases have been shown to be distributed in methanotroph genomes (Greening et al., 2016). While H_2 oxidation was originally implicated in energy conservation in response to N_2 fixation (Takeda, 1988), more recent findings indicate that H_2 serves a multifaceted role in the growth and survival of these bacteria. Of the verrucomicrobial methanotrophs, the activity of respiratory-linked group 1d hydrogenases can provide sufficient energy to sustain chemolithoautotrophic growth on H_2 alone (Mohammadi et al., 2016; Carere et al., 2017). Further, mixotrophic growth (H_2 and CH_4) in the thermoacidophile *Methylacidiphilum* sp. RTK17.1 has been observed under O_2-limiting conditions and is proposed to provide a competitive advantage over obligate methanotrophy at oxic/anoxic soil boundaries within geothermal environments (Carere et al., 2017). This suggests that the additional energetic input of H_2 may counter the effect of otherwise unbalanced growth conditions.

The influence of H_2 metabolism on the production of intracellular energy reservoirs, commonly associated with unbalanced growth, within methanotrophic bacteria has yet to be elucidated. In this work, we investigate the effect of H_2 metabolism on glycogen production within the methanotroph, *Methylacidiphilum* sp. RTK17.1. Chemostat cultivation was performed during O_2-replete and O_2-limited cultivation, in the presence of NH_4^+ or N_2, with or without H_2 in the headspace, to determine the influence of H_2 metabolism on observed growth rates, biomass production characteristics and transcriptional regulation. We show that cellular growth rates, molar growth yields, and the allocation of resources between protein and glycogen production vary depending on the supply of H_2, O_2, and nitrogen (as NH_4^+ or N_2). Transcriptome data provided a basis of findings, showing significant differential regulation of operons encoding the group 1d [NiFe]-hydrogenase, methane monooxygenases, and nitrogenase between the conditions. In turn, these findings enhance understanding of the physiological strategies that methanotrophs use to grow and survive in different environments.

MATERIALS AND METHODS

Chemostat Cultivation of *Methylacidiphilum* sp. RTK17.1

Chemostat cultivation was performed to investigate the influence of H_2 metabolism on the growth and production of intracellular glycogen reservoirs in *Methylacidiphilum* sp. RTK17.1 with respect to unbalanced growth conditions (O_2 and nitrogen limitation). As previously described, a 1 l bioreactor (BioFlo 110; New Brunswick Scientific, Edison, NJ, United States) equipped with an InPro 6810 Polarographic Oxygen Sensor (Mettler-Toledo, Columbus, OH, United States) was used for all cultivations (Carere et al., 2017). Cultures were continuously incubated at pH 2.5, 50°C with stirring (800 rpm). The reactor was constantly maintained at a volume of 0.5 l with V4 mineral medium (Carere et al., 2017), prepared with or without NH_4Cl (0.4 g l^{-1}) addition (as necessary), and supplied at a constant flow rate of 10 ml h^{-1} ($D = 0.02$ h^{-1}). Custom gas mixtures were supplied to the chemostat at a rate of 10 ml min^{-1} and contained approximately (v/v) 3% CH_4 and 26% CO_2 for all experiments; O_2 at (v/v) 14.1% and 3.5%, respectively for O_2-replete and -limiting conditions, and H_2 at 0.4% (v/v). The balance of all gas mixtures was made up with N_2.

Cell densities were monitored at 600 nm using a Ultrospec 10 cell density meter (Amersham Bioscience, United Kingdom) with one unit of OD_{600} equivalent to 0.43 g l^{-1} cell dry weight for *Methylacidiphilum* sp. RTK17.1. Influent and effluent gas concentrations were monitored using a 490 micro GC equipped with a thermal conductivity detector (Agilent Technologies, United States). After achieving a steady-state condition as determined by OD_{600}, gas concentrations were monitored over several days and used as a basis to calculate growth and specific gas consumption rates. Biomass samples of *Methylacidiphilum* sp. RTK17.1 were harvested during steady-state operation for subsequent transcriptome sequencing, biomass cell dry weight determinations, intracellular glycogen, total protein and amino acid levels measurements.

Transcriptome Sequencing

Cell culture samples for transcriptome sequencing were harvested (10 ml) from steady-state chemostat experiments, pelleted by centrifugation at 5,000 x g (15 min, 4°C), suspended in 1 ml RNAlater Stabilization solution (Thermo Fisher Scientific) and then stored at −80°C until required for further analysis, as per the manufacturer's recommended protocols. The extraction and sequencing of RNA was performed by Macrogen Inc. (Seoul, Korea). Briefly, isolation of mRNA was performed using the RNeasy Mini kit (Qiagen) according to the manufacturer's protocol. Following total RNA extraction, ribosomal RNAs were removed using the Ribo-Zero rRNA removal kit (bacteria) and the quality of the remaining RNA was assessed using an Agilent 2100 Bioanalyzer (Agilent). Library construction was performed using the TruSeq Stranded Total RNA Sample Prep (microbe) Kit (Illumina) and sequencing was performed using an Illumina HiSeq2500 platform. From this, an average of 7,988,451 raw untrimmed reads were obtained for each of the five conditions sampled. These reads were then analyzed using the Artificial Intelligence RNA-Seq pipeline (Sequentia Biotech, Barcelona, Spain), as described elsewhere (Vara et al., 2019), which were reduced to an average of 7,287,318 following quality filtering and trimming. Retained paired-end reads (100 bp) were then mapped to the genome of *Methylacidiphilum infernorum* strain V4 (GCA_000019665.1) (Hou et al., 2008) using the 'different genotype' setting. An average of 80.01% reads were mapped to genes within the reference genome for the five experimental conditions (condition 1: O_2 limiting, N_2, no H_2 addition; condition 2: O_2 limiting, N_2, H_2 addition; condition 3: O_2 limiting, NH_4^+, H_2 addition; condition 4: O_2 replete, NH_4^+, H_2 addition; condition 5: O_2 replete, NH_4^+, no H_2 addition). Following this, differential gene expression profiles and accompanying statistical analysis was performed to investigate regulation using the edgeR (Robinson et al., 2010) tool available within the Artificial Intelligence RNA-Seq pipeline. Synonymous conditions were grouped as replicates for differential gene expression analysis during oxygen limiting (conditions 1, 2, and 3) and oxygen excess (conditions 4 and 5) growth. Likewise, conditions were grouped as replicates for differential gene expression analysis under nitrogen fixing (N_2; conditions 1 and 2) and nitrogen excess (NH_4^+; conditions 3, 4, and 5) growth conditions, respectively. Where provided, expression values are given as FPKM (Fragments per Kilobase Million; **Supplementary Table S1**) (Mortazavi et al., 2008). Raw and processed transcriptome sequence files (accession numbers GSM3872525-GSM3872529) were subsequently deposited into the Gene Expression Omnibus (GEO[1]) for archival storage.

Characterization of Biomass

Effluent biomass, produced during experimental steady-state chemostat operation, was collected and stored at 4°C over a period of 7 days for all biomass characterization studies. Following collection of approximately 2 l culture, cells were pelleted (5,000 × *g*, 20 min, 4°C) and stored at −20°C until required. Characterization of *Methylacidiphilum* sp. RTK17.1 biomass (crude protein, ash content, amino acid composition) was performed at the Massey University Nutrition Laboratory (accredited to ISO 17025; New Zealand) according to the official methods of analysis of the Association of Official Analytical Communities (AOAC, 2005) international. Briefly, total crude protein and ash content (% w/w) were determined via the Dumas method (AOAC method 968.06) (Ebeling, 1968) and furnace methods, respectively (AOAC method 942.05) (Thiex et al., 2012). Amino acid profile determination of acid-stable residues was performed via reverse-phase high performance liquid chromatography (HPLC) separation using AccQ derivatization of biomass (60–140 mg) samples following oxidization with performic acid and hydrolysis with hydrochloric acid as described in AOAC method 994.12 (AOAC, 2005).

The concentration of glycogen within crude cell extracts of *Methylacidiphilum* sp. RTK17.1 was determined using a Dionex ICS 3000 HPLC equipped with a Biorad Aminex HPX-87H column and a Shodex RI-101 refractive index detector. Triplicate

[1]https://www.ncbi.nlm.nih.gov/geo/

cell pellets, dried to constant weight (5–15 mg), were suspended in 1M NaOH (0.9 ml) and disrupted by boiling lysis for 1 h within sealed screw top Micro Tubes (Thermo Fisher Scientific). The efficacy (>99%) of cell lysis was confirmed microscopically. Crude extracts were then incubated with amyloglucosidase (35 U/ml crude) from *Aspergillus niger* (Sigma-Aldrich), following acidification with acetate buffer (0.1 ml) to pH 4.8, for 8 h at 45°C to convert intracellular glycogen reservoirs into glucose. Following this, the resulting glucose was quantified by HPLC and normalized against a standard curve of known glycogen content (Sigma) that had been contemporaneously treated with amyloglucosidase. To account for non-glycogen derived glucose in cell samples, extracts that did not undergo amyloglucosidase treatment were similarly analyzed by HPLC in parallel. Total intracellular glycogen content was then expressed as a function of cell dry weight (% w/w). Observed differences in growth and biomass characteristics were analyzed for statistical significance using the Tukey's honest significance test tool available in Prism v7.0a (Graphpad Software, Inc.).

RESULTS

Hydrogen Availability Differentially Affects Growth and Biomass Allocation Depending on Oxygen and Nitrogen Availability

The growth characteristics and biomass production of *Methylacidiphilum* sp. RTK17.1 was compared in chemostats in four different conditions that differed in O_2, nitrogen (NH_4^+/N_2), and H_2 supply. Results from these experiments are provided in **Table 1**.

Under nitrogen-replete conditions (i.e., NH_4^+ present in the medium), *Methylacidiphilum* sp. RTK17.1 displayed many of the same growth characteristics in response to O_2 availability as found previously (Carere et al., 2017) and results were consistent with similar studies on *M. fumarolicum* SolV (Khadem et al., 2012a). The observed rate of steady-state biomass production (mg l^{-1} h^{-1}) of *Methylacidiphilum* sp. RTK17.1) decreased by 33.1% following the transition from O_2-replete to O_2-limiting cultivation (*p-value*: <0.0001). This decrease in growth rate was accompanied by a 30.4% reduction in the volumetric rate (mmol l^{-1} h^{-1}) of CH_4 consumption and a 19-fold increase in the observed rate of H_2 oxidation (*p-value*: <0.0001). With respect to specific gas consumption rates normalized against biomass production (mmol $gCDW^{-1}$ h^{-1}), observed rates of CH_4 consumption did not change significantly (*p-value*: 0.988), whereas H_2 consumption increased 36-fold (*p-value*: <0.0001). Intracellular glycogen content was observed to increase dramatically from 11.26 (± 0.14)% during O_2-replete growth to 20.23 (± 0.77)% (w/w; *p-value*: < 0.0001) during O_2-limiting cultivation.

We observed significant changes in these parameters when *Methylacidiphilum* sp. RTK17.1 was cultivated under O_2-limitation depending on H_2 and nitrogen supply. In the presence of H_2, observed rates of *Methylacidiphilum* sp. RTK17.1 biomass production decreased by 8.61% (*p-value*: 0.019) during N_2-fixation compared to growth on NH_4^+ replete media. In comparison, removal of H_2 from the headspace resulted in an 18.67% reduction in the observed rate of biomass production compared to cells cultured in NH_4^+-replete media (from 5.57 to 4.33 mg l^{-1} h^{-1}; **Table 1**; *p-value*: < 0.0001). These results suggest the activity of respiratory-linked aerobic H_2 oxidation may, at least partially, serve to offset the energetic demand imposed by N_2 fixation. In support of this, onset of nitrogen limitation in cultures actively respiring H_2 did not significantly increase the production of intracellular glycogen (*p-value*: 0.999). Following the removal of H_2 from the reactor feedgas, however, internal glycogen content significantly increased from 20.00 (± 2.93)% to 48.86 (± 4.32)% (w/w; *p-value*: < 0.0001). This corresponds to a 2.03 fold increase in the volumetric production rate of glycogen (**Table 1**). In the absence of CH_4, at 4°C, cellular glycogen reservoirs were depleted within 100 days (**Supplementary Figure S1**).

The total protein and amino acid content of *Methylacidiphilum* sp. RTK17.1 biomass produced during steady-state growth was also determined (**Figure 1**). A maximum total protein content of 53.9 (± 2.69)% (w/w) was achieved during growth under O_2-replete conditions with NH_4^+ as a readily available source of nitrogen. Compared to O_2-replete growth, a minor but insignificant decrease in total protein content of biomass coincided with reduced O_2 availability (51.2 ± 2.56%), and in the transition from NH_4^+ to N_2 as a source of nitrogen (51.9 ± 2.56%). Consistent with the observation that glycogen production increased in the absence of H_2 (under O_2-limiting, N_2-fixing growth conditions), the least total protein content of biomass (42.5 ± 8.94%) was observed in conditions where energy availability is likely to constrain cell growth (i.e., O_2-limiting, N_2-fixing, no H_2; *p-value*: 0.018; **Figure 1A**). Observed changes in the concentration of specific amino acid residues under all of the growth conditions were generally consistent with the changes associated with total protein determinations (**Figure 1C**). For each of the experimental conditions, glutamic acid, leucine, aspartic acid, lysine and alanine were the amino acids in greatest abundance whereas methionine, histidine and cysteine were the least abundant residues.

Transcriptome Analysis Reveals Changes in Hydrogenase, Nitrogenase, and Methane Monooxygenase Expression Between the Conditions

Transcriptome analysis was performed on chemostat grown cultures of *Methylacidiphilum* sp. RTK17.1 to determine whether genes associated with energy metabolism (CH_4 or H_2), glycogen synthesis, N_2 or CO_2 fixation were regulated in response to O_2 or nitrogen availability (**Figure 2**). For these experiments, to resolve the possible influence of H_2 on transcriptional responses, a fifth chemostat condition (condition 5: O_2 replete, NH_4^+, no H_2 addition) was added to the four growth conditions described in **Table 1**. In response to O_2 limitation, 36 genes were identified as significantly upregulated (*p-value*: <0.001; False discovery rate (FDR): < 0.05) and 36 genes were significantly downregulated

TABLE 1 | Growth and productivity characteristics of *Methylacidiphilum* sp. RTK17.1 during chemostat cultivation.

Growth condition [a,b,c]	O_2-limited, N_2 no H_2 addition	O_2-limited, N_2 H_2 addition	O_2-limited, NH_4^+ H_2 addition	O_2-replete, NH_4^+ H_2 addition
Biomass productivity:				
mg l^{-1} h^{-1}	4.33 (± 0.10)	5.09 (± 0.19)	5.57 (± 0.50)	8.32 (± 0.10)
CH_4 consumption rate:				
mmol l^{-1} h^{-1}	0.76 (± 0.05)	0.69 (± 0.06)	0.89 (± 0.05)	1.28 (± 0.10)
mmol gCDW^{-1} h^{-1}	3.31 (± 0.21)	2.73 (± 0.27)	3.18 (± 0.13)	3.22 (± 0.05)
$Y_{CDW/CH4}$ (g mol^{-1})	5.73 (± 0.35)	7.39 (± 0.74)	6.29 (± 0.25)	6.52 (± 0.11)
H_2 consumption rate:				
mmol l^{-1} h^{-1}	–	0.19 (± 0.01)	0.20 (± 0.01)	0.01 (± 0.01)
mmol gCDW^{-1} h^{-1}	–	0.71 (± 0.10)	0.71 (± 0.08)	0.02 (± 0.01)
Glycogen content:				
% CDW	48.86 (± 4.32)	20.00 (± 2.93)	20.23 (± 0.77)	11.26 (± 0.14)
mg glycogen l^{-1} h^{-1}	2.12 (± 0.19)	1.04 (± 0.15)	1.13 (± 0.04)	0.94 (± 0.01)

[a]Feedgas was continuously supplied at a rate of 10 ml min^{-1} with the following compositions (where applicable;% v/v): O_2-replete, 14.1%; O_2-limiting, 3.5%, H_2 0.4%. For all experiments excess CH_4 was supplied at 3.2%, CO_2 at 26% with the balance made up with N_2. O_2 saturations in the medium were 57.5 and 0.17% for the O_2-replete and O_2-limiting conditions, respectively. [b]A dilution rate of 0.02 h^{-1} (10 ml h^{-1}) was maintained for all experiments, with NH_4^+ supplied at an influent concentration of 0.4 g l^{-1} where applicable. [c]Replicate numbers for each growth condition correspond to n = 6, n = 6, n = 4 and n = 7 moving from the leftmost column to rightmost column, respectively. The standard deviation from the average of these measurements is shown in brackets.

(*p-value*: < 0.001; FDR: < 0.05). Subunits of the particulate methane monooxygenase operon (*pmoCAB1*), corresponding to *M. infernorum* V4 loci Minf_1509–1511, displayed the greatest degree of transcriptional upregulation (average: 9.8 Log_2FC, *p-value*: < 0.0001) in response to O_2 limitation. In contrast, the closely related and immediately proximal *pmoCAB2* operon (homologous to *M. infernorum* V4 loci Minf_1506–1508) that was highly expressed during O_2 replete growth, was strongly downregulated during O_2-limited growth (average: −4.0 Log_2FC, *p-value*: < 0.0001). Interestingly, transcripts for a third putative and relatively divergent *pmoCAB3* operon were not detected under the experimental conditions tested.

Expression of the complete complement of genes necessary for the oxidation of CH_4 to CO_2, carbon assimilation via the Calvin-Benson-Bassham cycle, and ATP production via aerobic respiration were detected in all conditions tested (**Figure 2C** and **Supplementary Table S1**). However, with exception of a 1.78-fold (*p-value*: < 0.0001) downregulation of a *moxY*-like gene (Minf_1448) that encodes a methanol utilization control sensor protein, no significant differences in expression level in these pathways were observed across conditions. With respect to glycogen metabolism, all genes necessary for glycogen synthesis, storage and degradation were expressed, but did not display evidence of transcriptional regulation (**Supplementary Table S1**). Consistent with the onset of H_2 oxidation in chemostat cultures, genes encoding for the large and small subunits of the Group 1d respiratory [NiFe] hydrogenase, and its associated cytochrome *b* subunit, were upregulated by 3.5-, 3.6-, and 2.9-fold respectively (to a maximum of 3105 FPKM) in response to O_2 limitation (**Figures 2A,C**). Likewise, genes associated with hydrogenase maturation, nickel incorporation and nickel transport were also significantly upregulated (**Supplementary Table S1**). In contrast, the cytosolic Group 3b [NiFe] hydrogenase was constitutively transcribed at low levels (FPKM < 125).

We further analyzed RNA-seq data to investigate the influence of nitrogen limitation on transcriptional regulation within *Methylacidiphilum* sp. RTK17.1. During chemostat cultivation in the absence of a supplied nitrogen source (NH_4^+), 66 genes were upregulated (*p-value*: < 0.001; FDR: < 0.02) and 13 genes were downregulated (*p-value*: < 0.001; FDR: < 0.05) when compared to nitrogen excess growth conditions. Consistent with the onset of N_2 fixation, a seven-gene operon encoding nitrogenase structural subunits and cofactor biosynthesis proteins (*nifHDKENX*, Minf_1870–1876) was upregulated (average 6.4 Log_2FC; **Figures 2B,C**). In addition, numerous other genes involved in nitrogenase transcriptional regulation (*nifA*, Minf_0464), cofactor biosynthesis (*nifB*, Minf_0453), stabilization (*nifW*, Minf_0472), and nitrate (Minf_1096) and NH_4^+ transport (Minf_1075) were also significantly upregulated (**Supplementary Table S1**). Hydrogenase expression was not significantly different between the conditions, being high for the Group 1d [NiFe]-hydrogenase and low for the Group 3b [NiFe]-hydrogenase.

DISCUSSION

The accumulation and storage of carbon and energy as polymeric reserves is a common strategy employed by microorganisms during unbalanced growth to fortify them against periods of environmental starvation (Wilson et al., 2010). Nitrogen limitation is often cited as triggering the accumulation of carbon-rich reserve polymers (Wanner and Egli, 1990), but there is a lack of detailed understanding of the underlying mechanisms responsible for their production. As with many heterotrophic species, methanotrophs often produce carbon-rich polymers; however despite the prevalence of glycogen production within the Gammaproteobacteria methanotrophs (Pieja et al., 2011a), research has primarily focused on the physiology of polyhydroxybutyrate storage in the Alphaproteobacteria methanotrophs (Pieja et al., 2011a,b; Sundstrom and Criddle, 2015). The requirement for organic carbon compounds to

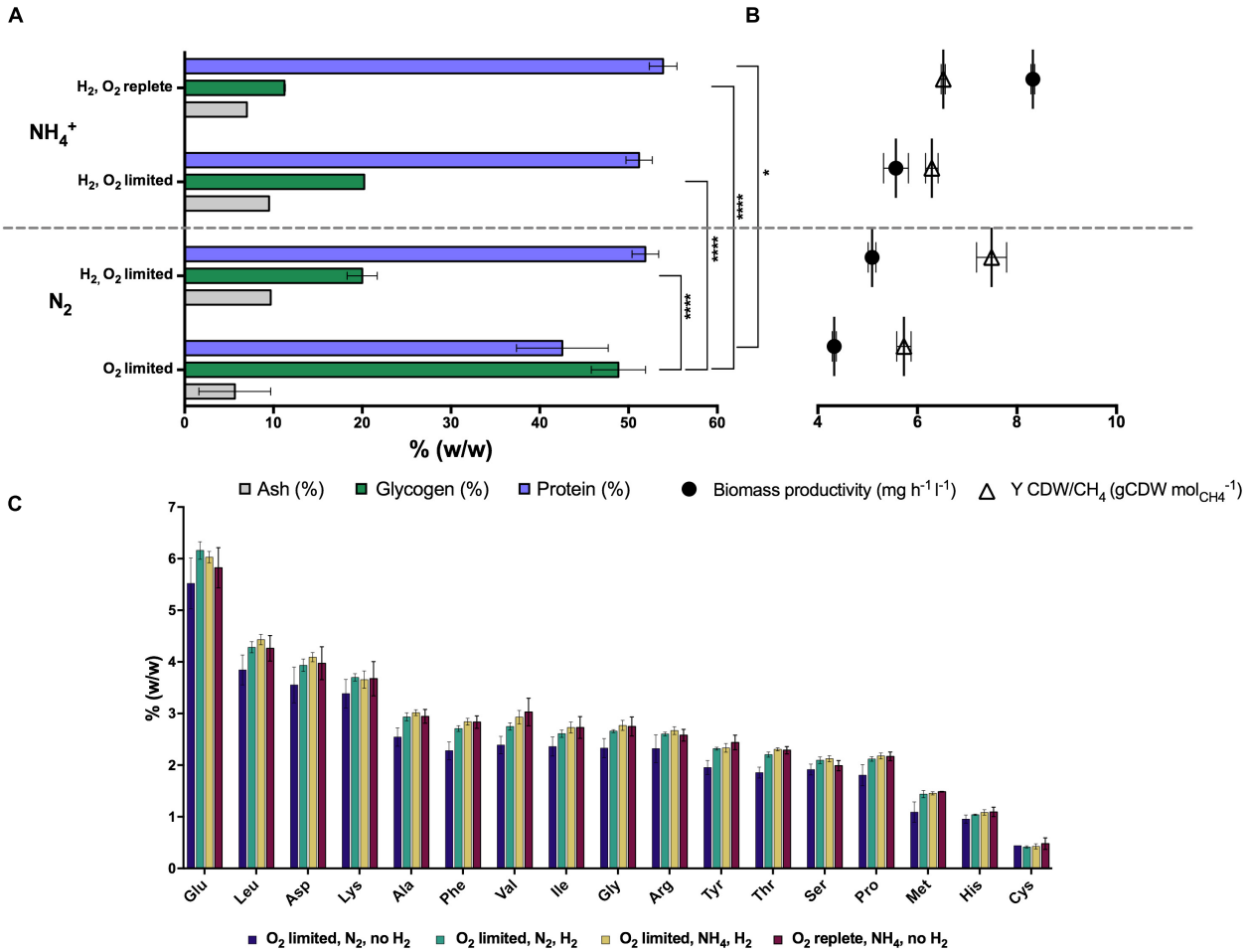

FIGURE 1 | The production of intracellular glycogen in chemostat grown cultures of *Methylacidiphilum* sp. RTK17.1 is influenced by O_2 availability, and H_2 and nitrogen metabolism. **(A)** Total protein, ash and glycogen content of cells, **(B)** observed growth rates and biomass yields (CDW: cell dry weight), and **(C)** amino acid content profiles are shown relative to total biomass. For all chemostat growth conditions, *Methylacidiphilum* sp. RTK17.1 excess CH_4 was continuously supplied (3% v/v, 10 ml min^{-1}). Displayed values represent the average of minimum triplicate samples, with error bars illustrating the standard deviation. Significant differences in cellular glycogen and protein content are shown next to squared brackets (****p-value < 0.0001, *p-value < 0.05).

provide both the respiratory energy and carbon necessary for anabolic processes for methanotrophs makes it difficult to untangle the roles of nitrogen, carbon, and energy availability (e.g., ATP) in the production of intracellular glycogen. However, as verrucomicrobial methanotrophs fix CO_2 for carbon and supplement their energy requirements via the oxidation of H_2 (Mohammadi et al., 2016; Carere et al., 2017), this affords an opportunity (obfuscated by the Type I and II methanotrophs) to investigate the influence of nitrogen, carbon, and energy availability independently.

Our findings show that H_2 oxidation influences the production of intracellular glycogen reservoirs in the thermoacidophilic methanotroph, *Methylacidiphilum* sp. RTK17.1. During chemostat experiments, the maximum glycogen content of *Methylacidiphilum* sp. RTK17.1 occurred within cells grown in the absence of H_2, under nitrogen- and O_2- limiting growth conditions [48.86 (± 4.32)%; **Table 1** and **Figure 1A**]. With respect to other studies reporting on the production of carbon storage polymers in methanotroph species, the glycogen content values observed for *Methylacidiphilum* sp. RTK17.1 are generally congruent. In the closely related thermoacidophile, *Methylacidiphilum fumarolicum* SolV, a maximum glycogen content of 36% (w/w) was observed (Khadem et al., 2012a) in nitrogen-limited, batch grown cells and a similar value (33% w/w) has been reported in the halotolerant methanotroph *Methylotuvimicrobium alkaliphilum* 20Z [formerly *Methylomicrobium alkaliphilum* 20Z (Khmelenina et al., 1999; Orata et al., 2018)]. A maximum of 42.8 (± 17.5)% (w/w) glycogen has been reported in the industrially promising methanotroph, *Methylotuvimicrobium buryatense* 5GB1 [formerly *Methylomicrobium buryatense* 5GB1 (Orata et al., 2018)], during batch-growth on methanol, with up to 13.1 (± 4.0)% (w/w) glycogen reported during O_2-limited chemostat growth on methane (Gilman et al., 2015).

The variability in reported glycogen content within methanotrophs (intraspecies) and between experimental

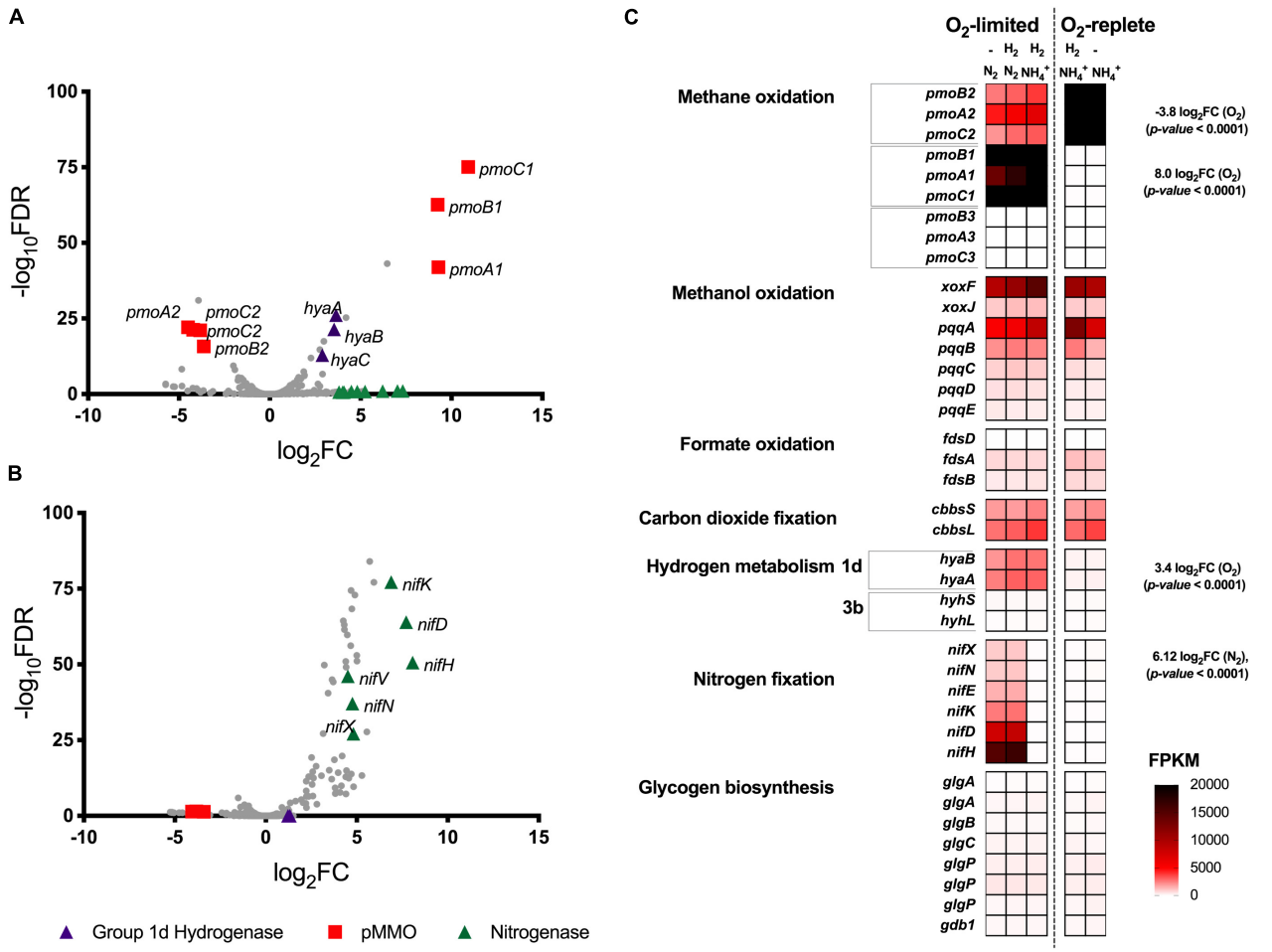

FIGURE 2 | Differential gene expression profiles of chemostat-grown cultures of *Methylacidiphilum* sp. RTK17.1 grown under O_2-replete and O_2-limiting conditions in the presence of ammonium (NH_4^+) or under N_2-fixing conditions. **(A)** Volcano plot showing differential gene expression changes following the transition from oxygen replete to O_2-limited growth. **(B)** Volcano plot showing differential gene expression changes following the transition from nitrogen-replete (NH_4^+) to N_2-fixing growth conditions. Both volcano plots compare data generated from the same five transcriptomes with fold-change values (log_2FC) and false discovery rates (FDR) calculated using O_2-replete and nitrogen excess as reference conditions, respectively. Each gene is represented by a gray dot and genes of interest are highlighted as per the legend. **(C)** Heat map of transcript abundance for key genes encoding the structural subunits of enzymes participating in methane oxidation (*pmoBAC;* particulate methane monooxygenase), methanol oxidation (*xoxFJ;* methanol dehydrogenase, *pqqABCDE;* pyrroloquinoline biosynthesis), formate oxidation (*fdsDAB*; formate dehydrogenase), carbon-dioxide fixation (*cbbsSL*; Rubisco), hydrogen metabolism (*hyaBA and hyhSL;* encoding group 1d and 3b [NiFe]-hydrogenases respectively), nitrogen fixation (*nifXNEKDH; nitrogenase*), and glycogen biosynthesis (*glgAABCPPP1*). The fragment counts per kilobase million transcripts (FPKM) are shown for steady-state cultures. O_2-replete, O_2-limiting, nitrogen-replete (NH_4^+), N_2-fixing and the supplementation of H_2 into the feed gas during chemostat operation is indicated.

trials (interspecies) is almost certainly a consequence of both underlying physiological characteristics and the inherent challenges associated with characterizing dynamic batch growth environments. We therefore sought to perform a series of carbon-excess (CO_2 and CH_4) steady-state experiments to gain insight into the mechanisms governing glycogen production in *Methylacidiphilum* sp. RTK17.1. With respect to O_2 and nitrogen limitation, rates of growth (inferred from observed biomass productivity rates), and changes to glycogen, and to a lesser extent total protein and amino acid contents, were consistent with a cell's expected response to unbalanced growth conditions. While previous studies have reported significant changes to the amino acid composition of *Staphylococcus aureus* cultures in response to variable environmental conditions (Alreshidi et al., 2015, 2016), we observed no change to the relative abundance of specific amino acid residues in *Methylacidiphilum* sp. RTK17.1 cultures under the conditions tested. Nevertheless, a 144% increase in glycogen content was observed during unbalanced growth following the removal of H_2 gas supply. Depriving *Methylacidiphilum* sp. RTK17.1 cultures of the respiratory energy gains afforded from H_2 gas oxidation is demonstrative of how this strain dynamically allocates carbon, nitrogen and energy resources.

The observation that *Methylacidiphilum* sp. RTK17.1 cells produce glycogen and grow more slowly in response to oxygen limitation is consistent with the occurrence of glycogen

within the obligate chemolithoautotroph *Hydrogenovibrio marinus* when grown on H_2 and CO_2 under O_2-limiting conditions (Nishihara et al., 1993). Similarly, production of polyhydroxybutyrate (PHB) has been reported within heterotrophically grown cultures of *Azotobacter beijerinckii* in response to oxygen limitation (Senior et al., 1972). We speculate that in the absence of sufficient oxygen, both glycogen and PHB reserves likely serve to not only store carbon and energy, but to maintain intracellular redox state. It is also plausible that the anabolic activities required for cell division (i.e., protein, DNA and RNA synthesis) were constrained by ATP availability under O_2-limiting conditions. Given protein synthesis requires approximately 19 times more ATP (mmol ATP (g macromolecule)$^{-1}$) than for saccharide polymerization (Stouthamer, 1979; Russell and Cook, 1995; Russell, 2007), even considering the ATP requirements of CO_2 fixation, glycogen biosynthesis likely represents an energetic *'cost'* savings for *Methylacidiphilum* sp. RTK171 compared to the ATP-demands of cell growth. These modest increases to intracellular glycogen content in response to O_2 limitation are unlikely to negatively impact biomass yields (Y_{ATP}; Russell and Cook, 1995) while also benefiting cell survivability during periods of starvation. The additional burden imposed by nitrogen limitation not only created unbalanced growth conditions with respect to carbon and nitrogen, but also increased the cell's ATP requirement via the nitrogenase reaction ($N_2 + 8H^+ + 16ATP \rightarrow 2NH_3 + H_2 + 16ADP$). Under these growth conditions, glycogen accounted for nearly half of *Methylacidiphilum* sp. RTK17.1 cell mass. Supplementing CH_4 oxidation with an alternative source of respiratory energy (H_2), however, was sufficient to offset the ATP burden imposed by N_2 fixation and consequently the production of intracellular glycogen was reduced and growth rates increased.

An alternative explanation for our chemostat observations is that synthesis of glycogen during energy-limiting conditions serves as a strategy for 'metabolic anticipation'. The combined conditions of low O_2, nitrogen, and H_2 availability are highly limiting for a cell and further resource deprivation is likely to trigger a transition from growth to persistence. Thus, disproportionately allocating biomass into storage compounds under this condition may serve as a 'bet-hedging' strategy to enable longer-term survival when conditions worsen. Indeed, the synthesis and storage of intracellular carbon polymers is commonly associated with an increase in viability during periods of environmental starvation. As with PHB, glycogen catabolism supplies reduced electron carriers (e.g., NADH) into the respiratory chain, thereby enabling the continuation of metabolic processes in the absence of an exogenous energy supply (e.g., CH_4 or H_2). A reduced lag phase following CH_4 starvation has previously been linked to the catabolism of glycogen reservoirs within the methanotroph *M. fumarolicum* SolV (Khadem et al., 2012a). Likewise, in *Methylacidiphilum* sp. RTK17.1 cultures, we interpret depletions in cellular glycogen content throughout prolonged incubations at 4°C (in the absence of CH_4) as evidence it was being consumed to promote survival (**Supplementary Figure S1**). Within oxic/anoxic habitats, it seems evident that *Methylacidiphilum* sp. RTK17.1 distributes carbon, energy and nitrogen resources during methanotrophic or mixotrophic growth to fulfill the metabolic demands imposed for cell persistence and/or proliferation (Hanson and Hanson, 1996). Similar phenomena of metabolic anticipation have been observed in other species, for example mycobacteria, which accumulate storage compounds such as triacylglycerols during the early hypoxic response (Daniel et al., 2004; Eoh et al., 2017).

While hydrogenase, methane monooxygenase and nitrogenase all displayed evidence of significant transcriptional regulation in response to O_2 and nitrogen limitation, the genes associated with glycogen metabolism were constitutively expressed. These results are consistent with previous findings within the verrucomicrobial methanotrophs (Khadem et al., 2010; Khadem et al., 2012a; Mohammadi et al., 2016; Carere et al., 2017) and suggests the enzymes associated with glycogen metabolism may be allosterically regulated in response to high carbon (i.e., fructose 1,6-bisphosphate) and/or energy contents (i.e., ATP/AMP), as described in other bacterial species (Wilson et al., 2010). Consistent with other verrucomicrobial methanotrophs (Dunfield et al., 2007; Pol et al., 2007; Op den Camp et al., 2009), *Methylacidiphilum* sp. RTK17.1 also possesses three phylogenetically distinct *pmoCAB* operons. Based on observed ratios of non-synonymous versus synonymous substitution rates in *pmoA* orthologs, it has been proposed that the pMMOs encoded in *Methylacidiphilum spp.* serve functionally distinct roles (Op den Camp et al., 2009). The observation that *Methylacidiphilum* sp. RTK17.1 transcriptionally regulates pMMO expression in response to oxygen availability therefore supports this hypothesis and is congruent with reports of differential expression in response to oxygen limitation (Khadem et al., 2012a) and during growth on methanol (Erikstad et al., 2012). Finally, it is noteworthy to include that the transcriptional upregulation of the Group 1d [NiFe] hydrogenase occurred in response to O_2 limitation; whereas nitrogenase upregulation was induced by nitrogen availability. The transcriptional decoupling of these two enzymes is further evidence that the physiological role of H_2 oxidation in methanotrophs (Mohammadi et al., 2016; Carere et al., 2017) is distinct from recycling H_2 produced during the nitrogen fixation reaction (Bont, 1976; Dixon, 1976; Chen and Yoch, 1987). Collectively, these findings indicate while H_2 oxidation is sufficient to partially offset the energetic costs associated with N_2 fixation, the regulation of this enzyme is transcriptionally uncoupled from nitrogen availability.

DATA AVAILABILITY

The raw and processed transcriptome sequence files (accession numbers GSM3872525–GSM3872529) were deposited into the Gene Expression Omnibus (GEO; https://www.ncbi.nlm.nih.gov/geo/) for archival storage.

AUTHOR CONTRIBUTIONS

CRC, CG, and MS conceived the study. CRC, MS, CG, CC, DG, and BM contributed to the experimental design. CRC,

BM, CC, and HP conducted the bioreactor and wet lab experiments. CRC and HP performed the glycogen analysis. CRC, MS, and CG performed the transcriptome experiments and analysis. CRC, CG, MS, and DG wrote the manuscript with input from BM, HP, and CC.

FUNDING

This work was supported by separate MBIE Strategic Science Investment Funds granted to GNS Science (CRC, MS, and HP) and Scion (DG, BM, and CC). CRC and CG were further supported by The Royal Society of New Zealand (Marsden Grant GNS1601). CC, DG, BM, and MS were also supported by an MBIE Smart Ideas Grant (C05X1710). CG was further supported by an ARC DECRA Fellowship (DE170100310).

ACKNOWLEDGMENTS

Ngāti Tahu–Ngāti Whaoa are acknowledged as the iwi having mana whenua (customary rights) over the Rotokawa geothermal field, *Methylacidiphilum* sp. RTK17.1, and associated microorganisms. We thank Ngāti Tahu–Ngāti Whaoa Runanga Trust and Tauhara North 2 Trust for their support of our research. We also thank Prof. Peter Dunfield for valuable comments during the preparation of this manuscript.

SUPPLEMENTARY MATERIAL

The Supplementary Material for this article can be found online at: https://www.frontiersin.org/articles/10.3389/fmicb.2019.01873/full#supplementary-material

REFERENCES

Alreshidi, M. M., Dunstan, R. H., Gottfries, J., Macdonald, M. M., Crompton, M. J., Ang, C.-S., et al. (2016). Changes in the cytoplasmic composition of amino acids and proteins observed in staphylococcus aureus during growth under variable growth conditions representative of the human wound site. *PLoS One* 11:e0159662. doi: 10.1371/journal.pone.0159662

Alreshidi, M. M., Dunstan, R. H., Macdonald, M. M., Smith, N. D., Gottfries, J., and Roberts, T. K. (2015). Metabolomic and proteomic responses of *Staphylococcus aureus* to prolonged cold stress. *J. Proteom.* 121, 44–55. doi: 10.1016/j.jprot.2015.03.010

AOAC (2005). *Official Methods of Analysis of AOAC Int. 18th Ed., Method 994.12*. Arlington, VA: AOAC international.

Bonafonte, M. A., Solano, C., Sesma, B., Alvarez, M., Montuenga, L., Garcia-Ros, D., et al. (2000). The relationship between glycogen synthesis, biofilm formation and virulence in *Salmonella* enteritidis. *Fems Microbiol. Lett.* 191, 31–36. doi: 10.1016/s0378-1097(00)00366-9

Bont, J. A. (1976). Hydrogenase activity in nitrogen-fixing methane-oxidizing bacteria. *Antonie Van Leeuwenhoek* 42, 255–259. doi: 10.1007/bf00394122

Bourassa, L., and Camilli, A. (2009). Glycogen contributes to the environmental persistence and transmission of *Vibrio cholerae*. *Mol. Microbiol.* 72, 124–138. doi: 10.1111/j.1365-2958.2009.06629.x

Carere, C. R., Hards, K., Houghton, K. M., Power, J. F., Mcdonald, B., Collet, C., et al. (2017). Mixotrophy drives niche expansion of Verrucomicrobial methanotrophs. *ISME J.* 11, 2599–2610. doi: 10.1038/ismej.2017.112

Chen, Y. P., and Yoch, D. C. (1987). Regulation of two nickel-requiring (inducible and constitutive) hydrogenases and their coupling to nitrogenase in *Methylosinus trichosporium* OB3b. *J. Bacteriol.* 169, 4778–4783. doi: 10.1128/jb.169.10.4778-4783.1987

Crombie, A. T., and Murrell, J. C. (2014). Trace-gas metabolic versatility of the facultative methanotroph *Methylocella silvestris*. *Nature* 510, 148–151. doi: 10.1038/nature13192

Daniel, J., Deb, C., Dubey, V. S., Sirakova, T. D., Abomoelak, B., Morbidoni, H. R., et al. (2004). Induction of a novel class of diacylglycerol acyltransferases and triacylglycerol accumulation in *Mycobacterium tuberculosis* as it Goes into a dormancy-like state in culture. *J. Bacteriol.* 186, 5017–5030. doi: 10.1128/jb.186.15.5017-5030.2004

Dedysh, S. N., and Dunfield, P. F. (2010). "Facultative methane oxidizers," in *Handbook of Hydrocarbon and Lipid Microbiology*, ed. K. N. Timmis, (Berlin: Springer-Verlag), 1967–1976. doi: 10.1007/978-3-540-77587-4_144

Dedysh, S. N., Knief, C., and Dunfield, P. F. (2005). *Methylocella* species are facultatively methanotrophic. *J. Bacteriol.* 187, 4665–4670. doi: 10.1128/jb.187.13.4665-4670.2005

Dixon, R. O. D. (1976). Hydrogenases and efficiency of nitrogen-fixation in aerobes. *Nature* 262, 173–173. doi: 10.1038/262173a0

Dunfield, P. F., Yuryev, A., Senin, P., Smirnova, A. V., Stott, M. B., and Hou, S. (2007). Methane oxidation by an extremely acidophilic bacterium of the phylum Verrucomicrobia. *Nature* 450, 879–882. doi: 10.1038/nature06411

Ebeling, M. E. (1968). The dumas method for nitrogen in feeds. *J. Assoc. Off. Anal. Chem.* 51, 766–770.

Eidels, L., and Preiss, J. (1970). Carbohydrate metabolism in *Rhodopseudomonas capsulata* enzyme titers, glucose metabolism, and polyglucose polymer synthesis. *Arch. Biochem. Biophys.* 140, 75–89. doi: 10.1016/0003-9861(70)90011-1

Eoh, H., Wang, Z., Layre, E., Rath, P., Morris, R., Branch Moody, D., et al. (2017). Metabolic anticipation in *Mycobacterium tuberculosis*. *Nat. Microbiol.* 2, 17084–17084. doi: 10.1038/nmicrobiol.2017.84

Erikstad, H.-A., Jensen, S., Keen, T. J., and Birkeland, N.-K. (2012). Differential expression of particulate methane monooxygenase genes in the Verrucomicrobial methanotroph '*Methylacidiphilum kamchatkense*' Kam1. *Extremophiles* 16, 405–409. doi: 10.1007/s00792-012-0439-y

Eshinimaev, B. T., Khmelenina, V. N., Sakharovskii, V. G., Suzina, N. E., and Trotsenko, Y. A. (2002). Physiological, biochemical, and cytological characteristics of a haloalkalitolerant methanotroph grown on methanol. *Microbiology* 71, 512–518.

Gibbons, R. J., and Kapsimalis, B. (1963). Synthesis of intracellular iodophilic polysaccharide by streptococcus-mitis. *Arch. Oral Biol.* 8, 319–329. doi: 10.1016/0003-9969(63)90024-4

Gilman, A., Laurens, L. M., Puri, A. W., Chu, F., Pienkos, P. T., and Lidstrom, M. E. (2015). Bioreactor performance parameters for an industrially-promising methanotroph *Methylomicrobium buryatense* 5GB1. *Microb. Cell Fact.* 14:182. doi: 10.1186/s12934-015-0372-8

Greening, C., Biswas, A., Carere, C. R., Jackson, C. J., Taylor, M. C., and Stott, M. B. (2016). Genome and metagenome surveys of hydrogenase diversity indicate H2 is a widely-utilised energy source for microbial growth and survival. *ISME J.* 10, 761–777. doi: 10.1038/ismej.2015.153

Hanczar, T., Csaki, R., Bodrossy, L., Murrell, C. J., and Kovacs, K. L. (2002). Detection and localization of two hydrogenases in *Methylococcus capsulatus* (Bath) and their potential role in methane metabolism. *Arch. Microbiol.* 177, 167–172. doi: 10.1007/s00203-001-0372-4

Hanson, R. S., and Hanson, T. E. (1996). Methanotrophic bacteria. *Microbiol. Rev.* 60, 439–471.

Hou, S., Makarova, K. S., Saw, J. H. W., Senin, P., Ly, B. V., Zhou, Z., et al. (2008). Complete genome sequence of the extremely acidophilic methanotroph isolate V4, *Methylacidiphilum infernorum*, a representative of the bacterial phylum Verrucomicrobia. *Biol. Direct* 3:26. doi: 10.1186/1745-6150-3-26

Keltjens, J. T., Pol, A., Reimann, J., and Den Camp, H. (2014). PQQ-dependent methanol dehydrogenases: rare-earth elements make a difference. *Appl. Microbiol. Biotechnol.* 98, 6163–6183. doi: 10.1007/s00253-014-5766-8

Khadem, A. F., Pol, A., Jetten, M. S. M., and Op Den Camp, H. J. M. (2010). Nitrogen fixation by the Verrucomicrobial methanotroph '*Methylacidiphilum*

fumariolicum' SolV. *Microbiology* 156, 1052–1059. doi: 10.1099/mic.0.036061-0

Khadem, A. F., Van Teeseling, M. C. F., Van Niftrik, L., Jetten, M. S. M., Op Den Camp, H. J. M., and Pol, A. (2012a). Genomic and physiological analysis of carbon storage in the Verrucomicrobial methanotroph "Ca. *Methylacidiphilum Fumariolicum*" SolV. *Front. Microbiol.* 3:345. doi: 10.3389/fmicb.2012.00345

Khadem, A. F., Wieczorek, A. S., Pol, A., Vuilleumier, S., Harhangi, H. R., and Dunfield, P. F. (2012b). Draft genome sequence of the volcano-inhabiting thermoacidophilic methanotroph *Methylacidiphilum fumariolicum* strain SolV. *J. Bacteriol.* 194, 3729–3730. doi: 10.1128/JB.00501-12

Khmelenina, V. N., Kalyuzhnaya, M. G., Sakharovsky, V. G., Suzina, N. E., Trotsenko, Y. A., and Gottschalk, G. (1999). Osmoadaptation in halophilic and alkaliphilic methanotrophs. *Arch. Microbiol.* 172, 321–329. doi: 10.1007/s002030050786

Kirschke, S., Bousquet, P., Ciais, P., Saunois, M., Canadell, J. G., and Dlugokencky, E. J. (2013). Three decades of global methane sources and sinks. *Nat. Geosci.* 6, 813–823. doi: 10.1073/pnas.1814297116

Knief, C. (2015). Diversity and habitat preferences of cultivated and uncultivated aerobic methanotrophic bacteria evaluated based on pmoA as molecular marker. *Front. Microbiol.* 6:1346. doi: 10.3389/fmicb.2015.01346

Knief, C., Lipski, A., and Dunfield, P. F. (2003). Diversity and activity of methanotrophic bacteria in different upland soils. *Appl. Environ. Microbiol.* 69, 6703–6714. doi: 10.1128/aem.69.11.6703-6714.2003

Linton, J. D., and Cripps, R. E. (1978). The occurrence and identification of intracellular polyglucose storage granules in *Methylococcus* NCIB 11083 grown in chemostat culture on methane. *Arch. Microbiol.* 117, 41–48. doi: 10.1007/bf00689349

McMeechan, A., Lovell, M. A., Cogan, T. A., Marston, K. L., Humphrey, T. J., and Barrow, P. A. (2005). Glycogen production by different *Salmonella enterica* serotypes: contribution of functional glgC to virulence, intestinal colonization and environmental survival. *Microbiol. SGM* 151, 3969–3977. doi: 10.1099/mic.0.28292-0

Mohammadi, S., Pol, A., Van Alen, T. A., Jetten, M. S. M., and Op Den Camp, H. J. M. (2016). *Methylacidiphilum fumariolicum* SolV, a thermoacidophilic 'Knallgas' methanotroph with both an oxygen-sensitive and -insensitive hydrogenase. *ISME J.* 11, 945–958. doi: 10.1038/ismej.2016.171

Mortazavi, A., Williams, B. A., Mccue, K., Schaeffer, L., and Wold, B. (2008). Mapping and quantifying mammalian transcriptomes by RNA-Seq. *Nat. Meth.* 5, 621–628. doi: 10.1038/nmeth.1226

Nishihara, H., Igarashi, Y., Kodama, T., and Nakajima, T. (1993). Production and properties of glycogen in the marine obligate chemolithoautotroph, *Hydrogenovibrio marinus*. *J. Ferment. Bioeng.* 75, 414–416. doi: 10.1016/0922-338x(93)90087-o

Op den Camp, H. J., Islam, T., Stott, M. B., Harhangi, H. R., Hynes, A., and Schouten, S. (2009). Environmental, genomic and taxonomic perspectives on methanotrophic Verrucomicrobia. *Environ. Microbiol. Rep.* 1, 293–306. doi: 10.1111/j.1758-2229.2009.00022.x

Orata, F. D., Meier-Kolthoff, J. P., Sauvageau, D., and Stein, L. Y. (2018). Phylogenomic Analysis of the Gammaproteobacterial methanotrophs (Order Methylococcales) calls for the reclassification of members at the genus and species levels. *Front. Microbiol.* 9:3162. doi: 10.3389/fmicb.2018.03162

Pieja, A. J., Rostkowski, K. H., and Criddle, C. S. (2011a). Distribution and Selection of Poly-3-hydroxybutyrate production capacity in methanotrophic Proteobacteria. *Microb. Ecol.* 62, 564–573. doi: 10.1007/s00248-011-9873-0

Pieja, A. J., Sundstrom, E. R., and Criddle, C. S. (2011b). Poly-3-hydroxybutyrate metabolism in the type II methanotroph *Methylocystis parvus* OBBP. *Appl. Environ. Microb.* 77, 6012–6019. doi: 10.1128/aem.00509-11

Pol, A., Heijmans, K., Harhangi, H. R., Tedesco, D., Jetten, M. S. M., and Den Camp, H. (2007). Methanotrophy below pH 1 by a new Verrucomicrobia species. *Nature* 450, 874–878. doi: 10.1038/nature06222

Preiss, J. (1984). Bacterial glycogen synthesis and its regulation. *Annu. Rev. Microbiol.* 38, 419–458. doi: 10.1146/annurev.micro.38.1.419

Robinson, M. D., Mccarthy, D. J., and Smyth, G. K. (2010). edgeR: a bioconductor package for differential expression analysis of digital gene expression data. *Bioinformatics* 26, 139–140. doi: 10.1093/bioinformatics/btp616

Russell, J. B. (2007). The energy spilling reactions of bacteria and other organisms. *J. Mol. Microb. Biotech.* 13, 1–11. doi: 10.1159/000103591

Russell, J. B., and Cook, G. M. (1995). Energetics of bacterial growth: balance of anabolic and catabolic reactions. *Microbiol. Rev.* 59, 48–62.

Senior, P. J., Beech, G. A., Ritchie, G. A., and Dawes, E. A. (1972). The role of oxygen limitation in the formation of poly-B-hydroxybutyrate during batch and continuous culture of *Azotobacter beijerinckii*. *Biochem. J.* 128, 1193–1201. doi: 10.1042/bj1281193

Shah, N. N., Hanna, M. L., Jackson, K. J., and Taylor, R. T. (1995). Batch cultivation of *Methylosinus trichosporium* OB3B: IV. Production of hydrogen-driven soluble or particulate methane monooxygenase activity. *Biotechnol. Bioeng.* 45, 229–238. doi: 10.1002/bit.260450307

Singh, B. K., Bardgett, R. D., Smith, P., and Reay, D. S. (2010). Microorganisms and climate change: terrestrial feedbacks and mitigation options. *Nat. Rev. Microbiol.* 8, 779–790. doi: 10.1038/nrmicro2439

Stouthamer, A. H. (1979). "The search for correlation between theoretical and experimental growth yields," in *International Review Of Biochemistry*, Vol. 21, ed. J. R. Quayle, (Baltimore, MD: University Park Press), 1–48.

Strong, P. J., Kalyuzhnaya, M., Silverman, J., and Clarke, W. P. (2016). A methanotroph-based biorefinery: potential scenarios for generating multiple products from a single fermentation. *Bioresour. Technol.* 215, 314–323. doi: 10.1016/j.biortech.2016.04.099

Sundstrom, E. R., and Criddle, C. S. (2015). Optimization of methanotrophic growth and production of poly(3-Hydroxybutyrate) in a high-throughput microbioreactor system. *Appl. Environ. Microbiol.* 81, 4767–4773. doi: 10.1128/AEM.00025-15

Takeda, K. (1988). Characteristics of a nitrogen-fixing methanotroph, *Methylocystis* T-1. *Antonie Van Leeuwenhoek* 54, 521–534. doi: 10.1007/bf00588388

Tavormina, P. L., Ussler, W., Joye, S. B., Harrison, B. K., and Orphan, V. J. (2010). Distributions of putative aerobic methanotrophs in diverse pelagic marine environments. *ISME J.* 4, 700–710. doi: 10.1038/ismej.2009.155

Thiex, N., Novotny, L., and Crawford, A. (2012). Determination of ash in animal feed: AOAC official method 942.05 revisited. *J. AOAC Int.* 95, 1392–1397. doi: 10.5740/jaoacint.12-129

Vara, C., Paytuví-Gallart, A., Cuartero, Y., Le Dily, F., Garcia, F., Salvà-Castro, J., et al. (2019). Three-dimensional genomic structure and cohesin occupancy correlate with transcriptional activity during spermatogenesis. *Cell Rep.* 28, 352–367.e9. doi: 10.1016/j.celrep.2019.06.037

Wanner, U., and Egli, T. (1990). Dynamics of microbial growth and cell composition in batch culture. *FEMS Microbiol. Lett.* 75, 19–43. doi: 10.1016/0378-1097(90)90521-q

Wilson, W. A., Roach, P. J., Montero, M., Baroja-Fernández, E., Muñoz, F. J., Eydallin, G., et al. (2010). Regulation of glycogen metabolism in yeast and bacteria. *FEMS Microbiol. Rev.* 34, 952–985. doi: 10.1111/j.1574-6976.2010.00220.x

Conflict of Interest Statement: The authors declare that the research was conducted in the absence of any commercial or financial relationships that could be construed as a potential conflict of interest.

frontiers in Microbiology

ORIGINAL RESEARCH
published: 22 November 2019
doi: 10.3389/fmicb.2019.02749

Putative Iron-Sulfur Proteins Are Required for Hydrogen Consumption and Enhance Survival of Mycobacteria

*Zahra F. Islam†, Paul R. F. Cordero† and Chris Greening**

School of Biological Sciences, Monash University, Clayton, VIC, Australia

Aerobic soil bacteria persist by scavenging molecular hydrogen (H_2) from the atmosphere. This key process is the primary sink in the biogeochemical hydrogen cycle and supports the productivity of oligotrophic ecosystems. In *Mycobacterium smegmatis*, atmospheric H_2 oxidation is catalyzed by two phylogenetically distinct [NiFe]-hydrogenases, Huc (group 2a) and Hhy (group 1h). However, it is currently unresolved how these enzymes transfer electrons derived from H_2 oxidation into the aerobic respiratory chain. In this work, we used genetic approaches to confirm that two putative iron-sulfur cluster proteins encoded on the hydrogenase structural operons, HucE and HhyE, are required for H_2 consumption in *M. smegmatis*. Sequence analysis show that these proteins, while homologous, fall into distinct phylogenetic clades and have distinct metal-binding motifs. H_2 oxidation was reduced when the genes encoding these proteins were deleted individually and was eliminated when they were deleted in combination. In turn, the growth yield and long-term survival of these deletion strains was modestly but significantly reduced compared to the parent strain. In both biochemical and phenotypic assays, the mutant strains lacking the putative iron-sulfur proteins phenocopied those of hydrogenase structural subunit mutants. We hypothesize that these proteins mediate electron transfer between the catalytic subunits of the hydrogenases and the menaquinone pool of the *M. smegmatis* respiratory chain; however, other roles (e.g., in maturation) are also plausible and further work is required to resolve their role. The conserved nature of these proteins within most Hhy- or Huc-encoding organisms suggests that these proteins are important determinants of atmospheric H_2 oxidation.

Keywords: hydrogenase, *Mycobacterium*, atmospheric H_2, iron-sulfur protein, hydrogen cycle

OPEN ACCESS

Edited by:
Patricia Coutinho Dos Santos, Wake Forest University, United States

Reviewed by:
Oliver Lenz, Technische Universität Berlin, Germany
Constanze Pinske, Martin Luther University of Halle-Wittenberg, Germany
Katherine A. Black, Cornell University, United States

***Correspondence:**
Chris Greening
chris.greening@monash.edu

†These authors have contributed equally to this work

Specialty section:
This article was submitted to Microbial Physiology and Metabolism, a section of the journal Frontiers in Microbiology

Received: *25 April 2019*
Accepted: *12 November 2019*
Published: *22 November 2019*

Citation:
Islam ZF, Cordero PRF and Greening C (2019) Putative Iron-Sulfur Proteins Are Required for Hydrogen Consumption and Enhance Survival of Mycobacteria. Front. Microbiol. 10:2749. doi: 10.3389/fmicb.2019.02749

INTRODUCTION

Over the last decade, various studies have revealed that aerobic bacteria conserve energy during persistence through aerobic respiration of atmospheric hydrogen (H_2) (Constant et al., 2010; Greening et al., 2014b, 2015a; Meredith et al., 2014; Liot and Constant, 2016; Islam et al., 2019). This process is now recognized to be important for biogeochemical and ecological reasons. Gas-scavenging soil bacteria serve as the primary sink in the global hydrogen cycle and are responsible

for the net consumption of approximately 70 million tonnes of H_2 each year (Constant et al., 2009; Ehhalt and Rohrer, 2009; Greening et al., 2014a; Piché-Choquette et al., 2018). More recently, it has been inferred that this process supports the productivity and biodiversity of various ecosystems, especially low-carbon soils (Lynch et al., 2014; Kanno et al., 2015; Khdhiri et al., 2015; Greening et al., 2016; Ji et al., 2017; Bay et al., 2018; Kessler et al., 2019; Piché-Choquette and Constant, 2019). Atmospheric H_2 oxidation appears to be a widespread trait among soil bacteria. To date, bacteria from three phyla have been experimentally shown to oxidize atmospheric H_2, Actinobacteriota (Constant et al., 2008, 2010; Greening et al., 2014a; Meredith et al., 2014), Acidobacteriota (Greening et al., 2015a; Myers and King, 2016), and Chloroflexota (Islam et al., 2019). However, genomic and metagenomic studies have indicated at least 13 other phyla encode enzymes that can mediate this process (Greening et al., 2016; Carere et al., 2017; Ji et al., 2017; Piché-Choquette et al., 2017).

The genetic basis and physiological role of atmospheric H_2 oxidation is now largely understood. This process has been most comprehensively studied in the genetically tractable soil actinobacterium *Mycobacterium smegmatis* (Greening and Cook, 2014). In this organism, atmospheric H_2 oxidation is mediated by two membrane-bound, oxygen-tolerant hydrogenases, Huc (group 2a [NiFe]-hydrogenase, also known as Hyd1 or cyanobacterial-type uptake hydrogenase) and Hhy (group 1h [NiFe]-hydrogenase, also known as Hyd2 or actinobacterial-type uptake hydrogenase) (Berney et al., 2014b). Additionally, *M. smegmatis* encodes a third [NiFe]-hydrogenase, Hyh (Hyd3), which mediates fermentative H_2 production during hypoxia (Berney et al., 2014a). Both H_2-oxidizing hydrogenases contain a large subunit containing the [NiFe] active site (HucL, HhyL) and a small subunit containing three iron-sulfur clusters (HucS, HhyS), as well as potential additional subunits (Berney et al., 2014b; Cordero et al., 2019b). These two hydrogenases are upregulated in stationary-phase cells, including in response to organic carbon limitation (Berney and Cook, 2010; Berney et al., 2014b). Consistently, when the structural subunits of these hydrogenases are deleted, strains show reduced growth yield and impaired long-term survival during starvation (Berney and Cook, 2010; Berney et al., 2014a; Greening et al., 2014b). Similar findings have been made in *Streptomyces avermitilis*; the sole hydrogenase of this organism, Hhy, is exclusively expressed in exospores and strains lacking this enzyme exhibit severe survival defects (Constant et al., 2010; Liot and Constant, 2016). Given these findings, it is proposed that bacteria shift from growing on organic compounds to persisting on atmospheric trace gases. Indeed, theoretical calculations indicate that the energy derived from atmospheric H_2 oxidation (0.53 ppmv) can sustain the maintenance of 10^7 to 10^8 cells per gram of soil (Conrad, 1999).

Despite this progress, little is currently known about the biochemical basis of atmospheric H_2 oxidation. One outstanding question is how electrons derived from H_2 oxidation are transferred to the respiratory chain. Most classes of respiratory uptake hydrogenases are predicted to be co-transcribed with a cytochrome *b* subunit (Greening et al., 2016; Søndergaard et al., 2016). For example, such subunits interact with the prototypical oxygen-tolerant hydrogenases (group 1d [NiFe]-hydrogenases) of *Escherichia coli* and *Ralstonia eutropha*; they anchor the hydrogenase to the membrane and transfer electrons from the hydrogenase small subunit to the quinone pool (Frielingsdorf et al., 2011; Volbeda et al., 2013). However, we did not detect equivalent proteins in the operons encoding the structural subunits of Huc (MSMEG_2261–2270) or Hhy (MSMEG_2722 – 2718) in *M. smegmatis* (**Supplementary Figure S1**) (Berney et al., 2014b). Putative iron-sulfur proteins, tentatively annotated as HucE (MSMEG_2268) and HhyE (MSMEG_2718), were encoded downstream of the hydrogenase structural subunits and may potentially fulfill this role instead (Berney et al., 2014b; Greening et al., 2015b). In this work, we characterized the effects of deleting these genes on hydrogenase activity, growth, and survival in *M. smegmatis*. We also investigated their broader conservation in hydrogenase-encoding bacteria.

MATERIALS AND METHODS

Bacterial Strains and Growth Conditions

All bacterial strains and plasmids used in this study are listed in **Supplementary Table S1**. *Escherichia coli* TOP10 was maintained on lysogeny broth (LB) agar plates (10 g L^{-1} tryptone, 5 g L^{-1} NaCl, 5 g L^{-1} yeast extract, 15 g L^{-1} agar), while *Mycobacterium smegmatis* mc^2155 (Snapper et al., 1990) and derived mutants were maintained on LB agar plates supplemented with 0.05% (w/v) Tween 80 (LBT). For broth culture, *E. coli* was grown in LB. *M. smegmatis* was grown in either LBT or in Hartmans de Bont (HdB) minimal medium (Hartmans and De Bont, 1992) supplemented with 0.2% (w/v) glycerol. In all cases, liquid cultures were grown in rotary incubators at 37°C with agitation (200 rpm).

Mutant Strain Construction

Allelic exchange mutagenesis was used to produce markerless deletions of the genes encoding two putative iron-sulfur proteins, *hucE* (MSMEG_2268) and *hhyE* (MSMEG_2718) (**Supplementary Figure S2**). Briefly, a fragment containing fused left and right flanks of the MSMEG_2268 (1800 bp) and MSMEG_2718 (3098 bp) genes were synthesized by GenScript. These fragments were cloned into the *Spe*I site of the mycobacterial shuttle plasmid pX33 (Gebhard et al., 2006) to yield the constructs pX33-*huc*E and pX33-*hhy*E (**Supplementary Table S1**). These constructs were propagated in *E. coli* TOP10 and transformed into wild-type *M. smegmatis* mc^2155 cells by electroporation. Gentamycin (5 μg mL^{-1} for *M. smegmatis* or 20 μg mL^{-1} for *E. coli*) was used in selective solid and liquid medium to propagate pX33. Creation of the double iron-sulfur cluster mutant (Δ*hucE*Δ*hhyE*) was achieved by transformation of Δ*hhyE* electrocompetent *M. smegmatis* mc^2155 with the pX33-*huc*E construct. Briefly, to allow for permissive temperature-sensitive vector replication, transformants were incubated on LBT gentamicin plates at 28°C until colonies were visible (5–7 days). Resultant catechol-positive colonies were subcultured onto fresh LBT gentamicin plates and incubated at 40°C for 3–5 days to facilitate integration of the recombinant plasmid

flanks into the chromosome. The second recombination event was facilitated by subculturing catechol-reactive and gentamicin-resistant colonies onto LBT agar plates supplemented with 10% sucrose (w/v) and incubating at 40°C for 3–5 days. Catechol-unreactive colonies were subsequently screened by PCR to discern wild-type revertants from Δ*hucE*, Δ*hhyE* and Δ*hucE*Δ*hhyE* mutants. Primers used for the generation of mutants and for screening are listed in **Supplementary Table S2**.

Complementation Vector Construction

The genes for the putative iron-sulfur proteins were amplified by PCR and the resulting fragments were cloned into the constitutive expression plasmid pMV261 *via Pst*I/*Hin*dIII site for *hucE* and *Bam*HI/*Hin*dIII site for *hhyE* (Stover et al., 1991) to yield the constructs pMV*hucE* and pMV*hhyE* (**Supplementary Table S1**). Sequence fidelity of the genes was verified through Sanger sequencing and insertion of the genes into the vector was confirmed through restriction-digestion analysis (**Supplementary Figure S3**). The plasmid constructs were propagated in *E. coli* DH5α and transformed into *M. smegmatis* cells by electroporation. Vector pMV*hucE* was transformed into *M. smegmatis* wild-type and Δ*hucE* strains, while pMV*hhyE* was transformed into wild type and Δ*hhyE* mutant. In addition, an empty pMV261 was transformed into wild-type, Δ*hucE*, and Δ*hhyE* strains. These seven *M. smegmatis* strains were used for complementation experiments in respirometry and activity staining. Kanamycin (20 μg mL^{-1} for *M. smegmatis* or 50 μg mL^{-1} for *E. coli*) was used in selective solid and liquid medium to propagate pMV261. Primers used for the generation of the constructs are listed in **Supplementary Table S2**.

Respirometry Measurements

Cultures of wild-type, derived mutants, and complemented mutant strains of *M. smegmatis* were grown in 125 mL aerated conical flasks containing 30 mL HdB medium supplemented with 0.2% glycerol. Respirometry measurements were performed with mid-stationary phase cells, i.e., 72 h post OD_{max} (∼3.0). A Unisense H_2 microsensor electrode was polarized at + 800 mV for 1 h using a Unisense multimeter and calibrated against standards of known H_2 concentration. Gas-saturated PBS was prepared by bubbling the solution with 100% (v/v) of either H_2 or O_2 for 5 min. The 1.1 mL microrespiration assay chambers were sequentially amended with stationary-phase cultures (0.9 mL, OD_{600} = 3.0), H_2-saturated PBS (0.1 mL), and O_2-saturated PBS (0.1 mL). Chambers were stirred at 250 rpm, 37°C. Changes in H_2 concentration were recorded using Unisense Logger Software, and upon observing a linear change in H_2 concentration, rates of consumption were calculated over a period of 20 s, which corresponds to the most linear uptake of hydrogen by the cells. Oxidation rates were normalized against total protein concentration, which was determined by the bicinchoninic acid method (Smith et al., 1985) with bovine serum albumin standards.

Activity Staining

Cultures of wild-type, derived mutants, and complemented mutant strains of *M. smegmatis* were grown in 2.5 L aerated conical flasks containing 500 mL HdB medium supplemented with 0.2% glycerol. For Huc activity staining, cultures of wild-type, Δ*hucS*, Δ*hucE*, Δ*hucS*Δ*hhyL*, Δ*hucE*Δ*hhyE*, and complemented Δ*hucE* and wild-type *M. smegmatis* (either with empty pMV261 or complementation vector pMV*hucE*) were harvested by centrifugation (10,000 × *g*, 10 min, 4°C) at early-stationary phase (24 h post OD_{max}, ∼3.0) (Cordero et al., 2019b). For Hhy activity staining, cultures of wild-type, Δ*hhyL*, Δ*hhyE*, Δ*hucS*Δ*hhyL*, Δ*hucE*Δ*hhyE*, and complemented Δ*hhyE* and wild-type *M. smegmatis* (either with empty pMV261 or complementation vector pMV*hhyE*) were harvested by centrifugation at mid-stationary phase (72 h post OD_{max}, ∼3.0) (Cordero et al., 2019b). Harvested cultures were washed in phosphate-buffered saline solution (PBS; 137 mM NaCl, 2.7 mM KCl, 10 mM Na_2HPO_4, 2 mM KH_2PO_4, pH 7.4), and resuspended in 16 mL lysis buffer (50 mM Tris-Cl, pH 8.0, 1 mM PMSF, 2 mM $MgCl_2$, 5 mg mL^{-1} lysozyme, 40 μg mL^{-1} DNase, 10% glycerol). Resultant cell suspensions were passed through a Constant Systems cell disruptor (40,000 psi, four times), with unbroken cells removed by centrifugation (10,000 × *g*, 20 min, 4°C) to yield whole-cell lysates. Protein concentration was determined using a bicinchoninic acid assay with bovine serum albumin standards. Next, 20 μg of each whole-cell lysate was loaded onto two native 7.5% (w/v) Bis-Tris polyacrylamide gels prepared as described elsewhere (Walker, 2009) and run alongside a protein standard (NativeMark Unstained Protein Standard, Thermo Fisher Scientific) for 1.5 h at 25 mA. One gel was stained overnight at 4°C with gentle agitation using AcquaStain Protein Gel Stain (Bulldog Bio) for total protein determination. The other gel was incubated for hydrogenase activity staining in 50 mM potassium phosphate buffer (pH 7.0) supplemented with 500 μM nitroblue tetrazolium chloride (NBT) in an anaerobic jar amended with an anaerobic gas mixture (5% H_2, 10% CO_2, 85% N_2 v/v) overnight at room temperature.

Growth and Survival Assays

Cultures of wild type and derived mutants of *M. smegmatis* were inoculated into 125 mL conical flasks containing 30 mL LBT medium (initial OD_{600} of 0.001), in six biological replicates. Growth was monitored by measuring optical density at 600 nm (1 cm cuvettes; Eppendorf BioSpectrometer Basic); when OD_{600} was above 0.5, cultures were diluted ten-fold in LBT before measurement. Specific growth rate during mid-exponential growth was calculated for each replicate using GraphPad Prism (non-linear regression, exponential growth equation, least squares fit). The long-term survival of the cultures was determined by counting colony forming units (CFU mL^{-1}) of cultures 21 days post-OD_{max}. Cultures were serially diluted in HdB containing no carbon source and spotted on to agar plates in technical quadruplicates. After incubation at 37°C for 3 days, the resultant colonies were counted.

Sequence and Phylogenetic Analysis

Sequences homologous to *M. smegmatis* HucE (MSMEG_2268) and HhyE (MSMEG_2718) were retrieved by protein BLAST (Altschul et al., 1990) using the National Center

for Biotechnology Information (NCBI) Reference Sequence (RefSeq) database (Pruitt et al., 2007). The retrieved hits were cross-referenced with the hydrogenase database (HydDB) (Søndergaard et al., 2016) in order to determine which organisms co-encode HucE with HucL and HhyE with HhyL. For downstream phylogenetic and motif analysis, sequences were filtered to remove truncated HucE/HhyE proteins and retain one protein sequence per genus. This resulted in a representative subset of 52 full-length HucE and 26 full-length HhyE sequences. The retrieved sequences were aligned using ClustalW in MEGA7 (Kumar et al., 2016). The phylogenetic relationships of these sequences were visualized on a maximum-likelihood tree based on the Poisson correction method and bootstrapped with 100 replicates. In addition, WebLogo (Crooks et al., 2004) was used to analyze the conserved motifs containing cysteine and histidine residues predicted to bind iron-sulfur clusters. The web-based software Properon (M. Milton[1]) was used to generate to-scale genetic organization diagrams of the group 1h and group 2a [NiFe]-hydrogenases, with genes labeled according to the nomenclature in HydDB (Søndergaard et al., 2016).

RESULTS

HucE and HhyE Are Predicted to Be Iron-Sulfur Proteins Associated With Group 2a and Group 1h [NiFe]-Hydrogenases

We investigated the diversity of putative iron-sulfur cluster proteins associated with [NiFe]-hydrogenases by conducting a homology-based search using the amino acid sequences of HucE (MSMEG_2268) and HhyE (MSMEG_2718) from *M. smegmatis* (**Supplementary Figure S1**). Homologous sequences were retrieved from 14 phyla and 104 genera of bacteria (**Supplementary Figure S4** and **Supplementary Table S3**).

The evolutionary relationships of these proteins were visualized on a maximum-likelihood phylogenetic tree (**Figure 1**). All retrieved sequences fall into two robustly supported clades, the HucE proteins associated with group 2a [NiFe]-hydrogenases (Huc) and the HhyE proteins associated with group 1h [NiFe]-hydrogenases (Hhy), that share approximately 27% amino acid identity. HhyE proteins were encoded by various atmospheric H_2 oxidizers, including *Streptomyces* (Berney and Cook, 2010), *Rhodococcus* (Meredith et al., 2014), *Pyrinomonas* (Greening et al., 2015a), and *Thermogemmatispora* (Islam et al., 2019). HucE proteins were encoded by various Cyanobacteria, which are known to recycle H_2 produced during the nitrogenase reaction *via* group 2a [NiFe]-hydrogenases (Houchins and Burris, 1981; Tamagnini et al., 2002), as well as genera capable of aerobic hydrogenotrophic growth such as *Nitrospira* (Koch et al., 2014), *Pseudonocardia* (Grostern and Alvarez-Cohen, 2013), and *Acidithiobacillus* (Schröder et al., 2007). Of the hydrogenase-positive species surveyed, 9.5% lacked HucE and HhyE, including *Thermomicrobium* (Islam et al., 2019) and *Methylacidiphilum* (Mohammadi et al., 2017) species known to synthesize mid-affinity group 1h [NiFe]-hydrogenases. In contrast, no HucE or HhyE sequences were retrieved from organisms that lack hydrogenases.

Multiple sequence alignments show that HucE and HhyE proteins contain highly conserved motifs potentially involved in binding iron-sulfur clusters (**Supplementary Figures S5, S6**). Both HucE and HhyE contain a CxxC motif within a domain homologous to NifU proteins (Yuvaniyama et al., 2000). The C-terminus of HhyE proteins contains two CxxC motifs typical of iron-sulfur proteins (e.g., rubredoxins). In contrast, the HucE proteins contain an C-terminal motif $CxH(x_{15-18})CxxC$ that matches the signature motif of Rieske iron-sulfur clusters (Schmidt and Shaw, 2001) (**Supplementary Figure S6**). A subset of the species surveyed contain truncated HucE and HhyE proteins that contain the NifU-like domain, but lack the C-terminal domains (**Supplementary Figures S4, S5**).

HucE and HhyE Are Essential for H_2 Oxidation in *Mycobacterium smegmatis*

We used allelic exchange mutagenesis to generate markerless single and double mutants of the *hucE* and *hhyE* genes in *M. smegmatis*, i.e., Δ*hucE*, Δ*hhyE*, and Δ*hucE*Δ*hhyE*. Gene deletion was confirmed by PCR targeting chromosomal sequences adjacent to the flanking regions used for homologous recombination (**Supplementary Figure S2**). Assays were used to compare H_2 oxidation of these strains with the wild-type strain and strains containing previously generated deletions of the hydrogenase structural subunits, i.e., Δ*hucS*, Δ*hhyL*, and Δ*hucS*Δ*hhyL*, that lack hydrogenase activity (Berney and Cook, 2010; Berney et al., 2014b; Greening et al., 2014a).

We first used a H_2 electrode to measure rates of aerobic H_2 respiration mediated by whole cells of each strain. There were significant differences in the rate of H_2 oxidation for all deletion strains compared to the wild type (**Figure 2A**). Loss of *hucE* and *hhyE* resulted in reductions of 1.8-fold and 8.4-fold, respectively; such reductions were statistically indistinguishable from those observed in the mutants of the hydrogenase structural subunits *hucS* and *hhyL*. Deletion of both iron-sulfur proteins (Δ*hucE*Δ*hhyE*) or both hydrogenase structural subunits (Δ*hucS*Δ*hhyL*) caused complete cessation of H_2 oxidation, highlighting that these two hydrogenases are solely responsible for H_2 oxidation and that the putative iron-sulfur proteins are indispensable for this process. The low-level negative rates in Δ*hucE*Δ*hhyE* and Δ*hucS*Δ*hhyL* strains most likely reflect drift of the electrode rather than actual H_2 production by Hyh (Hyd3), since this hydrogenase is only upregulated during hypoxia (Berney et al., 2014a). We successfully complemented the Δ*hucE* and Δ*hhyE* strains by reintroducing the *hucE* and *hhyE* genes on the episomal plasmid pMV261 (Stover et al., 1991) (**Figure 2B**); in contrast, introducing the empty vector caused no effect and neither did introducing the complementation vectors in a wild-type background. This restoration of Huc and Hhy activities in complemented iron-sulfur protein deletion mutants strongly indicate that HucE and HhyE are essential for

[1]https://zenodo.org/record/3519494#.Xb4CnJozZPY

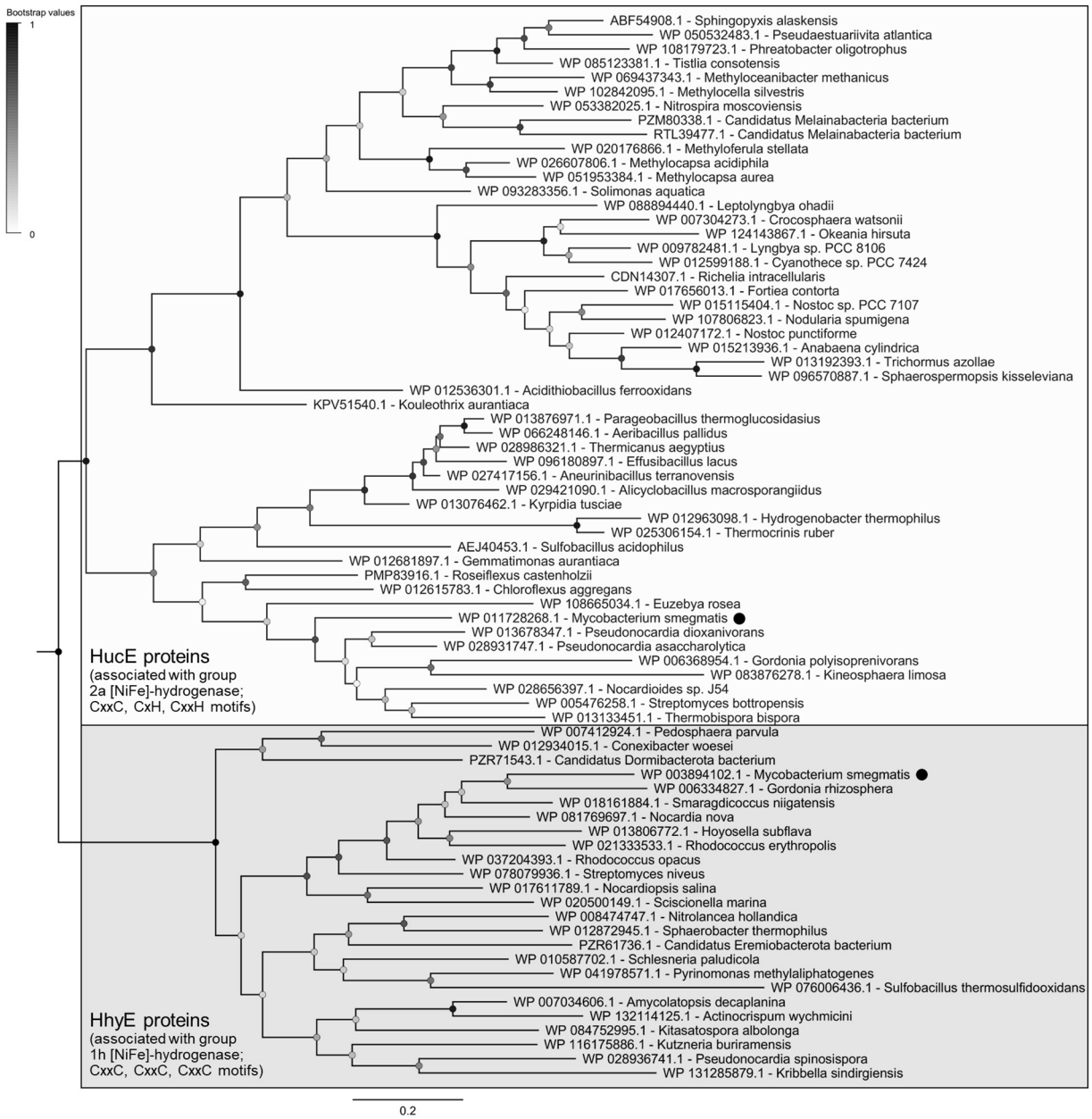

FIGURE 1 | Phylogenetic tree of HucE and HhyE proteins associated with group 2a and 1h [NiFe]-hydrogenases. The tree visualizes the evolutionary relationships between a representative subset of 52 full-length HucE and 26 full-length HhyE sequences. The proteins encoded by *Mycobacterium smegmatis* are emphasized. The tree was constructed using the maximum-likelihood method (gaps treated with partial deletion), bootstrapped with 100 replicates, and rooted at the mid-point. The sequences used to create this tree are provided in **Supplementary Table S3**.

H_2 oxidation. Moreover, the similarity in H_2 oxidation rates between the strains containing deletions of the catalytic subunits, compared to the putative iron-sulfur proteins, is consistent with HucE and HhyE being functionally linked with the Huc and Hhy hydrogenases, respectively.

In an interrelated assay, we performed activity staining of the Huc and Hhy hydrogenases using whole-cell lysates of wild-type and deletion mutant strains, with and without the complementation vectors, in the presence of the artificial electron acceptor nitroblue tetrazolium chloride. In the Huc activity staining gel (**Figure 3A**), three bands were observed in the whole-cell lysates of wild-type strains, with or without complementation vectors: the top high-MW band, middle mid-MW band, and bottom low-MW band. Both the high-MW and low-MW bands correspond to Huc activity (Cordero et al., 2019b) and these bands were not observed in strains lacking either *hucS* or *hucE*. However, Huc activity was restored when the Δ*hucE* strain was complemented by episomal expression of *hucE*. For Hhy activity

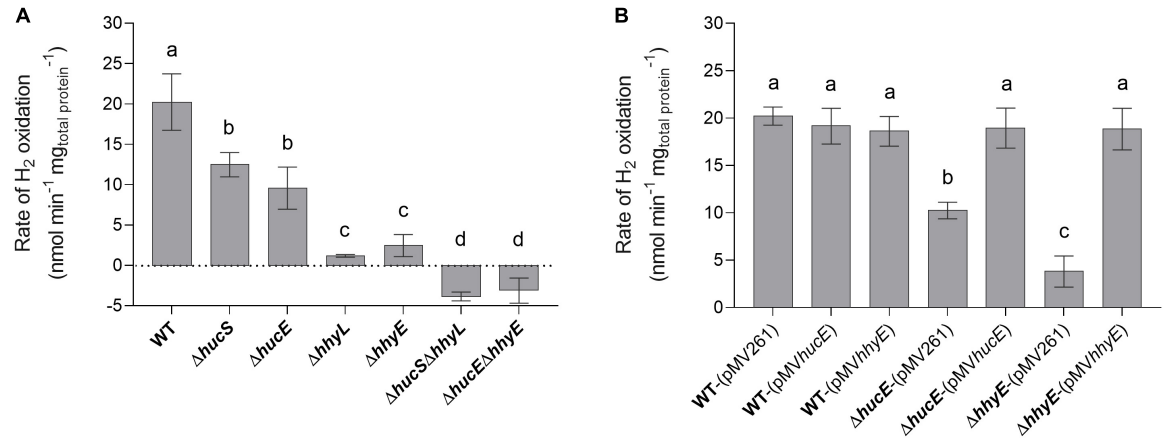

FIGURE 2 | Hydrogen oxidation by wild-type, derived mutants, and complemented mutant strains of *M. smegmatis*. H_2 uptake by whole cells in mid-stationary phase (72 h post OD_{max} ~3.0) was measured amperometrically using a Unisense H_2 electrode. **(A)** Comparison of the rates of H_2 oxidation between wild-type, single and double mutants of the iron-sulfur proteins (Δ*hucE*, Δ*hhyE*, Δ*hucE*Δ*hhyE*), and single and double mutants of hydrogenase structural subunits (Δ*hucS*, Δ*hhyL*, Δ*hucS*Δ*hhyL*). **(B)** Rates of H_2 oxidation in Δ*hucE* and Δ*hhyE* strains complemented with expression of *hucE* and *hhyE*, respectively. Controls include wild-type, Δ*hucE*, and Δ*hhyE* strains transformed with empty vector pMV261 and wild-type strain transformed with complementation vectors pMV*hucE* and pMV*hhyE*. Error bars show standard deviations of three biological replicates and values labeled with different letters are significantly different ($p < 0.05$) based on a one-way ANOVA.

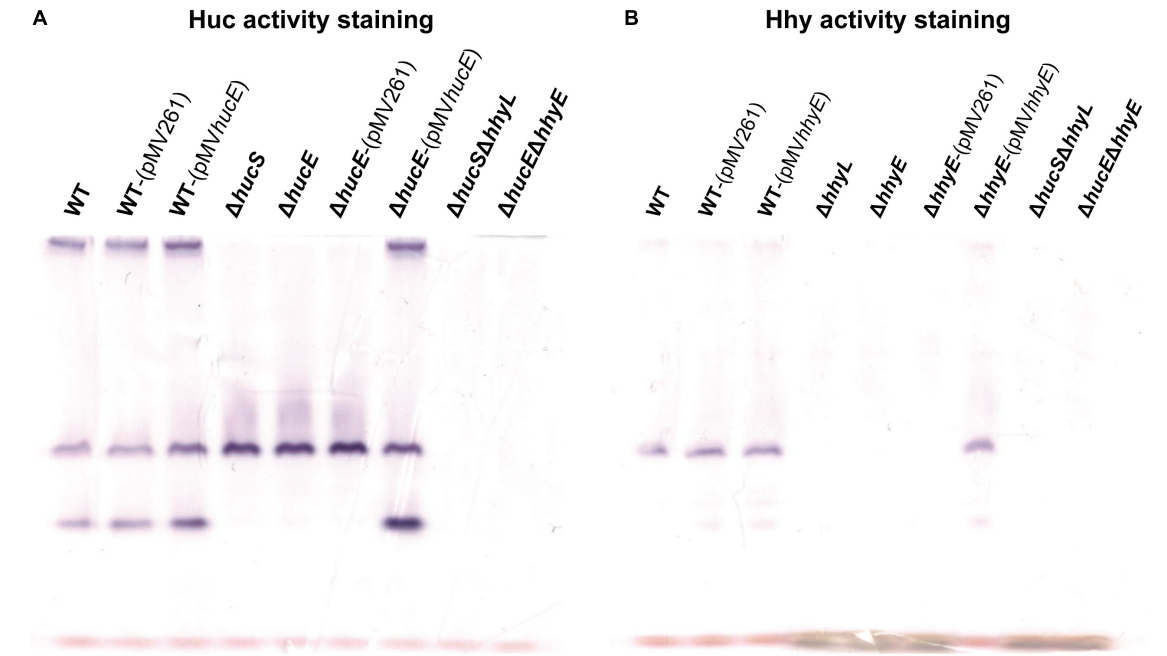

FIGURE 3 | Hydrogenase activity staining in wild-type, derived mutants, and complemented mutant strains of *M. smegmatis.* Whole-cell lysates were used for zymographic staining of H_2 uptake in a H_2-rich atmosphere with nitroblue tetrazolium as artificial electron acceptor. **(A)** Huc activity staining of cultures of wild-type, Δ*hucS*, Δ*hucE*, Δ*hucS*Δ*hhyL*, Δ*hucE*Δ*hhyE*, and complemented Δ*hucE* and wild-type *M. smegmatis* (either with empty pMV261 or complementation vector pMV*hucE*) harvested at early-stationary phase (24 h post OD_{max} ~3.0). **(B)** Hhy activity staining of cultures of wild-type, Δ*hhyL*, Δ*hhyE*, Δ*hucS*Δ*hhyL*, Δ*hucE*Δ*hhyE*, and complemented Δ*hhyE* and wild-type *M. smegmatis* (either with empty pMV261 or complementation vector pMV*hhyE*) harvested at mid-stationary phase (72 h post OD_{max} ~3.0). The original gels and Coomassie stain are shown in **Supplementary Figure S7**.

staining (**Figure 3B**), a mid-sized MW band was be observed in all wild-type strains. This band, which is the same middle band observed in the Huc activity stain (**Figure 3A**), corresponds to Hhy activity (Greening et al., 2014a; Cordero et al., 2019b). No Hhy staining was detected with the loss of either *hhyL* or *hhyE*, but complementation of the Δ*hhyE* strain with *hhyE* restored Hhy activity. The similarity in the staining bands observed between Δ*hucS* and Δ*hucE* strains or between Δ*hhyL* and Δ*hhyE*

indicate that the putative iron-sulfur proteins HucE and HhyE, like their respective hydrogenase core subunits HucS and HhyL, are important for hydrogenase activity. The artificial electron acceptor cannot compensate for the loss of HucE/HhyE and neither can HucE for HhyE nor HhyE for HucE. This further supports the model that HucE and HhyE form a functional association with Huc and Hhy, respectively.

HucE and HhyE Mutant Strains Have Significant Growth and Survival Defects

Previous genetic studies have shown that the hydrogenases modestly increase growth yield and long-term survival of *M. smegmatis* (Berney and Cook, 2010; Greening et al., 2014b). We therefore tested whether these findings extended to the putative iron-sulfur proteins by analyzing the growth rate, growth yield, and long-term survival of the seven aforementioned strains when cultured aerobically on rich media (LBT). In line with previous findings (Berney et al., 2014a; Greening et al., 2014b), no significant differences in specific growth rate were observed between the strains (**Figure 4A**). However, there was a 10% reduction in the specific growth yield of the HhyE mutant compared to the wild-type strain ($OD_{max\,wt} = 4.19 \pm 0.21$; OD_{max} $\Delta hhyE = 3.81 \pm 0.09$; $p = 0.008$) (**Figure 4B**). This phenotype extended to the double mutant strain ($\Delta hucE\Delta hhyE$) and again phenocopied single and double mutants lacking the *hhyL* gene.

We also tested whether the strains were defective in long-term survival by counting colonies of aerobic cultures 21 days following OD_{max}. There were significant reductions in the survival of most strains compared to the wild-type (**Figure 4C**). Cell counts were approximately two-fold lower for the $\Delta hhyE$ and $\Delta hhyL$ strains ($p < 0.02$), and four-fold lower for the double mutant strains ($p < 0.002$), relative to the wild-type. These findings agree with previous reports that atmospheric H_2 oxidation by the hydrogenases enables *M. smegmatis* to survive energy starvation (Greening et al., 2014b) and further supports that the putative iron-sulfur proteins contribute to this function. For reasons currently unclear, no phenotypes were observed for the $\Delta hucE$ strain.

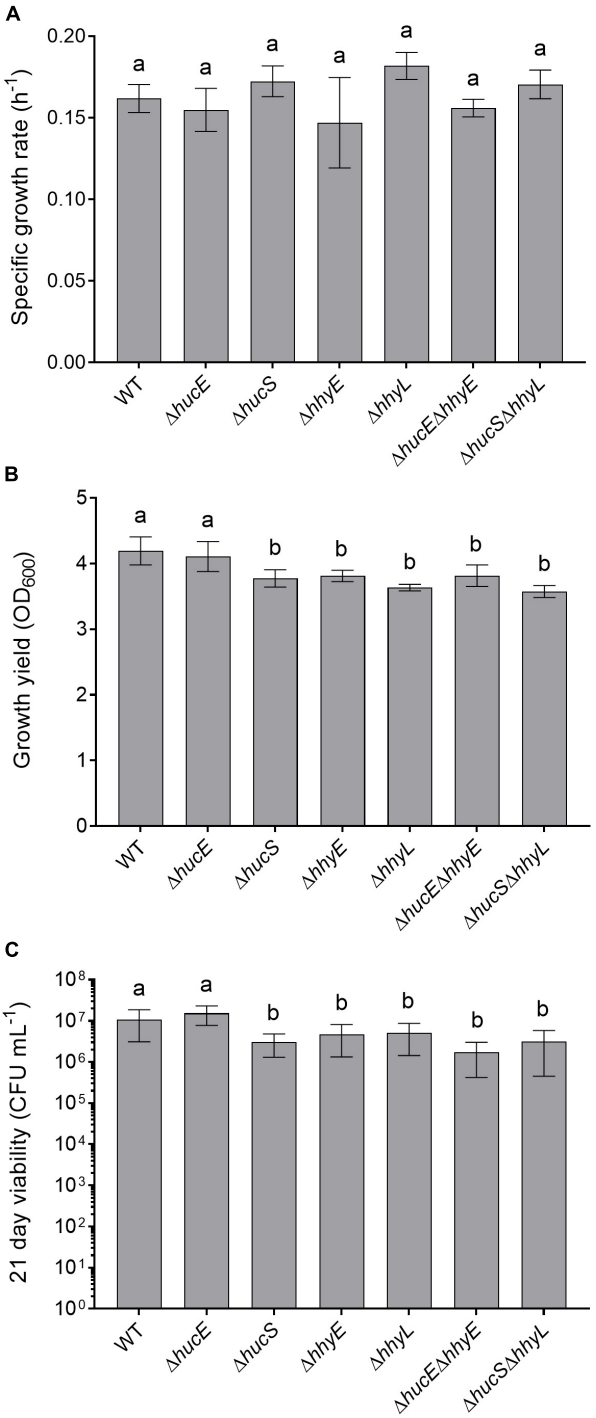

FIGURE 4 | Comparison of growth and survival between wild-type and mutant strains of *M. smegmatis*. Seven strains were grown on lysogeny broth supplemented with Tween80 (LBT): wild-type, single and double mutants of the iron-sulfur proteins ($\Delta hucE$, $\Delta hhyE$, $\Delta hucE\Delta hhyE$), and single and double mutants of hydrogenase structural subunits ($\Delta hucS$, $\Delta hhyL$, $\Delta hucS\Delta hhyL$). **(A)** Specific growth rate (μ) during exponential phase. **(B)** Final growth yield (OD_{max}) at 24 h post-stationary phase. **(C)** Long-term survival (CFU mL^{-1}) at 21 days post-stationary phase. Error bars show standard deviations of six biological replicates. Values labeled with different letters are significantly different ($p < 0.05$) based on a one-way ANOVA.

DISCUSSION

In summary, this study shows that HucE and HhyE are required for the enzymatic activity and physiological function of the mycobacterial uptake hydrogenases. Strains lacking these proteins showed no hydrogenase activity in either amperometric or zymographic assays. Furthermore, they exhibited growth and survival phenotypes similar to those of knockouts of hydrogenase structural subunits (Berney and Cook, 2010; Greening et al., 2014b); as with the structural subunit mutants, these phenotypes are relatively minor, likely reflecting the numerous survival mechanisms present in *M. smegmatis* such as the ability to persist on carbon monoxide (Cordero et al., 2019a). Despite some sequence similarity between the two proteins, they are non-redundant, as there was no compensation in hydrogenase activity in

the single mutant strains. The genomic survey and phylogenetic analysis indicate that *hucE* and *hhyE* genes co-evolved with the genes encoding the structural subunits of the group 2a and group 1h [NiFe]-hydrogenases. Their detection in the genomes of most but not all characterized high-affinity H_2 oxidizers indicate they are important but overlooked mediators of atmospheric H_2 oxidation. They are also associated with the group 2a [NiFe]-hydrogenases of H_2-recycling Cyanobacteria and various aerobic hydrogenotrophic bacteria that are not currently known to oxidize atmospheric H_2.

This study lends some support to the hypothesis that these proteins serve as the immediate electron acceptors for the group 2a and group 1h [NiFe]-hydrogenases. There are broadly five lines of evidence that support this hypothesis: (i) the presence of highly conserved motifs for binding iron-sulfur clusters, (ii) the essentiality of these proteins for the function of these hydrogenases, (iii) their association with the structural rather than maturation operons of the hydrogenases (Berney et al., 2014b), (iv) co-localization of HhyL, HhyS, and HhyE subunits on native polyacrylamide gels (Cordero et al., 2019b), and (v) their genomic association with hydrogenases that lack known electron transfer subunits (e.g., cytochrome *b* subunits). With the respect to the latter point, it is interesting that these proteins are conserved in Cyanobacteria, given the immediate electron acceptors of their uptake hydrogenases have long remained enigmatic (Tamagnini et al., 2002). It is also notable that HucE proteins encode the signature motifs of a Rieske iron-sulfur cluster. Given their unusual ligands, these clusters have a higher standard redox potential (E_o' > −150 mV) than most iron-sulfur clusters (e.g., ferredoxins) (Brown et al., 2008). They would therefore be well-poised to accept the relatively high-potential electrons derived from atmospheric H_2 and transfer them to menaquinone. Consistently, zymographic studies suggest that the high-affinity hydrogenases operate at higher redox potential than prototypical hydrogenases, given they are reactive with the nitroblue tetrazolium (E_o' = −80 mV) but not viologen compounds (E_o' = −360 mV) (Pinske et al., 2012; Greening et al., 2014a).

While this study demonstrates HucE and HhyE are important for mycobacterial hydrogenase activity, further work is ultimately needed to resolve their respective function. While a role in electron transfer is most plausible, we have not demonstrated that these proteins interact with the hydrogenases and it is notable that the artificial electron acceptor nitroblue tetrazolium chloride cannot compensate for their absence. In this regard, other roles are also possible and compatible with the available evidence, for example as specific assembly factors and/or structural scaffolds for the hydrogenases. For example, it has been demonstrated that a rubredoxin-related protein is important for aerobic maturation of the group 1d [NiFe]-hydrogenase in *R. eutropha* (Fritsch et al., 2014). Furthermore, it is possible that other hypothetical proteins downstream of HucE and HhyE may also serve as electron acceptor candidates, in particular MSMEG_2717 that shares homology to PHG067, the proposed electron acceptor of *R. eutropha* (Schäfer et al., 2013). Biochemical studies, including studying the redox chemistry of these proteins and their interactions with the as-yet-unpurified hydrogenases, are now required to distinguish these possibilities and develop a sophisticated understanding of their function.

DATA AVAILABILITY STATEMENT

All datasets generated for this study are included in the article/**Supplementary Material**.

AUTHOR CONTRIBUTIONS

CG conceived, designed, and supervised the study. CG and ZI were responsible for the phylogenetic analysis and analyzed the data. ZI and PC were responsible for the knockout generation, hydrogen electrode measurements, and activity staining. PC was responsible for the complementation experiments. ZI was responsible for the phenotypic assays. ZI, PC, and CG wrote the manuscript.

FUNDING

This work was supported by an ARC DECRA Fellowship (DE170100310; awarded to CG), an Australian Government Research Training Program Stipend (awarded to ZI), and a Monash University Doctoral Scholarship (awarded to PC).

ACKNOWLEDGMENTS

We thank Dr. Rhys Grinter and the three peer reviewers for their helpful feedback.

SUPPLEMENTARY MATERIAL

The Supplementary Material for this article can be found online at: https://www.frontiersin.org/articles/10.3389/fmicb.2019.02749/full#supplementary-material

REFERENCES

Altschul, S. F., Gish, W., Miller, W., Myers, E. W., and Lipman, D. J. (1990). Basic local alignment search tool. *J. Mol. Biol.* 215, 403–410. doi: 10.1016/S0022-2836(05)80360-2

Bay, S., Ferrari, B., and Greening, C. (2018). Life without water: how do bacteria generate biomass in desert ecosystems?. *Microbiol. Aust.* 39, 28–32. doi: 10.1071/MA18008

Berney, M., and Cook, G. M. (2010). Unique flexibility in energy metabolism allows mycobacteria to combat starvation and hypoxia. *PLoS One* 5:e8614. doi: 10.1371/journal.pone.0008614

Berney, M., Greening, C., Conrad, R., Jacobs, W. R., and Cook, G. M. (2014a). An obligately aerobic soil bacterium activates fermentative hydrogen production to survive reductive stress during hypoxia. *Proc. Natl. Acad. Sci. U.S.A.* 111, 11479–11484. doi: 10.1073/pnas.1407034111

Berney, M., Greening, C., Hards, K., Collins, D., and Cook, G. M. (2014b). Three different [NiFe] hydrogenases confer metabolic flexibility in the obligate aerobe *Mycobacterium smegmatis*. *Environ. Microbiol.* 16, 318–330. doi: 10.1111/1462-2920.12320

Brown, E. N., Friemann, R., Karlsson, A., Parales, J. V., Couture, M. M.-J., Eltis, L. D., et al. (2008). Determining rieske cluster reduction potentials. *JBIC J. Biol. Inorg. Chem.* 13:1301. doi: 10.1007/s00775-008-0413-4

Carere, C. R., Hards, K., Houghton, K. M., Power, J. F., McDonald, B., Collet, C., et al. (2017). Mixotrophy drives niche expansion of verrucomicrobial methanotrophs. *ISME J.* 11, 2599–2610. doi: 10.1038/ismej.2017.112

Conrad, R. (1999). Soil microorganisms oxidizing atmospheric trace gases (CH4, CO, H2, NO). *Indian J. Microbiol.* 39, 193–203. doi: 10.1128/AEM.00275-17

Constant, P., Chowdhury, S. P., Pratscher, J., and Conrad, R. (2010). Streptomycetes contributing to atmospheric molecular hydrogen soil uptake are widespread and encode a putative high-affinity [NiFe]-hydrogenase. *Environ. Microbiol.* 12, 821–829. doi: 10.1111/j.1462-2920.2009.02130.x

Constant, P., Poissant, L., and Villemur, R. (2008). Isolation of *Streptomyces* sp. *PCB7*, the first microorganism demonstrating high-affinity uptake of tropospheric H2. *ISME J.* 2, 1066–1076. doi: 10.1038/ismej.2008.59

Constant, P., Poissant, L., and Villemur, R. (2009). Tropospheric H2 budget and the response of its soil uptake under the changing environment. *Sci. Total Environ.* 407, 1809–1823. doi: 10.1016/j.scitotenv.2008.10.064

Cordero, P. R. F., Bayly, K., Leung, P. M., Huang, C., Islam, Z. F., Schittenhelm, R. B., et al. (2019a). Atmospheric carbon monoxide oxidation is a widespread mechanism supporting microbial survival. *ISME J.* 13, 2868–2881. doi: 10.1038/s41396-019-0479-8

Cordero, P. R. F., Grinter, R., Hards, K., Cryle, M. J., Warr, C. G., Cook, G. M., et al. (2019b). Two uptake hydrogenases differentially interact with the aerobic respiratory chain during mycobacterial growth and persistence. *J. Biol. Chem.* (in press). doi: 10.1074/jbc.RA119.011076

Crooks, G. E., Hon, G., Chandonia, J.-M., and Brenner, S. E. (2004). WebLogo: a sequence logo generator. *Genome Res.* 14, 1188–1190. doi: 10.1101/gr.849004

Ehhalt, D. H., and Rohrer, F. (2009). The tropospheric cycle of H2: a critical review. *Tellus B* 61, 500–535. doi: 10.1111/j.1600-0889.2009.00416.x

Frielingsdorf, S., Schubert, T., Pohlmann, A., Lenz, O., and Friedrich, B. (2011). A trimeric supercomplex of the oxygen-tolerant membrane-bound [NiFe]-hydrogenase from *Ralstonia eutropha* H16. *Biochemistry* 50, 10836–10843. doi: 10.1021/bi201594m

Fritsch, J., Siebert, E., Priebe, J., Zebger, I., Lendzian, F., Teutloff, C., et al. (2014). Rubredoxin-related maturation factor guarantees metal cofactor integrity during aerobic biosynthesis of membrane-bound [NiFe] hydrogenase. *J. Biol. Chem.* 289, 7982–7993. doi: 10.1074/jbc.M113.544668

Gebhard, S., Tran, S. L., and Cook, G. M. (2006). The Phn system of *Mycobacterium smegmatis*: a second high-affinity ABC-transporter for phosphate. *Microbiology* 152, 3453–3465. doi: 10.1099/mic.0.29201-0

Greening, C., Berney, M., Hards, K., Cook, G. M., and Conrad, R. (2014a). A soil actinobacterium scavenges atmospheric H2 using two membrane-associated, oxygen-dependent [NiFe] hydrogenases. *Proc. Natl. Acad. Sci. U.S.A.* 111, 4257–4261. doi: 10.1073/pnas.1320586111

Greening, C., Villas-Bôas, S. G., Robson, J. R., Berney, M., and Cook, G. M. (2014b). The growth and survival of *Mycobacterium smegmatis* is enhanced by co-metabolism of atmospheric H2. *PLoS One* 9:e103034. doi: 10.1371/journal.pone.0103034

Greening, C., Biswas, A., Carere, C. R., Jackson, C. J., Taylor, M. C., Stott, M. B., et al. (2016). Genomic and metagenomic surveys of hydrogenase distribution indicate H2 is a widely utilised energy source for microbial growth and survival. *ISME J.* 10, 761–777. doi: 10.1038/ismej.2015.153

Greening, C., Carere, C. R., Rushton-Green, R., Harold, L. K., Hards, K., Taylor, M. C., et al. (2015a). Persistence of the dominant soil phylum *Acidobacteria* by trace gas scavenging. *Proc. Natl. Acad. Sci. U.S.A.* 112, 10497–10502. doi: 10.1073/pnas.1508385112

Greening, C., Constant, P., Hards, K., Morales, S. E., Oakeshott, J. G., Russell, R. J., et al. (2015b). Atmospheric hydrogen scavenging: from enzymes to ecosystems. *Appl. Environ. Microbiol.* 81, 1190–1199. doi: 10.1128/AEM.03364-14

Greening, C., and Cook, G. M. (2014). Integration of hydrogenase expression and hydrogen sensing in bacterial cell physiology. *Curr. Opin. Microbiol.* 18, 30–38. doi: 10.1016/j.mib.2014.02.001

Grostern, A., and Alvarez-Cohen, L. (2013). RubisCO-based CO2 fixation and C1 metabolism in the actinobacterium *Pseudonocardia dioxanivorans* CB1190. *Environ. Microbiol.* 15, 3040–3053. doi: 10.1111/1462-2920.12144

Hartmans, S., and De Bont, J. A. (1992). Aerobic vinyl chloride metabolism in *Mycobacterium aurum* L1. *Appl. Environ. Microbiol.* 58, 1220–1226.

Houchins, J. P., and Burris, R. H. (1981). Comparative characterization of two distinct hydrogenases from *Anabaena* sp. strain 7120. *J. Bacteriol.* 146, 215–221.

Islam, Z. F., Cordero, P. R. F., Feng, J., Chen, Y.-J., Bay, S., Gleadow, R. M., et al. (2019). Two Chloroflexi classes independently evolved the ability to persist on atmospheric hydrogen and carbon monoxide. *ISME J.* 13, 1801–1813. doi: 10.1038/s41396-019-0393-0

Ji, M., Greening, C., Vanwonterghem, I., Carere, C. R., Bay, S. K., Steen, J. A., et al. (2017). Atmospheric trace gases support primary production in Antarctic desert surface soil. *Nature* 552, 400–403. doi: 10.1038/nature25014

Kanno, M., Constant, P., Tamaki, H., and Kamagata, Y. (2015). Detection and isolation of plant-associated bacteria scavenging atmospheric molecular hydrogen. *Environ. Microbiol.* 18, 2495–2506. doi: 10.1111/1462-2920.13162

Kessler, A. J., Chen, Y.-J., Waite, D. W., Hutchinson, T., Koh, S., Popa, M. E., et al. (2019). Bacterial fermentation and respiration processes are uncoupled in permeable sediments. *Nat. Microbiol.* 4, 1014–1023. doi: 10.1038/s41564-019-0391-z

Khdhiri, M., Hesse, L., Popa, M. E., Quiza, L., Lalonde, I., Meredith, L. K., et al. (2015). Soil carbon content and relative abundance of high affinity H2-oxidizing bacteria predict atmospheric H2 soil uptake activity better than soil microbial community composition. *Soil Biol. Biochem.* 85, 1–9. doi: 10.1016/j.soilbio.2015.02.030

Koch, H., Galushko, A., Albertsen, M., Schintlmeister, A., Gruber-Dorninger, C., Lucker, S., et al. (2014). Growth of nitrite-oxidizing bacteria by aerobic hydrogen oxidation. *Science* 345, 1052–1054. doi: 10.1126/science.1256985

Kumar, S., Stecher, G., and Tamura, K. (2016). MEGA7: molecular evolutionary genetics analysis version 7.0 for bigger datasets. *Mol. Biol. Evol.* 33, 1870–1874. doi: 10.1093/molbev/msw054

Liot, Q., and Constant, P. (2016). Breathing air to save energy – new insights into the ecophysiological role of high-affinity [NiFe]-hydrogenase in *Streptomyces avermitilis*. *Microbiologyopen* 5, 47–59. doi: 10.1002/mbo3.310

Lynch, R. C., Darcy, J. L., Kane, N. C., Nemergut, D. R., and Schmidt, S. K. (2014). Metagenomic evidence for metabolism of trace atmospheric gases by high-elevation desert Actinobacteria. *Front. Microbiol.* 5:698. doi: 10.3389/fmicb.2014.00698

Meredith, L. K., Rao, D., Bosak, T., Klepac-Ceraj, V., Tada, K. R., Hansel, C. M., et al. (2014). Consumption of atmospheric hydrogen during the life cycle of soil-dwelling actinobacteria. *Environ. Microbiol. Rep.* 6, 226–238. doi: 10.1111/1758-2229.12116

Mohammadi, S., Pol, A., van Alen, T. A., Jetten, M. S. M., and Op den Camp, H. J. M. (2017). Methylacidiphilum fumariolicum SolV, a thermoacidophilic "Knallgas" methanotroph with both an oxygen-sensitive and -insensitive hydrogenase. *ISME J.* 11, 945–958. doi: 10.1038/ismej.2016.171

Myers, M. R., and King, G. M. (2016). Isolation and characterization of *Acidobacterium ailaaui* sp. nov., a novel member of Acidobacteria subdivision 1, from a geothermally heated Hawaiian microbial mat. *Int. J. Syst. Evol. Microbiol.* 66, 5328–5335. doi: 10.1099/ijsem.0.001516

Piché-Choquette, S., and Constant, P. (2019). Molecular hydrogen, a neglected key driver of soil biogeochemical processes. *Appl. Environ. Microbiol.* 85:e02418-18. doi: 10.1128/AEM.02418-18

Piché-Choquette, S., Khdhiri, M., and Constant, P. (2017). Survey of high-affinity H2-oxidizing bacteria in soil reveals their vast diversity yet underrepresentation in genomic databases. *Microb. Ecol.* 74, 771–775. doi: 10.1007/s00248-017-1011-1

Piché-Choquette, S., Khdhiri, M., and Constant, P. (2018). Dose-response relationships between environmentally-relevant H2 concentrations and the biological sinks of H2, CH4 and CO in soil. *Soil Biol. Biochem.* 123, 190–199. doi: 10.1016/j.soilbio.2018.05.008

Pinske, C., Jaroschinsky, M., Sargent, F., and Sawers, G. (2012). Zymographic differentiation of [NiFe]-hydrogenases 1, 2 and 3 of *Escherichia coli* K-12. *BMC Microbiol.* 12:134. doi: 10.1186/1471-2180-12-134

Pruitt, K. D., Tatusova, T., and Maglott, D. R. (2007). NCBI reference sequences (RefSeq): a curated non-redundant sequence database of genomes, transcripts and proteins. *Nucleic Acids Res.* 35, D61–D65. doi: 10.1093/nar/gkl842

Schäfer, C., Friedrich, B., and Lenz, O. (2013). Novel, oxygen-insensitive group 5 [NiFe]-hydrogenase in *Ralstonia eutropha*. *Appl. Environ. Microbiol.* 79, 5137–5145. doi: 10.1128/AEM.01576-13

Schmidt, C. L., and Shaw, L. (2001). A comprehensive phylogenetic analysis of Rieske and Rieske-type iron-sulfur proteins. *J. Bioenerg. Biomembr.* 33, 9–26.

Schröder, O., Bleijlevens, B., de Jongh, T. E., Chen, Z., Li, T., Fischer, J., et al. (2007). Characterization of a cyanobacterial-like uptake [NiFe] hydrogenase: EPR and FTIR spectroscopic studies of the enzyme from *Acidithiobacillus ferrooxidans*. *JBIC J. Biol. Inorg. Chem.* 12, 212–233. doi: 10.1007/s00775-006-0185-7

Smith, P. K., Krohn, R. II, Hermanson, G. T., Mallia, A. K., Gartner, F. H., Provenzano, et al. (1985). Measurement of protein using bicinchoninic acid. *Anal. Biochem.* 150, 76–85. doi: 10.1016/0003-2697(85)90442-7

Snapper, S. B., Melton, R. E., Mustafa, S., Kieser, T., and Jacobs, W. R. J. (1990). Isolation and characterization of efficient plasmid transformation mutants of *Mycobacterium smegmatis*. *Mol. Microbiol.* 4, 1911–1919. doi: 10.1111/j.1365-2958.1990.tb02040.x

Søndergaard, D., Pedersen, C. N. S., and Greening, C. (2016). HydDB: a web tool for hydrogenase classification and analysis. *Sci. Rep.* 6:34212. doi: 10.1038/srep34212

Stover, C. K., De La Cruz, V. F., Fuerst, T. R., Burlein, J. E., Benson, L. A., Bennett, L. T., et al. (1991). New use of BCG for recombinant vaccines. *Nature* 351:456.

Tamagnini, P., Axelsson, R., Lindberg, P., Oxelfelt, F., Wünschiers, R., and Lindblad, P. (2002). Hydrogenases and hydrogen metabolism of cyanobacteria. *Microbiol. Mol. Biol. Rev.* 66, 1–20. doi: 10.1128/mmbr.66.1.1-20.2002

Volbeda, A., Darnault, C., Parkin, A., Sargent, F., Armstrong, F. A., and Fontecilla-Camps, J. C. (2013). Crystal structure of the O2-tolerant membrane-bound hydrogenase 1 from *Escherichia coli* in complex with its cognate cytochrome b. *Structure* 21, 184–190. doi: 10.1016/j.str.2012.11.010

Walker, J. M. (2009). "Nondenaturing polyacrylamide gel electrophoresis of proteins," in *The Protein Protocols Handbook*, ed. J. M. Walker, (Totowa, NJ: Humana Press), 171–176. doi: 10.1007/978-1-59745-198-7_20

Yuvaniyama, P., Agar, J. N., Cash, V. L., Johnson, M. K., and Dean, D. R. (2000). NifS-directed assembly of a transient [2Fe-2S] cluster within the NifU protein. *Proc. Natl. Acad. Sci. U.S.A.* 97, 599–604. doi: 10.1073/pnas.97.2.599

Conflict of Interest: The authors declare that the research was conducted in the absence of any commercial or financial relationships that could be construed as a potential conflict of interest.

Advantages of publishing in Frontiers

OPEN ACCESS
Articles are free to read for greatest visibility and readership

FAST PUBLICATION
Around 90 days from submission to decision

HIGH QUALITY PEER-REVIEW
Rigorous, collaborative, and constructive peer-review

TRANSPARENT PEER-REVIEW
Editors and reviewers acknowledged by name on published articles

Frontiers
Avenue du Tribunal-Fédéral 34
1005 Lausanne | Switzerland

Visit us: www.frontiersin.org
Contact us: info@frontiersin.org | +41 21 510 17 00

REPRODUCIBILITY OF RESEARCH
Support open data and methods to enhance research reproducibility

DIGITAL PUBLISHING
Articles designed for optimal readership across devices

FOLLOW US
@frontiersin

IMPACT METRICS
Advanced article metrics track visibility across digital media

EXTENSIVE PROMOTION
Marketing and promotion of impactful research

LOOP RESEARCH NETWORK
Our network increases your article's readership